Rhenium and Osmium PNP Pincer Complexes for Nitrogen Fixation and Nitride Transfer

Dissertation

for the award of the degree

"Doctor rerum naturalium"

of the Georg-August-Universität Göttingen

within the doctoral program of the Georg-August University School of Science (GAUSS)

submitted by

Florian Wätjen, M. Sc.

from Papenburg, Germany

Göttingen, 2019

Thesis Committee

Prof. Dr. Sven Schneider
Institut für Anorganische Chemie, Georg-August-Universität Göttingen

Prof. Dr. Franc Meyer
Institut für Anorganische Chemie, Georg-August-Universität Göttingen

Members of Examination Board

1. Reviewer	Prof. Dr. Sven Schneider Institut für Anorganische Chemie, Georg-August-Universität Göttingen
2. Reviewer	Prof. Dr. Franc Meyer Institut für Anorganische Chemie, Georg-August-Universität Göttingen
Further members of the Examination Board:	Prof. Dr. Ricardo Mata Institut für Physikalische Chemie, Georg-August-Universität Göttingen Prof. Dr. Inke Siewert Institut für Anorganische Chemie, Georg-August-Universität Göttingen Prof. Dr. Dietmar Stalke Institut für Anorganische Chemie, Georg-August-Universität Göttingen Dr. Michael John Institut für Organische und Biomolekulare Chemie, Georg-August-Universität Göttingen

Date of oral examination: 27.09.2019

In The Beginning There Was Silence And Darkness
All Across The Earth
Then Came The Wind And A Hole In The Sky
Thunder And Lightning Came Crashing Down
Hit The Earth And Split The Ground
Fire Burned High In The Sky

From Down Below Fire Melted The Stone
The Ground Shook And Started To Pound

*The Gods Made **Heavy Metal***
And They Saw That It Was Good

— **Manowar**
"The Gods Made Heavy Metal" on "Louder Than Hell"

First of all, I want to thank my supervisor Prof. Dr. Sven Schneider for providing me with interesting and challenging scientific "nuts to crack" and the great degree of freedom but also of support I got during the last years. Your enthusiasm for our research is inspiring and infectious.
Furthermore I want to thank Prof. Dr. Franc Meyer for kindly assuming the part of my second supervisor and referee of this thesis.

My gratitude goes to *Thomas Auth* for the memorable time during his practical lab course as well as to my bachelor student *Jan Christian Becker*.

I thank *Dr. Christian Würtele* and *Dr. Christian Volkmann* (X-ray), *Dr. Markus Finger* and *Prof. Dr. Vera Krewald* (DFT, CASSCF), *Dr. Milan Orlita* (magnetic IR), as well as *Dr. Michael John* and *Ralf Schöne* (NMR) for their scientific contributions to this thesis as well as for the helpful and instructive discussions.

The analytical laboratories and the mass department of the our faculty for there efforts in measuring my samples.

I thank *Mirko Paulikat* and *Stefan Ortgies* for providing me with their LaTeX templates, as well as *Ricardo Langner* who wrote the in here used cleanthesis template. Additionally, I want to highlight the work of the numerous coders out there developing free software (like Linux, Orca, Inkscape, LaTeX or vim, just to name a few) which I used quite heavily.

A probably unusual peculiarity of this thesis are the incorporated quotes from heavy metal lyrics at the beginning of each chapter. These are chosen to highlight certain aspects of each chapter and are my personal homage to the many (heavy) metal bands, the music of which accompanied me throughout my entire PhD period (and if scientific papers can open with *Monty Python* quotes, a small non-scientific personal note in a thesis should be fine).[1]

My special thanks go to the whole *AK Schneider group*. I've spend some marvelous years with you in the lab and beyond and I will keep this (unfortunately limited) time in good memory. Especially *Josh Abbenseth*, *Sarah Bete*, *Jan Gerkens*, *Sebastian Kopp*, *Felix Schneck* and *Richt van Alten* made this time an unforgettable experience.

Last but not least I thank *Lisa Wätjen*, my wife and best friend. Your motivation carried me through the tougher times of my PhD and your wanderlust is the reason why I write these lines in the shadow of an olive tree in south France rather than in a stuffy office. For this and everything else, I love you!

Contents

Part I

Introduction

1

Molecular dinitrogen, nitrogenase and the *Haber-Bosch* process

> *And no one, just no one, no one will break this*
>
> — **Heaven Shall Burn**
> "Endzeit" on "Iconoclast"

Nitrogen is one of the main elements in organic matter, next to hydrogen, carbon and oxygen, being incorporated in almost every bio-relevant molecule. Consequently, life on earth relies to a great extend on the availability of readily metabolizable nitrogen sources. Since nitrogen is continuously removed from the nutrient cycle by embedding in sediments or release of N_2 by sequential nitrification and denitrification of ammonia, processes to make molecular dinitrogen accessible for living organisms are essential to life.[2] Molecular nitrogen gas constitutes about 78 % of earth's atmosphere, making it the most abundant unbound element available. However, dinitrogen features an exceptionally strong N≡N triple bond, with a bond dissociation enthalpy (BDE) of 941 kJ mol^{-1} comparable to acetylene (962 kJ mol^{-1}) or carbon monoxide (1070 kJ mol^{-1}), the only diatomic molecule with a higher BDE than N_2.[3] Additionally, cleaving the first bond already requires almost half of the entire BDE (i.e. 410 kJ mol^{-1} while for acetylene it is only 222 kJ mol^{-1}, thus less than one quarter) and in contrast to CO, N_2 does not have a dipole moment. Both features render potential conversions highly demanding as they add an even higher kinetic barrier on top of the already challenging thermodynamic requirements. Many other properties like a proton affinity lower than that of methane (N_2: 493.8 kJ mol^{-1}, CH_4: 543.5 kJ mol^{-1}) or an ionization potential comparable to that of argon (N_2: 15.58 eV, Ar: 15.75 eV) and an extremely high energy gap between the highest occupied molecular orbital (HOMO) and the lowest unoccupied molecular orbital (LUMO) (10.82 eV) make redox chemistry almost impossible and are in line with the inertness of dinitrogen.[4]

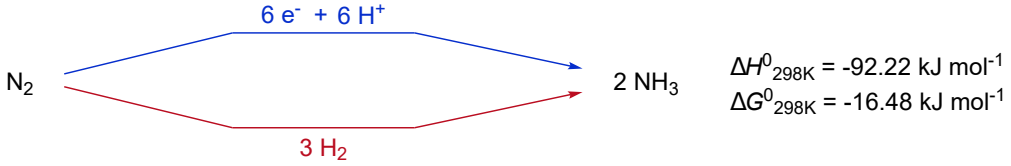

Scheme 1.1. Synthesis of ammonia via sequential proton and electron transfer (*top*) or direct reaction with H_2 (*bottom*).

While these properties highlight the difficulties connected to N_2 fixation, there are actually some conversions which are at least thermodynamically feasible, with the conversion to ammonia being the most prominent example (see Scheme 1.1). In order to achieve nitrogen fixation in nature, sophisticated enzymes evolved, the so-called nitrogenases, found in bacteria, which form ammonia in approx. 2.5×10^{11} kg / year.[5] The catalytically active center in the most thoroughly investigated nitrogenase enzyme is a [7Fe-9S-Mo-C-homocitrate] cluster, the iron-molybdenum cofactor (FeMo-co), which was recently proven to contain an interstitial carbon atom.[6,7] Additionally, nitrogenase systems that are based on a [VFe] or a pure [Fe] cofactor are known.[8] Under optimal conditions, nitrogen fixation by these enzymes follows a stepwise $6\,H^+$ / $6\,e^-$ reduction of N_2 to ammonia according to the following reaction:

$$N_2 + 8\,e^- + 16\,\text{MgATP} + 8\,H^+ \longrightarrow 2\,NH_3 + H_2\uparrow + 16\,\text{MgADP} + 16\,P_i$$

The "waste" of two H^+ and two e^- to produce H_2 from the so-called E_4 state has been proposed to be due to reductive activation of the FeMo-co necessary for initial N_2 binding and N_2H_2 formation.[9] Afterwards, protons and electrons are delivered in an alternating pathway (i.e. $NH{=}NH \xrightarrow[e^-]{H^+} NH_2{-}NH \xrightarrow[e^-]{H^+} NH_2{-}NH_2 \xrightarrow[e^-]{H^+} NH_3\uparrow + NH_2 \xrightarrow[e^-]{H^+} NH_3\uparrow$) to release two equivalents of ammonia (compare Scheme 3.1).

Until the early 20th century, enzymes remained the main source of fixed nitrogen. This changed drastically with the development of laboratory scale ammonia production by *Fritz Haber*, patented 1908, and the subsequent upscaling of this process to a multi-ton ammonia plant by *Carl Bosch*. The resulting *Haber-Bosch* process utilizes heterogeneous iron or ruthenium, which are the most active catalysts next to highly expensive osmium or radioactive uranium.[10] The mechanism of ammonia formation in this reaction is fundamentally different from the pathway in nitrogenase enzymes. Initially, the dihydrogen as well as dinitrogen molecules undergo full bond scission at the surface to form chemisorbed H and N atoms, which then react in a *Langmuir-Hinshelwood* type mechanism to form ammonia. By the formation of surface bound nitrides, the high energy demand for N≡N bond cleavage is compensated and the reaction $N_2 \longrightarrow 2\,N_{ad}$ is exothermic by $\Delta H^0 = -17\,\text{kJ mol}^{-1}$ (see Figure 1.1).[11] In these plants, 300 to 500 °C and pressures up to 300 atm are employed in order to drive the reaction, especially the rate determining N_2 chemisorption. Including all industrially necessary steps, e.g. hydrogen production by steam reforming, purification or the process itself, synthesis of ammonia requires roughly 485 kJ mol^{-1} and at a world production of roughly 140 Mt per year overall about 1.4 % of the world energy production are consumed in this process.[10,12]

The high energy demand of this process as well as the related scientific challenges have triggered several decades of intense research efforts to the development of alternative, more environmentally friendly processes. Apart from homogeneous approaches, which will be

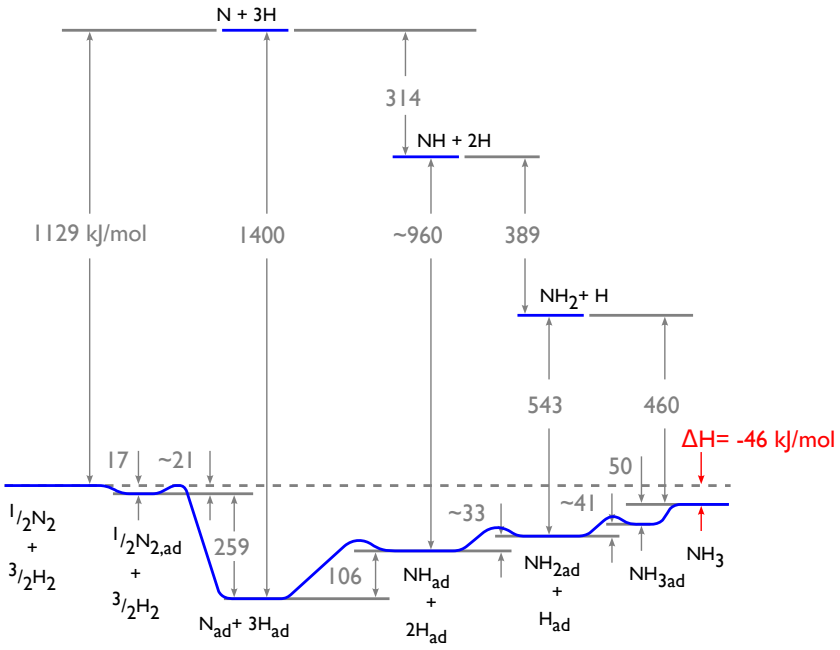

Fig. 1.1. Potential energy surface of ammonia formation in the iron catalyzed *Haber-Bosch* process.[11] Energies are given in kJ mol^{-1}.

covered in Section 3.1, especially the field of heterogeneously catalyzed electrochemical ammonia synthesis from N_2 and water has very recently gained a lot of attraction as an appealing approach where the necessary energy can potentially be derived from renewable resources.[13,14]

While the major part of industrially synthesized ammonia is used for production of fertilizers (approx. 88 %)[12] and therefore builds the foundation of modern agriculture, it also is the main source for the formation of industrially relevant organic molecules, building blocks and fine chemicals containing nitrogen atoms. In this context, the development of homogeneous catalysts which follow a *Haber-Bosch* type reaction, i.e. which undergo initial spitting of N_2 into terminal nitrido complexes, provides a promising approach. Since a broad range of functionalization reactions is available for transition metal nitride complexes,[15] such N_2 derived nitrides open the possibility of directly incorporating N_2 into higher value organic molecules, omitting the superfluous step of ammonia production. These functionalization reactions require well defined reaction centers and tuning of the active environment and therefore homogeneous transition metal complexes are predestined and can be assumed to perform with much better selectivity and efficiency than heterogeneous systems.

Consequently, homogeneous transition metal complexes involved in N_2 fixation schemes as well as possibilities of N-X bond formation and functionalization of nitrides in general will be the focus of this introduction.

2

Binding of dinitrogen to transition metal complexes

> *Believe that together*
> *We can change for the best*
>
> — **Architects**
> "Untitled II" on "Lost Forever // Lost Together"

In general, dinitrogen is a rather poor ligand, acting as a weak σ-donor and an even weaker π-acceptor. However, ever since the discovery of the very first N_2 complex in 1965, i.e. $[Ru(NH_3)_5N_2]^{2+}$,[17] various binding modes of molecular dinitrogen to transition metal complexes have been reported in literature. Overall, N_2 complexes can be classified in four main groups, i.e. (I) end-on terminal (η^1-N_2), (II) end-on bridging (μ-η^1:η^1-N_2), (III) side-on bridging (μ-η^2:η^2-N_2) and (IV) side-on-end-on bridging (μ-η^2:η^1-N_2), of which (I) is the most dominant coordination mode observed (see Figure 2.1). In these complexes, the bond order between the two nitrogen atoms can vary drastically either due to partial reduction by the metal center(s) or after subsequent protonation and reduction to N_2H_X ligands. In order to judge the degree of activation in these complexes, the N-N bond distances as well as

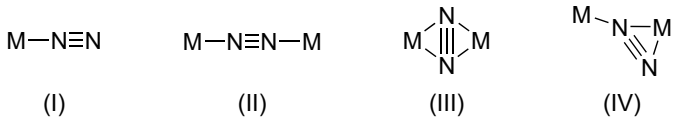

Fig. 2.1. Main classes of N_2 binding modes in complexes found in literature.

Tab. 2.1. Bond lengths and stretching vibrations for free N_2 and coordinated moieties in different reduction states.[16]

(coordinated) N-N moiety	bond lenght / Å	stretching vibration / cm^{-1}
free N_2	1.10	2331
N≡N	1.10 - 1.20	2331 - 1700
$[N{\equiv}N]^-$	n.a.	n.a.
free N_2H_2	1.25	1583/1529
$[N{=}N]^{2-}$	1.20 - 1.35	1700 - 1200
$[N{=}N]^{3-}$	1.40	1040 - 989
free N_2H_4	1.45	885
$[N{-}N]^{4-}$	1.40 - 1.60	1100 - 700

stretching vibrations are commonly employed as characteristic properties,[18,19] which should be inversely correlated according to *Badger*'s rule.[20] The typically observed parameters are summarized in Table 2.1. In general, the different degrees of activation are often restricted to the different binding motifs. For example, terminal N_2 complexes are always rather unactivated with an intact N≡N triple bond, whereas higher degrees of activation, i.e. N_2^{2-} or N_2^{4-} ligands, are found in dinuclear complexes (especially in side-on bridged complexes).

2.1 End-on bound N_2

As stated above, the vast majority of transition metal complexes do form mononuclear, terminal, end-on bound N_2 complexes, often with a d^6 electronic configuration of the metal center.[21] The bonding in such complexes can be understood as a combination of σ donation of the N_2 lone pair into a suitable, empty d-orbital and a π backdonation from filled d-orbitals into the $N^{\pi^*}N$ orbitals, comparable to the situation found in CO (see Figure 2.2). However, due to the large HOMO-LUMO gap in N_2 (see Section 1) the overlap is often rather poor and activation of the N≡N bond occurs only to a minor degree.

Fig. 2.2. Orbital interactions between the metal center and the N_2 ligand in terminal end-on bound complexes.

A higher degree of activation is typically found in dinuclear complexes featuring an end-on bridging N_2 ligand (i.e. coordination mode (II), see Figure 2.1). The very first complex with such a μ-η^1:η^1 dinitrogen ligand, i.e. $[(\mu\text{-}N_2)\{Ru(NH_3)_5\}_2]^{(BF_4)_4}$, was discovered in 1968 by *Taube* and coworkers.[22] Ever since, several such complexes were characterized.[16,18,19] The interaction with two metal centers at the same time can lead to significant charge transfer of the metal atoms to the N_2 bridge and thus to a decrease of the N-N bond order. This was first rationalized by molecular orbital (MO) considerations regarding the {MNNM} core by *Gray* and *Chatt* for complexes in an (idealized) fourfold symmetry.[23,24] This picture was later adopted by *Fryzuk* and veryfied by means of semi-empirical calculations, while *Bercaw* and *Cummins* developed a closely related MO scheme for complexes in threefold symmetry.[25–27] Combining the proposals and findings made in this work, a quite elaborate picture evolves (see Scheme 2.1). Assuming the {MNNM} core to be oriented along the z-axis, the frontier molecular orbitals (FMOs) of such dimers are constructed from the metal d orbitals and nitrogen p orbitals. The metal d_{xz} and d_{yz} as well as the nitrogen p_x and p_y orbitals are combined to form four sets of twofold degenerated, perpendicular π MOs, i.e. $1e_u$, $1e_g$, $2e_u$, $2e_g$. The metal d_{z^2} and nitrogen p_z orbitals can be combined into a σ

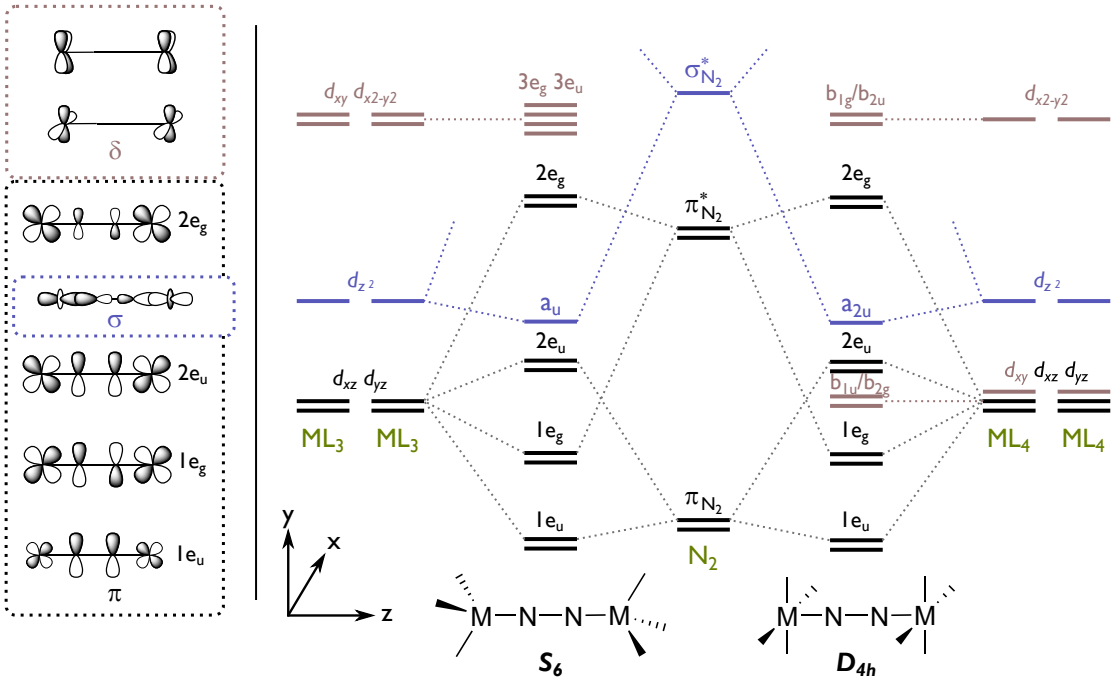

Scheme 2.1. The frontier molecular orbital scheme of end-on bridging dinuclear N_2 complexes, comprised of σ (*blue*), π (*black*) and δ (*red*) symmetric molecular orbitals.[16]

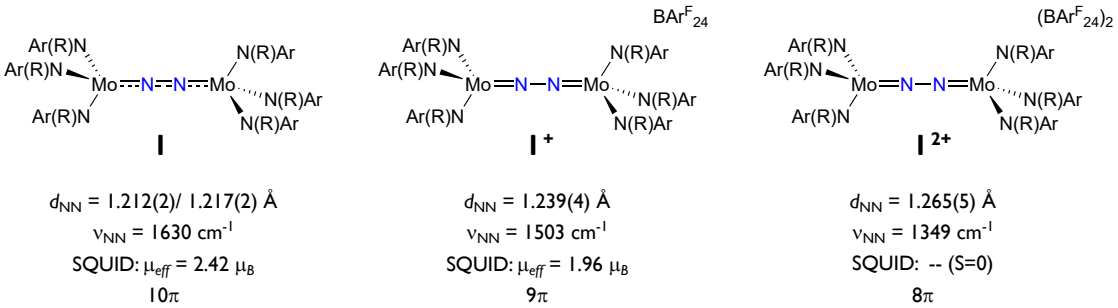

d_{NN} = 1.212(2)/ 1.217(2) Å
ν_{NN} = 1630 cm^{-1}
SQUID: μ_{eff} = 2.42 μ_B
10π

d_{NN} = 1.239(4) Å
ν_{NN} = 1503 cm^{-1}
SQUID: μ_{eff} = 1.96 μ_B
9π

d_{NN} = 1.265(5) Å
ν_{NN} = 1349 cm^{-1}
SQUID: -- (S=0)
8π

Fig. 2.3. Redox series of $\mathbf{I}^{n+}$ (n = 0-2, Ar = 3,5-($C_6H_3(Me)_2$), R = $C(CD_3)_2CH_3$).[27,28]

space, of which only the $M^{\sigma}N^{\sigma^*}N^{\sigma}M$ orbital (of a_u or a_{2u} symmetry, depending on the point group) is of relevance to the FMO space. Additionally, there are the δ symmetric MOs derived from the metal d_{xy} and $d_{x^2-y^2}$ orbitals, which do vary quite significantly in the different dimers. In *Cummins*'s S_6 symmetric dimer [(μ-N_2){Mo(N(R)Ar)$_3$}$_2$] (**I**, Ar = 3,5-($C_6H_3(CH_3)_2$), R = $C(CD_3)_2CH_3$), the amide donors interact strongly with the δ orbitals, raising them energetically high within the virtual orbital space.[27] However, in N_2 dimers with fourfold rotation symmetry, these orbitals are orthogonal to the ligand donor orbitals and therefore drop in energy, eventually becoming available for population.

As can be seen from the qualitative MO pictures in Scheme 2.1, the π symmetric e_u orbitals are mainly of N-N bonding character, while the e_g orbitals are mainly antibonding with respect to the N_2 bridge and their population should reduce the N-N bond order. Due to rather poor orbital overlap, the $1e_u$ orbital is predicted to be mainly located at the N_2 bridge, while the $2e_g$ orbital is rather metal centered. Consequently, population of these orbitals

contribute only to a minor degree to activation of the N-N bond.[29] In contrast to this, the $1e_g$ and $2e_u$ orbitals are rather delocalized and *Cummins* and coworkers proved the influence of population of the latter by preparation of the redox series $\mathbf{I}^{n+}$ (n = 0, 1, 2) (see Figure 2.3).[27,28] In neutral **I**, the constructed MO scheme in Scheme 2.1 is filled with a total of 10 electrons (two per nitrogen, three per formal Mo(III) center), ending up with a 10π electronic configuration in the {MNNM} core and both $2e_u$ orbitals being singly occupied. This electronic structure is confirmed by superconducting quantum interference device (SQUID) measurements (see Figure 2.3). A comparison of the Raman shifts of the N-N stretching vibrations with the crystallographically determined N-N bond distances shows a decrease of the N-N bond order upon oxidation, in line with a stepwise depopulation of a MO with N-N bonding character (i.e. $2e_u$).

This picture is also consistent with the bond metrics of *Taube*'s D_{4h} symmetric dimer $[(\mu\text{-}N_2)\{Ru(NH_3)_5\}]^{(BF_4)_4}$, which exhibits an almost unactivated N_2 bridge ($d(N{\equiv}N)$ = 1.124(15) Å, $\nu_{N\equiv N} = 2100\,cm^{-1}$), in line with the expected $12\pi4\delta$ configuration and thus full population of the $2e_u$ orbitals.[22,23,30] Also, the $8\pi3\delta$ electron complex $[\{(PMe_2Ph)_4ClRe\}(\mu\text{-}N_2)\{MoCl_4(OMe)\}]$ shows a quite high degree of activation ($d(N{=}N)$ = 1.21 Å, $\nu_{N\equiv N} = 1600\,cm^{-1}$).[31]

Another interesting redox series by *Chirik* and coworkers was published for $[(\mu\text{-}N_2)\{(^{Ph}Tpy)(PPh_2Me)_2Mo\}_2]^{(BAr^F_{24})_n}$ ($\mathbf{II}^{n+}$, n = 0 - 4, ^{Ph}Tpy = 4'-Ph-2,2',6'2''-terpyridine).[32] Starting from the formal Mo(I)/Mo(I) dication, which should exhibit a $10\pi4\delta$ electronic configuration,[1] reversible one- and two-electron reductions and oxidations were possible. From investigation of all resulting complexes, the authors developed a closely related electronic structure, but pertubated by mixing with the terpyridine ligand π system, which lifts the degeneracy of the $M^{\pi*}\text{–}N^{\pi}\text{–}N^{\pi*}\text{–}M$ orbitals and thus leads to a singlet ground state for the dication. Interestingly, oxidation (= depopulation of an N-N bonding orbital) as well as reduction (= population of an N-N antibonding orbital) does lead to further activation of

[1] These are just formal oxidation states. A computationally study suggests the system to be best decribed as two Mo(II) centers bridged by an N_2^{2-} ligand.

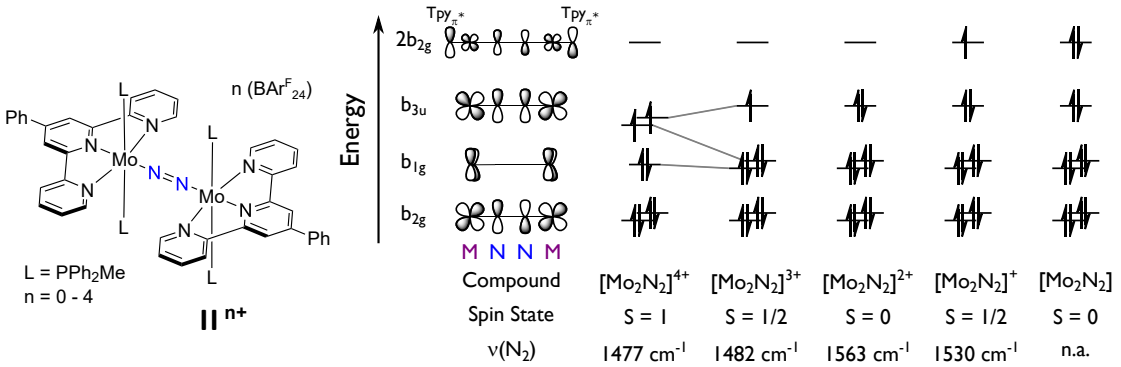

Fig. 2.4. *Left*: *Chirik*'s molybdenum terpyridine complex redox series. *Right*: Qualitative FMO scheme of all five accessible redox states and the corresponding spin states and N-N stretching vibrations.

the N_2 bridge. In contrast to *Cummins*' system, no splitting of the N_2 bridge was observed and no N centered functionalization reactions are reported. In recent, very sophisticated studies, the photophysics of this system were investigated and the terpyridine ligand was shown to act as a light harvesting moiety where excitation leads to an initial metal-ligand charge transfer (MLCT) to the terpyridine ligand followed by inter system crossing (ISC) which shifts electron density to the N_2 bridge via *Fermi*-resonance coupling between the terpyrindine breathing and the N_2 stretching vibrational modes.[33,34] However the excited-state lifetimes are pretty short (τ = 23-26 ps) rendering photoinduced bimolecular reactivity of this molecule unlikely.

The influence of different metals on the activation of N_2 was investigated thoroughly by *Sita* and coworkers, who reported eight different transition metal complexes bridged by an N_2 ligand with identical supporting ligands, i.e. [(μ-N_2){M(Cp^*)(am)}$_2$] (M = Ti, Zr, Hf, V, Nb, Ta, Mo, W; am = N(^{i}Pr)C(Me)N(^{i}Pr)).[35–38] From all these complexes despite the Zr and Hf compounds, end-on μ-η^1:η^1-N_2 complexes could be obtained and structurally characterized (Me group of the am ligand is exchanged with NMe_2 in the Zr and Ph in the Nb complex). The degree of activation of the dinitrogen bridge is expressed in the significantly deviating N-N bond distances (see Table 2.2). The authors describe the Ti complex as formal Ti(III) centers with d^1 electron count, bridged by an N_2^{2-} ligand. The higher homologues, i.e. the Zr and Hf complexes are more easily oxidized and can reach the formal M(IV) oxidation state, yielding formally N_2^{4-} bridges and ending in a side-on μ-η^2:η^2 coordination mode.[36] The group 5 complexes initially all form end-on bridging N_2 dimers, of which the Nb and Ta complexes are shown to undergo thermal rearrangement into bridging bis-nitrido complexes proposed to proceed via the μ-η^2:η^2 coordination mode, which reflects the reduced reduction potential upon moving from group 4 to 5. The remarkable thermal stability of the vanadium complex towards this reaction was explained by the authors as being due to a changes in the ground state electronic structure, comparable to the effects discussed by *Mindiola* for a related system.[39] Moving further right to group 6, i.e. the Mo and W complexes, the N-N bond distances again become shorter and formulation of the

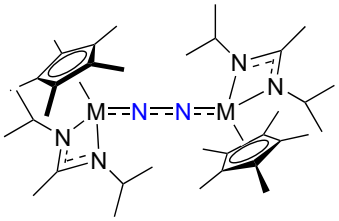

Fig. 2.5. Isostructural complexes of Ti, V, Nb, Ta, Mo and W, prepared by *Sita*.

Tab. 2.2. Coordination modes and bond lengths in *Sita*'s M(Cp^*)(am) N_2 complexes.

metal	coordination mode	N-N bond distance / Å
Ti[35]	μ-η^1:η^1-N_2	1.270(2)
Zr[36]	μ-η^2:η^2-N_2	1.518(2)
Hf[36]	μ-η^2:η^2-N_2	1.611(4)
V[37]	μ-η^1:η^1-N_2	1.225(2)
Nb[37]	μ-η^1:η^1-N_2	1.300(3)
Ta[38]	μ-η^1:η^1-N_2	1.313(4)
Mo[35]	μ-η^1:η^1-N_2	1.267(2)
W[35]	μ-η^1:η^1-N_2	1.277(8)

complexes as being comprised of M(IV) metal centers with a d^2 electron count, bridged by N_2^{2-} ligands were proposed.[35]

Consequently, slight changes in the systems employed to bind and activate N_2 can have a large influence on the actual degree of activation, requiring careful design and fine-tuning to obtain the wanted results. This is also highlighted in Section 3.2.

2.2 Side-on bound N_2

So far, no isolable mononuclear complex with a side-on bound N_2 ligand has been reported. η^2 coordination of N_2 to a single metal center has only been suggested based on electron paramagnetic resonance (EPR) spectroscopic results for the complex $[Zr(\eta^5\text{-}C_5H_4R')_2(N_2)R]$ (R = $CH(SiMe_3)_2$, R' = H or Me),[40] based on infrared (IR) spectra of matrix isolated product of Co atoms with N_2 at 10 K,[41] based on the observation of intramolecular, non-dissociative end-to-end isomerization of $[Ru(NH_3)_5(^{14}N^{15}N)]Br_2$[42] and $[Re(Cp)(CO)_2(^{14}N{\equiv}^{15}N)]$,[43,44] and was eventually structurally characterized by X-ray diffraction as meta-stable state after single-crystal to single-crystal irradiation of $[Os(NH_3)_5(N_2)](PF_6)_2$.[45] And even on bimetallic systems, until 1988, only two clusters with a tetrahedral, non-planar Ni_2N_2 core supported by Li ions were reported.[46–48]

The first structurally characterized side-on $\mu\text{-}\eta^2{:}\eta^2$ N_2 bridged complex with the dinitrogen ligand being coordinated in plane with the two metal centers, i.e. $[(\mu\text{-}\eta^2{:}\eta^2\text{-}N_2)\{Sm(Cp^*)_2\}_2]$ was published in 1988.[49] Only two years after, *Fryzuk* and coworkers were able to isolate and characterize the complex $[(\mu\text{-}\eta^2{:}\eta^2\text{-}N_2)\{ZrCl(N(SiMe_2CH_2P^iPr_2))\}_2]$ (**III**).[50] Based on this result and the finding that substitution of the chloride ligand in this complex with a Cp ligand resulted in isomerization to the end-on bridged dimer **IV**, the authors developed

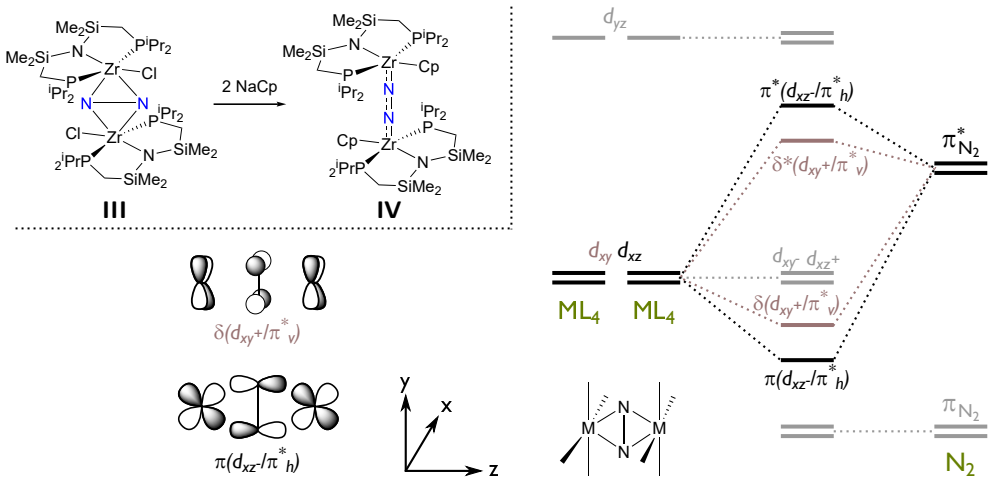

Fig. 2.6. *Top left*: Isomerization of *Fryzuk*'s side-on bridged N_2-dimer by exchange of the Cl^- with a Cp^- ligand. *Main*: FMO scheme of a side-on bridged N_2-dimer.

a bonding scheme for side-on bridged N_2 dimers which allowed to rationalize the respective preferences of the N_2 coordination mode.[25]

In general the more prevalent end-on bridging coordination mode is favorable, as here the metal centers and N_2 bridge do form solely σ- and π-interactions (compare Scheme 2.1), whereas in the side-on coordination mode, one π-interaction is replaced with a δ MO combination, which can be regarded as unfavorable simply due to poorer orbital overlap, analog to considerations in metal-metal multiple bonding.[51] However, if one of the d orbitals needed for π bonding is not available (e.g. due to interaction with strong field ligands), the δ bond can act as a "fallback" option to stabilize the system (see Figure 2.6). Two bonding orbital combinations can be constructed, one π symmetric combination of the d_{xz} and the π_h^* MO of the ligand as well as a δ symmetric combination of the d_{xy} orbitals and the π_v^* MO of the N_2 moiety. In their specific case, *Fryzuk* and coworkers argued that the PNP amide π-donor and chloride σ-donor in **III** interact too strongly with the d_{yz} orbitals, raising them in energy and making them unavailable for π-bonding with the N_2 bridge. When the chloride is exchanged with a Cp^- ligand, this interacts considerably with the d_{xy} orbital required for the δ bond, and the end-on bridging mode becomes more favorable again. This is also expressed in an exceptionally long Zr-N_{amide} bond length in **IV** (d(Zr-N) = 2.303(3) and 2.306(3) Å), indicating a reduced bond order and thus weaker interaction with the d_{yz} orbital. This picture was later qualitatively confirmed by density functional theory (DFT) calculations.[52] Despite these electronic influence, sterics were also shown to be of considerable importance in zirconocene complexes (see Scheme 2.2). A series of $Zr(Cp^X)_2$-N_2 complexes was made by *Bercaw* ([(μ-η^1:η^1-N_2){$Zr(C_5Me_5)_2(N_2)$}2] (**V**))[53] and *Chirik* ([(μ-η^1:η^1-N_2){$Zr(C_5Me_5)(C_5Me_4H)(N_2)$}2] (**VI**), [(μ-$\eta^2$:$\eta^2$-$N_2$){$Zr(C_5Me_4H)_2$}2] (**VII**))[54,55] of which only the latter, sterically least crowded complex forms a side-on bridged N_2 dimer.

One of the main differences between end-on and side-on coordinated dinuclear dimers is their reactivity. While the only reported N_2 centered reactivity of the former is their cleavage into nitrides (see Section 3.2.1), side-on bridged N_2 ligands often exhibit a much higher degree of activation and can be reactive towards N-X bond formation (X = H, B, C, Si; see Section 3.3).[56]

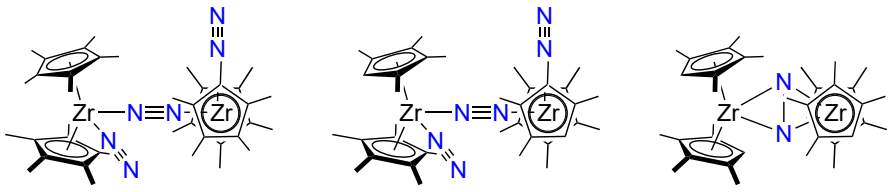

V **VI** **VII**

Scheme 2.2. Different coordination modes of N_2 in zirconocene complexes controlled by the steric bulk of the Cp-ligands.

3 Reactions of dinitrogen complexes

> *You've got to cut the cord*
> *Cut the cord and wake up!*
>
> — **The Agonist**
> "Disconnect Me" on "Eye of Providence"

3.1 Ammonia formation

In light of the unmatched importance of industrial ammonia production by the *Haber-Bosch* process, the discovery of molecular dinitrogen complexes naturally sparked hopes for the development of homogeneous catalysts capable of the same reaction. By now, this goal has been matched by a number of systems (even though with much less efficiency) and has been thoroughly reviewed in several recent publications.[56–59] However, for most of the time (1972 - 2003), only stochiometric conversion to ammonia was known, pioneered by the work of *Chatt* and coworkers, who reported protonation of $[M(N_2)_2(dppe)_2]$ (M = Mo, W; dppe = $Ph_2PCH_2CH_2PPh_2$) with HCl to form an N_2H_2 ligand,[60] followed by the report on ammonia formation after protonation of $[M(N_2)_2(PR_3)_4]$ (M = Mo, W; PR_3 = $PMePh_2$ or PMe_2Ph).[61] This discovery and intensive follow-up research led to the formulation of the *Chatt* cycle for ammonia formation from terminally bound N_2 which is depicted in Scheme 3.1.[62,63] This cycle, which is also discussed as the most likely mechanism of ammonia formation by the nitrogenase enzymes, starts with stepwise protonation and reduction of the *terminal* nitrogen atom (for which this is also called the *distal pathway*) until reaching

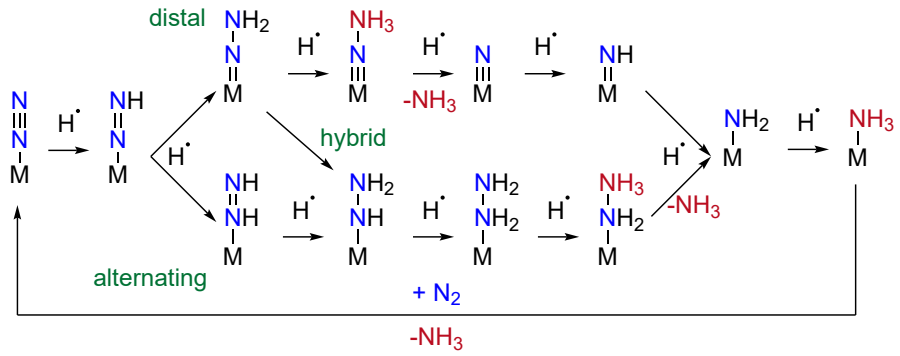

Scheme 3.1. Discussed mechanisms for ammonia formation from terminal bound N_2 by transfer of H^+/e^- (marked as $H^\bullet$).

the [M≡N–NH_3] state, from which the first equivalent of ammonia is released. Only then, the remaining metal nitride is stepwise protonated and reduced until a second equivalent of ammonia is released. Such a cycle can only produce ammonia, while for formation of hydrazine, an alternating pathway is required. In addition to this achievement, the authors were furthermore able to perform the first N–C bond formation from N_2 by reaction with acetyl chlorides.[64,65]

The next major breakthrough after these finding was marked by the first report of a well-defined molecular system with a single metal center which is able to catalyze ammonia formation, i.e. *Schrock*'s [Mo(N_2)(HIPTN_3N)] (**VIII**, HIPTN_3N^{3-} = [{3,5-(2,4,6-$^{i}Pr_3C_6H_2$)$_2$ $C_6H_3NCH_2CH_2$}$_3$N]$^{3-}$), which does react with Co(Cp^*)$_2$ and LuH(BAr^F_{24}) and is capable of forming up to 8 equivalents of ammonia with respect to Mo.[66] The reaction most likely follows a reduction scheme which is comparable to the *Chatt* cycle, which is backed up by a number of independently synthesized potential intermediates which are also catalytically active as well as by DFT calculations.[63,67–70] This large availability of characterized intermediates renders *Schrock*'s catalyst the best understood systems and even though much better performing catalysts are known by now, there are still ongoing efforts to aquire data on even the most unstable intermediates.[71] Notably, this work includes one of only two literature known parent imido complexes derived from dinitrogen, i.e. [Mo(NH)(HIPTN_3N)]$^{0/+}$.[67]

A slightly different situation might be at hand in the iron catalyzed ammonia formation reported by *Peters* and coworkers, who prepared a series of trigonal pyramidal complexes [Fe(N_2)(XP_3^{iPr})]$^-$ (**IX**, XP_3^{iPr} = X(2-*i*Pr_2P-C_6H_4)$_3$, X = B, C, Si), of which the first two are catalytically active.[72–74] In this system, a hybrid mechanism between the distal and the alternating pathway (i.e. alternating protonation of both N atoms) has been proposed based on the disproportionation of [Fe=N–NH_2] and [Fe=N–NH_2]$^+$ to [Fe–N_2] and [Fe–NH_2–NH_2]$^+$, where after formation of the [M=N–NH_2] moiety, the metal bound ni-

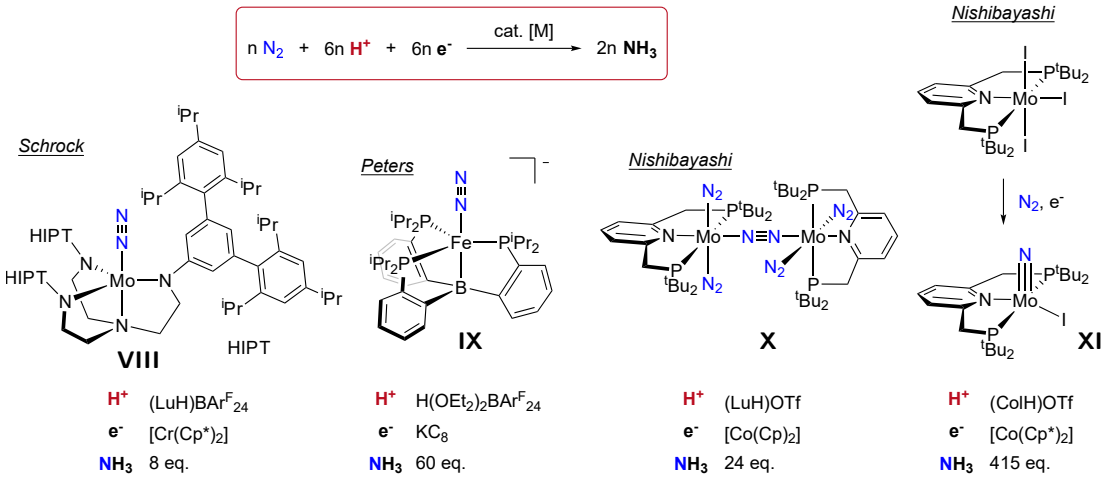

Fig. 3.1. Pioneering molecular catalysts mediating protonation/reduction cycles for ammonia production from N_2.

trogen is protonated before the terminal one. However, later studies contradicted these results, as the formation of a terminal nitrido complex $[Fe(N)(BP_3^{iPr})]^+$ was observed to form from threefold protonation of $[Fe(N_2)(BP_3^{iPr})]^{2-}$, accompanied by the release of equimolar amounts of NH_3.[75] Furthermore, *Peters* could show that the commonly used reduction / protonation agent pair, $Co(Cp_2^*)$ and lutidinium salts (LuH^+), might actually act as a proton coupled electron transfer (PCET) reagent in the catalyses, where instead of stepwise protonation and reduction of the N_2 complexes one Cp^* ring is first protonated, followed by an H atom transfer to the substrate.[76]

A very interesting observation regarding the pathway of ammonia formation was reported by *Nishibayashi* and coworkers. They developed the second ever reported catalytic system for ammonia production, $[(\mu\text{-}N_2)\{Mo(N_2)_2(PNP)\}_2]$ (**X**, PNP = 2,6-$(CH_2P^tBu_2)_2NC_5H_5$), which is obtained by reduction of the trichloro-complex $[MoCl_3(PNP)]$ in the presence of dinitrogen.[77] Treatment with $Co(Cp)_2$ and LuH^+ under N_2 atmosphere resulted in formation of 12 equivalents NH_3 per Mo center. This reaction is supposed to undergo a distal pathway protonation and reduction scheme at one of the terminally bound N_2 ligands. Variation of the *para* substituent of the pyridine ligand as well as computational investigation of the reaction led to the conclusion, that the initial protonation to M−N=NH is rate determining and intermetallic charge transfer from the second Mo in the dimer was proposed to be crucial for stabilizing this intermediate.[58,78] When the pyridine moiety was exchanged with an N-heterocyclic carbene (NHC), i.e. in the complexes $[(\mu\text{-}N_2)\{Mo(N_2)_2(PCP)\}_2]$ (PCP = 1,3-bis((di-*tert*-butylphosphino)methyl)benzimidazol-2-ylidene or 1,3-bis(2-(di-*tert*-butylphosphino)ethyl)imidazol-2-ylidene), especially the former, i.e. the benzimidazole based complex performed remarkably well in catalysis with 115 turnovers per Mo center.[79] Based on DFT calculations, this was attributed to the NHC acting not only as σ donor but also as π acceptor, which was considered beneficial for the reaction. However, when in the pyridine complex the chloride ligands of the precursor are exchanged with iodide, a significantly different mechanism comes into play. Upon reduction under N_2, the complex undergoes initial N≡N bond scission to form the terminal nitrido complex [Mo(N)I(PNP)] (**XI**), presumably via an $\mu\text{-}\eta^1{:}\eta^1$ bridged dimer.[80] The system still is catalytic but stepwise protonation and reduction to ammonia takes place only *after* the N_2 splitting step, raising the question on whether such initial cleavage reactions might also play a role in the previously reported systems. In addition to these mechanistic considerations, in their latest contribution, *Nishibayashi* and coworkers were also able to significantly tweak the turn-over-numbers of their catalysts by using SmI_2/H_2O as PCET reagents, obtaining up to 2175 equivalents NH_3 per Mo center.[81]

3.2 Initial full dinitrogen cleavage

3.2.1 Thermal N_2 cleavage from end-on bound dimers

The initial full cleavage of the N≡N triple bond reported by *Nishibayashi* for his iodide complex **XI** is unique for systems which catalyze the production of ammonia. However, it is by far not the first example of an initial N_2 cleavage by dinuclear transition metal catalysts. In fact, the very first report on such a reaction dates back to 1995, when *Cummins* and coworkers reported their dimolybdenum complex **I** (see Section 2.1) to undergo selective N≡N bond cleavage to form the corresponding nitrido complex $[Mo(N)(N(R)Ar)_3]$ (**XII**) at room temperature.[27,82] This reaction was thoroughly investigated and can be rationalized based on the MO scheme developed earlier for these end-on bridged dimers (see Section 2.1, Scheme 2.1).

Comparison of the FMO scheme of the dimer and the monomer reveals that while the dimer has an electronic structure with 10π and 6σ electrons in the $\{MNNM\}$ core, the formation of two monomers requires a total of 8π and 8σ electrons ($M\overset{\sigma}{-}N$ and the lonepairs at the two nitride ligands). Consequently, the former a_u orbital with $M\overset{\sigma}{-}N\overset{\sigma^*}{-}N\overset{\sigma}{-}M$ character in the dimer drops dramatically in energy and becomes an occupied, bonding, $1b_u$ symmetric $M\overset{\sigma}{-}N$ orbital in the nitride complexes. In order to achieve this and to obtain electron transfer from the π orbital space into a formally orthogonal σ orbital, the splitting needs to proceed via a *zig-zag* transition state, which breaks the symmetry, lifts the degeneracy of the orbital sets and allows for the required mixing of the orbitals (i.e. $3b_u$ and $2b_u$, see Scheme 3.2). These symmetry considerations were later reproduced by DFT calculations on a truncated model (i.e. $[(\mu\text{-}N_2)\{Mo(NH_2)_3\}_2$).[83]

This electronic requirements can also explain why the mono- and dicationic complexes $\mathbf{I}^+$ and $\mathbf{I}^{2+}$ do not undergo splitting into terminal nitrides, even though the N_2 ligand is stronger activated (vida supra).[27] From these dimers, no closed shell nitrides can be obtained, which is energetically unfavorable and thus, the N_2 cleavage becomes thermodynamically uphill.

Variations of this system have led to some valuable insights regarding the requirements for N_2 activation. The effect of the ligands on the electronic structure is well exemplified by comparing *Cummins*' dimeric complex with those prepared by *Schrock* (i.e. $[(\mu\text{-}N_2)\{Mo(N(CH_2CH_2NR)_3)\}_2]$ (**XIII**, $R = SiMe_3$)) and *Floriani* ($[(\mu\text{-}N_2)\{MoMes_3\}_2]$, **XIV**).[84–86] Both dimers feature a $\mu\text{-}\eta^1{:}\eta^1$ bridging N_2 ligand, just as in *Cummins*' complex. Nevertheless, both systems are thermally stable and do not split into the corresponding nitrides, even though they do formally feature the same oxidation state of the metal and exhibit threefold rotation symmetry, rendering them isoelectronic to **I**.

Schrock's dimeric molybdenum complex also features three amide donor ligands. However, they are connected via an amine, which acts as an additional σ donor in *trans* position with respect to the N_2 bridge. This should on the one hand destabilize σ-bonding in the

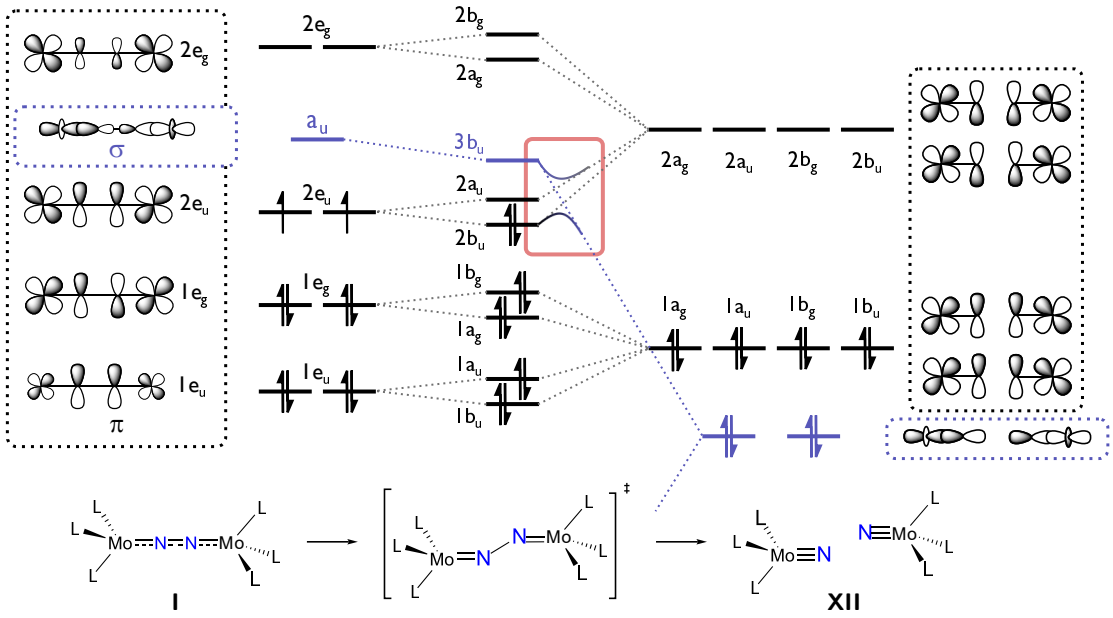

Fig. 3.2. FMO scheme the the thermal splitting of formal Mo(III) derived dimer **I** into terminal nitrido complexes **XII**.

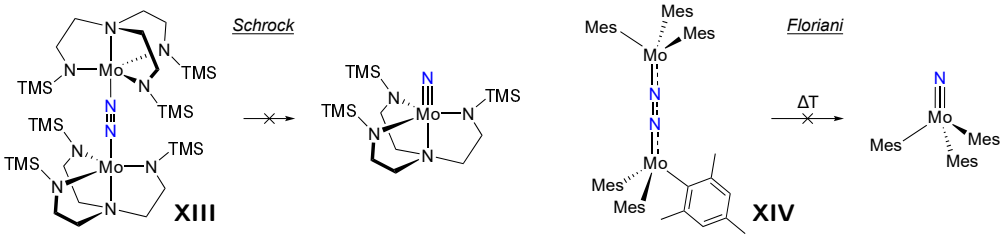

Fig. 3.3. Mo(III) based N_2 dimers by *Schrock* and *Floriani*, which are isoelectronic to *Cummins*' dimer but do not undergo thermal N_2 splitting.

nitride complex and on the other raise the a_u orbital energetically, therefore hampering the required orbital mixing in the transition state. Additionally, extensive theoretical studies on a truncated model by *Stranger* initially indicated amide rotation to be of importance for the N_2 scission, which would obviously be prevented by the amide link to the amine.[87] Later studies on the full model revealed this rotation is largely suppressed in the complexes with the bulky amides and therefore might not have a significant effect anyways.[88]

In *Floriani*'s dimer **XIV**, the most prominent difference is the replacement of π-donating amide with pure σ-donating aryl ligands.[86] While no detailed electronic structure considerations were addressed, a possible explanation for the thermal stability of the dimer might be the reduced π and σ donor strength of the aryl groups compared to the amide ligands in *Cummins*' system. This should lowerthe $2e_u$ in energy and increase the energetic gap to the a_u orbitals (see Scheme 2.1) which prevents mixing of the two orbitals and electron transfer in the transition state as discussed above. However, the complex is reported to undergo photochemical splitting of N_2, which is discussed in Section 3.2.3.

A strong influence on the product formation was found for the steric bulk of the amide ligands in *Cummins*' starting platform [Mo(N(^{t}Bu)Ar)$_3$] (**XV**). When small lignads like NMe_2^-, $NMeEt^-$ or NEt_2^- are employed, the corresponding Mo(III) trisamide complexes undergo dimerization reactions forming Mo≡Mo triple bonds, which prevents any further reactivity towards dinitrogen.[89] When the *tert*-butyl groups in **XV** are replaced with *iso*-propyl groups, the initially formed complex is [Mo(H)(η^2–Me$_2$C=NAr)(N(^{i}Pr)Ar)$_2$] (**XVII**), where one ^{i}Pr group is activated by the metal forming a hydride species (see Scheme 3.2 *top*).[90] This C-H activation was shown to be fully reversible, and under a dinitrogen atmosphere, a nitrido-bridged dimer [(μ-N){Mo(N(^{i}Pr)Ar)$_3$}$_2$] (**XVIII**) could be isolated as main product, which is believed to form by initial N_2 cleavage into the corresponding nitrido complexes and fast follow-up reaction with excess starting complex. DFT calculations on the system confirmed that such a dimerization is kinetically and thermodynamically favorable for the smaller ligand, but unfavorable for the more bulky *tert*-butyl based ligand. Increasing the steric shielding even further (i.e. using N(Ad)Ar, Ad = adamantyl) fully shuts down the observable N_2 chemistry at the Mo(III) stage and [Mo(N(Ad)Ar)$_3$] was reported to be stable indefinitely under N_2 atmosphere.[91] This series clearly shows how minor changes in ligand size can significantly impact the chemistry of the entire system and are therefore a highly important parameter in the design of new systems.

In order to elucidate the mechanism not only of the splitting but also of the dimer assembly in *Cummins*' dimer, intermediates of the reaction were trapped experimentally.[91] While the starting complexd **XV** is stable towards NaHg under Ar, a new species Na(THF)$_x$[Mo(N_2)(N(^{t}Bu)Ar)$_3$] (**XVI**) is readily formed under a N_2 atmosphere, suggesting the unobserved neutral mononuclear N_2 complex to be the electron accepting complex (see Scheme 3.2 *bottom*). This anionic complex could then be further functionalized by addition of MeOTs, $SiMe_3Cl$ or PhCOCl, undergoing N-C or N-Si coupling at the terminal nitrogen atom. Interestingly, the dimer-formation was shown to be redox-catalyzed by reductants, and the

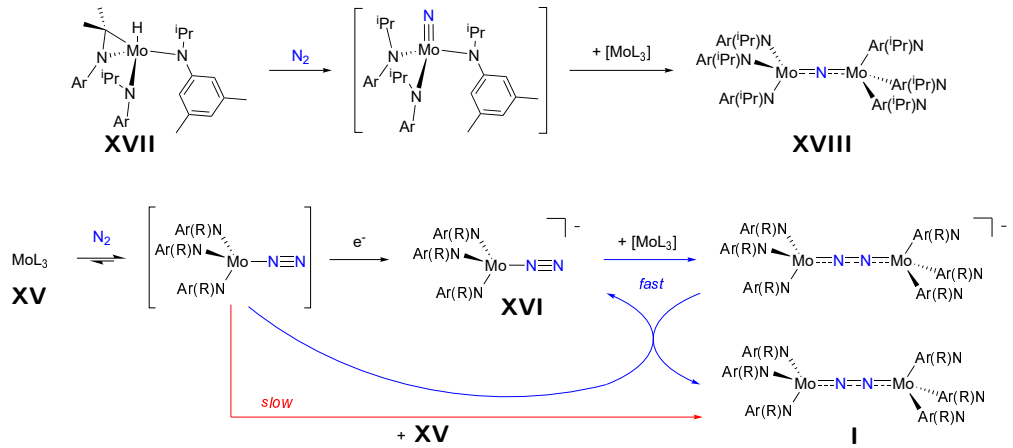

Scheme 3.2. *Top*: Reducing the steric bulk in *Cummins*' original Mo complex leads to exclusive formation of a μ-N bridged dimer from a hydride resting state. *Bottom*: Small amounts of reducing agents were found to redox-catalyze the formation of the neutral dimer **I**.

authors proposed that binding of a second metal fragment **XV** to the anionic N_2 complex **XVI** would be much faster than in the neutral case, followed by reduction of a neutral N_2 adduct by the formed anionic dimer (see Scheme 3.2 *bottom*).[91] It is also reported that the slow formation of the dimer can be significantly enhanced not only by reductant, but also by the addition of N-heterocyclic bases.[92] The authors ascribed this to a spin state change from quartet to doublet upon coordination of the base to the $[Mo(N(^tBu)Ar)_3]$ precursor and subsequent fast N_2 binding. This is also in line with the very recent publication on N_2 splitting by $[Mo(OSi(O^tBu)_3)_3]$ reported by *Copéret* and coworkers.[93] Here a corresponding end-on μ-N_2 bridged dimer forms within 30 s and in the product, one silylether ligand arm acts as additional ligand, coordinating *trans* to the N_2 ligand and consequently might have a comparable effect to external ligands in *Cummins*' system.

The very first (and to the present day exclusive) example of N_2 bond cleavage by a group 7 transition metal complex was published by *Schneider* and coworkers in 2014. The Re(III) complex $[ReCl_2(PNP^{tBu})]$ (**XIX**) was shown to split dinitrogen upon one-electron reduction under a dinitrogen atmosphere to yield Re(V) nitrido complex $[Re(N)Cl(PNP^{tBu})]$ (**XXI**).[94] This splitting was initially proposed to proceed via the dimeric complex $[(\mu\text{-}N_2)\{ReCl(PNP^{tBu})\}_2]$ (**XX**), which exhibits a $10\pi 4\delta$ electron count in the {MNNM} core, fully consistent with the above discussed mechanism.[1] An in-depth follow-up investigation of the reaction, especially by means of cyclic voltammetry, allowed for the construction of a mechanistic proposal for the dimer formation and splitting.[2] According to this model, after initial reduction to an anionic Re(II) complex, N_2 is bound, followed by chloride loss and a second reduction step to formal Re(I) complex $[Re(N_2)Cl(PNP^{tBu})]^-$.[95] This species then binds to a Re(III) fragment and comproportionats to yield the dimeric complex **XX**, which renders the formation an overall $EC^{Cl}C^{N_2}EC^{[Re]}$ mechanism. Importantly, it is shown that N_2 is bound and activated at the Re(II) stage. While the two systems are not entirely comparable due to different reaction conditions (especially with respect to addition of reductant), the role of "overreduced" Re(I) and Mo(II) species in *Schneider*'s system and *Cummins*' reported redox-catalysis for promoting dimer formation is strikingly similar.

[1] The dimer **XX** is actually characterized and proven to be an intermediate in the formation of **XXI** within this thesis (see Part II Section 2.1).

[2] The characterization of the thermal splitting of **XX** to **XXI** is part of this thesis and will therefore be discussed in Part II Section 2.1.

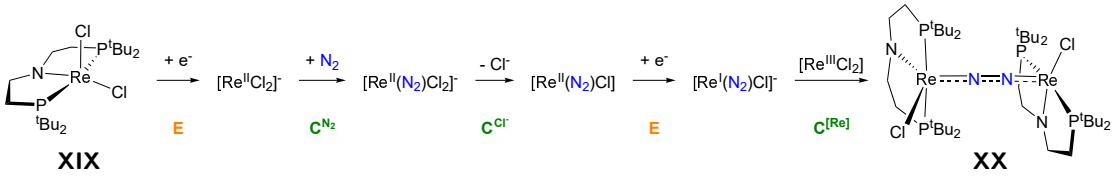

Scheme 3.3. Formation of the Re μ-N_2 dimer **XX** via an $EC^{Cl}C^{N_2}EC^{[Re]}$ mechanism.

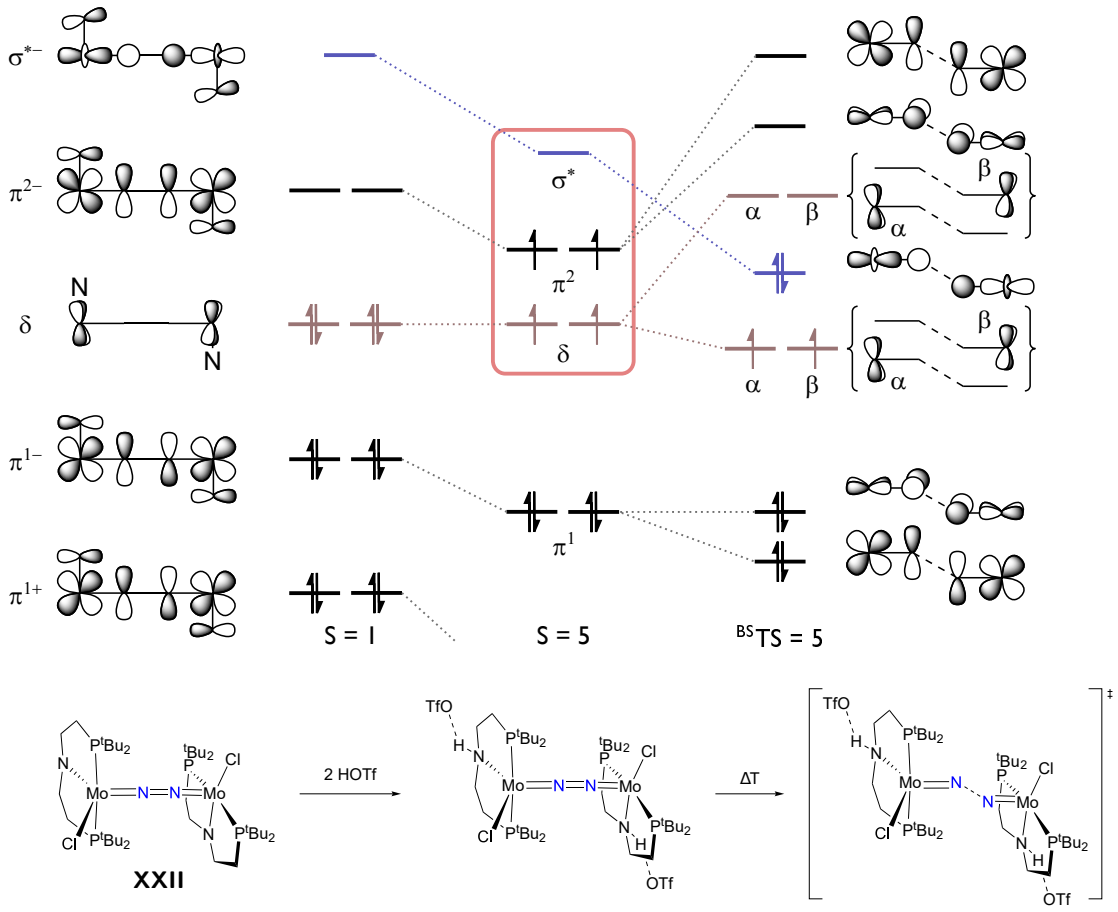

Fig. 3.4. Protonation coupled dinitrogen splitting via spin state change in a Mo dimer.

In 2017, *Schneider* and coworkers further reported N_2 splitting from the formal Mo(II) dinitrogen bridged dimer $[(\mu\text{-}N_2)\{MoCl(PNP^{tBu})\}_2]$ (**XXII**, $PNP^{tBu} = N(CH_2CH_2P^tBu_2)_2^-$).[96] Due to the idealized fourfold rotational symmetry, that dimer exhibits a $8\pi4\delta$ electronic configuration in the $\{MNNM\}$ core, which disqualifies it for splitting according to the considerations made before. And indeed, no thermal splitting was observed. However, twofold protonation of the PNP amide moiety results in splitting into the corresponding terminal nitrido complexes, which is counter intuitive at first glance since protonation should remove electron density from the metal centers, which are already short by one electron each for splitting. The authors identified a spin-state change from singlet to quintet due to quenched π-donation of the ligand upon protonation (identified by *Evan*'s measurement and computations), which led to population of the "$2e_u$" orbitals and significantly reduced the energy gap of the new HOMO to the "a_{2u}" orbital, enabeling thermal splitting (see Scheme 3.4).

Another example illustrating both the subtle influence of ligand variation as well as the complexity of some splitting mechanisms is provided by the group of *Holland*. They prepared a series of iron β-diketiminate complexes $[FeCl(Ln)]_{1or2}$ (**XXIII^{Ln}**, Ln = RC(C(R')N(2,6-R"$_2$C$_6$H$_3$))$_2$, with L1: R = H, R' = ^{t}Bu, R" = ^{i}Pr; L2: R = H, R' = Me, R" = ^{i}Pr; L3: R = R' = R" = Me), of which the L1 and L2 complexes do form end-on, dinitrogen bridged

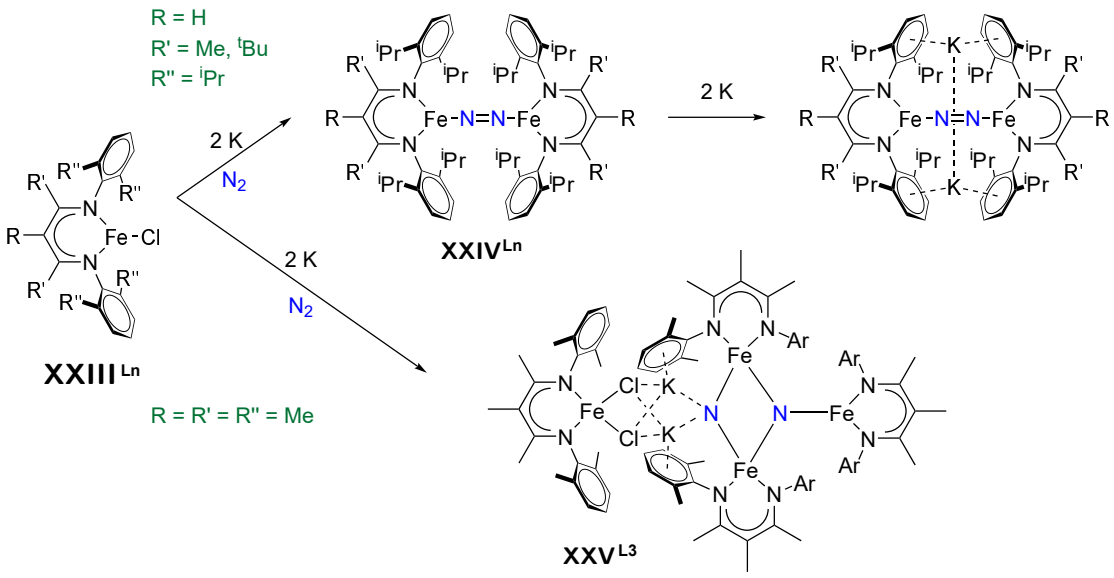

Scheme 3.4. Steric control by ligand bulk of multinuclear N_2 splitting by an Fe complex.

dimers upon reduction with K, i.e. $[(\mu\text{-}N_2)\{Fe(L)\}_2]$ (**XXIV^{Ln}**), which can be reduced further by two electrons with the potassium cations being intercorporated into the molecular structure by coordination to the aryl substituents (see Scheme 3.4).[97,98] In contrast to this, utilizing the least bulky ligand L3 resulted in full cleavage of the N_2 ligand into bridging nitrides by formation of a $[Fe_4(L_3)_4(\mu\text{-}N)_2Cl_2K_2]$ cluster (**XXV^{L3}**), from which ammonia could be released by protonolysis.[99] DFT calculations indicate initial formation of an end-on dimer analog to the systems utilizing L1 and L2, followed by side-on coordination of a third Fe(L3) fragment to the N_2 ligand.[100] The potassium cations are found to act as promotors in the reaction and to stabilize the splitting by ~10 kcal mol^{-1}, rendering this interaction indispensable to achieve splitting. However, potassium is not unique in this behavior and sodium and rubidium also resulted in N_2 splitting, while caesium yielded a cyclic $[Fe_3(\mu\text{-}N_2)_3]$ cluster with intact N_2 ligands. Interestingly, the N_2 splitting was found to be reversible as addition of CO gas to **XXV^{L3}** resulted in formation of 4 eq $[Fe(CO)_3(L_3)]$ accompanied by release of N_2.[101]

3.2.2 Thermal N_2 cleavage from side-on bound dimers

Apart from the splitting of end-on bridged dinitrogen complexes into terminal nitrides, initial splitting in side-on bridged dimers to yield two bridging nitrides has also been reported, but is investigated in less detail. In side-on bridging N_2 complexes, typically a much higher degree of activation can be observed (*vide supra*) and the transition into bridging nitrides is almost fluent. The first example reported on full N≡N cleavage was published by *Cloke* and coworkers and occurred upon one-electron reduction of [VCl(N'N_2)] (N'N_2 = $Me_3SiN(CH_2CH_2NSiMe_3)_2^{2-}$) resulting in $[V(\mu\text{-}N)(N'N_2)]_2$.[102] This complex features an intranuclear N-N distance of $d(N\cdots N) = 2.50(2)$ Å, thus proving full dinitrogen splitting

and the origin of the nitrides from N_2 was unequivocally confirmed by labeling with $^{15}N_2$. Detailed spectroscopic and theoretical investigations were performed in order to understand the electronic structure of the resulting nitrido complex.[103]
Additionally, the reaction pathway which leads to splitting was analyzed by DFT methods.[104] They confirmed initial side-on coordination to a single V(II) [V(N'$_2$)] fragment to be favorable over an end-on coordination mode. This was predicted to be required for electron transfer from the metal into the N$\overset{\sigma^*}{-}$N orbital. Again, a 10π electron count in the {MNNM} core seems to be required for achieving the splitting.

3.2.3 Photochemical N_2 cleavage

Almost 25 years past since *Cummins*' discovery of thermal N_2 splitting by molecular transition metal complexes and an impressive number of related systems undergoing thermal N≡N bond cleavage has been published ever since.[16,56] In contrast to these achievements, the prospect of using (visible) light as an energy source to achieve dinitrogen splitting as been addressed significantly less. However, photoinduced cleavage can potentially provide access to nitrides whose generation is thermally uphill and which might therefore exhibit increased reactivity. This would be highly desirable for achieving follow-up N-functionalization as most nitrides obtained from N_2 splitting are quite stable and unreactive (see Section 4.2.1). Probably the first discussion of the potential of photochemistry in transition metal mediated N_2 fixation can be found in a contribution from *Fischler* and *Gustorf* from 1975.[105] They suggested that photoexcitation in an Fe−N≡N complex should in principle be dominated by two transitions: *a*) a d-d transition from a Fe$\overset{\pi}{-}$N≡N into a Fe$\overset{\sigma^*}{-}$N≡N orbital, sigificantly weakening the M$\cdots$N$_2$ bond strength and *b*) a MLCT transition from the Fe$\overset{\pi}{-}$N≡N into a Fe−N$\overset{\pi^*}{\equiv}$N orbital, transfering electron density into an antibonding ligand orbital and thus potentially increasing the ligand centered reactivity, e.g. towards protonation. Along these lines it is interesting to note, that *Peters* and coworkers indeed reported enhanced turnover rates under irradiation with an Hg lamp for their Fe-based ammonia formation catalysts [Fe(N$_2$)(BP$_3^{iPr}$)]$^-$ (**IX**, see Section 3.1), even though the authors assigned this effect to photochemical regeneration of a H_2-poisoned iron dihydride complex by reducitve elimination of H_2.[106]

Until today, only five examples of photochemical N_2 cleavage are known, which are summarized in Scheme 3.5. The very first example was reported by *Floriani* and coworkers in 2001.[86] As discussed above, their end-on bridging N_2 dimer [(μ-N$_2$){MoMes$_3$}$_2$] (**XIV**) is thermally stable in refluxing benzene (see Section 3.2.1). However, when the complex was irradiated with ultraviolet (UV) light (λ = 365 nm), selective formation of a μ-N bridged dimer [(μ-N){MoMes$_3$}$_2$] (**XXVI**) was formed. The authors proposed photochemical cleavage into the terminal nitrides, followed by formation of an [Mo≡N−Mo−N≡N−Mo−N≡Mo] chain (with Mo = MoMes$_3$) by adduction fromation of two nitrides with one dimer, from which the centeral N_2 moiety is extruded.

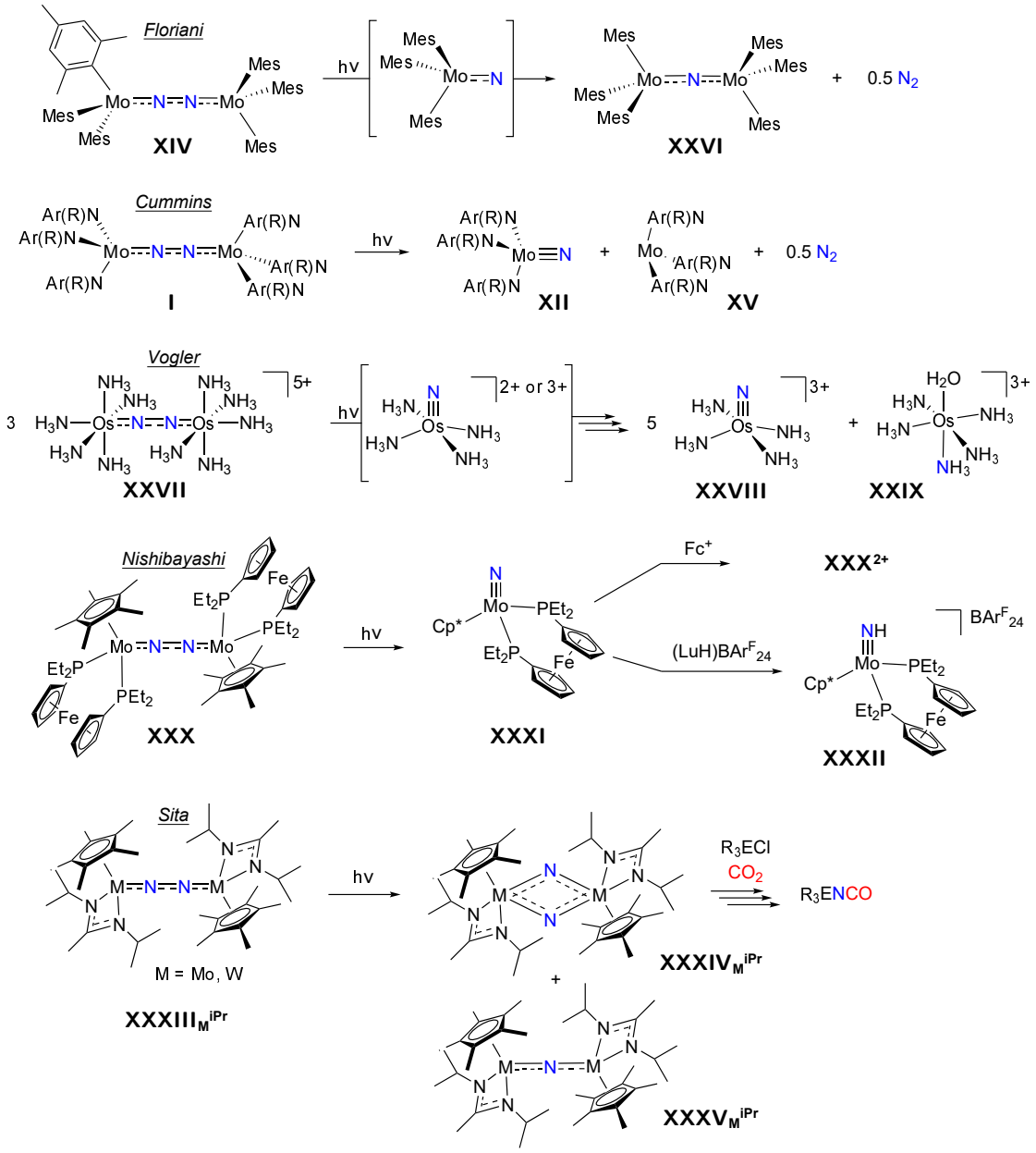

Scheme 3.5. Summary of all five literature known examples of photochemical dinitrogen cleavage.

In 2008, *Cummins* and coworkers also reported the photolysis of their dimer **I** at −78 °C (at which the dimer is thermally stable) by irradiating a pronounced absorption band at 544 nm to produce an equimolar mixture of the nitride [MoN(N(^{t}Bu)Ar)$_3$] (**XII**) and the starting complex [Mo(N(^{t}Bu)Ar)$_3$] (**XV**).[28] Competitive N≡N and Mo–N$_2$ bond cleavage analog to the proposal by *Fischler* and *Gustorf*[105] was proposed as a possible mechanism and the authors suggested that a similar situation might also be the case for *Floriani*'s isoelectronic system. The non-occurance of a bridging nitride complex in *Cummins*' system can rationlized by the large ligand sterics rendering such a dimerization unfavorable.[107] This is the only photochemical reaction available which was studied in detail using time-resolved electronic absorption pump-probe experiments.[108] The study revealed initial excitation into

an exited triplet state followed by full relaxation into the ground state within 300 fs by internal conversion (IC), excluding excited state photochemistry. Instead, N≡N or Mo–N_2 bond dissociation occur from a vibrationally hot ground state after IC and have to compete with vibrational energy relaxation (VER), resulting in a low quantum-yield of ~2 % for each splitting channel. Since formation of the nitride and the N_2 extrusion product will have different activation barriers, their equimolar formation is explained by a nonstatistical energy distribution after IC.

In 2010, *Kunkely* and *Vogler* reported on the photolysis of the mixed valent Os(II)/Os(III) complex $[(\mu\text{-}N_2)\{Os(NH_3)_5\}_2]^{5+}$ (**XXVII**) in aqueous solution, a complex which is strongly related to the very first bridging N_2 complex by *Taube* (see Section 2.1).[22,109] Solely based on ultraviolet/visible (UV/vis) absorption data, the authors claim an initial photodissociatiaon into an Os(VI) (**XXVIII**) and an Os(V) tetraamine nitrido complex, accompanied by the release of two equivalents of ammonia ligands. The Os(V) complex is supposed to be unstable and undergo further disproportionation into the Os(VI) and an Os(IV) nitride, of which the latter disproportionates again and forms **XXVIII** and an $[Os^{III}(NH_3)_5(H_2O)]^{3+}$ complex (**XXIX**) where one of the amine ligands is obtained from the nitride and protons, leading to an overall conversion of N_2 to ammonia in a maximum of 17 %. Interestingly, the photolysis of one-electron oxidized Os(III)/Os(III) dimer is reported to undergo quantitative N_2 release rather than N≡N bond scission, again showing both processes to be feasible under photochemical conditions.[109] As an extension to this work, the authors also reported the dimer photolysis in the presence of ClO_2 to yield $[Os^{II}(NH_3)_5(NO)]^{3+}$, as well as the photolysis of monomeric $[Os(NH_3)_5(N_2)]^{2+}$ under O_2 and H_2O to yield $[Os^{VI}N(NH_3)_4]^{3+} + NO_2^-$ and $[Os^{VI}N(NH_3)_4]^{3+} + N_2H_4 + OH^-$, respectively.[110–112] Despite the characterization of these reactions being based a lot on experience and chemical intuition, this system was investigated in a sophisticated theoretical study by *Krewald* and *González* using multireference CASPT2/CASSCF methods.[113] Splitting of the N_2 bridge was simulated by stepwise increase of the N≡N bond length of **XXVII** in a linear fashion (neglecting the proposed *zig-zag* structure, *vide supra*) and evolution of the electronic structure was analyzed, revealing the $M\overset{\sigma}{-}N\overset{\sigma^*}{-}N\overset{\sigma}{-}M$ orbital to dramatically decrease in energy along the reaction coordinate becoming first singly, then doubly occupied, in agreement with the qualitative picture developed by *Cummins* (see Figure 3.2).

An important step for utilizing photochemical dinitrogen splitting for N_2 fixation was made in 2014, when *Nishibayashi* and coworkers reported a Mo N_2 dimer which does undergo photolytical N_2 cleavage into terminal nitrides which could subsequently be functionalized further.[114] The thermally stable, formal Mo(I) based dimer $[(\mu\text{-}N_2)\{Mo(Cp^*)(depf)\}_2]$ (**XXX**, depf = 1,1'-bis(diethylphosphino)ferrocene), which exhibits a $10\pi4\delta$ electronic configuration in the {MNNM} core, does cleave the N≡N bond to yield the corresponding terminal nitride complex in 33 % yield. Wavelength selective irradiation indicated a pronounced absorption band at 748 nm to be *inactive* in the splitting process, whereas irradiation with

$\lambda > 400$ nm led to conversion. Using time-dependent density functional theory (TDDFT) calculations, a transition between 400 and 450 nm with significant electron loss between the nitrogen atoms was identified which might be relevant for the photolysis. When the obtained nitride [Mo(N)(Cp^*)(depf)] (**XXXI**) is oxidized by one electron, N-N coupling to the dicationic μ-N_2 bridged dimer is observed, in line with *Cummins* findings that splitting of a 8π system would be uphill (see Section 3.2.1). Importantly, the neutral nitride can be protonated at the nitride using (LuH)BAr^F_{24} to yield the only other reported parent imido complex derived from N_2 (**XXXII**) despite the one by *Schrock* (see Section 3.1), accompanied by partial H_2 generation and formation of the dicationic dimer. Treating the nitride with an excess of $Co(Cp^*)_2$ and (LuH)BAr^F_{24} gave ammonia in 37 % yield based on Mo, indicating photogenerated nitrido complexes to have a potential in N_2 fixation.[115]

A even more versatile example was provided in 2015 by *Sita* and coworkers, who could show their thermally stable Mo and W N_2 dimers [(μ-N_2){M(Cp^*)(am)}$_2$] (**XXXIII$_M^{iPr}$**, am = N(^{i}Pr)C(Me)N(^{i}Pr), M = Mo or W) to be photolyzed into a 1:1 mixture of the bis-nitride and mono-nitride bridged dimers [(μ-N)$_2${M(Cp^*)(am)}$_2$] (**XXXIV$_M^{iPr}$**) and [(μ-N){M(Cp^*)(am)}$_2$] (**XXXV$_M^{iPr}$**).[116] The occurance of the mono-μ-N bridged dimer is reminiscent of the observations by *Floriani* and *Cummins*, whereas the bis-μ-N bridged dimer was shown to be formed as well by reductive dimerization of [M(N)(Cp^*)Cl(am)], suggesting terminal nitrides to be the initial photoproduct. Irradiation in the presence of R_3ECl (R = Me, Ph; E = C, Si, Ge) resulted in concomitant formation of [MCl_2(Cp^*)(am)] and [M(N=ER_3)(Cp^*)(am)]. The imido complex was then shown to react with CO_2 to form isocyanide derivatives R_3ENCO and the oxo complexes [M(O)(Cp^*)(am)] and detailed reactivity studies resulted in the development of a three-step synthetic cylce for the generation of isocyanides from N_2, CO_2 and R_3ECl. This work marked the first and so far only example of direct incorporation of photochemically obtained nitrides into organic molecules and thus underpins the potential of this approach especially in generating reactive nitrido complexes which are thermally hard to produce.

3.3 Nitrogen functionalization in side-on coordinated complexes

While splitting into terminal nitrides is the only N_2 functionalization reaction known for the end-on μ-η^1:η^1 coordination mode, dinuclear complexes with a μ-η^2:η^2 side-on coordinated N_2 bridge are also known to undergo N-E bond formation reactions.[16,56] In particular, the groups of *Chirik* and *Fryzuk* reported remarkable reactivity of side-on bound dizirconium complexes (see Figure 3.5). *Fryzuk*'s complex [(μ-η^2:η^2-N_2){Zr(P_2N_2)}$_2$] (**XXXVI**, P_2N_2 = PhP($CH_2SiMe_2NSiMe_2CH_2$)$_2$PPh) was reported to undergo heterolytic H_2 cleavage to form one N-H bond and a bridging zirconium hydride.[117] Additionally, the same complex also

cleaves the related Si-H bond in $^{n}BuSiH_3$ to yield a N-Si bond and again a bridging hydride. Later, also reaction with arylalkynes were reported, leading to N-C bond formation.[118] *Chirik* and coworkers achieved a quite comparable reaction with their $[(\mu\text{-}\eta^2\text{:}\eta^2\text{-}N_2)\{Zr(Cp')_2\}_2]$ complex (**VII**, Cp' = C_5HMe_4, see Section 2.2), however in this complex two equivalents of H_2 are added forming $[((\mu\text{-}\eta^2\text{:}\eta^2\text{-}NH)_2)\{Zr(H)(Cp')_2\}_2]$ (**XXXVII**).[55] Heating this complex under a H_2 atmosphere to 85 °C eventually resulted in release of 10-15 % ammonia, marking the first and still exclusive example of full N_2 hydrogenolysis to NH_3 mediated by a molecular transition metal complex. The Hf analog furthermore reacts with CO_2 to undergo twofold N-C bond formation at one N atom and subsequent workup with excess Me_3SiI results in release of the hydrazine derivative $(Me_3Si)_2N{-}N(CO_2SiMe_3)_2$.[119] Similar reactions with CO or CO_2 were reported on closely related systems, suggesting the use of these gases to promote further reactivity as a general strategy.[56] Comparable reactivity was also obtained by *Sita* and coworkers on their zirconium and hafnium complexes $[(\mu\text{-}\eta^2\text{:}\eta^2\text{-}N_2)\{M(Cp^*)(am)\}_2]$ complex (see Section 2.2, including H_2 clevage, silylation with $PhSiH_3$ and alkylation with EtBr (the latter only in case of Hf).[36]

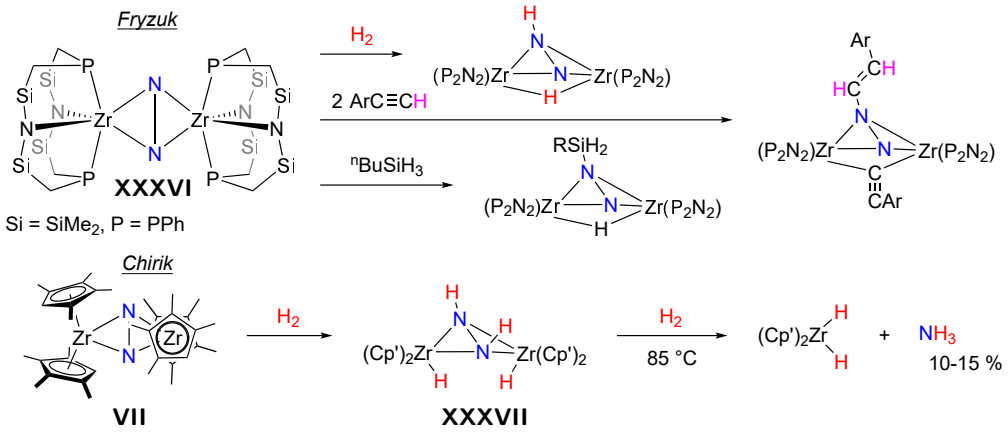

Fig. 3.5. Examples of direct functionaization of side-on bound N_2 by *Fryzuk* and *Chirik*.

4 Reactivity and functionalization of transition metal nitrides

> *Get me out of here!*
> *I've been lost in the dark!*
> *Get me out of here!*
> *Now!*
>
> — **Gojira**
> "The Cell" on "Magma"

4.1 General bonding considerations

Terminal transition metal nitride complexes have been known for more than a century, with the first example, i.e. $K[OsO_3N]$, dating back to 1847.[120] Thus, this field of chemistry is much older than transition metal dinitrogen chemistry and an overwhelming number of examples is known.[15] However, the vast majority of these nitrides is derived from nitrogen sources other than dinitrogen itself, typically via ammonia deprotonation and decomposition of azide or hydrazine and its derivatives.[15,121] Metal-nitride bonds are generally considered triple bonds consisting of one σ and two π bonds and the nitride is both a strong σ- and strong π-donor.

An elaborated picture for the electronic structure of such complexes with metal-ligand multiple bonds was developed by *Gray* and *Ballhausen* for an octahedral vanadyl oxo ion, i.e. $[V(O)(H_2O)_5]^{2+}$, and can be adopted for octahedral nitride complexes as well.[122] The strong donor properties of the nitrido complex lead to an energetic increase of all metal d orbitals with a z component, resulting in the MO splitting displayed in Figure 4.1 *center*. According to this scheme, all but the d_{xy} orbital are antibonding and population of these leads to reactive, unstable compounds. As an immediate consequence, only transition metal nitrides with a d^0-d^2 electron count should be able to form stable octahedral transition metal nitrides, which is the reason for the scarce occurance of late transition metal nitrido complexes.[123–125] This electronic limitation is exemplified by the report on the first terminal iron nitride, obtained after laser photolysis of an iron azide supported by a phorphyrine ligand at 30 K and characterized by resonance *Raman* measurements.[126] The produced Fe(V) d^3 nitrido species is unstable and local heating afforded the N-N coupling product.[127] Similar results were obtained by *Wieghardt* and *Neese* for cyclam supported iron azide complexes

and in depth spectroscopic and theoretical analysis of the formed Fe(V) nitrides indeed indicated a doublet ground state with a $(d_{xy})^2$ $(d_{xz},\ d_{yz})^1$ electronic configuration.[128,129] Later, a high valent octahedral Fe(VI) nitride was synthesized which was stable indefinitely at 77 K and marks the second ever reported Fe(VI) complex besides $[FeO_4]^{2-}$.[130]

The formation of stable nitrides with a higher d electron count can be achieved by removal of ligands and symmetry reduction, either to a tetrahedral geometry with a threefold rotation axis or a square planar geometry with twofold rotation symmetry. In threefold geometry, the $d_{x^2-y^2}$ as well as the d_{z^2} orbitals drop in energy, but only the former drops enough to become non-bonding and thus available for population (see Figure 4.1 *left*). Consequently, most transition metal nitrides with a d^4 electron count (in particular iron complexes) adopt a tetrahedral geometry (see Figure 4.2 *left*).[75,131–134] The first example, i.e. $[Fe(N)(PhBP_3^{iPr})]$ (**XXXVIII**^{iPr}, $PhBP_3^{iPr-} = PhB(CH_2CH_2P^iPr_2)_3^-$), was reported by *Peters* and coworkers and exhibits a singlet ground state and an electronic configuration evaluted by DFT calculations in full agreement with the proposed FMO scheme in Figure 4.1.[131] Later *Smith* and *Meyer* independently reported on closely related carbene stabilized Fe(IV) nitrido complexes (**XXXIX** and **XL**), both of which exhibited electronic configurations in agreement with the observations made by *Peters*.[132,133] These complexes exhibit unusually short Fe≡N bond lengths (**XXXVIII**^{Cy}: d(Fe-N) = 1.55 Å,[135], **XXXIX**: d(Fe-N) = 1.512(1) Å, **XL**: d(Fe-N) = 1.526(2) Å), indicative of a rather high covalency of the iron-nitrogen triple bond.

In a square-planar coordination geometry, where the M≡N bond is oriented along the x-axis, the d_{z^2} decreases drastically in energy and becomes non-bonding, allowing for taking up two

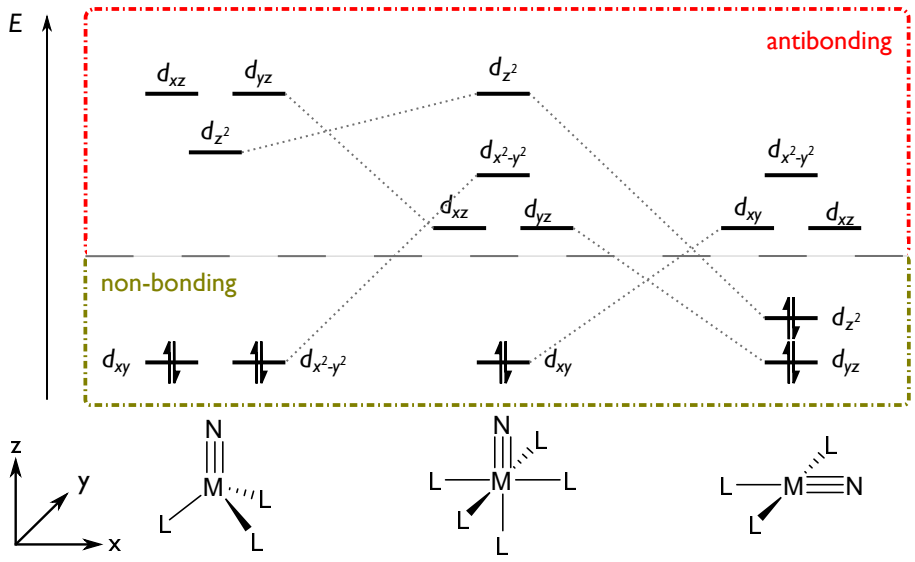

Fig. 4.1. Qualitative FMO schemes of transition metal nitrido complexes in octahedral (*center*) as well as tetrahedral (*right*) and square-planar (*right*) coordination geometries, allowing for an d electron count up to d^2 and d^4, respectively.

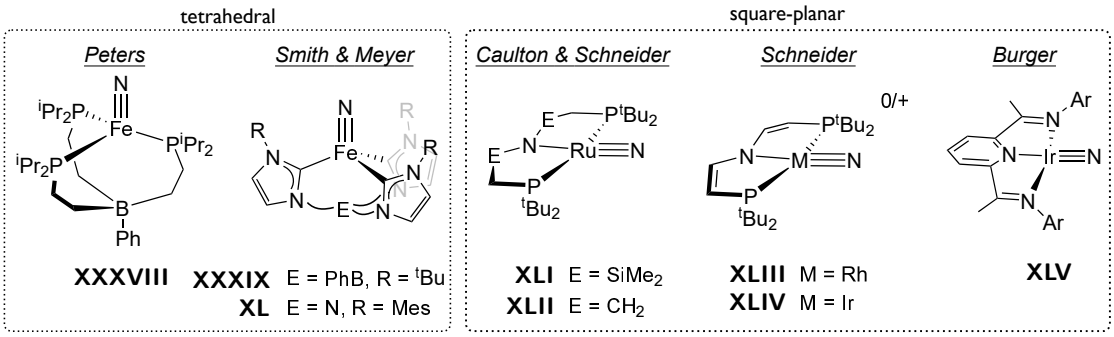

Fig. 4.2. Summary of important d^4-d^6 transition metal nitrido complexes which adopt either a tetrahedral (*left*) or square-planar coordination geometry (*right*).

additional electrons and thus for a d^4 electron count (see Figure 4.2 *right*). As can be seen in Figure 4.1, the d_{z^2} orbital in such a complex becomes the HOMO, while the LUMO and LUMO+1 are still dominated by antibonding π combinations of the d_{xz} and d_{yz} orbitals with the nitride ligand. Consequently, the FMOs of such as system exhibit similar energies, occupation number and symmetry as in a d^2 octahedral nitrido complex, rendering it isolobal to the latter.[136] The first realization of this strategy was reported by *Caulton* and coworkers in 2005 who were able to synthesize the stable Ru(IV) nitrido complex [Ru(N)(PNP^{tBu}_{Si})] (**XLI**, PNP^{tBu}_{Si} = $N(SiMe_2CH_2P^tBu_2)_2^-$) from an azide.[137] The most striking feature in this complex is the small N–Ru≡N angle ($\measuredangle$(N-Ru-N) = 155.86(13)°), which was assigned to the pincer amide and the nitride both being strong π donors which are thus interacting with the same set of orbitals. An analog Ru complex with a slightly modified ligand, i.e. [Ru(N)(PNP^{tBu})] (**XLII**, PNP^{tBu-} = $N(CH_2CH_2P^tBu_2)_2^-$) was later reported by *Schneider* and coworkers, featuring a similarly bent Ru≡N moiety ($\measuredangle$(N-Ru-N) = 147.3(2)°).[138] Remarkably, this coordination geometry even allowed for the synthesis of (meta)stable group 9 nitrido species with d^4 and even d^5 electron count, including $[M(N)(P{=}N{=}P^{tBu})]^{0/+}$ ($P{=}N{=}P^{tBu-}$ = $N(CHCHP^tBu_2)_2^-$; M = Rh (**XLIII**), Ir (**XLIV**)), Ir(N)(PDI)] (**XLV**, PDI = pyridinediimino).[139–141]

4.2 Reactivity of transition metal nitrides

In general, transition metal nitrides can be classified by their principal reactivity towards external reagents, being either nucleophilic or electrophilic. In a simple bonding picture, the difference can originate from the relative energies of the metal and nitrogen orbitals involved in forming the M≡N bond (see Figure 4.3).[142] If the metal d orbitals are rather high in energy compared to the nitrogen p orbitals, the resulting π bonding orbital, is more nitrogen centered, and the nitride is consequently expected to be nucleophilic. On the other hand, if the metal d orbitals are lower in energy, the π^* orbital becomes nitrogen centered and the nitride can be expected to be rather electrophilic. Based on these very simple considerations, early transition metal complexes can be expected to form rather nucleophilic nitrides, while

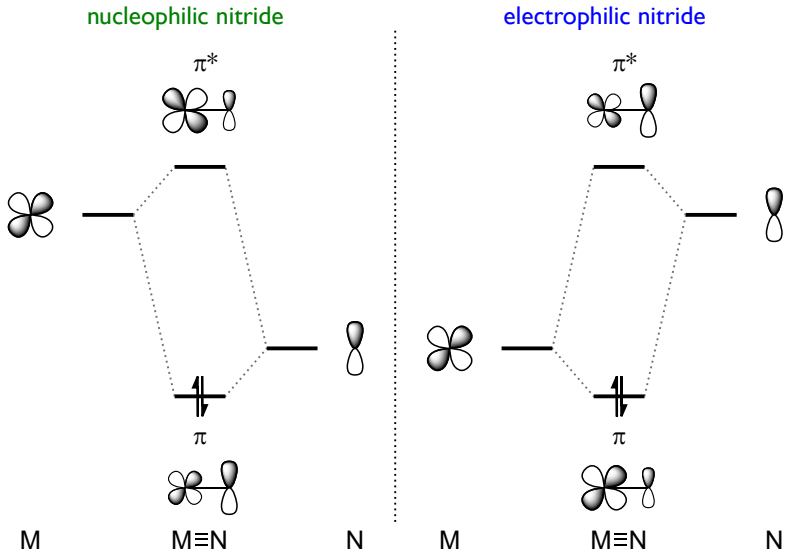

Fig. 4.3. Simplified MO scheme rationalizing the difference between an nucleophilic nitride (*left*) and an electrophilic nitride complex (*right*).

moving to the right along the periodic table should increase the electrophilicity of M≡N complexes. This trend was qualitatively exemplified by means of DFT calculations connected with population analyses on $[M(N)Cl_4]^{2-}$ and [M(N)(salen)] complexes (M = V, Cr, Mn, Fe), which found decreasing negative charges at the nitride ligand upon moving to late transition metals.[143] This bonding picture is of course insufficient to describe all effects influencing a nitride's reactivity like ligand influences, but can give a very simplified explanation for observed trends. A quite instructive example in this regard was published by *Mayer* and coworkers. They reported on the complexes $[Os(N)X_2(Tp)]$ (**XLVI**, Tp = trispyrazolylborate, X = Cl or Ph), of which the chloro complex is electrophilic and reacts with *Grignard* reagents to form N-C bonds and coordinated HNR^- amide ligands after aqueous workup.[144] When reacted with triarylboranes, the chloro complex does undergo electrophilic insertion into the B-C bond and $[Os(N(Ar)BAr_2)Cl_2(Tp)]$ is formed.[145] This is in stark contrast to the second complex, where the chloride ligands are exchanged with phenyl ligands. Reaction of $[Os(N)Ph_2(Tp)]$ with *Grignard* compounds occurs only very slowly and with the borane, a simple *Lewis* adduct rather than the B-C insertion product is formed, indicating a more nucleophilic behavior.[146] DFT calculations on model complexes show the near-degenerate

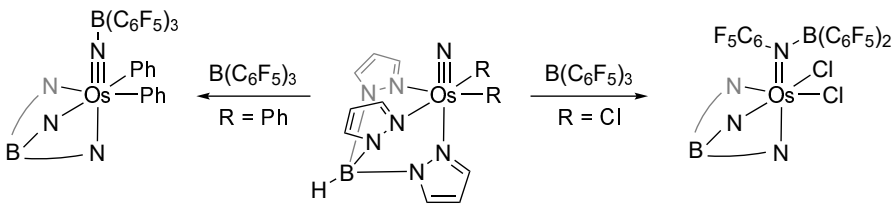

XLVI

Scheme 4.1. Switching between nucleophilic (*left*) and electrophilic (*right*) reactivity of an Os(*vi*) nitride through ligand exchange.

LUMO and LUMO+1 to be the antibonding $M^{\pi^*}N$ orbitals, which are rather low in energy and are significantly N-centered in the chloro complex. Upon exchanging the chlorides with more σ-donating phenyl groups, these orbtials rise in energy, explaining the reduced electrophilicity in the resulting complex.
This example clearly shows on the one hand that especially group 8 transition metal nitrides are just on the border between electrophilic and nucleophilic behavior and on the other, that even subtle changes of the supporting ligand framework can have a substantial influence on the obtained reactivty.

4.2.1 Dinitrogen derived terminal nitrides and functionalization beyond ammonia formation

All terminal nitrido complexes derived from full N_2 bond cleavage are nucleophilic, which is partly due to the overwhelming majority of them being based on early to mid transition metals.[59] Indeed, the only reports of N_2 derived terminal nitrides beyond group 7 are *Kunkeley* and *Vogler*'s $[Os(N)(NH_3)_4]^{3+}$ (**XXVIII**, see Section 3.2.3) and *Peters*' iron complex $[Fe(N)(BP_3^{iPr})]^+$ (see Section 3.1), of which only the former is proposed to be obtained after initial full bond cleavage.[16] Consequently, so far only electrophiles have been employed in functionalization of these complexes, and in most cases, quite strong reactants were needed to obtain any nitride centered reactivity at all.
Interestingly, the most obvious nucleophilic reactivity, i.e. acting as a *Brønsted* base, is hardly observed, with the examples of *Schrock* and *Nishibayashi* being the only so far reported parent imido complexes obtained after N_2 splitting (see Section 3.1 and 3.2.3).[67,114]
In contrast to this, the reaction with other electrophiles is much more common and the ubiquitous example of *Cummins*' Mo nitride **XII** is a good representative for this type of chemistry. Various adducts with *Lewis* acids have been reported, especially with EX_3 (X = F ; E = B / X = Cl ; E = B, Al, Ga, In / X = Br ; E = Al / X = I ; E = Al) and ECl_2 (E = Ge, Sn).[147] However, in these reactions hardly any influence on the Mo≡N bond distance was found and the resulting complexes often decomposed back to the starting materials within 3 h at room temperature (RT). In contrast to this, using MeI, Me_3SiOTf or Ph(CO)OTf resulted in formation of stable imido complexes $[Mo(NR)(N(^tBu)Ar)_3]^X$ (**XLVII**) with a linear Mo=N–E angle (E = C, Si) and a significantly increase Mo=N bond length (**XII**: d(Mo-N) = 1.651(4) Å, $\mathbf{XLVII_{R=SiMe_3}}$: d(Mo-N) = 1.715(6) Å.).[28,147] The methylated complex could be further deprotonated to yield a linear ketimido complex $[Mo(NCH_2)(N(^tBu)Ar)_3]$ (**XLVIII**), with a long Mo=N bond (d(Mo-N) = 1.777(4)Å), ranging between a single and a double bond, and reaction with an additional equivalent of MeI yielded the ethylimdo complex.
In a follow up study, the authors further reported on full conversion of the nitride to a cyanide ligand.[148] Initial reaction with $MeOCH_2Cl$ and $^iPr_3SiOTf$ afforts $[Mo(\equiv N-CH_2OMe)(N(^tBu)Ar)_3]^+$ (**XLIXa**) and deprotonation yielded the imido complex $[Mo(-N=CHOMe)(N(^tBu)Ar)_3]$

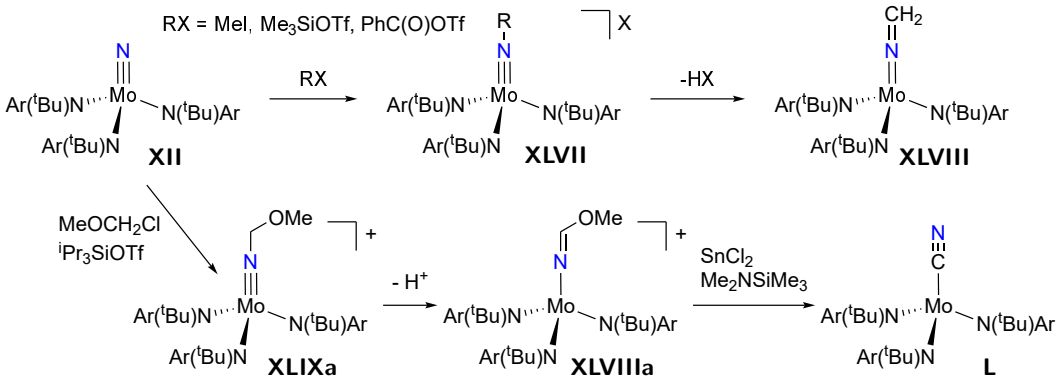

Scheme 4.2. Functionalization schemes of the N_2 derived nitride complex **XII**.

(**XLVIIIa**). Subsequent reaction with $SnCl_2$ and Me_2NSiMe_3 results in formation of the cyanide complex [Mo(CN)(N(^{t}Bu)Ar)$_3$] (**L**). Importantly, this process includes reduction of the Mo(VI) nitrido to an Mo(IV) cyanide complex with the reduction equivalents steming from the ligand C-H bonds rather than an external reduction source, an approach which was later also used by *Schneider* and coworkers (*vide infra*).

The first report of the incorporation of N_2 derived nitrogen into an organic molecule came from *de Vries* and coworkers, who reported the direct release of trifluoroacetamide from reaction of *Cummins*' nitrido complex **XII** with trifluoroacetic acid, accompanied by partial degradation of the amide ligands to an imide, releasing isobutene and protons from one of the *tert*-butyl groups (see Scheme 4.3, *top*).[149]

In 2016, *Mézailles* and coworkers published a paper on splitting of N_2 upon two-electron reduction of [MoCl$_3$(PPP)] (**LI**, PPP = PhP(CH$_2$CH$_2$PCy$_2$)$_2$) into the corresponding nitride complexes, which was proposed to proceed via an unobserved μ-η^1:η^1 N_2 bridged dimer **LII** (in fact, a related dimer, i.e. [(μ-N$_2$){Mo(N$_2$)$_2$(PPP)}] was previously observed and shown to be an active catalyst in the generation of silylamines from N_2) (see Scheme 4.3, *bottom*).[150,151] After successful dinitrogen cleavage into [Mo(N)I(PPP)] (**LIII**) (in the presence of NaI), the obtained nitride could be reacted with substituted silanes to form Mo-H and N-Si bonds. Importantly, the reaction with HSiMe$_2$(CH$_2$CH$_2$)Me$_2$SiH resulted in inital 1,2-addition of one Si-H group to the Mo≡N moiety and heating to 80 °C released the bis(silyl)amine after intramolecular reaction with the second Si-H moiety. The suspected concomitant formation of [Mo(H)I(PPP)] (**LIV**) could not be directly proven, but a PMe$_3$ adduct was isolated from the reaction mixture after addition of the phosphine, proving rereduction of the metal center to Mo(II), with the reduction equivalents originating from the reactant itself rather than from an external electron source. Rather recently, the authors reported a closely related reaction, in which the N_2 derived nitride was functionalized by HBPin to give triborylamine N(BPin)$_3$ in high yields, again accompanied by formation of Mo hydride complexes.[152] Unfortunately, closing the cycle has not been achieved so far in neither of the two reactions.

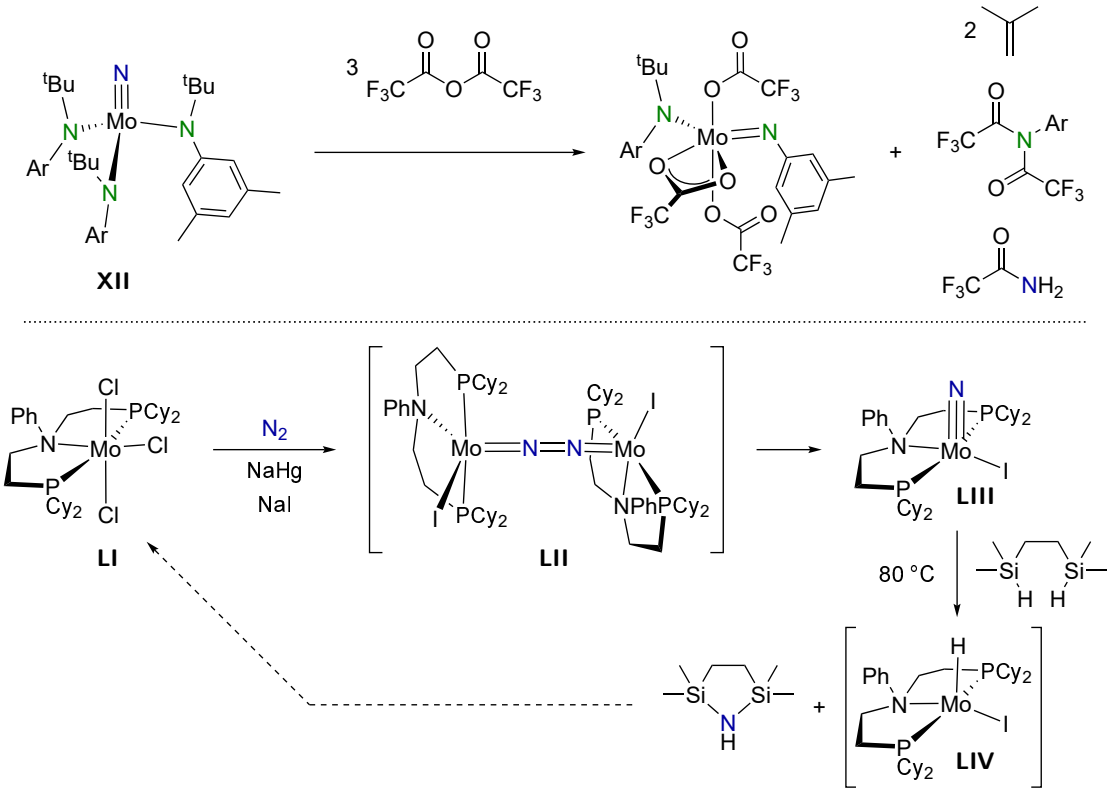

Scheme 4.3. *Top*: Release of an amide from *Cummins*' nitrido complex, accompanied by ligand degradation. *Bottom*: Conversion of a Mo nitride to a bissilylamine with simultaneous rereduction of the metal center.

Cummins went a step further as he not only achieved incorporation of the nitrido ligand into an organic molecule, but at the same time was able to regenerate the starting Mo complex, thus closing a synthetic cycle (see Scheme 4.4). After acylation of the nitride **XII** with *in situ* generated acyl triflates, the obtained imido complexes can be reduced using Mg in the presence of Me_3SiOTf to affort the ketimido complexes $[Mo(N{=}C(R)OSiMe_3)(N(^tBu)Ar)_3]$ (**LV**; R = Ph, ^{t}Bu, Me). Subsequent reaction with $SnCl_2$ or $ZnCl_2$ results in clean formation of the corresponding nitrile compounds R–C≡N and $[MoCl(N(^tBu)Ar)_3]$ (**XV**) of which the later could be cleanly rereduced to the Mo(III) starting complex **XV**. This way, a synthetic cylce for the synthesis of nitrogen containing organic molecules directly from N_2 was realized for the first time, even though it is already apparent that the required reactants (acyl triflates, Mg(0)) are not compatible with each other and thus prevent catalytic turnover.

A slightly different approach was used by the group of *Schneider* and coworkers, who reported the formation of acetonitrile from N_2 in the coordination sphere of a rhenium complex (see Scheme 4.5). The Re(V) nitrido complex $[Re(N)Cl(PNP^{tBu})]$ (**XXI**) obtained from splitting of N_2 (see Section 3.2.1 and Scheme 3.3) was initially reported to undergo nucleophilic N-C bond formation with MeOTf.[94] In a subsequent study, the authors published the ethylation with *in situ* prepared EtOTf yielding $[Re(NEt)Cl(PNP^{tBu}]^{OTf}$ (**LVI**) followed by stepwise deprotonation ultimately leading to the release of acetonitrile.[153] Initial deprotonation yields

the ketimido complex [Re(N=CHMe)Cl(PNP^{tBu})] (**LVII**), in which bond distances and angle (d(Re-N) = 1.822(4) Å, d(N=C) = 1.273(7) Å, ∡(Re=N=C) = 174.3(5)°) suggest a pronounced heterocummulene character. A second deprotonation in the presence of 2 equivalents of CN^{t}Bu resulted in almost quantitative release of acetonitrile accompanied by the formation of [Re(CN^{t}Bu)$_2$(PNP^{tBu})] (**LVIII**), a formal Re(I) complex. This is remarkable in that respect that the reduction equivalents necessary for this Re(V) → Re(I) conversion are obtained from the C-H bonds (2 e$^-$ each) of the ethyl group rather than from an external reductant. Alternatively, external oxidants can be utilized to circumvent the need of π-accepting ligands to stabilize the Re(I) species. Using a combination of Ag^+ and 2,4,6-tris-*tert*-butylphenoxy radical (TTBP) to formally remove 2 e$^-$/H$^+$ from **LVIII** results in the vinylimide complex [Re(NCHCH$_2$)Cl(PNP^{tBu})]$^+$ (**LIX**), which is a tautomer of the corresponding acetonitrile complex. Addition of a chloride source could trigger acetonitrile release and reformation of starting complex **XIX**. Alternatively, direct conversion of **LVII** could be achieved with *N*-chlorosuccinimide (NCS). To test, whether this latter, one-step conversion necessarily proceeds via the vinyl imido tautomer, the reaction was also performed after benzylation.[154] The benzyl imido analog to **LVII**, which is inherently *unable* to undergo such a tautomerization gives similar yields of benzonitrile upon reaction with NCS, rendering this not a prerequisit for the observed reactivity.

Interestingly, in a very recent study, **XXI** was oxidized at the ligand backbone with 3-chloroperbenzoic acid and subsequently at the metal center to form the nitroxide Re(VI)

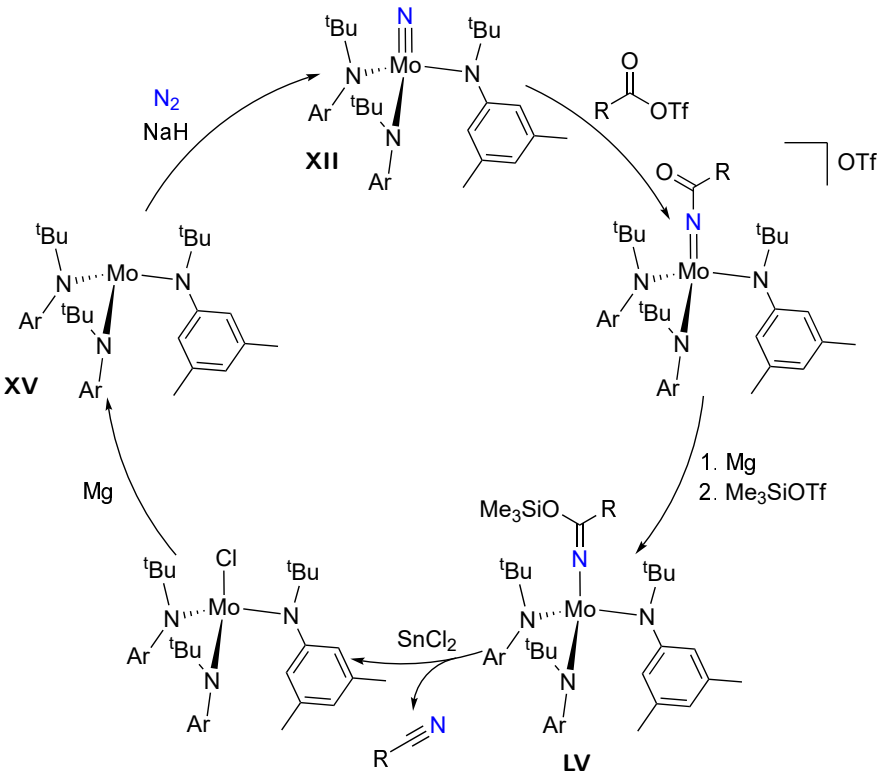

Scheme 4.4. Synthetic cylce for the conversion of dinitrogen into nitriles developed by *Cummins* and coworkers.

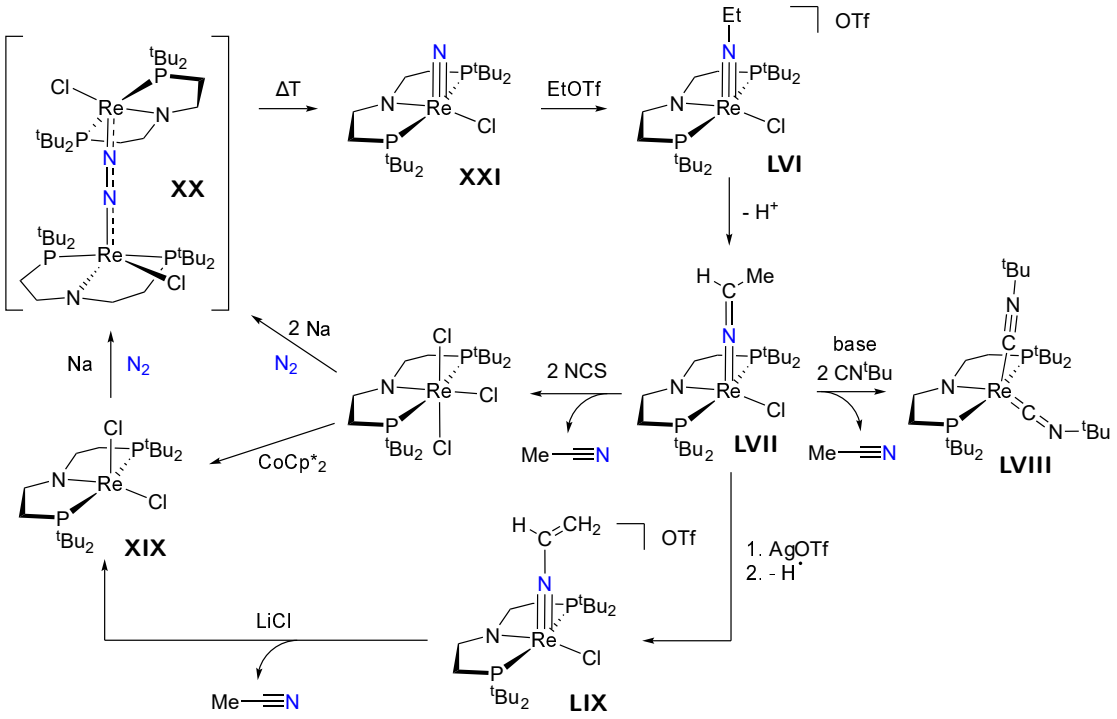

Scheme 4.5. Synthetic cycle for acetonitrile formation from N_2 as employed by *Schneider* and coworkers.

complex $[ReNCl(P^{O}NP^{tBu})]^{PF6}$.[155] These oxidations now lead to an *umpolung* of the nitride reactivity, which does form (unstable) phosphoraneiminato complexes with various phosphines, rendering it electrophilic.

The probably most efficient synthetic cycle for N_2 functionalization to organic molecules was reported by *Sita* and coworkers (see Scheme 4.6). The Mo and W end-on bound dimeric complexes $\mathbf{XXXIII_{Mo}}^{\mathbf{iPr}}$ (M = Mo, W) were already discussed for their ability to undergo photochemical N_2 cleavage (see Section 3.2.3). By reducing the steric strain of the ligand (replacing the *iso*-propyl groups with ethyl groups) the authors were able to switch from a photochemical to a thermal splitting pathway.[156] Again, bis-μ-nitrido bridged complexes are obtained and the Mo congener is shown to react with Me_3SiCl to form the silylimido complexes $[M(=NSiMe_3)(Cp^*)(am)]$ ($\mathbf{LX_{Mo}}^{\mathbf{Et}}$) and the starting complex $\mathbf{LXI_{Mo}}^{\mathbf{Et}}$. In a later study, the imido complex was reported to undergo further reaction with alcohols and Me_3SiCl and forms $\mathbf{LXI_{Mo}}^{\mathbf{Et}}$, $HN(SiMe_3)_2$ and $ROSiMe_3$, thus closing the synthetic cycle upon release of disilylamine.[157] It is exciting to note that the used chemicals (i.e. Me_3SiCl and ROH) are chemically compatible with the complexes $\mathbf{LXI_{Mo}}^{\mathbf{Et}}$ and $\mathbf{XXXIII_{Mo}}^{\mathbf{Et}}$. A system allowing for turnover therefore seems to depend only on finding a suitable reductant.

From the above discussed examples of synthetic cycles for N_2 functionalization, some important aspects and strategies can be derived:
An inherent problem of transition metal complexes which are capable of splitting the N≡N triple bond is their tendency to form very strong M≡N triple bonds in the corresponding

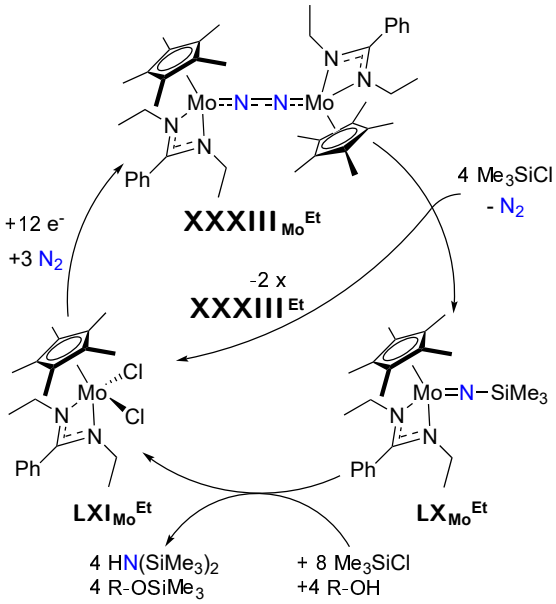

Scheme 4.6. Synthetic cycle for bis-silylamine generation from a Mo(Cp*)(am) complex developed by *Sita*.

nitrides, which drives the reaction in the first place. This problem was accurately expressed by *Fryzuk* and *Shaver*: 'The problem with developing a viable process coupling nitride formation with the production of useful nitrogen-containing materials is the inherent stability of the metal nitrides generated. Reactions of nitrides employ harsh reagents to effect moderate changes.'[158]

This stability can in principle be met by two strategies. One the one hand, forming products with strong N-X bonds, like nitriles containing a N≡C triple bond can account at least partially for the energy-demand of cleaving the strong M≡N triple bond and can thus facilitate the incorporation of dinitrogen into organic products. On the other hand, it seems desirable to find transition metal complexes which do undergo N≡N bond cleavage but result in less stabilized compounds which are therefore more easily functionalized. As will be shown in the next section, especially nitrido complexes of late transition metals are often very reactive and do undergo quite rich transformations. Developing compounds based on these metals for N_2 fixation therefore seems a promising approach.

4.2.2 Low valent nitrido complexes from other nitrogen sources

As discussed in Section 4.2, most early to mid transition metal complexes exhibit nucleophilic reactivity at the nitride. This behavior changes quite significantly for the nitrido complexes formed by late transition metals (i.e. group 8 or 9). Unfortunately, these compounds are so far not available by direct activation of dinitrogen but rather from other sources (mostly by decomposition of azides). Nevertheless, their reactivity is versatile.

The only reported Fe(VI) nitrido complex prepared by *Wieghardt* is only stable at 77 K and yields an Fe(III) species upon warming, so no defined reactivity is known for this complex.[130]

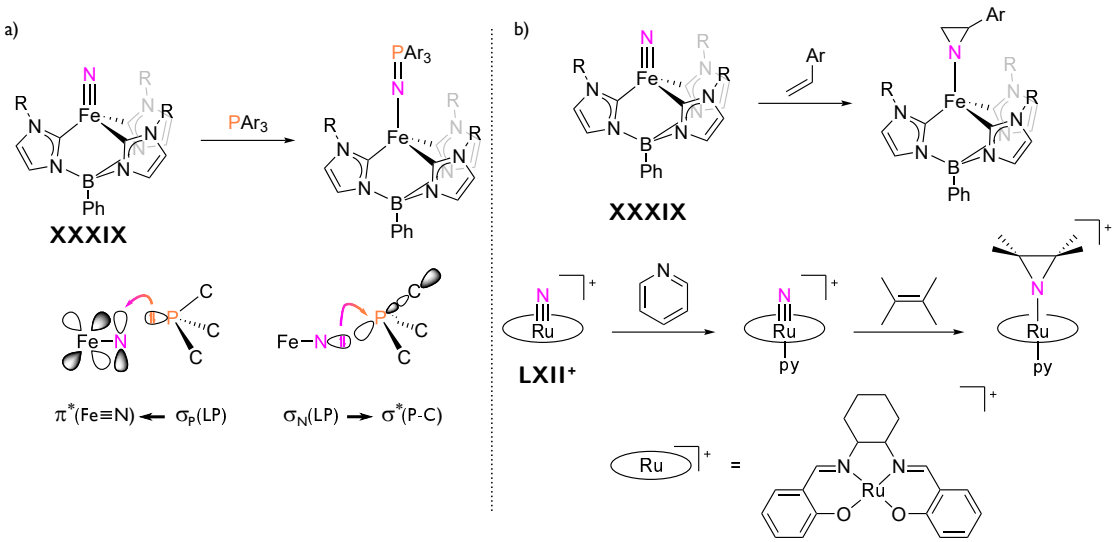

Scheme 4.7. *a*) Reaction of **XXXIX** with PAr_3 determined by two mutual donor-acceptor interactions. *b*) Alkene aziridination mediated by **XXXIX** (*top*) and **LXII** (*bottom*).

This is different in the case of tetrahedral Fe(IV) nitrido complexes. The complexes presented in Section 4.1 are described as being rather electrophilic. In particular, *Peters* as well as *Smith* reported their complexes **XXXVIII** and **XXXIX** to undergo electrophilic coupling with phosphines to phosphoraneiminato ligands.[131,133] However, this reaction, which is often reported to be archtypical for an electrophilic nitride was later investigated in detail by *Smith* and coworkers. By following the kinetics of the reaction with substituted triphenylphosphines, a *Hammett* analysis revealed the counter intuitive trend that electron-poorer phosphines do react *faster* than electron richer congeners.[159] This could be explained by DFT calculations which revealed a dual nature of the reaction transition state in which on the one hand the phosphine centered lone pair donates electron density into the $Fe^{\pi^*}N$ orbital, but on the other hand, the nitride centered lone pair donates also into a $P^{\sigma^*}C$ bond of the phosphine (see Scheme 4.7 *a*). This ambiphilicity was also proposed to be important for the reported N-C bond formation with CO and CN^tBu.[160] Furthermore, reaction with 1-hydroxyl-2,2,6,6-tetramethylpiperidine (TEMPOH) was reported to yield ammonia and the Fe(II) complex [Fe(tempo)(PhB(MesIm)$_3$)].

In a rather recent work, *Smith* and coworkers further reported their iron complex to be potent of alkene aziridination.[161] Reaction of **XXXIX** with various styrenes results in equilibrium mixtures of the nitride and the Fe(II) aziridino complexes and combined theoretical and mechanistical investigations pointed towards an asynchronous radical addition as the most likely pathway (see Scheme 4.7 *b, top*).[162]

The only other example of direct alkene aziridination by a terminal nitride stems from an Ru(VI) salen complex, i.e. $[Ru(N)(salchda)]^{PF_6}$ (**LXII**, salchda = *N,N'*-bis(salicylidene)-*o*-cyclohexyldiamine dianion) reported by *Lau* and coworkers (see Scheme 4.7 *b, bottom*).[163] Aziridination of alkenes only takes place in the presence of pyridine or 1-methylimidazole and kinetic measurements indicated coordination of the base to the Ru to be the initial step of

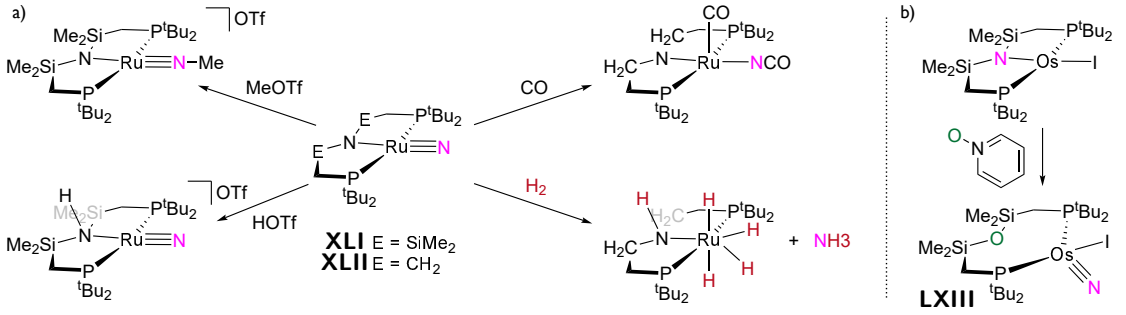

Scheme 4.8. *a*) Nucleophilic Ru(IV) nitrido complexes **XLI** and **XLII**. *b*) Synthesis of the only literature known Os(IV) nitrido complex **LXIII**.

the reaction. This example shows quite clearly how the variation of a *trans* ligand can alter the reactivity of a nitride. In comparison, Os(VI) nitrido complex *cis*-$[Os(N)Cl_2(terpy)]^+$ has been reported to insert into the C=C bond of stilbene, yielding η^2 coordinated azaallenium complexes.[164,165]

In line with this example ruthenium(VI) nitrido complexes are in general electrophilic.[15,121,125] This changes quite drastically with change of the oxidation states. The two Ru(IV) complexes reported by *Caulton* and *Schneider*, i.e. **XLI** and **XLII**, both show defined nucleophilic reactivity (see Scheme 4.8 *a*). Reaction of **XLI** with HOTf and MeOTf is proposed to yield $[Ru(N)(HPNP^{tBu}_{Si})]^{OTf}$ and $[Ru(NMe)(PNP^{tBu}_{Si})]^{OTf}$, respectively, based on 1D-nuclear magnetic resonance (NMR) data and hints from an unrefined X-ray diffraction study.[166] Furthermore, reaction with two equivalents of NO resulted in the formation of $[Ru(NO)(PNP^{tBu}_{Si})]$ and N_2O, where the former nitride is transferred to N_2O, as indicated by ^{15}N labeling.[167] *Schneider*'s related complex **XLII** does undergo N-C coupling with CO to yield $[Ru(NCO)(CO)(PNP^{tBu})]$, which is indicated by preliminary computational results to result from a direct electrophilic attack of CO at the nitride (see Scheme 4.8 *a*).[138] Importantly, the complex is also reactive towards H_2 and does undergo full hydrogenolysis to give ammonia in 80 % yield and $[Ru(H)_4(HPNP^{tBu})]$, the latter of which could be reconverted into the starting complex $[RuCl_2(HPNP^{tBu})]$ by application of vacuum, addition of HCl and a second evacuation. The mechanism of the hydrogenation reaction was investigated quite thoroughly by computational calculations and the minimum energy pathway revealed metal-ligand cooperative heterolytic H_2 splitting over the $Ru{-}N_{backbone}$ bond to be a key step in this reaction.

The sole low-valent osmium nitrido complex ever reported is *Caulton*'s Os(IV) complex $[Os(N)I(POP^{tBu}_{Si})]$ (**LXIII**, $POP^{tBu}_{Si} = O(SiMe_2CH_2P^tBu_2)_2$) which was obtained rather coincidental by reaction of $[OsI(PNP^{tBu}_{Si})]$ with pyridine-*N*-oxide (see Scheme 4.8 *b*).[168] N/O exchange at the oxophilic position in the ligand backbone resulted in formation of this distorted tetrahedrally coordinated complex ($\tau_4' = 0.674$;[1] $d(Os\cdots O) = 3.14$ Å, thus the ligand oxygen is not bound). However, no follow-up reactivity of this complex is reported.

[1] Calculated according to Ref [169] and the structure data deposited at The Cambridge Crystallographic Data Center, CCDC-778422.

The above described reaction of a nitrido ligand with H_2 is very rare. Among the only other reports is *Burger*'s complex **XLV**, one of the few examples of isolated group 9 nitrido complexes, which reacts with H_2 to yield [Ir(NH_2)(PDI)] (or analogously with R_3SiH to give the Ir–N(SiR_3)H product).[139,170,171] Despite this reaction, the complex exhibits electrophilic reactivity, as indicated by the formation of an NO ligand with Me_3NO as single electron donor. Thermolysis of the complex for extended time resulted in intramolecular C–H activation, whereas attempts to isolate the rhodium congener of the complex (**LXIV**) always resulted in a twofold ligand activation (see Scheme 4.9 *a*).[172] While no final explanation for this difference could be provided, the authors suggested **XLV** to directly insert into the C–H bond, while the Rh complex might first abstract an H atom, generating a biradical, which can then rearrange so that the second *iso*-propyl group can be activated as well.
Similarly, the group of *Schneider* reported on the synthesis of Ir (**XLIV$^{0/+}$**) and Rh (**XLIII**) nitrido species (see Scheme 4.9 *b*).[140,141] The d^4 complex **XLIV$^+$** is thermally stable and can be isolated. It is reported to react with Me_3NO to yield the corresponding nitrosyl complex $[Ir(NO)(P{=}N{=}P^{tBu})]^+$, hence it is electrophilic as well.[140] However, the neutral, formal d^5 complex **XLIV** can only be characterized at low temperatures in frozen toluene. The complex exhibits a singly occupied molecular orbital (SOMO) and spin density which resemble the Ir^{π^*}–N orbital, with almost equal spin populations on the metal and the nitrido complex. Upon warming, the complex is shown to undergo N–N coupling to form a dimeric, μ-$\eta^1{:}\eta^1$ N_2 bridged complex **LXV**, a reaction which is the microscopic reverse of the above discussed N_2 splitting reactions. In a follow-up study, the authors further prepared the mono and dicationic dimers $[(\mu\text{-}N_2)\{Ir(P{=}N{=}P^{tBu})\}_2]^{+/2+}$ (**LXV^{n+}**, n = 1-2), which were shown to be thermally stable as well.[173] DFT calculations revealed the cationic complex **XLIV$^+$** to be stabilized only kinetically and coupling to **LXV^{2+}** should in theory be downhill for this complex as well. Considering the isolobal relation between square-planar d^n and octahedral d^{n-2} compounds and thus the formal 10π electronic configuration of the {MNNM} core of of **LXV^{2+}**, this example clearly shows the limitations of the MO considerations regarding the prerequisites for N_2 cleavage made in Section 3.2.1. The low stability of late transition metal nitrides can render splitting unfeasible, even though the formally required electronic configuration is provided. Similar behavior is also observed for the Rh congener, however

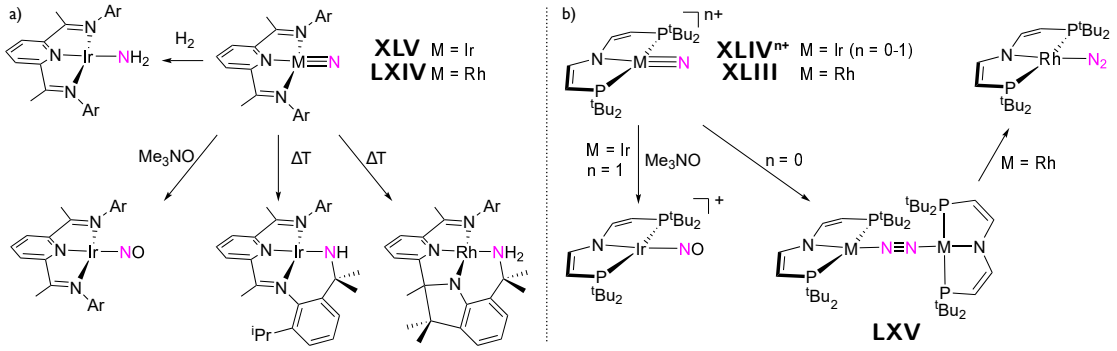

Scheme 4.9. Electrophilic group 9 transition metal nitrido complexes reported by *Burger* (*a*) and *Schneider* (*b*).

here no nitride could be isolated and the coupled dimer even reacts further with atmospheric N_2 (from azide decomposition) to form $[Rh(N_2)(P{=}N{=}P^{tBu})]$.[141]

5 Scope of this work

Terminal nitrides have been shown to undergo various nitrogen functionalization reactions, leading to a large zoo of available N-E bond formation schemes as well as the possibility to incorporate metal bound nitrides into organic molecules. Especially low-valent nitrides of late transition metal complexes were proven to exhibit remarkable reactivity, often even towards comparably unactivated substrates.
With the advent of full dinitrogen bond cleavage by transition metal complexes into terminal nitrides, these reactions become a promising toolbox to directly utilize N_2 for N-functionalization of relevant molecules, ultimately omitting the generation of ammonia in the *Haber-Bosch* process. However, the currently available systems suffer from the formation of extremely strong M≡N bonds, hampering N-centered reactivity.

This thesis falls within the intersection of both areas of research:

- Supported by a PNP pincer ligand, the previously synthesized, unprecedented **square-planar Os(IV) nitrido complex** [Os(N)(PNP^{tBu})] (**3**) is investigated in terms of reactivity. As group 8 transition metal nitrides have previously been reported to exhibit reactivity just on the borderline between **electrophilicity** and **nucleophilicity**, distinguishing these two principal reactivities will be emphasized.

- Due to their increased reactivity with respect to early transition metal nitrides, Os≡N compounds derived from N_2 are promising yet elusive candidates for dinitrogen functionalization. By molecular orbital considerations, d^2 and d^4 compounds can be imagined as possible splitting products and thus **Os(VI) nitrido complexes related to 3** will be prepared. The prospects of **accessing these target molecules by N_2 cleavage** will be evaluated. Especially, reaction conditions aiming for a formal 10π electron count in the $\{$MNNM$\}$ core of a potential dimeric intermediate will be tested.

- The previously reported dinitrogen splitting by Re complex [ReCl$_2$(PNP^{tBu})] (**XXI**) will be explored further in terms of the actual splitting reaction as well **follow-up functionalization** of the obtained nitride. In particular, observing and identifying potential **intermediates of the N_2 splitting** reaction of the original system will be attempted in order to gain further insight into the process and to provide experimental evidence for the theoretical predictions made in the original paper about the nature of the intermediary μ-N_2 bridged dimer.

- In light of the oxidative conditions needed for acetonitrile release in this Re system, the pincer ligand will be modified to meet these conditions. Established procedures for **ligand backbone oxidation to the vinylamido based P=N=P pincer** will be employed and the resulting complex will be tested towards N_2 activation and functionalization.

- The prevalent problem of nitride overstabilization after N_2 splitting will be addressed. Theoretical results indicate reduction of the steric bulk of the pincer ligand to be a promising approach to obtaining a more reactive nitride. Therefore, a **Re(III) platform with the *iso*-propyl substituted PNP pincer ligand** will be synthesized from which the ability of this complex in **N_2 coordination, activation and functionalization** will be investigated in an attempt to optimize the previously developed synthetic cycle and approaching real, catalytic turnover.

Part II

Results and Discussion

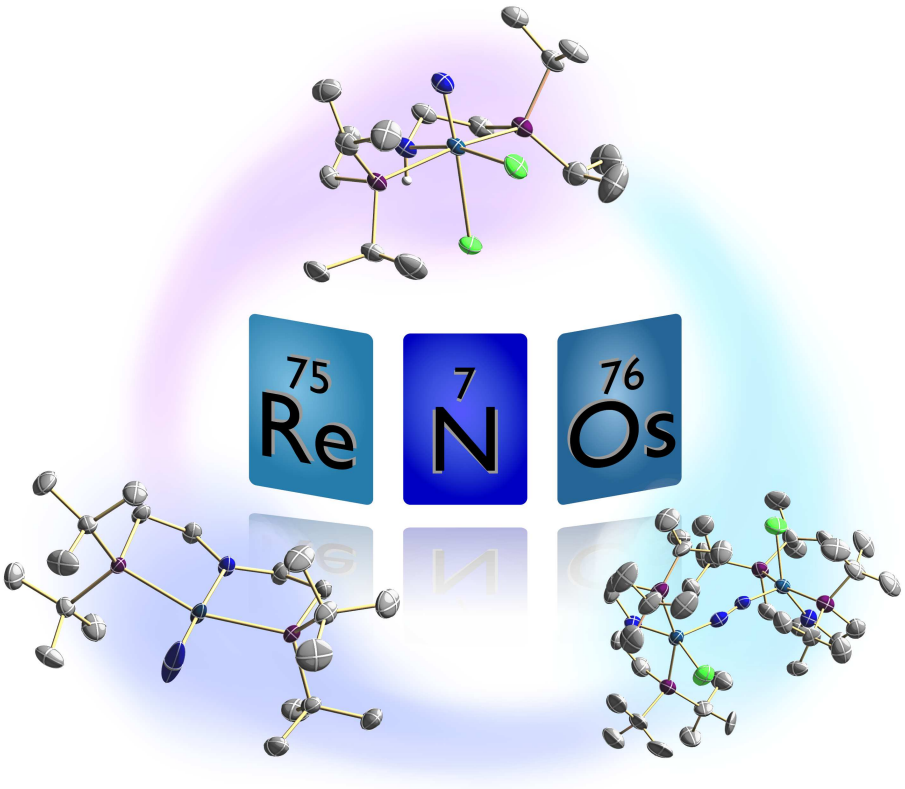

1

Low valent osmium nitride complexes with a PNP pincer ligand

> *You build me up, you break me down*
> *Until I'm falling to pieces.*
> *The price I pay to live this way,*
> *And the fantasy stays alive.*
>
> — **Dream Theater**
> "Build Me Up, Break Me Down" on "A Dramatic Turn of Events"

Parts of this chapter (especially Section 1.1 as well as 1.2) have been published in: F. Schendzielorz, M. Finger, C. Volkmann, C. Würtele, S. Schneider, "A Terminal Osmium(IV) Nitride: Ammonia Formation and Ambiphilic Reactivity", *Angew. Chem. Int. Ed.* **2016**, *55*, 11417-11420.

The successful synthesis of low-valent nitride complexes of late transition metals and their interesting and sometimes unprecedented reactivity motivated the attempt to get access to the first osmium complex in this group (compare Part I Section 4.2.2).

The synthesis and characterization of the first square-planar Os(IV) nitrido complex [OsN(PNP$^{t\mathrm{Bu}}$)] (**3**) was already established in the master's thesis of *Florian Schendzielorz* and is summarized and extended in Section 1.1, including a synthetic route to the analytically pure complex as well as improved understanding of the involved species.

The unexplored reactivity of this unique compound is investigated in Section 1.2, with the main emphasis on the distinction of **3** being rather nucleophilic or electrophilic. Nitride centered nucleophilic reactivity towards classic *Lewis* acids as well as a reaction with ambiphilic PMe_3 are found and theoretical investigation of the latter lead to the description of **3** as an ambiphile. Additionally, it is shown that hydrogenolysis leads to full cleavage of the Os≡N bond and concomitant formation of ammonia.

An exploration of the redox chemistry of **3** and related compounds is presented in Section 1.3. Attempts to access a hypothetical Os(V) nitride by oxidation of the Os(IV) complex or by reduction of corresponding Os(VI) nitrides were not successful, pointing to an inherent instability of the target molecule.

Finally, Section 1.4 summarizes the largely unsuccessful efforts to bind, activate or even split dinitrogen in the coordination sphere of the previously developed platform. Two stable Os(II) complexes evolve from this investigation, one of which at least bears an N_2 ligand.

1.1 A square planar osmium(IV) nitride complex

Large parts of the synthesis and characterization of the square planar osmium(IV) nitrido complex **3** have already been reported in the master's thesis of *Florian Schendzielorz* and will therefore be described only briefly.[174] The synthesis starts with initial formation of an unidentified complex from $HPNP^{tBu}$ and $OsCl_2(PPh_3)_3$, which converts over time to the Os(IV) complex $[OsHCl_2(PNP^{tBu})]$ (**1**) by net oxidative addition of the pincer NH moiety to the Os center. Reaction of **1** with NaN_3 leads to formation of an intermediate hydride complex, which was proposed to be $[OsHClN(PNP^{tBu})]$ ($\mathbf{2}_{old}$) in the thesis. *In situ* deprotonation with potassium *tert*-butoxide (KO^tBu) yields the square planar Os(IV) complex $[Os(N)(PNP^{tBu})]$ (**3**) (see Scheme 1.1).

Subsequent investigations revealed the proposal of $\mathbf{2}_{old}$ being an uncharged complex to be rather unlikely. Based on DFT calculations, it was assumed that after chloride dissociation the coordination site *trans* to the hydride is vacant and consequently the nitride also resides in this position in $\mathbf{2}_{old}$. However, performing the synthesis of **2** in the presence of KPF_6 gave identical NMR signatures, even though PF_6^- clearly served as a counteranion according to the NMR data. Hence, the complex is most likely cationic, i.e. $[Os(N)(H)(PNP^{tBu})]^{Cl}$ ($\mathbf{2}^{Cl}$) or $[Os(H)(N)(PNP^{tBu})]^{PF6}$ ($\mathbf{2}^{PF_6}$), depending on whether KPF_6 is added during the synthesis or not. The use of the PF_6^- salt also allowed for isolation of analytically pure $\mathbf{2}^{PF_6}$, as well as the synthesis of analytically pure **3** by deprotonation with KO^tBu, both of which was not possible previously due to partial complex decomposition. Complex $\mathbf{2}^+$ features a well isolated Os–H stretching vibration in the IR spectrum at $\tilde{\nu}_{\nu(Os-H)} = 2056\,cm^{-1}$, which is significantly shifted to lower wavenumbers compared to **1** (**1**: $\tilde{\nu}_{\nu(Os-H)} = 2216\,cm^{-1}$). Unfortunately, no single crystals suitable for X-ray diffraction measurements could be obtained.

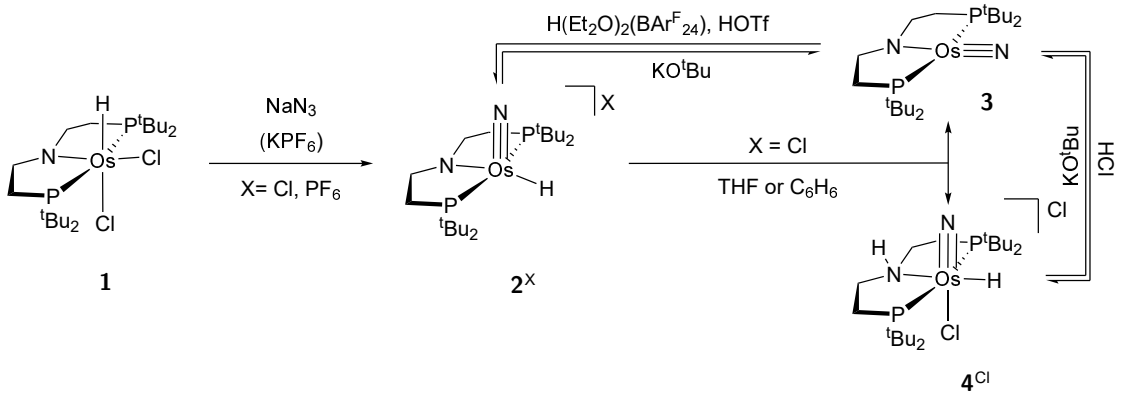

Scheme 1.1. Revised scheme for the synthesis of **3**. If KPF_6 is added to the reaction of **1** with NaN_3, $\mathbf{2}^{PF_6}$ is formed, otherwise $\mathbf{2}^{Cl}$ is obtained.

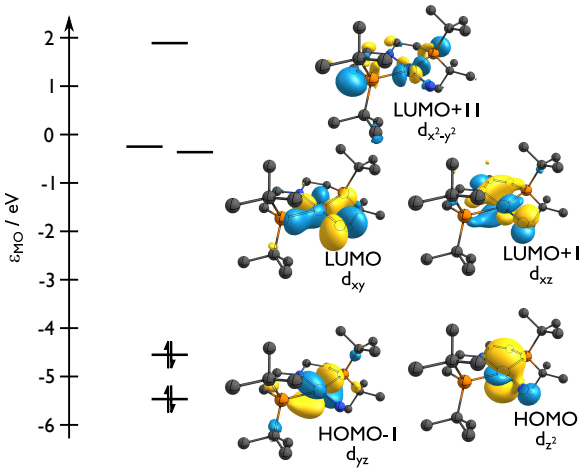

Fig. 1.1. FMO scheme of **3** reproducing the qualitative scheme in Part I Figure 4.1.

It is noteworthy that $\mathbf{2}^{+}$ is the first reported osmium complex bearing a hydride as well as a nitride at the same metal center. Such a species might be of interest as a possible intermediate in the hydrogenolysis under basic conditions of an Os(VI) nitrido complex (HBPB)Os(N)Cl_2 (HBPB$^-$ = 2,6-bis(benzimidazolyl)pyridine) with H_2 in presence of KOH_{aq} reported by *Hashiguchi* and coworkers.[175]

Additionally, the instability of $\mathbf{2}^{\mathbf{Cl}}$ and the product(s) formed from it have to be revised. While a dichloromethane (DCM) solution of $\mathbf{2}^{\mathbf{Cl}}$ was stable for at least some days, the observation was made that in benzene or tetrahydrofurane (THF), spontaneous decomposition into the square planar nitride **3** and one additional species **4** takes place, of which the latter can be converted into **3** by addition of base. This process (i.e. $\mathbf{2}^{\mathbf{Cl}} \rightarrow \mathbf{3} + \mathbf{4}$) can also be induced in DCM by irradiation with a Hg(Xe) arc lamp equipped with a long wave pass filter for $\lambda > 305$ nm and the formation of **4** was assigned to an isomerization of $\mathbf{2}_{old}$ in the original thesis. However, the suggested structure of that isomer was just as unlikely as the initial proposal for **2** itself. Instead, it was found that the full reprotonation of **3** with HCl in THF leads to formation of **4** and requires addition of 2 equivalents (eqs) for full conversion, pointing to the reaction of **2** being a dissociation of $\mathbf{2}^{\mathbf{Cl}}$ rather than an isomerization. ^{1}H NMR data revealed signals corresponding to an NH proton ($\delta_{^1H} = 6.35$ ppm) as well as an osmium hydride ($\delta_{^1H} = -2.52$ ppm). These two signals, the formation by disproportionation of $\mathbf{2}^{\mathbf{Cl}}$ and the low solubility of the compound it benzene or even THF all point towards it being [OsH(N)Cl(HPNP$^{t\mathrm{Bu}}$)]^{Cl} ($\mathbf{4}^{\mathbf{Cl}}$).
If acids with non-coordinating anions like $H(Et_2O)_2(BAr^F_{24})$ (BAr^F_{24} = tetrakis{3,5-(trifluoromethyl)phenyl}borate) or HOTf are used for protonation of **3**, $\mathbf{2}^{\mathbf{X}}$ (X = BAr^F_{24}, OTf) is reobtained. This is in contrast to the protonation of the related ruthenium complex [Ru(N)($PNP^{t\mathrm{Bu}}_{Si}$)] (see Part I Section 4.2.2)[138] which is protonated at the pincer amide and thus reflects the higher metal basicity of osmium *versus* (vs.) ruthenium. This matches the proposed FMO scheme derived from the *Gray-Ballhausen* scheme (see Part I Section 4.1), which predicts the d_{z^2} orbital to be the HOMO and thus the most basic side in the

complex. Indeed, inspecting the FMOs of a DFT derived model,[1] the expected d-orbital splitting is reproduced accordingly (see Figure 1.1).

1.2 Functionalization of square planar osmium(IV) nitride **3**

[Os(N)(PNP$^{t\text{Bu}}$)] (**3**) represents the first reported square planar Os(IV) nitride complex and the second Os(IV) nitride at all. The only other example published by *Caulton* and coworkers is tetrahedrally coordinated [Os(N)I(PNP$^{t\text{Bu}}_{\text{Si}}$)] (**LXIII**, see Part I Section 4.2.2) was obtained rather coincidentally and no further studies of this product were performed. Consequently, the general reactivity of complex **LXIII** and especially its behavior towards nucleophilic and electrophilic reagents was of fundamental interest.

Protonation of the metal to form **2**$^+$ already identified the most nucleophilic side of the complex (see Section 1.1). When the steric bulk of the used *Lewis* acid is increased, the steric bulk of the pincer ligand prevents reactions at the metal center and the nitride becomes the reactive side as examplified by the reaction with tris-{3,5-(trifluoromethyl)phenyl}borane (BAr$^{\text{F}}_{18}$) or Me_3SiBr (see Figure 1.2). Mixing **3** with BAr$^{\text{F}}_{18}$ led to an immediate color change to yellow and clean conversion to [Os(NBAr$^{\text{F}}_{18}$)(PNP$^{t\text{Bu}}$)] (**5**). A single resonance in the ^{31}P{^{1}H} NMR spectrum at $\delta_{^{31}\text{P}} = 98.2$ ppm and retained C_{2v} symmetry according to the ^{1}H NMR spectrum provided good evidence for the successful and clean formation of **5**. Single crystals grown from benzene allowed for the determination of the molecular structure by X-ray diffraction measurements and confirmed the connectivity as a nitride-borane adduct. The osmium center is coordinated in a square planar geometry ($\tau_4' = 0.06$)[169] The Os≡N bond is significantly elongated with respect to parent **3** (**5**: d(Os1-N2) = 1.7257(17) Å; **3**: d(Os1-N2) = 1.683(2) Å), while the bond to the ligand amide is shortened (**5**: d(Os1-N1) = 1.9958(18) Å; **3**: d(Os1-N1) = 2.0573(17) Å), reflecting the reduced *trans* influence. The rather linear coordination of the nitride ($\measuredangle$(Os1-N2-B1) = 167.77(15)°) points to a retention of a significant triple bond character of the Os≡N bond.

Analogously, **3** can also be reacted with Me_3SiOTf or Me_3SiBr, whereas $SiMe_3Cl$ did not lead to any reaction. While both former reagents initially gave the same product, slow decomposition was observed over time. However, starting with a solution of **3** and Na(BAr$^{\text{F}}_{24}$), slow addition of Me_3SiBr gave clean and persistent formation of analytically pure [Os(NSiMe$_3$)(PNP$^{t\text{Bu}}$)]$^{\text{BAr}^{\text{F}}_{24}}$ (**6**$^{\mathbf{BAr^F_{24}}}$). Similar to **5**, **6**$^{\mathbf{BAr^F_{24}}}$ exhibits C_{2v} symmetry on the NMR timescale, as indicated by a single resonance for the *tert*-butyl groups in the ^{1}H NMR spectrum at $\delta_{^1\text{H}} = 1.55$ ppm as well as a singlet in ^{31}P{^{1}H} NMR spectrum at $\delta_{^{31}\text{P}} = 106.9$ ppm. Nitride centered reactivity and a resulting square planar coordination geometry is confirmed by ^{1}H nuclear *Overhauser* effect spectroscopy (NOESY) giving cross peaks in the resulting spectrum between the Me_3Si and the *tert*-butyl groups, as well as by the molecular structure

[1] PBE0/D3BJ/RIJCOSX/def2-TZVPP

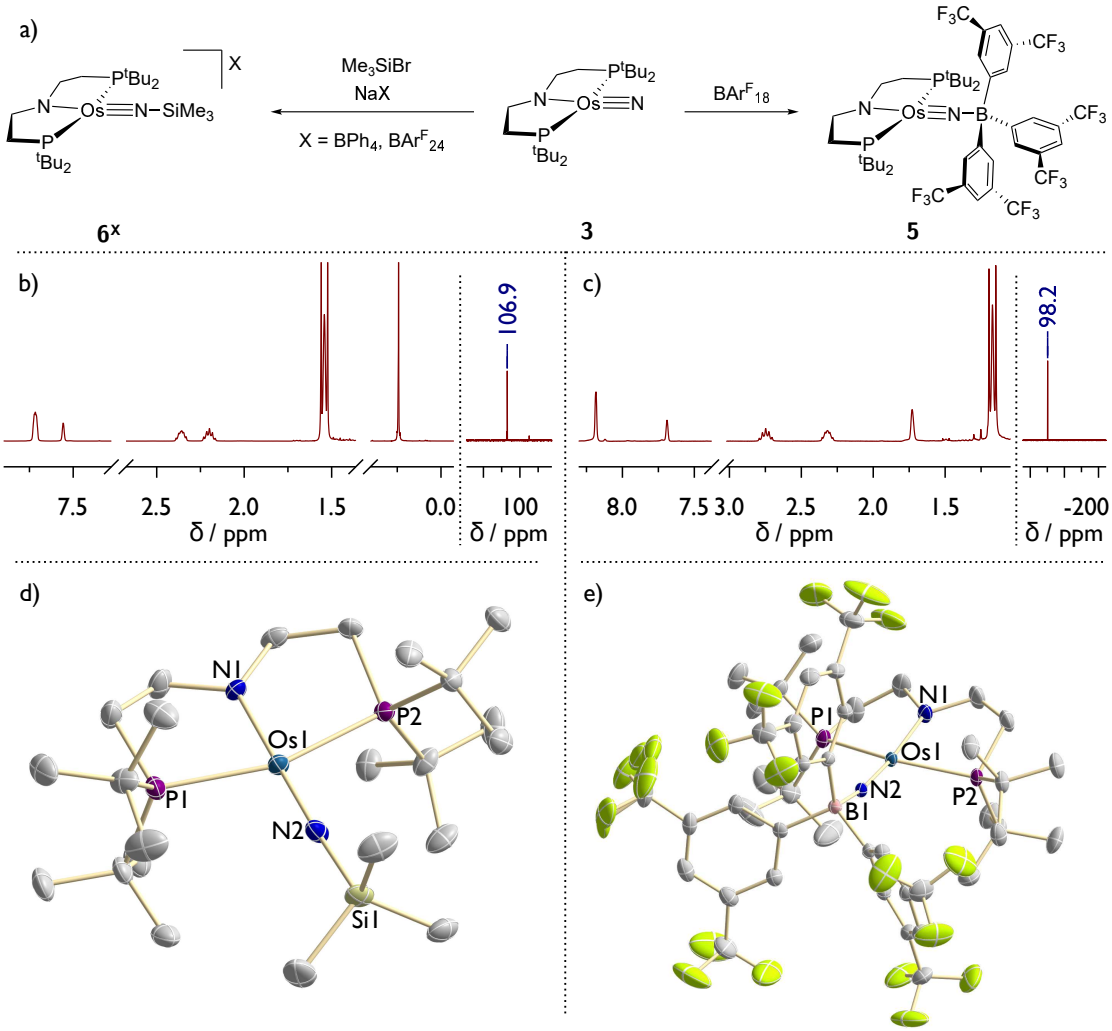

Fig. 1.2. *a*) Synthesis of **5** (*right*) and $\mathbf{6^X}$ (*left*) from **3**. *Middle*: ^{1}H (*left*) and ^{31}P$\{^{1}$H$\}$ (*right*) NMR spectra of $\mathbf{6^{BAr^F_{24}}}$ (*b*) and **5** (*c*). *Bottom*: Molecular structure of $\mathbf{6^{BAr^F_{24}}}$ (*d*) and **5** (*e*) obtained by single crystal X-ray diffraction measurements. All H atoms, the anion and a cocrystallized DCM molecule in $\mathbf{6^{BAr^F_{24}}}$ are omitted for clarity. Anisotropic displacement parameters are set to 50 % probability. Selected bond lengths [Å] and angles [°]: $\mathbf{6^{BAr^F_{24}}}$: Os1-N1 1.988(3), Os1-N2 1.733(4), N2-Si1 1.797(4), P1-Os1-P2 160.80(4), N1-Os1-N2 177.78(17), Os1-N2-Si1 176.0(3). **5**: Os1-N1 1.9958(18), Os1-N2 1.7257(17), N2-B1 1.567(3), P1-Os1-P2 153.67(6), N1-Os1-N2 169.75(8), Os1-N2-B1 167.77(15).

derived by X-ray diffraction measurements on single crystals. The osmium center is coordinated in a square planar coordination environment ($\tau_4' = 0.07$)[169] and again the nitride is coordinated almost linearly ($\measuredangle$(Os1-N2-Si1) = 177.78(17) °) and exhibits an elongated Os≡N distance (d(Os1-N2) = 1.733(4) Å), in line with an activated triple bond.

The only other group of Os(IV) hydrocarbon based imido complexes prepared by *Schrock* and coworkers exhibit similar structural parameters, i.e. a linear coordiantion of the imido ligand,[176,177] whereas azidoimido and cyanoimido complexes by the group of *T. J. Meyer* were considerably bend.[178,179]

In contrast to this, using intermediate sized electrophiles like methyl triflate or methyl iodide did not give selective reactions, but rather complex mixtures of different compounds, of

which only $\mathbf{2}^+$ could be identified spectroscopically. However the occurrence of a triplet in the ^{1}H NMR spectrum at $\delta_{^1\mathrm{H}} = 2.61$ ppm ($^3J_{\mathrm{HP}} = 4.2$ Hz, becomes a singlet in $^1\mathrm{H}\{^{31}\mathrm{P}\}$ NMR) suggests at least partial methylation at the osmium center, as it is reminiscent of e.g. the spectrum of [Re(N)Me(PNP$^{t\mathrm{Bu}}$)] prepared by *Isabel Klopsch*.[180] Apparently, the steric shielding of the pincer is insufficient to prevent such reactivity. Further increasing the ligand bulk might improve the selectivity in this respect (e.g. using the adamantyl based pincer).

Also other tested electrophiles like acetyl chloride or trifluoroacetic anhydride led to conversion of **3**, even though these reactions were not selective and the products were not identified. No reactions were observed with pure nucleophiles like 1-hexen, 1-hexyne, MeMgCl or even with bulky ambiphiles like PPh_3.[2] Therefore the principal reactivity of **3** must be considered nucleophilic. However, when **3** was reacted with PMe_3, slow reaction to a new product **7** was observed. Two singlets in the $^{31}\mathrm{P}\{^1\mathrm{H}\}$ NMR spectrum at $\delta_{^{31}\mathrm{P}} = 43.9$ and 22.1 ppm with a 2:1 ratio and retained C_{2v} symmetry according to the ^{1}H NMR spectrum suggested formation of a phosphoraneiminato complex [Os(NPMe$_3$)(PNP$^{t\mathrm{Bu}}$)]. Spatial proximity between the new N=PMe$_3$ moiety and the *tert*-butyl groups of the ligand was confirmed by a ^{1}H NOESY spectrum. This was further substantiated by starting from **3** with 50 % ^{15}N labeled nitride. In this reaction, the signal intensity of the singlet at $\delta_{^{31}\mathrm{P}} = 22.1$ ppm dropped by 50 % and a new doublet arose at $\delta_{^{31}\mathrm{P}} = 22.1$ ppm with a coupling constant of $^1J_{\mathrm{P}^{15}\mathrm{N}} = 22.7$ Hz. Additionally, a new doublet was detected in the $^{15}\mathrm{N}\{^1\mathrm{H}\}$ NMR spectrum at $\delta_{^{15}\mathrm{N}} = -126.5$ ppm, exhibiting an identical coupling constant. The reaction did not go to completion as indicated by NMR spectroscopy which showed the formation of **7** to plateau at an equilibrium concentration with an estimated equilibrium constant of $K_c = 150\ \mathrm{M}^{-1}$ ($\Delta G^0 = -12.4\ \mathrm{kJ\,mol}^{-1}$). Indeed, removal of all volatiles and subsequent redissolving of the obtained complex led to reformation of **3** and liberation of free PMe_3, proving the reaction to be fully reversible. This reverse reaction represents a rather unique way of nitride formation, exemplified only once by the group of *Abram* reporting the reaction of $[Tc(O)Cl_4]^-$ with $Me_3SiNPPh_3$ to form $[Tc(N)Cl_2(PPh_3NH)_2]$.[181] Attempts to drive the reaction to completion by addition of a large excess of the phosphine resulted in partial decomposition of the complexes. Consequently, **7** could not be isolated as a pure compound. Nevertheless, single crystals obtained from the reaction mixture allowed determination of the molecular structure by X-ray diffraction measurements and thus for the unequivocal confirmation of the structural assignment made above. The osmium center is still coordinated in a square planar coordination environment ($\tau_4' = 0.02$).[169] In contrast to **5** and **6**$^{\mathbf{BAr^F_{24}}}$, the osmium-nitride bond is significantly elongated (d(Os1-N2) = 1.968(2) Å). In combination with the short N=P bond length of the newly formed ligand (d(N2-P3) = 1.532(2) Å) in line with a double bond, this confirms formation of a phosphoraneiminato ligand.

While PMe_3 is often described as a nucleophile in literature, *Smith* and coworkers showed by *Hammett* analysis of the adduct formation of a tetrahedral tris(carbene)borate Fe(IV) nitride with triarylphosphines that these can also also act as electron acceptors by backbonding into

[2] For a discussion of the ambiphilicity of phosphines see below as well as Part I Section 4.2.2.

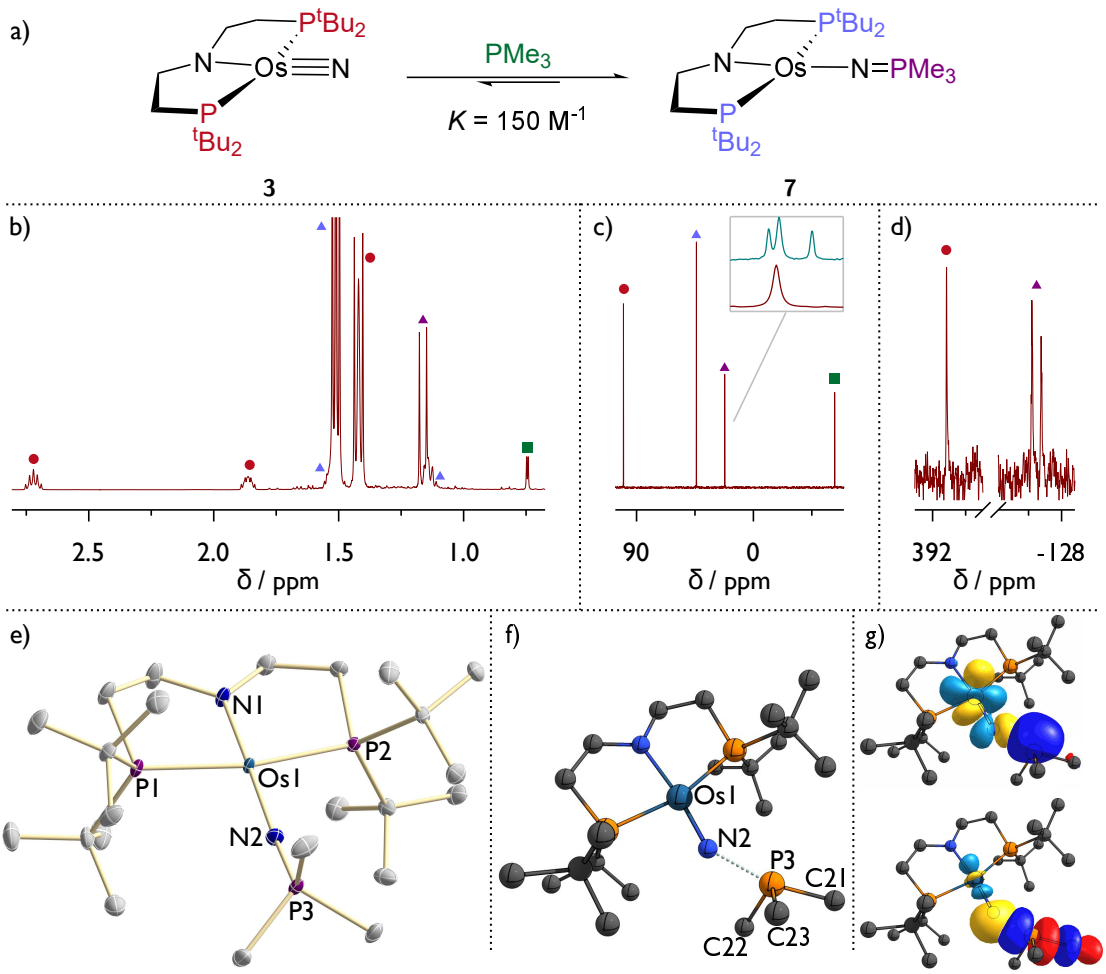

Fig. 1.3. *a*) Equilibrium reaction between **3** + PMe_3 and **7**. *Middle*: NMR spectra of the equilibrium mixture with color coded compounds: **3** (*red circle*), free PMe_3 (*green square*) and **7** with independently marked PNP pincer (*violet triangle*) and phoshphoraneiminato ligand (*pink triangle*). Shown are *b*) the ^{1}H, *c*) the $^{31}P\{^{1}H\}$ (with comparison of the phosphoraneiminato signal resulting from [Os(^{14}N)(PNP^{tBu})] (*bottom*) and [Os($^{14/15}$N)(PNP^{tBu})] (*top*) in the inset) and *d*) the $^{15}N\{^{1}H\}$ NMR spectra from the reaction with [Os($^{14/15}$N)(PNP^{tBu})]. *e*) Molecular structure of **7** obtained by single crystal X-ray diffraction measurements. All H atoms are omitted for clarity. Anisotropic displacement parameters are set to 50 % probability. Selected bond lengths [Å] and angles [°]: Os1-N1 1.920(2), Os1-N2 1.968(2), N2-P3 1.532(2), P1-Os1-P2 167.09(2), N1-Os1-N2 178.63(11), Os1-N2-P3 173.57(17). *f*) DFT derived geometry of the transition state for the reaction of **3** with PMe_3. All H atoms are omitted for clarity. Selected bond lengths [Å] and angles [°]: Os1-N2 1.755, N2-P3 2.104, P3-C21 1.914, P3-C22 1.852, P3-C33 1.853, Os1-N2-P3 146.92, N2-P3-C21 164.66, N2-P3-C22 92.47, N2-P3-C23 92.65. *g*) Donor-acceptor interactions dominating the bond formation between the phosphine and the nitride according to a natural bonding orbital (NBO) analysis. *Top*: Dominant donation for the phosphine lone pair into a $Os^{\pi^*}N$ MO. *Bottom*: Backdonation of the nitride centered lone pair into a $P^{\sigma^*}C$ MO.

$P^{\sigma^*}C$ MOs (see Part I Section 4.2.2).[159] This raised the question of the nature of the reaction between **3** and PMe_3. Since PPh_3 was unreactive, a *Hammett* plot was impossible in the present case. Therefore, a computational analysis of the reaction was performed to shed some light on it (see Part III Section 3.3 for details). The almost thermoneutral reaction was confirmed ($\Delta G^0 = -13.2\,kJ\,mol^{-1}$) and a rather high activation barrier was found ($\Delta G^{\ddagger}$

$= 60.2\,\mathrm{kJ\,mol^{-1}}$), which is in agreement with the long timescale of reaction equilibration. Closer analysis of the transition state revealed an interesting picture reminiscent of the findings by *Smith*. The Os-N···P angle strongly deviates from linearity ($\measuredangle$(Os1-N2-P3) = 147°), indicating an nucleophilic attack of the phosphine lone pair at the LUMO of **3**. Additionally, the phosphine is strongly tilded with one N···P-C angle approaching linearity ($\measuredangle$(N2-P3-C21) = 164.7°) resulting in a disphenoidal phosphine coordination. The corresponding P−C bond is elongated (d(P3-C21) = 1.914 Å, d(P3-C22) = 1.852 Å, d(P3-C23) = 1.853 Å), as a result from backdonation of the nitride lone pair into the P^{σ^*}−C MO. Both donor-acceptor interactions could also be identified in an NBO analysis, rendering a clear identification of an electrophilic vs. nucleophilic nature of the reaction non-trivial. Comparison of the natural population analysis (NPA) of both the reactants as well as the transition state revealed a net charge transfer of $0.3\,e^-$ from the phosphine to the nitride, making the electrophilic interaction of the nitride the dominant contribution to the reaction. Hence, **3** is not only a nucleophile but can exhibit electrophilic reactivity under certain circumstances, rendering it an ambiphile.

In addition to this ambiphilicity, **3** could also be shown to cleanly react with H_2 gas, when heated to 100 °C over several hours. As the immediate reaction product, [OsH_4($HPNP^{tBu}$)] (**8**) could be identified and isolated in 74 % yield (see Figure 1.4). A broad singlet in the ^{1}H NMR spectrum at $\delta_{^1H}$ = 4.88 ppm as well as three broad signals between $\delta_{^1H}$ = −6.00 - −14.33 ppm which split into four distinct and sharp signals at −50 °C correspond to the NH atom and the four hydrides. In the IR spectrum, the NH as well as the OsH stretching vibrations were found at $\tilde{\nu}$ = 3294.7 cm^{-1} (ν_{N-H}), 2013.6 cm^{-1}, 2071.5 cm^{-1}, 2044.0 cm^{-1} and 1852.6 cm^{-1} (ν_{Os-H}) (see Figure 1.4 *f*). H_2 was unambiguously confirmed as source of these H atoms when the reaction was performed with D_2. All corresponding signals vanished from the ^{1}H NMR spectrum, the ND stretching vibration was shifted to $\tilde{\nu}$ = 2455.5 cm^{-1} and the OsD stretching vibrations were shifted into the fingerprint region and could therefore not be identified unequivocally. Single crystals suitable for X-ray diffraction measurements gave a molecular structure of **8** confirming the NMR and IR based assignments (see Figure 1.4 *e*). All four OsH atoms are found from the residual density map and the protonation of the backbone N is clearly evident by the pyramidal coordination ($\Sigma_{\measuredangle}$(N1) = 350.5°). Two long (d(H1-H2) = 2.11(7) Å) and one short (d(H2-H2') = 1.70(9) Å) intramolecular distances between the H-atoms underpinned the formulation as hydrides with one compressed dihydride moiety. This assignment is also in line with the proposal by *Gusev* and coworkers on the analogous complex [OsH_4($HPNP^{iPr}$)] or the related complex [OsH_4(PNP^{tBu})] (PNP = κ^3-$C_5NH_3$2,6-(CH_2PR_2)$_2$) prepared by *Goldman* and coworkers.[182,183]

The fate of the nitride ligand was elucidated by closer analysis of the ^{1}H NMR spectrum of the reaction mixture. A broadened triplet at $\delta_{^1H}$ = 0.33 ppm ($^1J_{^1H^{14}N}$ = 42.8 Hz) could be identifed which gives a cross peak in the ^{1}H-^{14}N-HMQC spectrum at $\delta_{^{14}N}$ = -388.0 ppm, characteristic for ammonia (see Figure 1.4 *d*). If $^{14/15}$*N*-**3** with 50 % ^{15}N labeled nitride was used, the ^{1}H NMR resonance became very broad at RT, due to overlapping $^{14}NH_3$ and

$^{15}NH_3$ signals, but gave sharp signals at −50 °C with a cleanly identifiable ^{15}N-^{1}H doublet ($^{1}J_{^{1}H^{15}N} = 61.2$ Hz), fully in agreement with the expected ratio of J-coupling constants ($\gamma_{^{15}N}/\gamma_{^{14}N} = -1.41$) (see Figure 1.4 *c*). Indophenolic titration according to a literature procedure allowed for quantification of the formed ammonia to 79.4 %, matching the yield of **8** (see also resulting spectra in Part III, Section 1.2, Figure 1.1).[184]

While full hydrogenolysis of a nitride ligand to ammonia is rare, it is not unprecedented. The ruthenium complex analogous to **3**, i.e. [Ru(N)(PNP^{tBu})] (**XLII**), prepared by *Schneider* and coworkers, was also described to undergo full hydrogenolysis to form NH_3 (see Part I, Section 4.2.2).[138] Furthermore, a variation of **3**, i.e. the congener with fully oxidized ligand backbone [OsN(P=N=P^{tBu})], was developed by the *Schneider* group as a follow up of the in here presented results, which also reacts with H_2 to give NH_3 and **8**.[185] Additionally, *Hashiguchi*

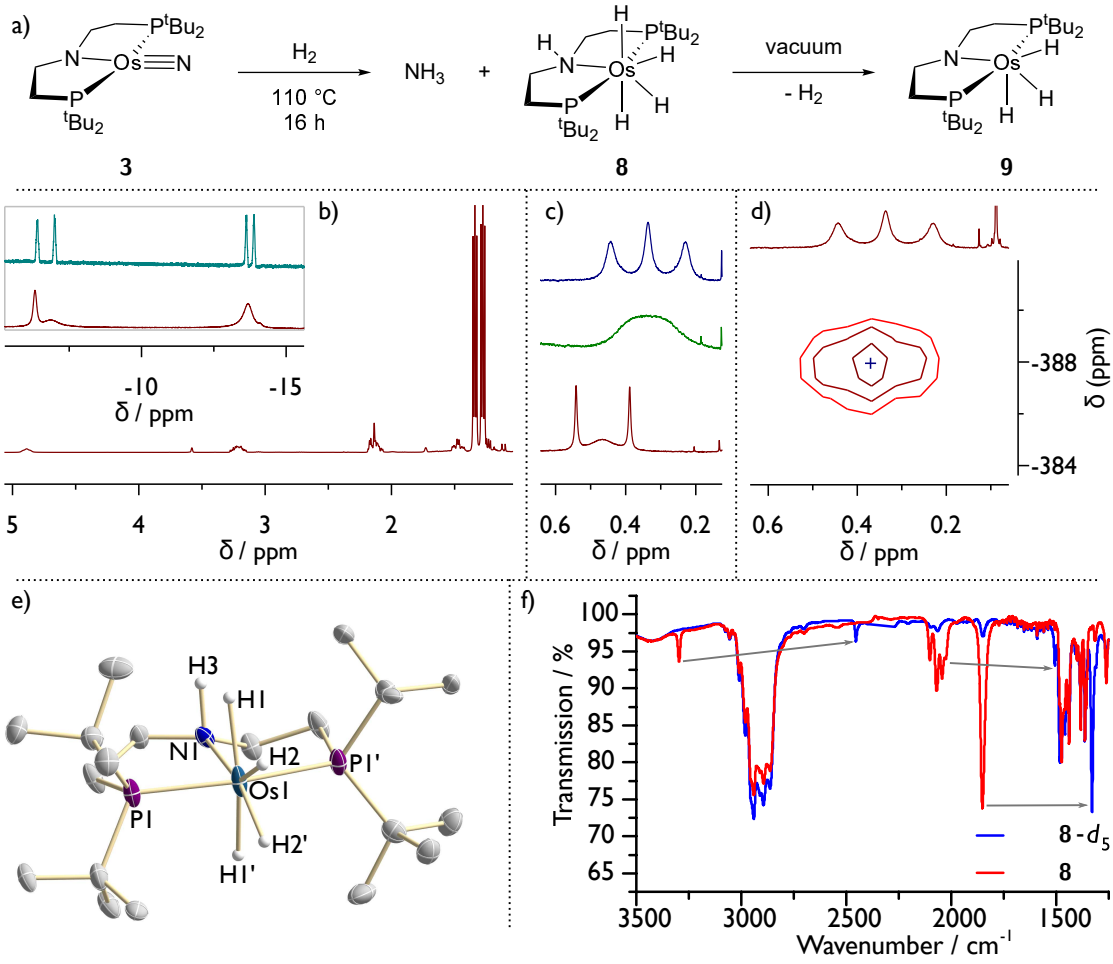

Fig. 1.4. *a*) Hydrogenation of **3** to form ammonia and **8**. Applying vacuum to a solid sample leads to H_2 loss and formation of **9**. *b*) ^{1}H NMR spectrum of **8**. *Inset*: Hydride region at RT (*bottom*) and −50 °C (*top*). *c*) ^{1}H NMR region of the NH_3 signal of the reaction mixture (*top*) and of a reaction starting from $^{14/15}N$-**3** at RT (*middle*) and at −50 °C (*bottom*). *d*) ^{1}H-^{14}N HMQC NMR of the reaction mixture. *e*) Molecular structure of **8** obtained by single crystal X-ray diffraction measurements. All carbon bound H atoms are omitted for clarity. Anisotropic displacement parameters are set to 50 % probability. Selected bond lengths [Å]: Os1-N1 2.210(5), Os1-H1 1.78(5), Os1-H2 1.77(5), H1-H2 2.11(7), H2-H2' 1.70(9). *f*) IR spectrum of **8** (*red*) and **8**-d_5 obtained from the reaction with D_2 (*blue*).

and coworkers reported increased formation of NH_3 upon base accelerated hydrolysis of an Os(VI) nitride when the Ar atmosphere was replaced with H_2.[175] The actual mechanism of the hydrogenation of **3** is unknown, but can be expected to be quite comparable to **XLII**, for which a DFT derived mechanism is available. This indicated the presence of potentially highly reactive intermediates like e.g. [Ru(NH)(HPNP$^{t\text{Bu}}$)], the product of the first metal-ligand cooperative H_2 addition. In a first attempt to trap some intermediates, the reaction was performed in the presence of 10 eq styrene. However, rather than projected aziridination or amination of the olefin, simple and quantitative hydrogenation to ethylbenzene was observed. This could indicate either **3** or **8** to be quite potent hydrogenation catalysts. In fact, the *iso*-propyl substituted analog to **8**, [OsH_4(HPNP$^{i\text{Pr}}$)], was reported to be an efficient catalyst for transfer hydrogenation and dehydrogenative coupling of alcohols.[182]

Finally, **8** could be shown to undergo reversible H_2 loss by applying vacuum to the solid sample, just as it was reported for [Ru(N)(PNP$^{t\text{Bu}}$)].[138] While the product was not fully characterized, the ^{1}H NMR spectrum pointing to a C_{2v} symmetry and the appearance of a single hydride peak integrating to three protons relative to the *tert*-butyl groups at $\delta_{^1\text{H}} = -13.64$ ppm is fully inline with loss of one H_2 molecule and formation of [OsH_3(PNP$^{t\text{Bu}}$)] (**9**), analog to the reported Ru compound and *Gusevs iso*-propyl based complex.

1.3 Redox chemistry of osmium(IV) and osmium(VI) nitrido complexes

The cyclic voltammetry (CV) data of [Os(N)(PNP$^{t\text{Bu}}$)] (**3**), which were previously reported,[174] revealed a quasi-reversible oxidation at $E_{1/2} = -0.75$ V vs. Fc/Fc^+. Concentration dependent measurements indicated a reduced reversibility at higher concentrations of **3**, especially at low scan rates, suggesting a bimolecular follow-up reaction. This could indicate a potential coupling of the cationic nitride complexes to form a dimer, in line with previous reports by *Taube* and *Meyer*.[186–188] Considering the isolobal relationship between square-planar d^4 and octahedral d^2 nitrido complexes, such a coupling would be analogous to the observation by *Nishibayashi* of his complex [Mo(N)(Cp*)(depf)] (**XXXI**) coupling to the dimer [(μ-N_2){Mo(Cp*)(depf)}$_2$] (**XXX**) upon one-electron oxidation (see Part I, Section 3.2.3).[114] Furthermore, N$\cdots$N coupling reactions from Os(V) nitrido complexes are well known in the literature.[42,189,190] Consequently, the chemical oxidation of **3** was investigated to elucidate potential formation of a dimeric compounds.

Initial attempts using [Fe(Cp)$_2$]PF_6 resulted in the formation of little [Os(N)H(PNP$^{t\text{Bu}}$)]$^+$ (**2**$^+$), along the formation of a doublet in ^{31}P{^{1}H} NMR spectroscopy at $\delta_{^{31}\text{P}} = 96.5$ ppm ($J_{\text{PF}} = 20.5$ Hz), tentatively attributed to activation of the PF_6^- anion. Replacing the anion with BAr^F_{24} indeed gave no sign of such species. Instead, almost equimolar amounts of hydride species **2**$^+$ and an unidentified C_S symmetric compound with a resonance singlet at $\delta_{^{31}\text{P}} = 98.1$ ppm in the ^{31}P{^{1}H} NMR spectrum were obtained. However, the nature of that

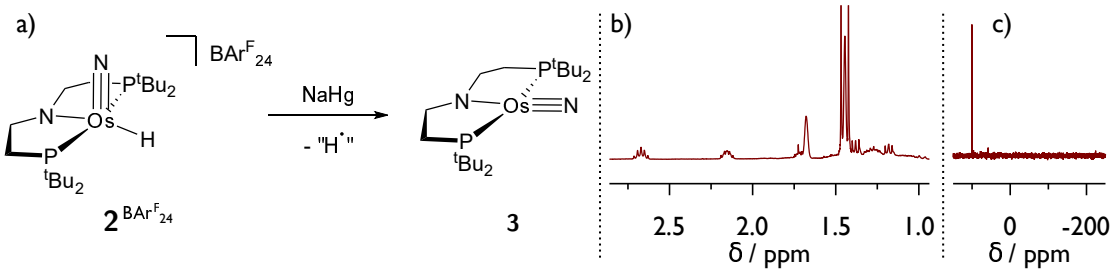

Fig. 1.5. *a*) Reduction of **2**$^{\mathbf{BAr^F_{24}}}$ with 1 eq NaHg. *b*) ^{1}H and *c*) ^{31}P$\{^1$H$\}$ NMR spectra indicate clean formation of **3**.

species currently remains unclear as well. Another attempt using the trityl cation as oxidant resulted in almost quantitative formation of **2**$^+$. While non of these reactions yielded an expected C_{2v} symmetric complex according to ^{1}H NMR spectroscopy, it is noteworthy that also no sign of any paramagnetic complexes was observed. The initially formed open-shell species can therefore be assumed to be highly reactive. Attempts with mild oxidants and non-coordinating anions, like [Fe(Cp*)$_2$](BAr$^F_{24}$) were not performed but might be promising candidates for selective reactions. A second approach aiming for an osmium(V) nitride which could undergo coupling reactions was the one-electron reduction of **2**$^{\mathbf{BAr^F_{24}}}$. If that osmium(VI) nitride complex was mixed with 1 eq NaHg, surprisingly quantitative and clean formation of **3** was observed, suggesting formal H-atom loss from the Os(V) stage, even though no H_2 could be detected in the NMR (see Figure 1.5).

When **3** was reacted with 1.0 eq NCS, which can act as one or two-electron oxidant, a more desired reaction was observed. Mixing the two reactants resulted in immediate and selective formation of a new, diamagnetic, C_S symmetric compound, which slowly decomposed at RT over several hours. This suggested a two-electron oxidation and therefore indicated the potential formation of a succinimide anion. Consequently, addition of a proton source after the successful reaction resulted in selective formation of analytically pure Os(VI) nitride [Os(N)Cl(PNP^{tBu})]^X (**10^X** (X = anion of the used acid). The complex resonates at $\delta_{^{31}P}$ = 96.2 ppm in the ^{31}P$\{^1$H$\}$ NMR spectrum, is C_S symmetric on the NMR timescale and bears no other proton containing group but the PNP pincer according to the ^{1}H NMR spectrum. It is interesting to note that the recorded spectra are slightly different when HCl was used as acid, instead of those with non-coordinating anions, suggesting the formation of an octahedrally coordinated nitride [Os(N)Cl$_2$(PNP^{tBu})] (**10-Cl**) (see Figure 1.6).
Since **10**$^+$ does not bear a hydride ligand anymore, reduction of this complex can not lead to H$^•$ loss and might therefore be more suitable to initiate a potential coupling reaction. However, the reaction of **10**$^{\mathbf{BAr^F_{24}}}$ with Co(Cp*)$_2$ at RT leads now to the formation of equimolar amounts of **3** and **10-Cl**, which is the result of a formal disproportionation reaction of the formed Os(V) nitride (see Scheme 1.2).

Due to the higher oxidation state of **10**$^{\mathbf{BAr^F_{24}}}$ the complex can be assumed to be rather electrophilic and its behavior towards styrene was tested. However, no reaction with up to

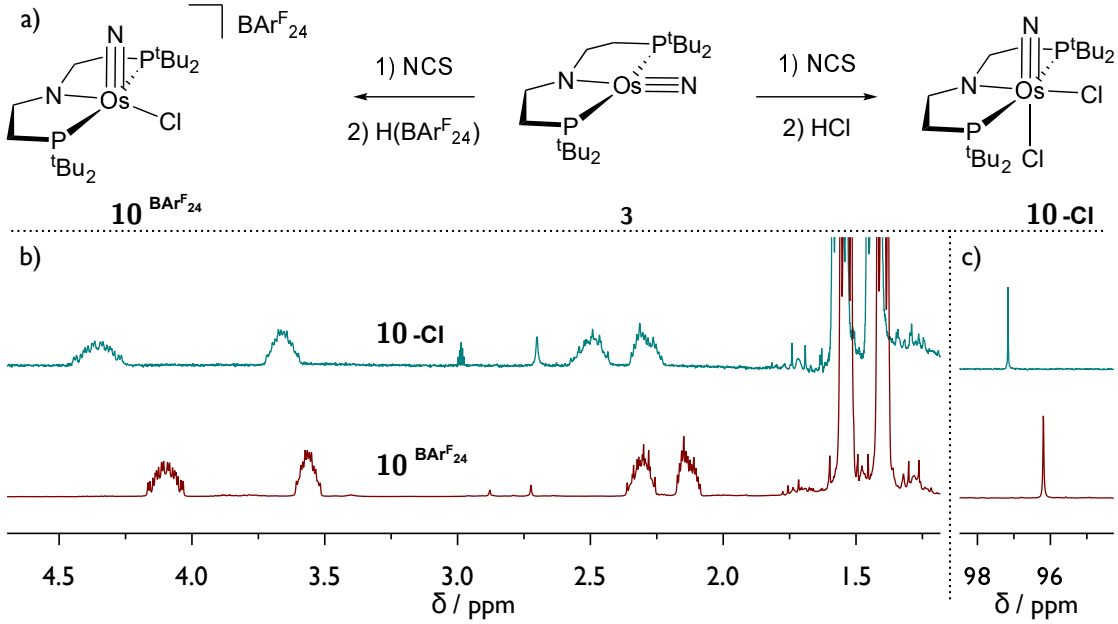

Fig. 1.6. *a*) Syntheses of **10-Cl** and **10**$^{\mathbf{BAr^F_{24}}}$ from **3** and NCS. The ^{1}H (*b*) and ^{31}P{^{1}H} (*c*) NMR spectra show clearly distinguishable compounds, suggesting chloride coordination in **10-Cl**.

10 eq was observed. One way to increase nitride centered reactivity was published by *Lau* and cowokers who observed alkene aziridination reaction by [Ru(N)(salchda)]^{PF_6} (**LXII**), initiated by coordination of a ligand (pyridine) in *trans* position to the nitride (see Part I, Section 4.2.2).[163] Adopting this strategy, **10**$^{\mathbf{BAr^F_{24}}}$ and 10 eq styrene were mixed with pyridine as well as the strong σ-donor ligand CN^{t}Bu. While the former reagent is also unreactive, mixing **10**$^{\mathbf{BAr^F_{24}}}$ with one equivalent CN^{t}Bu, resulted in only 50 % conversion. Furthermore, the reaction was observed to be fully independent of styrene being present or not. Full conversion was achieved upon addition of another equivalent or by starting the reaction with an excess of CN^{t}Bu right away. Moreover, ^{31}P{^{1}H} NMR spectroscopy revealed the formation of two new complexes **11a** and **11b** in an estimated ratio of 1:0.2, each with inequivalent P atoms and very small coupling constants (J_{PP} = 11.6 and 6.7 Hz). While the two products were not isolated from each other and no clean samples were obtained, ^{1}H NMR measurements suggest the species to be C_S symmetric with the pincer being in plane with the mirror plane. Additionally, a doublet at $\delta_{^1H}$ = 7.92 ppm (J_{HP} = 17.1 Hz) can be identified, which collapses to a singlet in the ^{1}H{^{31}P} NMR spectrum. Full NMR characterization of the complexes is still pending. Nevertheless, single crystals suitable for

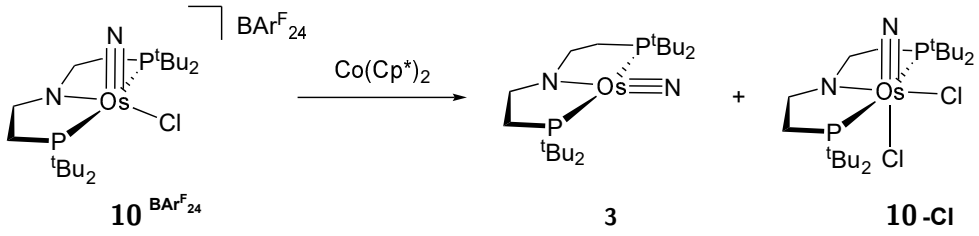

Scheme 1.2. Disproportionation of **10**$^{\mathbf{BAr^F_{24}}}$ upon reduction.

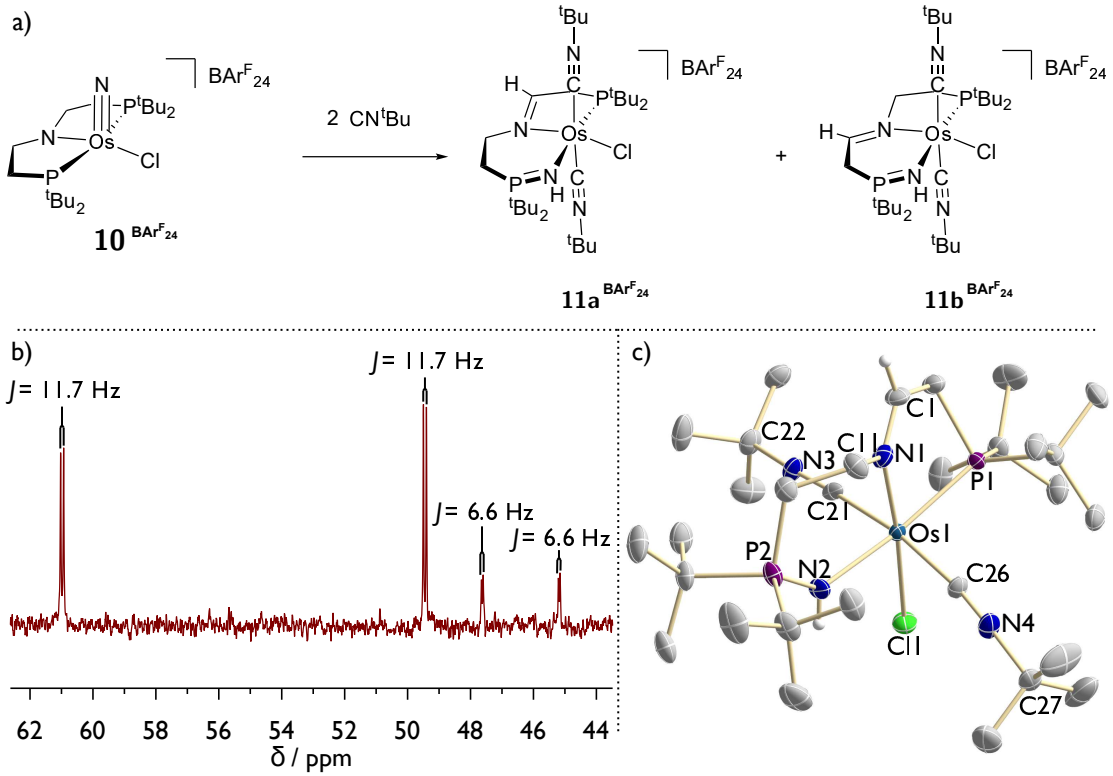

Fig. 1.7. *a*) Reaction of $\mathbf{10}^{\mathbf{BAr^F_{24}}}$ with 2 eq CN^{t}Bu and the most likely formed products $\mathbf{11a}^{\mathbf{BAr^F_{24}}}$ and $\mathbf{11b}^{\mathbf{BAr^F_{24}}}$. *b*) ^{31}P{^{1}H} NMR spectrum of $\mathbf{11a}^{\mathbf{BAr^F_{24}}}$ and $\mathbf{11b}^{\mathbf{BAr^F_{24}}}$. *c*) Molecular structure of one of the two isomers obtained by single crystal X-ray diffraction measurements. All H atoms but the NH and imine CH atoms, as well as the anion are omitted for clarity. Anisotropic displacement parameters are set to 50 % probability. Selected bond lengths [Å] and angles [°]: Os1-N1 2.058(2), Os1-N2 2.175(2), P2-N2 1.592(2), N1-C1 1.308(4), N1-C11 1.447(4), C21-N3 1.177(4), C26-N4 1.146(3), Os1-N2-P2 132.15(15), C26-N4-C27 170.0(3), C21-N3-C22 171.8(3), N1-Os1-Cl1 175.19(7), P1-Os1-N2 171.64(7), C21-Os1-C26 170.68(11).

X-ray diffraction measurements could be obtained and revealed one of the species to be [Os(CN^{t}Bu)$_2$Cl{N(CH$_2$CH$_2$P^{t}Bu$_2$)(=CHCH$_2$P(^{t}Bu)$_2$=NH)}]$^{\mathrm{BAr^F_{24}}}$, i.e. the product of nitride insertion into the Os–P bond, accompanied by CH activation of the backbone and imine formation. The osmium center is coordinated octahedrally by the newly formed PNN^H pincer, the chloride and two isocyanide ligands in *trans* position to each other, leading to the overall observed C_S symmetry. Both isocyanides are almost linear ($\measuredangle$(Os-C-N) = 170.0(3) and 171.8(3)°) and feature similar C≡N bond length (d(C–N) = 1.177(4) and 1.146(3) Å), indicating a modest degree of backbonding. The newly formed imino phosphorane features a P=N bond length of d(P2-N2) = 1.592(2) Å, in line with a double bond. This imino phosphorane moiety formation also perfectly matches the small coupling constants in ^{31}P{^{1}H} NMR, as these are now ^3J coupling constants. The NH proton was found from the residual density map and most likely corresponds to the doublet at $\delta_{^1\mathrm{H}}$ = 7.92 ppm in the ^{1}H NMR spectrum. The two N-C bond distances in the backbone strongly differ (d(N1-C1) = 1.308(4) Å, d(N1-C11) = 1.447(4) Å), which is in line with an intramolecular CH bond activation and imine formation in the pincer backbone.

Similar insertion reactions into metal-ligand bonds are rare and have been reported for Fe,[191] Co[192,193] and Ni.[194] In all these cases, the insertion products were obtained by thermal or photolytic decomposition of complexes featuring nitride precursors (azides or dbabh = 2,3:5,6-dibenzo-7-azabicyclo[2.2.1]hepta-2,5-diene) and the formation of transient nitrido species remained only hypothetical, with initial insertion of the precursor and subsequent loss of the leaving groups standing to reason. In the present case no defined mechanism is available, and several possible pathways could play a role, including *intra*molecular CH activation directly by the nitride and subsequent insertion into the Os–P bond; initial insertion, followed by β-hydride elimination and shift to the P=N ligand, or even initial insertion followed by *inter*molecular CH activation. Slightly different barriers for the formation of the *syn* or *anti* isomers $\mathbf{11a}^{\mathbf{BAr^F_{24}}}$ and $\mathbf{11b}^{\mathbf{BAr^F_{24}}}$ with respect to the newly formed imine in the backbone and the phosphoraneiminino ligand might than explain the appearance of the two different signal sets as observed by $^{31}P\{^1H\}$ NMR.
Even though this reaction is not full characterized yet, its occurance is promising and further trapping experiments could open access to a rather unique way of nitride functionalization reactions. Especially if at some point N_2 activation should become feasible at this platform, closer investigation of the reaction at hand might become of greater interest.

1.4 Attempts of dinitrogen activation

The $\{Os(PNP^{tBu})\}$ platform might be a promising candidate for N_2 activation and functionalization, as pointed out in Part I, Section 5. Therefore, the potential of **1** and derived compounds with respect to N_2 activation was thoroughly investigated and will be discussed in this section. Three different targets of hypothetical N_2 splitting pathways were identified and independently synthesized from azide source, i.e. $\mathbf{2^X}$, **3** and $\mathbf{10^X}$ (see Section 1.1 and 1.3 for syntheses and characterization of these complexes). Starting from **1** and the thereof derived monocationic complex $[OsClH(PNP^{tBu})]^{\mathbf{X}}$ ($\mathbf{12^X}$), overall five different strategies were developed for how the target molecules might be obtained from N_2 (see Figure 1.3 and Table 1.1). According to the considerations expounded in Part I, Section 3.2.1, a $10\pi(4\delta)$ electronic configuration of a $\{MNNM\}$ core should be necessary for efficient splitting of N_2 into terminal nitrides. Consequently, an Os(III) dinitrogen bridged dimer in an idealized D_{4h} geometry which is isoelectronic to the formal Re(II) compound **XX** should be an ideal candidate for splitting into the Os(VI) nitride complexes $\mathbf{2}^+$ and $\mathbf{10}^+$. This was attempted by one-electron reduction of the starting complexes under a dinitrogen atmosphere (I), by *in situ* deprotonation and subsequent one-electron oxidation (III *b*) or by single hydrogen atom abstraction with TTBP under a dinitrogen atmosphere (III *a*).
Despite this MO rationalized approach, splitting attempts to directly obtain Os(IV) nitrido complex **3** were followed as an alternative pathway, taking into account the isolobal relationship between octahedral d^n and square-planar d^{n+2} complexes. In related Ir complexes, splitting was calculated to be thermodynamically uphill, but was assumed to potentially

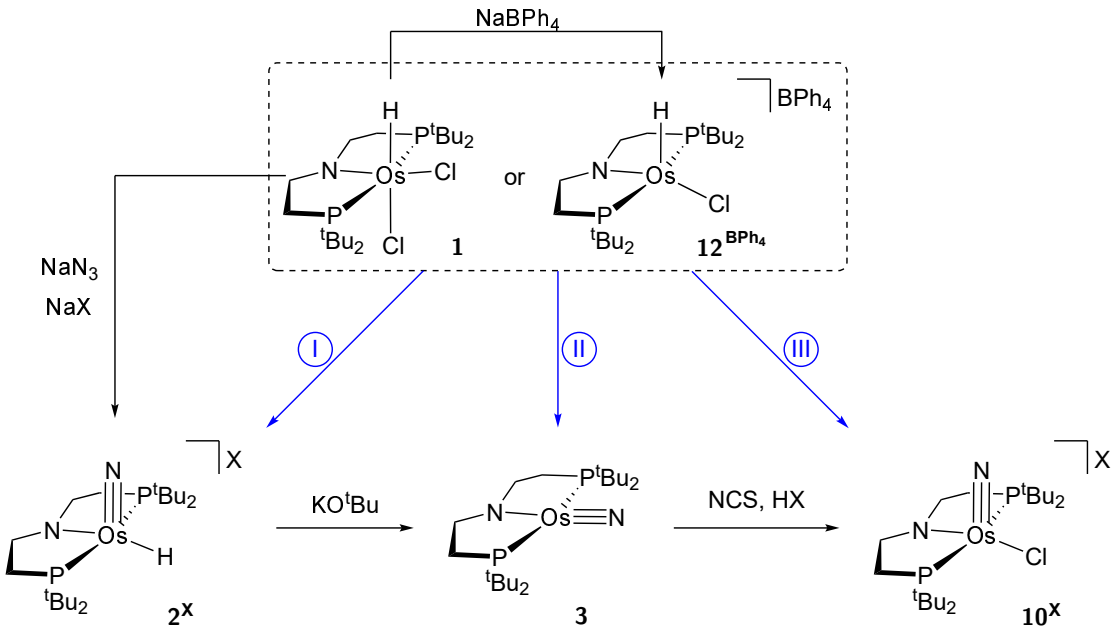

Scheme 1.3. Summary of the reaction strategies I, II or III detailed in Table 1.1, which were envisioned to potentially lead to N_2 splitting with the osmium platform.

Tab. 1.1. Explanation of strategies I, II or III depicted in Scheme 1.3 and the list of tested reagents. Most reactions were carried out under various conditions (solvent, temperature).

I	$+ e^- + N_2$	*Reductants*: NaHg, $CoCp_2$, $Co(Cp^*)_2$
II *a*	$+ 3\ e^- + N_2$	*Reductants*: NaHg, KC_8
II *b*	$+$ base $+ e^- + N_2$	*Bases*: KO^{t}Bu, KHMDS, NEt_3, DBU. *Reductants*: NaHg, KC_8
III *a*	$- H^\bullet + N_2$.	*Oxidants*: TTBP, 1,4-benzoquinone
III *b*	$+$ base $- e^- + N_2$	*Bases*: KO^{t}Bu, KHMDS. *Oxidants*: Fc^+, $^{Ac}Fc^+$, Ag^+, magic blue

result in an almost thermoneutral splitting product. For this, the starting complexes were either reacted with an excess of KC_8 in order to reduce all the way down to an Os(I) fragment (II *a*), or treated *in situ* with a base and then with KC_8, all under dinitrogen atmosphere (III *b*).

Most of these reactions gave mixtures of several, unidentifiable species and will therefore not be discussed here in detail. Most importantly, in more than 60 different reactions, no sign for any of the three different target compounds could be identified, suggesting an inherent problem of the chosen system. In many reactions, especially in those which involved bases, C_1 symmetric species bearing hydride ligands and signals between 5 - 8 ppm in the ^{1}H NMR spectrum could be identified as part of the product mixtures, suggesting β-hydride elimination from the ligand. This points to a rather low stability of low coordinated Os(II) compounds towards intramolecular CH activation as one major issue, which is in line with the few literature reports on square-planar Os(II) complexes.[168,195] Yet it is noteworthy that reaction of **1** with KO^{t}Bu at $-80\,°C$ resulted in a defined color change from green to violet, indicating an initial clean reaction product persistent at low temperatures. Warming these reaction to $T > -50\,°C$ already leads to color change to brown. Unfortunately, no NMR data on this violet species are available.

It was possible to gain access to two stable Os(II) complexes when additional ligands were introduced via two different routes (see Figure 1.8 *a*). On the one hand, reaction of **1** with 3 eq KC_8 under a dinitrogen atmosphere in THF gives selective reaction to a new complex **13**. The ^{1}H NMR spectrum reveals a hydride signal at $\delta_{^1H} = -26.88$ ppm and C_s symmetry on the NMR timescale (see Figure 1.8 *b*). A single resonance in the $^{31}P\{^1H\}$ NMR at $\delta_{^{31}P} = 85.9$ ppm is split into a doublet ($^2J_{HP} = 8.7$ Hz), attributed to insufficient decoupling of the hydride signal (see Figure 1.8 *c*). Two bands in the attenuated total reflection infrared (ATR-IR) spectrum at $\tilde{\nu} = 2114.5\,cm^{-1}$ (ν_{Os-H}) and $2007.7\,cm^{-1}$ ($\nu_{N\equiv N}$) support **13** to be the Os(II) hydride dinitrogen complex [OsH(N_2)(PNP^{tBu})] (see Figure 1.8 *d*).
The identification of this complex explained why the strategy II *a* was unsuccessful. Apparently, **13** can not be reduced any further, not even with KC_8. Unfortunately, oxidation of **13** by one electron also gave no signal of the Os(VI) hydride nitride complex **2**$^+$, which is why the complex was not further investigated.
Stabilization of an Os(II) complex by addition of an electron-acceptor ligand appears to be an attractive option to prevent unwanted backbone activation. However the presence of a hydride in any hypothetical splitting product can be considered undesirable, as for example **2**^{Cl} is known to decompose into **3** and **4**^{Cl} (see Section 1.1). Consequently, a similar route to stabilize the deprotonation product of **1** was investigated. A sequence of chloride abstraction using $NaBPh_4$, *tert*-butylisocyanide coordination and deprotonation was finally developed, yielding [OsHCl(PNP^{tBu})]^{BPh_4} (**12**^{BPh_4}), [OsHCl(CN^{t}Bu)(PNP^{tBu})]^{BPh_4} (**14**^{BPh_4}) and [OsCl(CN^{t}Bu)(PNP^{tBu})] (**15**) (see Figure 1.8 *a*). Successful chloride abstraction in the first step is most evident by the shift of the hydride signal from $\delta_{^1H} = -4.48$ ppm to -20.8 ppm and the fact, that **12**^{BPh_4} becomes unstable towards DCM, which is different from parent **1**. Overall, the signals of **12**^{BPh_4} are often quite broad, in ^{1}H as well as $^{31}P\{^1H\}$ NMR spectroscopy. Successful coordination of CN^{t}Bu to form **14**^{BPh_4} again becomes evident from the ^{1}H NMR spectrum, showing a backshifting of the hydride signal to $\delta_{^1H} = 0.30$ ppm as well as the appearance of a new singlet integrating to nine protons at $\delta_{^1H} = 1.47$ ppm, overlapping with the resonance of one of the *tert*-butyl groups. Importantly, at this stage the stochiometry of the isocyanide ligand needed to be controlled with care, because already a minor excess leads to formation of side products which could not be separated from the main complex. Finally, deprotonation using KO^{t}Bu resulted in formation of **15**, which exhibits no signal corresponding to a hydride or the anion anymore but still contains a single CN^{t}Bu group. Further spectroscopic measurements on these compounds are not available at this point. However, all three complexes were confirmed by liquid injection field desorption ionization (LIFDI) mass spectrometry and single crystals suitable for X-ray diffraction measurements allowed to determine the molecular structure of the final complex **15**, suggesting a successful synthetic route (see Figure 1.8 *g*). The osmium center is coordinated in a square pyramidal coordination geometry ($\tau_5 = 0.06$)[196] with the isocyanide ligand adopting the apical position. The isocyanide moiety is strongly bent ($\measuredangle$(Os1-C21-N2) = 170.1(2)°, $\measuredangle$(C21-N2-C22) = 141.3(3)°), indicating a significant amount of backbonding. Such highly bent isocyanides were observed before for isoelectronic W(0) and Re(I) complexes.[153,197]

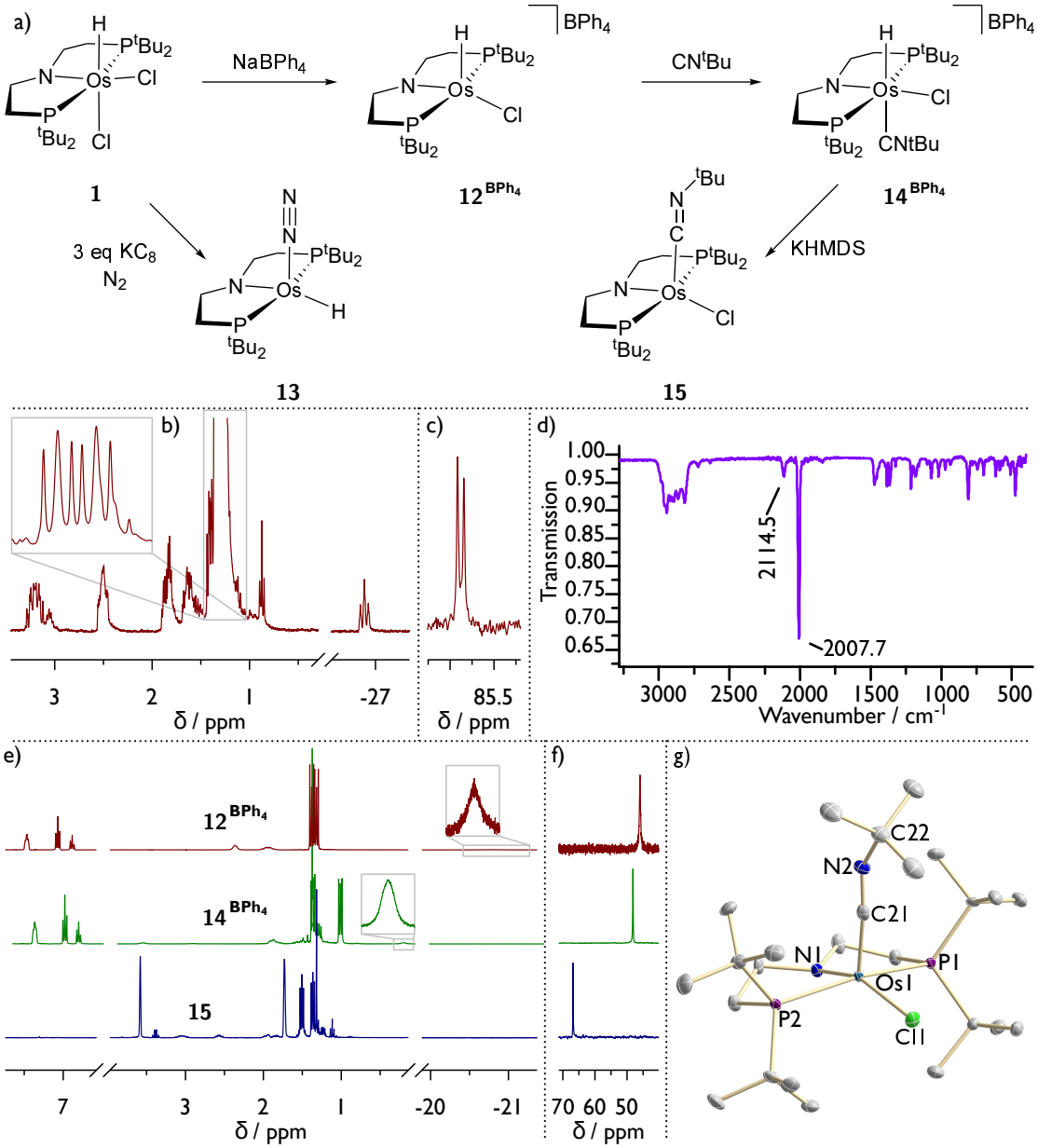

Fig. 1.8. *a*) Synthesis scheme describing the syntheses of Os(II) complexes **13** and **15**. *Middle*:) ^{1}H (*b*) and ^{31}P{^{1}H} (*c*) NMR spectrum as well as IR spectrum (*d*) of **13**. *Bottom*: ^{1}H (*e*) and ^{31}P{^{1}H} (*f*) NMR spectra of $\mathbf{12}^{\mathbf{BPh_4}}$ (*red*), $\mathbf{14}^{\mathbf{BPh_4}}$ (*green*) and **15** (*blue*). *g*) Molecular structure of **15** obtained by single crystal X-ray diffraction measurements. All H atoms are omitted for clarity. Anisotropic displacement parameters are set to 50 % probability. Selected bond lengths [Å] and angles [°]: Os1-N1 1.972(2), Os1-Cl1 2.4639(7), Os1-C21 1.838(3), C21-N2 1.206(4), P1-Os1-P2 161.66(3), N1-Os1-Cl1 157.95(7), Os1-C21-N2 170.1(2), C21-N2-C22 141.3(3).

This is in line with a slight elongation of the N≡C bond in that moiety (d(C21-N2) = 1.206(4) Å) compared to unactivated isocyanides like $\mathbf{11}^{\mathbf{BAr^F_{24}}}$ (see Section 1.3).

Preliminary reactivity studies suggest an instability of **15** in the presence of sodium salts with different outcomes under Ar or N_2. However, these reaction were hardly selective and lacked reproducibility. The appearance of many different signals in the high field region of

the ^{1}H NMR spectrum suggested hydride formation and thus backbone activation under these conditions. Thus, also this complex was not investigated further.

1.5 Summary

At the beginning of this thesis, it was known how the square-planar Os(IV) nitride **3** could be synthesized, including most of the characterization. However, the nature of the intermediates and involved species was only discussed on a rather speculative basis. Continued research provided a refined picture, especially on the nature of the initially formed Os(VI) nitrido complex $\mathbf{2}^{+}$, and its disproportionation if chloride was the counteranion. Eventually, these results allowed for improving the synthesis of **3**.

Exploration of the principal reactivity of **3** showed nitride centered reactivity towards large *Lewis* acids like Me_3Si^{+} or BAr^{F}_{18}, whereas exposure to smaller electrophiles result in metal centered reactivity, highlighting the importance of the steric shielding by the *tert*-butyl groups. Contrary to this, **3** is inert towards most nucleophiles. However, upon mixing with PMe_3, the reversible formation of a phosphoraneiminato ligand is observed. Theoretical investigations by DFT calculations and NBO analysis proved the reaction to feature a dual nature push pull interaction between both reactants, with the electrophilic properties of **3** dominating, rendering it an ambiphile.
Additionally, full hydrogenolysis of **3** was proven to yield NH_3 and polyhydride complex **8**.

Attempts to synthesize an Os(V) nitride species by either oxidation of **3** or reduction of $\mathbf{2}^{+}$ or $\mathbf{10}^{+}$ gave either non-selective reactions in the former or full reduction down to **3** in the latter case. In this context, $\mathbf{10}^{+}$ was found to react with two equivalents of $CN^{t}Bu$ undergoing backbone CH activation and insertion of the nitride into an Os–P bond, forming an phosphoraneimine moiety. This reaction shows how the nitride centered reactivity can be increased through addition of *trans* ligands and might be exploited in further functionalization schemes.

Finally, extensive investigation of potential N_2 activation schemes gave no sign of nitride formation at any stage, pointing to some inherent problems of the system at hand. Backbone CH activation seemed to be a major problem. In the cause of this research, two Os(II) complexes **13** and **15** could be obtained and were tested towards N_2 splitting as well, yet unsuccessful.

2

Extensions of the [$ReCl_2(PNP^{tBu})$] platform

> *The extension of existence to a further level of Being*
>
> — **Vader**
> "Xeper" on "Litany"

In previous work, the rhenium PNP pincer complex [$ReCl_2(PNP^{tBu})$] (**XIX**) was shown to be a potent platform for N_2 activation and functionalization (see Part I Section 4.2.1). Notably, the reductive splitting into nitrido complex [$ReCl(N)(PNP^{tBu})$] (**XXI**) and the subsequent functionalization with alkyl triflates resulted in synthetic cycles for nitrile formation.[94,153]

The nature of the proposed intermediate of the dinitrogen splitting process, i.e. [$(\mu\text{-}N_2)\{ReCl(PNP^{tBu})\}_2$] (**XX**), was previously only predicted from DFT calculations. However, during the reduction of **XIX** a color change to deep red was observed which vanished rapdily at RT, indicating a short-lived, yet observable intermediate. Investigations which led to the spectroscopic, structural and thermodynamic characterization of this dimer **XX** are described in Section 2.1.

The above mentioned nitrile formation was achieved after ethylation and benzylation of the nitrido complex **XXI**. Interestingly, previous work indicated that following a similar route with the methylated complex [$Re(NMe)Cl(PNP^{tBu})]^+$ (**16**) led to intermolecular C–C coupling instead of cyanide formation.[180] This reaction was investigated further and is described in Section 2.2.

The synthetic cycles which lead to nitrile formation require strong reductants for the initial Re(III/II) reduction to enable N_2 activation on the one hand, and oxidants for the subsequent functionalization on the other. In the strive for developing catalytic systems, electrochemistry provides a promising alternative to chemical reactants which would enable to apply reductive and oxidative conditions to a bulk solution simultaneously. However, any potential system for such a scenario should be inert to oxidative stress, i.e. side reactions leading to decomposition should be avoided. Previous work in our group identified the oxidation of the ligand backbone, forming $N(CHCHPR_2)_2^-$ ($P{=}N{=}P^-$), as strategy to easily access a versatile platform which is less sensitive to oxidative decomposition. Therefore, the preparation of

complex [$ReCl_2$(P=N=P^{tBu})] (**21**) as well as its application in N_2 activation, splitting, and functionalization is described in Section 2.3.

2.1 Characterization of μ-N_2 bridged Re dimer **XX**

Part of this section has been published in: B. M. Lindley, R. S. van Alten, M. Finger, F. Schendzielorz, C. Würtele, A. J. M. Miller, I. Siewert, S. Schneider, "Mechanism of Chemical and Electrochemical N_2 Spitting by a Rhenium Pincer Complex", *J. Am. Chem. Soc.* **2018**, *140*, 7922-7935.

The splitting of N_2 by **XIX** under reductive conditions was proposed to proceed via dinuclear, μ-N_2 bridged dimer **XX**, the structure of which was predicted by DFT calculations.[94] These computations also pointed to a significant activation barrier for the actual splitting step and thus suggested a considerable lifetime of the dimer, giving rise to the question whether it could be at least spectroscopically observable.

A first evidence of a short-lived, yet observable, intermediate had already been reported in terms of a color change during the reaction from violet (**XIX**), via deep red (intermediate **XX**) to yellow (**XXI**) within minutes at RT. Reduction of **XIX** under N_2 atmosphere at $-40\,°C$ preserved the red color and low temperature NMR measurements revealed, despite several minor side products, two new doublets in the $^{31}P\{^1H\}$-NMR spectrum at $\delta_{^{31}P} = 16.5$ and -115.3 ppm which featured a mutual coupling constant of $^2J_{PP} = 234$ Hz (see NMR spectra in Figure 2.1). Warming the sample to RT and monitoring the process showed clean conversion of the newly formed species into **XXI** proving it to be an actual intermediate in the N_2 splitting process. In the ^1H-NMR spectrum, a new set of paramagnetically shifted, yet sharp signals with resolved J-coupling constants was observed. A total of eight signals for backbone protons between $\delta_{^1H} = 12.2$ and -16.7 ppm could be identified, while an identification of the *tert*-butyl groups was not fully possible as they became very broad at low temperatures (probably due to dynamic effects). These data are in agreement with a single new complex **XX** exhibiting a C_2 symmetric dimer structure resembled by the DFT-predicted structure as well as the analogous Mo complex [(μ−N_2){MoCl(PNP^{tBu})}$_2$] (**XXII**).[96] However, an attempt to further substantiate the dimeric nature of **XX** by $^{31}P\{^1H\}$-diffusion ordered spectroscopy (DOSY) was not successful. The T_1 relaxation time of these doublets

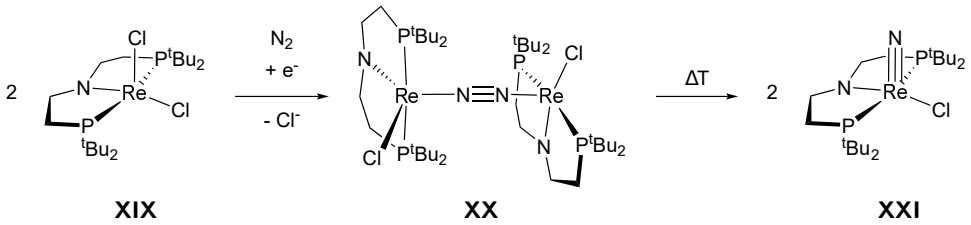

XIX **XX** **XXI**

Scheme 2.1. Thermal dinitrogen splitting after reduction of **XIX** proceeds via dimeric, μ-N_2 bridged complex **XX** to yield terminal nitrido complex **XXI**.

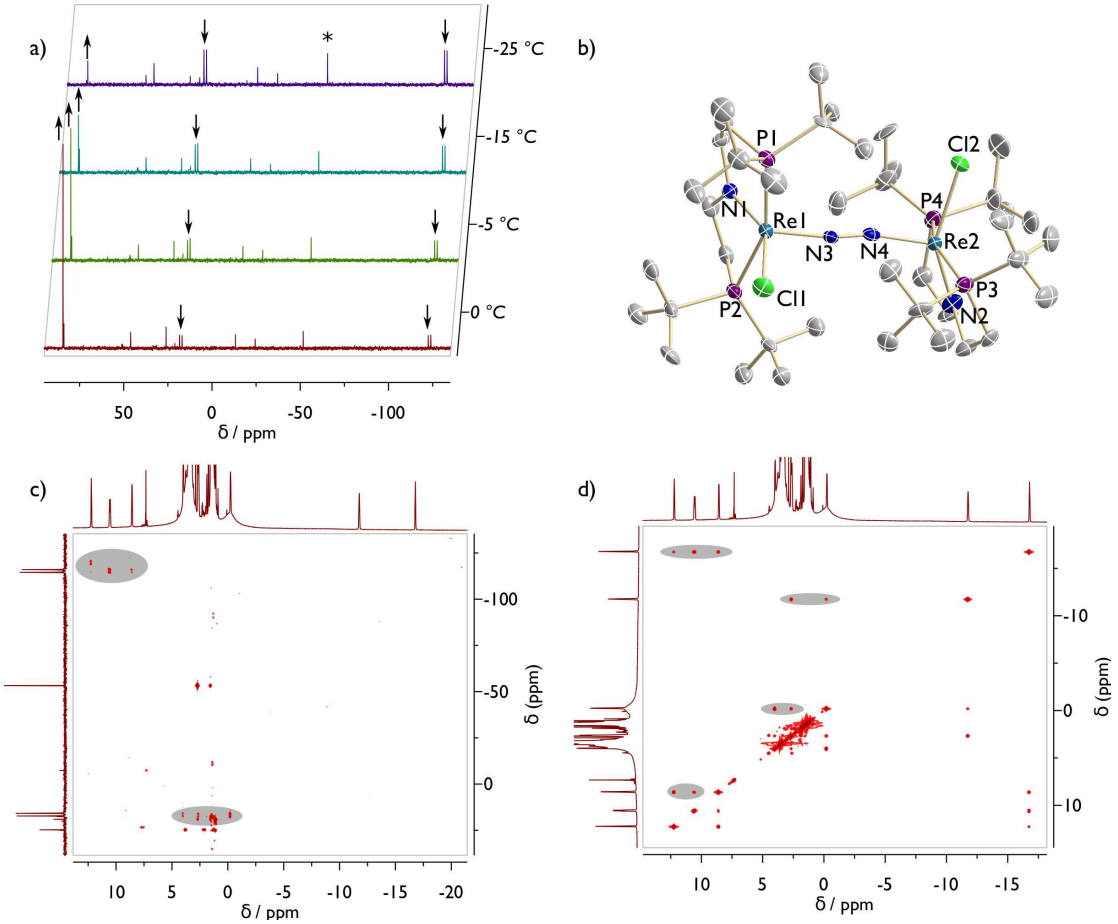

Fig. 2.1. Characterization of N_2 bridged dimer **XX**: *a*) Reaction monitoring of an *in situ* prepared solution of **XX** ($\delta_{^{31}P}$ = 16.5 and -115.2 ppm) to **XXI** ($\delta_{^{31}P}$ = 84.4 ppm) by warming from −25 °C to 0 °C. Signals corresponding to the dimer decrease (arrow down) while the peak of the nitride rises (arrow up). The peak marked with an asterisk corresponds to residual **XIX**. *b*) Molecular structure of **XX** obtained by single crystal X-ray diffraction measurements. H-atoms as well as co-crystallized pentane, **XIX** and **XXI** are omitted for clarity. Anisotropic displacement parameters are set to 50 % probability. Selected bond lengths [Å] and angles [°]: Re1-N1 1.937(7), Re1-N3 1.861(8), Re1-P1 2.406(3), Re1-P2 2.405(3), Re1-Cl1 2.463(3), Re2-N2 1.949(8), Re2-N4 1.886(8), Re2-P3 2.409(3), Re2-P4 2.406(3), Re2-Cl2 2.455(3), N3-N4 1.202(10), N1-Re1-N3 118.0(3), P1-Re1-P2 157.38(9), N1-Re1-Cl1 146.3(2), N2-Re2-N4 119.3(3), P3-Re2-P4 156.28(9), N2-Re2-Cl2 146.6(3), Cl1-Re1-Re2-Cl2 112.06. *c*) ^{1}H-^{31}P-HMBC NMR spectrum. The cross peaks corresponding to **XX** are highlighted in gray. *d*) ^{1}H-^{1}H-COSY NMR spectrum of **XX** showing cross peaks for all eight paramagnetically shifted backbone signals (highlighted in gray) (both 2D-NMR spectra were recorded at −50 °C).

was estimated by inversion recovery to 15 ms, which was too fast for the available DOSY measurements. The unusually strongly shifted ^{31}P- and ^{1}H-NMR signals are most likely a result of significant spin-orbit coupling (SOC) of low-lying, yet isolated excited states into the ground state and the resulting temperature independent paramagnetism (TIP), analogous to the effects discussed in Section 3.1.2.

Even though the thermal instability of **XX** rendered its isolation impossible, after many attempts to crystallize the compound, single crystals suitable for X-ray diffraction measure-

ments could be obtained from diffusing pentane into a THF solution at −40 °C (see Figure 2.1).

The two independent Re centers are coordinated in a distorted square pyramidal coordination environment (τ_5(Re1) = 0.185 and τ_5(Re2) = 0.161)[196] with rather long Re–N_2 bonds (1.861(8) and 1.886(8) Å). The N≡N bond (1.202(10) Å) indicates slight activation of the dinitrogen moiety and the two {PNPReCl} fragments are twisted with respect to each other by 112.06 °, perfectly mirroring the structural features of the predicted structure in the first publication on this complex. The molecule co-crystallized with superimposed 0.5 molecules of **XIX** and **XXI** each, reflecting the presence of both in the *in situ* prepared solution, as indicated by $^{31}P\{^1H\}$-NMR spectroscopy (see Figure 2.1 a).

Despite dimeric complex **XX** is not being formed exclusively, once its formation has finished it seems to cleanly react to **XXI** (the byproducts of the dimer formation remain basically unchanged during formation of **XXI**, see Figure 2.1 *a*). Encouraged by this finding, a first effort was made to monitor the kinetics of this reaction by variable temperature nuclear magnetic resonance (VT-NMR) spectroscopy. Initial results indicated the reaction to proceed via a first-order reaction. Later, this analysis was finalized by *Richt van Alten*, confirming the reaction order and leading to values of $\Delta H^{\ddagger} = 100.4 \pm 4.1$ kJ mol^{-1} and $\Delta S^{\ddagger} = 59 \pm 13$ J mol^{-1} K^{-1}.[95]

Interestingly, it was noted before that in the synthesis of **XX**, using NaHg as a reductant gave much higher yields than Co(Cp*)$_2$, even though the reduction potential of the latter should be sufficient for quantitative reduction ($E_{1/2}$(Co(Cp)$_2$) = −1.84 V vs. Fc/Fc$^+$, $E_{1/2}$(**XIX**) = −1.90 V. A close analysis of the NMR spectra after reduction revealed a side product (**17**) corresponding to a $^{31}P\{^1H\}$-NMR signal at $\delta_{^{31}P}$ = 29.8 ppm which forms exclusively when Co(Cp*)$_2$ is used as a reductant but not with alkali metals. A higher yield in **17** can be obtained, if an excess of Co(Cp*)$_2$ is used and ^{1}H-NMR spectroscopy indicated a C_S-symmetric species bearing a hydride ($\delta_{^1H}$ = −9.28 ppm, t, $^2J_{HP}$ = 12.9 Hz). Furthermore, **17** is formed also in the absence of N_2 and requires two equivalents of reductant for quantitative conversion. All these observations are in agreement with the formation of the Re–H species [ReHCl(PNP^{tBu})] (**17**) (see Figure 2.2 *a*). The origin of the hydride can be explained considering the reported PCET reactivity of Co(Cp*)$_2$ forming [Co(Cp*)(C$_5$Me$_4$(CH$_2$))], even though the latter complex was not found in the NMR spectra.[198] **17** exhibits only limited stability, as it showed significant decomposition if stored for extended time (days) in solution. Nevertheless, X-ray structure determination was possible from single crystals grown from cold pentane. **17** exhibits a square-pyramidal coordination geometry (τ_5 = 0.022)[196] with the hydride in apical position. The Re–H bond distance is in agreement with a hydride ligand (d(Re–H) = 1.70(2)Å) and planar coordination of the backbone nitrogen indicates an intact amide ligand. Overall, the formation of **17** can explain the reduced yield of dinitrogen splitting utilizing Co(Cp*)$_2$, as it is the product of an off-pathway consuming two equivalents of reductant.

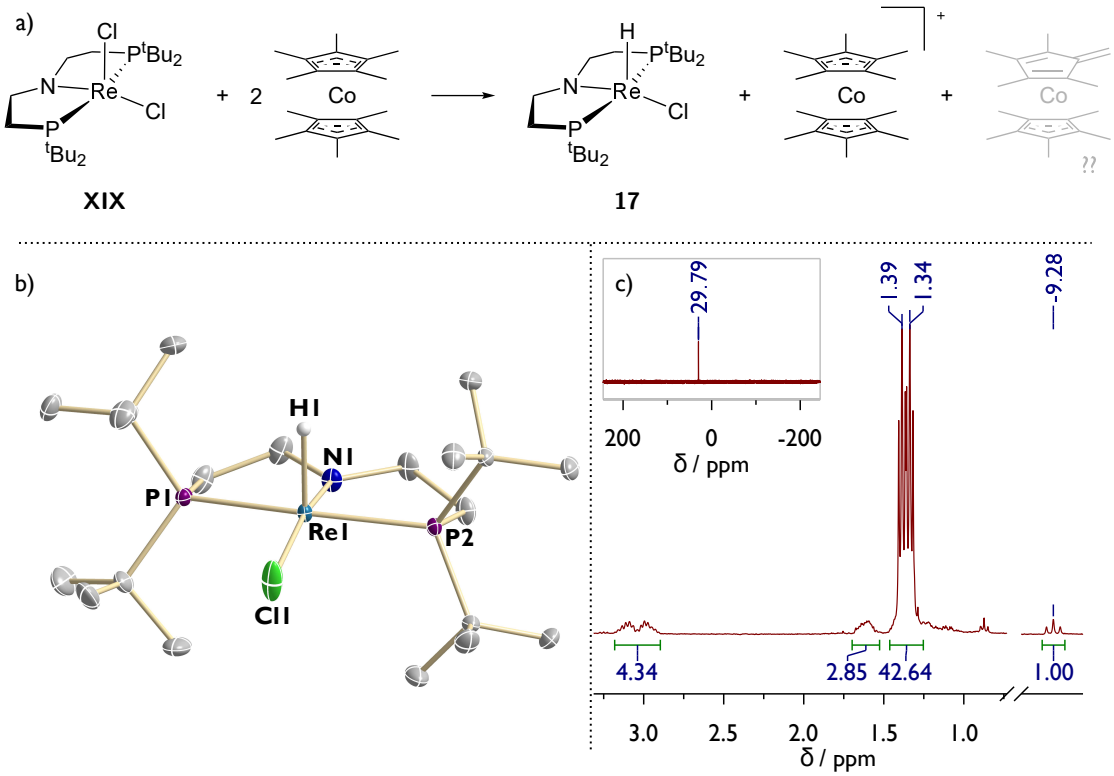

Fig. 2.2. *a*) Synthesis scheme for the formation of **17** by PCET reaction of **XIX** and $Co(Cp^*)_2$. *b*) Molecular structure of **17** obtained by single crystal X-ray diffraction measurements. All H-atoms despite the Re-H are omitted for clarity. Anisotropic displacement parameters are set to 50 % probability. The isotropically refined Re—H was found from the residual density map. Selected bond lengths [Å] and angles [°]: Re1-N1 1.9107(18), Re1-P1 2.3520(5), Re1-P2 2.3641(5), Re1-Cl1 2.3995(6), Re1-H1 1.70(2), P1-Re1-P2 165.963(18), N1-Re1-Cl1 167.33(6), Cl1-Re1-H1 93.6(8). *c*) ^{1}H-NMR spectrum of **17** showing the hydride resonance signal at -9.28 ppm. *Inset*: $^{31}P\{^1H\}$-NMR of **17**.

2.2 Intermolecular C-C coupling of $[Re(NCH_2)Cl(PNP^{tBu})]^+$ (**18**$^+$)

The first report of functionalization of **XXI** described methylation at the nitride with MeOTf yielding $[Re(NMe)Cl(PNP^{tBu})]^{OTf}$ (**16**^{OTf}).[94] In analogy to later reported nitrile formation after ethylation by sequential deprotonation and oxidation,[153] the release of cyanide from **16**^{OTf} could be imagined. However, it was found that after deprotonation to $[Re(NCH_2)Cl(PNP^{tBu})]$ (**18**), oxidation with AgOTf results in various compounds with the main product most likely being the dicationic product from intermolecular C—C coupling of of the ketimido CH_2 moieties, $[(N,N\text{—}C_2H_4N_2)\{ReCl(PNP^{tBu})\}_2]^{(OTf)_2}$ (**19**$^{(OTf)_2}$).[180] The appearance of several byproducts was attributed to chloride abstraction from **18** rather than mere oxidation. Thus, a much cleaner reaction was obtained after exchanging the chloride ligand in **18** with a methyl group to form **18**^{Me} and subsequent oxidation (see Scheme 2.2). Via this route single crystals suitable for molecular structure determination were obtained, confirming the suggested dinuclear nature of **19**$^{Me,\ (OTf)_2}$.

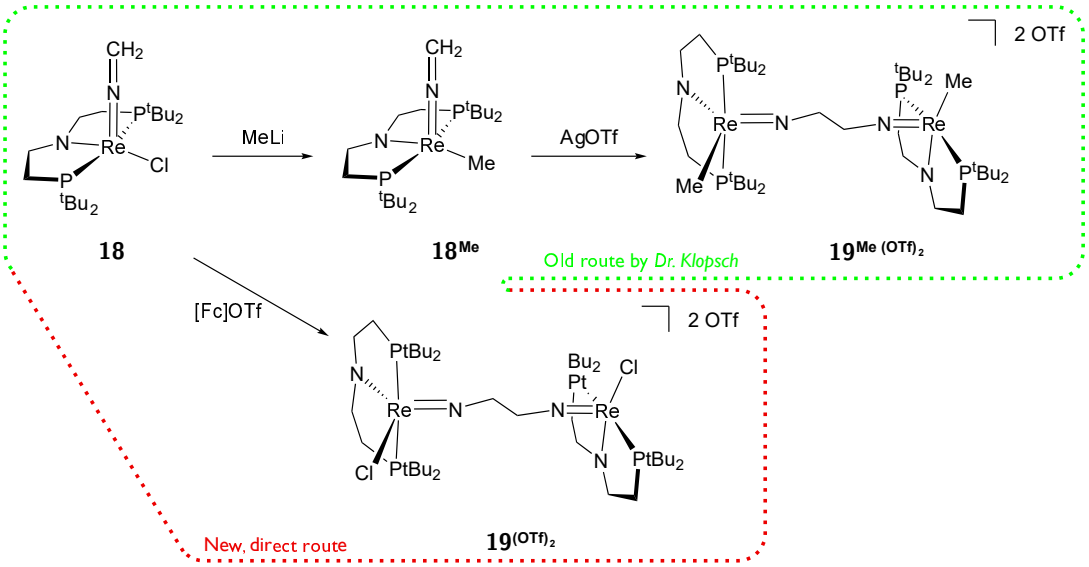

Scheme 2.2. Previously reported oxidative intermolecular coupling of ketimide complexes $\mathbf{18}^{\mathbf{Me}}$ with AgOTf and newly developed route directly from **18** with $[Fe(Cp)_2]^{OTf}$.

This radical coupling provides an interesting entry into new, N_2 derived organic molecules. To omit unnecessary steps, the initially explored reaction starting from chloro complex **18** was reinvestigated. Previous work suggested that the precipitation of AgCl likeley is a problem, therefore alternative pathways to the above described procedure were considered. Unfortunately, the most appealing approach, i.e. direct H atom abstraction from $\mathbf{16}^+$ rather than stepwise deprotonation and oxidation, did not give the wanted result (**16** stayed fully intact upon mixing with equimolar amounts of TTBP, even after gentle heating). Therefore, the use of oxidants other than silver salts was tried. CV data of **18** show a reversible oxidation wave at −0.50 V vs. Fc^+/Fc,[180] thus rendering ferrocenium salts suitable oxidants with much reduced tendency for salt exchange.

Oxidation with $[Fe(Cp)_2]PF_6$ in DCM showed already cleaner conversion to one major species which exhibits C_s symmetry on the NMR time scale and displays a singlet in $^{31}P\{^1H\}$-NMR at $\delta_{^{31}P} = 90.2$ ppm as well as in ^{1}H-NMR spectroscopy for the N−CH_2 group ($\delta_{^1H} = 3.31$ ppm, analog to $\mathbf{19}^{\mathbf{Me,\ (OTf)_2}}$). However, full conversion is not achieved and remarkably, $\mathbf{16}^+$ is obtained as side product, hinting to either an H^+ source prior to oxidation or the presence of an H atom donor. Changing the anion from PF_6^- to OTf^- and replacing DCM with Na/K dried THF finally resulted in analytically pure coupling product $\mathbf{19}^{\mathbf{(OTf)_2}}$ in 61 % isolated yield (see Section 2.2.3). Single crystals suitable for X-ray diffraction were obtained from layering a concentrated toluene solution with hexamethyldisiloxane (HMDSO) (see Figure 2.3).

The two independent Re centers are found in a distorted square pyramidal coordination environnment (τ_5(Re1) = 0.295 and τ_5(Re2) = 0.1475).[196] The Re−N_{imide} bonds are significantly shorter than in the parent ketimide complex **18** (d(Re−N) = 1.723(2) Å, 1.720(2) Å vs. 1.8365(16) Å in **18**) while the corresponding N−C bonds became much longer (d(N−C) = 1.448(3) Å, 1.441(3) Å vs. 1.248(3) Å in **18**). Combined with a now bent Re−N−C moi-

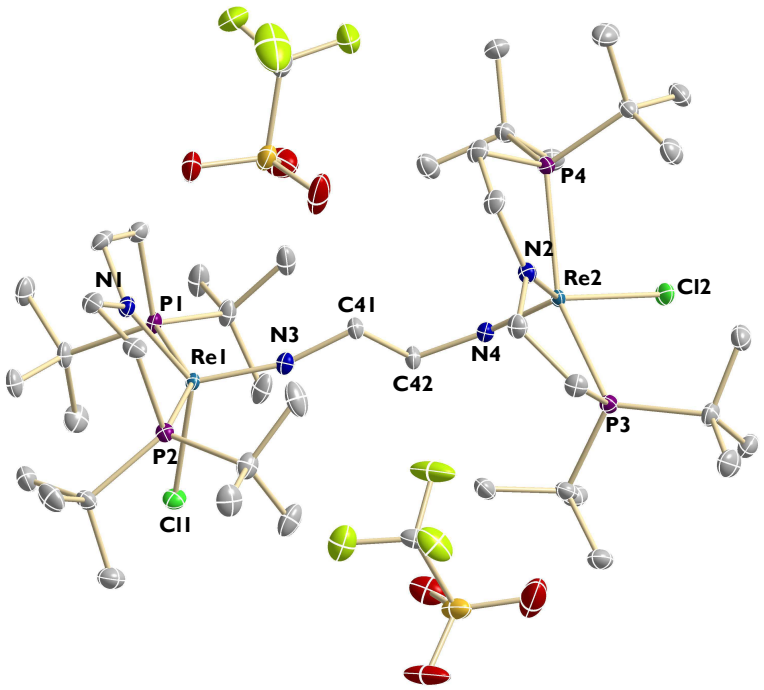

Fig. 2.3. Molecular structure of $\mathbf{19^{(OTf)_2}}$ obtained by single crystal X-ray diffraction measurements. H-atoms are omitted for clarity. Anisotropic displacement parameters are set to 50 % probability. Selected bond lengths [Å] and angles [°]: Re1-N1 1.942(2), Re1-N3 1.723(2), N3-C41 1.448(3), N1-Re1-N3 117.37(9), N1-Re1-Cl1 133.66(6), P1-Re1-P2 151.36(2), Re1-N3-C41 163.63(18), Re2-N2 1.9298(19), Re2-N4 1.720(2), N4-C42 1.441(3), N2-Re2-N4 110.31(9), N2-Re2-Cl2 140.61(6), P3-Re2-P4 149.46(2), Re2-N4-C42 160.24(17).

ety ($\measuredangle$(Re−N−C) = 163.63(18)°, 160.24(17)°vs. 172.56(16)°in **18**), all these parameters are in agreement with the formation of an imido ligand.

Adding stochiometric amounts of water to $\mathbf{19^{(OTf)_2}}$ did not result in a hydrolysis to the oxo complex $[Re(O)Cl(PNP^{tBu})]^+$ ($\mathbf{20^+}$) as confirmed by comparision with an authentic sample prepared by reaction of **XIX** with $NaBPh_4$ and Me_3NO (see Section 2.2.4). Instead, no reaction was observed, not even upon heating. On the other hand, reaction with base, especially with potassium bis(trimethylsilyl)amide (KHMDS), led to conversion. First, two new signals in $^{31}P\{^1H\}$-NMR were observed at $\delta_{^{31}P}$ = 69.5 ppm and 69.5 ppm, which were converted to a singlet at 84.2 ppm upon addition of more equivalents of base. However, the exact stochiometry of this reaction as well as the identity of the product are unknown.

While a new route to $\mathbf{19^{(OTf)_2}}$ has been developed and the complex is now synthetically accessible, further investigations concerning its follow-up chemistry and potential release of nitrogen containing organic molecules are still pending.

2.3 Effect of the backbone oxidation to the P=N=P platform

Part of this section has been published in: J. Becker, "Rhenium-vermittelte N_2-Funktionalisierung", *Bachelor thesis*, Georg-August-Universität Göttingen, **2017**.

2.3.1 Synthesis and dinitrogen splitting

The cycle for nitrile generation from N_2, mediated by **XIX**, requires a sequence of reductive (for N_2 splitting) and oxidative (for N_2 functionalization) steps. Thus, its realization can be envisioned by means of electrochemistry, where both conditions can be applied simultaneously without the redox agents reacting with each other. However, such an approach would require the {Re(PNP)} fragment to be rugged towards reductive and oxidative conditions. While no {PNP} decomposition has been observed even with very harsh reductants such as KC_8, previous experiments indicated ligand backbone oxidation to be a viable side reaction under certain conditions. Hence, the backbone oxidized complex [$ReCl_2$(P=N=P^{tBu})] (**21**) (P=N=P^{tBu} = {N(CHCHP*t*Bu_2)$_2$}$^-$) was synthesized according to previous developed procedures[180] as an attempt to harden **XIX** towards oxidative conditions, and its behavior in N_2 activation and functionalization was investigated.

Stirring **XIX** with excess TTBP at 50 °C in benzene resulted in formation of **21**. A paramagnetic side product which most likely results from over-oxidation to Re(IV) center could be converted to the desired product by addition of small quantities of $Co(Cp)_2$. **21** could be isolated in analytical purity after sublimation of the formed phenol and excess $Co(Cp)_2$ in 63 % isolated yield (see Scheme 2.3).

NMR spectroscopic investigation show that **21** exhibits a C_{2v} symmetry on the NMR timescale with a backbone signal pattern characteristic for the fully oxidized ligand.[195,199,200] Especially the downfield shift of the CH group next to the amide as well as the peak separation $\Delta\delta > 2$ ppm of the α- and β-protons are typical of vinylamines[201] and characteristic

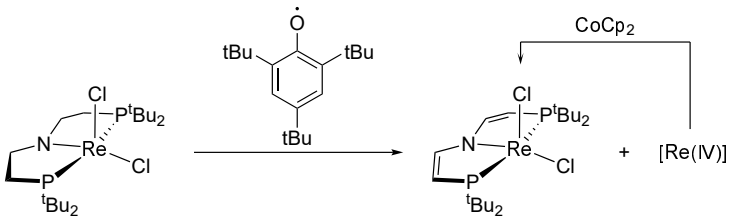

XIX **21**

Scheme 2.3. Synthesis of [$ReCl_2$(P=N=P^{tBu})] (**21**).

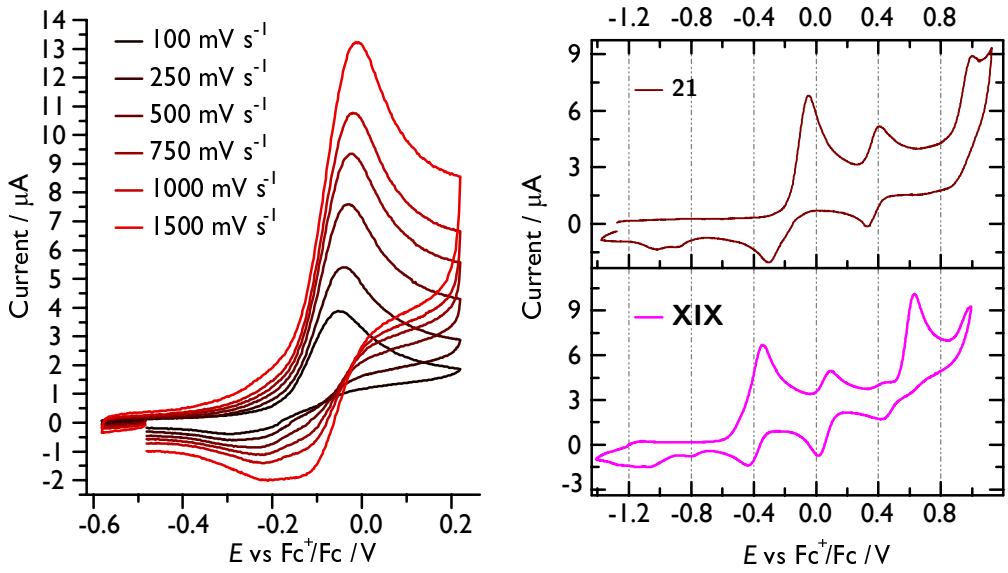

Fig. 2.4. *Left*: CV measurements of Re(IV/III) oxidation of **21** at various scan rates. *Right*: Comparison of the anodic region of **XIX** (*bottom*) and **21** (*top*) at 100 mV s^{-1}. All spectra are recorded in THF with 10^{-3} M complex, 0.1 M $N^nBu_4PF_6$, working electrode (WE): glassy carbon (GC), reference electrode (RE): Ag-wire, counter electrode (CE): Pt-wire.

for this ligand. Notably, the $^{31}P\{^1H\}$-NMR spectrum shows a tremendous high field shift of the resonance peak to $\delta_{^{31}P} = -275.6$ ppm. Again, this shift is most likely a result TIP (see Section 3.1.2 for a detailed discussion). Unfortunately, no single crystals suitable for X-ray structure determination could be obtained.

Closer investigation of the CV data of compounds **XIX** and **21** reveals very similar traces (see Figure 2.4 *right*). The first oxidation event is shifted anodically by almost 300 mV (**XIX**: $i_{p,a} = -0.34$ V vs. Fc^+/Fc; **21**: $i_{p,a} = -0.05$ V; both at 100 mV s^{-1}), in line with the reduced amide donor strength. Also the other two oxidation events are shifted in the same direction. However, while these results suggest increased stability of the complex towards oxidative conditions, it has to be noted that for **XIX**, the first oxidation wave is fully reversible, as long as the second event is not scanned as well. In contrast to this, the first oxidation event of **21** is irreversible even at higher scan rates, at least in the absence of an external chloride source (see Figure 2.4, *left*). So even though the potential of the first oxidation is indeed shifted anodically, in terms of chemical stability $\mathbf{21}^+$ must be considered *less* stable than $\mathbf{XIX}^+$, at least under the conditions of the CV experiments.

Nevertheless, investigations concerning the N_2 cleavage and functionalization capabilities of **21** were investigated to see if the modified ligand backbone has a significant influence in this field. Chemical reduction with $Co(Cp^*)_2$ under N_2 atmosphere leads to formation of a mixture of products, as indicated by $^{31}P\{^1H\}$ and ^1H-NMR spectroscopy. In this mixture, the Re(V) nitrido species [Re(N)Cl(P=N=P^{tBu})] (**22**) could be identified in approx. 60 % spectroscopic yield, based on comparison with an authentic sample prepared in analytical purity by the reaction of **21** with 5 eq $(Me_3Si)N_3$ in 72 % yield (see Figure 2.5 a). Furthermore, LIFDI mass spectra of the reaction mixture confirmed formation of nitrido complex **22**. **22**

resonates at $\delta_{^{31}P} = 71.8$ ppm in the $^{31}P\{^{1}H\}$-NMR spectrum and exhibits C_S symmetry in the ^{1}H NMR.

Single crystals suitable for X-ray diffraction measurements were obtained (see Figure 2.5 *c*). The Re(V) center is coordinated in a slightly distorted square-pyramidal geometry with the nitrido ligand in the apical position ($\tau_5 = 0.15$).[196] The Re≡N bond length (d(Re-N2) = 1.647(18) Å) lies in a typical range of a metal-nitrogen triple bonds and is in very good agreement with the DFT-optimized structure of parent [Re(N)Cl(PNP$^{t\text{Bu}}$)] (**XXI**) (d(Re-N)$_{\text{DFT}}$ = 1.65 Å; unfortunately no X-ray structure of that complex is available). Additionally, the flat ligand backbone and short C–C distances (d(C1-C2) = 1.35(2) Å) show the vinyl moiety to be still intact.

While the occurance of dinitrogen splitting from **21** is not too surprising, given its similarity with **XIX**, it still is only the second example ever reported of a rhenium complex capable of this reaction.

The observed anodic shift of redox events in **21** attributed to the less donating ligand motivated an investigation of the electrochemical properties of **22** to see if this effect also makes the Re(V/IV) redox couple accessible (see Figure 2.6). CV measurements revealed a reversible Re(V/VI) oxidation at $E_{1/2} = +0.21$ V vs. Fc/Fc^{+} which is significantly anodically

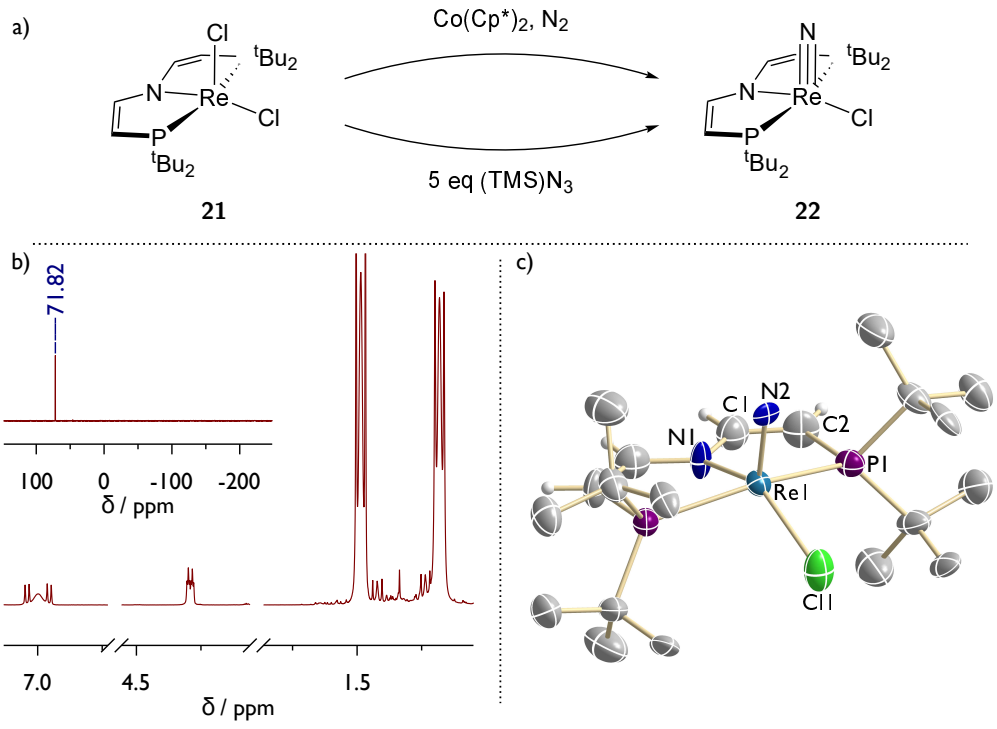

Fig. 2.5. *a*) Synthesis scheme for **22** via N_2 splitting or TMS azide as nitrogen source. *b*) ^{1}H-NMR spectrum of **22** (*inset*: $^{31}P\{^{1}H\}$-NMR spectrum). *c*) Molecular structure of **22** obtained by single crystal X-ray diffraction measurements. Selected H atoms are omitted for clarity. Anisotropic displacement parameters are set to 50 % probability. Selected bond lengths [Å] and angles [°]: Re1-N1 2.106(13), Re1-N2 1.647(18), Re1-Cl1 2.395(7), C1-C2 1.35(2), N1-Re1-N2 109.2(5), P1-Re1-P1# 155.11(13), N1-Re1-Cl1 145.9(2).

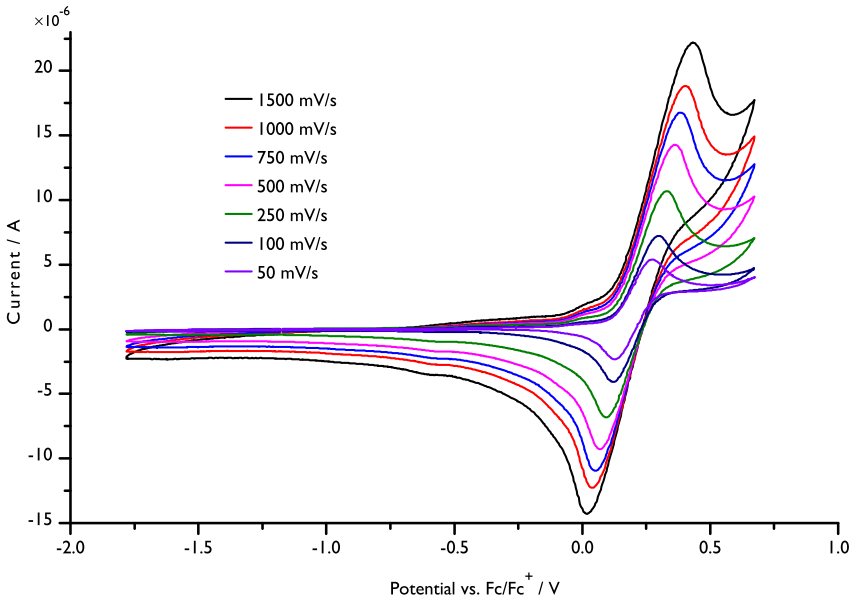

Fig. 2.6. CV measurements of **22** in THF at different scan rates (10^{-3} M **22**, 0.1 M $N^nBu_4PF_6$, WE: GC, RE: Ag-wire, CE: Pt-wire).

shifted with regard to the parent nitride ($E_{1/2}$(**XXI**) $= -0.09$ V).[180] Unfortunately, no reduction event occurs until potentials as negative as $E_{p,c} = -3.3$ V. Thus, the reduced π-donation of the ligand does *not* provide and entry into reductive nitride functionalization.

2.3.2 Nitride functionalization

In order to increase the electrophilic character of **22**, its reactivity towards acids was investigated. Introducing a cationic charge should facilitate reduction of the nitrido complex and could therefore open up a route to ammonia synthesis following well known stepwise protonation and reduction schemes. Reacting nitride complex **22** with 1 eq of HOTf or $HBAr^F_{24}$ ($HBAr^F_{24} = H(OEt_2)_2[B\{_{4,5}\text{-}(CF_3)_2C_6H_3\}_4]$) leads to clean and selective formation of the monoprotonated complex $[Re(N)Cl(P^H{=}N{=}P^{tBu})]^X$ (**23**^{X}) with **X** being the resulting anions from the acids ($P^H{=}N{=}P^{tBu} = \{^-N(CHCH_2PtBu_2)(CHCHPtBu_2)\}$). The protonation of one vinylidene moiety of the pincer breaks the symmetry of the complex, leading to the formation of two doublets in $^{31}P\{^1H\}$-NMR at $\delta_{^{31}P} = 70.0$ and 73.0 ppm, respectively, with a mutual coupling constant of $^2J_{PP} = 148.1$ Hz (see Figure 2.7). ^{1}H NMR shows five resonances of CH protons between $\delta_{^1H} = 9.5$ and 3.5 ppm, with a large coupling constant of $^2J_{HH} = 21.3$ Hz between the protons of the CH_2 group. In CV measurements, **23** again exhibits a reversible oxidation wave at $E_{1/2} = +0.24$ V vs. Fc/Fc^+, suggesting that the oxidation is metal centered and thus not affected by the ligand centered protonation. At potentials below -2.0 V, a new reduction feature appears. However, the slope of the wave is rather shallow and resembles the appearance of proton reduction waves of organic

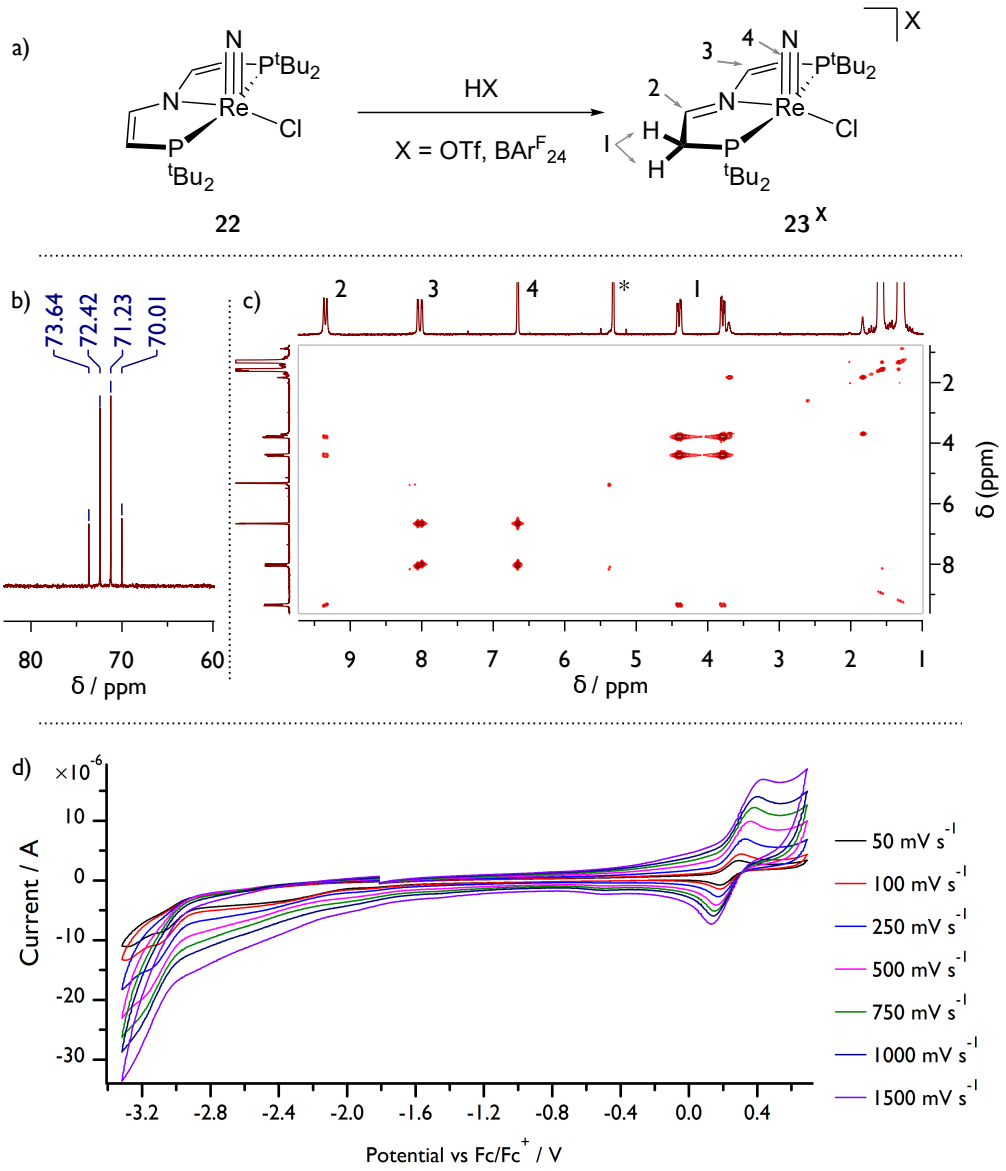

Fig. 2.7. *a*) Synthesis scheme for **23^{OTf}** via protonation of **22**. *b*) $^{31}P\{^1H\}$ NMR spectrum of **23^{OTf}**. *c*) ^1H-^1H COSY showing the coupling between the five backbone protons and allow for full assignment (in combination with other 2D-techniques). Solvent signals are marked with an asterisk. *d*) CV measurements of **23^{OTf}** in THF at different scan rates (10^{-3} M **23^{OTf}**, 0.1 M N^{n}Bu$_4$PF$_6$, WE: GC, RE: Ag-wire, CE: Pt-wire).

acids. Therefore, protonation to **23^X** did not yield the desired effects and the approach was abandoned.

As can be suggested from the electrochemical investigations, the very negative potential for reduction of **22** is reflected in its inertness towards electron donating reagents. All attempted reactions with nucleophiles like Me_3NO, PMe_3, alkenes, as well as CO gave no detectable conversion, not even at elevated temperatures. Again, this behavior is completely analogous to parent nitride **XXI**.

Following this similarity, C–N bond formation on **22** was achieved by methylation with

strongly electrophilic MeOTf. Stirring in chlorobenzene at 60 °C gave analytically pure [Re(NMe)Cl(P=N=P$^{t\mathrm{Bu}}$)]$^{\mathrm{OTf}}$ (**24$^{\mathbf{OTf}}$**) in 80.5 % yield. **24** retains a C_S symmetry on the NMR timescale and resonates at $\delta_{^{31}\mathrm{P}}$ = 88.8 ppm in ^{31}P{^{1}H}-NMR spectroscopy. *N*-Methylation was confirmed by ^{1}H-^{1}H NOESY where a cross peak appeared solely between the methyl group (singlet at $\delta_{^1\mathrm{H}}$ = 2.70 ppm) and one *tert*-butyl group, but not with the backbone protons (see Figure 2.8 *c*). Unfortunately, no single crystals suitable for an X-ray structure determination could be obtained, despite several attempts.

Deprotonation of **24$^{\mathbf{OTf}}$** with NEt_3 gave spectroscopically almost pure ketimido complex [Re(N=CH$_2$)Cl(P=N=P$^{t\mathrm{Bu}}$)] (**25**) in approximately 50 % yield after workup. Attempts with stronger bases like KO^{t}Bu or KHMDS gave either decomposition in the former, or formation of non-separable side products in the latter case. **25** exhibits a single resonance in ^{31}P{^{1}H}-NMR and displays C_S symmetry in the ^{1}H-NMR spectrum. The two ketimido protons could be identified by ^{1}H-^{13}C heteronuclear single quantum coherence (HSQC) spectroscopy as two broad singlets at $\delta_{^1\mathrm{H}}$ = 1.74 and 1.63 ppm, indicating the rotation around the Re=N=C moiety to be hindered at RT (see Figure 2.8).

Interestingly, in both complexes **24$^{\mathbf{OTf}}$** and **25**, the more highfield shifted ^{1}H NMR signal belonging to a *tert*-butyl group is significantly broadened (see Figure 2.8 *b* ($\delta_{^1\mathrm{H}}$ = 1.29 ppm) for **24$^{\mathbf{OTf}}$** and *d* ($\delta_{^1\mathrm{H}}$ = 1.25 ppm) for **25**). VT-NMR spectra indicate this effect to be due to dynamic behavior in solution, however, the nature of these dynamics is not yet understood and will need further investigation. Given the so far observed similarity between the alkyl and vinyl based pincer systems, no further investigation of **25** or its follow-up reactivity was conducted. Nitrile release as observed after alkylation of **XXI** can be considered rather likely and would only be of interest if this reaction could be achieved electrochemically (following the previously proposed scheme of fully electrochemially driven dinitrogen splitting and functionalization).

Apart from the described C–N bond formation, the well defined and apparently reversible oxidation of **22** to a Re(VI) stage rendered redox chemistry a promising approach to further functionalize the N_2 derived nitride. Oxidation could in theory alter the nitride centered reactivity from nucleophilic (but only towards very harsh reagents) to become rather electrophilic. Initial DFT calculations of neutral **22** and its monooxidized analogue **26$^+$** revealed very little change in structural parameters (root-mean-square deviation (of atomic positions) (RMSD) = 0.042, also: see Figure 2.9 *c*).[1] Furthermore, an NBO analysis indicated a slightly decreased population at the nitride (**22**: 7.40 e$^-$, **26$^+$**: 7.32 e$^-$) and a reduced Wiberg bond order (**22**: 2.52, **26$^+$**: 2.47). These results encouraged the actual synthesis of the monooxidized nitride complex.

Mixing of **22** with 1 eq $AgSbF_6$ in THF results in immediate color change to deep red. Full conversion of the starting material, clearly evident by ^{31}P{^{1}H} NMR spectroscopy, is accompanied by the formation of a very broad, paramagnetic peak in ^{1}H NMR spectrum between $\delta_{^1\mathrm{H}}$ = 7-1 ppm, indicating the formation of $S = 1/2$ compound [Re(N)Cl(P=N=P$^{t\mathrm{Bu}}$)]$^{\mathbf{SbF_6}}$

[1] The RMSD value was calculated by using the ChemCraft software package.

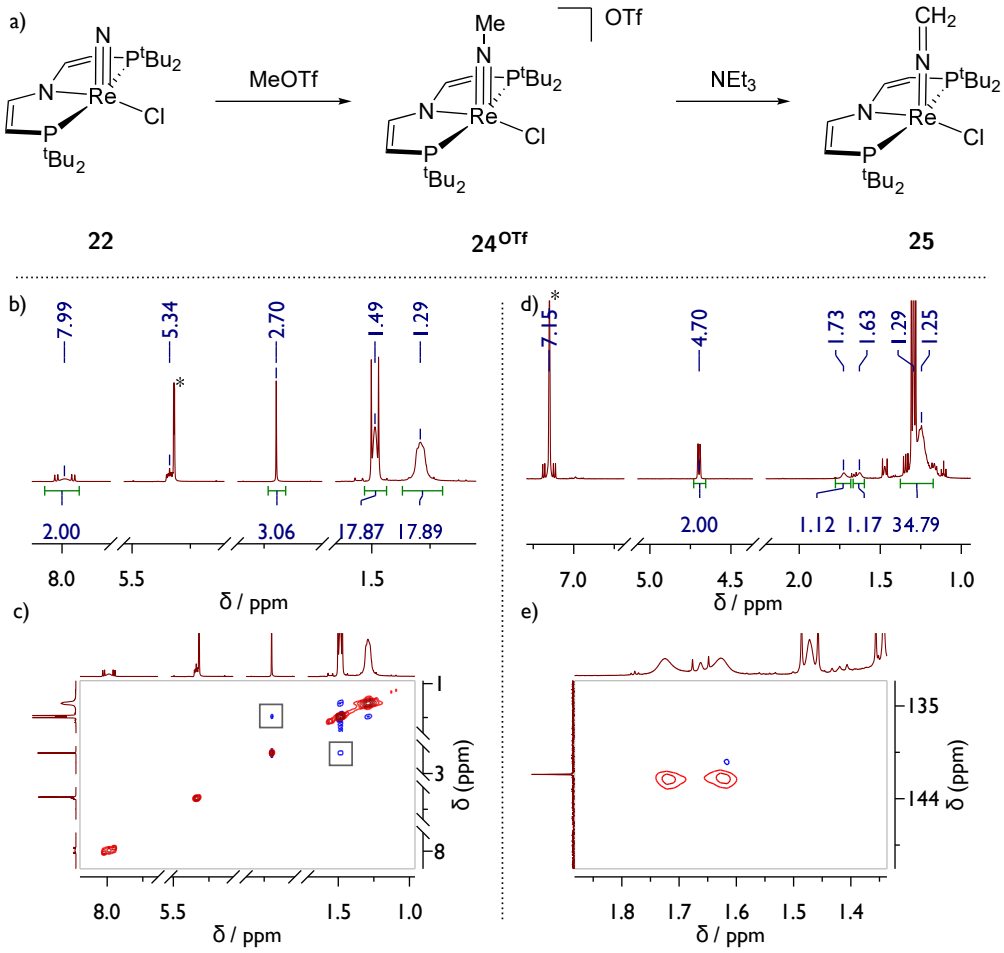

Fig. 2.8. *a*) Synthesis scheme for alkylation of **22** with MeOTf to $\mathbf{24^{OTf}}$ and subsequent deprotonation to **25**. *b*) ^{1}H-NMR spectrum of $\mathbf{24^{OTf}}$ in CD_2Cl_2 (solvent signal - marked with an asterisk - is overlapping with one backbone signal). *c*) ^{1}H-^{1}H NOESY of $\mathbf{24^{OTf}}$ showing cross-peaks between the methyl group with only one *tert*-butyl group. *d*) ^{1}H NMR spectrum of **25** (solvent signal - marked with an asterisk - is overlapping with one backbone signal). For readability, spectral regions without compound signals are not shown. *d*) ^{1}H-^{13}C HSQC spectrum of **25** identifying the two broadened protons of the CH_2 group.

($\mathbf{26^{SbF_6}}$). Unfortunately, minor amounts of monoprotonated nitride $\mathbf{23^{+}}$ are formed as a side-product which could not be separated from the product due to very similar solubility behavior. This probably indicates impurities in the oxidant which thus requires further purification before usage. While further analytics are still pending and the protic impurity $\mathbf{23^{+}}$ prevented detailed studies of the reactivity of $\mathbf{26^{SbF_6}}$ towards nucleophiles, the formation of the target molecule is rather likely and the stability of the solution was confirmed by ^{1}H NMR spectroscopy over several days, substantiating the previous findings from CV measurements. Hence, future investigation of this pathway could be of interest for modifying and extending the range of possible functionalization schemes for dinitrogen derived rhenium nitrides.

Overall, it could be shown, that the vinyl based pincer ligand exhibits basically identical reactivity compared with its parent alkyl counterpart. Reductive N_2 activation and splitting with chemical reductants seems to proceed with comparable efficiency for PNP based **XIX**

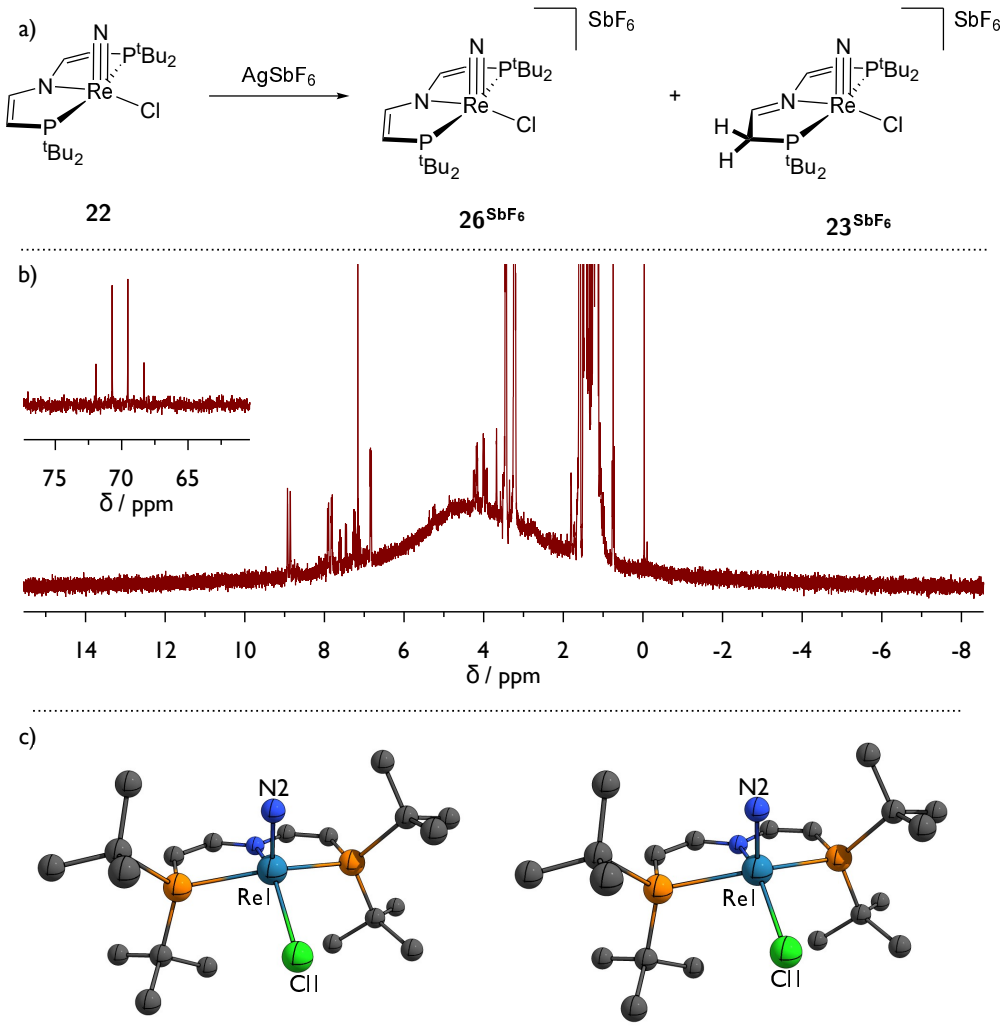

Fig. 2.9. *a*) Synthesis of **26**^{SbF_6} with minor formation of **23**^{SbF_6}. *b* ^{1}H NMR spectrum of **26**^{SbF_6}. *Inset*: ^{31}P$\{^1$H$\}$ NMR showing the signal of **23**^{SbF_6}. *c*) DFT (RI-PBE|D3BJ|def2-SVP) optimized gas phase structures of **22** (left) and **26**$^+$ (right) with the following structural parameters: **22**: Re1-N2 1.664 Å, Re1-Cl1 2.434 Å, τ_5 0.15. **26**: Re1-N2 1.661 Å, Re1-Cl1 2.321 Å, τ_5 0.06.

and P=N=P based **21**, although the former was shown to be more efficient with alkali metals, whereas the latter works better with Co(Cp*)$_2$. The hypothesis of increased electrophilic reactivity of the resulting nitride **22** due to reduced electron donations of the pincer amide could not be confirmed. Rather, the only successful functionalization at the nitride was achieved by using highly reactive MeOTf, just as it was known for parent **XXI**, while protonation occured at the pincer backbone. Subsequent deprotonation of the methylated complex to form the ketimido complex **25** provided access to a platform, from which electrochemical oxidative nitrile release might be explored. However, investigation of such reactions will need to be part of a following project. Finally, first experimental evidence on a fully reversible chemical oxidation of **22** to its monocationic Re(VI) stage were gathered, pointing to stable and potentially isolable complex **26**$^+$, which could open interesting alternatives in the accessible nitride functionalization schemes.

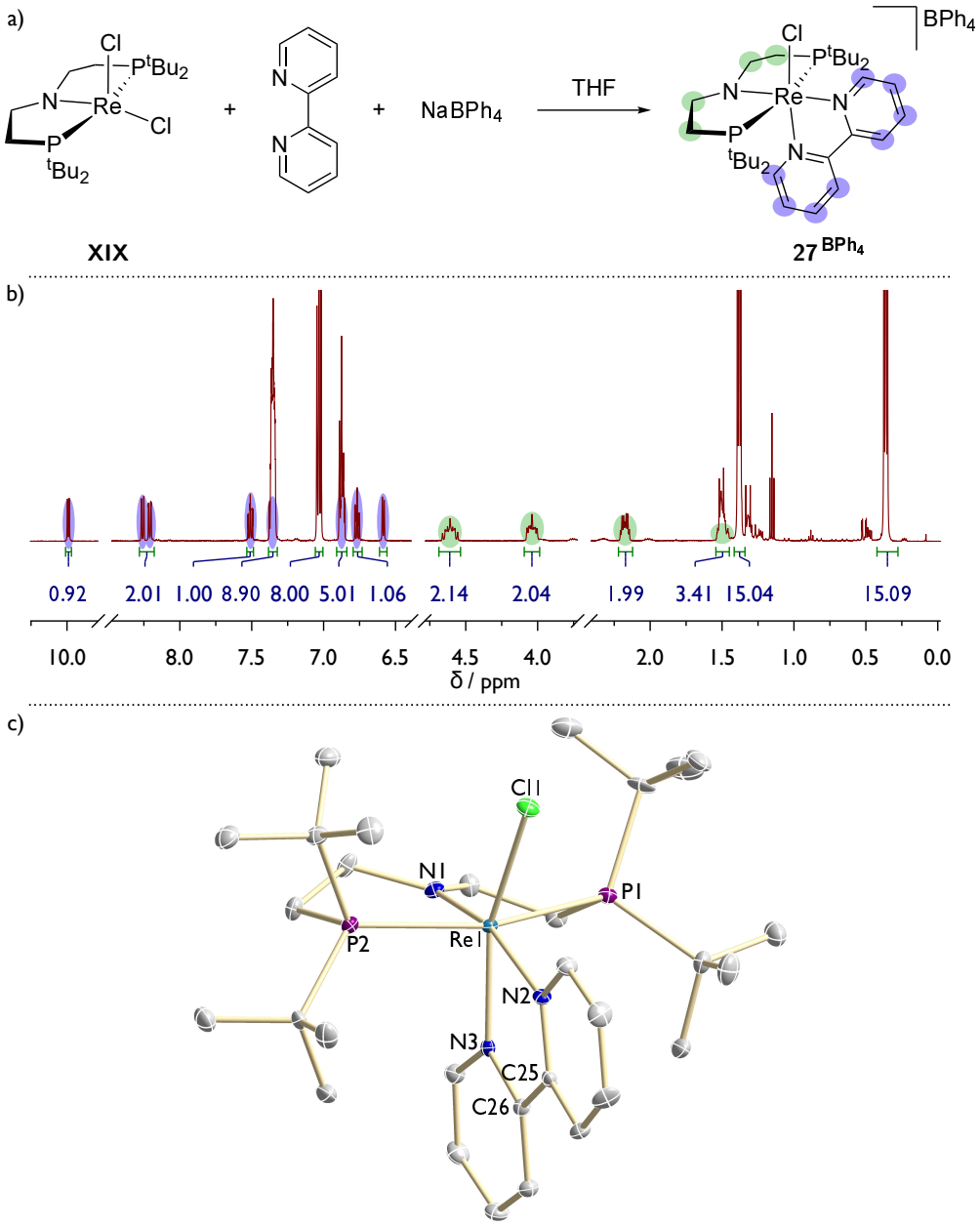

Fig. 2.10. *a*) Synthesis of 2,2'-bipyridine (bipy) complex **27**^{BPh_4}. *b*) ^{1}H NMR spectrum of **27**^{BPh_4} in CD_2Cl_2. Aromatic signals belonging to the bipy ligand are marked in violet (partially overlapping with those of the anion), signals of the pincer backbone are marked in green. *c*) Molecular structure of **27**^{BPh_4} obtained by single crystal X-ray diffraction measurements. H atoms, a cocrystallized solvent molecule and the anion are omitted for clarity. Anisotropic displacement parameters are set to 50 % probability. Selected bond lengths [Å] and angles [°]: Re1-N1 1.911(3), Re1-N2 2.185(3), Re1-N3 2.096(3), Re1-Cl1 2.3781, P1-Re1-P2 161.21(3), Cl1-Re1-N3 159.14(7), N1-Re1-N2 165.54(10), N2-C25-C26-N3 -4.1(4).

2.4 Ligand exchange reactions from [$ReCl_2(PNP^{tBu})$]

The non-reducability of the rhenium nitride complexes with both the saturated and the unsaturated ligand backbone (**XXI** and **22** respectively) necessitated the incorporation of other strategies to facilitate electron-storage on these complexes. A well-known approach to circumvent this problem is the usage of redox non-innocent ligands which can serve as an electron-reservoir upon reduction. A possible reaction could include reduction of the complex with the non-innocent ligand being the electron acceptor side, subsequent protonation and formation of a parent imide in an overall PCET type reaction. bipy is a workhorse in this type of chemistry and previously been successfully employed in our group by *Josh Abbenseth*. Stirring of [$ReCl_2(PNP^{tBu})$] (**XIX**) with 1 eq bipy and $Na(BPh_4)$ in THF at 60 °C overnight resulted in formation of a new, deep red complex which exhibits C_S symmetry on the NMR timescale and does not dissolve in pentane or Et_2O anymore, unlike the starting complex, indicating the formation of a cationic complex. Full NMR analysis as well as LIFDI mass spectrometry identified the new complex to be $[Re(bipy)Cl(PNP^{tBu})]^{BPh_4}$ (**27^{BPh_4}**) (see Figure 2.10). A characteristic feature is a significant high-field shift of one of the *tert*-butyl groups in the complex, due to the aromatic ring current in the bipy moiety ($\delta_{^1H}$ = 0.36 ppm, see Figure 2.10). Crystals suitable for X-ray structure analysis could be obtained from THF/Et_2O diffusion. The Re center is coordinated octahedrally by the two nitrogen donors of the bipy ligand, the PNP pincer and the chloride. The amide nature of the pincer nitrogen donor can be verified by its planar coordination G($\Sigma(\measuredangle_{N1}) = 359.9°$) and the bipy ligand is coordinated perpendicular to the pincer with both aromatic rings being coplanar ($\phi_{N2-C25-C26-N3} = -4.1(4)°$).

Unfortunately, attempts to reduce the complex with NaHg under N_2 atmosphere did not lead to the selective formation of one new compound, as would be expected from dinitrogen splitting. Instead, two new diamagnetic species are formed, as indicated by $^{31}P\{^1H\}$-NMR signals at $\delta_{^{31}P}$ = 49.9 ppm (singlet) and 32.7 / 26.5 ppm (two doublets, $^2J^{PP}$ = 206.3 Hz). Reduction of **27^{BPh_4}** under Ar gave rather selectively one diamagnetic product, potentially bearing a hydride ligand as indicated by a triplet in the ^1H-NMR spectrum at $\delta_{^1H}$ = 4.56 ppm ($^2J_{HP}$ = 17.9 Hz). These two distinctly different results indicate N_2 to take part in the reaction. No further investigation of the reaction was performed during this thesis, but if splitting is actually possible, the platform could offer an entry into reductive functionalization of a Re(V) nitride.

2.5 Summary

In previous work the rhenium complex [$ReCl_2(PNP^{tBu})$] (**XIX**) was shown to be a versatile platform for N_2 activation and functionalization reactions. Based on this finding, several

variations and extensions of the known research were added, in order to broaden the understanding as well as the applications of this system.

Importantly, the dimeric, μ-N_2 bridged Re-complex **XX** resulting from reduction of **XIX** under N_2 atmosphere could be characterized spectroscopically to large extends as well as by X-ray structure analysis. The clean thermal conversion of **XX** to nitrido complex [Re(N)Cl(PNP^{tBu})] (**XXI**) was proven by means of NMR spectroscopy and following this process at various temperatures allowed for a fist estimation of activation parameters to $\Delta H^{\ddagger} \approx 110\,\mathrm{kJ\,mol^{-1}}$, which is in reasonable agreement with the originally published DFT calculated barrier of $\Delta H^{\ddagger} = 84.4\,\mathrm{kJ\,mol^{-1}}$.[94]
Additionally the hydride complex [ReHCl(PNP^{tBu})] (**17**) could be identified and characterized as a side product of the reduction of **XIX** with Co(Cp*)$_2$, serving as an explanation for the experimentally observed reduced yield of **XXI** when using this reductant.

Furthermore, the oxidative C–C coupling of ketimido complex [Re(NCH$_2$)Cl(PNP^{tBu})] (**18**) which was proposed by *Dr. Isabel Klopsch* was developed into a clean and reproducable reaction and the product could be isolated and fully characterized. Even though no continuative reactions were investigated, this coupling opens a route to new, nitrogen containing organic molecules as well as odd-electron nitride functionalization schemes and should thus be followed more thoroughly in the future.

With this latter reaction as well as the known, oxidative nitrile release reactions from [Re(NR)Cl(PNP^{tBu})]$^+$ (R = Et, Bn) in mind, the vinylamido congener of **XIX**, i.e. [ReCl$_2$(P=N=P^{tBu})] (**21**) was synthesized and investigated towards N_2 functionalization reactions. CV data suggest a only slightly increased stability of **21** in comparison with parent **XIX**, but successful N_2 splitting encouraged further investigation of its functionalization capabilities. Overall, the vinylamido PNP pincer based system turned out to exhibit very similar reactivity to the alkyl based pincer, with hardly any differences in redox chemistry, stability, N_2 activation and splitting behavior or nucleophilicity of the corresponding nitrido complexes. Thus, the products of protonation (with H(OEt$_2$)$_2$(BAr$^F_{24}$)), methylation (with MeOTf) and oxidation (with Ag(SbF$_6$)) were investigated and the resulting products were characterized (despite the oxidized nitride **26^{SbF_6}**). By doing so, a promising starting point for further investigation of potential electrochemical functionalization pathways, where oxidative and reductive conditions can be applied simultaneously to a reaction mixture, was developed.

Finally, the non-reducability of the Re(V) nitrido complexes **XXI** and **22** was addressed by an attempt to introduce the potentially redox non-innocent ligand 2,2'-bipyridine. The complex [Re(bipy)Cl(PNP^{tBu})]^{BPh_4} (**27^{BPh_4}**) was successfully synthesized and characterized. Preliminary experiments revealed it to reaction to different products upon reduction under Ar or N_2. Investigations concerning the identification of the resulting products are still pending.

3

Rhenium complexes of *iso*-propyl based PNP pincer ligands for dinitrogen activation

> *All we need is lightning,*
> *With power and might*
>
> — **Lordi**
> "Hard Rock Halleluja" on "The Arockalypse"

Parts of this chapter (Section 3.1.1 and well as major parts of Section 3.3) have been published in: F. Schendzielorz, M. Finger, J. Abbenseth, C. Würtele, V. Krewald, S. Schneider, "Metal-Ligand Cooperative Synthesis of Benzonitrile by Electrochemical Reduction and Photolytic Splitting of Dinitrogen", *Angew. Chem. Int. Ed.* **2019**, *58*, 830-834.

Successful [$ReCl_2(PNP^{tBu})$] (**XIX**) mediated synthesis of organic nitriles from dinitrogen (see Part I Scheme 4.5 and corresponding section) inspired further research to improve the system. One of the major drawbacks of this conversion is the need to work with strong, alkali metal based reductants as well as strong oxidants like Ag salts or NCS. Additionally, highly reactive electrophiles are necessary (i.e. alkyl triflates) to obtain any nitride centered functionalization. This implies non-compatible reaction conditions, preventing one pot mixtures and therefore rendering catalytic turnover of such a system very unlikely.
Consequently, new ways to tune the properties responsible for these reaction requirements are needed. One option to potentially increase the nucleophilicity of the nitride and thus enhance its reactivity towards weaker electrophiles is indicated by DFT calculations (see Figure 3.1). If the splitting of the N_2 bridged dimer [$(\mu\text{-}N_2)\{ReCl(PNP^{tBu})\}_2$] (**XX**) is computed, it is found to proceed via a modest transition state (which rendered the spectroscopic observation of this dimer possible, see Section 2.1) and results in the strongly exergonic splitting product [$Re(N)Cl(PNP^{tBu})$] (**XXI**) (ΔG^0 = -98.3 kJ mol^{-1}). In this reaction the very strong N≡N triple bond is exchanged with two very strong Re≡N triple bonds, eventually leading to an overstabilization of the reaction product. From this thermodynamic sink, harsh reaction conditions are needed to obtain nitride centered reactivity, which is also commonly observed in other systems and can therefore be regarded as a general problem.[16] However, if the steric bulk of the ligand is reduced *in silico* by exchanging the *tert*-butyl residues with methyl groups, this has a major impact on the calculated thermodynamics of the reaction.

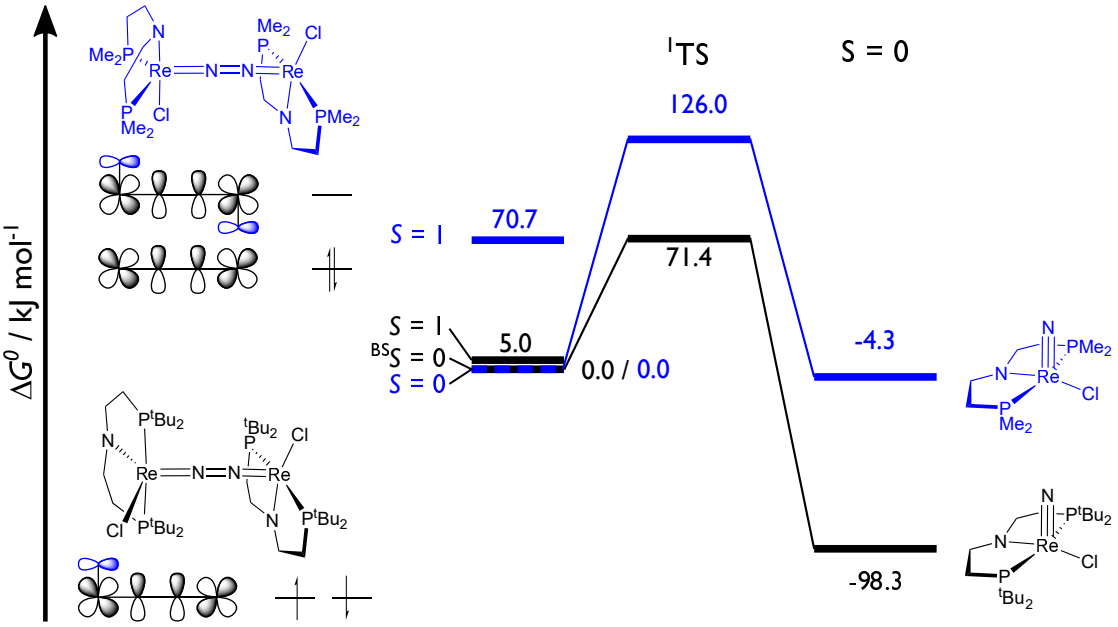

Fig. 3.1. Comparison of the DFT computed thermal dinitrogen splitting from **XX** (*black*) with *in silico* simulated **28** (*blue*) into the corresponding nitrido complexes (PBE/D3BJ/RI/def2-TZVP||PBE/D3BJ/RI/def2-SV(P)).[1]

On the one hand, in the ground state geometry one {ReCl(PNP^{Me})} fragment is found to be rotated by 90° with respect to the *tert*-butyl analog, accompanied by a change from a broken symmetry open shell singlet $^{BS}S = 0$ in **XX** to a closed shell singlet $S = 0$ in the methyl-PNP based dimer [(μ-N$_2$){ReCl(PNP^{Me})}$_2$] (**28**). This change in electronic structure can be understood considering the MO scheme of **XX** (also see Scheme 2.1). The rotation of the pincer results in the amido donor interacting solely with one of the orthogonal sets of π orbitals, thereby lifting their degeneracy and stabilizing the $S = 0$ state as ground state. On the other hand, splitting now results in an almost thermoneutral nitride ($\Delta G^0 = -4.3\,\text{kJ mol}^{-1}$) which can be expected to be more reactive than in the *tert*-butyl substituted system. At the same time, the kinetic barrier for the splitting is computed to become much higher, which should lead to a more stable, potentially isolable dimer.
Based on these results, reducing the steric bulk of the pincer ligand seemed to be a promising approach to increase the reactivity of the N$_2$ derived nitride complex. For this, changing to the *iso*-propyl based pincer HPNP^{iPr} was favored over HPNP^{Me}, because it is already significantly smaller than the *tert*-butyl based ligand but unlike the latter can still shield the metal center to some degree, preventing potentially unwanted side-reactions (*Tolman* cone angles: $\Theta_{P(^tBu)_2Et} = 165°$, $\Theta_{P(^iPr)_2Et} = 151°$, $\Theta_{P(Me)_2Et} = 123°$).[202]

In this chapter, the synthesis and chemistry of rhenium complexes with the *iso*-propyl based PNP pincer ligand will be described. To this end, Section 3.1 details the synthesis and

[1]The DFT calculations presented in Figure 3.1 were performed by *Dr. Markus Finger*. The data on the *tert*-butyl system were published previously,[94] while the data on the Me based system are unpublished.

properties of starting complex [$ReCl_3$(HPNP^{iPr})] (**29**) and discusses its remarkable electronic structure and spectroscopic features.

A route to the formal deprotonation product [$ReCl_2$(PNP^{iPr})] (**30**) via H atom abstraction to form [$ReCl_3$(PNP^{iPr})] (**31**) and subsequent reduction is reported in Section 3.2, as well as the resulting N_2 coordination/activation chemistry of **30** and the attempts to split dinitrogen with this platform.

Section 3.3 finally describes the N_2 activation with the amine based pincer, i.e. the formation of [(μ-N_2){$ReCl_2$(HPNP^{iPr})}$_2$] (**36**) and its photolysis into the corresponding nitride complexes [Re(N)Cl_2(HPNP^{iPr})] (**37**). The nitride exhibits defined nucleophilic reactivity towards *Lewis* acids as exemplified by the reaction with HOTf or BAr^F_{18} (BAr^F_{18} = tris{3,5-bis(trifluoromethyl)phenyl}borane). Imporantly, the reaction with benzoyl chloride results in a metal-ligand cooperative cleavage of the Re≡N bond, formation of a benzamide/benzonitrile mixture and [$ReCl_3$(P=NP^{iPr})] (**40**). The latter can be regenerated to reform **29** via electrolysis and thus a synthetic cycle for N_2 fixation is obtained.

3.1 The starting platform - [$ReCl_3$(HPNP^{iPr})] (**29**)

3.1.1 Synthesis and characterization

Initial attempts to synthesize the amide complex [$ReCl_2$(PNP^{iPr})] (**30**), analog to the *tert*-butyl system were not successful. Reactions of precursor [$ReCl_3(PPh_3)_2$(MeCN)] with HPNP^{iPr} in the presence of the bases NEt_3, KO*t*Bu or KHMDS did not lead to the formation of an isolable product, but rather to an inseparable mixture of different compounds (for further information, see Section 3.2.1). However, when [$ReCl_3(PPh_3)_2$(MeCN)] and HPNP^{iPr} were refluxed overnight in toluene without base, clean formation of the new complex [$ReCl_3$(HPNP^{iPr})] (**29**) was observed in 70 % isolated yield. Apparently, **29** is less acidic than the *tert*-butyl counterpart and therefore, partial deprotonation of the complex by non-coordinated HPNP^{iPr} does not take place before full complexation.

29 displays uniquely strongly shifted NMR signals (see Figure 3.2 *b* and *c*), e.g. the N*H* signal resonates at $\delta_{^1H} = 154.45$ ppm, the backbone CH_2 protons between $\delta_{^1H} = 8.31$ and -10.44 ppm, the ^{15}N signal of the backbone amine, identified by ^{1}H-^{15}N HSQC, exhibits a signal at $\delta_{^{15}N} = -1226.5$ ppm and the ^{31}P{^{1}H} NMR shows a singlet at $\delta_{^{31}P} = -1525.9$ ppm, which is likely to be the strongest highfield shift for a trialkylphosphine ligand ever reported in literature. Despite these shifts into spectral regions which are typical for paramagnetic compounds, all signals exhibit well resolved J_{HH} and J_{HP}-coupling, pointing to a non-trivial electronic structure, which is discussed in detail in Section 3.1.2. The molecular structure

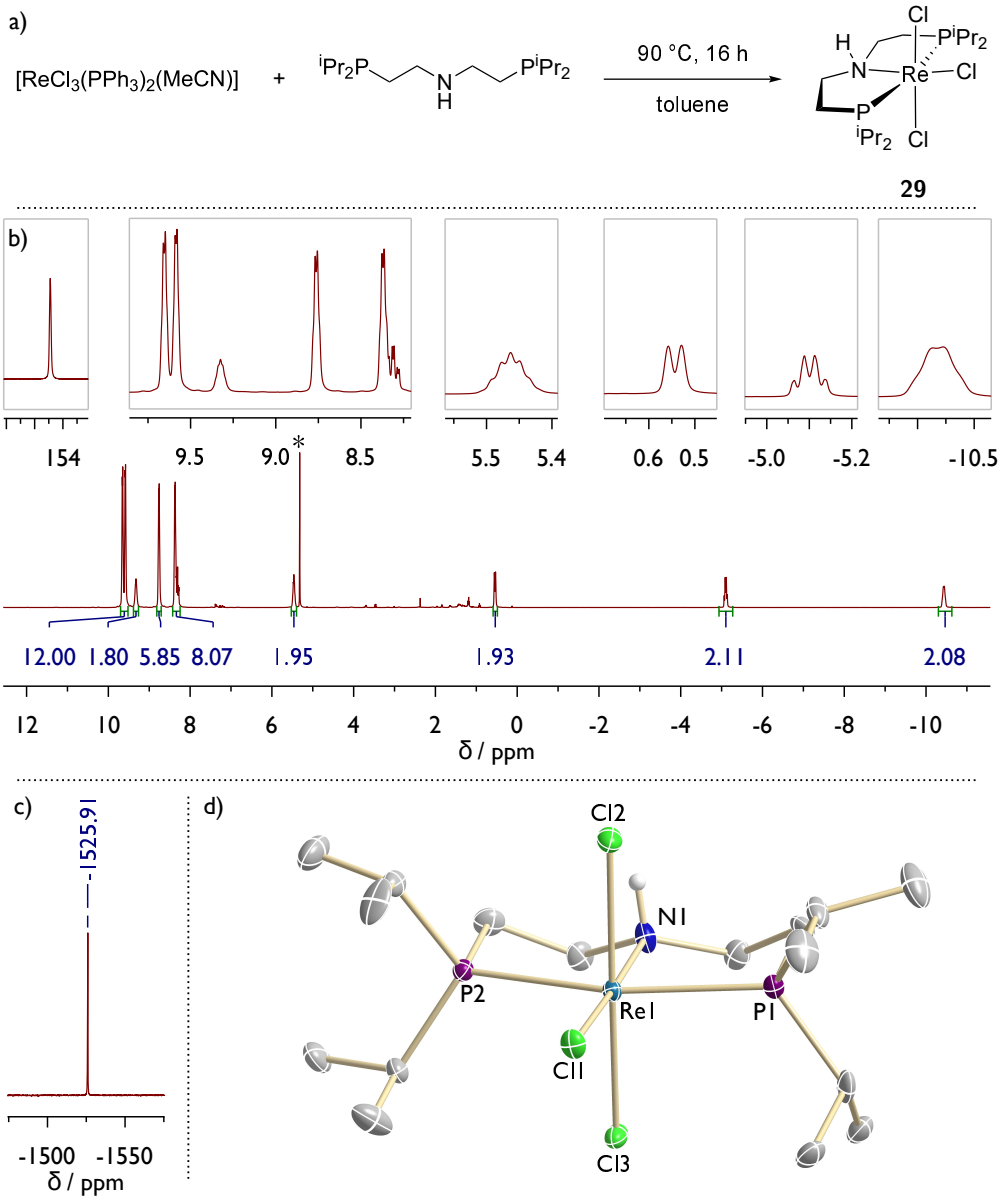

Fig. 3.2. *a*) Synthesis of **29**. *b*) ^{1}H NMR spectrum of **29**. *Insets*: Magnification of the individual signals. *c*) ^{31}P{^{1}H} NMR spectrum of **29**. *d*) Molecular structure of **29** obtained by single crystal X-ray diffraction measurements. All H atoms but the NH proton are omitted for clarity. Anisotropic displacement parameters are set to 50 % probability. Selected bond lengths [Å] and angles [°]: Re1-N1 2.158(6), Re1-Cl1 2.4117(18), Re1-Cl2 2.3791(18), Re1-Cl3 2.3725(17), P1-Re1-P2 161.58(6), N1-Re1-Cl1 177.47(18), Cl2-Re1-Cl3 174.73(7).

of **29** could be determined by X-ray diffraction measurements of single crystals (see Figure 3.2 *d*). The Re center is found to be octahedrally coordinated by the PNP pincer and three chloride ligands. The backbone nitrogen displays defined pyramidal coordination ($\Sigma(\measuredangle_{\mathrm{N1}})$ = 342.1°) and the NH proton was found from the residual density map and isotropically refined.

In cyclic voltammetry measurements, **29** shows a Re(IV/III) oxidation wave at $E_{1/2}$ = −0.24 V vs. Fc^{+}/Fc as well as a quasi-reversible wave with an estimated reduction potential

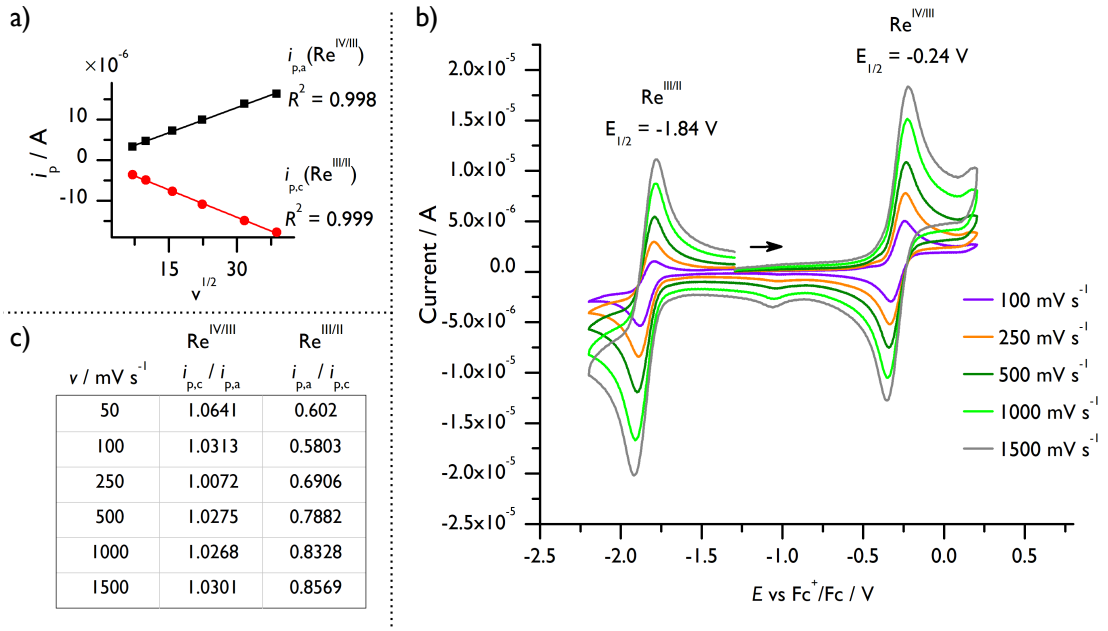

v / mV s^{-1}	Re$^{IV/III}$ $i_{p,c}$ / $i_{p,a}$	Re$^{III/II}$ $i_{p,a}$ / $i_{p,c}$
50	1.0641	0.602
100	1.0313	0.5803
250	1.0072	0.6906
500	1.0275	0.7882
1000	1.0268	0.8328
1500	1.0301	0.8569

Fig. 3.3. *a*) Plot and linear fit of i_p vs. $v^{1/2}$ ($i_{p,a}$ for the Re(IV/III) couple and $i_{p,c}$ for the Re(III/II) couple.) *b*) CV measurements of first oxidation and reduction of **29** in THF at different scan rates (10^{-3} M **29**, 0.1 M N^{n}Bu$_4$PF$_6$, WE: GC, RE: Ag-wire, CE: Pt-wire). *c*) Scan rate dependent ratio between forward and backward peak current of both waves.

of $E_{1/2} = -1.84$ V. Plotting the anodic peak current $i_{p,a}$ vs. $v^{1/2}$ for the oxidation and the cathodic peak current $i_{p,c}$ vs. $v^{1/2}$ for the reduction according to the *Randles-Sevcik* equation (see equation (eq.) 1.1 in Section 1.2), electrochemical reversibility and fast electron transfer to freely diffusing complexes can be assumed for both redox processes. A constant, scan-rate independent ratio of the forward and backward peak current close to unity proves chemical reversibility of the oxidation, while a pronounced decrease of that ratio with slower scan-rates shows the reduction to be irreversible. This irreversibility is tentatively ascribed to chloride loss after the reduction as observed for [ReCl$_2$(PNP^{tBu})] (**XIX**).[95] However, a CV series with varying chloride concentrations would be necessary to prove this assumption. Reactivity which follows from the reduction of **29** is described in Sections 3.2.3 and 3.3.1.

3.1.2 The electronic structure of **29**

The strongly shifted NMR signals of **29** described in Section 3.1.1, in particular the presence of a ^{31}P resonance at $\delta_{^{31}P} = -1525.9$ ppm, are reminiscent of previously published work on the osmium(II) PNP pincer complex [OsCl(P=N=P^{tBu})].[195] This complex exhibits a peak in ^{31}P{^{1}H} NMR spectroscopy at $\delta_{^{31}P} = -978.2$ ppm and a TIP, as indicated by a linear behaviour in the $\chi_M T$ vs. T plot derived from SQUID magnetometry, with a constant susceptibility of χ_M(TIP) = 1030·10^{-6} cm^3 mol^{-1}. Such behavior has been ascribed to the second-order Zeeman effect which arises from mixing of the thermally isolated ground state (i.e. $k_B T << \Delta E$, with ΔE describing the energy difference between the ground state and

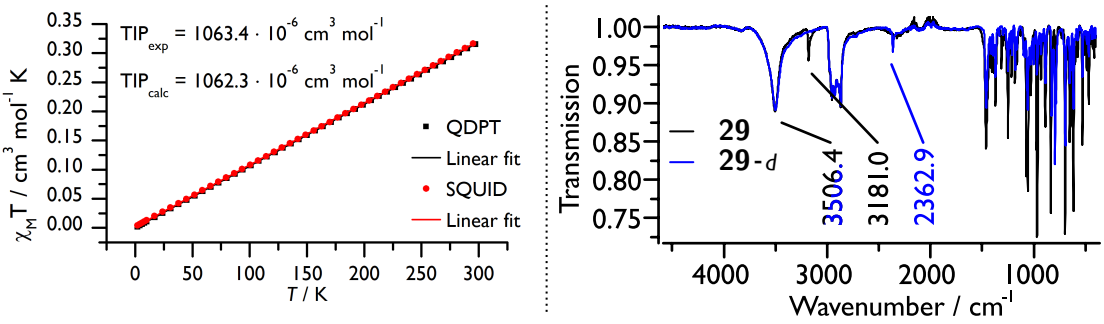

Fig. 3.4. *Left*: Temperature-dependent molar susceptibility data of **29** determined experimentally by SQUID magnetometry (*red*) as well as computationally by QDPT/NEVPT2/CASSCF calculations (*black*). *Right*: ATR-IR spectrum of **29** (*black*), compared with the spectrum of **29-*d*** (*blue*).

the first excited state) with excited states in the presence of a magnetic field.[203] Indeed, multireference calculations on the Os(II) complex indicated the complex to exhibit rather strong SOC effects. A similar situation for **29** seems very likely, as TIP is a known phenomenon especially for octahedrally coordinated heavy metal complexes with a d^4 electron configuration like Re(III).[204]

In order to gain insight into the electronic structure of the system at hand, its magnetic behavior was evaluted by means of SQUID magnetometry (see Figure 3.4). Over a temperature range of 2-295 K, complex **29** exhibits a strong TIP as indicated by a linearly increasing $\mathcal{X}_M T$ vs. T curve, corresponding to a molar susceptibility of $\mathcal{X}_M$(TIP) = 1063.4·10^{-6} cm^3 mol^{-1}, which is only marginally different from the value obtained for [OsCl(P=N=P$^{t\text{Bu}}$)]. Therefore, it seems not to be possible to draw a simple, linear correlation between experimentally determinable TIP and ^{31}P NMR shifts which one might be tempted to assume.

Nevertheless, **29** obviously features strong SOC effects. To back up these data, theoretical calculations were performed (see Part III, Section 3.4 for further details on the exact methods and settings used). To this end, the X-ray structure of **29** was used as a starting point and optimized for both the S=0 and S=1 state without any constraints. The derived PBE0/RIJCOSX/D3BJ/def2-TZVP||PBE/RI/D3BJ/def2-SVP energies indicated the S=1 state to be favorable by $\Delta G = -36.5$ kJ mol^{-1}, which obviously does not reflect the experimental findings. Hence, higher level calculations were needed. The DFT-predicted minimal energy structure was the geometry used for all further calculations.

The SQUID data show **29** to exhibit electronic states which are rather close in energy to the ground state. Such quasi-degenerate systems are poorly described by single-reference methods like DFT or coupled cluster (CC). Therefore, complete active space self consistent field (CASSCF) calculations were performed on this system, as they are capable of describing strongly statically correlated systems and serve as starting point for multi-reference methods like N-electron valence state perturbation theory (NEVPT2) or quasi-degenerate perturbation

theory (QDPT). Starting in the SVP basis, a CASSCF(14,10) calculation[2] was set up which included the five metal-centered d-orbitals as well as the five ligand based MOs balancing the active space (i.e. the bonding orbitals corresponding to the antibonding d-space, see Figure 3.5). Inclusion of further, chloride centered orbitals, which are dominated by Cl p orbitals and are basically non-bonding, did not lead to significant variation of the results (no improvement of the overall energy, negligible influence on excited state energies). Preliminar results based on a reduced CASSCF(4,5) active space including only the d orbitals indicate that the overall picture is only slightly affected by the ligand based orbitals. However, having a balanced active space was considered good practice and since the (14,10) space was computationally perfectly feasible, this was used.

The final set of orbitals was obtained after reconverging the CASSCF(14,10) calculation in the TZVP basis averaging over a total of 50 singlet, 45 triplet and 5 quintet states (i.e. over all possible excitations within the d orbitals) and the obtained energies were corrected for dynamic correlation by means of NEVPT2. The triplet ground state is confirmed with

[2] Throughout this thesis, for the active space of the performed calculations the following notation will be employed: method($n_{\text{active electrons}}$,$n_{\text{active orbitals}}$).

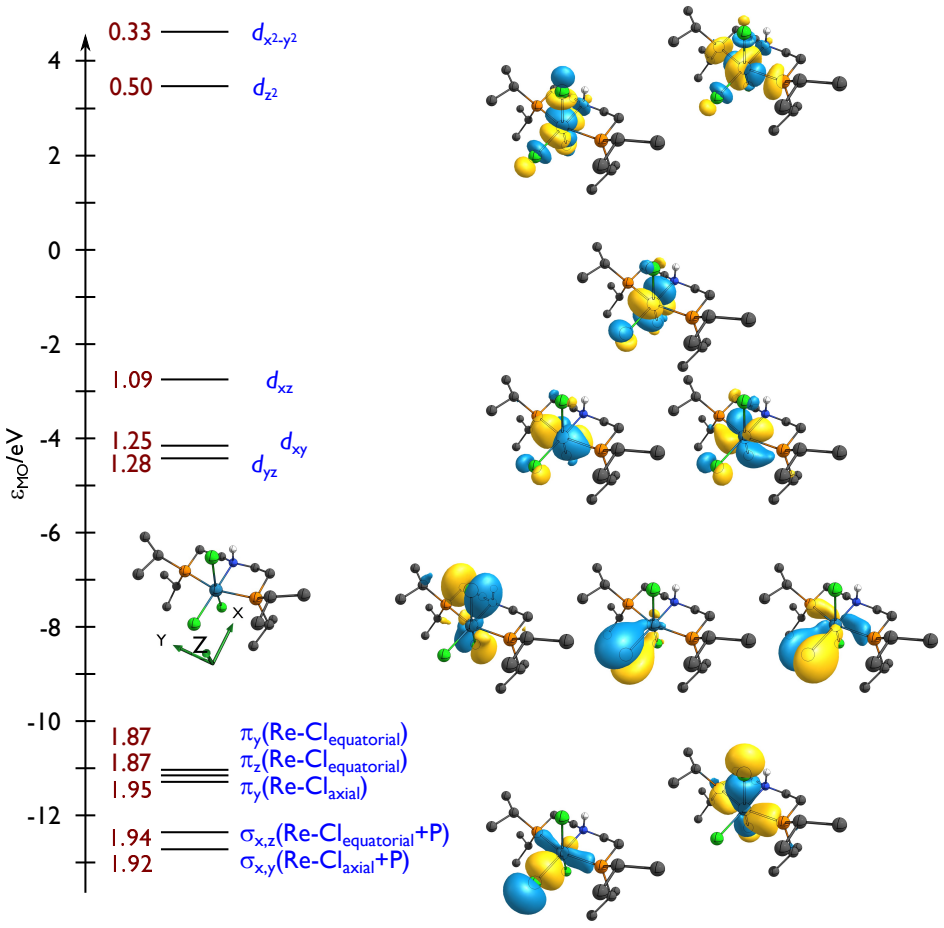

Fig. 3.5. MO scheme of **29** from a stage-averaged CASSCF(14,10) calculation in the triple-ζ basis averaging over 50 singlet, 45 triplet and 5 quintet states. Occupation numbers (*red*), orbital labels (*blue*) and orbital plots at an isovalue of 0.04 are given as well.

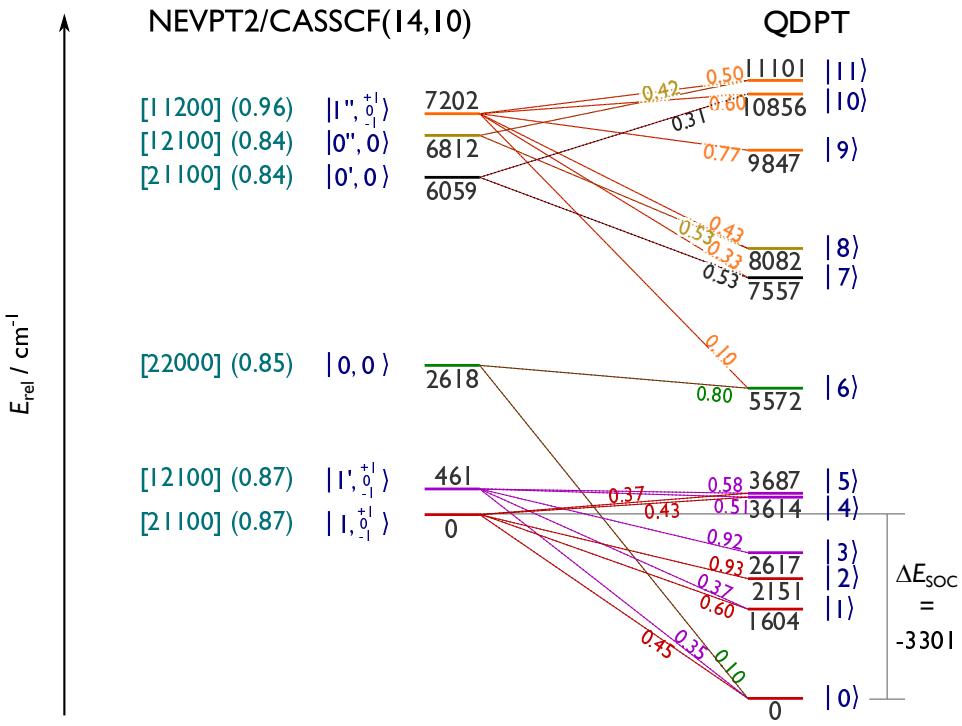

Fig. 3.6. State-energy diagramm of **29** based on a NEVPT2/CASSCF(14,10) calculation. Non-relativistic states $|S, M_S\rangle$ (blue) and their dominant configuration [XXXXX] with the respective weights in brackets (turquoise) are given (*left*), where each X corresponds to the occupation of the d-orbitals in energetically increasing order (the ligand orbitals are fullly occupied in all configurations and are thus omitted). Spin-orbit states derived from QDPT treatment (*right*) are color-coded according to the dominant spin-free state and individual contributions are given (weights $\geq$ 10 %, on the dashed lines). State energies are given in cm^{-1} respective to the ground states.

a $(d_{yz})^2$, $(d_{xy})^1$, $(d_{xz})^1$ electron configuration (87 % weight), while the first exited triplet, which lies only 5.5 kJ mol^{-1} above the ground state is mainly composed of the corresponding $(d_{yz})^1$, $(d_{xy})^2$, $(d_{xz})^1$ (87 % weight), reflecting the near-degeneracy of the d_{xy} and d_{yz} orbitals. However, if these states were subjected to a SOC calculation by means of a QDPT treatment, the degeneracy of each state is lifted. The lowest eigenstate is stabilized by $\Delta E_{\mathrm{SOC}} = -3301\,\mathrm{cm}^{-1}$ and features considerable multireference character, i.e. it is mainly composed from $|1\rangle$ (45 % weight), $|1'\rangle$ (35 % weight) and $0\rangle$ (10 % weight) (see Figure 3.6).

The strong SOC effect, especially on the ground state are in good agreement with the observed TIP from magnetometry (see Figure 3.4) and simulated SQUID data from the QDPT calculation reproduce the TIP value exactly ($\mathcal{X}_M T_{\mathrm{QDPT}} = 1062.3{\cdot}10^{-6}\,\mathrm{cm}^3\,\mathrm{mol}^{-1}$). The computed SOC stabilization energy is comparable to that of [OsCl(P=N=P$^{t\mathrm{Bu}}$)] ($\Delta E_{\mathrm{SOC}} = -9.2\,\mathrm{kcal\,mol}^{-1} \approx -3200\,\mathrm{cm}^{-1}$) and would therefore support a linear correlation of ΔE_{SOC} and $\mathcal{X}_M$(TIP). However, further data would be needed to underpin this suggestion.
Interestingly, the SOC calculation predicted significant oscillator strengths for the $|0\rangle \rightarrow |4\rangle$ and $|0\rangle \rightarrow |5\rangle$ electronic excitations, with very low excitation energies close to the near

infrared (NIR)/mid infrared (MIR) limit (3614 cm^{-1} and 3687 cm^{-1}, respectively) (see Part III, Table 3.12). And indeed, ATR-IR on a solid sample as well as regular transmission IR measurements in Nujol revealed a very prominent and broad peak at 3507 cm^{-1} with a small shoulder at slightly lower energies, which is in very good agreement with the calculations. While the band shape and central frequency strongly reminds of water, this result was verified with different batches, each of which were pure by elemental analysis and showed no sign for water in the NMR spectra, excluding this to be the source of the signal. Additionally, and H/D exchange at the backbone amine by stirring with D_2O[3] proved the smaller and sharper peak at $\tilde{\nu} = 3181\,cm^{-1}$ to be the N–H stretching vibration (ν_{N-D}: $\tilde{\nu} = 2363\,cm^{-1}$; $\Delta\tilde{\nu}_{harm.\ osz.} = 858\,cm^{-1}$).

IR measurements with an applied magnetic field and plotting of the obtained data as $T_B/T_{B=0}$ allowed to unambiguously identify the observed spectroscopic feature as an electronic absorption, detectable with a regular MIR spectrometer (see Figure 3.7, *left*). All vibrational absorptions, which by nature are not influenced by an magnetic field, are canceled out in this spectrum and only electronic excitations which are perturbed by the field become visible. However, the shift is so small that a quantification of the effect is difficult, which is in line with the simulations of the effect by QDPT calculations, where by applying a field along the y-axis a maximum shift of $\leq 1\,cm^{-1}$ at 10 T is predicted (see Figure 3.7 *right* and Part III Section 3.4.5).

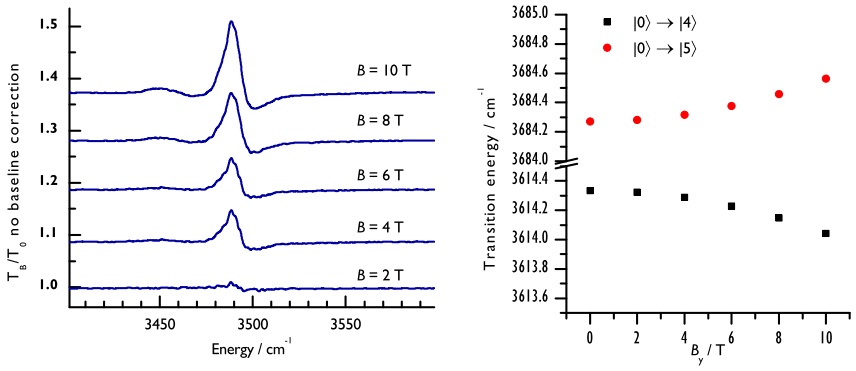

Fig. 3.7. *Left*: Relative change of IR transmission in applied field, plotted as $T_B/T_{B=0}$. The original y-intercept (1) of each spectrum is manipulated so that the spectra appear stacked. *Right*: QDPT simulated influence of a magnetic field on the energies of the states $|4\rangle$ and $|5\rangle$.

3.2 Amide based pincer chemistry

3.2.1 A route to [$ReCl_2(PNP^{iPr})$] (**30**)

As discussed in Section 3.1.1, the synthesis of [$ReCl_2(PNP^{iPr})$] (**30**) was not possible using the same procedure as for the related *tert*-butyl substituted derivative **XIX**. Similarly,

[3] See Part III Section 2.3.1 for details.

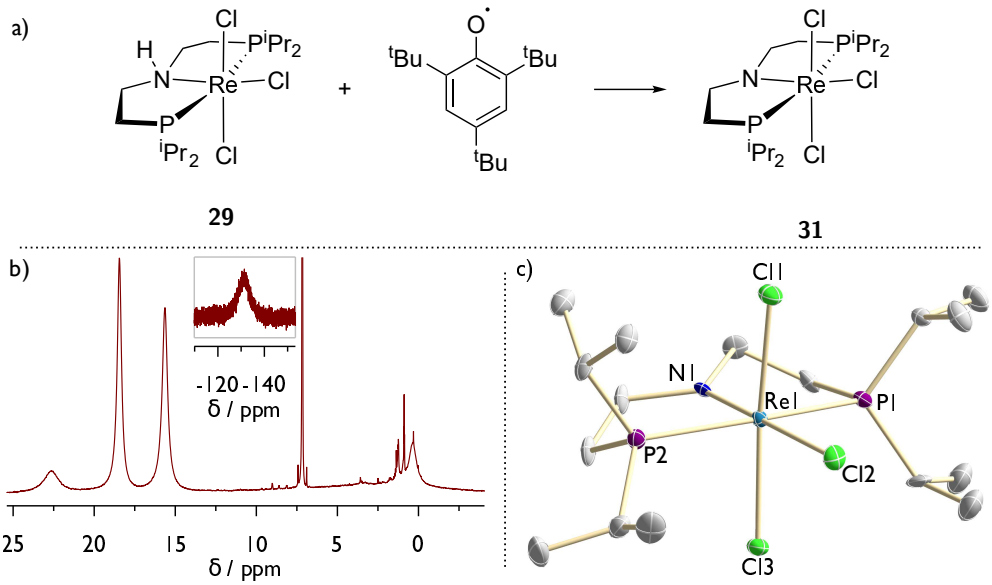

Fig. 3.8. *a*) Synthesis of complex **31**. *b*) ^{1}H NMR spectrum of **31** in C_6D_6. *c*) Molecular structure of **31** obtained by single crystal X-ray diffraction measurements. H atoms are omitted for clarity. Anisotropic displacement parameters are set to 50 % probability. Selected bond lengths [Å] and angles [°]: Re1-N1 1.902(7), Re1-Cl1 2.379(2), Re1-Cl2 2.429(2), Re1-Cl3 2.369(2), N1-Re1-Cl2 178.7(2), P1-Re1-P2 163.48(8), Cl1-Re1-Cl3 174.01(8).

reactions of **29** with bases did not lead to an isolable complex in most cases. The only seemingly selective reaction was observed when KHMDS was used, however that reaction did not proceed clean enough to allow for isolation of the new complex. This is most likely due to the strong tendency of **30** to bind a sixth ligand whenever possible, as will be discussed later in this section. As an alternative to deprotonation of **29**, the synthesis of **30** can be envisioned by stepwise H-atom abstraction (from the NH moiety of the ligand) and subsequent reduction. Stirring **29** with 1 eq of TTBP in benzene resulted in a color change to deep red. [$ReCl_3(PNP^{iPr})$] (**31**) could be isolated as the sole product of the reaction in 63 % yield. The ^{1}H NMR spectrum shows broad, paramagnetically shifted signals, while the $^{31}P\{^{1}H\}$ NMR spectrum shows no resonance. The expected $S = 1/2$ spin state is supported by *Evans'* method,[205] which yielded an effective magnetic moment of $\mu_{eff} = 1.37 \pm 0.14\,\mu_B$ in CD_2Cl_2 at RT, which is in reasonable agreement with the expected spin-only value of $\mu_{eff} = 1.73\,\mu_B$, thus confirming the formal oxidation of the metal center to Re(IV). For the CH_3 groups of the molecule, two large signals integrating to 12 protons each could be identified, pointing to a C_{2v} symmetry on the NMR timescale. In the molecular structure derived from X-ray diffraction measurements the Re atom is coordinated octahedrally by the PNP pincer and the Cl ligands. Successful H-atom abstraction from the amine moiety is confirmed by planar coordination of the pincer nitrogen atom ($\Sigma(\measuredangle_{N1}) = 359.8°$), accompanied by a shortening of the Re–N distance (**31**: d(Re1–N1) = 1.902(7) Å; **29**: 2.158(6) Å), supporting the amide nature of the ligand.

Since **31** was prepared as precursor for the synthesis of Re(III) compound **30**, its electrochemical properties were investigated by means of CV measurements. A quasi-reversible reduction was found at $E_{1/2} = -1.06$ V vs. Fc^+/Fc. Analysis of the scan rate dependence

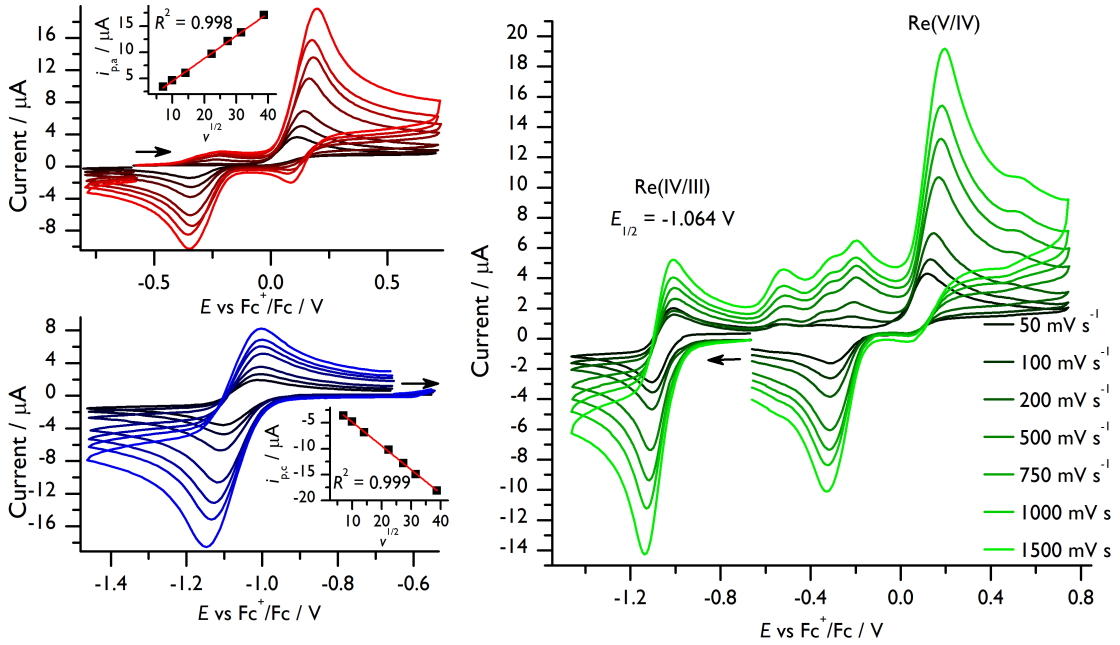

Fig. 3.9. *Green*: CV measurements of **31** in THF at different scan rates (10^{-3} M **31**, 0.1 M $N^nBu_4PF_6$, WE: GC, RE: Ag-wire, CE: Pt-wire). *Red*: Re(V/IV) oxidation. *Blue*: Re(IV/III) reduction. *Insets*: Plot and linear fit of i_p vs. $v^{1/2}$.

Tab. 3.1. Peak analysis of reduction and oxidation of **31**. $^{\Delta E_{sample}}/_{\Delta E_{ref}}$ is the peak separation as a ratio to the peak separation of the internally added decamethylferrocene standard. All potentials are reported against Fc^+/Fc.

	Re(IV/III)			Re(V/IV)	
v / mV s^{-1}	$E_{1/2}$ / V	$^{i_{p,an}}/_{i_{p,cat}}$	$^{\Delta E_{sample}}/_{\Delta E_{ref}}$	E_{an} / V	$i_{p,an}$ / µA
50	-1.057	0.81	1.00	0.113	3.43
100	-1.057	0.78	1.00	0.131	4.63
200	-1.057	0.75	1.00	0.140	6.05
500	-1.062	0.73	1.11	0.163	9.66
750	-1.066	0.70	1.00	0.181	12.10
1000	-1.071	0.65	1.10	0.176	13.78
1500	-1.075	0.66	1.00	0.194	17.07

of $i_{p,c}$ according to the *Randles-Sevcik* equation (see Part III, Section 1.2, eq. 1.1) gives a linear relationship between $i_{p,c}$ and $v^{1/2}$, indicating electrochemically reversible electron transfer to a freely diffusing analyte. The ratio of $\frac{i_{p,a}}{i_{p,c}}$ *decreases* upon *increasing* scan rate v, indicating a first-order reversible chemical follow-up reaction after electrochemically reversible electron transfer in comparable timescale to the CV experiment.[206] Assuming the immediate reaction to be chloride loss, this reaction would therefore be much slower than in the case of the *tert*-butyl substituted congener [$ReCl_3(PNP^{tBu})$], where no reverse peak could be observed even in the presence of 50 eq chloride ions at high scan rates.[207] The oxidation is also proven to be electrochemically reversible according to the linear relationship between $i_{p,a}$ and $v^{1/2}$. However, a reverse-peak appeared only at $v = 1500$ mV s^{-1}, and a

new reduction feature around −0.4 V indicates a rather selective EC mechanism after initial oxidation to a new product.

While these results suggest $CoCp_2$ to be a proper reductant for simple Re(IV/III) reduction, actually using this reagent led to basically blank *in situ* NMR spectra and the formation of a precipitate which was unsoluble in THF. A possible explanation would be the formation of insoluble $[ReCl_3(PNP^{iPr})][Co(Cp)_2]$ rather than precipitation of $[Co(Cp)_2]Cl$. However, this is only a working hypothesis and needs further investigation. Therefore, Na(Hg) was used as a reductant. Reduction of **31** with Na(Hg) did give selective conversion of the starting material. Interestingly, two different complexes of C_{2v} symmetry on the NMR timescale were obtained depending on whether the reaction was conducted in THF ($\delta_{^{31}P} = -14.5$ ppm, deep orange) (**32**) or in non-coordinating solvents like benzene, toluene or 1,4-dioxane ($\delta_{^{31}P} =$ 9.9 ppm, deep violet) (**30**) (see Figure 3.10 *b*). The first complex is largely uncharacterized, despite the molecular structure obtained from X-ray diffraction measurements on single crystals grown from THF/Et_2O (see Figure 3.10 d). Complex **32** is found to be octahedrally coordinated $[ReCl_2(thf)(PNP^{iPr})]$ where a THF molecule binds at the vacant coordination side *trans* to the amide, resulting from chloride dissociation after reduction. The planar coordination of the PNP amide ligand ($\Sigma(\measuredangle_{N1}) = 360.0°$) and the presence of only two chloride ligands confirm successful reduction to a Re(III) species. Nevertheless, applying vacuum to the complex caused release of that ligand and (rather clean, but not exclusive) formation of **30**, which prevented isolation or further characterization of **32**.

If **31** is reduced in toluene (or other non-coordinating solvents), the reaction takes longer (several hours, attributed to reduced activity of the amalgam in low polarity solvents), but yields a clean complex identified as $[ReCl_2(PNP^{iPr})]$ (**30**). NMR analysis indicates spectroscopically clean formation of a C_{2v} symmetric complex. The deep violet color resembles that of *tert*-butyl substituted complex **XIX** and the LIFDI mass is in agreement with the proposed structure. Single crystals grown by slow evaporation of a toluene solution allowed for molecular structure determination by X-ray diffraction measurements. The Re center in **30** is five-fold coordinated and adopts a distorted trigonal bipyramidal coordination geometry with the two phosphorous atoms in axial position ($\tau_5 = 0.677$).[196] The short Re−N distance ($d_{Re1\text{-}N1} = 1.873(4)$ Å) and planar coordination of the nitrogen atom ($\Sigma(\measuredangle_{N1}) =$ 360.0°) confirm the amide nature of the PNP ligand.
At this point, it interesting to note that all compounds within the steric variation series of $[ReCl_2(PNP^{iPr})]$ (**30**, this work), $[ReCl_2(PNP^{tBu})]$ (**XIX**, reference [94]) and $[ReCl_2(PNP^{Ad})]$ (**30-Ad**, unpublished work by *Lukas Alig*)[4] are coordinated by closely related ligands and could thus be expected to exhibit similar electronic structures (the variation of the trialkylphosphine donor strength can be assumed to be neglectible upon interchanging R = *i*Pr, *t*Bu and Ad).[208] Contrary to this assumption, the three complexes resonate at highly

[4] I appreciate *Lukas'* permission to include the ^{31}P NMR shift as well as the τ_5 value of his complex **30-Ad** in this discussion. Further information on this complex can be expected to be found in his thesis.

different ^{31}P NMR shifts ($\delta_{^{31}P}$ = 10.0 ppm (**30**), −51.5 ppm (**XIX**) and −412.5 ppm (**30-Ad**)). One might be tempted to assume this to be due to increasing influence of spin orbit coupling and a resulting TIP. However, the comparsionn of [OsCl(P=N=P^{tBu})] and **29** did already indicate that a direct linear correlation between ^{31}P NMR shifts and TIP is not likely (see Section 3.1.2 for further details). A striking difference within the series is the change in coordination geometry from distorted trigonal bipyramidal in **30** (τ_5 = 0.677) to distorted

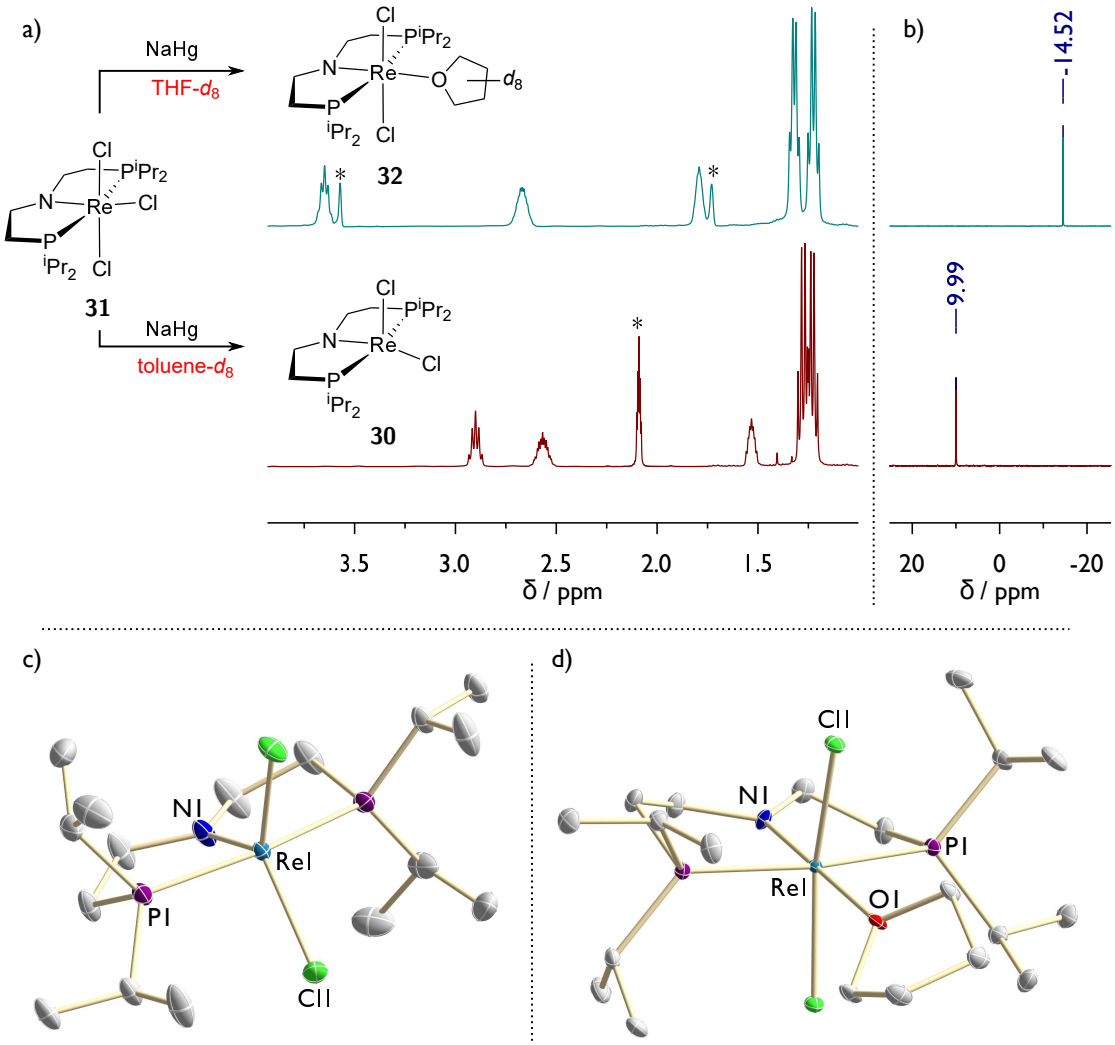

Fig. 3.10. *a*) Reaction scheme and ^{1}H NMR spectra of the reduction of **31** in THF and toluene leading to the formation of **32** and **30**, respectively. Residual solvent signals are marked with asterisks. *b*) ^{31}P{^{1}H} NMR spectra of **32** (*top*) and **30** (*bottom*) in THF-d_8 and toluene-d_8, respectively. *c*) Molecular structure of **30** obtained by single crystal X-ray diffraction measurements. The asymmetric unit contains a half molecule. H atoms are omitted for clarity. Anisotropic displacement parameters are set to 50 % probability. Selected bond lengths [Å] and angles [°]: Re1-N1 1.873(4), Re1-Cl1 .3272(7), Re1-P1 2.3731(7), Cl1-Re1-Cl#1 126.07(4), P1-Re1-P#1 166.66(4), N1-Re1-Cl1 116.97(2). *d*) Molecular structure of **32** obtained by single crystal X-ray diffraction measurements. The asymmetric unit contains a half molecule. H atoms are omitted for clarity. Anisotropic displacement parameters are set to 50 % probability. Selected bond lengths [Å] and angles [°]: Re1-N1 1.900(3), Re1-O1 2.264(2), Re1-P1 2.3725(6), Re1-Cl1 2.4097(5), N1-Re1-O1 180.0, P1-Re1-P#1 166.07(3), Cl1-Re1-Cl#1 164.22(3).

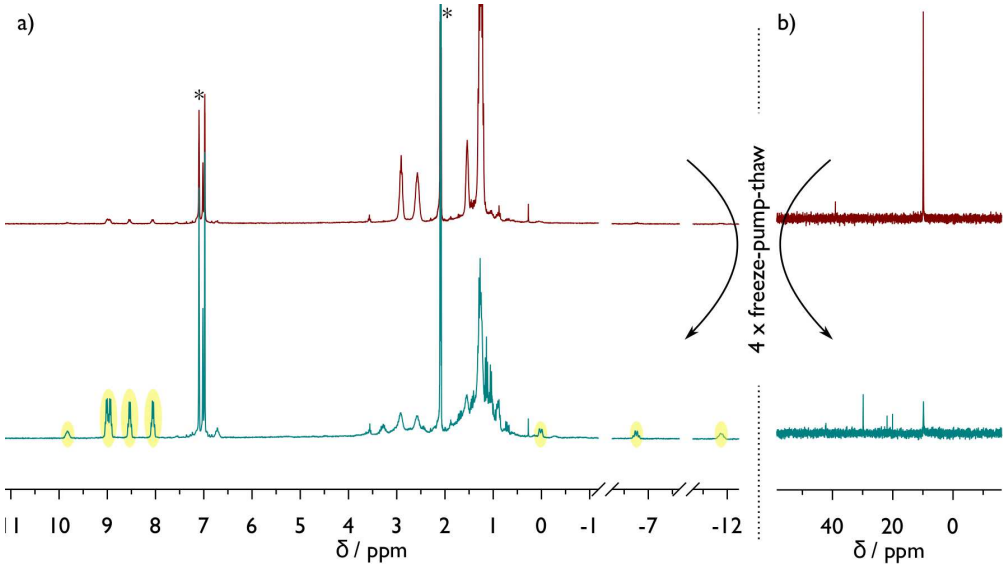

Fig. 3.11. Changes in the ^{1}H (*a*) and ^{31}P$\{^{1}$H$\}$ (*b*) NMR spectra of a solution of **30** in toluene-d_8 after four *freeze-pump-thaw* cycles, demonstrating the instability of the complex to even these conditions. Residual solvent signals are marked with asterisks. The yellow shaded ^{1}H NMR signals can be assigned to the starting complex **29**, although the origin of its formation is unclear.

square pyramidal ($\tau_5 = 0.371$ and 0.261 in **XIX** and **30-Ad**, respectively). This change in geometry should directly influence the d-orbital splitting and thus have a defined influence on the electronic structure. However, detailed (theoretical) investigation of the underlying effects is necessary to draw founded conclusions.

Nevertheless, **30** can be considered to be the exact, sterically less encumbered analog to PNP$^{t\text{Bu}}$ complex **XIX** and thus the proper candidate to test the proposed effects of reduced steric shielding on N_2 activation as outlined at the beginning of this chapter (3). However, despite several attempts, clean isolation of **30** could not be achieved. The main reason for this can be found in a remarkable instability of the complex towards almost any conditions. While a toluene solution was stable for at least several days, irreversible decomposition of **30** was observed upon solvent removal or even simple freezing and thawing of the solution (see Figure 3.11). Therefore, only *in situ* prepared samples were used for all further investigations, which could be separated from Hg and precipitated NaCl by simple filtration. This was proven to be a viable approach by measuring elemental analysis of a filtered and lyophilized sample. Even though lyophilization induced partial complex decomposition as proven by NMR spectroscopy, the fitting analysis combined with clean spectroscopy *prior* to removal of the solvent point to a clean solution containing only **30** after filtration.

3.2.2 Dinitrogen chemistry with [ReCl$_2$(PNP$^{i\text{Pr}}$)] (**30**)

30 shows a high tendency to bind a sixth ligand, as exemplified by the formation of a THF complex or the non-trivial synthesis of the penta-coordinated complex **30**. This can be

attributed to the reduced steric shielding of the metal center and is in line with previous results on the corresponding [$RuCl_2$(HPNP^R)] complexes (R = *i*Pr, *t*Bu).[209,210] Accordingly, when **30** is exposed to an N_2 atmosphere, the color changes immediately from deep violet to brown-orange, indicating fast reaction with dinitrogen at the Re(III) oxidation state. The NMR spectra reveal largely broadened signals, with the $^{31}P\{^1H\}$ NMR signal vanishing almost in the spectral noise, at a similar shift as pure **30**. However, if the sample is cooled (−15 - −50 °C), a new set of signals forms (see Figure 3.12 *a*). Warming the sample back to RT results in reformation of the previous, broad signals and when the sample is heated (up to 75 °C) or when Ar is bubbled through the solution, **30** becomes the main species again. Hence, the reaction with N_2 is dynamic, fully reversible and thus most likely mere coordination chemistry. The following discussion therefore focuses on the identity of the species which are present at low temperatures under an N_2 atmosphere.

The $^{31}P\{^1H\}$ NMR spectrum reveals five new signals, i.e. two doublets at $\delta_{^{31}P}$ = 1.3

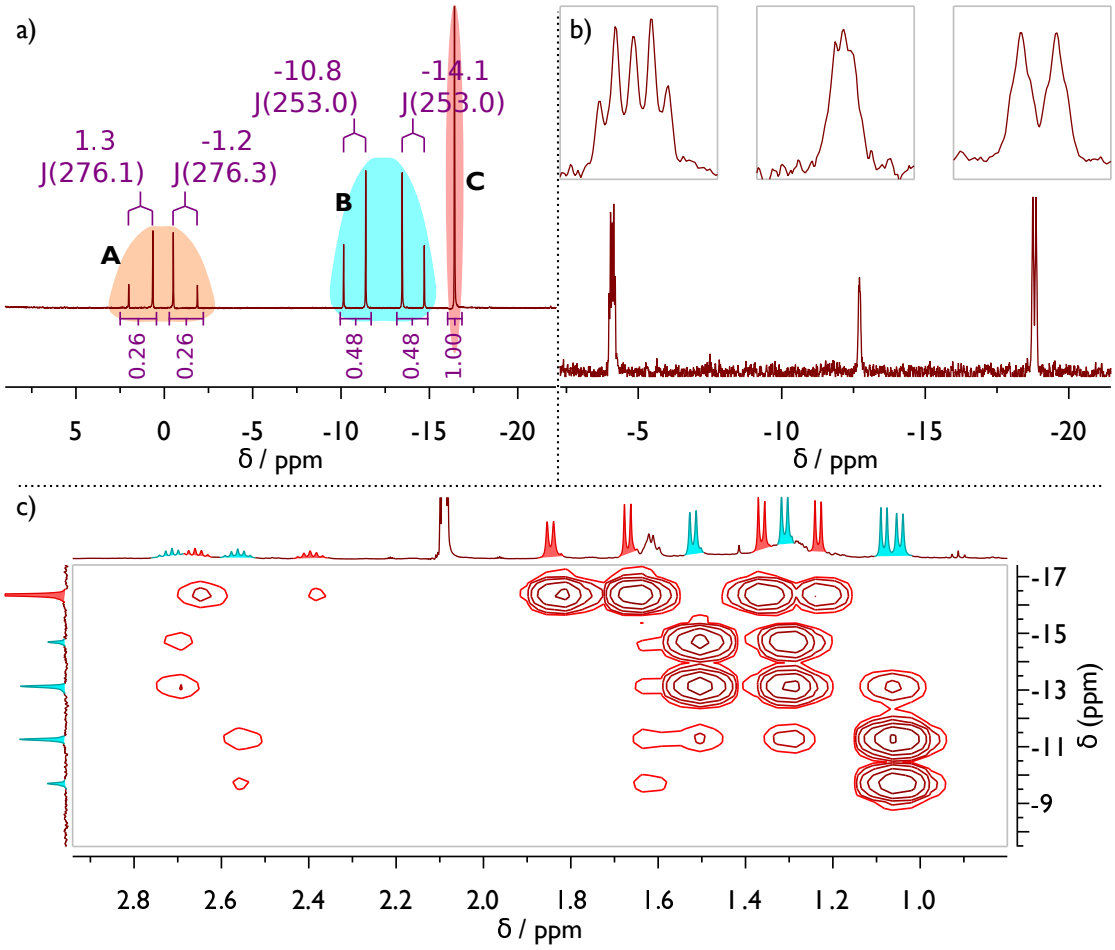

Fig. 3.12. Low temperature NMR spectroscopy of the reaction of **30** with N_2. *a*) $^{31}P\{^1H\}$ NMR spectrum, showing three pincer fragments. Coupling constants are given in Hz. *b*) $^{15}N\{^1H\}$ NMR spectrum, recorded inverse gated. *c*) ^1H-^{31}P heteronuclear multiple bond correlation (HMBC) revealing both, fragment **B** (*turquoise*) and **C** (*red*) to feature a mirror plane within and orthogonal to the pincer plane, respectively. For better readability, the ^1H NMR trace was substituted with the $^1H\{^{31}P\}$ NMR spectrum.

and -1.2 ppm with a mutual coupling $^{2}J_{PP} = 276.2$ Hz (denoted **A** in the following), two doublets at $\delta_{^{31}P} = -10.8$ and -14.1 ppm with a mutual coupling of $^{2}J_{PP} = 253.0$ Hz (denoted **B**) and a singlet at $\delta_{^{31}P} = -16.4$ ppm (denoted **C**), indicating three different PNP-pincer ligands, two with inequivalent phosphorous atoms as well as one with equivalent phosphorous atoms. Importantly, the ratio **B**:**C** was found to be close to 1:1 in every single spectrum that was measured, while the ratio **A**:**B**/**C** changed between the experiments. The coupling constants are typical for *trans* coupling of the pincer ligand in an asymmetric environment, whereas the constant 1:1 ratio of **B** and **C** indicates either some kind of connectivity between these fragments or a dissociation of one intermediate into two products. The origin of these varying ratios was not investigated, yet it is noteworthy that **A** was the minor product in all measurements and most of the times the signals were less intense than in the exemplary spectrum in Figure 3.12 *a*.

Therefore the focus of further investigations was on the nature of **B** and **C**, which was further elucidated using 2D-NMR spectroscopy. By ^{1}H-^{31}P HMBC spectroscopy, coupling of **B** and **C** to two inequivalent *iso*-propyl groups (one CH and two CH_3 signal) each could be detected. Therefore, both pincer ligands are coordinated in a C_S symmetric environment, but with orthogonal mirror planes (i.e. once within the ligand plane (**B**) and once perpendicular to it (**C**). An identification of the *i*Pr signals belonging to the ^{31}P signal **A** was not possible, due to the low concentration. If **30** was placed under an atmosphere of $^{15}N_2$ gas, at low temperatures three signals were identified by ^{15}N$\{^{1}$H$\}$ NMR spectroscopy at $\delta_{^{15}N} = -4.1$ ppm (dt, $J = 5.5$ and 2.6 Hz), -12.7 ppm (s) and -18.8 ppm (d, $J = 5.7$ Hz with non-resolved shoulders which can be estimated to a coupling constant of ≈ 1.5 Hz) (see Figure 3.12 *b*). Again, the signals at $\delta_{^{15}N} = -4.1$ and -18.8 ppm integrate in a 1:1 ratio, while the signal at $\delta_{^{15}N} = -12.7$ ppm integrates to 0.4. This matches the ratio between **B**/**C** vs. **A** determined by ^{31}P$\{^{1}$H$\}$ NMR spectroscopy. The coupling constants indicates the resonances at $\delta_{^{15}N} = -4.1$ and -18.8 ppm to belong to a single, asymmetrically coordinated N_2 ligand, while the signal at -12.7 ppm must belong to an N_2 ligand in a symmetric coordination environment. Notably, under $^{15}N_2$, in the ^{31}P$\{^{1}$H$\}$ NMR spectrum the resonance at $\delta_{^{31}P} = -16.4$ ppm splits into a doublet with $J_{PN} = 2.6$ Hz, matching the small coupling of the signal at $\delta_{^{15}N} = -4.1$ ppm and thereby proving binding of the N_2 ligand to fragment **C**.

Finally, the sample was subjected to an ^{1}H$\{^{31}$P$\}$ NOESY as well as a ^{31}P$\{^{1}$H$\}$ DOSY measurement (see Figure 3.13). The NOESY revealed small cross peaks between *i*Pr groups belonging to **B** and **C**, indicating both fragments to actually belong to a single compound **33a**. This was confirmed by the low temperature ^{31}P-DOSY measurement, which was performed first at -30 °C on a sample of **30** in toluene under Ar. Then N_2 gas was bubbled through the solution and the sample was remeasured under N_2 at the same temperature. The data shows all three pincer moieties to have the same diffusion coefficient of $D = 1.89 \cdot 10^{-6}$ cm^2 s^{-1}, while pure **30** has a coefficient of $D = 2.61 \cdot 10^{-6}$ cm^2 s^{-1}. Since these values are derived in toluene-d_8 at -30 °C, for comparision with the previously published diffusion constant of *tert*-butyl substituted complex **XIX** ($D = 9.1 \cdot 10^{-6}$ cm^2 s^{-1} in THF-d_8

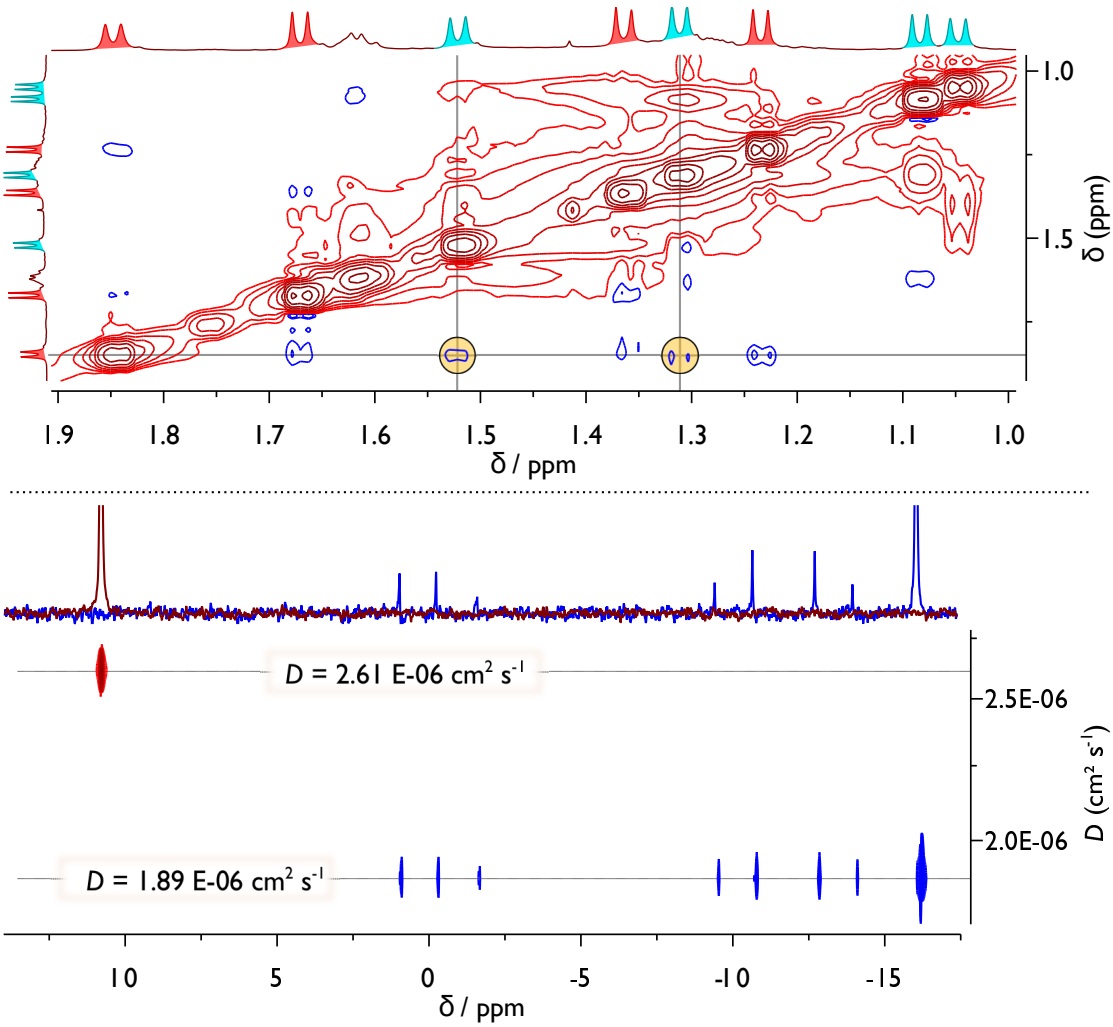

Fig. 3.13. Low temperature ^{1}H-NOESY (*top*) and ^{31}P-DOSY (*bottom*) of the reaction of **30** with N_2 in toluene-d_8. The NOESY shows cross peaks between *i*Pr groups belonging to the fragments **B** and **C** while the DOSY shows smaller diffusion coefficients for **A**, **B** and **C** (blue), compared to **30** (red) (all measured at -30 °C).

at RT)[95] the *Stokes* radii for all three diffusion constants were calculated according to the *Stokes-Einstein* equation:

$$D = \frac{k_\mathrm{B} T}{6\pi\eta r} \tag{3.1}$$

where D is the diffusion constant, k_B is *Boltzmann's* constant, T is the temperature, η is the dynamic viscosity of the solvent at that temperature and r is the *Stokes* radius, i.e. the radius a spherical particle with that D would have. The restriction of this equation to spherical particals limits its use for quantitative radii determination, however since the molecules discussed here do not deviate too much from that geometry, eq. 3.1 can be used in reasonable approximation of qualitative analysis. With $\eta_{\text{toluene, -30 °C}} = 1.39\,\text{mP s}$ and $\eta_{\text{THF, 25 °C}} = 0.456\,\text{mP s}$,[211,212] the following *Stokes* radii could be calculated: r(**XIX**) = 4.95 Å, r(**30**) = 4.48 Å and r(**33a**) = 6.69 Å.

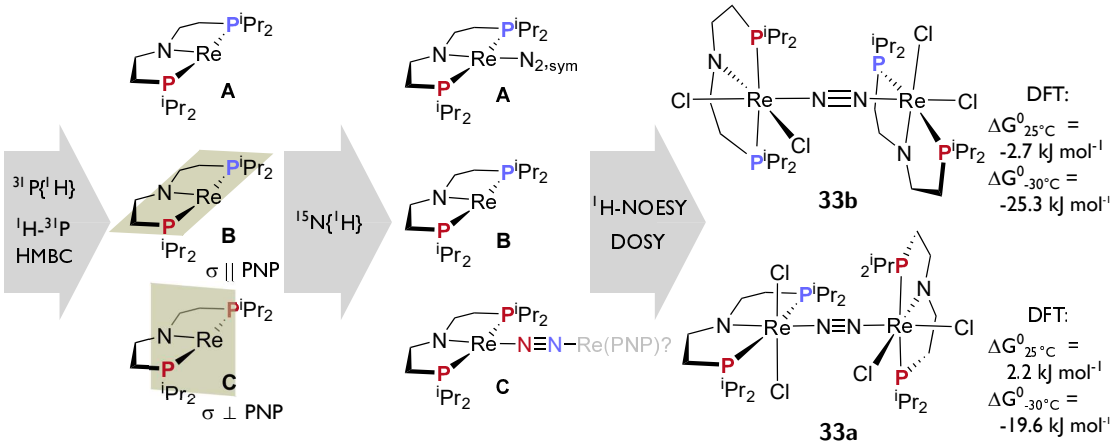

Fig. 3.14. Summary of structure determination of **33a** and **33b** by low temperature NMR spectroscopy and computational analysis of the thermochemistry of the formation of **33a** and **33b** at different temperatures.

All these data form a coherent picture of the reaction of **30** with N_2, which is summerized in Figure 3.14:

- The reversible nature of the reaction tendentially indicates simple coordination of N_2. The formation of the product(s) only at low temperatures points to an entropic penalty of the reaction, in line with a dimerization process.
- ^{31}P NMR as well as ^{1}H-^{31}P HMBC spectra allow for identification of three pincer fragments and their symmetry planes.
- ^{15}N NMR spectroscopy proves N_2 binding to fragment **C**, while binding of the same ligand to **B** is suggested by a triplet-like shoulders of the second signal of similar intensity. If **A** coordinates N_2 it has to be bound symmetrically.
- NOESY and ^{31}P-DOSY reveal all three fragments to belong to dimers, with **B** and **C** actually being two sides of the same dimer.

Consequently, **A** most likely corresponds to $[(\mu\text{-}N_2)\{ReCl_{2,cis}(PNP^{iPr})\}_2]$ (**33b**), a symmetric analog of the previously observed *tert*-butly substituted analog **XX** (see Section 2.1) but with additional chloride ligands *trans* to the N_2 bridge. On the other hand, **B** and **C** are the two sides of an asymmetrical dimer $[\{ReCl_{2,cis}(PNP^{iPr})\}(\mu\text{-}N_2)\{ReCl_{2,trans}(PNP^{iPr})\}]$ (**33a**) as depicted in Figure 3.14. These suggestions are supported by DFT calculations,[5] which reveal the binding of N_2 to form dimer **33a** and **33b** to be favorable at $-30\,°C$ by $\Delta G^0 = -19.6$ and $-25.3\,kJ\,mol^{-1}$, respectively. At $25\,°C$, the reaction is computed to be almost thermoneutral ($\Delta G^0 = 2.2$ and $-2.7\,kJ\,mol^{-1}$), fully consistent with the experimental observation. Coordination of N_2 to **30** either *cis* or *trans* to the amido ligand was calculated to be uphill in all cases. Unfortunately, neither **33a** nor **33b** could be crystallized to allow for X-ray diffraction, despite various attempts. Hence, no molecular structures could be determined experimentally.

[5] PBE0/D3BJ/RIJCOSX/def2-TZVP/CPCM(toluene)||PBE/D3BJ/RI/def2-SVP

3.2.3 Assessment of dinitrogen activation capabilities

The fact that dinitrogen binding and dimer formation already occurs straightforward at the Re(III) oxidation state encouraged a thorough investigation of the abilities of **30** to activate and/or split N_2 under reductive conditions.
In order to be able to evaluate the success or failure of a reaction, the expected product of successful splitting, [Re(N)Cl(PNP^{iPr})] (**34**) was synthesized by deprotonation of [Re(N)Cl$_2$(HPNP^{iPr})] (**37**).[6] Stirring **37** with 1 eq KO^{t}Bu in benzene resulted in clean formation of a new, diamagnetic, species with a single resonance in the $^{31}P\{^1H\}$ NMR spectrum at $\delta_{^{31}P} = 74.7$ ppm (see Figure 3.15). ^{1}H NMR spectroscopy revealed **34** to exhibit C_S symmetry in solution and the lack of a signal corresponding to an NH proton indicated successful deprotonation. LIFDI mass spectrometry confirmed the proposed molecular composition and finally single crystals obtained from chlorobenzene/pentane diffusion allowed for a X-ray diffraction measurement to determine the molecular structure of **34**. The Re center is coordinated in a distorted square pyramidal coordination geometry with the nitride ligand in apical position ($\tau_5 = 0.30$)[196]. The Re≡N bond length (d(Re1-N2) = 1.666(2) Å) is in full agreement with a nitride ligand and does indicate only moderate bond elongation as compared to d(Re≡N) = 1.647(18) Å in compound **22** (see Section 2.3.1) or d(Re≡N) = 1.643(6) Å in **XXI**,[155] most likely due to the distorted geometry. The short distance to the backbone nitrogen donor (d(Re1-N1) = 2.0086(18) Å) and the planar coordination of the nitrogen atom ($\Sigma(\measuredangle_{N1}) = 352.6°$) support the formulation as an amide.

With this target molecule in hand, different routes to potential N_2 splitting were investigated. The Re(III)/Re(III) dimer(s) **33b**/**33a** were treated with chloride abstracting agents (NaX, with X = BPh_4^-, OTf^-) to stabilize the dimers analog to literature known 8π electron systems. Additionally, acids (HOTf, H(OEt$_2$)$_2$(BAr$^F_{24}$)) were added, aiming to split analog to the Mo system reported in the *Schneider* group[96]. Both approaches did not lead to any selective reaction (see Section 3.2.1 for a discussion of these strategies). Thus those reactions were focused were solutions of **30** under N_2 were treated with various reductants (Co(Cp*)$_2$, NaHg, KC_8, Na(NAP) (NAP = naphthalenide)). The necessity of *in situ* preparation of the Re complex meant a uncertainty in these reactions, since the stochiometry of the reductant had to be chosen based on assuming quantitative formation of **30**. Nevertheless, a consistent picture evolved during these attempts: reduction of **30** under N_2 resulted in complex decomposition and formation of various unknown species under all tested conditions (including initial dimer formation at low temperatures and subsequent addition of a reductant). This also applies to reactions starting from **31** with two equivalents of the reductant. In all of these mixtures, no signal was found which could indicate the formation of the desired nitride complex **34**. Instead, the actual composition of products changed between the reactions, and hardly any similarities in the product distribution was observed by comparing $^{31}P\{^1H\}$ NMR spectra of different runs.

[6] See Section 3.3.2 for further information on the synthesis and properties of this complex.

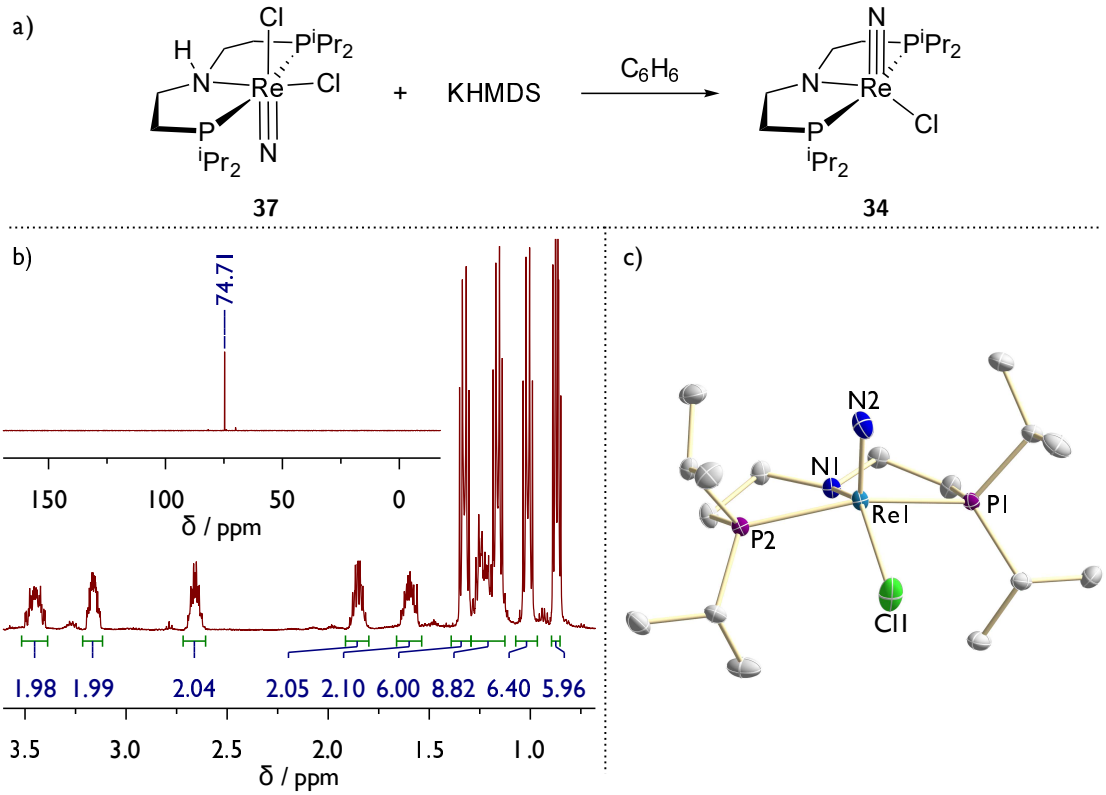

Fig. 3.15. *a*) Synthesis of **34** by deprotonation of **37**. *b*) ^{1}H NMR spectrum of **34** in C_6D_6. *Inset*: the corresponding $^{31}P\{^{1}H\}$ NMR spectrum. *c* Molecular structure of **34** obtained by single crystal X-ray diffraction measurement. A cocrystallized chlorobenzene molecule and all H atoms are omitted for clarity. Anisotropic displacement parameters are set to 50 % probability. Selected bond lengths [Å] and angles [°]: Re1-N1 2.0086(18), Re1-N2 1.666(2), Re1-Cl1 2.4248(6), N1-Re1-Cl1 137.43(6), P1-Re1-P2 155.43(2), N1-Re1-N2 111.37(9).

The sole exception was a broad peak at $\delta_{^{31}P} \approx 33$ ppm which appeared in many spectra in significant amounts (although never as an exclusive product). Single crystals could be isolated from one of the reaction mixtures, which revealed the Re(I) *bis*-N_2 complex [ReCl(N_2)$_2$(HPNP^{iPr})] (**35**) to be one of the reaction products by X-ray diffraction. While the origin of the NH proton (or hydrogen atom) is unclear so far, the presence of a Re(I) species in the mixture is of particular interest with regard to the findings that the *t*Bu based μ-N_2 bridged dimer **XX** is most likely formed *via* an ECCEC mechanism (E denoting an electron transfer step, C denoting a chemical step), consisting of inital Re(III/II) reduction (E), N_2 binding (C), chloride loss (C), *Re(II/I) reduction (E)* and final binding of another Re(III) species and comproportionation (C) to the dimer.[95]

Targeted synthesis of **35** by twofold reduction of amine trichloride precursor **29** with NaHg in THF under a dinitrogen atmosphere resulted in a single resonance in the $^{31}P\{^{1}H\}$ NMR spectrum at $\delta_{^{31}P} = 34.5$ ppm in benzene, thus confirmed the broad peak observed in almost all reduction attempts of **30** to correspond to **35** (in THF, the ^{31}P resonance occasionally showed significant broadening, especially in the presence of side products). The ^{1}H NMR spectrum shows a C_S symmetric complex with the NH proton resonating at $\delta_{^{1}H} = 2.90$ ppm.

The ν(N-H) as well as two ν(N≡N) stretching vibrations were found in the IR spectrum at $\tilde{\nu}$ = 3152.6 and 2038.8 / 1936.1 cm^{-1}, respectively. Compared to the stretching vibration of free N_2 (ν(N≡N) = 2359 cm^{-1})[213] these are rather typical stretching vibrations for Re(I) complexes with *end-on* bound N_2 ligands and indicate quite a signifcant amount of π-backbonding.[214] This is also reflected in a surprisingly cathodic reversible oxidation potential of −0.23 V vs. Fc^+/Fc corresponding to the Re(I/II) couple and deviating only marginally from the Re(III/IV) potential in **29** ($E_{1/2}$ = -0.24 V vs. Fc^+/Fc, see Section 3.1.1). Nevertheless, the CV included no reduction wave except for an irreversible wave as

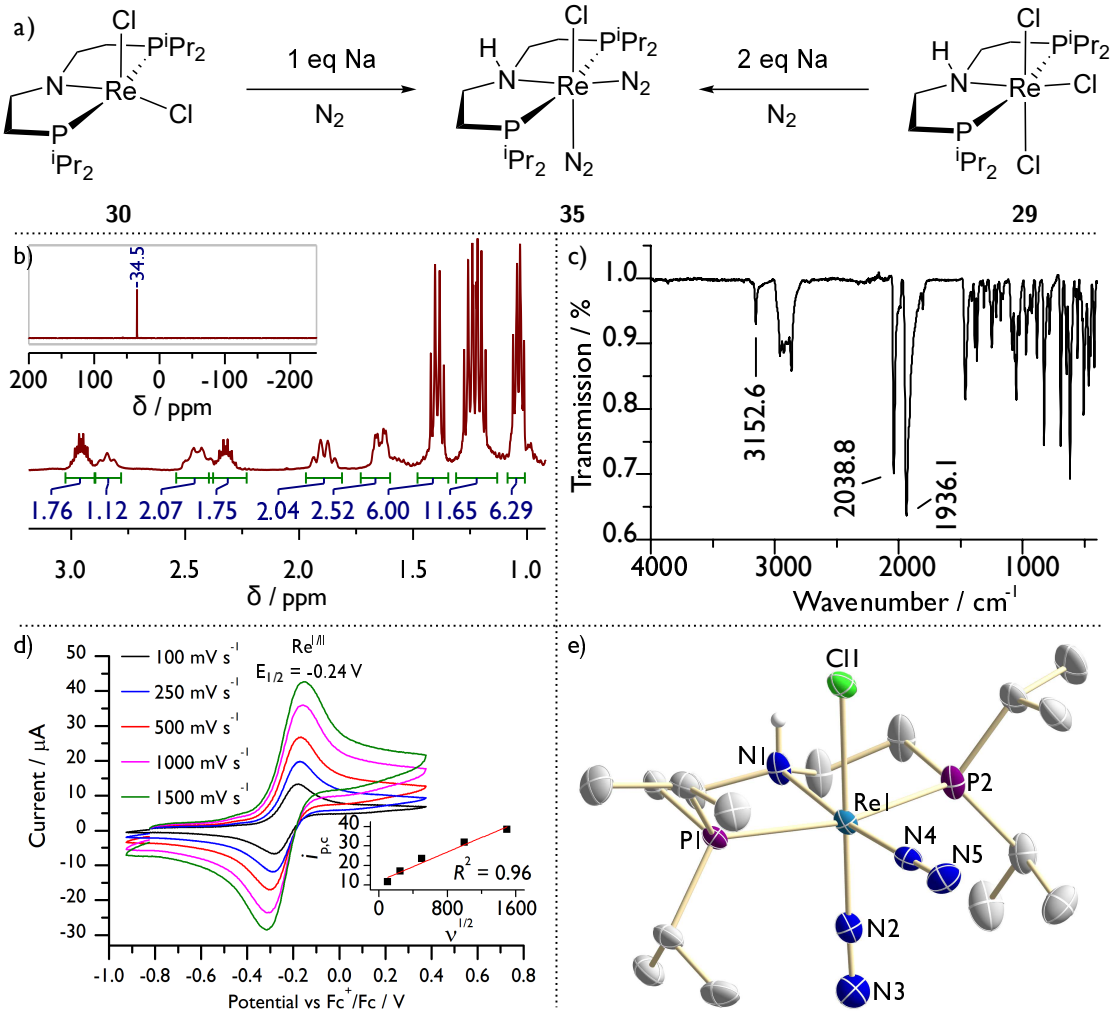

Fig. 3.16. *a*) Synthesis of **35** either by reducing **30** (formally by one electron, product is obtained among others) or by twoelectron reduction of **29**, both under N_2 atmosphere. *b*) ^{1}H and ^{31}P{^{1}H} (*inset*) NMR spectra of complex **35** in C_6D_6. *c*) ATR-IR spectrum of **35** with marked NH and N≡N stretching vibrations. *d*) CV measurements of Re(II/I) oxidation of **35** in THF at different scan rates (10^{-3} M in **35**, 0.1 M in $N^nBu_4PF_6$, WE: GC, RE: Ag-wire, CE: Pt-wire). *Inset*: Plot and linear fit of $i_{p,c}$ vs. $v^{1/2}$. *e*) Molecular structure of **35** obtained by single crystal X-ray diffraction measurements. Carbon bonded H atoms are omitted for clarity. Anisotropic displacement parameters are set to 50 % probability. Selected bond lengths [Å] and angles [°]: Re1-N1 2.188(3), Re1-N2 1.909(3), N2-N3 1.124(4), Re1-N4 1.969(3), N4-N5 1.090(4), Re1-Cl1 2.4994(8), Re1-N2-N3 175.13(12), Re1-N4-N5 179.0(3), N1-Re1-N4 173.86(11), Cl1-Re1-N2 178.57, P1-Re1-P2 161.23(3).

cathodic as −3.34 V. The molecular structure of **35** shows the Re center to be coordinated octahedrally, with two N_2 ligands binding *end-on* and *cis* to each other. The N≡N bond distances (d(N2-N3) = 1.124(4) Å and d(N4-N5) = 1.090(4) Å) as well as the Re–N≡N binding angles (∡(Re1-N2-N3) = 175.2(3)°, ∡(Re1-N4-N5) = 179.0(3)°) are slightly different , reflecting the different amounts of backbonding indicated by the IR absorptions. The amine nature of the PNP pincer is shown by a rather long Re-N bond distance (d(Re1-N1) = 2.188(3) Å) and a pyramidal coordination of the pincer nitrogen atom ($\Sigma(\measuredangle_{N1})$ = 341.4°). The formation of this product clearly indicates that overreduction could be an issue in the present system. One possible explanation for it's formation could be the following scenario: The initial reduction of a Re(III) complex is followed by chloride loss, leading to a Re(II) complex with an open coordination side. Due to the high tendency of the *iso*-propyl substituted pincer complex to be coordinated octahedrally, this complex can be expected to bind a second N_2 ligand, which leads to an anodic shift of it's reduction potential, as it is observed for **35** resulting in a potential inversion and thus in overreduction. Nevertheless, Re(I) N_2 complex represents an interesting compound to investigate the Re(I)-Re(III) comproportionation proposed for the parent *tert*-butyl based system (see Part I Section 3.2.1).[95] Especially in combination with the high ligand affinity of the Re(III) dichloro complex **30**, the formation of a mixed valent Re(I)/Re(III) dimer appears quite likely. As a matter of facts, this very dimer could be crystallized from the reaction mixture of an splitting attempt, i.e. from a mixture in which **30** is the starting material and **35** is known to be formed in significant amounts (see Figure 3.17). Unfortunately, the X-ray data were insufficient for unambiguous bond-length and angle determination, however the basic connectivity within the molecule can be treated as given. In line with the preceding discussion, the more activated, i.e. more electron-rich, N_2 ligand in **35** becomes the μ-bridging ligand in the dimer. Notably, the pincer and ligand orientation in this complex resembles the proposed structure

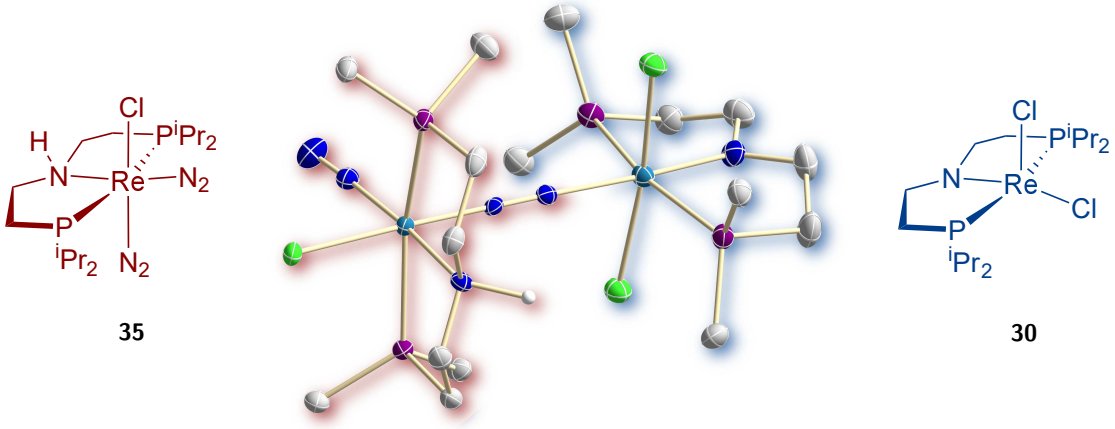

Fig. 3.17. Molecular structure obtained by X-ray diffraction measurements of a mixed valent dimer composed of Re(I) fragment **35** and Re(III) fragment **30** crystallized from a reaction mixture. The X-ray diffraction data quality does not allow for a detailed bond lengths and angle determination. CH_3 groups and all carbon bonded H atoms are omitted for clarity.

of the asymmetric Re(III)/Re(III) dimer **33a**, there based solely on NMR data. To date, neither further analysis or targeted synthesis of the mixed-valent dimer is available, nor is it known whether such a dimer would undergo dinitrogen splitting reactivity, e.g. under basic conditions. However, as synthetic routes to both building blocks are known, this would be an interesting problem to be solved in the future.

3.3 Amine based pincer chemistry

3.3.1 A thermally stable, μ-N_2 bridged Re(II) dimer and its photochemistry

Theoretical computations presented in this section were performed by Dr. Markus Finger (DFT) and Prof. Dr. Vera Krewald (TDDFT).

The overreduction of the N_2 dimers **33b**/**33a** to Re(I) complex **35** can potentially occur due to the reaction proceeding through an coordinationally unsaturated Re(II) complex, as discussed above. Consequently, the direct reduction of octahedrally coordinated amine complex **29** was attempted, because here reduction and subsequent chloride loss would allow for only one N_2 molecule to bind to the metal center. When [ReCl(N_2)$_2$(HPNP^{iPr})] (**35**) was formed by twofold reduction of **29**, the observation was made that this proceeds via a deeply blue colored intermediate, before the actual, orange complex is formed. This corresponds to the reduction wave around −1.84 V vs. Fc/Fc^+ in the CV of **29** and therefore to a single electron reduction (see Figure 3.3). Purposeful synthesis of the blue intermediate by reaction with 1 eq Co(Cp*)$_2$ under an N_2 atmosphere resulted in clean formation of a new complex, which again featured paramagnetically shifted but sharp NMR signals with resolved J couplings, similar to those observed for **29**. Two mutually coupling doublets in the $^{31}P\{^1H\}$ NMR spectrum ($\delta_{^{31}P} = -370.6$ and −380.4 ppm, $^2J_{PP} = 237.0$ Hz), eight signals for inequivalent methyl groups, and a mole peak of 1152.2 determined by LIFDI spectrometry are all in agreement with this species being the μ-N_2 bridged dimer [(μ-N_2){ReCl$_2$(HPNP^{iPr})}$_2$] (**36**), an amine pincer based analog of **XX** with a corresponding $10\pi4\delta$ electron configuration. If the reaction is carried out under fully labeled $^{15}N_2$, a singlet can be detected in $^{15}N\{^1H\}$ NMR

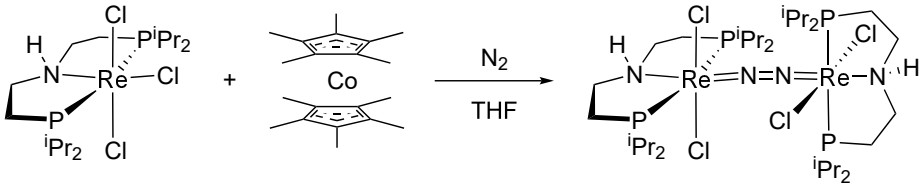

29 **36**

Scheme 3.1. Synthesis of **36** by reduction of **29** under an N_2 atmosphere.

spectroscopy with a strongly highfield shifted resonance at $\delta_{^{15}N}$ = -1113.0 ppm. While the IR spectrum of **36** does not show any sign for an N_2 band, the resonance Raman spectrum ($\lambda_{exc.}$ = 632.8 nm) shows a very prominent band at $\tilde{\nu}$ = 1733.3 cm^{-1}, which shifts to $\tilde{\nu}$ = 1675.2 cm^{-1} in the $^{15}N_2$ labeled complex, in perfect agreement with the harmonic oscillator approximation for an N_2 stretching vibration, which predicts a shift of $\Delta\tilde{\nu}(^{14}N_2\text{-}^{15}N_2)$ = 58.7 cm^{-1}. Since the complex is intensely colored, the UV/vis absorption spectrum was recorded. A strong band at λ = 578 nm (ϵ = 12294 M^{-1} cm^{-1}), assigned to a $\pi \rightarrow \pi^*$ transition in the μ-N_2 ligand by TDDFT calculations (*vide infra*), as well as an even stronger band peak at λ = 336 nm (ϵ = 38027 M^{-1} cm^{-1}) were found as characteristic features of **36**. X-ray diffraction data on single crystals confirmed the molecular structure of **36** as a dimer with the two Re centers being bridged by a μ-N_2 ligand (see Figure 3.18 *c*). Two

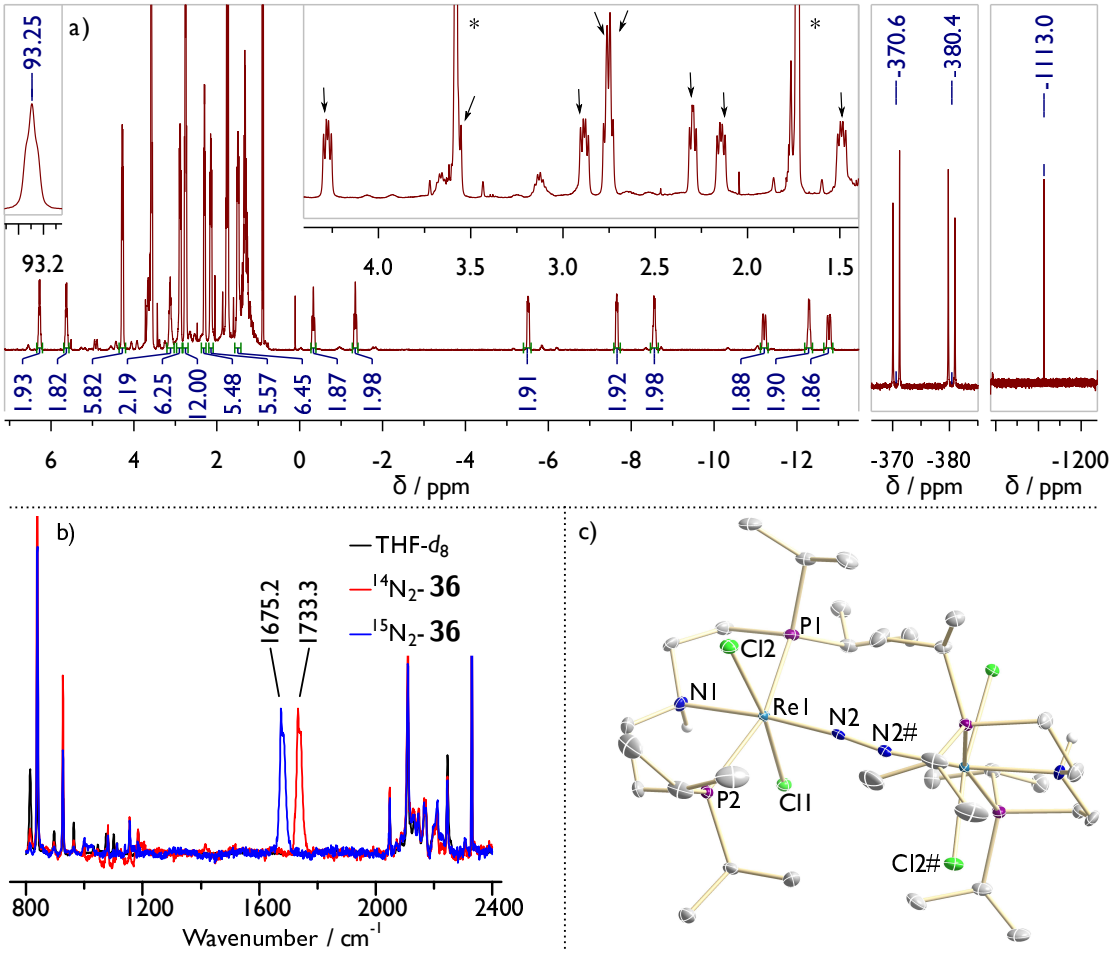

Fig. 3.18. *a*) NMR spectra of **36**: *left* = ^{1}H-NMR, arrows in the inset mark the eight *i*Pr groups; *middle* = $^{31}P\{^1H\}$-NMR spectrum; *right* = $^{15}N\{^1H\}$-NMR spectrum of **36**, synthesized under $^{15}N_2$ atmosphere. *b*) Resonance raman spectrum ($\lambda_{exc.}$ = 632.8 nm) of **36** (*red*) and $^{15}N_2$-**36** (*blue*). *c*) Molecular structure of **36** obtained by single crystal X-ray diffraction measurements. All H atoms but the NH proton are omitted for clarity. Anisotropic displacement parameters are set to 50 % probability. Selected bond lengths [Å] and angles [°]: Re1-Cl1 2.4530(7), Re1-Cl2 2.4271(8), Re1-N1 2.212(3), Re1-N2 1.906(2), N2-N2# 1.169(5), Cl1-Re1-Cl2 170.72(3), P1-Re1-P2 160.33(3), N1-Re1-N2 171.84(10), Re1-N2-N2# 171.5(3), Cl1-Re1-Re1#-Cl2# 75.5.

chloride ligands and the HPNP ligand complete the octahedral coordination environment of both metal centers. The N≡N bond distance of d(N2-N2#) = 1.169(5) Å is slightly shorter than in the *tert*-butyl pincer based dimer **XX** (d(N3-N4) = 1.202(10) Å, see Section 2.1), indicating a moderate activation of the ligand, which is also reflected in the stretching vibrations. As a striking difference to the *tert*-butyl pincer based dimer **XX**, the pincer nitrogen atom is coordinated *trans* to the N_2 bridge. Since the pincer $\{ReCl_2(HPNP^{iPr})\}$ fragments are twisted towards each other by 75.5°, the N–H moieties are the reason for the observed C_2, breaking the otherwise obtainable C_{2v} symmetry. Consequently, the rotation of the two fragments against each other seems to still be slow on the NMR timescale, indepedent of the reduced ligand bulkiness. Evaluation of the electrochemical properties of **36** by means of CV measurements show the dimer to undergo three redox events, a irreversible reduction and two fully reversible oxdiations (see Figure 3.19). All events show fast electron transfer to freely diffusing reactants according to the analysis of the forward peak current i_p vs. $v^{1/2}$ (using the *Randles-Sevcik* equation, see Equation 1.1). Chemical reversibility for both oxidations is further shown by a scan-rate independent ratio of the forward and backward peaks close to unity, while the ratio of $i_{p,c}$ of the reduction vs. $i_{p,a}$ of the first oxidation suggests more than one electrons are passed to the analyte (the decrease of that ratio with higher scan-rates could indicate an ECE mechanism, were both E steps have idenctical or even inverted potentials - however, closer analysis would be needed for a precise statement).

In contrast to **XX**, **36** exhibits a remarkable thermal stability, i.e. heating overnight to 60 °C did not lead to any sample decomposition detectable by NMR spectroscopy. To rationalize this, the thermal splitting was investigated computationally by *Dr. Markus Finger*. The shifted NMR signals of **36** are reminiscent of those of **29**, hence it can be assumed that TIP, induced by SOC, might play a role in describing the electronic structure of the dimer at hand. While basically DFT is inherently unable to accurately describe such compounds, the size of the system renders application of higher-level calculations extremely challenging. Therefore DFT[7] remained the method of choice for this study, keeping in mind that the results have to be treated with some care.

DFT resonably well reproduced the X-ray geometry of the dimer ($RMSD_{Cl,N,P,Re}$ = 0.139) and similar to **29**, the triplet ground state was found to be favorable over the open shell singlet state by $\Delta G^0 = -34\,kJ\,mol^{-1}$. Splitting by simply increasing the N≡N bond distance proceeds via the well-known zig-zag transition state (see Part I Section 3.2.1 for further details) with an estimated barrier of $\Delta G^{\ddagger} = 175\,kJ\,mol^{-1}$ and results in an dichloro nitride complex (**37**^{trans}) where the nitrido ligand is coordinated *trans* to the pincer amine donor. This product is still uphill by $\Delta G^0 = +9\,kJ\,mol^{-1}$ and features an extremely long Re–NH bond distance of 2.53 Å, resulting from the strong *trans* influence of the nitride. Isomerization of **37**^{trans} to either **37**$^{cis\text{-}1}$ with the Re≡N bond being *syn* to the N–H bond or to **37**$^{cis\text{-}2}$ with the Re–Cl bond being *syn* to the N–H bond results in product stabilization of ΔG^0

[7] M06/def2TZVP/SMD(THF)||PBE/D3BJ/RI/def2SVP(def2TZVP for Re, P, N, Cl).

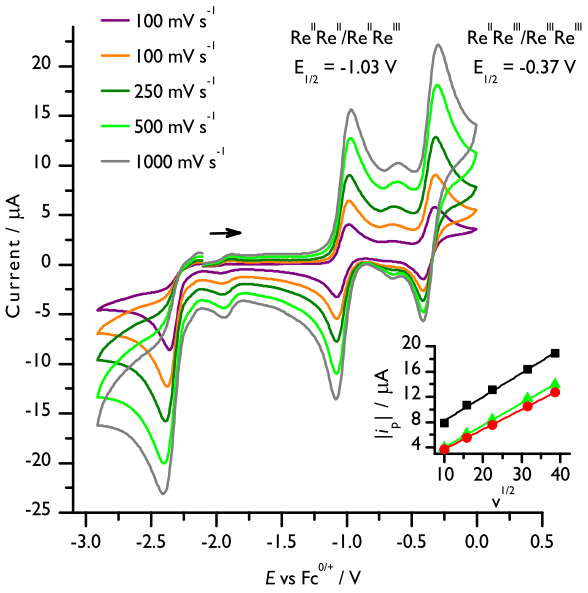

Fig. 3.19. CV measurements of two reversible oxidations and one irreversible reduction of **36** in THF at different scan rates (10^{-3} M **36**, 0.1 M $N^nBu_4PF_6$, WE: GC, RE: Ag-wire, CE: Pt-wire). *Inset*: Plot and linear fit of i_p vs. $v^{1/2}$ ($i_{p,a}$ for first oxidation in green, $R^2 = 0.999$; $i_{p,a}$ for second oxidation in red, $R^2 = 1.000$; $i_{p,c}$ for first reduction in black, $R^2 = 0.995$).

Tab. 3.2. Peak current analysis of the forwards peak of the first and second oxidation as well as the first reduction.

v / mV s^{-1}	$\frac{i_{p,c}}{i_{p,a}}$ (first ox.)
100	1.006
250	0.989
500	1.005
1000	1.056
1500	1.102
	$\frac{i_{p,c}}{i_{p,a}}$ (second ox.)
100	1.039
250	1.059
500	1.076
1000	1.002
1500	1.006
	$\frac{i_{p,c}}{i_{p,a}^{\text{firstox}}}$ (red.)
100	2.015
250	1.757
500	1.558
1000	1.398
1500	1.353

$= -46$ and -89 kJ mol^{-1}, respectively. This can easily be rationalized on the one hand since isomerization reduces the *trans* repulsion to the nitride ligand, as chloride is a much weaker donor than an amine and on the other hand because in **37**$^{cis\text{-}2}$, the coordination of the chloride ligand *trans* to the nitride can additionally be stabilized by an *intra*-molecular hydrogen bond to the N–H proton. Overall, the DFT derived scheme can explain the thermal stability by a significantly increased activation barrier, as compared to **XX** ($\Delta G^{\ddagger}$ = 113 kJ mol^{-1}). This increased activation barrier can be rationalized, as the amine ligand *trans* to the N_2 bridge in **36** raises the energy of the a_{2u} symmetric $M\overset{\sigma}{-}N\overset{\sigma^*}{-}N\overset{\sigma}{-}M$ orbital and thereby reduces its mixing with orbitals of the π system in the transition state, which is required for splitting (see Part I Figure 3.2). Additionally, no π donor is interacting with the π-MO space anymore which lowers the energy of the frontier orbitals and thus even further increases the MO energy gap. The influence of the *trans* ligand might also serve as an explanation for the comparison of *Cummins*' N_2 dimer complex **I** (see Part I, Section 2.1 and 3.2.1)[27,28,82] with *Schrock*'s [(μ-N_2){Mo(N(CH_2CH_2NR)$_3$)}$_2$] complex (R = C_6F_5)[84,85] of which only the former splits N_2, while the latter, which features a *trans* amine ligand, does not.

In a nutshell, thermal population of the a_{2u} symmetric $M\overset{\sigma}{-}N\overset{\sigma^*}{-}N\overset{\sigma}{-}M$ orbital through mixing with the HOMOs in a zig-zag transition state is not possible in **36**. Therefore alternative

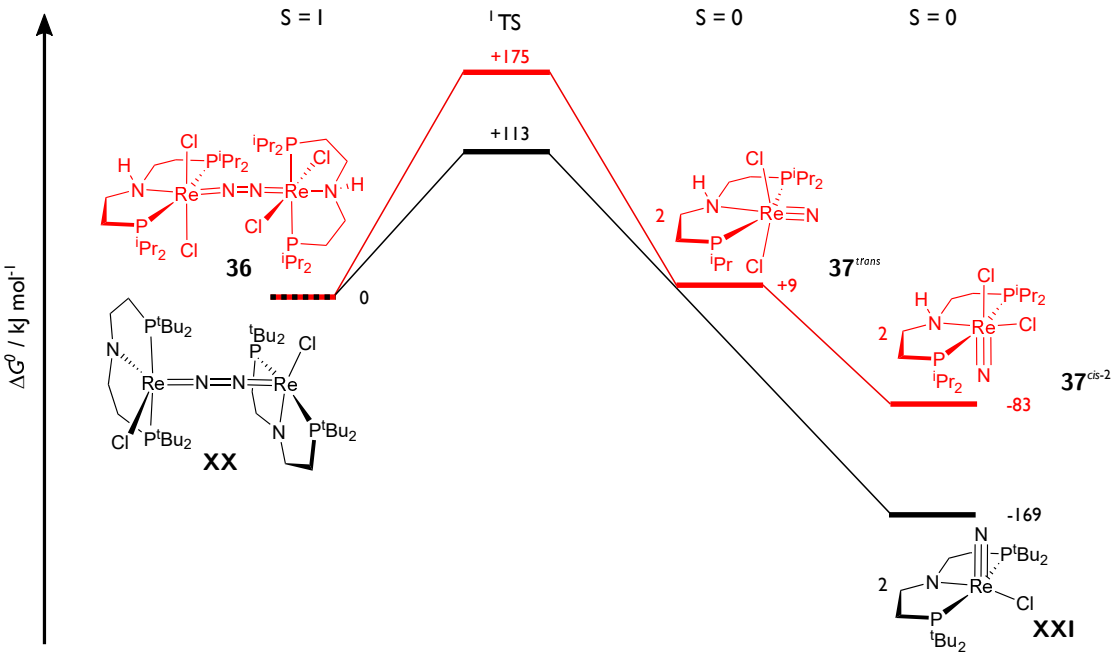

Fig. 3.20. DFT calculated thermodynamic scheme for the splitting of **XX** and **36** into the corresponding nitrido species.

ways for intramolecular electron transfer into the N–N antibonding MO space are needed. A well established possibility for achieving this is electronic excitation by absorption of photons. Consequently, a sample of **36** in THF was irradiated with a Hg(Xe) arc lamp equipped with a long wave pass filter for $\lambda > 305$ nm, leading to a gradual color change from blue to orange. In the UV/vis spectrum, a decay of all bands could be observed while NMR measurements indicated the formation of a single, diamagnetic, C_S symmetric species in 95 % spectroscopic yield, determined against an internal standard. Further spectroscopic characterization as well as preparation of an authentic sample via the reaction of **29** with an azide source revealed this species to be the splitting product [Re(N)Cl_2(HPNP^{iPr})] (**37**), where the two chloride ligands are oriented *cis* to each other and the N–H in *anti* orientation towards the Re≡N bond, which was also predicted by DFT to be the thermodynamically favored isomer (*vide supra*). This is a quite rare finding, as so far only five other system have been reported, which also do undergo photolytic splitting of dinitrogen, non of which bears a rhenium atom (see Part I Section 3.2.3).[28,86,109,114,116] The high selectivity of the photochemical dinitrogen splitting is an unique feature among these systems, especially because it seems to not suffer from M–N_2 bond cleavage which is an often observed or hypothesized side reaction.

To identify the productive range for this process, wavelength-dependent irradiations were performed. When a long wave pass filter for $\lambda > 420$ nm was used, no conversion could be observed, excluding the pronounced absorption at 578 nm to be relevant for the photolysis. Rather, irradiation with a 390 nm LED (FWHM = 11 nm) leads to successful conversion of **36** to **37**, indicating the small shoulder around $\lambda \approx 400$ nm to contain the transitions which are relevant for the reaction. The quantum yield of this reaction was determined to be very low (0.36 %) (see Section 1.2 for further details on the determination).

At this point, only little can be said about the excited state dynamics, by which the reaction proceeds. Based on the above hypothesized influence of the *trans* ligand on the thermal splitting pathway, photochemically induced chloride dissociation and subsequent thermal splitting was standing to reason. This could be excluded in so far as chloride concentration dependent photolysis did not lead to any distinguishable differences in the reaction kinetics. Therefore chloride dissociation (which likely *has* to occur at some point on the route to **37**) must take place only after the rate determining step of the reaction, which is believed to be the actual splitting step. However, other pathways can be envisioned to play a role during this process (e.g. phosphine dissociation, metal-nitrogen bond cleavage) and detailed analysis of the process (i.e. by transient spectroscopy) will be necessary to elucidate the actual mechanism. A first hint on the underlying processes can be derived from TDDFT calculations which were performed to gain inside into the nature of the relevant transitions in the experimentally identified, productive region (see Figure 3.21). The calculations reasonably well reproduced the spectroscopic features of the experimental electronic excitation spectrum. The excitation energies are all slightly overestimated, leading to a blueshift in the calculated spectrum, which is quite regularly observed in TDDFT calculations.[215] As mentioned above, the prominent absorption at 578 nm is identified as an excitation within the

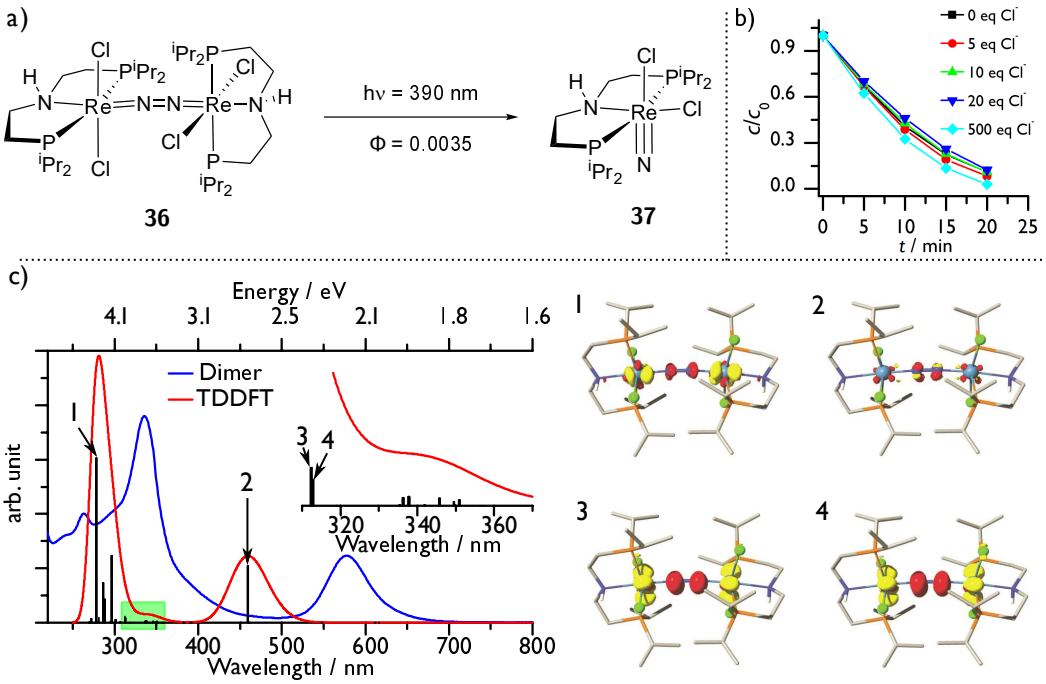

Fig. 3.21. *a*) Photolytic splitting of **36** into the corresponding nitride species **37** with a 390 nm LED, proceeding with a quantum yield of 0.36 %. *b*) Time-dependent concentration decay of **36** by photolysis ($\lambda > 305$ nm) in the presence of various concentrations of $NHex_4Cl$. *c*) Experimental (*blue*) vs. TDDFT calculated (*red*) electronic absorption spectrum of **36**. *Bottom right*: The electron difference densities of the marked excitations, with 1 and 2 being mainly located within the Re—N—N—Re moiety, while 3 and 4 are of considerable charge transfer from the metal centered δ orbitals into the Re—N—N—Re π^*-π^*-π^* orbital (see Figure 3.4 in Section 3.5 for the corresponding natural transition orbitals). Electron depletion is colored yellow, electcron gain in red.

Re−N−N−Re π manifold ($Re^{\pi}N^{\pi^*}N^{\pi}Re \rightarrow Re^{\pi^*}N^{\pi}N^{\pi^*}Re$). Closer investigation of the photolytically active region allowed for identification of two weak absorptions ($f_{osc} \leq 0.02$) with a pronounced MLCT character from the metal-centered, nonbonding δ orbitals into the $Re^{\pi^*}N^{\pi^*}N^{\pi^*}Re$ orbital. As a hypothetical effect from such an MLCT, increased flexibility of the M−N−N−M core could facilitate the splitting process. Additionally, the induced charge separation already resembles the situation in the final products, which might also be beneficial. Interestingly, the complex $[(\mu\text{-}N_2)\{Mo(Cp^*)(PP)\}_2]$ (PP = $Fe(1\text{-}PEt_2\text{-}C_5H_4)_2$) prepared by *Nishibayashi* and coworkers, which also does undergo photolytic splitting of the bridging dinitrogen ligand, exhibits very similar UV/vis spectroscopic features with a pronounced absorption at 748 nm located within the N-N fragment and a shoulder at 394 nm, which is associated with a loss of electron density between the two nitrogen atoms and is speculated to be the productive transition.[114]

It is noteworthy, that of those systems which are reported to undergo photoinduced N_2 bond scission, only two exhibit a 10π (0δ) electronic configuration of the {MNNM} core (i.e. the examples by *Cummins* and *Floriani*, see Part I Section 3.2.3),[28,86] while all others, including the in here presented complex **36**, have filled δ orbitals. The conclusion of *Cummins* from transient spectroscopy that the vibrationally hot ground state after IC rather than an excited state is relevant to N_2 splitting in his and probably also in *Floriani*'s dimer thus raises the question whether filled δ symmetric orbitals at the metal center might be a general requirement for photoinduced dinitrogen splitting.[216] However, the current availability of data on this subject is scarce, and more detailed investigation of the underlying excited state dynamics in these systems will be needed.

3.3.2 An octahedral rhenium nitride complex and nitrogen centered, nucleophilic reactivity

Complex $[Re(N)Cl_2(HPNP^{iPr})]$ (**37**) exhibits a single resonance in $^{31}P\{^1H\}$ NMR spectra at $\delta_{^{31}P} = 36.1$ ppm (see Figure 3.22, *c*). ^{1}H-NMR reveals it to be a C_S symmetric compound with a prominant peak corresponding to the NH moiety at $\delta_{^1H} = 4.93$ ppm (see Figure 3.22 *b*). When a labeled sample $^{15}N_2$-**36** is irradiated, in the $^{15}N\{^1H\}$ NMR spectrum of the product a singlet is detectable at $\delta_{^{15}N} = 383.8$ ppm, confirming **37** to be a nitride species. Single crystals grown from DCM/Et_2O allowed for molecular structure determination by X-ray diffraction measurements (see Figure 3.22 *a*). The Re center is found to be coordinated in an octahedral coordination sphere. The nitride ligand occupies an apical position in *anti* orientation to the N−H group and the chloride, which is bound *trans* to it exhibits a significantly elongated Re−Cl bond distance when compared with the second chloride (d(Re1-Cl4) = 2.6712(7) Å, d(Re1-Cl3) = 2.4309(7) Å). The small angle between the pincer backbone, the metal center and the chloride ($\measuredangle$(N3-Re2-Cl4) = 78.68(7)°), as well as the rather short distance to the backbone N−*H* atom (d(Cl4-H112) = 2.5596(1) Å) suggest some

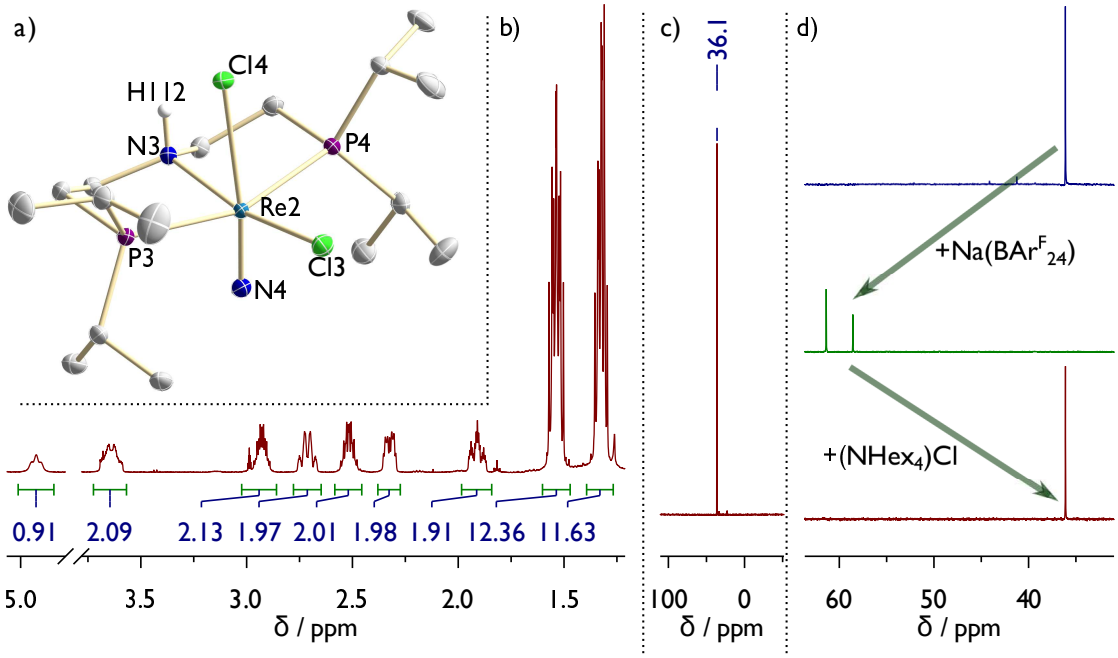

Fig. 3.22. *a*) Molecular structure of **37** obtained by single crystal X-ray diffraction measurements. All H atoms but the NH proton, a second, disordered nitride molecule, a DCM and a Et_2O molecule which all cocrystallized in the unit cell are omitted for clarity. Anisotropic displacement parameters are set to 50 % probability. Selected bond lengths [Å] and angles [°]: Re2-N3 2.159(2), Re2-N4 1.669(2), Re2-Cl3 2.4309(7), Re2-Cl4 2.6712(7), Cl4-H112 2.5596(1), N3-Re2-N4 92.65(11), P3-Re2-P4 159.92(2), Cl3-Re2-Cl4 88.23(2), N3-Re2-Cl4 78.68(7). *b*) ^{1}H NMR spectrum of **37** in CD_2Cl_2. *c*) $^{31}P\{^1H\}$ NMR spectrum of **37** in CD_2Cl_2. *d*) $^{31}P\{^1H\}$ NMR spectra of **37** (*blue*), **37** after addition of 1 eq of Na(BAr$^F_{24}$) (BAr$^F_{24}$ = tetrakis{3,5-(trifluoromethyl)phenyl}borate) (*green*) and after subsequent addition of $(NHex_4)Cl$(*red*).

degree of intramolecular hydrogen bonding to stabilize the coordination of the chloride. This is in stark contrast to the analog *tert*-butly based complex [Re(N)Cl(HPNP^{tBu})]^{Cl}, prepared by protonation of **XXI** with HCl, where the chloride was found to be non-coordinating in the X-ray structure.[94] The influence of the additional *trans* ligand in **37** is also reflected by a slightly elongated Re≡N bond distance as compared to the *tert*-butyl system (d(Re≡N) = 1.669(2) Å vs. 1.642(4) Å in [ReNCl(HPNP^{tBu})]^{Cl}), which suggests a higher degree of activation of the nitride. To exclude the coordination of the second chloride to be solely due to packing effects in the solid state, chloride dependent NMR spectra of **37** were recorded (see Figure 3.22 *d*). After addition of 1 eq of Na(BAr$^F_{24}$) as a chloride abstraction agent, **37** was cleanly converted into two new species as indicated by two singlets in the $^{31}P\{^1H\}$ NMR spectrum ($\delta_{^{31}P}$ = 58.6 and 61.4 ppm), which are also matched in ^{1}H NMR spectra. Although the new species are not fully characterized, they are tentatively assigned to the formation of two isomers of the cation obtained from chloride abstraction, with the N–H bond being oriented either *syn* or *anti* to the Re≡N moiety. In fact, the two isomers are found to be almost thermoneutral according to DFT calculations (ΔG^0 = 3.7 kJ mol^{-1}, see Section 3.6 for further details), as the intramolecular hydrogen bond to the *trans* chloride is removed, which stabilizes the *anti* isomer in **37** (compare Section 3.3.1). Subsequent

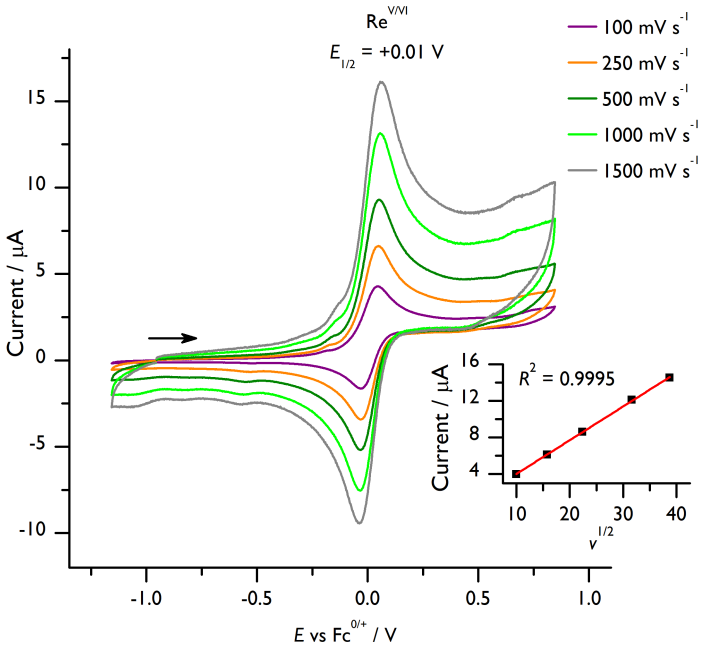

Fig. 3.23. CV measurements of Re(V/VI) oxidation **37** in THF at different scan rates (10^{-3} M **37**, 0.1 M $N^nBu_4PF_6$, WE: GC, RE: Ag-wire, CE: Pt-wire). *Inset*: Plot and linear fit of $i_{p,a}$ vs. $v^{1/2}$.

Tab. 3.3. Full peak analysis of the Re(V/VI) oxidation wave. v is the scan rate in mV s^{-1}, $i_{p,a}$ the anodic peak current in µA and ΔE is the peak separation given as ratio to peak separation of the internal standard.

v	$i_{p,a}$	$\left\lvert\frac{i_{p,c}}{i_{p,a}}\right\rvert$	ΔE
100	3.98	0.81	1.28
250	6.13	0.74	1.27
500	8.61	0.78	1.22
1000	1.21	0.76	1.24
1500	1.45	0.76	1.15

addition of 1.1 eq of $(NHex_4)Cl$ quantitatively restored **37**, proving the chloride abstraction to be reversible.

Recording the electrochemical response by CV measurements revealed a single oxidation as the only redox event. Linear behavior of the forward peak current with $v^{1/2}$ indicate fast electron transfer to freely diffusing complexes, while an constant peak current ratio and a peak separation comparable to that of the internal standard suggest chemical reversibility of the reaction. The fact that the forward peak current is slightly higher than the backward peak current is assigned to a small impurity identified by a preshoulder of the forwards peak, which leads to a (constant) offset of the current. Consequently, the reduced donation of amine pincer ligand in **37** as compared to the amide ligand in the *tert*-butyl analog **XXI** does not lead to any significant changes in the redox behavior of the complex and initial reduction to a Re(IV) nitride is not possible.

The absence of any reduction wave in the CV of **37** rendered an electrophilic reactivity of this complex rather unlikely and also treatment with hydrogen or carbon monoxide gas did not lead to any reactions, not even at elevated temperatures (60 °C, overnight). Therefore, the reactivity studies of the nitride focused on its nucleophilic behavior. Inital attempts to protonate **37** with acids like (LuH)OTf ($pK_a^{THF} = 7.2$) or $(PhNH(Me)_2)OTf$ ($pK_a^{THF} = 4.9$)[217] did also not lead to any reaction, showing the nitride to be a fairly weak base. However, reaction with strong *Lewis* acids like HOTf ($pK_a^{MeCN} = 2.6$)[77] or BAr^F_{18} (BAr^F_{18} = tris{3,5-bis(trifluoromethyl)phenyl}borane) do lead to immediate conversion to new com-

plexes as indicated by new singlets in the $^{31}P\{^{1}H\}$-NMR spectrum at $\delta_{^{31}P} = 30.2$ ppm and 23.9 ppm, respectively.

In the reaction with HOTf, the NMR signals were found to be very broad in many cases, independent of whether the samples were measured in CD_2Cl_2 or THF-d_8. Nevertheless, full assignment of all NMR signal was possible, by cooling the sample to −35 °C. Despite the expected signals belonging to the *iso*-propyl groups and ligand backbone, a broadened triplet at 4.96 ppm and a broad singlet at 14.24 ppm were found in the ^{1}H NMR spectrum which integrated to one proton each. The ^{1}H-^{15}N-HSQC spectrum contains two cross peaks, one for the pincer backbone NH at $\delta_{^{1}H} = 4.96$ ppm / $\delta_{^{15}N} = -330.0$ ppm and one for a Re≡N−H proton at $\delta_{^{1}H} = 14.24$ ppm / $\delta_{^{15}N} = 18.1$ ppm, proving successful nitride centered protonation and the formation of *cis*-[Re(NH···OTf)Cl_2(HPNP^{iPr})] (**cis-38**···**OTf**). The molecular structure of **cis-38**···**OTf** derived from X-ray diffraction measurements of single crystals confirms the compound to be an octahedrally coordinated parent imido complex with the triflate anion forming a hydrogen bond to the corresponding proton. The Re≡NH bond distance (d(Re$_1$−N$_2$) = 1.692(5) Å) is only slightly elongated in comparison to nitrido complex **37** (Δd(Re≡N) = 0.02 Å), but the deviation of the Re≡N−H angle (∡(Re1-N2-H112) = 167(5)°) from linearity and the significantly shortened Re−Cl bond length of the *trans* chloride ligand (**cis-38**···**OTf**: d(Re1-Cl2) = 2.4600(14), **37**: d(Re2-Cl4) = 2.6712(7) Å) still substantiate the imido nature of the NH ligand.

The formation of **cis-38**···**OTf** highlights the advantage of the reduced ligand sterics which allow for binding of a sixth ligand *trans* to the nitride. Since the Re center of **37** is coordinated octahedrally and the backbone nitrogen is already protonated, the nitride remains the only basic side of the molecule, rendering imido formation most favorable. Additionally, the fact that both chlorides are coordinating omits the formation of a dication, which would have been necessary in the case of the *tert*-butyl complex [Re(N)Cl(HPNP^{tBu})]^{Cl}. This is further underpinned by the finding that the two isomers formed from chloride abstraction from **37** are unreactive even towards H(Et$_2$O)$_2$(BAr$^{F}_{24}$).

While parent imido compounds are not unprecedented (see ref. [218] and references [12-35] therein), to date only three other examples in the coordination sphere of rhenium were reported, with Re≡NH bond distances of 1.664(3)-1.712(8) Å.[219–221] Additionally, there are only two literature examples of stable parent imido complexes derived from dinitrogen splitting, even though they are regularly discussed as intermediates in transition metal catalyzed dinitrogen fixation to ammonia.[68,114]

The reason for the broadend NMR signals is unclear at this point, but might be due to a fast equilibrium between different isomers of **38^{OTf}**. Indeed, in the $^{31}P\{^{1}H\}$ NMR spectrum of an analytically pure sample at −40 °C, a small, similarly broadened singlet at 44.9 ppm can be found, which might correspond to such an isomer (see inset in Figure 3.22 *c*). Computational evaluation[8] of different isomers also points to this possibility (see Part III Section 3.7 for

[8] DFT: PBE0/D3BJ/RIJCOSX/def2-TZVPP or PBE/D3BJ/RI/def2-TZVPP with CPCM(THF) or CPCM(DCM)||PBE/D3BJ/RI/def2-SVP.

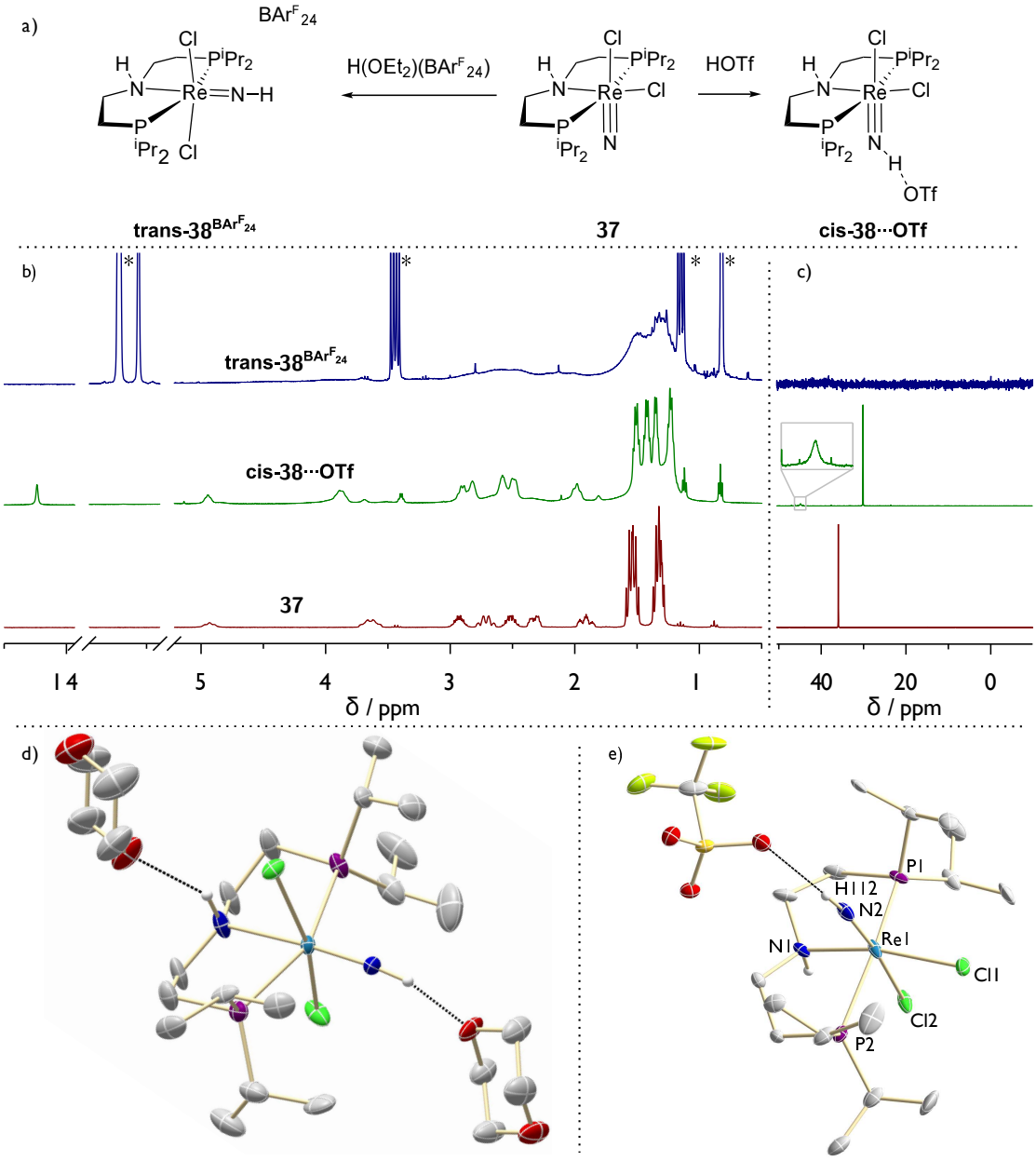

Fig. 3.24. *a*) Protonation of **37** to parent imido complexes **cis-38···OTf** (*right*) and **trans-38$^{BAr^F_{24}}$** (*left*) by HOTf and H(OEt$_2$)(BAr$^F_{24}$), respectively. *b*) ^{1}H-NMR spectra (**cis-38···OTf** was measured at −35 °C; signals marked with asterisks in the spectrum of **trans-38$^{BAr^F_{24}}$** correspond to the anion, Et$_2$O from the acid and PMe$_3$ which was added as internal standard in a capillary). *c*) ^{31}P{^{1}H}-NMR spectra (**cis-38···OTf** was measured at −35 °C). *d*+*e*) Molecular structures of **trans-38$^{BAr^F_{24}}$** (*d*) and **cis-38···OTf** (*e*) obtained by single crystal X-ray diffraction measurements. All H atoms but the NH protons as well as disordered atoms, the BAr$^F_{24}$ anion and a cocrystallized solvent molecules are omitted for clarity. Anisotropic displacement parameters are set to 50 % probability. Selected bond lengths [Å] and angles [°]: **trans-38$^{BAr^F_{24}}$**: Re1-N1 2.298(5), Re1-N2 1.706(5), Re1-Cl1 2.3929(13), Re1-Cl2 2.4094(15), N1-Re1-N2 175.4(2), Cl1-Re1-Cl2 163.27(5), Re1-N2-H112 170(5), P1-Re1-P2 156.41(6). **cis-38···OTf**: Re1-N1 2.164(5), Re1-N2 1.692(5), Re1-Cl1 2.473(12), Re1-Cl2 2.4600(14), N1-Re1-N2 90.8(2), Cl1-Re1-Cl2 87.7(3), Re1-N2-H112 167(5), P1-Re1-P2 164.3(3).

details). Investigated were the imido complex isomers with *cis*- and *trans*-chlorides, each of them with and without hydrogen bonding to the triflate anion (i.e. **cis-38^{OTf}**, **cis-38···OTf**, **trans-38^{OTf}** and **trans-38···OTf**). For the reaction of **37** with HOTf, the crystallized isomer **cis-38···OTf** (i.e. with an apical NH moiety and a hydrogen-bound triflate anion) is found to be very close in energy with the cationic *trans*-chloro analog with a non-coordinating anion **trans-38^{OTf}**. Actually, when a DCM solvent model is used, **trans-38^{OTf}** is even favored ($\Delta G^0 = -1.9\,\mathrm{kJ\,mol^{-1}}$ (PBE), $-6.5\,\mathrm{kJ\,mol^{-1}}$ (PBE0)), while with the THF model **cis-38···OTf** is sightly more stable ($\Delta G^0 = -6.5\,\mathrm{kJ\,mol^{-1}}$ (PBE), $-2.7\,\mathrm{kJ\,mol^{-1}}$ (PBE0)). Interestingly, a hydrogen bond between the imido hydrogen atom in the *trans* isomer and the triflate anion (i.e. isomer **trans-38···OTf**) is thermodynamically unfavorable in all calculations, and in these structures the proton is found to be localized at the triflate anion, rather than at the nitride. Furthermore, when only the isomers **cis-38^{OTf}** and **trans-38^{OTf}** are compared (i.e. neglecting the possibility of hydrogen bond formation), **trans-38^{OTf}** is predicted to be the more stable anion in all cases.
These results would also be in line with the observation that the peak broadening strongly depends on the reaction conditions and the acid. To test these computational results, protonation of **37** was repeated with the strong acid $H(OEt_2)_2(BAr^F_{24})$, which features a non-coordinating anion. Unfortunately, the NMR spectra in these reactions were almost not interpretable due to extreme line broadening. Selectivity of the reaction is nevertheless proven by subsequent treatment of the reaction mixture with NEt_3, which leads to regeneration of starting complex **37** by more than 90 % and single crystals allowed for molecular structure determination by X-ray diffraction. Indeed, the non-coordinating anion results in isomerization to the imido complex **trans-38$^{BAr^F_{24}}$**, with the two chloride ligands being oriented *trans* to each other and the imido group being coordinated *trans* to the pincer NH functionality. The Re≡N bond is slightly elongated in comparison with **cis-38···OTf** (d(Re1-N2) = 1.706(5) Å) as a direct influence of the stronger *trans* donor ligand, also expressed in the elongated Re–N_{PNP} bond (**cis-38···OTf**: d(Re1-N1) = 2.164(5) Å, **trans-38$^{BAr^F_{24}}$**: d(Re1-N1) = 2.298(5) Å). The imido moiety is tendentially linear, but the angle must not be interpreted to much due to the large error of that specific value ($\measuredangle$(Re1-N2-H112) = 170(5)°). Consequently, the choice of the anion has a significant influence on the molecular structure. The fact that the crystal structure of **trans-38$^{BAr^F_{24}}$** contains hydrogen bonded dioxane molecules, while the structure of **cis-38···OTf** features a THF molecule which does not form any hydrogen bond further highlights how sensitive this effect is to small changes.

An indication on whether this *cis-trans* isomerization occurs after protonation or if **37** itself might already exhibit such an equilibrium (only strongly on the *cis* side) is obtained from the reaction with BAr^F_{18}. A new signal in the ^{31}P NMR spectrum at $\delta_{^{31}P} = 23.9$ ppm as well as the ^{1}H NMR spectrum show clean conversion to a new C_S symmetric complex with an intact NH proton at $\delta_{^1H} = 4.98$ ppm and a slight shift of those signals corresponding to the borane, indicating coordination. This complex can be assumed to be the *cis* chloro complex $[Re(NBAr^F_{18})Cl_2(HPNP^{iPr})]$ (**cis-39**) analog to **38^{OTf}**. Surprisingly, the complex turned out

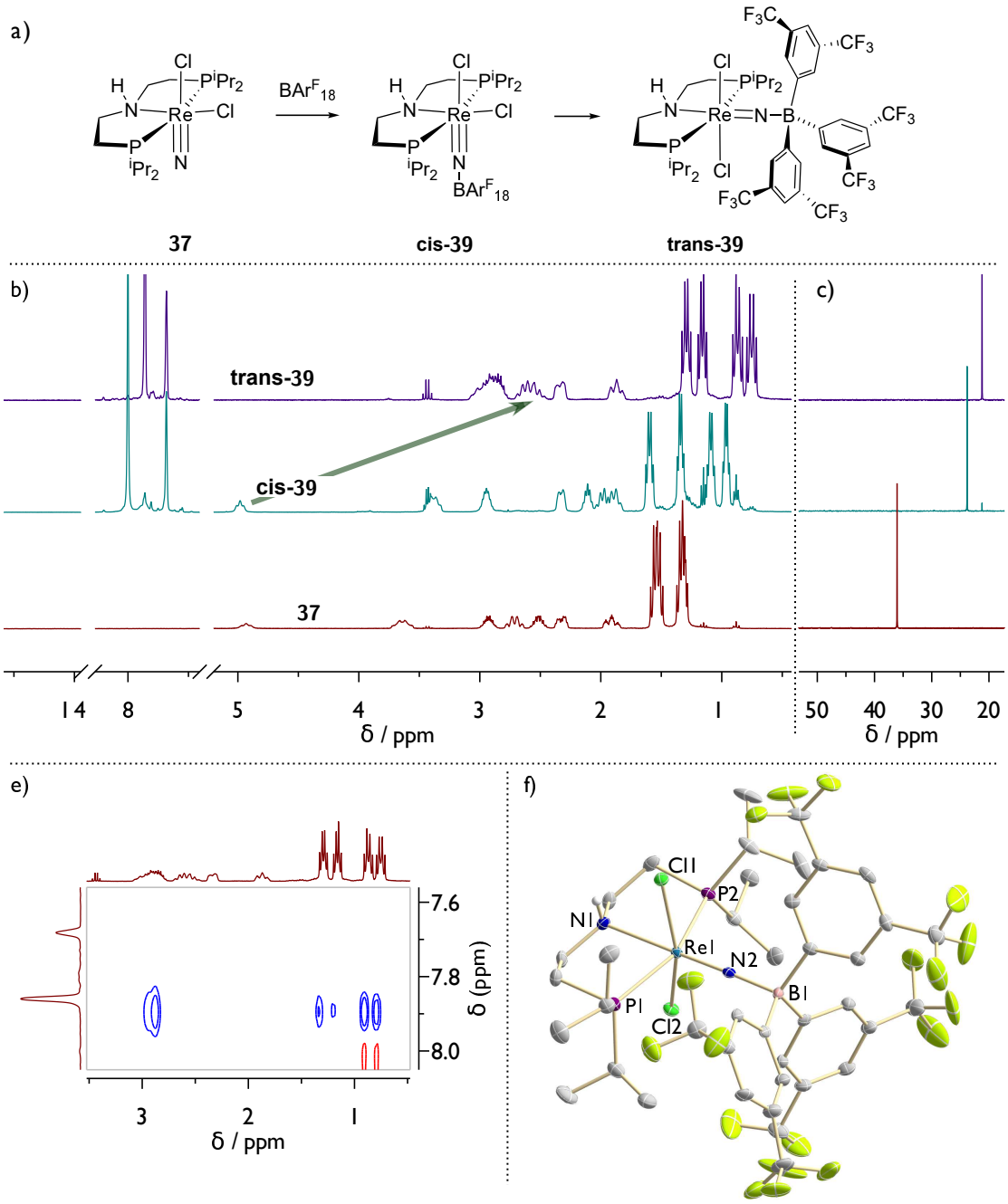

Fig. 3.25. *a*) Synthesis of **cis-39** and isomerization to **trans-39**. *b*) ^{1}H-NMR spectra. The green arrow highlights the sift of the pincer NH proton upon isomerization. *c*) ^{31}P{^{1}H}-NMR spectra. *d*) NOESY spectrum of **trans-39** showing cross peaks between the aromatic protons and all *iso*-propyl groups. *e*) Molecular structure of **trans-39** obtained by single crystal X-ray diffraction measurements. All H atoms but the NH proton as well as disordered atoms are omitted for clarity. Anisotropic displacement parameters are set to 50 % probability. Selected bond lengths [Å] and angles [°]: Re1-N1 2.341(3), Re1-N2 1.705(3), Re1-Cl1 2.4311(9), Re1-Cl2 2.3788(9), N2-B1 1.568(5), N1-Re1-N2 176.93(13), Cl1-Re1-Cl2 159.55(3), Re1-N2-B1 175.5(3), P1-Re1-P2 156.22(3).

to be unstable at RT, undergoing a selective follow-up reaction overnight to a new species with a resonance at $\delta_{^{31}P} = 21.2$ ppm. The ^{1}H NMR spectrum also revealed all signals to be shifted of which the NH proton exhibits the largest shift to $\delta_{^{1}H} = 2.51$ ppm. According to LIFDI mass spectrometry, the new complex still is a simple borane-nitride adduct, so the chemical composition did not change but rather the complex isomerized. Indeed, cross peaks in the NOESY spectrum indicate spacial proximity between the aromatic protons of the borane and all four signals belonging to the *iso*-propyl groups, indicating an isomerization to the *trans*-chloro complex [Re(NBAr$^{F}_{18}$)Cl$_2$(HPNP^{iPr})] (**trans-39**), resembling the structure of **trans-38$^{BAr^{F}_{24}}$**. This is also in good agreement with the observed shifts in the ^{1}H NMR spectrum, since the effect on the pincer NH proton can be assumed to be strongest. This assignment was confirmed by X-ray diffraction analysis of single crystals of **trans-39**. The Re center was indeed found in an octahedral coordination environment, again with the two chloride ligands oriented *trans* to each other and the N–BAr$^{F}_{18}$ moiety in *trans* position to the pincer amine donor. The bond lengths and angles are very similar to those of **trans-38$^{BAr^{F}_{24}}$** (d(Re1-N1) = 2.341(3) Å and d(Re1-N2) = 1.705(3) Å, **38^{OTf}**: d(Re1-N1) = 2.164(5) Å), reflecting the mutual *trans* influence of two strong donors, and the Re=N–B angle is again closer to linearity than in **cis-38···OTf** ($\measuredangle$(Re1-N2-B1) = 175.5(3)°).

No reactivity studies have been performed on **trans-** or **cis-39**. In contrast, very preliminary reactions of **cis-38···OTf** with excess of Co(Cp)$_2$ or Co(Cp*)$_2$ (4 eq) and (Ph$_2$NH$_2$)OTf (5 eq) were executed, in an attempt to form ammonia. While the reaction with Co(Cp)$_2$ seemed to yield rather selectively an unknown, paramagnetic species, the reaction with Co(Cp*)$_2$ resulted in a ^{1}H NMR spectrum which appeared to be identical with [ReCl$_3$(HPNP^{iPr})] (**29**). However, since no additional chloride source was added, the reaction is unbalanced and rather formation of a cationic analog with (non)coordinating triflate might have occured. In the end, even though these results do look quite promising with regard to potential ammonia formation, only NMR data are available on those reactions and no attempts to detect ammonia were made, leaving a lot of room for further research before any conclusions can be drawn.

3.3.3 Metal-ligand cooperative benzamide / benzonitrile formation

This nitride centered reactivity raised the question in how far **37** exhibits improved reactivity towards carbon centered electrophiles. One of the main motivations for using the *iso*-propyl ligand was the hope to access a more reactive nitride than with the *tert*-butyl ligand. Therefore the reactivity of **37** towards acyl chlorides was tested, which are less reactive than previously utilized alkyl triflates. In fact, heating **37** with benzoyl chloride or acetyl chloride in 1,4-dioxane to 90 °C overnight does lead to conversion to main one new complex. While the reaction seems to proceed analogous in with both reagents (identical spectroscopic signature for the obtained Re complex in the ^{1}H and $^{31}P\{^{1}H\}$ NMR spectra), the reaction with

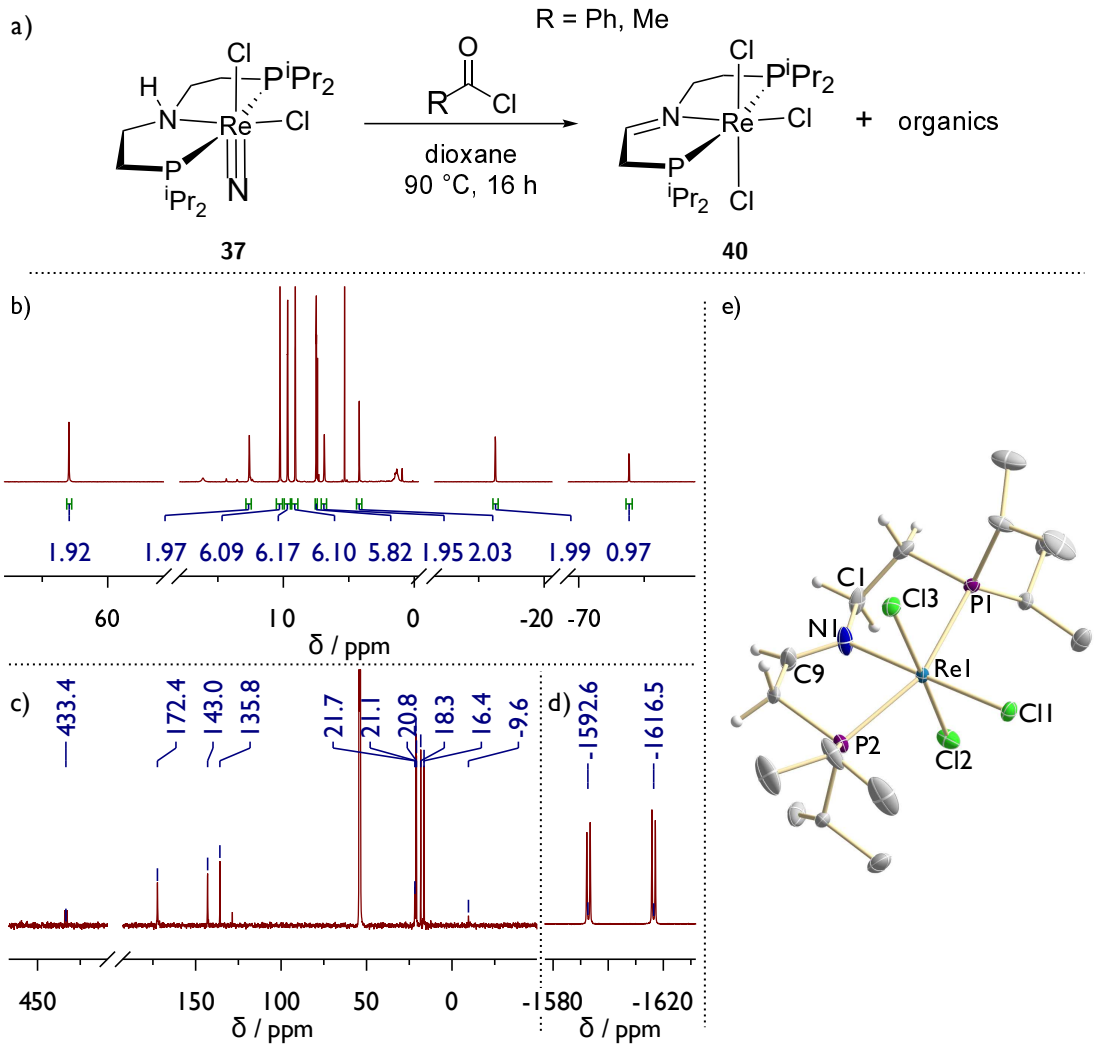

Fig. 3.26. *a*) Reaction of **37** acetyl chlorides to **40** and organic compouds. *b*) ^{1}H NMR spectrum of **40**. *c*) ^{13}C{^{1}H} NMR spectrum of **40**. *d*) ^{31}P{^{1}H} NMR of **40**. *e*) Molecular structure of **40** obtained by single crystal X-ray diffraction measurements. All H atoms but the backbone protons are omitted for clarity. Anisotropic displacement parameters are set to 50 % probability. Selected bond lengths [Å] and angles [°]: Re1-N1 2.109(5), Re1-Cl1 2.3970(13), Re1-Cl2 2.3686(13), Re1-Cl3 2.3958(13), N1-C1 1.460(7), N1-C9 1.299(7), P1-Re1-P2 159.78(5), N1-Re1-Cl1 177.88(14), Cl2-Re1-Cl3 176.41(5).

acetyl chloride was not further investigated and all data reported here refer to the reaction with benzoyl chloride. The new Re complex features two new doublets in ^{31}P{^{1}H} NMR at $\delta_{^{31}\mathrm{P}} = -1592.6$ and -1616.5 ppm with a mutual coupling constant of $^{2}J_{\mathrm{PP}} = 248$ Hz. In the ^{1}H NMR spectrum, four signals corresponding to *iso*-propyl groups (i.e. two inequivalent groups) identify the complex to exhibit C_S symmetry on the NMR timescale with the mirror plane being coplanar with the PNP pincer ligand. Additionally, four signals arising from the pincer backbone with a ratio of 2:2:2:1 resonate in a range of 63 - -74 ppm and no NH proton could be identified, suggesting an oxidation of the pincer backbone to an imine (i.e. N(=CHCH$_2$P*i*Pr$_2$)(CH$_2$CH$_2$P*i*Pr) (P=NP$^{i\mathrm{Pr}}$). Despite being strongly shifted, all signals are very sharp and exhibit resolved J-couplings, reminiscent of the spectra of Re(III)

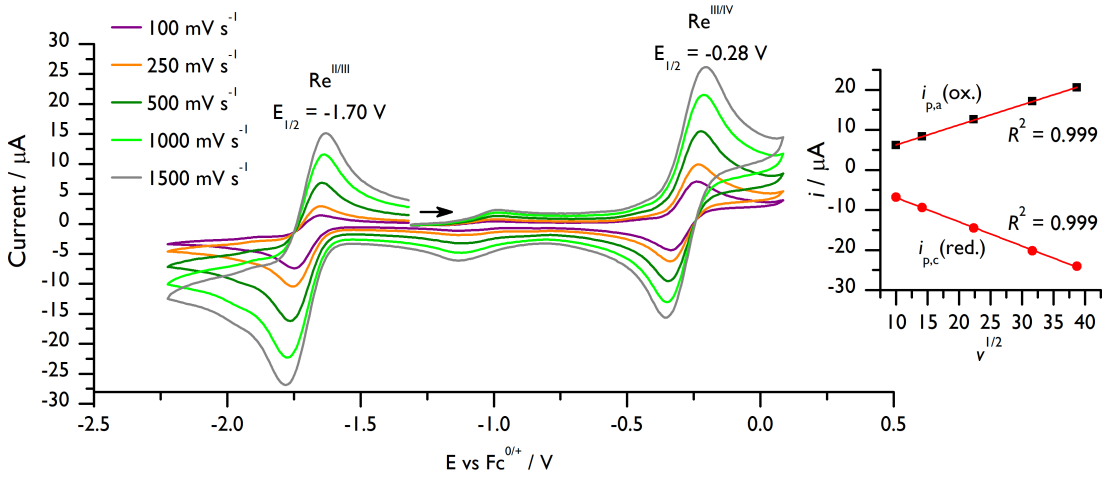

Fig. 3.27. CV measurements of reversible oxidation and quasi-reversible reduction of **40** in THF at different scan rates (10^{-3} M **40**, 0.1 M $N^nBu_4PF_6$, WE: GC, RE: Ag-wire, CE: Pt-wire). *Inset*: Plot and linear fit of $i_{p,a}$(oxidation) and $i_{p,c}$(reduction) vs. $v^{1/2}$.

Tab. 3.4. Peak analysis for the oxidation and reduction of **40**. ΔE denotes the peak separation of the oxidation wave as ratio of the peak separation of subsequent added ferrocene.

	oxidation		reduction		
v / mV s^{-1}	$i_{p,a}$ / µA	$\left\|\frac{i_{p,c}}{i_{p,a}}\right\|$	$i_{p,c}$ / µA	$\left\|\frac{i_{p,a}}{i_{p,c}}\right\|$	ΔE
100	6.13	1.051	-6.83	0.507	1.000
200	8.30	1.077	-9.38	0.564	1.083
500	12.64	1.087	-14.47	0.726	1.154
1000	17.11	1.098	-20.17	0.809	1.067
1500	20.53	1.076	-24.08	0.857	1.125

complex **29**. In the $^{13}C\{^1H\}$ NMR spectrum, two strongly shifted signals arise at $\delta_{^{13}C}$ = 433.4 and −9.6 ppm. Decoupling of the entire proton range was not possible, resulting in the signal at $\delta_{^{13}C}$ = 433.4 ppm to be split into a doublet, which collapsed to a singlet when the decoupler was set to the proton signal at $\delta_{^1H}$ = −73.9 ppm. Finally, LIFDI mass spectrometry, independent synthesis by reaction of **29** with 2 eq TTBP and X-ray diffraction measurements on single crystals all confirmed the newly formed complex to be the backbone oxidized Re(III) complex [$ReCl_3$(P=NP^{iPr})] (**40**). In the X-ray structure, the Re center is coordinated octahedrally by the P=NP^{iPr} and three chloride ligands. Backbone oxidation to the imine is supported by one significantly shortened N=C bond (d(N1-C9) = 1.299(7) Å, d(N1-C1) = 1.460(7) Å), a planar coordination of the nitrogen atom ($\Sigma(\measuredangle_{N1})$ = 359.55°) and a Re–N bond distance which is too long for an amide ligand (d(Re1-N1) = 2.109(5) Å). The electrochemical response of **40** in CV measurements is also quite similar to that of **29**. A reversible Re(III/IV) oxdiation wave at $E_{1/2}$ = −0.28 V vs. Fc/Fc^+ and a quasi-reversible reduction wave at $E_{1/2}$ = −1.70 V are found, in line with the Re(III) formulation. Linear development of the forward peak current with $v^{1/2}$ shows both process to be induced by fast electron transfer to freely floating molecules in solution. The reversibility of the oxidation is

reflected by a peak separation almost identical to that of ferrocene as well as an invariant ratio of the backward to the forward peak current close to unity, while for the reduction this ratio clearly decreases with lower scan rates, indicating an irreversible chemical follow-up process after reduction.

The strong shifts in NMR spectroscopy most likely arise from a comparable TIP resulting from SOC, just as in the amine complex **29** (compare Section 3.1.2). This is not surprising, since **40** is an octahedrally coordinated d^4 complex and the donor abilities of the imine vs. and amine ligand can be assumed to be comparable, so no big influence on the ligand field is to be expected.

The observed formation of **40** raises the question about the fate of the nitrido ligand. The formal Re(V/III) reduction is accompanied by the backbone oxidation by two electrons and removal by two protons. Considering benzoyl chloride as the most likely source of the additional chloride ligand in **40**, either the formation of benzamide or benzonitrile and water are suitable possiblities to balance the reaction. If the solvent of a neat reaction mixture is removed *in vacuo* and the products are analyzed in THF-d_8, the aromatic region of the ^{1}H NMR spectrum reveals signals for benzoic acid and benzamide ($\delta_{^1\mathrm{H}} = 8.11$ and 7.81 ppm, both in THF-d_8). If the reaction was performed directly in toluene-d_8 rather than 1,4-dioxane, equimolar formation of benzonitrile (with respect to benzoic acid) was detectable. However, these latter reactions gave reduced overall yields. The occurance of all three products can be rationalized by assuming initial electrophilic attack of the benzoyl chloride at the nitride

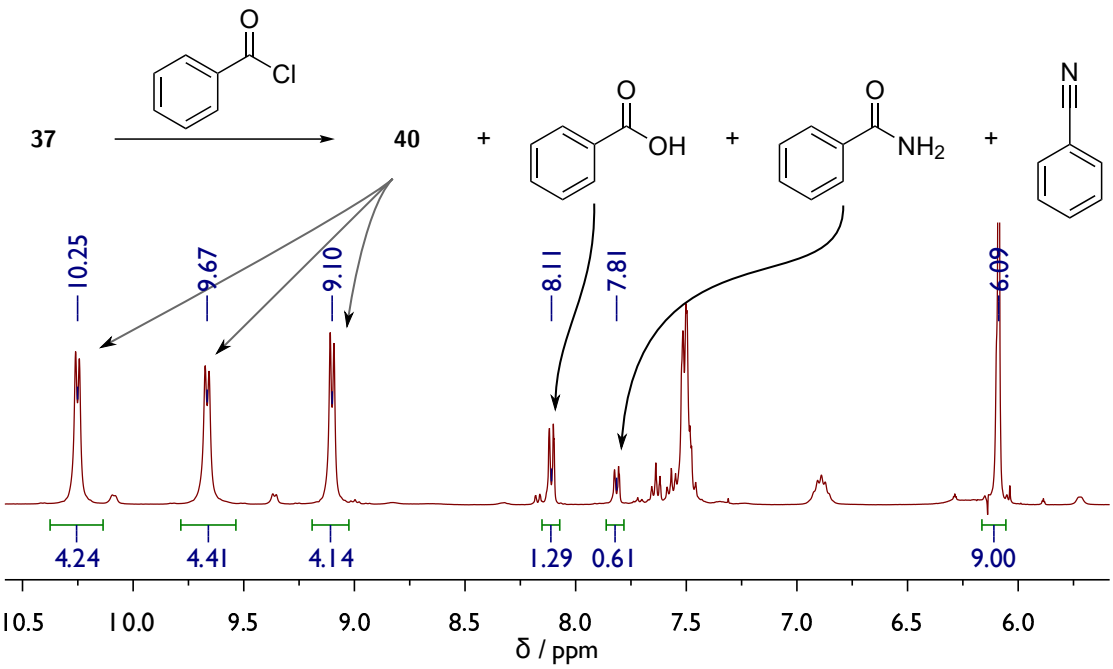

Fig. 3.28. ^{1}H NMR quantification of the formation of **40** (71 % yield), benzoic acid (64.5 %, $\delta(\mathrm{H}_{ortho}) = 8.11$ ppm) and benzamide (30.5 %, $\delta(\mathrm{H}_{ortho}) = 7.81$ ppm) from the reaction of **37** with 2 eq benzoyl chloride. 1,3,5-trimethoxybenzene ($\delta(\mathrm{CH}_{arom.}) = 6.09$ ppm) was used as internal standard (3 eq).

and subsequent release of benzamide and formation of **40**. Afterwards, benzamide itself can react with benzoyl chloride to form benzoic acid and benzonitrile while releasing HCl.[222] In fact, simply mixing commercial benzamide and benzoyl chloride and heating in 1,4-dioxane gave almost identical product distributions. If the reaction was performed at higher temperatures (110 °C), also tribenzamide was formed to minor degree. All organic products were identified by comparison to commercial samples.

In this reaction, the pincer ligand acts as a two electron, two proton reservoir enabling the one-pot synthesis of benzamide by PCET. This convenient reactivity of the PNP pincer ligand is not unprecedented. The group of *A. J. M. Miller* reported a quite analogous reaction (see Scheme 3.2). Starting from the square-planar Ru(IV) nitride complex [Ru(N)(PNP^{tBu})] originally reported by the *Schneider* group,[138] monoprotonation with a luthidinium salt results in the amine-pincer complex [Ru(N)(HPNP^{tBu})]$^+$. Subsequent treatment with carboxylic acids like benzoic acid leads to conversion of the nitrido ligand into an amine with concomitant oxidation of the amine pincer to the imine variant, resulting in [Ru(NH$_3$)(κ^2–O$_2$CAr)(P=NP^{tBu})]$^+$.[223] A DFT derived mechanism of the reaction identified the possibility of the benzoic acid / benzoate anion to act as a chelate and thereby serving as a proton shuttle to be of significant importance. A comparable role could be imagined for the C=O moiety of the benzoyl chloride after inital attack at the nitride. To further evaluate the importance of that functional group, additional experiments will be necessary. Especially, nitride methylation with e.g. MeOTf and subsequent heating in presence of a chloride salt could give further insights.

Both above discussed reactions reveal the PNP pincer ligands to have a certain potential as PCET agents in nitride functionalization. In applied systems, this reactivity could be quite valuable, but only if the pincer ligand could also be restored, making it act as a real proton and electron relay. While the group of *Miller* was unable to achieve re-reduction of the ligand, sequential addition of Li(HBEt$_3$) and (Ph$_2$NH$_2$)Cl to **40** could restore amine complex **29** in 61.8 % yield. In this reaction, the addition of Li(HBEt$_3$) is accompanied by the formation of hydride-bearing side products as indicated by ^{1}H NMR spectroscopy. Upon acid addition, these hydride complexes then reform the imine complex **40**, which limits the possible yields for the reaction via this route. Despite this limiation, a hydride and proton source are neither compatible with each other nor with the so far used reagents in this synthetic cylce (i.e. (Ph$_2$NH$_2$)Cl vs. Co(Cp*)$_2$ and Li(HBEt$_3$) vs. benzoyl chloride).

Therefore, possibilities to electrochemically re-reduce **40** in the presence of a proton source

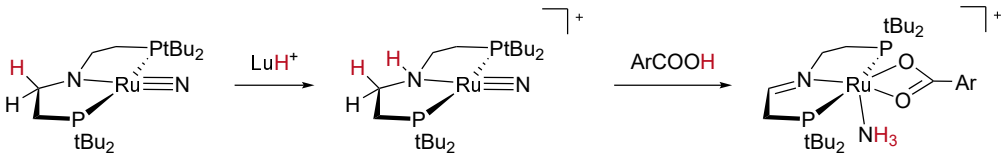

Scheme 3.2. Metal-ligand cooperative, PCET mediated ammonia formation at a Ru(IV) nitrido complex, reported by *Miller* and coworkers.

were investigated. Initially, (LuH)BAr^F_{24} was used for this reaction, which resulted in very nice cyclic voltammograms clearly differing from those of the pure complex. However, it was found that the N_2 bridged dimer **36**, which would be the ultimate target in an electrolysis setup, is not stable towards acids with such high acidity ($pK_a^{THF} = 7.2$) or even weaker acids like $(HNEt_3)BAr^F_{24}$ ($pK_a^{THF} = 12.5$).[217] On the other hand, too weak acids like phenol ($pK_a^{THF} = 29.2$)[224] did not lead to any changes in the CV data. Finally, benzoic acid ($pK_a^{THF} = 25.1$)[225] was found to be the sweet spot, which was weak enough to not react with **36** but at the same time resulted in the same electrochemical response as the stronger acids. Titration of 0 - 15 eq of benzoic acid to **40** resulted in a strong increase of the initial reduction current up to doubling the starting value. This is associated with the appearance of a second, quasi reversible reduction wave at approximately the same potential as the reduction feature of **29**, indicating the formation of that complex. The formation of **29** can be understood as an ECEC mechanism. After initial reduction, protonation leads to formation of a new complex, presumable the Re(IV) amide complex **31**. This has a reduction potential which is anodically shifted with respect to **40** (i.e. -1.16 V vs. Fc/Fc^+, see Figure 3.9) and can therefore be reduced a second time at the same potential as the first reduction, turning that response into a two-electron wave. Subsequent second protonation then results in formation of **29** and the appearance of the corresponding redox wave.

Even though these results were very promising, after an actual CPE of **40** in the presence

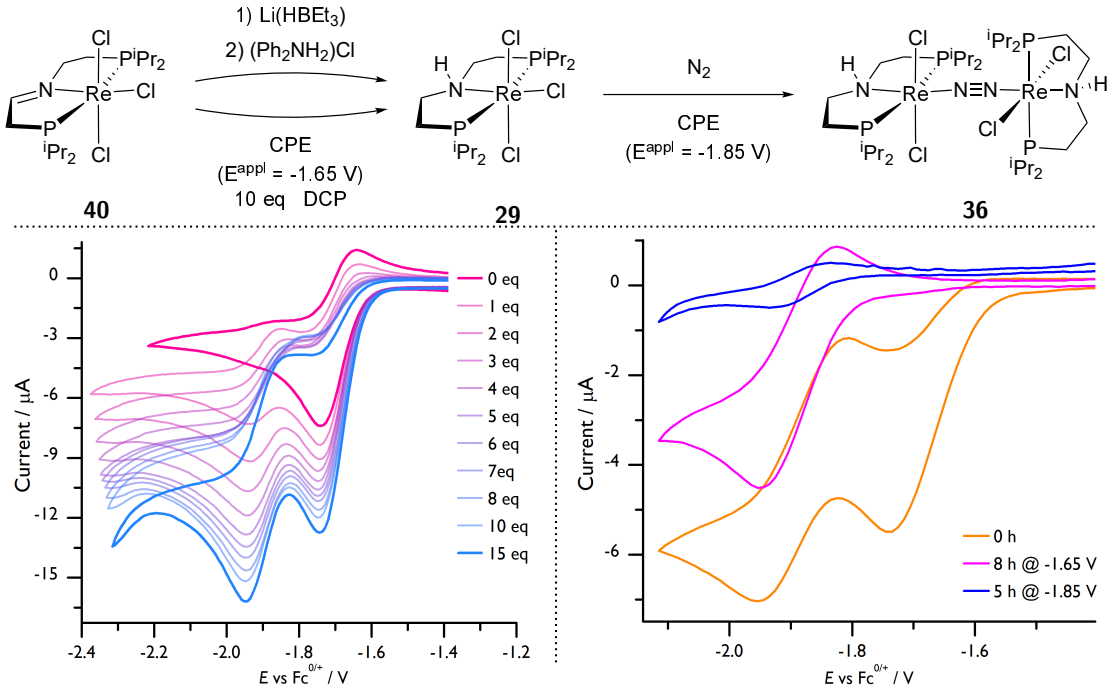

Fig. 3.29. *Top*: Regeneration of **29** from **40** via chemical reagents or electrolysis in presence of 2,6-dichlorophenol (DCP). *Bottom left*: CV measurements of **40** in presence of 0-15 eq of benzoic acid in THF at 100 mV s^{-1} (10^{-3} M **40**, 0.1 M $N^nBu_4PF_6$, WE: GC, RE: Ag-wire, CE: Pt-wire). *Bottom right*: CV of **40** under an N_2 atmosphere in the presence of 10 eq DCP before electrolysis (orange), after 8 h controlled potential electrolysis (CPE) at -1.65 V vs. Fc/Fc^+ (*pink*) and after another 5 h CPE at -1.85 V (*blue*).

of 10 eq of benzoic acid at the half-wave potential of the first reduction feature, **29** could not be identified spectroscopically. Instead, at least three other complexes with strongly shifted NMR signals are found, pointing to the formation of other Re(III) species. This was ascribed to the fact that the simultaneously formed benzoate anions can be very potent chelating ligands and might therefore interfere with the reaction. Exchanging benzoic acid with 2,6-dichlorophenol, which exhibits an almost identical pK_a value (p$K_a{}^{THF} = 25.1$)[224] but is a less potent ligand, results in identical CV measurements and if the CPE is performed with this acid, formation of target amine complex **29** can be observed in almost quantitative yields (99 %), determined by ^{1}H NMR integration vs. an internal standard. Thus, electrochemical regeneration of the PNP pincer ligand is not only feasible, but even outperforms the "chemical" pathway with Li(HBEt$_3$) and (Ph$_2$NH$_2$)Cl.
To further improve the so far obtained synthetic cycle, as last step the direct reduction of **40** all the way to the μ-N$_2$ bridged dimer **36** was attempted, thus providing all reduction equivalents needed in this conversion from the electrochemical setup. Therefore, the electrolysis was repeated under a dinitrogen atmosphere in two sequential steps. First, the solution was electrolyzed at the half-wave potential of the first reduction wave to *in situ* generate **29** until in-between-measured control CVs showed no sign of the starting complex anymore. Afterwards, the electrolysis potential was changed to the half-wave potential of the newly formed reduction wave and the solution was again electrolyzed until that peak disappeared, leading to a characteristic, deep blue coloring of the solution, indicative of dimer formation. In these reactions, a total of 1.8 e$^-$ in the first and 1.5 e$^-$ in the second step are transferred per Re atom. The formation of dimer **36** was confirmed by NMR and quantified by UV/vis spectroscopy to 69.7 %, based on starting complex **40**. An attempt to directly photolyze the obtained solution with an 390 nm LED led to formation of nitride complex **37** as the only detectable product. However the yield dropped to 14 %. Similarly poor yields were also obtained when the entire electrolysis was performed under continuous irradiation. The fact that these yields are considerably lower than after photolysis of isolated **36** highlights the importance to better understand the photochemistry of this or comparable dimers.

3.4 Summary

The successful synthesis and characterization of a new rhenium trichloro complex supported by an *iso*-propyl based PNP pincer ligand (**29**) is reported. **29** exhibits unusually spectroscopic features and a large TIP from SOC. This is due to a rather complex electronic structure, dominated by a quasi-degenerate triplet ground state and resulting spin-orbit coupling effects, as rationalized by QDPT/NEVPT2/CASSCF(14,10) calculations.

Starting from this new platform, a route to [ReCl$_2$(PNP^{iPr})] **30** is developed and the ability of that complex towards N$_2$ activation in analogy to the previously reported *tert*-butyl counterpart is investigated. Due to the reduced ligand sterics, **30** shows a high tendency to bind a

sixth ligand, as exemplified by the reversible low temperature dimer formation with N_2, without the need for any additional reagents. Unfortunately, N_2 splitting was not achieved with this complex, despite several attempts. Instead, the Re(I) complex $[ReCl(N_2)_2(HPNP^{iPr})]$ could be identified as one of several reduction products, indicating overreduction to be a problem.

In contrast to this, direct reduction of the amine complex **29** under N_2 yields a thermally stable, μ-N_2 bridged formal Re(II) dimer $(\mu\text{-}N_2)\{ReCl_2(HPNP^{iPr})\}_2]$, which exhibits a remarkable thermal stability, but does undergo clean photochemical splitting into the corresponding nitride complexes. The nitride complex **37** is then shown exhibit nitride centered, nucleophilic reactivity, resulting in borylation as well as protonation. Importantly, reaction with benzoyl chloride is shown to yield the imine complex $[ReCl_3(P{=}NP^{iPr})]$ as well as benzamide. In this rare metal-ligand cooperative nitride functionalization, the pincer ligand serves as a $2\,e^- / 2\,H^+$ donor. By controlled potential electrolysis in the presence of the weak acid 2,6-dicholorphenol, full regeneration of the ligand backbone could be achieved and eventually also dimer **36** could be obtained, closing the synthetic cycle without the need for chemical reductants.

4 Conclusion and outlook

This thesis was devoted to further develop the available understanding of two main topics:

A) Low-valent late transition metal nitrides and their reactivity
B) Dinitrogen activation and cleavage by transition metal complexes and their functionalization

The targeted synthesis of [Os(N)(PNP$^{t\mathrm{Bu}}$)] (**3**) provides access to the second ever reported Os(IV) nitrido complex and thus to the first reactivity study on such a species.[174] In line with the higher d electron count in comparison with well established Os(VI) nitrides, **3** exhibits mainly nucleophilic reactivity. It was observed that small electrophiles, which are largely unaffected by the steric bulk of the pincer ligand, do react directly at the metal center, identifying the Os atom to be the most nucleophilic side, in accordance with the d_{z^2} orbital being the HOMO. This is especially highlighted by the protonation of **3** to give fully characterized [Os(N)(H)(PNP$^{t\mathrm{Bu}}$)]$^+$ (**2**$^+$), as well as reactions with MeI, were NMR data suggest an osmium methylated complex to be one of several formed products. Using electrophiles with increased steric bulk like Me_3Si^+ results in clean and selective formation of [Os(NSiMe$_3$)(PNP$^{t\mathrm{Bu}}$)]$^+$ (**6**$^+$).
In agreement with this mainly nucleophilic character of the nitride, no reactions were observed towards olefins, alkynes or *Grignard* reagents. However, slow reaction with PMe_3 was observed, leading to an equilibrium mixture between the free reactants and the phosphoraneiminato complex [Os(N=PMe$_3$)(PNP$^{t\mathrm{Bu}}$)] (**7**). It was previously shown by *Smith* and coworkers that phosphines can be ambiphilic, with the possibility to act as σ-acceptor into their P$\overset{\sigma^*}{-}$C orbital.[159] The same effect was identified for the reaction of **3** with PMe_3 in a computational analysis, revealing two mutual donor-acceptor interactions between the nitride and the phosphine coming into play in the transition state. Population analyses of all involved species indicated a net electron transfer from the phosphine to the nitride in the transition state, justifying the formulation of **3** to be an ambiphile.
When **3** was heated in toluene under a hydrogen atmosphere, hydrogenolysis of the nitride moiety to form ammonia and the polyhydride Os(IV) complex [Os(H)$_4$(HPNP$^{t\mathrm{Bu}}$)] (**8**) occured. Such direct reactions with H_2 are extremely rare (the selective formation of ammonia even more so) and emphasize the high reactivity of late transition metal nitrides.
Additionally, the Os(VI) nitride complex [Os(N)Cl(PNP$^{t\mathrm{Bu}}$)]$^+$ **10**$^+$) was synthesized. This complex showed an interesting increase of nitride reactivity upon coordination of a strongly

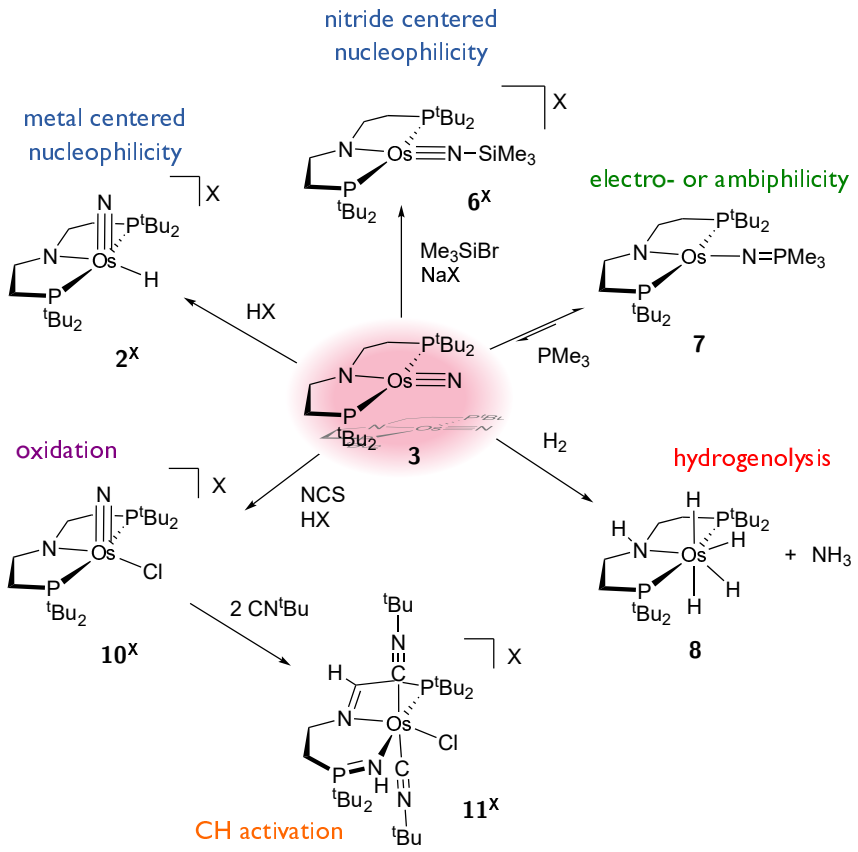

Scheme 4.1. Reactivity scheme of square planar Os(IV) nitrido complex **3**.

σ-donating isonitrile ligand, leading to backbone CH activation and insertion of the formed imide into an Os–P bond, yielding $\mathbf{11^X}$.

Even though every effort has been made to generate one of the nitrides **3**, $\mathbf{2^+}$ or $\mathbf{10^+}$ directly from dinitrogen, unfortunately no hint for successful splitting could be observed. Most reactions resulted in intractable mixtures of several compounds, with the selective formation of Os(II) complex $[OsH(N_2)(PNP^{tBu})]$ (**13**) under reductive conditions being among the only exceptions. In many reactions, especially those including bases for initial dehydrohalogenation, species were observed which most likely resulted from intramolecular CH activation, according to the NMR data. Interestingly, *Josh Abbenseth* prepared complementary osmium complexes with the fully oxidized ligand backbone which is inert towards β-hydride elimination from the backbone, i.e. $\{Os(P{=}N{=}P^{tBu})\}$.[195,226] However, neither Os(II) complex $[OsCl(P{=}N{=}P^{tBu})]$ nor Os(III) complex $[OsCl_2(P{=}N{=}P^{tBu})]$ are reported to give any reactions with N_2, which might be attributed to the reduced π-donor capabilities of the vinyl amide.

Since computational results indicate that N_2 splitting should in principal be feasible on the osmium platform, these results strongly point towards the need to modify the ligand in order to meet the requirements and properties of the system. One possibility to obtain a complex

which is unable to undergo β-hydride elimination and *also* features a strong amide donor would be to use a pincer ligand with CMe_2 instead of CH_2 groups next to the amide.
Synthesis of such a ligand can be envisioned by simply chlorination of literature known[227] $HN(CMe_2CH_2OH)_2$ with thionyl chloride to form $(H_2N(CMe_2CH_2Cl)_2)Cl$ and subsequent reaction with LiP^tBu_2 analog to the in here used procedures, with or without previous amine protection (see Scheme 4.2).
Another possibility to increase the reactivity towards N_2 would be to reduce the steric bulk of the ligand. The results obtained for the rhenium platform in Chapter 3 clearly show that the *iso*-propyl substituted pincer leads to significantly reduced shielding of the metal center and thus to an increased tendency to bind additional ligands. Investigations in connection with this proposal are already in progress, conducted by *Lukas Alig*. Also combinations of both approaches, i.e. smaller ligand substituents on pincer ligands which are inert towards CH activation (either the vinyl amido ligand or the CMe_2 substituted analog) should lead to significantly different, probably enhanced dinitrogen chemistry.

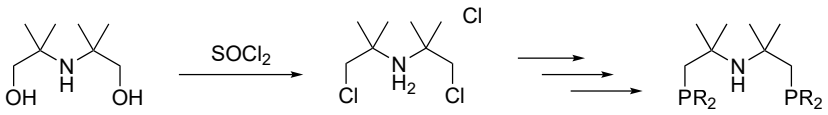

Scheme 4.2. Proposal for the synthesis of a new ligand designed to meet the problems which emerged during attempts to activate N_2 on the osmium platform.

The previously reported dinitrogen activation, cleavage and incorporation of the resulting nitrides into organic nitriles by rhenium complex **XIX** marked the first extension of dinitrogen cleavage chemistry to a group 7 element and raised a number of interesting questions, of which some were addressed in this thesis.
Characterization of the previously postulated complex $[(\mu\text{-}N_2)\{ReCl(PNP^{tBu})\}]$ (**XX**) was achieved by means of NMR data and X-ray diffraction. Monitoring the decay of the temperature labile complex by NMR spectroscopy revealed clean formation of the nitrido complex $[Re(N)Cl(PNP^{tBu})]$ (**XXI**). This way, **XX** was proven to be an actual intermediate in the reaction pathway to dinitrogen splitting. Repeating the experiments at various temperatures allowed for a first estimate of kinetic parameters and the activation barrier, which are in good agreement with the DFT calculations.[94] This analysis proved the proposed dinitrogen cleavage mechanism to occur via an end-on bridged N_2 dimer and once more underpinned the importance of a $10\pi(4\delta)$ electron count in the $\{MNNM\}$ core for this reactivity, fully in line with the considerations made in Part I Section 3.2.1.
Additionally, the rhenium platform was varied in several ways, to evaluate the potential of the system. Following a reaction analog to the reported acetonitrile release (see Part I Section 4.2.1) by methylation, deprotonation and oxidation of the ketimido complex $[Re(NCH_2)Cl(PNP^{tBu})]$ (**18**) resulted in C-C coupling. This reaction was achieved in a clean manner and the complex $[(N,N\text{-}C_2H_4N_2)\{ReCl(PNP^{tBu})\}_2]^{(OTf)_2}$ ($\mathbf{19^{(OTf)_2}}$) was fully characterized. While follow-up chemistry of this complex was not developed, it offers the possibility to incorporate two nitrogen atoms into the same molecule and thus could broaden

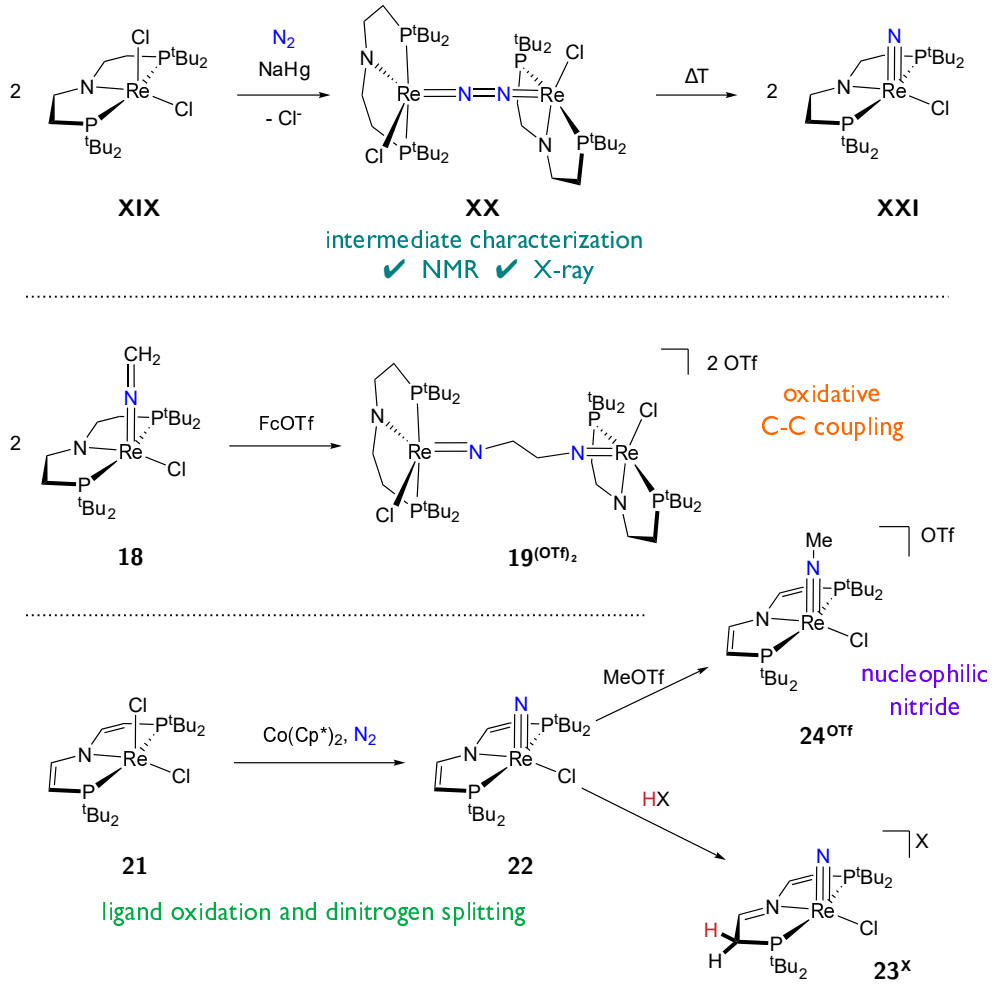

Scheme 4.3. Expansion of the understanding of rhenium mediated dinitrogen activaiton chemistry with *tert*-butyl substituted PNP pincer ligands.

the spectrum of accessible compounds. Therefore, further research on how to cleave off the obtained diimide would be of significant interest.

Overall, the development of a catalytic system capable of forming nitrogen containing organic molecules from N_2 is a long-standing challenge which is so far unmet. With regard to the oxidative conditions needed for nitrile release from **XXI**, a certain interest in improving the systems stability towards these conditions arose. Hence, the ligand backbone was oxidized to the vinyl amido pincer P=N=P, which was previously found to have beneficial influence on stabilizing oxidized species. Preparation of $[ReCl_2(P{=}N{=}P^{tBu})]$ (**21**) by oxidation of **XIX** with TTBP was achieved in good yields. Investigation of the redox properties of this compound in comparison with parent **XIX** indicated a significant anodic shift of the first oxidation potential, but at the same time a reduced stability of the resulting species, thus only partially meeting the targeted properties. Nevertheless, the dinitrogen activation and functionalization capabilities of this platform were evaluated and cleavage of dinitrogen under reductive conditions was achieved in moderate yields ($\approx 60\,\%$). Followup investigation of the functionalization chemistry indicated the nitride $[Re(N)Cl(P{=}N{=}P^{tBu})]$ to exhibit a reactivity highly comparable to that of the alkyl amido congener **XXI**. No reduction was

achieved up to very low potentials and also protonation (which is centered at the pincer ligand) did not lead to a significant shift in the redox potentials. Nitride centered methylation with methyl triflate to [Re(NMe)Cl(P=N=P^{tBu})]^{OTf} (**24^{OTf}**) as well as subsequent deprotonation to the ketimidio complex [Re(NCH$_2$)Cl(P=N=P^{tBu})] (**25**) occured fully analog to the parent system. Consequently, the new platform with the oxidized ligand performs comparably well in dinitrogen functionalization chemistry but does not lead to a significant improvement in terms of reactivity. This could become of importance in the future, given the possibility that functionalization schemes and potential catalytic cycles might be developed where backbone CH activation could become an actual issue.

In order to increase the reactivity of dinitrogen obtained nitrides, the steric shielding by the ligand framework is a highly important factor which needs to be controlled. This has already been demonstrated by *Cummins* and coworkers on their molybendum trisamide complexes, were significantly different reactivities were observed upon varying the sterics of the amide residues (see Part I Section 3.2.1). In general, tuning the steric bulk of the supporting ligands can be regarded as a tightrope walk between protection of the metal center from unwanted side-reactions and exposing the dinitrogen derived nitride towards reactants.
In this context, the synthesis of a complex analog to [ReCl$_2$(PNP^{tBu})] (**XIX**) but with the *iso*-propyl substituted ligand was attempted. The amine complex [ReCl$_3$(HPNP^{iPr})] (**29**) was prepared in good yields (70 %). Strongly shifted but sharp NMR signals with well resolved coupling constants indicated a non-trivial electronic structure, further substantiated by SQUID measurements, which revealed a large TIP. CASSCF calculations indeed showed **29** to feature a quasi-degenerated triplet ground state and multireference calculations by means of QDPT resulted in extensive mixing of the states by SOC.
29 provided a good starting platform for subsequent reactivity studies. Overall, the reduced steric shielding of the metal center resulted in a very high affinity towards even weak ligands. This became apparent during the attempts to dehydrohalogenate **29** in order to obtain [ReCl$_2$(PNP^{iPr})] (**30**). No isolable sample of **30** could be obtained with bases, and also the spectroscopically clean samples obtained from H atom abstraction from **29** to form [ReCl$_3$(PNP^{iPr})] (**31**) and subsequent reduction to **30** degraded upon solvent removal. **30** does form adducts with THF as well as with N$_2$, highlighting the high tendency of the system to bind a sixth ligand. Especially the latter reaction was investigated in detail and 2D-NMR data strongly indicate reversible formation of an equilibrium mixture of two N$_2$ containing dimers at low temperatures. A symmetric dimer [(μ-N$_2$){ReCl$_{2,cis}$(PNP^{iPr})}$_2$] (**33b**) and a asymmetric complex [{ReCl$_{2,cis}$(PNP^{iPr})}(μ-N$_2$){ReCl$_{2,trans}$(PNP^{iPr})}] (**33a**) were identified as the most likely products of this reaction. While the formation of these dimers was a promissing starting point, all attempts for subsequent cleavage of the dinitrogen moieties by reduction failed and no sign for the expected nitride was observed. From the mostly intractable reaction mixtures, the Re(I) complex [ReCl(N$_2$)$_2$(HPNP^{iPr})] (**35**) could be identified which pointed to overreduction as one unwanted side reaction in this system.
Therefore, direct reduction of amine complex **29** was performed under N$_2$, as here the

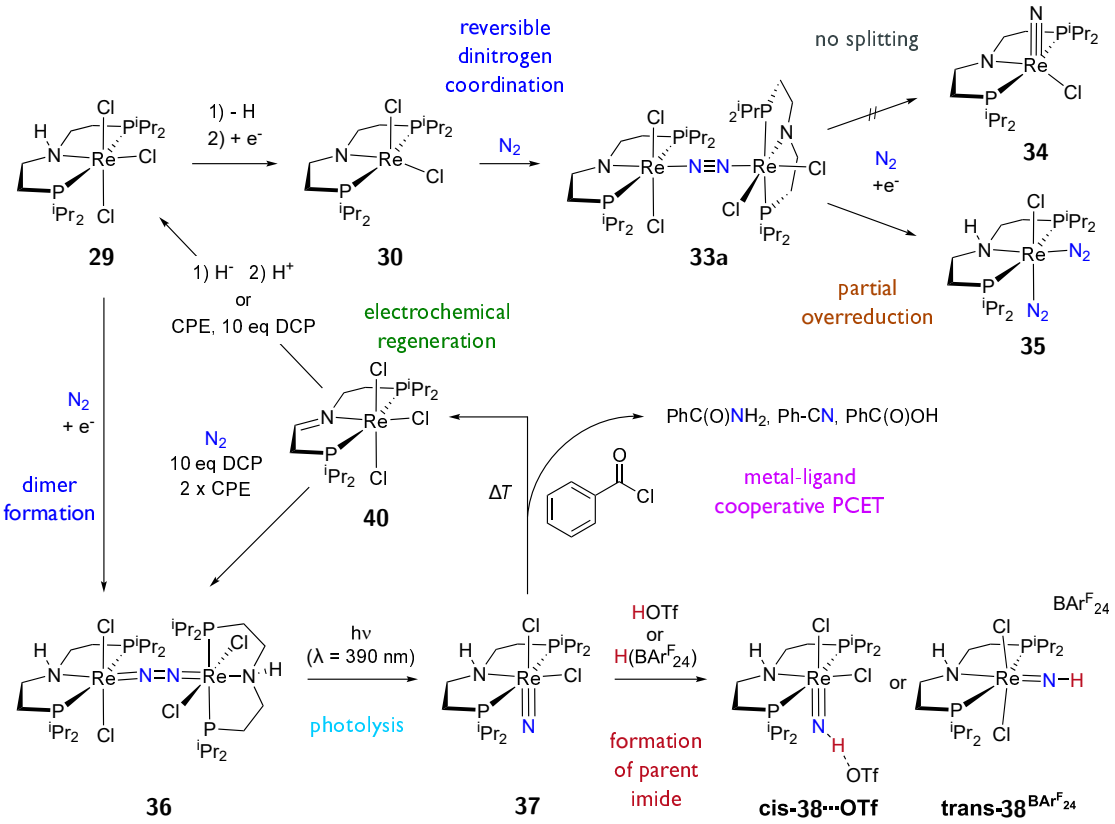

Scheme 4.4. Reaction scheme of a rhenium complex supported by a *iso*-propyl substituted PNP pincer ligand and it's dinitrogen chemistry developed within this thesis.

following chloride loss allows for binding of only one N_2 ligand and thus potential inversion should be less of an issue. This reduction led to isolation and characterization of the temperature stable μ-N_2 bridged N_2 dimer $[(\mu\text{-}N_2)\{ReCl_2(HPNP^{iPr})\}_2]$ (**36**). It's thermal stability is in stark contrast to the *tert*-butyl substitued dimer **XX** and can be explained by the octahedral coordination and thus the presence of a strong donor ligand *trans* to the N_2 bridge. This ligand raises the a_u symmetric MO $M^{\sigma}\!-\!N^{\sigma^*}\!-\!N^{\sigma}\!-\!M$ signficantly in energy, making it less available for mixing with the complex's HOMOs and thus increases the activation barrier. Population of the antibonding MO space was therefore sought by photoinduced electronic excitation and indeed, irradiation with a violet LED allowed for selective N_2 cleavage into the corresponding nitrides $[Re(N)Cl_2(HPNP^{iPr})]$ (**37**). TDDFT calculations point towards an MLCT from the metal centered, non-bonding δ orbitals into the $Re^{\pi^*}\!-\!N^{\pi^*}\!-\!N^{\pi^*}\!-\!Re$ MOs to be of importance for this reaction. There are only two system (by *Cummins* and *Floriani*) which do undergo photolytic N_2 scission and do not feature filled δ symmetric orbitals. Given the similarities between both systems and the fact, that *Cummins* reported the splitting in his complex to occur from a vibrationally hot ground state rather than from an excited state, the question stands to reason if such populated δ orbitals are a general requirement for the observed reactivity. This particular question and as well as the entire excited state dynamics are still to be explored and should be addressed in future projects.

The nitride complex **37** obtained from photochemical N_2 cleavage features a number of important properties. On the one hand, the smaller pincer ligand and the resulting affinity to form coordinatively saturated complexes leads to the *trans* chloride ligand being coordinated, which is in contrast to $[Re(N)Cl(HPNP^{tBu})]^{Cl}$, where the chloride was found to be non-coordinating. This renders the nitride the only nucleophilic side in the complex, allowing for N centered protonation to form a rare parent imido complex $[Re(NH)Cl_2(HPNP^{iPr})]^+$ (**38**$^+$). Starting from an octahedral and thus uncharged complex was found to be essential for this reaction. Interestingly, DFT calculations indicated a strong influence of the anion on the preferred geometry and indeed, using HOTf and $H(Et_2O)_2(BAr^F_{24})$ resulted in formation of **cis-38**$\cdots$**OTf** and **trans-38**$^{\mathbf{BAr^F_{24}}}$, as identified by NMR measurements in the former and X-ray diffraction in both cases. The formation of these imido complexes might provide an entry to ammonia formation reactions and closer investigation of followup reactions, also on the influence of the **cis-** vs. the **trans-** isomer are advisable.
Despite the protonation, reaction with benzoyl chloride resulted in selective formation of Re(III) imine complex $[ReCl_3(P{=}NP^{iPr})]$ (**40**) accompanied by the formation of a mixture of benzamide, benzonitrile and benzoic acid. In this metal-ligand cooperative nitride functionalization, the amine pincer ligand acts as a $2\,H^+/2\,e^-$ reservoir for PCET reactivity. Regeneration of the original amine complex **29** was achieved either by stepwise addition of a hydride and a proton source in approximately 62 % yield or almost quantitatively by CPE in the presence of weakly acidic 2,6-dichlorophenol. Furthermore, continued electrolysis under N_2 without intermediate workup led to direct reformation of dimer **36** in 70 % yield.

While this leads to a quite efficient three-step synthetic cycle for nitrogen incorporation into organic nitriles, still no catalytic turnover could be achieved. This is mainly due to two aspects: On the one hand, nitride complex **37** still requires harsh reaction conditions to be functionalized (i.e. 100 °C overnight), which is not compatible with the other reaction conditions, on the other hand, photolysis of dimer **36** is only selective in pure solvent, but drops dramatically in yield when other substrates (electrolyte, benzoyl chloride, DCP) are present. The latter issue requires extensive studies of the excited state dynamics of the system to better understand the relevant processes while the former might be met by further increasing the nitrides reactivity, for example by introduction of stronger *trans* ligands, which was previously found to be beneficial (compare Part I Section 4.2.2 and Part II Section 1.3). A potentially promissing modification would be the introduction of an additional residue in the pincer ligand to form $N(R)(CH_2CH_2P^iPr_2)_2$ where R can hold a number of anionic donor atoms (see Figure 4.1). The possible benifits of such a ligand are examplified by DFT calculations[1] on the model complex $[(\mu\text{-}N_2)\{ReCl(^{Me}NPNP^{iPr})\}_2]$ ($^{Me}NPNP^{iPr}$ = $(MeN^-CH_2CH_2)N(CH_2CH_2P^iPr_2)_2$):

- The strongly π-donating amide donor would raise the δ symmetric orbitals, which are predicted to be the donor orbitals in the photochemical process, significantly in

[1] M06/def2TZVP/SMD(THF)||PBE/D3BJ/RI/def2SVP, see Part III Section 3.8.

energy, eventually becoming the HOMOs and thus leading to an overall $12\pi 2\delta$ electron count. The influence on thermal and photochemical splitting behavior could provide important insight into molecular dinitrogen activation.

- If the presumably high kinetic barrier for splitting ($\Delta G^{\ddagger}_{\mathrm{DFT}} = +240\,\mathrm{kJ\,mol^{-1}}$) can be overcome by photoexcitation, the tetradentate nature of the ligand would force an obtained nitride ($\Delta G^{0}_{\mathrm{DFT}} = -68\,\mathrm{kJ\,mol^{-1}}$) to be coordinated *trans* to the amine (comparable to **37**^{trans}, see Figure 3.20), which should greatly enhance the nitride centered reactivity, as expressed in the model nitride methylation with MeOTf ($\Delta G^{0}_{\mathrm{DFT}} = -99\,\mathrm{kJ\,mol^{-1}}$, **37**: $\Delta G^{0} = -74\,\mathrm{kJ\,mol^{-1}}$).

Further variation of the new ligand arm could then allow to fine tune the systems properties to optimize the behavior (e.g. by using N-hetrocyclic donors like (substituted) pyrroles).

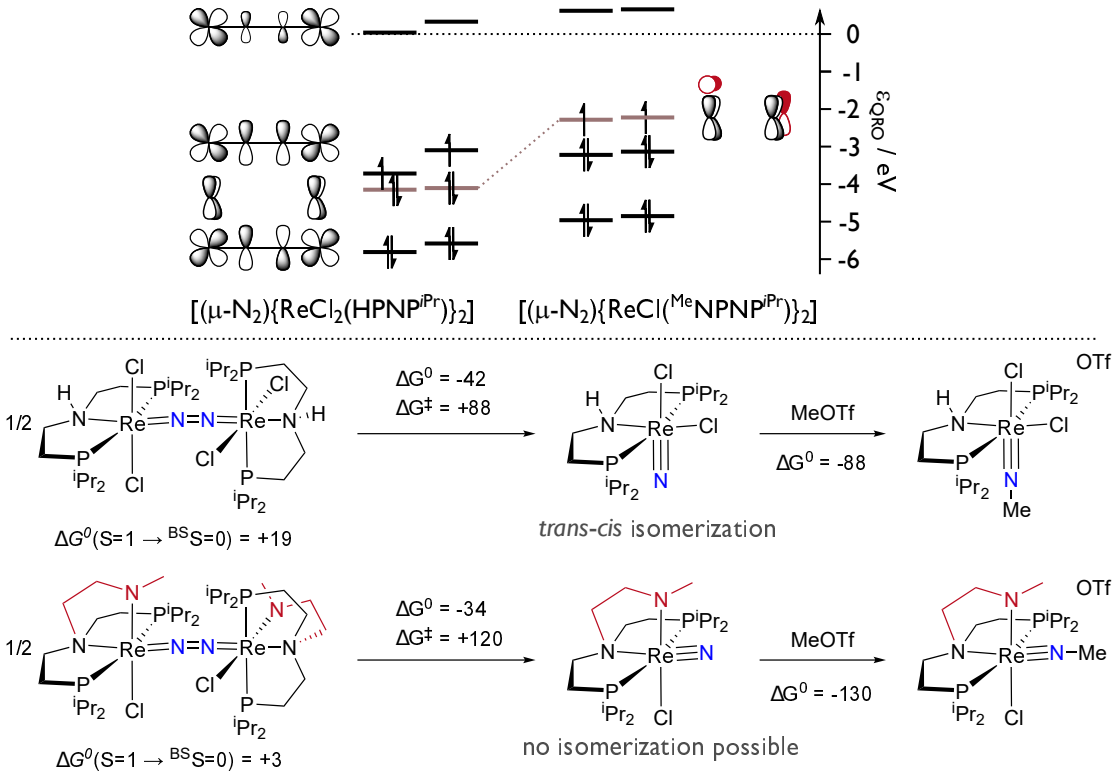

Fig. 4.1. Influence of an additional amide donor arm at the PNP pincer on the N_2 activation of a rhenium system closely related to **36**. *Top*: quasi-restricted orbital (QRO) scheme of **36** (*left*) and [(μ-N$_2$){ReCl(MeNPNP^{iPr})}$_2$] (*right*), demonstrating the influence of an additional amide donor on the δ symmetric MOs. *Bottom*: DFT derived data (in kJ mol^{-1}) for N_2 cleavage and functionalization in both systems.

Part III

Experimental details

1 Materials and Methods

> *We walk this earth*
> *With fire in our hands*
>
> — **Arch Enemy**
> Doomsday Machine - Nemesis

1.1 General synthesis and materials

All synthetic procedures were performed under an inert atmosphere of Ar or N_2 (both 5.0, Linde gas) using standard *Schlenk* and glovebox techniques, unless otherwise noted. Purification of H_2 gas (6.0, Linde gas) was obtained by passing the gas through a high capacity moisture filter (Pure Gas Products) followed by a steel coil, cooled with liquid N_2 to freeze out potential impurities.
All glasware was cleaned by KOH/*iso*-propanol baths, washed with deionized water and dried at 120 °C. Before usage, all vessels were evacuated at a Schlenk line with periodically applied heat. Small scale reactions ($\leq$ 10 mg) were typically performed in J-Young NMR tubes.

All solvents were purchased in HPLC quality (Merck) and used as obtained from an MBraun Solvent Purification System. THF and toluene were further purified by stirring over Na/K alloy for serveral days. Deuterated solvents were obtained from Eurisotop GmbH and dried by stirring over Na/K (C_6D_6, toluene-d_8, THF-d_8) or CaH_2 (CD_2Cl_2, CD_3CN). D_2O was degassed. CN^tBu, HOTf, MeOTf, Me_3SiBr, PhC(O)Cl and PMe_3 were distilled under an Ar atmosphere before usage, whereas ferrocene, KO^tBu, Me_3NO, naphthalene, PPh_3 and 2,4,6-tris-*tert*-butylphenol were sublimed. NEt_3 was dried over KoH and distilled. All other chemicals were used as purchased without further purification.

XIX, **XXI**, **18**, **21**,[180], **1**, $\mathbf{2^{Cl}}$,[174], the ligands $HPNP^{tBu}$ and $HPNP^{iPr}$,[228], $ReCl_3(MeCN)(PPh_3)_2$,[229,230], NaHg,[231] KC_8,[232] 2,4,6-tris-*tert*-butylphenoxy radical,[233], $Na(BAr^F_{24})$ and $H(Et_2O)_2(BAr^F_{24})$,[234], [PPN]N_3,[235] $[Fc]^{OTf}$,[236] and BAr^F_{18}[237] have been synthesized according to published procedures.

1.2 Analytical methods

Crystallographic details

Suitable single crystals for X-ray structure determination were selected from the mother liquor under an inert gas atmosphere and transferred in protective perfluoro polyether oil on a microscope slide. The selected and mounted crystals were transferred to the cold gas stream on the diffractometer. The diffraction data were obtained at 100 K on a BRUKER D8 three-circle diffractometer, equipped with a PHOTON 100 CMOS detector and an INCOATEC microfocus source with Quazar mirror optics (Mo-Kα radiation, $\lambda = 0.71073$ Å).
The data obtained were integrated with SAINT and a semi-empirical absorption correction from equivalents with SADABS was applied. The structure was solved and refined using the BRUKER SHELX 2014 software package.[238–241] All non-hydrogen atoms were refined with anisotropic displacement parameters. All C-H hydrogen atoms were refined isotropically on calculated positions by using a riding model with their U_{iso} values constrained to 1.5 U_{eq} of their pivot atoms for terminal sp^3 carbon atoms and 1.2 times for all other atoms.

Cyclic voltammetry

Electrochemical data were recorded either on a METROHM PGSTAT101 using the NOVA 2.0 software (all data measured under argon) or a GAMRY 600 reference Potentiostat using the GAMRY software (all data measured under N_2). The cyclic voltammetry (CV) data were recorded in a UV/vis cell equipped with a glassy carbon ($\varnothing = 1.6$ mm) working electrode (WE), a Pt wire as counter electrode (CE) and a Ag wire as pseudo-reference electrode (RE). Referencing was performed against the Fc^+/Fc couple. All experiments were performed in 0.1 M $N^nBu_4PF_6$ in THF.

During the second half of this thesis, CV data were compensated for internal resistance (iR). In these cases, the scan rate dependence of the peak currents i_p was analyzed according to the *Randles-Sevcik* equation:

$$i_p = 0.446nFAC^0 \left(\frac{nFvD_o}{RT}\right)^{1/2} \tag{1.1}$$

where n is the number of transferred electrons, F is *Faraday's* constant, A is the electrode surface in cm^2, C^0 is the bulk concentration of the analyte in mol cm^{-3}, v is the scan rate in V s^{-1} and D_o is the diffusion coefficient of the oxidized species in cm^2 s^{-1}.[242] This equation is valid for freely diffusing (i.e. non-absorbed) analyte in solution which undergoes fast, electrochemically reversible electron transfer. Thus deviations from linearity of a plot of i_p vs. $v^{1/2}$ can indicate quasi-reversible electron transfer (accompanied by a scan rate dependent

peak-to-peak separation) or adsorption of the analyte on the electrode surface (which should have a constant peak-to-peak separation).

All controlled potential electrolysis (CPE) experiments were performed in a three-neck cell with reticulated vitreous carbon as WE, a Pt wire as CE in a fritted sample holder compartment with Fc^{*+}/Fc^{*} as sacrificial reductant and a Ag wire as RE in a compartment separated by a fritted sample holder from the main solution. The solution was stirred during electrolysis. All experiments were performed in 0.2 M $N^{n}Bu_4PF_6$ in THF.

Elemental analysis

Elemental analyses were obtained from the Analytical Laboratories at the Georg-August University Göttingen using an Elementar Vario EL 3 analyzer.

Indophenolic titration

After reaction of **3** with H_2 according to the procedure described in Section 2.1.7, all volatiles were transfered to a Schlenk tube containing HCl in Et_2O. This mixture was stirred for 10 min, all volatiles were removed *in vacuo* and the precipiate was analyzed for NH_4Cl according to a literature procedure.[184]

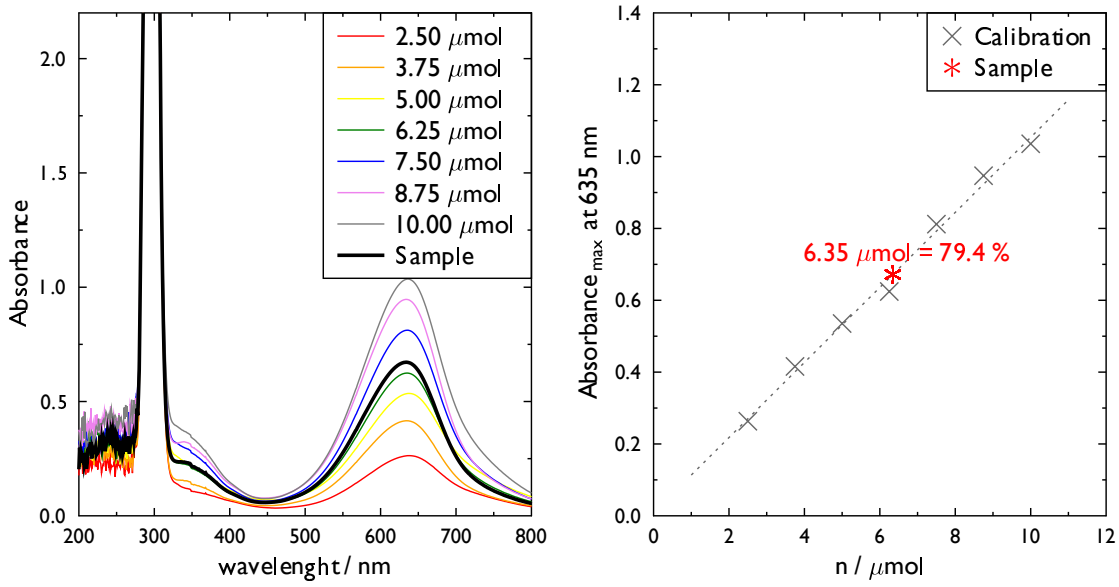

Fig. 1.1. Determination of the amount of NH_3 from the reaction of **3** with H_2 by indophenolic titration. *Left*: UV/vis spectra of the indophenol solutions of the calibration solutions (*colored*) and the actual sample (*black*). *Right*: Calibration curve and calculated yield of the reaction.

Irradiation and quantum yield determination

All photolysis experiments were performed using either a KESSIL PR160-390 LED (390 nm) or a 150 W Hg(Xe) arc lamp with lamp housing and arc lamp power supply from LOT-QUANTUM DESIGN GmbH. For the latter, IR radiation was eliminated by use of a water filter and photolyzed samples were kept at room temperature by a water bath. Wavelength selection was achieved using filter with a cutoff of 305 nm and 420 nm.

For the photolytic splitting of **36** into **37**, the quantum yield was determined for the irradiation with a 390 nm LED lamp. The quantum yield of any photon-induced chemical reaction is defined as

$$\Phi = \frac{n(\text{molecules reacted})}{n(\text{photons absorbed})} \tag{1.2}$$

If the total amount of photons emitted by a monochromatic light source per time per sample area is known, the number of absorbed photons can be derived from the absorbance of the sample at the wavelength of interest. This initial amount of photons is termed photon flux and can be derived for any given light source by photolysis of an chemical actinometer with a known quantum yield. The workhorse system in this respect is the photolysis of potassium ferrioxalate ($K_3[Fe(C_2O_4)_3]$), for which quantum yields are determined over a wide range of wavelengths and which proceeds according to the following equation:

$$2\,[Fe(C_2O_4)_3]^{3-} \xrightarrow{h\nu} 2\,[Fe(C_2O_4)]^{2-} + CO_2 + C_2O_4^{2-}$$

Formation of the Fe^{2+} compound can than be quantified by addition of phenanthroline which leads to the formation of an $[Fe(phen)_3^{2+}]$ complex which features a very pronounced absorption at 510 nm.

In the actual experiment, three aliquots of an aqueous solution of potassium ferrioxalate (12 mM, 2 mL) were placed in 20 cm distance of the lamp and photolyzed with 25 % power output for 15 s. Afterwards, to a portion of each photolyzed sample (1 mL) were added a sodium acetate buffer (0.1 M, pH = 3.5, 2 mL) and 1,10-phenanthroline solution (5 mM, 2 mL). The mixture was diluted to 10 mL and allowed to equilibrate for 1 h. Afterwards, the concentration of the formed Fe^{2+} phenanthroline complex was determined by UV/vis spectroscopy. All reactions were performed with strict exclusion of ambient light.
The photonflux of a light source at a given distance can be determined using the following equation:

$$I = \frac{k \cdot V \cdot A_{510\text{nm}}}{\Phi \cdot \epsilon_{510\text{nm}} \cdot d \cdot a \cdot t \cdot (1 - 10^{-A})} \tag{1.3}$$

where I is the photon flux in mol cm^{-2}, k is the dilution factor between photolyzed sample and analyzed solution (10), V is the total volume of photolyzed actinometer solution (0.002 L), $A_{510\text{nm}}$ is the absorbance of the formed Fe^{2+} phenanthroline complex at $\lambda = 510$ nm, $\epsilon_{510\text{nm}}$ is the corresponding molar attenuation coefficient in M^{-1} cm^{-2} ($1.11 \cdot 10^4$), Φ is the quantum

yield of the actinometer at 390 nm (1.18), d is the pathlength of the used UV/vis cuvette in cm, a is the area of irradiation in cm^2, and A is the initial absorbance of the ferrioxalate solution at the wavelength of irradiation (9.6). For the three samples, $A_{510\mathrm{nm}}$ was 0.401, 0.367 and 0.461, respectively, resulting in a photon flux of

$$I = 1.1948 \pm 0.1391 \cdot 10^{-6} \mathrm{mol\,min^{-1}\,cm^{-2}} \tag{1.4}$$

For the quantum yield determination, a solution of complex **36** in THF (2 mL, 4·10^{-5} M) was irradiated with the same setup (same cuvette dimension, same distance from the light-emitting diode (LED) lamp) for a total of 20 min. After every 2 min, the irradiation was stopped and the concentration of the dimer was determined by monitoring of the absorbance at $\lambda = 578$ nm. The quantum yield was determined by

$$\Phi = \frac{\Delta n_{t_x - t_{x-1}}}{n_{\mathrm{Photons,2min}} \cdot (1 - 10^{-A_m athrm390nm})} \tag{1.5}$$

where $\Delta n_{t_x - t_{x-1}}$ is the amount of **36** decomposed between two measurements, i.e. after irradiation for 2 min, $n_{\mathrm{Photons,2min}}$ is the amount of photons reaching the sample during 2 min ($4.7792 \cdot 10^{-6}$ mol in the above described setup, calculated by $n = I \cdot t \cdot A$) and $A_{390\mathrm{nm}}$ is the absorbance of the solution at 390 nm *at the beginning of each photolysis step*. To account for small absorption of the product at the same wavelength, this value is calculated from the initial absorbance, prior to the first irradiation, and the concentration of the dimer (i.e. referenced to the absorption at $\lambda = 578$ nm). This results in a quantum yield of 0.36±0.03 %.

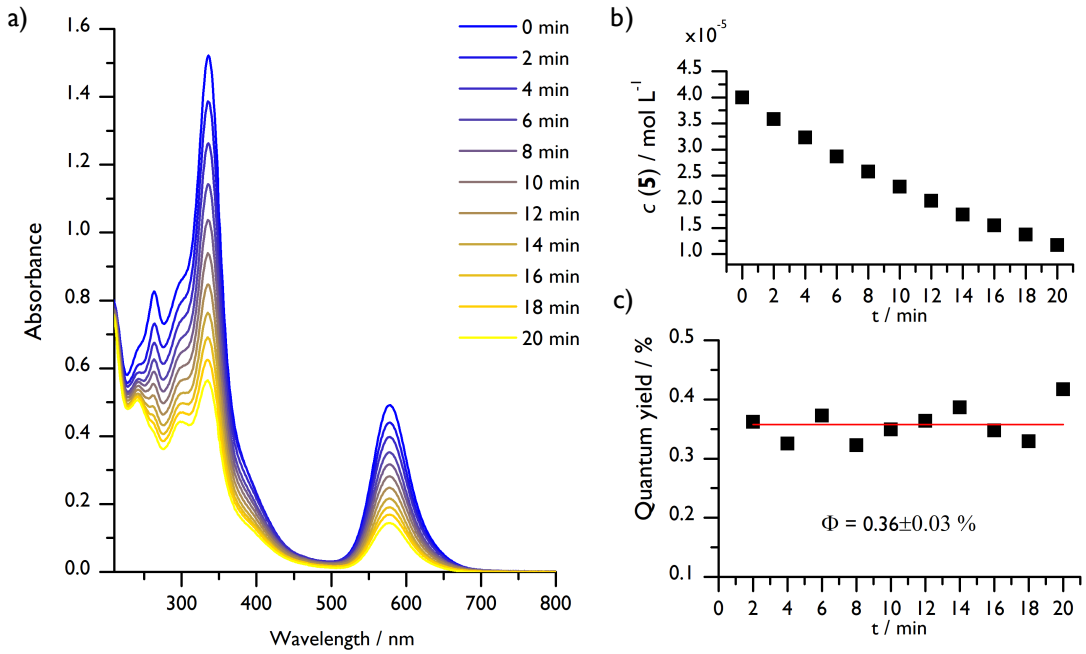

Fig. 1.2. Quantum yield determination of the photosplitting of **36** by 390 nm LED lamp. *a*) Decay of **36** during photolysis. *b*) Concentration profile of **36** during the reaction. *c*) Quantum yields between each irradiation interval.

Mass spectrometry

ESI mass spectra (on a BRUKER HCT ultra ESI-MS) and LIFDI (LINDEN CMS) mass spectra were measuerd by the Zentrale Massenabteilung, Fakultät für Chemie, Georg-August-Universität.

Nuclear magnetic resonance

NMR data were recorded on machines from BRUKER (AVANCE III 300, AVANCE III 400 or AVANCE 500 with a Prodigy broadband CryoProbe). All spectra were referenced to residual solvent signals (THF-d_8: $\delta_{^1\mathrm{H}} = 3.58$ ppm, $\delta_{^{13}\mathrm{C}} = 67.2$ ppm; C_6D_6: $\delta_{^1\mathrm{H}} = 7.16$ ppm, $\delta_{^{13}\mathrm{C}} = 128.1$ ppm; toluene-d_8: $\delta_{^1\mathrm{H}} = 2.08$ ppm, $\delta_{^{13}\mathrm{C}} = 20.4$ ppm; CD_2Cl_2: $\delta_{^1\mathrm{H}} = 5.32$ ppm, $\delta_{^{13}\mathrm{C}} = 53.8$ ppm). ^{15}N and ^{31}P chemical shifts are reported relative to external standards (nitromethane and phosphoric acid, respectively, both defining $\delta = 0.0$ ppm).
In general, signal multiplicity is denoted as broad (br), singlet (s), doublet (d), triplet (t), virtual triplet (vt) or heptet (hept). In complexes where both phosphorous atoms are equivalent, deriving coupling constants in the ^{1}H NMR data was often not possible, due to higher order coupling effects. In these cases, the resonances are described either as multiplet (m) or as spin system (spin-sys), if at least the $^3J_{\mathrm{HP}}$ coupling constant could be determined (i.e. for the *tert*-butyl signals, where $^3J_{\mathrm{HP}}$ corresponds to the separation of the outer peaks of a signal).

SQUID measurement

Temperature-dependent magnetic susceptibility measurements were carried out with a QUANTUM-DESIGN MPMS-XL-5 SQUID magnetometer equipped with a 5 T magnet in the range from 295 to 2.0 K at a magnetic field of 0.5 T. The powdered sample was contained in a Teflon bucket and fixed in a non-magnetic sample holder. Each raw data file for the measured magnetic moment was corrected for the diamagnetic contribution of the Teflon bucket according to $M^{dia}(\text{bucket}) = \mathcal{X}_g \cdot m \cdot H$, with an experimentally obtained gram susceptibility of the Teflon bucket. The molar susceptibility data were corrected for the diamagnetic contribution using the *Pascal* constants and the increment method according to *Haberditzl*.[243,244] Experimental data were modeled with the JULX program[245] for $S = 0$ including temperature independent paramagnetism (TIP) and paramagnetic impurities (PI, $S = 1/2$) according to $\mathcal{X}_{exp} = (1 - PI) \cdot \mathcal{X}_{\text{sample}} + PI \cdot \mathcal{X}_{PI} + TIP$.

UV/vis spectroscopy

UV/vis spectra were recorded in a cuvette equipped with a J-YOUNG cap at an AGILENT CARY 300 spectrometer using the SCAN software. Background measurements of the blank solvent were performed in an UV/vis cuvette identically constructed to the one of the actual measurement.

Vibrational spectroscopy

Standard IR spectra of pure compounds were recorded at a BRUKER ALPHA FT-IR spectrometer with the Platinum ATR module inside a glovebox. When a sample was prepared as KBr disk, it was diluted with solid KBr, pestled until a homogeneous mixture was obtained an pressed into a pellet. The disk was then measured at a THERMO SCIENCE NICOLET iZ10 at ambient conditions.
For IR measurements in the magnetic field, the spectra were recorded using a commercial Fourier transform spectrometer (VERTEX 80v) coupled to a superconducting coil delivering the field up to 11 T. To measure transmittance, the radiation of globar was delivered from the spectrometer using light-pipe optics to the sample (a mixture of the studied compound with KBr) inside the magnet and detected by a silicon composite bolometer (IRLABS) placed just below the sample. Both the sample and bolometer were surrounded by the helium exchange gas and cooled down to 4.2 K.
Resonance Raman (rR) spectra were measured using a HORIBA SCIENTIFIC LabRAM HR 800 spectrometer with open-electrode CCD detector in combination with a free space optical microscope and a He:Ne-laser (632.8 nm).

2 Synthesis

> *Ich bin meines Glückes Schmied*
> *Ich bau mir einen Prototyp*
> *Ich setz dich Stück für Stück zusammen*
>
> — **Eisbrecher**
> "Prototyp" on "Die Hölle muss warten"

2.1 Osmium compounds

2.1.1 $[Os(H)(N)(PNP^{tBu})]^{X}$ ($\mathbf{2^{X}}$)

*From reaction of **1** with NaN_3*:
$[OsHCl_2(PNP^{tBu})]$ (**1**) (150 mg, 241 µmol, 1.0 eq), KPF_6 (57.6 mg, 313 µmol, 1.3 eq) and NaN_3 (20 mg, 313 µmol, 1.3 eq) were diluted in DCM (10 mL) and EtOH (20 mL) and the solution was stirred for 1 h. The solvent was removed *in vacuo* and the yellow residue was extracted with DCM. The solution was concentrated to 1-2 mL, layered with pentane and stored in the freezer (-35 °C) overnight. $[Os(H)(N)(PNP^{tBu})]^{PF6}$ ($\mathbf{2^{PF_6}}$) was obtained as yellow crystals, which were collected and dried (153 mg, 215 µmol, 89.3 %).

^{1}H-NMR (400 MHz, CD_2Cl_2, 25 °C): δ (ppm) = 4.02-3.86 (m, 2H, NCH_2), 3.85-3.75 (m, 2H, NCH_2), 2.35-2.25 (m, 2H, PCH_2), 2.15-2.02 (m, 2H, PCH_2), 1.49 (spin-sys, $^{3}J_{HP}$ = 15.6 Hz, 18H, CH_3), 1.31 (spin-sys, $^{3}J_{HP}$ = 15.6 Hz, 18H, CH_3), -1.34 (t, $^{2}J_{HP}$ = 16 Hz, 1H, Os*H*). **^{13}C{^{1}H}-NMR** (100.7 MHz, CD_2Cl_2, 25 °C): δ (ppm) = 70.0 (virtual triplet (vt), AXX'A', N = $|^{2}J_{CP}+^{4}J_{CP}|$ = 6.2 Hz, NCH_2), 38.5 (vt, AXX'A', N = $|^{1}J_{CP}+^{3}J_{CP}|$ = 18.4 Hz, *C*$(CH_3)_3$), 36.6 (vt, AXX'A', N = $|^{1}J_{CP}+^{3}J_{CP}|$ = 27.8 Hz, *C*$(CH_3)_3$), 29.3 (m, *C*H_3), 28.9 (m, *C*H_3), 23.7 (vt, AXX'A', N = $|^{1}J_{CP}+^{3}J_{CP}|$ = 27.2 Hz, P*C*H_2). **^{31}P{^{1}H}-NMR** (162.0 MHz, CD_2Cl_2, 25 °C): δ (ppm) = 107.6 (s, *P*Os), -144.5 (hept, $^{1}J_{PF}$ = 711.8 Hz, *P*F_6). **Elemental anal.** Calc. for $C_{20}H_{45}F_6NOsP_3$: C, 33.8; H, 6.38; N, 3.94. Found: C, 33.27; H, 6.17; N, 3.90. **IR** (KBr): $\tilde{\nu}$ (cm^{-1}) = 2215.9 (ν_{Os-H})

*By protonation of **3***:
$[Os(N)(PNP^{tBu})]$ (**3**) (10.0 mg, 17.7 µmol, 1.0 eq) was dissolved in THF (2 mL) and H

$(Et_2O)_2(BAr^F_{24})$ (17.9 mg, 17.7 µmol, 1.0 eq) was added. After stirring for 5 min, the solvent was removed *in vacuo* and the residue was extracted with Et_2O. The solution was concentrated, layered with pentane and stored in the freezer at -35 °C overnight. [Os(H)(N)(PNP^{tBu})]$^{BAr^F_{24}}$ (**2**$^{BAr^F_{24}}$) was collected as yellow crystals and dried (19.7 mg, 13.8 µmol, 78 %).

The ^{1}H, $^{13}C\{^1H\}$ and $^{31}P\{^1H\}$-NMR spectra of the cation are identical with those of **2**^{PF_6}. **Mass spect.** (LIFDI), m/z (%) = 567.3 ([M$^+$]). **Elemental anal.** Calc. for $C_{52}H_{57}BF_{24}N_2OsP_2$: C,43.71; H, 4.02; N, 1.96. Found: C, 43.74; H, 4.27; N, 1.93.

2.1.2 [Os(N)(PNP^{tBu})] (**3**)

[Os(H)(N)(PNP^{tBu})]^{PF6} (**2**^{PF_6}) (103 mg, 145 µmol, 1.0 eq) was dissolved in THF (12 mL) andKO^tBu (16 mg, 145 µmol, 1.0 eq) in THF (2 mL) added dropwise. After stirring for 5 min, the solvent was removed and the deep red residue was extracted with pentane. [Os(N)(PNP^{tBu})] (**3**) was obtained as red powder (73 mg, 130 µmol, 89.9 %).

^{1}H-NMR (400 MHz, C_6D_6, 25 °C): δ (ppm) = 2.72 (m, 4H, NCH_2), 1.92 (m, 4H, PCH_2), 1.42 (spin-sys, $^3J_{HP}$ = 13.4 Hz, 36H, CH_3). **$^{13}C\{^1H\}$-NMR** (100.7 MHz, C_6D_6, 25 °C): δ (ppm) = 63.1 (vt, AXX'A', N=$|^2J_{CP}+^4J_{CP}|$ = 14.2 Hz, NCH_2), 36.4 (vt, $A_2XX'A'_2$, N=$|^1J_{CP}+^3J_{CP}|$ = 21.4 Hz, $C(CH_3)_3$), 29.7 ($A_6XX'A'_6$, N=$|^2J_{CP}+^4J_{CP}|$ = 2.6 Hz, CH_3), 25.3 (vt, AXX'A', N=$|^1J_{CP}+^3J_{CP}|$ = 24.2 Hz, PCH_2). **$^{15}N\{^1H\}$−NMR** (50.7 MHz, C_6D_6, 25 °C): δ (ppm) = 391.0 (s). **$^{31}P\{^1H\}$-NMR** (162.0 MHz, C_6D_6, 25 °C): δ (ppm) = 100.1 (s). **Elemental anal.** Calc. for $C_{20}H_{44}N_2OsP_2$: C, 42.53; H, 7.85; N, 4.96. Found: C, 42.60; H, 7.99; N, 4.84. **IR** (KBr): $\tilde{\nu}$ (cm^{-1}) = 999.2 ($\nu_{Os\equiv N}$). **^{15}N-3** (*from* $Na^{15}NN_2$): 966.9 ($\nu_{Os\equiv{}^{15}N}$). **Mass spec.** (ESI$^+$, THF): m/z = 567.2673 ([M+H]$^+$, calc. 567.2668).

2.1.3 [Os(H)(N)Cl($HPNP^{tBu}$)]^{Cl} (**4**^{Cl})

*By protonation of **3*** :
[Os(N)(PNP^{tBu})] (**3**) (6.0 mg, 10.6 µmol, 1.0 eq) in THF (0.6 mL) was treated with 2 eq HCl (2.0 M in Et_2O, 10.6 µL, 21.2 µmol). After stirring for 15 min, the solvent was removed *in vacuo* and the product was washed with Et_2O (2 × 0.5 mL). The selective formation of one product was observed and assigned to [Os(H)(N)Cl($HPNP^{tBu}$)]^{Cl} (**4**^{Cl}). Reaction of **3** with 1 eq HCl gave the same product exclusively with 50 % conversion.

*By disproportionation of **3***:
[Os(H)(N)(PNP^{tBu})]^{Cl} (**2**^{Cl}) was prepared as described above in DCM without KPF_6. After evaporation of the solvent the residue was dissolved in THF. Immediate reaction to **3** and **4**^{Cl} was detected by ^{31}P NMR spectroscopy.

^{1}H-NMR (300 MHz, CD_2Cl_2, 25 °C): δ (ppm) = 6.46-6.24 (singlet (s)$_{br}$, 1H, N*H*), 3.04-2.81 (m, 2H, CH_2), 2.69-2.54 (m, 2H, CH_2), 2.47-2.23 (m, 4H, CH_2), 1.72 (spin-sys, $^{3}J_{HP}$ = 15.0 Hz, 18H, CH_3), 1.60 (spin-sys, $^{3}J_{HP}$ = 15.2 Hz, 18H, CH_3), -2.52 (t, $^{2}J_{HP}$ = 14.6 Hz, 1H, Os*H*). **^{31}P{^{1}H}-NMR** (121.5 MHz, CD_2Cl_2, 25 °C): δ (ppm) = 65.0 (s).

2.1.4 [Os(NBAr$^{F}_{18}$)(PNP^{tBu})] (**5**)

[Os(N)(PNP^{tBu})] (**3**) (5.0 mg, 8.9 µmol, 1.0 eq) and BAr$^{F}_{18}$ (5.8 mg, 8.9 µmol, 1.0 eq) were mixed in benzene (0.5 mL) and stirred for 30 min. The solvent was removed *in vacuo*, the product was washed with pentane and Et_2O.

^{1}H-NMR (300 MHz, THF-d_8, 25 °C): δ (ppm) = 8.18 (s, 6H, CH_{ortho}), 7.69 (s, 3H, CH_{para}), 2.75 (m, 4H, NCH_2), 2.32 (m, 4H, PCH_2), 1.17 (spin-sys, $^{3}J_{HP}$ = 14.1 Hz, 36H, CH_3). **^{19}F{^{1}H}-NMR** (282.4 MHz, CD_2Cl_2, 25 °C): δ (ppm) = −63.5 (s). **^{31}P{^{1}H}-NMR** (121.5 MHz, CD_2Cl_2, 25 °C): δ (ppm) = 98.2(s).

2.1.5 [Os(NSiMe$_3$)(PNP^{tBu})]$^{BAr^{F}_{24}}$ (**6**$^{\mathbf{BAr^{F}_{24}}}$)

[Os(N)(PNP^{tBu})] (**3**) (10 mg, 17.7 µmol, 1.0 eq) and NaBAr$^{F}_{24}$ (15.7 mg, 17.7 µmol, 1.0 eq) were stirred in THF (2 mL). Me_3SiBr (2.3 µL, 2.7 mg, 17.7 µmol, 1.0 eq) in THF (0.5 mL) was added dropwise accompanied by a color change to deep green. After 15 min the solvent was removed *in vacuo* and the residue extracted with Et_2O. The solution was concentrated, layered with pentane and stored in the freezer at −35 °C overnight. The product was collected as green crystals and dried (16.7 mg, 11.2 µmol, 63.0 %).

^{1}H-NMR (400 MHz, CD_2Cl_2, 25 °C): δ (ppm) = 7.72 (m, 8H, H_{ortho}), 7.56 (m, 4H, H_{para}), 2.42-2.33 (m, 4H, PCH_2), 2.26-2.15 (m, 4H, NCH_2), 1.55 (spin-sys, $^{3}J_{HP}$ = 14.8 Hz, 36H, C(CH_3)$_3$), 0.25 (s, 9H, Si(CH_3)$_3$). **^{13}C{^{1}H}-NMR** (100.7 MHz, CD_2Cl_2, 25 °C): δ (ppm) = 161.7 (q, $^{1}J_{CB}$ = 49.7 Hz, B*C*), 134.8 (s, C_{ortho}), 128.8 (qq, $^{2}J_{CF}$ = 31.5 Hz, $^{3}J_{BC}$ = 2.9 Hz, C_{meta}), 124.5 (q, $^{1}J_{CF}$ = 272.8 Hz, *C*F$_3$), 117.4 (m, C_{para}), 67.9 (vt, AXX'A', N = $|^{2}J_{CP}+^{4}J_{CP}|$ = 13.8 Hz, N*C*H$_2$), 39.0 (vt, AXX'A', N = $|^{1}J_{CP}+^{3}J_{CP}|$ = 21.0 Hz, P*C*(CH$_3$)$_3$), 30.0 (m, C(*C*H$_3$)$_3$), 23.5 (vt, AXX'A', N = $|^{1}J_{CP}+^{3}J_{CP}|$ = 28.8 Hz, P*C*H$_2$), 1.6 (s, Si(*C*H$_3$)$_3$). **^{11}B{^{1}H}-NMR** (93.6 MHz, CD_2Cl_2, 25 °C): δ (ppm) = -6.61 (s). **^{19}F{^{1}H}-NMR** (282.3 MHz, CD_2Cl_2, 25 °C): δ (ppm) = -62.9 (s, C*F*$_3$). **^{31}P{^{1}H}-NMR** (162.0 MHz, CD_2Cl_2, 25 °C): δ (ppm) = 106.9 (s). **Elemental anal.** Calc. for $C_{55}H_{65}BF_{24}N_2OsP_2Si$: C, 44.01; H, 4.36; N, 1.87. Found: C, 43.99; H, 4.30; N, 1.85.

2.1.6 [Os(NPMe$_3$)(PNP^{tBu})] (**7**)

[Os(N)(PNP^{tBu})] (**3**) (20 mg, 35 µmol, 1.0 eq) was dissolved in C_6D_6 (0.6 mL) and PMe_3 (4.0 µL, 3.0 mg, 39 µmol, 1.1 eq) was added via variable volume pipette. The reaction solution was transferred into a NMR tube and shaken for 48 h for equilibrium formation. A mixture of the reactants and [Os(NPMe$_3$)(PNP^{tBu})] (**7**) was observed by NMR spectroscopy.

^{1}H-NMR (400 MHz, C_6D_6, 25 °C): δ (ppm) = 1.62-1.54 (m, 4H, P-CH_2), 1.57 (spin-sys, $^3J_{HP}$ = 11.8 Hz, 18H, C(-CH_3)$_3$), 1.24-1.16 (m, 4H, N-CH_2), 1.22 (d, $^2J_{PH}$ = 11.5 Hz, 9H, P(-CH_3)$_3$). **^{13}C{^{1}H}-NMR** (100.7 MHz, C_6D_6, 25 °C): δ (ppm) = 85.6 (vt, AXX'A', N = $|^2J_{CP}+^4J_{CP}|$ = 8.4 Hz, 2C, N-CH$_2$), 38.3 (vt, AXX'A', N = $|^1J_{CP}+^3J_{CP}|$ = 8.4 Hz, 2 C, C(-CH$_3$)$_3$), 32.7 (m, 12C, C(-CH$_3$)$_3$), 29.6 (vt, AXX'A', N = $|^1J_{CP}+^3J_{CP}|$ = 17.6 Hz, 2C, P-CH$_2$), 27.8 (d, $^1J_{PC}$ = 64.7 Hz, 3C, P-(CH$_3$)$_3$). **^{15}N{^{1}H}-NMR** (38.0 MHz, C_6D_6, 25 °C): δ (ppm) = −126.5 (d, $^1J_{15N\text{-}31P}$ = 22.6 Hz). **^{31}P{^{1}H}-NMR** (162.0 MHz, C_6D_6, 25 °C): δ (ppm) = 43.9 (s, 2P, Os-P), 22.1 (s, 1P, N=P). Using 50 % ^{15}N-labeled **7** the signal at 22.1 ppm was reduced by 50 % and an additional doublet arose: 22.1 (d, $^1J_{15N\text{-}31P}$ = 22.7 Hz).). **ATR-IR** (C_6H_6): $\tilde{\nu}$ (cm^{-1}) = 1240 ($\nu_{Os\text{-}N}$).

2.1.7 [OsH$_4$(HPNP^{tBu})] (**8**)

[Os(N)(PNP^{tBu})] (**3**) (46 mg, 82 µmol, 1.0 eq) was dissolved in toluene (8 mL) in a Teflon-stoppered tube. The solution was degased by three successive *freeze-pump-thaw* cycles and the tube was backfilled with H_2 gas (2 bar). The solution was stirred over 36 h at 110 °C. All volatiles were removed *in vacuo* and the remaining solid was washed with cold pentane (−10 °C) and lyophilized to obtain [OsH$_4$(HPNP^{tBu})] (**8**) as a yellow powder (34 mg, 61 µmol, 74 %).

^{1}H-NMR (400 MHz, THF-d_8, 25 °C): δ (ppm) = 4.88 (s_{br}, 1H, NH), 3.29-3.12 (m, 2H, NCH_2), 2.20-2.03 (m, 4H, NCH_2 + PCH_2), 1.53-1.40 (m, 2H, PCH_2), 1.33 (spin-sys, $^3J_{HP}$ = 11.8 Hz, 18H, CH_3), 1.27 (spin-sys, $^3J_{HP}$ = 12.0 Hz, 18H, CH_3), −6.00 - −6.66 (s_{br}, 1H, Os-H), −6.28 - −7.48 (s_{br}, 1H, OsH), −13.11 - −14.33 (s_{br}, 2H, Os-H). **^{13}C{^{1}H}-NMR** (100.7 MHz, THF-d_8, 25 °C): δ (ppm) = 59.4 (vt, AXX'A', N = $|^2J_{CP}+^4J_{CP}|$ = 8.0 Hz, NCH$_2$), 33.1 (vt, AXX'A', N = $|^1J_{CP}+^3J_{CP}|$ = 19.0 Hz, PC(CH$_3$)$_3$), 31.2 (vt, AXX'A', N = $|^1J_{CP}+^3J_{CP}|$ = 18.0 Hz, PC(CH$_3$)$_3$), 30.0 (m, CH$_3$), 29.9 (vt, AXX'A', N = $|^1J_{CP}+^3J_{CP}|$ = 14.2 Hz, PCH$_2$), 29.5 (m, CH$_3$). 79.4 (s). **Elemental anal.** Calc. for [$C_{20}H_{49}NOsP_2$] · (0.065 × C_6H_6): C, 43.66; H, 8.88; N, 2.50. Found: C, 44.12; H, 8.56; N, 2.59. **Mass spec.** (LIFDI, toluene): m/z = 555.2 ([M-H$_2$]$^+$) (558.2 from experiment with D_2).

2.1.8 $[OsH_3(PNP^{tBu})]$ (**9**)

A solid sample of lyophilized $[OsH_4(HPNP^{tBu})]$ (**8**) (5.0 mg, 9.0 µg, 1.0 eq) was heated to 110 °C under applied vacuum for 16 h. The solid was redissolved in C_6D_6 and measured.

^{1}H-NMR (300 MHz, CD_2Cl_2, 25 °C): δ (ppm) = 3.11-3.01 (m, 4H, NCH_2), 1.85-1.75 (m, 4H, PCH_2), 1.25 (spin-sys, $^3J_{HP}$ = 12.4 Hz, 36H, C(CH_3)$_3$), −13.64 (br, 3H, OsH_3). **^{31}P{^{1}H}-NMR** (121.5 MHz, CD_2Cl_2, 25 °C): δ (ppm) = 96.1 (s).

2.1.9 $[Os(N)Cl(PNP^{tBu})]BAr^F_{24}$ (**10$^{BAr^F_{24}}$**) and $[Os(N)Cl_2(PNP^{tBu})]$ (**10-Cl**)

*Synthesis of $[Os(N)Cl(PNP^{tBu})]BAr^F_{24}$ (**10$^{BAr^F_{24}}$**)*:
$[Os(N)(PNP^{tBu}]$ (**3**) (10.0 mg, 17.8 µmol, 1.0 eq) and *N*-chlorosuccinimide (2.4 mg, 17.8 µmol, 1.0 eq) are mixed in THF (1 mL) and stirred for 5 min. $H(Et_2O)_2\{BAr^F_{24}\}$ (18.0 mg, 17.8 µmol, 1.0 eq) is added and the mixture is stirred for another 15 min. The solvent is removed *in vacuo*, the product is extracted with Et_2O and washed with pentanes.

^{1}H-NMR (400 MHz, CD_2Cl_2, 25 °C): δ (ppm) = 7.73 (m, 8H, CH_{ortho}), 7.57 (m, 4H, CH_{para}), 4.18-4.01 (m, 2H, N−CHH), 3.62-3.50 (m, 2H, N−CHH), 2.37-2.25 (m, 2H, P−CHH), 2.18-2.08 (m, 2H, P−CHH), 1.54 (spin-sys, $^3J^{HP}$ = 16.0 Hz, 18H, C(CH_3)$_3$), 1.40 (spin-sys, $^3J^{HP}$ = 15.8 Hz, 18H, C(CH_3)$_3$). **^{13}C{^{1}H}-NMR** (100.6 MHz, CD_2Cl_2, 25 °C): δ (ppm) = 161.7 (q, $^1J_{CB}$ = 49.8 Hz, C_{ipso}), 134.7 (br, C_{ortho}H), 12R8.8(qq, $^2J_{CF}$ = 31.2 Hz, $^3J_{CB}$ = 2.9 Hz, $C_{meta}CF_3$), 124.5 (q, $^1J_{CF}$ = 272.3 Hz, CF_3), 117.4 (hept, $^3J_{CF}$ = 4.1 Hz, C_{para}H), 72.0 (s, N−CH_2), 39.1 (vt, AXX'A', N=|$^1J_{CP}$+$^2J_{CP}$| = 22.8 Hz, CMe$_3$), 38.1 (vt, AXX'A', N=|$^1J_{CP}$+$^2J_{CP}$| = 16.1 Hz, CMe$_3$), 28.7 (s, C(CH_3)$_3$), 27.7 (s, C(CH_3)$_3$), 23.1 (vt, AXX'A', N=|$^1J_{CP}$+$^2J_{CP}$| = 26.9 Hz, P−CH_2). **^{31}P{^{1}H}-NMR** (162.0 MHz, CD_2Cl_2, 25 °C): δ (ppm) = 96.2 (s). **Elemental anal.** Calc. for $C_{52}H_{56}BClF_{24}N_2OsP_2$: C, 42.68; H, 3.86; N, 1.91. Found: C, 43.24; H, 3.95; N, 2.02. **Mass spect.** (LIFDI), m/z (%) = 601.1 (100, $[M]^+$).

*Synthesis of $[Os(N)Cl_2(PNP^{tBu})]$ (**10-Cl**)*:
Synthesis was done analogous to the above described procedure, but using HCl in Et_2O instead of $H(Et_2O)_2\{BAr^F_{24}\}$.

^{1}H-NMR (300 MHz, CD_2Cl_2, 25 °C): δ (ppm) = 4.47-4.23 (m, 2H, N−CHH), 3.74-3.57 (m, 2H, N−CHH), 2.59-2.42 (m, 2H, P−CHH), 2.37-2.22 (m, 2H, P−CHH), 1.56 (spin-sys, $^3J^{HP}$ = 15.9 Hz, 18H, C(CH_3)$_3$), 1.43 (spin-sys, $^3J^{HP}$ = 15.6 Hz, 18H, C(CH_3)$_3$). **^{31}P{^{1}H}-NMR** (121.5 MHz, CD_2Cl_2, 25 °C): δ (ppm) = 97.2 (s). **Mass spect.** (LIFDI), m/z (%) = 601.2 (100, $[M\text{-}Cl]^+$).

2.1.10 $[Os(CN^tBu)_2Cl\{N(CH_2CH_2P^tBu_2)(=CHCH_2P(^tBu)_2=NH)\}]^{BAr^F_{24}}$ (**11a**$^{BAr^F_{24}}$ and **11b**$^{BAr^F_{24}}$)

$[Os(N)Cl(PNP^{tBu})]^{BAr^F_{24}}$ (**10**$^{BAr^F_{24}}$) (5.0 mg, 3.4 µmol, 1.0 eq) is dissolved in THF (0.5 mL). ^{t}BuNC (1.0 µ, 8.5 µmol, 2.5 eq) is added via Eppendorf pipette and the mixture is stirred overnight at RT. The solvent is removed *in vacuo* and the product is extracted with Et_2O.

$^{31}P\{^1H\}$-NMR (121.5 MHz, CD_2Cl_2, 25 °C): δ (ppm) = 62.5 (doublet (d), $^3J_{PP}$ = 11.6 Hz, **A**), 51.9 (d, $^3J_{PP}$ = 11.6 Hz, **A**), 49.0 (d, $^3J_{PP}$ = 6.4 Hz, **B**), 47.5 (d, $^3J_{PP}$ = 6.5 Hz, **B**). **Mass spect.** (LIFDI), m/z (%) = 767.2 (100, $[M]^+$), 731.2 (25, $[M\text{-}HCl]^+$), 684.2 (62, $[M\text{-}CN^tBu]^+$).

2.1.11 $[OsH(N_2)(PNP^{tBu})]$ (**13**)

$[OsHCl_2(PNP^{tBu})]$ (**1**) (5.0 mg, 8.0 µmol, 1.0 eq) and KC_8 (3.3 mg, 24.1 µmol, 3.0 eq) are suspended in THF (Na/K, 0.7 mL) under a dinitrogen atmosphere and stirred for 30 min. All volatiles are removed *in vacuo* and the product is extracted with pentane. $[OsH(N_2)(PNP^{tBu})]$ (**13**) is obtained as orange solid.

^{1}H-NMR (300 MHz, C_6D_6, 25 °C): δ (ppm) = 3.31-3.12 (m, 2H, N−C*H*H), 2.56-2.44 (m, 2H, N−CH*H*), 1.91-1.77 (m, 2H, P−C*H*H), 1.71-1.58 (m, 2H, P−CH*H*), 1.34 (spin-sys, $^3J_{HP}$ = 12.6 Hz, 18H, $C(CH_3)_3$), 1.28 (spin-sys, $^3J_{HP}$ = 12.6 Hz, 18H, $C(CH_3)_3$), −26.9 (triplet (t), $^2J_{HP}$ = 12.2 Hz, 1H, Os*H*). **$^{31}P\{^1H\}$-NMR** (121.5 MHz, C_6D_6, 25 °C): δ (ppm) = 85.9 (s). **ATR-IR**: $\tilde{\nu}$ (cm^{-1}) = 2114.5 (ν_{OsH}), 2007.7 ($\nu_{N\equiv N}$).

2.1.12 $[OsHCl(PNP^{tBu})]^{BPh_4}$ (**12**^{BPh_4})

$[OsHCl_2(PNP^{tBu})]$ (**1**) (33.0 mg, 53.0 µmol, 1.0 eq) and $NaBPh_4$ (20.0 mg, 58.3 µmol, 1.1 eq) are stirred for 20 min in THF (1 mL). Afterwards, all volatiles are removed *in vacuo*, the product is extracted with DCM, concentrated and crystallized by layering with Et_2O at −40 °C. $[OsHCl(PNP^{tBu})]^{BPh_4}$ (**12**^{BPh_4}) is obtained as green powder (33.0 mg, ≈70 %).

^{1}H-NMR (300 MHz, CD_2Cl_2, 25 °C): δ (ppm) = 7.51-7.43 (m, 8H, $C_{ortho}H$), 7.07 (t, $^3J_{HH}$ = 7.3 Hz, 8H, $C_{meta}H$), 6.88 (t, $^3J_{HH}$ = 7.2 Hz, 4H, $C_{para}H$), 2.45-2.28 (m, 4H, N−C*H*H), 2.06-1.81 (m, 4H, P−C*H*H), 1.38 (spin-sys, $^3J_{HP}$ = 14.5 Hz, 18H, $C(CH_3)_3$), 1.32 (spin-sys, $^3J_{HP}$ = 14.1 Hz, 18H, $C(CH_3)_3$), −20.79 (br, 1H, Os*H*). **$^{31}P\{^1H\}$-NMR** (121.5 MHz, CD_2Cl_2, 25 °C): δ (ppm) = 46.0 (s_{br}). **Mass spect.** (LIFDI), m/z (%) = 588.1 (100, $[M]^+$).

2.1.13 [OsHCl(CN^{t}Bu)(PNP^{tBu})]^{BPh_4} (**14^{BPh_4}**)

[OsHCl(PNP^{tBu})]^{BPh_4} (**12^{BPh_4}**) (20.0 mg, 22.1 µmol, 1.0 eq) and *tert*-butylisocyanide (2.5 µL, 1.8 mg, 22.1 µmol, 1.0 eq) are separately dissolved in DCM (2 mL each). The CN^{t}Bu solution is added dropwise to **12^{BPh_4}** at −0°C. The solution is stirred for 10 min, the solvent is removed *in vacuo* and the product is washed with Et_2O and dried. [OsHCl(CN^{t}Bu)(PNP^{tBu})]^{BPh_4} (**14^{BPh_4}**) is obtained as a spectroscopically clean yellow powder.

^{1}H-NMR (300 MHz, CD_2Cl_2, 25 °C): δ (ppm) = 7.50-7.41 (m, 8H, $C_{ortho}H$), 7.07 (t, $^3J_{HH}$ = 7.4 Hz, 8H, $C_{meta}H$), 6.89 (t, $^3J_{HH}$ = 7.2 Hz, 4H, $C_{para}H$), 1.46 (spin-sys, $^3J_{HP}$ = 13.9 Hz, 18H, $C(CH_3)_3$), 1.47 (s, 9H, C≡N−$C(CH_3)_3$), 1.10 (spin-sys, $^3J_{HP}$ = 12.9 Hz, 18H, $C(CH_3)_3$), 0.30 (br, 1H, Os*H*). **^{31}P{^{1}H}-NMR** (121.5 MHz, CD_2Cl_2, 25 °C): δ (ppm) = 48.2 (s). **Mass spect.** (LIFDI), m/z (%) = 671.2 (100, $[M]^+$), 635.3 (50, $[M\text{-}HCl]^+$).

2.1.14 [OsCl(CN^{t}Bu)(PNP^{tBu})] (**15**)

[OsHCl(CN^{t}Bu)(PNP^{tBu})]^{BPh_4} (**14^{BPh_4}**) (61.3 mg, 61.9 µmol, 1.0 eq) and KO^{t}Bu (7.2 mg, 64.2 µmol, 1.05 eq) are mixed in THF (5 mL) and stirred for 15 min. All volatiles are removed *in vacuo*, the product is extracted with pentane, concentrated and stored at −40 °C overnight. The solution is filtered and the residue is taken up in C_6H_6 and lyophilized. [OsCl(CN^{t}Bu)(PNP^{tBu})] (**15** is obtained as a red-brownish powder.

^{1}H-NMR (400 MHz, THF-d_8, 25 °C): δ (ppm) = 2.95-2.81 (m, 2H, N−C*H*H), 2.55-2.46 (m, 2H, N−CH*H*), 1.62-1.54 (m, 4H, P−CH_2), 1.46 (spin-sys, $^3J_{HP}$ = 12.8 Hz, 18H, $C(CH_3)_3$), 1.43 (spin-sys, $^3J_{HP}$ = 12.6 Hz, 18H, $C(CH_3)_3$), 1.40 (s, 9H, C≡N−$C(CH_3)_3$). **^{13}C{^{1}H}-NMR** (100.6 MHz, THF-d_8, 25 °C): δ (ppm) = 167.9 (t, $^2J_{CP}$ = 6.3 Hz, *C*≡N^{t}Bu), 69.8 (vt, AXX'A', N=$|^2J_{CP}+^4J_{CP}|$ = 9.6 Hz, NCH_2), 57.0 (s, C≡N−*C*Me_3), 37.4 (vt, AXX'A', N=$|^1J_{CP}+^3J_{CP}|$ = 21.2 Hz, P*C*Me_3), 36.3 (vt, AXX'A', N=$|^1J_{CP}+^3J_{CP}|$ = 17.6 Hz, P *C*Me_3), 33.2 (s, C≡N−$C(CH_3)_3$), 29.8 (m, PC$(CH_3)_3$), 29.8 (m, PC$(CH_3)_3$), 25.7 (vt, AXX'A', N=$|^1J_{CP}+^3J_{CP}|$ = 20.2 Hz, PCH_2). **^{31}P{^{1}H}-NMR** (162.0 MHz, THF-d_8, 25 °C): δ (ppm) = 66.8 (s). **Mass spect.** (LIFDI), m/z (%) = 670.1 (100, $[M]^+$).

2.2 Rhenium compounds based on the PNP^{tBu} ligand

2.2.1 [(μ-N_2){ReCl(PNP^{tBu})}$_2$] (**XX**)

In a typical experiment, [$ReCl_2$(PNP^{tBu})] (5.0 mg, 8.1 μmol, 1.0 eq) was mixed in solid state with NaHg (1.0 M, 125 mg, 9.2 μmol, 1.15 eq) in a J-Young NMR tube. The tube was connected to a condensation bridge and THF-d_8 was degassed and vacuum-transferred to the tube. The NMR tube was backfilled with N_2 gas, thawed and shaken in a -35 °C cooling bath for 10 min before the tube was placed in a cooled spectrometer for analysis. If a kinetic study was performed, a capillary with $P(OTMS)_3$ in toluene-d_8 was added at the very beginning of the reaction.

^{1}H-NMR (400 MHz, THF-d_8, −50 °C): δ (ppm) = 12.23 (m, 2H, CH_2), 10.56 (m, 2H, CH_2), 8.60 (m, 2H, CH_2), 4.00 (m, 2H, CH_2), 2.64 (m, 2H, CH_2), -0.22 (m, 2H, CH_2), -11.75 (m, 2H, CH_2), -16.74 (m, 2H, CH_2) (signals for the *tert*-butyl groups could not be identified at this temperature, as they became very broad due to some dynamic effects). **^{31}P{^{1}H}-NMR** (162.0 MHz, THF-d_8, −50 °C): δ (ppm) = 16.5 (d, $^2J_{PP}$ = 234.5 Hz), -115.3 (d, $^2J_{PP}$ = 234.2 Hz).

2.2.2 [ReHCl(PNP^{tBu})] (**17**)

[$ReCl_2$(PNP^{tBu})] (**XIX**) (16.1 mg, 26.1 μmol, 1.0 eq) and $Co(Cp^*)_2$ (17.2 mg, 52.1 μmol, 2.0 eq) were mixed in THF (Na/K, 1.0 mL) and stirred for 1.5 h. The solvent was removed *in vacuo* and the product is extracted with Et_2O. Afterwards the product was washed with cold pentane to yield rather clean [ReHCl(PNP^{tBu})] (**17**).

^{1}H-NMR (300 MHz, C_6D_6, 25 °C): δ (ppm) = 3.15-2.87 (m, 4H, CH_2), 1.69-1.49 (m, 2H, CH_2), 1.37 (spin-sys, $^3J_{HP}$ = 12.3 Hz, 18H, C(CH_3)$_3$), 1.32 (spin-sys, $^3J_{HP}$ = 12.0 Hz, 18H, C(CH_3)$_3$), -9.30 (t, $^2J_{HP}$ = 13.1 Hz, 1H, Re−H). The last CH_2 signal is superimposed by the *tert*-butyl signals and was thus not identified. **^{31}P{^{1}H}-NMR** (121.5 MHz, C_6D_6, 25 °C): δ (ppm) = 29.8.

2.2.3 [(*N*,*N*−$C_2H_4N_2$){ReCl(PNP^{tBu})}$_2$]$^{(OTf)_2}$ (**19$^{(OTf)_2}$**)

[Re(NCH_2)Cl(PNP^{tBu})] (**18**) (10.0 mg, 16.4 μmol, 1.0 eq) and [Fe$(Cp)_2$]OTf (5.5 mg, 16.4 μmol, 1.0 eq) are mixed in THF (dried over Na/K, 0.5 mL) and stirred for 1.5 h. Afterwards the solvent is removed *in vacuo*, the product is washed with Et_2O and recrys-

tallized from THF/Et_2O. $[(N,N{-}C_2H_4N_2)\{ReCl(PNP^{tBu})\}_2]^{2OTf}$ (**19$^{(OTf)_2}$**) is obtained as deep green powder (7.6 mg, 5.0 µmol, 61 % yield).

^{1}H-NMR (400 MHz, CD_2Cl_2, 25 °C): δ (ppm) = 4.45-4.29 (m, 4H, N−C*H*H−CH_2), 3.93-3.82 (m, 4H, N−CH*H*−CH_2), 3.31 (s, 4H, Re=N−CH_2) 2.55-2.42 (m, 4H, P−C*H*H−CH_2), 2.23-2.11 (m, 4H, P−CH*H*−CH_2), 1.47 (spin-sys, $^3J_{HP}$ = 14.6 Hz, 32H, C(CH_3)$_3$), 1.29 (spin-sys, $^3J_{HP}$ = 14.3 Hz, 32H, C(CH_3)$_3$). **^{13}C{^{1}H}-NMR** (100.6 MHz, CD_2Cl_2, 25 °C): δ (ppm) = 76.6 (s, N−*C*H_2−CH_2), 67.8 (s, Re=N−*C*H_2), 38.5 (vt, $^1J_{CP}$ = 10.5 Hz, *C*(CH_3)$_3$), 38.0 (vt, $^1J_{CP}$ = 8.7 Hz, *C*(CH_3)$_3$), 29.7 (m, both C(*C*H_3)$_3$), 24.2 (t, $^1J_{CP}$ = 11.2 Hz, P−*C*H_2−CH_2). **^{31}P{^{1}H}-NMR** (162.0 MHz, CD_2Cl_2, 25 °C): δ (ppm) = 90.2 (s). **Elemental anal.** Calcd. for $C_{44}H_{32}Cl_2F_6N_4O_6P_4Re_2S_2$: C, 34.80; H, 6.11; N, 3.69. Found: C, 35.09; H, 6.04; N, 3.46.

2.2.4 $[Re(O)Cl(PNP^{tBu})]^{BPh_4}$ (**20^{BPh_4}**)

$[ReCl_2(PNP^{tBu})]$ (**XIX**) (8.0 mg, 13.0 µmol, 1.0 eq), $NaBPh_4$ (4.4 mg, 13.0 µmol, 1.0 eq) and Me_3NO (1.0 mg, 13.0 µmol, 1.0 eq) are mixed in THF (dried over Na/K, 1 mL) and stirred overnight. All volatiles are removed *in vacuo*, the product is washed with Et_2O and extracted with DCM. $[Re(O)Cl(PNP^{tBu})]^{BPh_4}$ (**20^{BPh_4}**) is obtained as a green powder (9.6 mg, 10.5 µmol, 80.8 % yield).

^{1}H-NMR (500 MHz, CD_2Cl_2, 25 °C): δ (ppm) = 7.35 (m, 8H, H_{ortho}), 7.04 (t, $^3J_{HH}$ = 7.0 Hz, 8H, H_{meta}), 6.89 (t, $^3J_{HH}$ = 6.9 Hz, 4H, H_{para}), 3.99-3.88 (m, 2H, N−C*H*H−CH_2), 3.77-3.67 (m, 2H, N−CH*H*−CH_2), 2.35-2.25 (m, 2H, P−C*H*H−CH_2), 2.03-1.93 (m, 2H, P−CH*H*−CH_2), 1.50 (spin-sys, $^3J_{HP}$ = 15.2 Hz, 18H, C(CH_3)$_3$), 1.31 (spin-sys, $^3J_{HP}$ = 15.3 Hz, 18H, C(CH_3)$_3$). **^{13}C{^{1}H}-NMR** (125.8 MHz, CD_2Cl_2, 25 °C): δ (ppm) = 164.3 ($^1J_{CB}$ = 49.4 Hz, C_{ipso}), 137.2 ($^2J_{CB}$ = 1.3 Hz, C_{ortho}), 126.1 ($^3J_{CB}$ = 2.7 Hz, C_{meta}), 122.2 (s, C_{para}), 76.6 (vt, $^2J_{CP}$ = 2.0 Hz, N−*C*H_2−CH_2), 39.8 (vt, $^1J_{CP}$ = 11.1 Hz, P−*C*(CH_3)$_3$), 38.1 (vt, $^1J_{CP}$ = 7.1 Hz, P−*C*(CH_3)$_3$), 30.0 (C(*C*H_3)$_3$), 29.2 (C(*C*H_3)$_3$). **^{31}P{^{1}H}-NMR** (121.5 MHz, CD_2Cl_2, 25 °C): δ (ppm) = 97.7 (s). **Mass spect.** (LIFDI), m/z (%) = 598.3 (100).

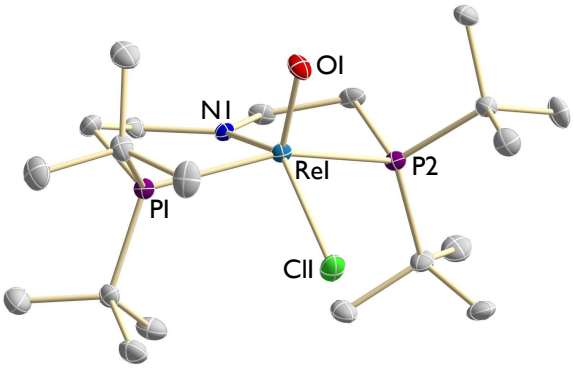

Fig. 2.1. Molecular structure of **37** obtained by single crystal X-ray diffraction measurements. All H atoms, a cocrystallized Et_2O molecule as well as the anion are omitted for clarity. Anisotropic displacement parameters are set to 50 % probability. Selected bond length [Å] and angles [°]: Re1-O1 1.681(3), Re1-N1 1.934(3), Re1-Cl1 2.3594(12), P1-Re1-P2 151.96(4), N1-Re1-Cl1 135.90(10), N1-Re1-O1 112.14(14).

2.2.5 $[ReCl_2(P{=}N{=}P^{tBu})]$ (**21**)

$[ReCl_2(PNP^{tBu})]$ (**XIX**) (120 mg, 194 µmol, 1.0 eq) and the 2,4,6-tri-*tert*-butylphenoxy radical (305 mg, 1.17 mmol, 6.0 eq) were mixed in dry benzene (15 mL) and stirred for 24 h at 50 °C. The solvent was removed *in vacuo* and the product was washed with excess pentane, until the washing solution was colorless. $Co(Cp)_2$ (7 mg, 37 µmol, 0.2 eq) was added and the product was dissolved in benzene and stirred for 2 h at RT. The reaction mixture was filtered, the benzene phase was lyophilized and remaining $Co(Cp)_2$ and 2,4,6-tri-*tert*-butylphenol were sublimed off overnight at 75 °C. $[ReCl_2(P{=}N{=}P^{tBu})]$ (**21**) was obtained as a brown powder (75.1 mg, 122.4 µmol, 63 % yield.

*Spectroscopic characterization matched the previously published features of **21**.*[180]

2.2.6 $[Re(N)Cl(P{=}N{=}P^{tBu})]$ (**22**)

From N_2:
Degassed THF (0.45 mL) was vacuum-transferred to a mixture of $[ReCl_2(P{=}N{=}P^{tBu})]$ (**21**) (5.0 mg, 8.1 µmol, 1.0 eq) and reductant ($Co(Cp^*)_2$: 3.0 mg, 9.0 µmol, 1.1 eq; NaHg (1 M): 121.3 mg, 9.0 µmol, 1.1 eq or KC_8: 1.1 mg; 8.1 µmol, 1.0 eq) in a J-Young NMR tube and placed under an N_2 atmosphere. After thawing of the solvent the mixture was stirred vigorously upon which the color gradually changed from dark brown to light brown. After 30 min at RT the solvent was removed, hexamethylbenzene (1 eq via 0.08 M stock solution in THF) was added and the solvent was removed again. The spectroscopic yield of the title compound was obtained by integration of the $P{=}N{=}P^{tBu}$ ligand backbone ^1H NMR signals

vs. the internal standard C_6Me_6 (maximum 60 % for $Co(Cp^*)_2$, 30 % for Na/Hg, 20 % for KC_8). [Re(N)Cl(P=N=P^{tBu})] (**22**) was not isolated via this route.

From azide:
[$ReCl_2$(P=N=P^{tBu})] (**21**) (25.0 mg, 40.7 µmol, 1.0 eq) was dissolved in THF (1 mL) and was added dropwise over a period of 5 min to a stirring solution of (TMS)N_3 (26.78 µL, 23.5 mg, 203 µmol, 5.0 eq) in THF (0.5 mL). The solution was stirred at RT for 1.5 h after which the solvent was removed *in vacuo*. After extraction with pentane (4 × 5 mL) and removal of the solvent, [Re(N)Cl(P=N=P^{tBu})] (**22**) was obtained as a light brown solid (17.4 mg, 29.3 µmol, 72 % yield).

^{1}H-NMR (400 MHz, C_6D_6, 25 °C): δ (ppm) = 7.00 ($A_9B_9CDXX'D'C'B'_9A'_9$, $N = |^3J_{DX} + ^5J_{DX'}| = 17.1$ Hz, $^3J_{DC} = 6.2$ Hz, 2H, NC*H*), 4.29 ($A_9B_9CDXX'D'C'B'_9A'_9$, $^3J_{CD} = 6.3$ Hz, $N = |^2J_{CX} + ^4J_{CX'}| = 2.2$ Hz, 2H, PC*H*), 1.49 ($A_9B_9CDXX'D'C'B'_9A'_9$, $^3J_{BX} = 7.0$ Hz, 18H, C(CH_3)$_3$), 1.18 ($A_9B_9CDXX'D'C'B'_9A'_9$, $^3J_{AX} = 7.2$ Hz, 18H, C(CH_3)$_3$). **^{13}C{^{1}H}-NMR** (125.8 MHz, C_6D_6, 25 °C): δ (ppm) = 170.3 (vt, $^2J_{CP} = 6.8$ Hz, 2C, N*C*H), 91.8 (vt, $^1J_{CP} = 20.9$ Hz, 2C, P*C*H), 36.7 (vt, $^1J_{CP} = 11.8$ Hz, 2C, *C*(CH$_3$)$_3$), 34.9 (vt, $^1J_{CP} = 10.3$ Hz, 2C, *C*(CH$_3$)$_3$), 29.4 (m, 6C, C(*C*H$_3$)$_3$), 28.5 (m, 6C, C(*C*H$_3$)$_3$). **^{31}P{^{1}H}-NMR** (162.0 MHz, C_6D_6, 25 °C): δ (ppm) = 71.8 (s). **Elemental anal.** Calc. for $C_{20}H_{40}ClN_2P_2Re$: C, 40.57; H, 6.81; N, 4.73. Found: C, 40.66; H, 6.73; N, 5.01. **Mass spect.** (LIFDI), m/z (%) = 592.1 (100).

2.2.7 [Re(N)Cl(P^H=N=P^{tBu})]^{OTf} (**23^{OTf}**)

Compound [Re(N)Cl(P=N=P^{tBu})] (**22**) (5.0 mg, 8.4 µmol, 1.0 eq) was dissolved in Et_2O (1.0 mL) and HOTf (0.74 µL, 8.4 µmol, 1.0 eq) was added via an Eppendorf pipette. Upon stirring for 1 h a red-brownish precipitate formed which was collected by filtration, washed with pentanes (3 × 2 mL) and dried *in vacuo* to give [Re(N)Cl(P^H=N=P^{tBu})]^{OTf} (**23^{OTf}**) (5.1 mg, 6.9 µmol, 82 %).

^{1}H-NMR (500 MHz, CD_2Cl_2, 25 °C): δ (ppm) = 9.35 (d, $^3J_{HP} = 20.9$ Hz, 1H, N=C*H*–CH$_2$), 8.02 (doublet of doublets (dd), $^3J_{HP} = 27.8$ Hz, $^3J_{HH} = 6.6$ Hz, 1H, N–C*H*=CH), 6.66 (d, $^3J_{HH} = 6.7$ Hz, 1H, P–C*H*), 4.40 (dd, $^2J_{HH} = 21.2$ Hz, $^2J_{HP} = 7.4$ Hz, 1H, P–C*H*–CH), 3.79 (dd, $^2J_{HH} = 21.2$ Hz, $^2J_{HP} = 7.7$ Hz, 1H, P–CH_2–CH), 1.60 (d, $^3J_{HP} = 15.6$ Hz, 9H, C(CH_3)$_3$), 1.57 (d, $^3J_{HP} = 15.9$ Hz, 9H, C(CH_3)$_3$), 1.32 (d, $^3J_{HP} = 14.7$ Hz, 9H, C(CH_3)$_3$), 1.28 (d, $^3J_{HP} = 14.8$ Hz, 9H, C(CH_3)$_3$). **^{13}C{^{1}H}-NMR** (125.8 MHz, CD_2Cl_2, 25 °C): δ (ppm) = 201.2 (s, N=*C*H–CH$_2$), 163.9 (d, $^2J_{CP} = 3.8$ Hz, N–*C*H=CH), 127.9 (d, $^1J_{CP} = 31.9$ Hz, *C*H–P), 41.0 (d, $^1J_{CP} = 22.5$ Hz, *C*H$_2$–P), 38.2 (dd, $^1J_{CP} = 18.7$ Hz, $^3J_{CP} = 3.7$ Hz, *C*(CH$_3$)$_3$)$_3$), 37.8 (dd, $^1J_{CP} = 15.5$ Hz, $^3J_{CP} = 3.9$ Hz, *C*(CH$_3$)$_3$)$_3$), 36.3 (d, $^1J_{CP} = 15.1$ Hz, *C*(CH$_3$)$_3$)$_3$), 36.0 (d, $^1J_{CP} = 18.1$ Hz, *C*(CH$_3$)$_3$), 29.1 (d, $^2J_{CP} = 3.3$ Hz,

C(CH_3)$_3$), 29.0 (d, $^2J_{CP}$ = 3.9 Hz, C(CH_3)$_3$), 28.7 (d, $^2J_{CP}$ = 4.1 Hz, C(CH_3)$_3$), 28.6 (d, $^2J_{CP}$ = 3.5 Hz, C(CH_3)$_3$). **^{31}P{^{1}H}-NMR** (121.5 MHz, CD_2Cl_2, 25 °C): δ (ppm) = 73.0 (d, $^2J_{PP}$ = 148.1 Hz), 70.0 (d, $^2J_{PP}$ = 148.1 Hz).

2.2.8 [Re(NMe)Cl(P=N=P$^{t\text{Bu}}$)]$^{\text{OTf}}$ (**24$^{\text{OTf}}$**)

Compound [Re(N)Cl(P=N=P$^{t\text{Bu}}$)] (**22**) (25.0 mg, 44.2 µmol, 1.0 eq.) and MeOTf (5.26 µL, 46.4 µmol, 1.1 eq.) were dissolved in chlorobenzene and heated to 80 °C for 12 h. After removal of all volatiles *in vacuo*, the product was washed with Et_2O and [Re(NMe)Cl(P=N=P$^{t\text{Bu}}$)]$^{\text{OTf}}$ (**24$^{\text{OTf}}$**) was obtained as brown solid (25.7 mg, 34.0 µmol, 80.5 %).

^{1}H-NMR (500 MHz, CD_2Cl_2, 25 °C): δ (ppm) = 7.99 (A_9B_9CDXX'D'C'B'$_9$A'$_9$, $N = |^3J_{DX} + ^5J_{DX'}|$ = 18.2 Hz, $^3J_{DC}$ = 6.5 Hz, 2H, NC*H*), 5.34 (m, superimposed with solvent, 2H, PC*H*), 2.70 (s_{br}, 3H, N–CH_3), 1.49 (A_9B_9CDXX'D'C'B'$_9$A'$_9$, $^3J_{AX}$ = 7.8 Hz, 18H, C(CH_3)$_3$), 1.29 (A_9B_9CDXX'D'C'B'$_9$A'$_9$, $^3J_{AX}$ = 6.6 Hz, 18H, C(CH_3)$_3$). **^{13}C{^{1}H}-NMR** (125.8 MHz, CD_2Cl_2, 25 °C): δ (ppm) = 172.9 (vt, $^2J_{CP}$ = 5.3 Hz, 2C, NCH), 99.1 (AXX'A', $^1J_{CP}$ = 22.6 Hz, $^3J_{CP}$ = 20.4 Hz, PCH), 61.9 (s, NCH_3), 40.2 (vt, $^1J_{CP}$ = 9.7 Hz, *C*(CH_3)$_3$), 39.6 (vt, $^1J_{CP}$ = 11.6 Hz, *C*(CH_3)$_3$), 30.2 (m, C(*C*H_3)$_3$), 28.9 (m, C(*C*H_3)$_3$). **^{31}P{^{1}H}-NMR** (202.4 MHz, CD_2Cl_2, 25 °C): δ (ppm) = 88.8 (s). **Elemental anal.** Calc. for $C_{22}H_{43}ClF_3N_2O_3P_2ReS$: C, 34.94; H, 5.71; N, 3.70. Found: C, 35.18; H, 5.71; N, 3.49. **Mass spect.** (LIFDI), m/z (%) = 607.2 (100).

2.2.9 [Re(N=CH$_2$)Cl(P=N=P$^{t\text{Bu}}$)] (**25**)

[Re(NMe)Cl(P=N=P$^{t\text{Bu}}$)]$^{\text{OTf}}$ (**24$^{\text{OTf}}$**) (20.0 mg, 26.5 µmol, 1.0 eq) was mixed with NEt_3 (5.5 µmL, 39.7 µmol, 1.5 eq) in THF (5 mL) and heated to 60 °C over 16 h. After evaporation of the solvent, the product was extracted with pentane and [Re(N=CH$_2$)Cl(P=N=P$^{t\text{Bu}}$)] (**25**) could be obtained as dark brown solid (9.1 mg, 15.0 µmol, 56.7 %).

^{1}H-NMR (500 MHz, C_6D_6, 25 °C): δ (ppm) = 7.16 (m, superimposed with solvent, 2H, NC*H*), 4.71 (A_9B_9CDXX'D'C'B'$_9$A'$_9$, $^3J_{CD}$ = 6.4 Hz, $N = |^2J_{CX} + ^4J_{CX'}|$ = 1.5 Hz, 2H, PC*H*), 1.74 (s_{br}, 1H, N=C*H*H), 1.63 (s_{br}, 1H, N=CH*H*), 1.30 (A_9B_9CDXX'D'C'B'$_9$A'$_9$, $^3J_{AX}$ = 6.8 Hz, 18H, C(CH_3)$_3$), 1.26 (s_{br}, 18H, C(CH_3)$_3$). **^{13}C{^{1}H}-NMR** (125.8 MHz, C_6D_6, 25 °C): δ (ppm) = 170.3 (vt, $^2J_{CP}$ = 7.7 Hz, NCH), 141.7 (t, $^3J_{CP}$ = 2.6 Hz, N=*C*H_2), 102.6 (vt, $^1J_{CP}$ = 17.0 Hz, PCH), 38.6 (vt, $^1J_{CP}$ = 10.0 Hz, *C*(CH_3)$_3$), 36.9 (vt, $^1J_{CP}$ = 8.6 Hz, *C*(CH_3)$_3$), 30.6 (m, C(*C*H_3)$_3$), 28.9 (m, C(*C*H_3)$_3$). **^{31}P{^{1}H}-NMR** (202.4 MHz, C_6D_6, 25 °C): δ (ppm) = 38.9 (s). **Mass spect.** (LIFDI), m/z (%) = 606.1 (100).

2.2.10 [Re(N)Cl(P=N=P$^{t\mathrm{Bu}}$)]$^{\mathrm{SbF_6}}$ (**26$^{\mathbf{SbF_6}}$**)

[Re(N)Cl(P=N=P$^{t\mathrm{Bu}}$)] (**22**) (5.0 mg, 8.4 µmol, 1.0 eq) and Ag($\mathrm{SbF_6}$) were dissolved in THF (1 mL) and stirred, upon which the solution turned red immediately. After stirring for 1.5 h the solution was filtered and the solvent was removed *in vacuo*. Despite the title compound [Re(N)Cl(P=N=P$^{t\mathrm{Bu}}$)]$^{\mathbf{SbF_6}}$ (**26$^{\mathbf{SbF_6}}$**) the product always contained **23$^{\mathbf{SbF_6}}$** as a side product.

^{1}H-NMR (300 MHz, $\mathrm{CD_2Cl_2}$, 25 °C): δ (ppm) = 7 - 2 ($\mathrm{s_{br}}$).

2.2.11 [Re(bipy)Cl(PNP$^{t\mathrm{Bu}}$)]$^{\mathrm{BPh_4}}$ (**27$^{\mathbf{BPh_4}}$**)

[$\mathrm{ReCl_2}$(PNP$^{t\mathrm{Bu}}$)] (**XIX**) (15.0 mg, 24.3 µmol, 1.0 eq), 2,2'-bipyridine (4.9 mg, 31.6 µmol, 1.3 eq) and $\mathrm{NaBPh_4}$ (10.8 mg. 31.6 µmol, 1.3 eq) are mixed in THF (dried over Na/K, 3 mL) and the reaction mixture is heated to 60 °C and stirred overnight. Afterwards the solvent is removed *in vacuo* and the product is extraced with DCM. Recrystallization from DCM/$\mathrm{Et_2O}$ at -40 °C afforded the target complex **27$^{\mathbf{BPh_4}}$** as spectroscopically clean, deep red solid (23.3 mg, 22.3 µmol, 91 % yield).

^{1}H-NMR (500 MHz, $\mathrm{CD_2Cl_2}$, 25 °C): δ (ppm) = 9.99 (d, $^3J_{\mathrm{HH}}$ = 6.2 Hz, 1H, 3-CH_{bipy}), 8.26 (d, $^3J_{\mathrm{HH}}$ = 7.9 Hz, 1H, 6-CH_{bipy}), 8.20 (d, $^3J_{\mathrm{HH}}$ = 8.3 Hz, 1H, 6'-CH_{bipy}), 7.51 (dd, $^3J_{\mathrm{HH}}$ = 8.3, 7.3 Hz, 1H, 5-CH_{bipy}), 7.37 - 7.33 (m, superimposed, 9H, C$H_{\mathrm{Ph},ortho}$, 4-CH_{bipy}), 7.03 (t, $^3J_{\mathrm{HH}}$ = 7.4 Hz, 8H, C$H_{\mathrm{Ph},meta}$), 6.91-6.84 (m, superimposed, 5H, C$H_{\mathrm{Ph},para}$, 4'-CH_{bipy}), 6.77 (dd, $^3J_{\mathrm{HH}}$ = 8.4, 7.2 Hz, 1H, 5'-CH_{bipy}), 6.59 (d, $^3J_{\mathrm{HH}}$ = 6.3 Hz, 1H, 3'-CH_{bipy}), 4.67-4.55 (m, 2H, N−CHH), 4.09-3.99 (m, 2H, N−CHH), 2.22-2.13 (m, 2H, P−CHH), 1.54-1.45 (m, 2H, P−CHH), 1.38 (spinsys, 18H, C(CH_3)$_3$), 0.36 (spinsys, 18H, C(CH_3)$_3$). **^{13}C{^{1}H}-NMR** (125.8 MHz, $\mathrm{CD_2Cl_2}$, 25 °C): δ (ppm) = 164.6 ($^1J_{\mathrm{BC}}$ = 49.3 Hz, 4C, B−C$_{ipso}$), 153.0 (s, 2'-$\mathrm{C_{bipy}}$), 150.5 (s, 2-$\mathrm{C_{bipy}}$), 149.8 (s, 3-$\mathrm{C_{bipy}}$), 145.0 (s, 3'-$\mathrm{C_{bipy}}$), 138.6 (s, 5-$\mathrm{C_{bipy}}$), 136.7 (s, 5'-$\mathrm{C_{bipy}}$), 136.5 (s, $\mathrm{C_{Ph,\ ortho}}$), 126.2 (s, $\mathrm{C_{Ph,\ meta}}$), 124.1 (s, 4'-$\mathrm{C_{bipy}}$), 123.4 (s, 4-$\mathrm{C_{bipy}}$), 122.8 (s, 6'-$\mathrm{C_{bipy}}$), 122.3 (s, $\mathrm{C_{Ph,\ para}}$), 121.9 (s, 6-$\mathrm{C_{bipy}}$), 86.9 (vt, $^2J_{\mathrm{CP}}$ = 3.9 Hz, N−CH$_2$), 42.5 (vt, $^1J_{\mathrm{CP}}$ = 8.7 Hz, C(CH$_3$)$_3$), 41.4 (vt, $^1J_{\mathrm{CP}}$ = 7.4 Hz, C(CH$_3$)$_3$), 32.1 (m, C(CH_3)$_3$), 29.6 (m, C(CH_3)$_3$), 28.3 (vt, $^1J_{\mathrm{CP}}$ = 7.7 Hz, P−CH$_2$). **^{31}P{^{1}H}-NMR** (162.0 MHz, $\mathrm{CD_2Cl_2}$, 25 °C): δ (ppm) = 2.1 (s). **Mass spect.** (LIFDI), m/z (%) = 738.2 (100).

2.3 Rhenium compounds based on the PNP^{iPr} ligand

2.3.1 [ReCl$_3$(HPNP^{iPr})] (**29**)

[ReCl$_3$(PPh$_3$)$_2$(NCMe)] (600 mg, 699 µmol, 1.00 eq) and HPNP^{iPr} (224 mg, 734 µmol, 1.05 eq) are suspended in toluene (dried over Na/K, 15 mL), stirred vigorously and heated to 90 °C overnight. After 16 h, the solution is cooled to −50 °C and filtered. The residue is washed with Et$_2$O until the washing solution is colorless and then extracted with CH$_2$Cl$_2$. The solvent is removed *in vacuo* and [ReCl$_3$(HPNP^{iPr})] (**29**) is obtained as a yellow powder (292 mg, 488 µmol, 70 %).

^{1}H-NMR (500 MHz, CD$_2$Cl$_2$, 25 °C): δ (ppm) = 154.45 (s,N*H*), 9.66 (m, 6H, CH(C*H*$_3$)$_2$), 9.59 (m, 6H, CH(C*H*$_3$)$_2$), 9.32 (m, 2H, C*H*(CH$_3$)$_2$), 8.76 (m, 6H, CH(C*H*$_3$)$_2$), 8.37 (m, 6H, CH(C*H*$_3$)$_2$), 8.31 (m, 2H, P-C*H*H-CH$_2$), 5.46 (m, 2H, C*H*(CH$_3$)$_2$), 0.54 (m, 2H, P-CH*H*-CH$_2$), −5.10 (m, 2H, N-C*H*H-CH$_2$), −10.44 (m, 2H, N-CH*H*-CH$_2$). **^{13}C{^{1}H}-NMR** (125.7 MHz, CD$_2$Cl$_2$, 25 °C): δ (ppm) = 160.9 (s, N-*C*H$_2$), 142.1 (s, *C*HMe$_2$), 132.1 (s, *C*HMe$_2$), 68.6 (s, P-*C*H2), 22.5 (s, *C*H$_3$), 22.2 (s, *C*H$_3$), 18.4 (s, *C*H$_3$), 16.8 (s, *C*H$_3$). **^{15}N{^{1}H}−NMR** (50.7 MHz, CD$_2$Cl$_2$, 25 °C): δ (ppm) = −1226.5 (s, *N*H). **^{31}P{^{1}H}-NMR** (202.6 MHz, CD$_2$Cl$_2$, 25 °C): δ (ppm) = 4−1525.9 (s). **CV**: $E_{1/2}$ vs Fc/Fc$^+$ (V) = −1.84 (Re(II/III)), −0.24 (Re(III/IV)). **Elemental anal.** Calc. for C$_{16}$H$_{37}$Cl$_3$NP$_2$Re (597.10): C, 32.14; H, 6.24; N, 2.34. Found: C, 32.16; H, 6.18; N, 2.37. **ATR-IR**: $\tilde{\nu}$ (cm^{-1}) = 3506.4 (br, electronic absorption), 3181.0 (ν_{N-H}. **Mass spect.** (LIFDI), m/z (%) = 596.9 (100).

*H/D exchange to synthesize **29-d***:
[ReCl$_3$(HPNP^{iPr})] (**29**) (6.0 mg, 10.0 µmol, 1.0 eq) is suspended in a DCM/D$_2$O mixture (0.4 mL / 0.1 mL) and stirred overnight. Afterwards the solvent is removed *in vacuo* and the spectroscopically clean product [ReCl$_3$(DPNP^{iPr})] (**29-*d***) is measured in CD$_2$Cl$_2$. The NMR spectra show basically identical signals to those of **29**. However, the signal corresponding to the NH proton is largely gone (∼ 2 % remaining) and the signals at $\delta_{^1H}$ = −5.10 and −10.44 ppm exhibit different coupling patterns.

^{2}H-NMR (46.1 MHz, CD$_2$Cl$_2$, 25 °C): δ (ppm) = 152.6 (s, N*D*). **ATR-IR**: $\tilde{\nu}$ (cm^{-1}) = 3506.4 (br, electronic absorption), 2362.9 (ν_{N-D}).

2.3.2 [ReCl$_3$(PNP^{iPr})] (**31**)

[ReCl$_3$(HPNP^{iPr})] (**29**) (30.0 mg, 50.2 µmol, 1.0 eq) and TTBP (14.4 mg, 55.2 µmol, 1.1 eq) are suspended in benzene (5 mL) and stirred at RT for 1.5 h, resulting in a deep red solution. All volatiles are removed *in vacuo*. The crude product is washed with pentane and

extracted with benzene. Lyophilization gives [$ReCl_3(PNP^{iPr})$] (**31**) as a red powder (19.0 mg, 31.8 µmol, 63 %).

^{1}H-NMR (400 MHz, CD_2Cl_2, 25 °C): δ (ppm) = 21.86 (b, 4H), 19.20 (br, 12H), 16.00 (br, 12H), 1.43 (br, 4H). **CV**: $E_{1/2}$ vs Fc/Fc^+ (V) = −1.16 ($Re(III/IV)$). **Elemental anal.** Calcd. for $C_{16}H_{36}Cl_3NP_2Re$ (596.98): C, 32.19; H, 6.07; N, 2.35. Found: C, 32.55; H, 6.04; N, 2.18.

2.3.3 [$ReCl_2$(thf)(PNP^{iPr})] (**32**) and [$ReCl_2(PNP^{iPr})$] (**30**)

In a typical experiment, [$ReCl_3(PNP^{iPr})$] (**31**) (10 mg, 16.8 µmol, 1.0 eq) and NaHg (1.0 M, 250 mg, 18.4 µmol, 1.1 eq) are stirred in either THF (to form **32**) or in toluene (to form **30**) (0.5 mL) for 4 h at RT. [$ReCl_2$(thf)(PNP^{iPr})] (**32**) becomes a deep orange solution while [$ReCl_2(PNP^{iPr})$] (**30**) becomes deep violet. Formed NaCl and remaining Hg is removed by filtration. Both complexes could not be isolated to instability towards vacuum and were thus used *in situ*.

In THF-d_8 (**32**):
^{1}H-NMR (400 MHz, THF-d_8, 25 °C): δ (ppm) = 3.73-3.60 (m, 4H, N−CH_2), 2.75-2.60 (m, 4HC*H*(CH_3)$_2$), 1.84-1.75 (m, 4H, P−CH_2), 1.39-1.27 (m, 12H, CH(C*H*$_3$)$_2$), 1.27-1.18 (m, 12H, CH(C*H*$_3$)$_2$). **^{31}P{^{1}H}-NMR** (162.0 MHz, THF-d_8, 25 °C): δ (ppm) = −14.5 (s).

In toluene-d_8 (**30**):
^{1}H-NMR (400 MHz, toluene-d_8, 25 °C): δ (ppm) = 2.97-2.86 (m, 4H, N−CH_2), 2.64-2.50 (m, 4HC*H*(CH_3)$_2$), 1.59-1.48 (m, 4H, P−CH_2), 1.35-1.17 (m, 24H, CH(C*H*$_3$)$_2$). **^{1}H{^{31}P}-NMR** (400 MHz, toluene-d_8, 25 °C): δ (ppm) = 2.97-2.86 (m, 4H, N−CH_2), 2.57 (heptet (hept), $^3J_{HH}$ = 7.3 Hz, 1.59-1.48 (m, 4H, P−CH_2), 1.28 (d, $^3J_{HH}$ = 7.2 Hz, 12H, CH(C*H*$_3$)$_2$), 1.23 (d, $^3J_{HH}$ = 7.2 Hz, 12H, CH(C*H*$_3$)$_2$). **^{13}C{^{1}H}-NMR** (100.6 MHz, toluene−d_8, 25 °C): δ (ppm) = 84.8 (vt, $^2J_{CP}$ = 5.4 Hz, 2C, N−*C*H_2), 33.5 (vt, $^1J_{CP}$ = 8.5 Hz, 2C, P−*C*H_2), 30.2 (vt, $^1J_{CP}$ = 11.1 Hz, 2C, *C*H(CH_3)$_2$), 19.0 (s, 4C, C(*C*H_3)$_2$), 18.3 (s, 4C, C(*C*H_3)$_2$). **^{31}P{^{1}H}-NMR** (162.0 MHz, CD_2Cl_2, 25 °C): δ (ppm) = 10.0 (s). **Mass spect.** (LIFDI), m/z (%) = 561.1 (100). **Elemental anal.** Calcd. for $C_{16}H_{36}Cl_2NP_2Re$ (561.5): C, 34.22; H, 6.46; N, 2.49. Found: C, 33,63; H, 5.97; N, 2.25. NMR spectroscopy revealed the formerly spectroscopically clean sample to be partially decomposed after drying it for the elemental analysis. Since the analysis as well as the initial spectra were fine, it is assumed that **30** is present exclusively and cleanly in the *in situ* prepared solution but decomposes partially when the solvent is removed.

2.3.4 [{ReCl$_{2,cis}$(PNP^{iPr})}(μ-N$_2$){ReCl$_{2,trans}$(PNP^{iPr})}] (**33a**) and [{ReCl$_{2,cis}$(PNP^{iPr})(μ-N$_2$)ReCl$_{2,cis}$(PNP^{iPr})}] (**33b**)

Through a freshly prepared solution of [ReCl$_2$(PNP^{iPr})] (**30**), N$_2$ gas is passed leading to an immediate color change from violet to deep brown. No isolation of the formed complexes was possible, but they could be identified by NMR spectroscopy at −30 °C (see Section 3.2.2 for a discussion).

[{ReCl$_{2,cis}$(PNP^{iPr})}(μ-N$_2$){ReCl$_{2,trans}$(PNP^{iPr})}] (**33a**, composed of *trans*-Cl fragment **B** and *cis*-Cl fragment **C**):
^{1}H{^{31}P}-NMR (500 MHz, toluene-d_8, −30 °C): δ (ppm) = 2.72 (hept, ^{3}J$_{HH}$ = 7.1 Hz, 2H, **B**, C*H*(CH$_3$)$_2$), 2.65 (hept, ^{3}J$_{HH}$ = 7.2 Hz, 2H, **C**, C*H*(CH$_3$)$_2$), 2.56 (hept, ^{3}J$_{HH}$ = 7.2 Hz, 2H, **B**, C*H*(CH$_3$)$_2$), 2.40 (hept, ^{3}J$_{HH}$ = 7.2 Hz, 2H, **C**, C*H*(CH$_3$)$_2$), 1.85 (d, $^3J_{HH}$ = 7.5 Hz, **C**, CH(C*H*$_3$)(CH$_3$)), 1.67 (d, $^3J_{HH}$ = 7.3 Hz, **C**, CH(C*H*$_3$)(CH$_3$)), 1.52 (d, $^3J_{HH}$ = 7.2 Hz, **B**, CH(C*H*$_3$)(CH$_3$)), 1.36 (d, $^3J_{HH}$ = 7.3 Hz, **C**, CH(C*H*$_3$)(CH$_3$)), 1.31 (d, $^3J_{HH}$ = 7.1 Hz, **B**, CH(C*H*$_3$)(CH$_3$)), 1.23 (d, $^3J_{HH}$ = 7.0 Hz, **C**, CH(C*H*$_3$)(CH$_3$)), 1.08 (d, $^3J_{HH}$ = 7.1 Hz, **B**, CH(C*H*$_3$)(CH$_3$)), 1.05 (d, $^3J_{HH}$ = 7.3 Hz, **B**, CH(C*H*$_3$)(CH$_3$)). **^{15}N{^{1}H}−NMR** (50.7 MHz, toluene-d_8, −30 °C): δ (ppm) = −4.1 (dt, $^1J_{NN}$ = 5.6 Hz, $^2J_{NP}$ = 2.6 Hz, Re$_{\mathbf{C}}$−N), −18.8 (d, $^1J_{NN}$ = 5.6 Hz, Re$_{\mathbf{B}}$−N), **^{31}P{^{1}H}-NMR** (202.5 MHz, toluene-d_8, −30 °C): δ (ppm) = −10.8 (d, $^2J_{PP}$ = 253.0 Hz, P$_{\mathbf{B}}$), −14.1 (d, $^2J_{PP}$ = 253.0 Hz, P$_{\mathbf{B}}$), −16.4 (s, 2P, P$_{\mathbf{C}}$). Under a ^{15}N{^{1}H} atmosphere, the singlet at -16.4 ppm is split into a doublet with $^2J_{PN}$ = 2.7 Hz.

[{ReCl$_{2,cis}$(PNP^{iPr})}(μ-N$_2$){ReCl$_{2,cis}$(PNP^{iPr})}] (**33b**, composed of two *cis*-Cl fragments **A**):
^{15}N{^{1}H}−NMR (50.7 MHz, toluene-d_8, −30 °C): δ (ppm) = −12.7 (s), **^{31}P{^{1}H}-NMR** (202.5 MHz, toluene-d_8, −30 °C): δ (ppm) = 1.3 (d, $^2J_{PP}$ = 276.2 Hz), −1.2 (d, $^2J_{PP}$ = 276.2 Hz).

2.3.5 [Re(N)Cl(PNP^{iPr})] (**34**)

[Re(N)Cl$_2$(HPNP^{iPr})] (**37**) (7.5 mg, 12.9 μmol, 1.0 eq) and KO^{t}Bu (1.4 mg, 12.9 μmol, 1.0 eq) are mixed in benzene (1 mL) and stirred overnight. All volatiles are removed *in vacuo* and the product is extracted with Et$_2$O. After recrystallization from a minimal amount of pentane at −80 °C, [Re(N)Cl(PNP^{iPr})] (**34**) can be isolated as orange solid.

^{1}H-NMR (500 MHz, C$_6$D$_6$, 25 °C): δ (ppm) = 3.51-3.39 (m, 2H, N−C*H*H), 3.20-3.12 (m, 2H, N−CH*H*), 2.70-2.61 (m, 2H, C*H*(CH$_3$)$_2$), 1.90-1.80 (m, 2H, C*H*(CH$_3$)$_2$), 1.65-1.55 (m, 2H, P−C*H*H), 1.37-1.30 (m, 6H, CH(C*H*$_3$)(CH$_3$)), 1.29-1.20 (m, 2H, P−CH*H*), 1.19-1.13 (m, 6H, CH(C*H*$_3$)(CH$_3$)), 1.04-0.98 (m, 6H, CH(C*H*$_3$)(CH$_3$)), 0.90-0.84 (m, 6H,

CH(CH_3)(CH$_3$)). **^{1}H{^{31}P}-NMR** (500 MHz, C_6D_6, 25 °C): δ (ppm) = 3.45 (ddd, J_{HH} = 10.9, 7.9, 2.8 Hz, 2H, N−C*H*H), 3.16 (ddd, J_{HH} = 11.2, 9.4, 6.3 Hz, 2H, N−CH*H*), 2.66 (hept, $^3J_{HH}$ = 7.1 Hz, 2H, C*H*(CH$_3$)$_2$), 1.85 (hept, $^3J_{HH}$ = 6.9 Hz, 2H, C*H*(CH$_3$)$_2$), 1.60 (ddd, J_{HH} = 14.3, 9.4, 7.9 Hz, 2H, P−C*H*H), 1.33 (d, $^3J_{HH}$ = 6.9 Hz, 6H, CH(CH_3)(CH$_3$)), 1.23 (ddd, J_{HH} = 14.3, 6.3, 2.7 Hz, 2H, P−C*H*H), 1.16 (d, $^3J_{HH}$ = 6.9 Hz, 6H, CH(CH_3)(CH$_3$)), 1.01 (d, $^3J_{HH}$ = 7.1 Hz, 6H, CH(CH_3)(CH$_3$)), 0.87 (d, $^3J_{HH}$ = 7.2 Hz, 6H, CH(CH_3)(CH$_3$)). **^{13}C{^{1}H}-NMR** (125.8 MHz, C_6D_6, 25 °C): δ (ppm) = 70.4 (vt, $^2J_{CP}$ = 4.3 Hz, 2C, N−*C*H$_2$), 25.1 (vt, $^1J_{CP}$ = 12.1 Hz, 2C, *C*H(CH$_3$)$_2$), 23.8 (vt, $^1J_{CP}$ = 12.3 Hz, 2C, P−*C*H$_2$), 21.8 (vt, $^1J_{CP}$ = 13.6 Hz, 2C, *C*H(CH$_3$)$_2$), 18.7 (s, 2C, CH(*C*H$_3$)(CH$_3$)), 18.4 (s, 2C, CH(*C*H$_3$)(CH$_3$)), 18.0 (s, 2C, CH(*C*H$_3$)(CH$_3$)), 16.6 (s, 2C, CH(*C*H$_3$)(CH$_3$)). **^{31}P{^{1}H}-NMR** (202.5 MHz, C_6D_6, 25 °C): δ (ppm) = 74.7 (s). **Mass spect.** (LIFDI), m/z (%) = 540.6 (100).

2.3.6 [ReCl(N$_2$)$_2$(HPNP^{iPr})] (**35**)

[ReCl$_3$(HPNP^{iPr})] (**29**) (5.0 mg, 8.4 µmol, 1.0 eq) and NaHg (1.0 M, xx mg, 17.6 µmol, 2.1 eq) mixed in THF (dried over Na/K, 1 mL) under an N_2 atmosphere and stirred for 2 h. The solution always contained at least one side product, the NMR signature of which pointed to a THF double CH activation product comparable to a previous published Ir compound.[228] Separation of this product was not achieved with a practial procedure and only once a rather clean batch of **35** was obtained by several recrystallizations but with overall yields below 15 %.

^{1}H-NMR (400 MHz, C_6D_6, 25 °C): δ (ppm) = 3.08-2.95 (m, 2H, C*H*(CH$_3$)$_2$), 2.89 (m$_{br}$, 1H, N*H*), 2.57-2.43 (m, 2H, XXX), 2.43-2.31 (m, 2H, C*H*(CH$_3$)$_2$), 2.02-1.87 (m, 2H, XXX), 1.75-1.65 (m, 2H, XXX), 1.51-1.40 (m, 6H, CH(CH_3)(CH$_3$)), 1.36-1.21 (m, 12H, superimposed 2 × CH(CH_3)(CH$_3$)), 1.14-1.04 (m, 6H, CH(CH_3)(CH$_3$)). **^{1}H{^{31}P}-NMR** (400 MHz, C_6D_6, 25 °C): δ (ppm) = 3.01 (hept, 2H, $^3J_{HH}$ = 7.3 Hz, C*H*(CH$_3$)$_2$), 2.89 (m$_{br}$, 1H, N*H*), 2.57-2.43 (m, 2H, XXX), 2.38 (hept, 2H, $^3J_{HH}$ = 7.2 Hz, 2H, C*H*(CH$_3$)$_2$), 2.02-1.87 (m, 2H, XXX), 1.75-1.65 (m, 2H, XXX), 1.45 (d, $^3J_{HH}$ = 7.4 Hz, 6H, CH(CH_3)(CH$_3$)), 1.30 (d, $^3J_{HH}$ = 7.1 Hz, 6H, CH(CH_3)(CH$_3$)), 1.26 (d, $^3J_{HH}$ = 7.4 Hz, 6H, CH(CH_3)(CH$_3$)), 1.09 (d, $^3J_{HH}$ = 7.1 Hz, 6H, CH(CH_3)(CH$_3$)). **^{31}P{^{1}H}-NMR** (162.0 MHz, C_6D_6, 25 °C): δ (ppm) = 34.5 (s). **CV**: $E_{1/2}$ vs Fc/Fc$^+$ (V) = −0.23 (Re(I/II)), −3.34 ($E_{p,a}$, irreversible). **ATR-IR**: $\tilde{\nu}$ (cm^{-1}) = 3152.6 ($\nu_{N\text{-}H}$), 2038.8 ($\nu_{N\equiv N}$), 1935.1 ($\nu_{N\equiv N}$). **Mass spect.** (LIFDI), m/z (%) = 583.2 (100).

2.3.7 [(µ-N$_2$){ReCl$_2$(HPNP^{iPr})}$_2$] (**36**)

[ReCl$_3$(HPNP^{iPr})] (**29**) (20.0 mg, 33.5 µmol, 1.0 eq) and Co(Cp*)$_2$ (15.4 mg, 46.8 µmol, 1.4 eq) are placed in a Schlenk tube. Degassed THF (2 mL) is vacuum-transferred to the

tube and the reaction is thawed under N_2 atmosphere in a −60 °C cooling bath. The reaction is stirred, slowly warmed to RT over 3 h and finally stirred at RT for an additional hour. After that, all volatiles are removed *in vacuo* and the product is washed with Et_2O and extracted with toluene. The solution is concentrated *in vacuo*, layered with Et_2O and stored at −80 °C for four days. [(μ-N_2){$ReCl_2$(HPNP^{iPr})}$_2$] (**36**) was isolated as a spectroscopically pure, deep blue powder (10.8 mg, 9.4 μmol, 56.0 %). A $^{15}N_2$-labeled sample was prepared analogously under a $^{15}N_2$ atmosphere.

^{1}H-NMR (500 MHz, THF−d_8, 25 °C): δ (ppm) = 93.23 (t, $^1J_{NH}$ = 11.4 Hz, 2H, N*H*), 6.28 (m, $^3J_{HH}$ = 7.4 Hz, 2H, C*H*Me$_2$), 5.63 (m, $^3J_{HH}$ = 7.4 Hz, 2H, C*H*Me$_2$), 4.28 (d, $^3J_{HP}$ = 13.6 Hz, $^3J_{HH}$ = 7.6 Hz, 6H, CH(CH_3)$_2$), 3.66 (m, $^3J_{HH}$ = 7.6 Hz, 2H, C*H*Me$_2$), 3.57 (m, overlapping with THF−d_8, 6H, CH(CH_3)$_2$), 3.13 (m, $^3J_{HH}$ = 7.3 Hz, 2H, C*H*Me$_2$), 2.88 (dd, $^3J_{HP}$ = 14.2 Hz, $^3J_{HH}$ = 7.6 Hz, 6H, CH(CH_3)$_2$), 2.76 (m, $^3J_{HH}$ = 7.2 Hz, 6H, CH(CH_3)$_2$), 2.75 (m, $^3J_{HH}$ = 7.1 Hz, 6H, CH(CH_3)$_2$), 2.30 (dd, $^3J_{HP}$ = 11.7 Hz, $^3J_{HH}$ = 7.1 Hz, 6H, CH(CH_3)$_2$), 2.14 (dd, $^3J_{HP}$ = 14.7 Hz, $^3J_{HH}$ = 7.6 Hz, 6H, CH(CH_3)$_2$), 1.49 (dd, $^3J_{HP}$ = 14.7 Hz, $^3J_{HH}$ = 7.6 Hz, 6H, CH(CH_3)$_2$), −0.33 (m, 2H, P-C*H*H-CH$_2$), −1.34 (m, 2H, P-C*H*H-CH$_2$), −5.51 (m, 2H, P-CH*H*-CH$_2$), −7.65 (m, 2H, P-CH*H*-CH$_2$), −8.57 (m, 2H, N-C*H*H-CH$_2$), −11.21 (m, 2H, N-CH*H*-CH$_2$), −12.30 (m, 2H, N-C*H*H-CH$_2$), −12.77 (m, 2H, N-CH*H*-CH$_2$). For the assignment of J_{HH} coupling constants, a ^{1}H{^{31}P} spectrum was measured. **^{13}C{^{1}H}-NMR** (125.8 MHz, THF−d_8, 25 °C): δ (ppm) = 162.0 (s, N-*C*H$_2$), 161.6 (s, N-*C*H$_2$), 147.7 (d, $^1J_{CP}$ = 18.9 Hz, *C*HMe$_2$), 136.0 (d, $^1J_{CP}$ = 19.4 Hz, *C*HMe$_2$), 84.0 (d, $^1J_{CP}$ = 19.6 Hz, P-*C*H$_2$), 82.4 (d, $^1J_{CP}$ = 20.1 Hz, P-*C*H$_2$), 65.4 (d, $^1J_{CP}$ = 17.3 Hz, *C*HMe$_2$), 49.7 (d, $^1J_{CP}$ = 17.6 Hz, *C*HMe$_2$), 36.2 (s, *C*H$_3$), 35.5 (s, *C*H$_3$), 21.9 (s, *C*H$_3$), 21.4 (s, *C*H$_3$), 20.9 (s, *C*H$_3$), 20.8 (s, *C*H$_3$), 18.8 (s, *C*H$_3$), 18.5 (s, *C*H$_3$). **^{15}N{^{1}H}−NMR** (50.7 MHz, THF−d_8, 25 °C): δ (ppm) = −999.6 (s, *N*H), −1113.0 (s, Re=N=N=Re). **^{31}P{^{1}H}-NMR** (202.5 MHz, THF−d_8, 25 °C): δ (ppm) = −370.6 (d, $^2J_{PP}$ = 236.9 Hz), −380.4 (d, $^2J_{PP}$ = 237.2 Hz). **CV**: $E_{1/2}$ vs Fc/Fc$^+$ (V) = −1.03 ($Re^{II}Re^{II}/Re^{II}Re^{III}$), −0.37 ($Re^{II}Re^{III}/Re^{III}Re^{III}$). **ATR-IR**: $\tilde{\nu}$ (cm^{-1}) = 3146.4 (ν_{N-H}). **Mass spect.** (LIFDI), m/z (%) = 1152.2 (100, [M]$^+$). **rRaman** (frozen THF solution, cm^{-1}): 1733.3 (**36**) / 1675.2 ($^{15}N_2$-**36**). **UV/Vis** (THF, RT): λ / nm (ϵ / M^{-1} cm^{-1}) = 578 (12293), 336 (38027).

2.3.8 [Re(N)Cl$_2$(HPNP^{iPr})] (**37**)

Route A – from azide as nitrogen source, as published: [$ReCl_3$(HPNP^{iPr})] (**29**) (30.0 mg, 50.2 μmol, 1.0 eq) and [N(PPh_3)$_2$]N_3 (29.1 mg, 50.2 μmol, 1.0 eq) are mixed in THF (6 mL) and stirred at 60 °C for 3 h. After that, the solvent is removed *in vacuo* and the product is extracted with toluene. The solution is concentrated and stored at −70 °C overnight. [Re(N)Cl$_2$(HPNP^{iPr})] (**37**) is obtained as orange crystals by filtration and washed with a minimal amount of cold toluene (24.5 mg, 42.5 μmol, 85 %).

^{1}H-NMR (500 MHz, CD_2Cl_2, 25 °C): δ (ppm) = 4.93 (t, $^{1}J_{NH}$ = 12.5 Hz, 1H, N*H*), 3.64 (m, 2H, N-C*H*H-CH_2), 2.93 (m, $^{3}J_{HH}$ = 7.3 Hz, 2H, C*H*Me_2), 2.71 (m, 2H, N-CH*H*-CH_2), 2.52 (m, $^{3}J_{HH}$ = 6.9 Hz, 2H, C*H*Me_2), 2.32 (m, 2H, P-C*H*H-CH_2), 1.91 (m, 2H, P-CH*H*-CH_2), 1.55 (m, $^{3}J_{HH}$ = 7.4 Hz, 6H, CH(CH_3)$_2$), 1.53 (m, $^{3}J_{HH}$ = 6.9 Hz, 6H, CH(CH_3)$_2$), 1.33 (m, $^{3}J_{HH}$ = 7.1 Hz, 6H, CH(CH_3)$_2$), 1.32 (m, $^{3}J_{HH}$ = 7.2 Hz, 6H, CH(CH_3)$_2$). For the assignment of J_{HH} coupling constants, a $^{1}H\{^{31}P\}$ spectrum was measured. **^{13}C{^{1}H}-NMR** (125.8 MHz, CD_2Cl_2, 25 °C): δ (ppm) = 62.7 (s, N-*C*H_2), 31.4 (AXY, N = $|^{1}J_{AX} + {}^{3}J_{AY}|$ = 24.6 Hz, P-*C*H_2), 27.7 (AXY, N = $|^{1}J_{AX} + {}^{3}J_{AY}|$ = 27.2 Hz, *C*HMe_2), 25.0 (AXY, N = $|^{1}J_{AX} + {}^{3}J_{AY}|$ = 20.2 Hz, *C*HMe_2), 21.3 (s, *C*H_3), 19.2 (s, *C*H_3), 18.3 (s, *C*H_3), 18.0 (s, *C*H_3). **^{15}N{^{1}H}−NMR** (50.7 MHz, CD_2Cl_2, 25 °C): δ (ppm) = −331.7 (s, *N*H); the ^{15}N chemical shift of the nitride ligand was obtained from ^{15}N-**37** obtained on route *B* (see below). **^{31}P{^{1}H}-NMR** (202.5 MHz, CD_2Cl_2, 25 °C): δ (ppm) = 36.1 (s). **CV**: $E_{1/2}$ vs Fc/Fc^{+} (V) = +0.01 (Re^{V}/Re^{VI}). **Elemental anal.** Calc. for $C_{16}H_{37}Cl_2N_2P_2Re$ (576.54): C, 33.33; H, 6.47; N, 4.86. Found: C, 33.27; H, 6.34; N, 4.24. **Mass spect.** (LIFDI), m/z (%) = 576.1 (100, $[M]^{+}$), 540.1 (60, $[M\text{-}Cl]^{+}$). **UV/Vis** (THF, RT): λ / nm (ϵ / M^{-1} cm^{-1}) = ∼484 (∼100), ∼405 (∼180), 325 (1540), 285 (2030), 237 (6194).

Route A – from azide as nitrogen source, improved: $[ReCl_3(HPNP^{iPr})]$ (**29**) (250.0 mg, 418 µmol, 1.0 eq) and NaN_3 (31.3 mg, 481 µmol, 1.15 eq) are mixed in DCM (5 mL) and EtOH (7.5 mL) and stirred at 60 °C for 16 h. The solvent is removed *in vacuo*, the product is washed with Et_2O and extracted with hot benzene (60 °C). $[Re(N)Cl_2(HPNP^{iPr})]$ (**37**) is obtained as orange solid (186 mg, 323 µmol, 77 %).

*Route B – photolysis of **36***: A solution of $[(\mu\text{-}N_2)\{ReCl_2(HPNP^{iPr})\}_2]$ (**36**) (5 mg) in THF (0.5 mL) is irradiated with either a Xe(Hg) lamp equipped with a water filter and a long wave pass filter ($\lambda > 305$ nm) or with a 390 nm LED lamp for 2 h. $[Re(N)Cl_2(HPNP^{iPr})]$ (**37**) is obtained in both cases in 95 % spectroscopic yield relative to an internal standard. Labeled $^{15}N_2$-**36** gives the corresponding ^{15}N nitride complex ^{15}N-**37**, which was used for ^{15}N NMR spectroscopic characterization. Using the Xe(Hg) lamp with a long wave pass filter ($\lambda >$ 420 nm) gave no detectable reaction. With a band gap filter ($\lambda = 337 \pm 10$ nm) very slow formation to minor splitting products were observed over several hours. NMR spectroscopic features as well as the LIFDI mass spectrum are identical with those of **37** obtained from route *A*.

^{15}N{^{1}H}−NMR (50.7 MHz, CD_2Cl_2, 25 °C): δ (ppm) = 383.8 (s, Re≡*N*).

2.3.9 $Re(NH)Cl_2(HPNP^{iPr})]^{OTf}$ (**38^{OTf}**)

$[Re(N)Cl_2(HPNP^{iPr})]$ (**37**) (20.0 mg, 34.7 µmol, 1.0 eq) is supsended in toluene and HOTf (3.65 µL, 6.3 mg, 41.6 µmol, 1.2 eq) is added with an Eppendorf pipette. The solution is

stirred for 16 h at RT. Afterwards all volatiles are removed *in vacuo*, the product is extracted with DCM, concentrated, layered with Et_2O and stored at −40 °C overnight. After filtration and removal of residual solvent, [Re(NH)Cl_2(HPNP^{iPr})]^{OTf}] (**38^{OTf}**) is obtained as analytically pure complex. However, due to the broad nature of the peaks, judging the spectroscopic purity of the complex is tricky. Additionally the linewidth of the peaks prevented measurement of a ^{1}H-^{1}H correlation spectroscopy (COSY) or a ^{1}H-^{13}C HMBC, therefore some peaks are assigned based on empirism (i.e. by comparsion with other spectra).

^{1}H-NMR (500 MHz, CD_2Cl_2, −35 °C): δ (ppm) = 14.25 (br, 1H, Re≡N−*H*), 4.96 (br, 1H, N_{PNP}−*H*), 3.98-3.80 (br, 2H, N−*H*H), 2.98-2.87 (br, 2H, N−H*H*), 2.87-2.78 (br, 2H, C*H*$(CH_3)_2$), 2.65-2.55 (br, 2H, C*H*$(CH_3)_2$), 2.55-2.45 (br, 2H, P−*H*H), 2.08-1.93 (br, 2H, P−*H*H), 1.56-1.48 (br, 6H, CH(CH_3)(C*H*$_3$)), 1.47-1.40 (br, 6H, CH(C*H*$_3$)(CH_3)), 1.40-1.33 (br, 6H, CH(CH_3)(C*H*$_3$)), 1.27-1.20 (br, 6H, CH(C*H*$_3$)(CH_3)). **^{13}C{^{1}H}-NMR** (125.8 MHz, CD_2Cl_2, −35 °C): δ (ppm) = 63.3 (br, N−*C*H_2), 30.9 (br, P−*C*H_2), 26.9 (vt, ABB'A', N = $|^1J_{AB}+{}^3J_{AB'}|$ = 28.9 Hz, *C*HMe_2), 25.2 (vt, ABB'A', N = $|^1J_{AB}+{}^3J_{AB'}|$ = 19.7 Hz, *C*HMe_2), 20.8 (br, CH(*C*H$_3$)(CH_3)), 17.9 (br, CH(CH_3)(*C*H$_3$)), 17.7 (br, CH(CH_3)(*C*H$_3$)), 17.5 (br, CH(*C*H$_3$)(CH_3)). **^{15}N{^{1}H}−NMR** (50.7 MHz, CD_2Cl_2, −35 °C): δ (ppm) = 18.1 (Re≡*N*−H), −329.8 (*N_{PNP}*−*H*). **^{31}P{^{1}H}-NMR** (202.5 MHz, CD_2Cl_2, −35 °C): δ (ppm) = 30.2 (br). **Elemental anal.** Calc. for $C_{17}H_{38}Cl_2F_3N_2O_3P_2ReS$ (726.61): C, 28.10; H, 5.27; N, 3.86. Found: C, 27.68; H, 5.03; N, 3.77.

2.3.10 [Re(NBAr$^F_{18}$)Cl_2(HPNP^{iPr})] (**39**)

[Re(N)Cl_2(HPNP^{iPr})] (**37**) (5.0 mg, 8.7 µmol, 1.0 eq) and tris{3,5-bis(trifluoromethyl)phenyl} borane (BAr$^F_{18}$) (5.6 mg, 8.7 µmol, 1.0 eq) are mixed in DCM and stirred for 5 min, during which the color of the solution changes to light blue. The solvent is removed *in vacuo*, the product is washed with pentane, extracted with Et_2O and dried under reduced pressure. *cis*-[Re(NBAr$^F_{18}$)Cl_2(HPNP^{iPr})] (**cis-39**) is obtained, which slowly converts into *trans*-[Re(NBAr$^F_{18}$)Cl_2(HPNP^{iPr})] (**trans-39**) overnight in solution.

cis-[Re(NBAr$^F_{18}$)Cl_2(HPNP^{iPr})] (**cis-39**):
^{1}H-NMR (400 MHz, CD_2Cl_2, 25 °C): δ (ppm) = 8.00 (s, 6H, C_{ortho}H), 7.68 (s, 3H, C_{para}H), 4.98 (br, 1H, N*H*), 3.42-3.34 (m, 2H, N−C*H*H), 2.95 (m, $^3J_{HH}$ = 7.4 Hz, 2H, C*H*Me_2), 2.38-2.27 (m, 2H, P−CH*H*), 2.11 (m, $^3J_{HH}$ = 7.2 Hz, 2H, C*H*Me_2), 2.05-1.93 (m, 2H, N−CH*H*), 1.93-1.81 (m, 2H, P−C*H*H), 1.60 (m, $^3J_{HH}$ = 7.4 Hz, 6H, CH(C*H*$_3$)(CH_3)), 1.34 (m, $^3J_{HH}$ = 7.4 Hz, 6H, CH(C*H*$_3$)(CH_3)), 1.09 (m, $^3J_{HH}$ = 7.2 Hz, 6H, CH(C*H*$_3$)(CH_3)), 0.96 (m, $^3J_{HH}$ = 7.3 Hz, 6H, CH(C*H*$_3$)(CH_3)). **^{31}P{^{1}H}-NMR** (162.0 MHz, CD_2Cl_2, 25 °C): δ (ppm) = 23.9 (s).

trans-[Re(NBAr$^{F}_{18}$)Cl$_2$(HPNP^{iPr})] (**trans-39**):
^{1}H-NMR (400 MHz, CD_2Cl_2, 25 °C): δ (ppm) = 7.86 (s, 6H, $C_{ortho}H$), 7.68 (s, 3H, $C_{para}H$), 3.03-2.96 (m, 2H, N−C*H*H), 2.96 (m, $^3J_{HH}$ = 7.3 Hz, 2H, C*H*Me$_2$), 2.84 (m, $^3J_{HH}$ = 7.3 Hz, 2H, C*H*Me$_2$), 2.56-2.51 (m, 2H, N−CH*H*), 2.51 (br, 1H, N*H*), 2.37-2.30 (m, 2H, P−CH*H*), 1.93-1.80 (m, 2H, P−C*H*H), 1.29 (m, $^3J_{HH}$ = 7.3 Hz, 6H, CH(CH_3)(CH$_3$)), 1.16 (m, $^3J_{HH}$ = 7.1 Hz, 6H, CH(CH_3)(CH$_3$)), 0.87 (m, $^3J_{HH}$ = 7.0 Hz, 6H, CH(CH_3)(CH$_3$)), 0.75 (m, $^3J_{HH}$ = 7.2 Hz, 6H, CH(CH_3)(CH$_3$)). **^{13}C{^{1}H}-NMR** (100.7 MHz, CD_2Cl_2, 25 °C): δ (ppm) = 152.2 (br, C_{ipso}), 134.8 (br, C_{ortho}H), 129.4 (quart, $^2J_{CF}$ = 32.2 Hz, $C_{meta}CF_3$), 124.2 (quart, $^1J_{CF}$ = 272.5 Hz, *C*F$_3$), 119.6 (hept, $^3J_{CF}$ = 4.0 Hz, C_{para}H), 47.2 (br, N−*C*H$_2$), 24.9 (vt, ABB'A', N = $|^1J_{AB}+^3J_{AB'}|$ = 27.1 Hz, P−*C*H$_2$), 24.6 (vt, ABB'A', N = $|^1J_{AB}+^3J_{AB'}|$ = 25.1 Hz, *C*HMe$_2$), 20.8 (vt, ABB'A', N = $|^1J_{AB}+^3J_{AB'}|$ = 24.6 Hz, *C*HMe$_2$), 19.4 (br, CH(*C*H$_3$)(CH$_3$)), 19.0 (br, CH(*C*H$_3$)(CH$_3$)), 18.2 (br, CH(*C*H$_3$)(CH$_3$)), 18.2 (br, CH(*C*H$_3$)(CH$_3$)). **^{15}N{^{1}H}−NMR** (50.7 MHz, CD_2Cl_2, 25 °C): δ (ppm) = −316.5 (s). **^{31}P{^{1}H}-NMR** (162.0 MHz, CD_2Cl_2, 25 °C): δ (ppm) = 21.2 (s). **Elemental anal.** Calc. for $C_{40}H_{46}BCl_2F_{18}N_2P_2Re$ (1226.66): C, 39.17; H, 3.78; N, 2.28. Found: C, 39.37; H, 3.88; N, 2.49.

2.3.11 [ReCl$_3$(P=NP^{iPr})] (**40**)

*Route A – oxidation of **29***: [ReCl$_3$(HPNP^{iPr})] (**29**) (40 mg, 66.9 µmol, 1.0 eq) and 2,4,6-tris-*tert*-butylphenoxy radical (35.0 mg, 133.8 µmol, 2.0 eq) are mixed in chlorobenzene (5 mL) and stirred at 60 °C overnight. After 16 h the solvent is removed *in vacuo*. The product is washed with Et_2O and benzene and subsequently extracted with DCM. The product [ReCl$_3$(P=NP^{iPr})] (**40**) is obtained as an orange powder (36.4 mg, 61.1 µmol, 91 %).

^{1}H-NMR (500 MHz, CD_2Cl_2, 25 °C): δ (ppm) = 62.96 (s, 2H, P-CH_2-CH), 12.60 (m, $^3J_{HH}$ = 7.3 Hz, 2H, C*H*Me$_2$), 10.25 (dd, $^3J_{HH}$ = 6.8 Hz, $^3J_{HP}$ = 10.0 Hz, 6H, CH(CH_3)$_2$), 9.67 (dd, $^3J_{HH}$ = 7.2 Hz, $^3J_{HP}$ = 13.3 Hz, 6H, CH(CH_3)$_2$), 9.09 (dd, $^3J_{HH}$ = 6.8 Hz, $^3J_{HP}$ = 12.7 Hz, 6H, CH(CH_3)$_2$), 7.49 (dd, $^3J_{HH}$ = 7.2 Hz, $^3J_{HP}$ = 15.1 Hz, 6H, CH(CH_3)$_2$), 6.87 (m, $^3J_{HH}$ = 7.1 Hz, 2H, C*H*Me$_2$), 4.20 (m, $^3J_{HH}$ = 6.2 Hz, 2H, P-CH_2-CH$_2$), −16.27 (m, $^3J_{HH}$ = 6.2 Hz, 2H, N-CH_2-CH$_2$), −73.85 (d, $^3J_{HP}$ = 14.6 Hz, 1H, N-C*H*-CH$_2$). J_{HH} coupling constants were assigned by ^{1}H{^{31}P} spectroscopy. **^{13}C{^{1}H}-NMR** (125.8 MHz, CD_2Cl_2, 25 °C): δ (ppm) = 433.4 (s, N-*C*H-CH$_2$), 172.4 (d, $^1J_{CP}$ = 16.2 Hz, *C*HMe$_2$), 143.0 (d, $^1J_{CP}$ = 16.6 Hz, *C*HMe$_2$), 135.8 (d, $^2J_{CP}$ = 7.0 Hz, N-*C*H$_2$-CH$_2$), 21.7 (d, $^1J_{CP}$ = 22.2 Hz, P-*C*H$_2$-CH$_2$), 21.1 (s, CH(*C*H$_3$)$_2$), 20.8 (s, CH(*C*H$_3$)$_2$), 18.3 (s, CH(*C*H$_3$)$_2$), 16.4 (s, CH(*C*H$_3$)$_2$), −9.6 (s, P-*C*H$_2$-CH). **^{31}P{^{1}H}-NMR** (202.5 MHz, CD_2Cl_2, 25 °C): δ (ppm) = −1592.6 (d, $^2J_{PP}$ = 247.6 Hz), −1616.5 (d, $^2J_{PP}$ = 248.1 Hz). **CV**: $E_{1/2}$ vs Fc/Fc$^+$ (V) = −1.70 (Re^{II}/Re^{III}), −0.28 (Re^{III}/Re^{IV}). **Elemental anal.** Calc. for $C_{16}H_{35}Cl_3NP_2Re$ (595.97): C, 32.25; H, 5.92; N, 2.35. Found: C, 32.56; H, 6.18; N, 2.39. **Mass spect.** (LIFDI), m/z (%) = 95.0 (100, [M]$^+$).

*Route B – reaction of **37** with benzoyl chloride*: In a typical experiment, [Re(N)Cl_2(HPNP^{iPr})] (**37**) (5.0 mg, 8.7 µmol, 1.0 eq) and benzoyl chloride (2.01 µL, 17.3 µmol, 2.0 eq) are mixed in 1,4-dioxane and heated to 80 °C for 15 h. All volatiles are subsequently removed *in vacuo* and 1,3,5-trimethoxybenzene (4.4 mg, 26.1 µmol, 3 eq) is added as internal standard. NMR spectroscopic examination in CD_2Cl_2 reveals the formation of [$ReCl_3$(P=NP^{iPr})] (**40**) in 71.0 % yield. NMR spectroscopic features as well as the LIFDI mass spectrum are identical with those of **40** obtained from route *A*.

The reaction is accompanied by the formation of benzamide (30.5 % spectroscopic yield) and equimolar amounts of benzoic acid and benzonitrile (64.5 % spectroscopic yield each), respectively. Benzonitrile can be detected when the reaction is carried out in toluene-d_8. Use of 1 eq benzoyl chloride resultes in incomplete conversion of **37**. Tribenzamide is observed in minor quantities as additional product if the reaction is carried out at 100 °C over 24 h or in THF for 65 h at 60 °C, respectively.

3 Computational details

> *I love my computer*
> *For all you give to me*
> *Predictable errors and no identity*
>
> — **Bad Religion**
> "I Love My Computer" on "The New America"

3.1 General procedure

For all independently carried out theoretical calculations, either the ORCA 3.0 or ORCA 4.0 program packages were used.[246,247] DFT calculations were performed utilizing the PBE or PBE0 functionals.[248,249] *Ahlrich's* double-ζ def2-SVP basis set (used in geometry optimizations and frequency calculations) as well as the triple-ζ def2-TZVP/def2-TZVPP (for single point calculations) were used for all elements but Os or Re, for which effective core potentials with the Stuttgart-Dresden 60 parameter sets replaced the inner shell $1s$-$4f$ orbitals.[250,251] In all DFT calculations, the RI-J (PBE)[252–255] and RIJCOSX (PBE0)[256] approximations together with the corresponding def2/J auxiliary basis sets[257] were used, and the obtained energies were corrected for dispersion with *Grimme's* D3 model[258] with *Becke-Johnson* damping.[259] In the ORCA nomenclature, the *TightOpt* and *TightSCF* convergence criteria were employed, the former only during geometry optimizations.
Frequency calculations were performed at the same level of theory as the geometry optimizations, verifying the obtained structures to be local minima or transition states (no or only one imaginary vibrational frequency, respectively). These calculations incorporated *Grimme's* quasi-RRHO aproach for low energy frequencies below 35 cm^{-1} in all calculations performed with ORCA 4.0.[260] If solution data were simulated, solvent effects were accounted for in the single point calculations with the COSMO (ORCA 3.0) or the CPCM continuum solvation models.[261,262] In these cases, the obtained *Gibb's* free energies were corrected for the difference between ideal gas standard conditions (1 atm, 298.15 K) used by ORCA and standard solution conditions (1 mol L^{-1}, 298.15 K):

$$G_{sol} = G_{gas} + RTln\frac{RT}{p}G_{sol} = G_{gas} + RTln(24.47)G_{sol} = G_{gas} + 7.93\,\mathrm{kJ\,mol^{-1}} \quad (3.1)$$

Final free energies were obtained by combining the higher level single point energies (triple-ζ PBE0) with the obtained free energies according to:

$$G = G_{\mathrm{double}\zeta} - E^{\mathrm{el}}_{\mathrm{double}\zeta} + E^{\mathrm{el}}_{\mathrm{triple}\zeta} \quad (3.2)$$

The results obtained from this approach are reported in the main text in the form "SinglePointMethod||FrequencyCalculationMethod". While the protonated HPNP pincer has only one possible conformation, the amide based, monoanionic PNP pincer ligand can adopt three different conformers, which exhibit slightly different energies. However, these were only compared when exact energies were needed, while during simple estimations, this effect was neglected. For the *iso*-propyl based PNP ligand it was found that rotation of the *iso*-propyl groups did not lead to a significant variation of the energy, therefore conformations were derived from X-ray structures of the compounds (if available) or from closely related complexes, rather than comparing all 81 additionally possible rotation conformers (three possible orientations for each *i*Pr group).
The output files were analyzed using the ChemCraft software package.[263]

3.2 Model of [Os(N)(PNP$^{t\mathrm{Bu}}$)] (**3**)and revised scan of the N–Os≡N bending mode

All calculations were performed with ORCA 3.0.3 according to the procedure described in Section 3.1.

Tab. 3.1. XZY geometry data for the DFT-derived structures of **3**.

	X	Y	Z		X	Y	Z
Os	-0.006854006	0.205414989	0.52005072	H	2.592067054	2.130772755	-2.255401385
P	-2.312891097	0.580036775	0.424485232	H	-2.753875543	2.129887616	-2.092107754
P	2.288611584	0.588687811	0.286122017	H	-2.669420515	0.803222424	-3.25405206
N	-0.012607445	2.283855916	0.342958922	H	-1.315204363	1.093899165	-2.144545362
N	0.002746125	-1.459589805	0.701208738	H	-1.52147959	-0.545922447	2.99263108
C	-1.193376841	3.10149957	0.183092865	H	-3.009270158	-0.359550347	3.954141307
C	-2.469222426	2.391767363	0.619826917	H	-2.178686079	1.057155868	3.292694483
C	1.151459279	3.108076311	0.113052804	H	2.345716359	1.096529818	3.160000952
C	2.45678748	2.401937279	0.462184018	H	3.179500857	-0.337394746	3.776479973
C	3.360787137	-0.129477791	1.648788945	H	1.630573897	-0.491542355	2.911483089
C	2.926684723	0.135317447	-1.419500745	H	2.580138865	-2.113620617	1.223529468
C	-3.313312592	-0.137597981	1.841228981	H	3.98363582	-2.073780506	2.301265528
C	-3.043219469	0.134791454	-1.244537931	H	4.208938378	-1.833199176	0.575049361
C	2.238377522	1.105969399	-2.381402282	H	4.648219874	1.586469091	2.095020352

C	-2.403695994	1.10650989	-2.237770937	H	5.322407336	0.482682341	0.888216137
C	-2.448696434	0.01806729	3.093437625	H	5.282548125	0.022124218	2.585789156
C	2.575684542	0.049891154	2.950214535	H	1.400966089	-1.396763231	-1.645925309
C	3.538602613	-1.624668168	1.409036077	H	2.9664351	-2.032937288	-1.147672176
C	4.726889616	0.53877522	1.797719665	H	2.748544987	-1.488927321	-2.809791925
C	2.479001937	-1.284447595	-1.768754105	H	4.816080605	1.234401774	-1.348379349
C	4.436243236	0.237286753	-1.583443982	H	4.695933299	0.013765212	-2.623267565
C	-3.533318622	-1.628187316	1.609450616	H	4.961596195	-0.487876604	-0.962727751
C	-4.656478115	0.555205398	2.0689134	H	-2.594375851	-2.13694092	1.382261992
C	-2.617677778	-1.285144817	-1.619493754	H	-4.244589558	-1.823901582	0.807036364
C	-4.55884438	0.243734706	-1.328729684	H	-3.947701736	-2.067438239	2.521383943
H	-1.29158506	3.433340822	-0.863727688	H	-4.541630138	1.599311175	2.365936862
H	-1.091191895	4.026384388	0.773977732	H	-5.178536822	0.044808874	2.883693101
H	1.08296729	4.029331642	0.714361901	H	-5.301763227	0.515566175	1.193062346
H	1.181052293	3.445181517	-0.936353279	H	-1.535392561	-1.400973194	-1.549437224
H	-3.349872214	2.785028827	0.107285685	H	-2.935837218	-1.485411536	-2.647371075
H	-2.619453231	2.552323469	1.688649928	H	-3.076684004	-2.034395105	-0.977813833
H	2.684706181	2.568516576	1.516090591	H	-4.920771228	1.243019635	-1.075616052
H	3.298057128	2.792008455	-0.114538905	H	-5.055225636	-0.478131684	-0.680860376
H	1.15563665	1.092309581	-2.235729422	H	-4.873951187	0.020709413	-2.353097625
H	2.454544841	0.801964813	-3.409193871				

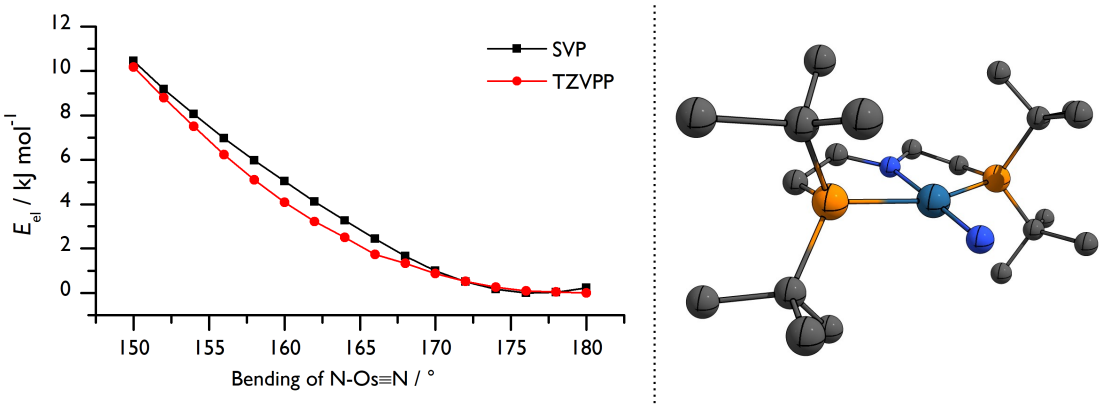

Fig. 3.1. *Left*: Relaxed surface scan of the N–Os≡N bending mode of **3**. *Right*: DFT-derived geometry of **3**.

3.3 Computational analysis of the reaction between **3** and PMe_3 to form **7**

All calculations were performed using ORCA 3.0.3 according to the procedure described in Section 3.1. Geometry optimization and single point energy calculations at the double- and triple-zeta basis set quality, respectively, were performed with three functionals: PBE-D3BJ, PBE0-D3BJ and M06. The obtained results were benchmarked against the experimentally available Gibbs free energy of the reaction as well as known stretching vibrations of **3** and

7 (see Table XX). PBE and M06 performed equally well with only ≈1 kJ mol^{-1} deviation in ΔG^0 and rather good agreement with the vibrational frequencies while PBE0 exhibited less satisfying agreement. Due to lower computational costs and less problems with small imaginary frequencies, PBE was chosen for all subsequent computations and the presented data was obtained with this functional. The NBO analysis was performed by *Dr. Markus Finger* (see Tables 3.3 and 3.4 as well as Figure 1.3).

Tab. 3.2. Benchmarking of the DFT calculations.

	PBE	PBE0	M06	Experimental
ΔG^0 (**3** + PMe_3 → **7** / kJ mol^{-1}	−13.2	−32.6	−11.3	−12.4
$\nu_{Os\equiv N}$(**3**) / cm^{-1}	1040.3	1093.2	1973.4	999
$\nu_{Os-N=P}$(**7**) / cm^{-1}	1259.5	1317.0	1304.2	1240

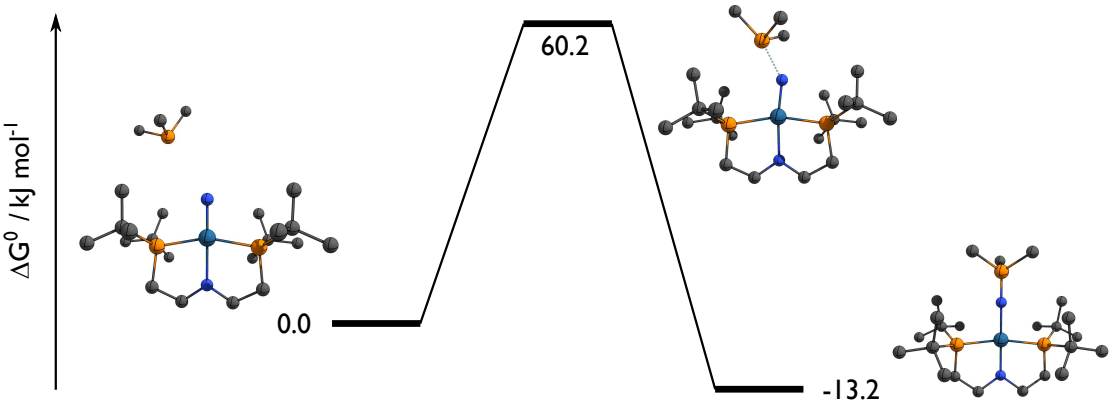

Fig. 3.2. Free Gibbs energy diagramm for the formation of **7** from **3** and PMe_3 (PBE/D3BJ/RI/def2-TZVPP||def2-SVP).

Tab. 3.3. Selected donor-acceptor interactions according to an NBO analysis of the transition state of the formation of **7** (PBE/D3BJ/RI/def2-TZVPP).

Bond	Polarization (NLMOs)	Hybridization	LMO-Bond orders	Energy kJ mol^{-1}
P ⟶ N	78.5 % (P3)	$sp^{0.71}$ (P3)	0.22 (N2-P3)	168.2
	11.2 % (N2)	p (N2)	-0.13 (Os1-N2)	
	6.7 % (Os1)	d (Os1)		
N ⟶ P	91.2 % (N2)	$sp^{0.40}$ (N2)	0.02 (Os1-N2)	142.4
	4.7 % (P3)	p (P3)	0.09 (N2-P3)	
	2.0 % (C21)	$sp^{2.34}$ (C21)	−0.04 (P3-C21)	
	0.9 % (Os1)	$sd^{0.18}$ (Os1)		

Tab. 3.4. Atomic charges obtained from NPA analysis of **3**, PMe_3, **TS**, and **7**, respectively, with atoms with minor changes in grey.

	def2-SVP	def2-TZVPP
	3	
Os	76.03	75.97
P_{PNP}	14.01	13.90
N_{PNP}	7.74	7.64
$N_{nitride}$	7.32	7.38
	PMe_3	
P	14.28	14.26
C	6.97	6.94
	TS	
Os	76.04	75.98
P_{PNP}	13.99/14.02	13.87/13.91
N_{PNP}	7.69	7.59
$N_{nitride}$	7.53	7.64
P_{PMe_3}	14.07	13.96
C21	6.98	6.97
C22/C23	6.96	6.95
	7	
Os	76.16	76.09
P_{PNP}	13.00	13.90
N_{PNP}	6.53	7.43
$N_{nitride}$	8.17	8.21
P_{PMe_3}	13.34	13.29

3.3.1 XYZ-Coordinates

Tab. 3.5. XYZ geometries of **3**, PMe_3 and **7** derived with the PBE0 functional.

	X	Y	Z		X	Y	Z
			3				
Os	-0.009576	0.174007	0.409504	H	2.726588	2.061792	-2.33299
P	-2.340317	0.563283	0.411803	H	-2.941195	2.227809	-2.044579
P	2.318477	0.562476	0.259128	H	-2.891951	0.931069	-3.258599
N	-0.011518	2.284852	0.261143	H	-1.478639	1.209081	-2.198294
N	-0.012147	-1.497198	0.475145	H	-1.447917	-0.649242	2.901646
C	-1.2015	3.091644	0.14433	H	-2.903877	-0.525841	3.948282

C	-2.447862	2.382776	0.672074	H	-2.108096	0.939582	3.318435
C	1.156717	3.084279	-0.016086	H	2.283191	1.154249	3.149347
C	2.454517	2.393773	0.399144	H	3.062579	-0.299353	3.823985
C	3.353129	-0.102827	1.694191	H	1.543554	-0.430785	2.869694
C	3.038634	0.082876	-1.421222	H	2.632305	-2.123747	1.284872
C	-3.304894	-0.189805	1.853509	H	4.014833	-2.029797	2.407139
C	-3.157644	0.189404	-1.250398	H	4.282595	-1.810317	0.672113
C	2.3759	1.023818	-2.432058	H	4.56009	1.682398	2.128363
C	-2.579838	1.207085	-2.237798	H	5.3328	0.556786	0.98603
C	-2.38333	-0.098107	3.074702	H	5.237557	0.152336	2.709717
C	2.50613	0.093575	2.956188	H	1.520621	-1.456052	-1.700182
C	3.579108	-1.600661	1.490124	H	3.061181	-2.091727	-1.086893
C	4.690873	0.619707	1.873582	H	2.942017	-1.58636	-2.785048
C	2.613541	-1.349212	-1.758923	H	4.909576	1.223969	-1.264578
C	4.555317	0.211734	-1.515107	H	4.872136	-0.006232	-2.54919
C	-3.571086	-1.667889	1.566263	H	5.073482	-0.507064	-0.866245
C	-4.614895	0.541974	2.157341	H	-2.644657	-2.192828	1.286361
C	-2.729258	-1.208029	-1.707198	H	-4.31523	-1.817649	0.771722
C	-4.678913	0.297775	-1.237615	H	-3.971362	-2.145489	2.475598
H	-1.368597	3.412218	-0.907189	H	-4.447598	1.588831	2.453205
H	-1.082129	4.041124	0.709623	H	-5.110934	0.043151	3.006773
H	1.100899	4.053729	0.524108	H	-5.317524	0.530688	1.314676
H	1.206208	3.363375	-1.091644	H	-1.632813	-1.279232	-1.75316
H	-3.373895	2.805252	0.250409	H	-3.14464	-1.399108	-2.711009
H	-2.501578	2.509619	1.763965	H	-3.088277	-2.000865	-1.039254
H	2.639301	2.585752	1.4665	H	-5.026321	1.291868	-0.914913
H	3.325792	2.78171	-0.151837	H	-5.146056	-0.457174	-0.591705
H	1.279722	1.010328	-2.316978	H	-5.061082	0.125823	-2.257905
H	2.623223	0.684734	-3.451567				

PMe_3

P	0.159556158	-0.432751689	-0.388611653	H	2.427822791	0.458942186	-0.602755251
C	1.98700487	-0.418691449	-0.106525875	H	2.438587528	-1.313306851	-0.560913824
C	-0.302087626	1.015348468	0.664290179	H	2.251208267	-0.390926714	0.964298085
C	-0.302848265	-1.818399708	0.744236338	H	0.057761211	-2.766098913	0.314962209
H	0.078670718	1.935807295	0.195270406	H	-1.398528738	-1.885110459	0.822033394
H	0.10700201	0.94594711	1.686735291	H	0.122839172	-1.704267435	1.755599137
H	-1.397668096	1.100848157	0.722351565				

transition state

Os	-0.07779724	0.361703503	0.387523649	H	-2.165753044	1.325548505	3.285235877
P	-2.405918612	0.733018986	0.402771766	H	2.082207937	1.120050398	3.160552722
P	2.256416282	0.643593665	0.279055274	H	3.023427034	-0.239178141	3.836761423
N	-0.070720883	2.392048884	0.182341972	H	1.553522796	-0.537347973	2.845819145
N	-0.270866354	-1.364740421	0.504400298	H	2.82597942	-2.050691736	1.278077668
C	-1.245548255	3.220295651	0.007871238	H	4.183987908	-1.826805931	2.417443047
C	-2.508643728	2.566996439	0.557184871	H	4.442750236	-1.57271072	0.684892917
C	1.121947359	3.173609458	-0.068166347	H	4.356054672	1.8995574	2.229348168
C	2.392354796	2.482192532	0.410506763	H	5.235112602	0.89986679	1.046996339
C	3.329048537	0.023832441	1.714049413	H	5.175105182	0.418582144	2.753092472
C	3.020300938	0.179886268	-1.386354589	H	1.567973632	-1.419961409	-1.611759409

C	-3.358498966	0.091955012	1.908548656	H	3.142034342	-1.985129783	-1.015063931
C	-3.293706323	0.300291798	-1.21158194	H	2.974071846	-1.519248485	-2.722083829
C	2.326778918	1.068651794	-2.423264291	H	4.826224013	1.419946637	-1.258717423
C	-2.732757704	1.252693154	-2.271103357	H	4.863719698	0.149434145	-2.501631852
C	-2.410231775	0.26822088	3.099720227	H	5.083041968	-0.283811542	-0.80136097
C	2.442648637	0.098766085	2.961241731	H	-2.709851988	-1.93138732	1.420960434
C	3.715186224	-1.43946172	1.497437218	H	-4.40549602	-1.596784365	0.969476219
C	4.588133723	0.865881892	1.933192898	H	-3.978262512	-1.83373803	2.671441419
C	2.6555559	-1.274402865	-1.694271691	H	-4.497213313	1.903235214	2.412269242
C	4.529133802	0.381897892	-1.47607012	H	-5.125624424	0.397674018	3.103496942
C	-3.626498919	-1.401354571	1.720014509	H	-5.395648986	0.756691769	1.388899779
C	-4.663722587	0.835765664	2.202196526	H	-1.811606228	-1.188524441	-1.740169395
C	-2.901997681	-1.120584657	-1.620537311	H	-3.384677181	-1.370502747	-2.580404463
C	-4.811473032	0.430273806	-1.15408304	H	-3.209557864	-1.874580322	-0.884701997
H	-1.385229223	3.48142282	-1.06228689	H	-5.136214579	1.436540988	-0.847017722
H	-1.101375955	4.1928754	0.522363568	H	-5.264488317	-0.301558809	-0.471992278
H	1.047349445	4.152986424	0.448636528	H	-5.22968572	0.235163868	-2.156095761
H	1.204235734	3.425320106	-1.146564844	P	0.587826864	-3.193568185	0.593713239
H	-3.420582308	2.974968886	0.093562544	C	1.770615181	-4.681053516	0.647534806
H	-2.579109088	2.76625284	1.636897773	H	2.418850863	-4.612645024	1.535071391
H	2.519060066	2.680238331	1.485214083	H	2.415717188	-4.663942921	-0.244916006
H	3.289537485	2.871303463	-0.096597749	H	1.231840379	-5.645181235	0.674352887
H	1.231051483	1.013122499	-2.314992585	C	-0.345228481	-3.782190646	-0.875980081
H	2.59880078	0.719056133	-3.433149457	H	0.357016306	-3.880399536	-1.717945371
H	2.634822154	2.121763075	-2.343289068	H	-1.119436786	-3.054619689	-1.140632968
H	-3.073127221	2.288864103	-2.127974803	H	-0.807869003	-4.76570814	-0.696075992
H	-3.078832315	0.923330939	-3.265025344	C	-0.383601706	-3.641682009	2.091174504
H	-1.63078925	1.237556247	-2.263868906	H	0.287311525	-4.088488145	2.839064031
H	-1.458739956	-0.255990604	2.928062032	H	-1.179042394	-4.369098275	1.864741311
H	-2.893949273	-0.130513194	4.007709956	H	-0.842068661	-2.735881836	2.508922306

7

Os	-0.008247756	0.399379046	0.320762425	H	-2.083574554	1.226232955	3.184811917
P	-2.311515854	0.65238043	0.312697481	H	2.063375344	1.233877724	3.188125713
P	2.29488371	0.650771474	0.317689059	H	2.864903495	-0.180526691	3.92219625
N	-0.007268199	2.322992312	0.164881754	H	1.426735802	-0.381000646	2.857281618
N	-0.010897579	-1.570597931	0.405745382	H	2.65252709	-1.980904187	1.364814416
C	-1.193296648	3.160536156	-0.011247476	H	3.965123014	-1.878478197	2.574043348
C	-2.470963774	2.492095144	0.466554933	H	4.332926113	-1.650783449	0.854988805
C	1.179655094	3.159414992	-0.010952066	H	4.414904762	1.853115913	2.324086991
C	2.456005138	2.490537745	0.469659152	H	5.299741213	0.7453894	1.249536093
C	3.29323695	0.033625637	1.811822333	H	5.0898228	0.345866874	2.964898937
C	3.180640877	0.225320606	-1.305629746	H	1.73069452	-1.359216345	-1.617696666
C	-3.314870524	0.033947151	1.802798999	H	3.29606366	-1.944264247	-1.012159612
C	-3.193467888	0.229778303	-1.313450298	H	3.162559773	-1.427004462	-2.704629667
C	2.563564363	1.14789458	-2.361362684	H	4.997331747	1.423702095	-1.027641319
C	-2.572548022	1.152994138	-2.366395228	H	5.091000128	0.190412691	-2.306827743
C	-2.379740925	0.180766663	3.007736321	H	5.189492528	-0.298459953	-0.6103288
C	2.35564425	0.186823574	3.014054269	H	-2.679807866	-1.981573007	1.352353383
C	3.579620411	-1.454651543	1.631308774	H	-4.35792715	-1.64465704	0.839260204
C	4.592191133	0.793281299	2.086955065	H	-3.995007777	-1.877591931	2.558605612

C	2.819757652	-1.213502469	-1.67724586	H	-4.431651064	1.855655139	2.317523366
C	4.694096231	0.400082085	-1.298272068	H	-5.11392924	0.348833563	2.951425858
C	-3.605794409	-1.452893058	1.617797018	H	-5.317045749	0.754474283	1.236637398
C	-4.611984123	0.797215897	2.076453632	H	-1.744818239	-1.356444954	-1.623643106
C	-2.833534928	-1.209166096	-1.685791969	H	-3.174049704	-1.420803149	-2.714327836
C	-4.706716033	0.406745633	-1.310138909	H	-3.312515849	-1.940226999	-1.022928459
H	-1.278732719	3.4510848	-1.077220016	H	-5.009180796	1.430643131	-1.039601458
H	-1.052208779	4.110441365	0.539465492	H	-5.205239173	-0.291546408	-0.624210801
H	1.038636399	4.110271155	0.538119127	H	-5.101024347	0.198564013	-2.320032114
H	1.26677347	3.448143372	-1.077285534	P	-0.008059966	-3.114369159	0.544046468
H	-3.360162753	2.889899422	-0.046859006	C	1.399121233	-4.056943729	-0.181777844
H	-2.603503636	2.693854863	1.53963848	H	2.340549589	-3.738109297	0.284318259
H	2.587223186	2.693632762	1.542640454	H	1.454785994	-3.843611294	-1.258853616
H	3.346334267	2.886696692	-0.043031626	H	1.272282387	-5.140539801	-0.036951754
H	1.463079067	1.090786246	-2.3320667	C	-1.413893036	-4.05696504	-0.1838218
H	2.907035538	0.83220862	-3.36106568	H	-2.355840782	-3.737454958	0.280781052
H	2.863261257	2.198156247	-2.226307414	H	-1.288249855	-5.140762405	-0.03945037
H	-2.871878852	2.203318542	-2.230973911	H	-1.467702872	-3.842805473	-1.260861422
H	-2.913401226	0.838795355	-3.367464018	C	-0.008009166	-3.627117861	2.294871935
H	-1.472186517	1.095067705	-2.334025941	H	0.878652296	-3.196913337	2.780817614
H	-1.452866382	-0.390589414	2.851877022	H	-0.001257252	-4.721033569	2.410808559
H	-2.892755246	-0.186624018	3.913749349	H	-0.901595271	-3.208115675	2.778000214

Tab. 3.6. XYZ geometries of **3**, PMe_3, the transition state and **7** derived with the PBE functional.

	X	Y	Z	X	Y	Z
			3			
Os	-0.008659244	0.16211101	0.51891145	H	2.643342433	2.163961747	-2.281992082
P	-2.341719665	0.558707662	0.420463175	H	-2.812346351	2.175520132	-2.121440057
P	2.315513411	0.555754803	0.286833154	H	-2.72627516	0.836281689	-3.304583592
N	-0.013176707	2.289081065	0.319750065	H	-1.356078791	1.111872221	-2.168723375
N	-0.003098279	-1.512488596	0.770740099	H	-1.480569754	-0.344270408	3.024093356
C	-1.206390662	3.101989236	0.156207222	H	-3.001653971	-0.377897102	4.008600682
C	-2.479262016	2.394710571	0.641643097	H	-2.37945532	1.165658804	3.347052452
C	1.169076259	3.099912903	0.082325519	H	2.525097489	1.176929717	3.20391014
C	2.468018375	2.392446383	0.492599313	H	3.179781794	-0.365719458	3.835367423
C	3.400140509	-0.172800789	1.681512411	H	1.604097932	-0.331120411	2.940970762
C	2.990630402	0.139953601	-1.452575676	H	2.517836565	-2.1573202	1.338646546
C	-3.345585122	-0.174420016	1.871946998	H	3.980735125	-2.146673762	2.378713925
C	-3.115632603	0.149932564	-1.278989526	H	4.154412783	-1.950870054	0.611277163
C	2.283311128	1.123629767	-2.405495548	H	4.731693857	1.575680191	1.903280919
C	-2.461868949	1.134947033	-2.268105172	H	5.423204979	0.266622854	0.892201407
C	-2.496877269	0.084027892	3.133176117	H	5.320330755	0.072364051	2.663733641
C	2.626549107	0.09396753	2.98850852	H	1.443114121	-1.384430435	-1.696552573
C	3.515471392	-1.692251425	1.478299407	H	3.023317912	-2.0592453	-1.192183158
C	4.791397854	0.47639931	1.773962987	H	2.80647396	-1.491835987	-2.877196314
C	2.541000277	-1.285813468	-1.818242895	H	4.870887155	1.286359123	-1.268312516
C	4.511495053	0.287589285	-1.590257478	H	4.795862721	0.163524022	-2.657323386
C	-3.475782555	-1.692722748	1.668918469	H	5.060058948	-0.483508785	-1.015412473

C	-4.727496746	0.477197066	2.048253138	H	-2.488715376	-2.159006263	1.470600313
C	-2.691328581	-1.275700069	-1.674424302	H	-4.1636601	-1.946337722	0.838692004
C	-4.641566111	0.301956127	-1.329617473	H	-3.889724641	-2.150209581	2.592540677
H	-1.331030793	3.411738567	-0.913253434	H	-4.657446174	1.575434881	2.181104583
H	-1.10549247	4.066251458	0.718578341	H	-5.205441302	0.068431295	2.964318032
H	1.103333748	4.065998122	0.646725162	H	-5.409495205	0.274634944	1.20303294
H	1.229589728	3.406096462	-0.993693649	H	-1.588593445	-1.377924819	-1.615510862
H	-3.392091124	2.803101162	0.160922167	H	-3.016773636	-1.476903951	-2.717444325
H	-2.588952403	2.540474108	1.734762354	H	-3.139901261	-2.050092388	-1.024979783
H	2.644095886	2.542237989	1.576400397	H	-4.97916915	1.300565998	-0.984447691
H	3.350545677	2.797470593	-0.044233065	H	-5.159376225	-0.469632456	-0.727537334
H	1.184997717	1.102977099	-2.242597504	H	-4.986438728	0.18274486	-2.379259426
H	2.487157839	0.821671299	-3.454621858				

PMe3

P	0.164564039	-0.429104852	-0.41167768	H	2.457002125	0.460809275	-0.611774057
C	2.006130075	-0.42115242	-0.113747865	H	2.457126834	-1.328019419	-0.564711557
C	-0.308839517	1.017537344	0.666888697	H	2.2628954	-0.392711361	0.966974117
C	-0.308705817	-1.816825444	0.741756214	H	0.04768641	-2.780661011	0.325602191
H	0.04777801	1.958043245	0.200569658	H	-1.413303605	-1.872708166	0.818699378
H	0.114989765	0.942252076	1.691297618	H	0.115448921	-1.687635458	1.760634124
H	-1.41345264	1.077516191	0.740459161				

transition state

Os	-0.080792582	0.351482594	0.411343928	H	-2.326206134	1.184940622	3.335823663
P	-2.416199428	0.718483945	0.397041935	H	2.261271054	1.386480614	3.137006703
P	2.256523446	0.668394587	0.258857514	H	3.065026926	-0.039189243	3.870232565
N	-0.08973921	2.408930419	0.228062905	H	1.536761012	-0.225689511	2.910480671
N	-0.298063006	-1.383037026	0.566207696	H	2.681906219	-1.972274375	1.382927548
C	-1.277525465	3.248704297	0.142749074	H	4.080312347	-1.805623446	2.509316249
C	-2.534817965	2.551125285	0.671996515	H	4.32876378	-1.642434522	0.746021583
C	1.095255642	3.19688742	-0.094184332	H	4.517961632	1.948425839	1.99450004
C	2.391588213	2.52246156	0.360994392	H	5.34293861	0.724959844	0.976716612
C	3.355400551	0.087652681	1.717124246	H	5.224021872	0.491318362	2.742962576
C	3.014789871	0.183402683	-1.429820837	H	1.552912734	-1.435143371	-1.590650911
C	-3.421129978	-0.02797673	1.842966639	H	3.164438292	-1.993958713	-1.050587377
C	-3.262324487	0.39161947	-1.290538868	H	2.921565492	-1.532352361	-2.764903029
C	2.290861801	1.069621031	-2.462733162	H	4.827829295	1.436564192	-1.289274757
C	-2.610607776	1.384526975	-2.273127758	H	4.855538608	0.20204912	-2.581256194
C	-2.518086034	0.122146404	3.083856716	H	5.098462116	-0.29351397	-0.883806552
C	2.501507142	0.315286074	2.980052195	H	-2.681818577	-2.01410251	1.281732541
C	3.626094952	-1.417724583	1.572198025	H	-4.38030041	-1.702161644	0.767920357
C	4.677671792	0.861765372	1.848654057	H	-4.014661388	-2.020139326	2.488356287
C	2.644212832	-1.282360751	-1.718162558	H	-4.629532109	1.758330792	2.314920656
C	4.52999914	0.397026539	-1.536483627	H	-5.23875643	0.229038582	3.003714458
C	-3.635486956	-1.525655087	1.568508453	H	-5.474322085	0.574442792	1.267753296
C	-4.761596241	0.677962156	2.105750676	H	-1.799845437	-1.172100251	-1.729440803
C	-2.899097463	-1.031218055	-1.750465411	H	-3.260790056	-1.183464052	-2.790005233
C	-4.783284291	0.592407013	-1.28940048	H	-3.358114102	-1.81376773	-1.117997866
H	-1.441604799	3.584106299	-0.911907254	H	-5.076608153	1.592264679	-0.909125654
H	-1.11894509	4.193643689	0.721081796	H	-5.307456688	-0.176507091	-0.689275182

H	1.031034875	4.202382782	0.392607852	H	-5.165791642	0.51151731	-2.32996169
H	1.134479076	3.410254002	-1.191598739	P	0.620056737	-3.274717899	0.649137095
H	-3.46234833	2.98391388	0.243963427	C	1.873205505	-4.721737414	0.617481525
H	-2.590827336	2.673414988	1.772261834	H	2.651425209	-4.54878907	1.388423821
H	2.554182991	2.738611744	1.435561791	H	2.372726731	-4.741699799	-0.372728837
H	3.276635658	2.904098062	-0.188556887	H	1.404466421	-5.713733087	0.800020858
H	1.190017533	1.000903076	-2.328587311	C	-0.575259032	-3.997035992	-0.567370351
H	2.544319302	0.718701527	-3.485803691	H	-0.095256805	-4.037717677	-1.565890114
H	2.593631479	2.132979932	-2.390921638	H	-1.468944779	-3.350560009	-0.631079913
H	-2.926178481	2.429762631	-2.086382052	H	-0.873474616	-5.025486383	-0.277782524
H	-2.916724557	1.124675466	-3.308819241	C	-0.12917804	-3.66142663	2.299308047
H	-1.503350856	1.327304519	-2.209578572	H	-0.557383272	-4.684790691	2.323294739
H	-1.532703499	-0.357691868	2.919817445	H	-0.918733644	-2.922148119	2.529079708
H	-3.020082936	-0.345321588	3.958391502	H	0.659463277	-3.592261276	3.075137191

7

Os	-0.008198029	0.385220732	0.328967592	H	-2.268167191	1.369160946	3.220008721
P	-2.317275148	0.64427089	0.317971029	H	2.245347935	1.367726329	3.225513341
P	2.301033697	0.642561689	0.323645614	H	2.888670272	-0.132047848	3.965385646
N	-0.00728192	2.321311655	0.171791122	H	1.410776378	-0.17645063	2.911336995
N	-0.00939362	-1.588832843	0.432976416	H	2.519440042	-1.970154677	1.458603171
C	-1.204585472	3.166668305	-0.009120929	H	3.876925111	-1.927523026	2.643772558
C	-2.486152059	2.499343603	0.480764939	H	4.216088251	-1.765630898	0.894100114
C	1.19107724	3.165749094	-0.006428697	H	4.566079962	1.812428582	2.137688063
C	2.470924434	2.497529161	0.486702846	H	5.391316133	0.501851841	1.23801642
C	3.31518903	0.019167843	1.833195292	H	5.12139497	0.350118266	2.996566616
C	3.204225946	0.242182001	-1.326828212	H	1.785146649	-1.391204114	-1.621874679
C	-3.335506475	0.021429326	1.824974297	H	3.392669374	-1.940778249	-1.050204118
C	-3.216773577	0.244654395	-1.334695055	H	3.199869221	-1.410796936	-2.747577435
C	2.540911077	1.160283071	-2.372938234	H	4.990726369	1.495505541	-0.990616119
C	-2.550287626	1.162304954	-2.379180956	H	5.115729363	0.350268198	-2.357910012
C	-2.432451494	0.286316276	3.04651404	H	5.253180463	-0.254942509	-0.684382424
C	2.409361472	0.284759851	3.052524273	H	-2.54014507	-1.968319674	1.451949089
C	3.494784931	-1.499090898	1.6917135	H	-4.23535239	-1.762646467	0.883529483
C	4.669063639	0.712563629	2.047308923	H	-3.900395151	-1.925011261	2.633970447
C	2.876475963	-1.212155708	-1.70263955	H	-4.585968795	1.815512662	2.126390221
C	4.719633084	0.473412276	-1.325918378	H	-5.144231423	0.353621924	2.984079124
C	-3.515743273	-1.496699312	1.682869235	H	-5.409925186	0.505384643	1.224889328
C	-4.689438211	0.715704049	2.035859558	H	-1.798220455	-1.389752421	-1.626666908
C	-2.889237392	-1.209910942	-1.709822696	H	-3.210476764	-1.408282122	-2.755476212
C	-4.732010053	0.477024085	-1.337384187	H	-3.407378552	-1.938189225	-1.058545751
H	-1.289566332	3.441219804	-1.087422441	H	-5.003153741	1.499274102	-1.002599262
H	-1.054616437	4.13106483	0.531114789	H	-5.267642844	-0.251015499	-0.69722836
H	1.040545626	4.130376914	0.533235918	H	-5.125727315	0.35431134	-2.370337324
H	1.278862596	3.439987446	-1.084585566	P	-0.009611692	-3.150977838	0.55597802
H	-3.383661824	2.894375771	-0.037247273	C	1.405431131	-4.098077824	-0.197180296
H	-2.617122444	2.70003243	1.562498475	H	2.359561867	-3.775032522	0.258634258
H	2.599333445	2.698211669	1.568744548	H	1.442568917	-3.876527155	-1.281322064
H	3.370022051	2.891847145	-0.029095963	H	1.277440135	-5.190139943	-0.054449631
H	1.434503246	1.075151678	-2.318409528	C	-1.423082573	-4.09697186	-0.201341722
H	2.869795928	0.856442998	-3.390127738	H	-2.378222949	-3.773424712	0.25200175

H	2.822484409	2.223628807	-2.23863829	H	-1.296220613	-5.189172967	-0.058693725
H	-2.831365495	2.225857562	-2.245493542	H	-1.457130054	-3.874959679	-1.285492742
H	-2.877004247	0.858765377	-3.397157689	C	-0.012219634	-3.690586007	2.314890999
H	-1.444079675	1.076320861	-2.322056514	H	0.885699334	-3.277823568	2.813138798
H	-1.43382334	-0.175511743	2.90766883	H	-0.012676556	-4.795264552	2.400860009
H	-2.91422625	-0.130284189	3.958171036	H	-0.91123035	-3.277254729	2.810684782

Tab. 3.7. XYZ geometries of **3**, PMe_3, the transition state and **7** derived with the M06 functional.

	X	Y	Z	X	Y	Z
3						
Os	-0.010775244	0.196459748	0.456484918	H	2.74625922	2.059626408	-2.337111194
P	-2.373807283	0.578130031	0.423676115	H	-3.001013802	2.225879446	-2.050768303
P	2.348856911	0.561749875	0.27173653	H	-2.957173141	0.921203912	-3.259164743
N	-0.010986206	2.321675522	0.299546381	H	-1.527377745	1.222093395	-2.228843784
N	-0.014039871	-1.472250233	0.525994898	H	-1.551683141	-0.631104496	2.983690292
C	-1.205898062	3.115344705	0.150013805	H	-3.044282596	-0.476561277	3.967218325
C	-2.463674478	2.408529471	0.663206855	H	-2.211950791	0.975444367	3.348657421
C	1.166517995	3.099877338	0.004172441	H	2.326483839	1.090917888	3.177130993
C	2.46572979	2.401239385	0.414115323	H	3.205036867	-0.322711572	3.822069491
C	3.417861234	-0.114768823	1.686410619	H	1.664993922	-0.536457328	2.925507896
C	3.062863823	0.082660453	-1.419940497	H	2.726060285	-2.15080613	1.267335476
C	-3.367922155	-0.16919344	1.857150985	H	4.113871038	-2.035249789	2.380002029
C	-3.185898311	0.186984719	-1.246219849	H	4.371232113	-1.80618176	0.645512538
C	2.404710608	1.015459842	-2.436307634	H	4.622784139	1.669531657	2.146895998
C	-2.631484307	1.204513953	-2.241941876	H	5.380237153	0.576473639	0.956472925
C	-2.488938144	-0.064293835	3.104755432	H	5.318847665	0.125205921	2.670899378
C	2.601462958	0.042503271	2.970737586	H	1.555846714	-1.47236967	-1.730946127
C	3.664733585	-1.605684464	1.466787145	H	3.090995315	-2.094305725	-1.081069145
C	4.750683085	0.612819391	1.857666767	H	3.001901775	-1.589871819	-2.781493069
C	2.650815501	-1.350278806	-1.760843861	H	4.942527034	1.220244453	-1.276189696
C	4.576826513	0.210426959	-1.53133898	H	4.877456583	0.004012444	-2.575324267
C	-3.615670282	-1.651935354	1.584383965	H	5.108814607	-0.521245789	-0.903971617
C	-4.693644817	0.541867526	2.126140681	H	-2.680406422	-2.182022679	1.334567413
C	-2.74858265	-1.205281663	-1.70365756	H	-4.345981633	-1.827487885	0.778584615
C	-4.707237338	0.268821657	-1.248520526	H	-4.032638736	-2.12034336	2.493934441
H	-1.357530955	3.422798731	-0.913257148	H	-4.555982178	1.594419581	2.426622828
H	-1.110005371	4.079924887	0.700523157	H	-5.204322622	0.035056508	2.965415643
H	1.133570952	4.081884279	0.530390726	H	-5.379465117	0.51489607	1.266762181
H	1.211175144	3.370189715	-1.079060751	H	-1.651887809	-1.268094963	-1.79387977
H	-3.3849545	2.841460722	0.233245144	H	-3.195959812	-1.414308282	-2.692696991
H	-2.53264022	2.542141441	1.756904302	H	-3.071302119	-2.003657812	-1.019059249
H	2.647511867	2.584505383	1.487254723	H	-5.083179874	1.252905989	-0.918389372
H	3.341327379	2.805195642	-0.125077904	H	-5.174576193	-0.507998398	-0.624330868
H	1.303857465	0.997626539	-2.345427218	H	-5.07287483	0.104129353	-2.278773882
H	2.669342676	0.677354138	-3.4544025				
			PMe_3				
P	0.144036134	-0.435898055	-0.42111999	H	2.424268235	0.464970621	-0.5878414
C	1.971986474	-0.418372004	-0.109338128	H	2.442124792	-1.309392746	-0.554785187

C	-0.298271819	1.006017339	0.656582869	H	2.209607418	-0.394613895	0.969991173
C	-0.299998363	-1.811148122	0.738741696	H	0.070168945	-2.765426258	0.329223248
H	0.097489606	1.931658407	0.20719046	H	-1.394547737	-1.891939221	0.833806845
H	0.118459511	0.907964468	1.675890991	H	0.136387018	-1.668517522	1.744157223
H	-1.392390214	1.112036987	0.7284702				

transition state

Os	-0.073840674	0.369449331	0.417357479	H	-2.26698353	1.286468507	3.322588094
P	-2.434166127	0.726239224	0.413086833	H	2.1295663	0.954994125	3.199478525
P	2.289207987	0.64697198	0.270902671	H	3.160051594	-0.384336401	3.784234673
N	-0.079286093	2.412072606	0.225351448	H	1.689987762	-0.71855693	2.809621783
N	-0.267882346	-1.364747112	0.560270991	H	3.024377896	-2.088943964	1.169903372
C	-1.261741616	3.231432702	0.056622059	H	4.368136024	-1.8164928	2.309842259
C	-2.528363276	2.565181636	0.587624631	H	4.612845826	-1.496557533	0.587215378
C	1.116182324	3.184165933	-0.040616004	H	4.358385851	1.894716047	2.284504879
C	2.391613495	2.492588008	0.430413455	H	5.267079577	1.004815777	1.033271075
C	3.410460341	0.004186352	1.674045033	H	5.250780432	0.423682431	2.710943266
C	3.058082254	0.226869192	-1.413605615	H	1.690692686	-1.461356073	-1.625626661
C	-3.415147807	0.057782392	1.897252203	H	3.317054429	-1.932166272	-1.072020219
C	-3.319096527	0.316361743	-1.220145705	H	3.076805042	-1.459591348	-2.76748248
C	2.331763342	1.083209752	-2.451310221	H	4.811594696	1.552050742	-1.327791843
C	-2.773808845	1.289859961	-2.264057607	H	4.881888884	0.268632814	-2.556330689
C	-2.514703902	0.230049003	3.122172236	H	5.156649417	-0.135735885	-0.856537341
C	2.545048907	-0.032619472	2.934947602	H	-2.727829027	-1.95959428	1.401117991
C	3.874676962	-1.425900526	1.401363455	H	-4.424588065	-1.640358651	0.924641139
C	4.629954201	0.889361318	1.923688045	H	-4.020686946	-1.883911858	2.631404347
C	2.768346649	-1.240934061	-1.728371587	H	-4.61000564	1.836384128	2.409389209
C	4.553913592	0.496946574	-1.524979247	H	-5.218672691	0.299553482	3.050787846
C	-3.656813225	-1.436236566	1.688613591	H	-5.454228789	0.686663296	1.336627562
C	-4.741277	0.767470027	2.169716329	H	-1.835309747	-1.165903836	-1.798495244
C	-2.926836276	-1.092281564	-1.661598608	H	-3.418587357	-1.322150163	-2.624627353
C	-4.837374149	0.42578988	-1.179792531	H	-3.232539057	-1.867128152	-0.94202626
H	-1.398764082	3.507560069	-1.015222744	H	-5.187926364	1.416471194	-0.842377967
H	-1.131554973	4.205043985	0.57950054	H	-5.297696691	-0.342269289	-0.539090748
H	1.055973956	4.172867517	0.467077752	H	-5.235684627	0.262859357	-2.198308994
H	1.190594677	3.431380048	-1.125507969	P	0.55094604	-3.167132614	0.649723341
H	-3.440490782	2.987731122	0.129638117	C	1.72319193	-4.684692637	0.677440158
H	-2.607111769	2.747992866	1.673197612	H	2.40667228	-4.622910932	1.541098304
H	2.506483565	2.670744872	1.513850642	H	2.334097878	-4.696154583	-0.241558067
H	3.290438148	2.910465686	-0.058088167	H	1.160811999	-5.636529275	0.738137694
H	1.235669312	0.969466568	-2.376551324	C	-0.427576928	-3.793216083	-0.77731375
H	2.645164076	0.760622186	-3.460800587	H	-0.896430988	-4.765973696	-0.548211486
H	2.57720057	2.154781553	-2.360639272	H	0.256542226	-3.940127173	-1.629937949
H	-3.127642855	2.322481626	-2.107662621	H	-1.204127584	-3.072458975	-1.065873448
H	-3.122801024	0.971213687	-3.263103014	C	-0.360641134	-3.613539296	2.191206989
H	-1.669295862	1.291989477	-2.273593535	H	0.327734612	-4.109299179	2.893646547
H	-1.560384413	-0.308839659	3.004232018	H	-1.194547566	-4.307959429	1.988723727
H	-3.040598584	-0.163587498	4.011586876	H	-0.768312801	-2.70796701	2.665307079

7

Os	-0.006148493	0.377652456	0.362921846	H	-2.142884015	1.28623873	3.184016814

P	-2.332157079	0.645512204	0.31332203	H	2.157099509	1.192532164	3.23536785
P	2.324991656	0.642391912	0.342578639	H	3.041687951	-0.190508316	3.936542574
N	-0.003014972	2.320542823	0.199931838	H	1.566795225	-0.452243711	2.941132569
N	-0.009645924	-1.602916244	0.441216132	H	2.767090068	-2.010248217	1.378506961
C	-1.185112772	3.151617033	-0.028683896	H	4.103654012	-1.867610719	2.559402486
C	-2.478441519	2.496025676	0.422327358	H	4.434815121	-1.638009345	0.833379321
C	1.185492701	3.157676929	0.039063684	H	4.492022155	1.854965619	2.327146817
C	2.464169511	2.488453121	0.510576245	H	5.355515994	0.777063781	1.199167323
C	3.375624417	0.027753486	1.812029513	H	5.204240007	0.341323272	2.913081918
C	3.210257941	0.257354802	-1.302390737	H	1.80228552	-1.361207745	-1.676316592
C	-3.367529558	0.069659944	1.809671373	H	3.360809261	-1.913325688	-1.011995065
C	-3.223694773	0.208450208	-1.315194249	H	3.276036031	-1.38746142	-2.708271313
C	2.577595105	1.176157727	-2.348414032	H	5.015184777	1.486745726	-1.032095466
C	-2.597621062	1.094060609	-2.393487508	H	5.092267348	0.291364969	-2.348546272
C	-2.464115345	0.241260513	3.032505523	H	5.252725247	-0.248109536	-0.672423663
C	2.481663186	0.154692065	3.046935472	H	-2.743737253	-1.972356301	1.422567015
C	3.687571393	-1.453000415	1.62269772	H	-4.422113511	-1.632596857	0.891843018
C	4.670366586	0.799913012	2.059457748	H	-4.064503973	-1.812747787	2.619260293
C	2.891438582	-1.184532827	-1.690990797	H	-4.496946952	1.899755289	2.284764054
C	4.718647118	0.463337446	-1.321340887	H	-5.187574262	0.395617876	2.919405644
C	-3.666444002	-1.418960095	1.665788049	H	-5.360693155	0.782224035	1.195676609
C	-4.667235931	0.836016902	2.047926003	H	-1.812425362	-1.410007049	-1.662351877
C	-2.90272179	-1.242059332	-1.667264831	H	-3.298391922	-1.47537633	-2.673714436
C	-4.73249911	0.410204526	-1.326479878	H	-3.357484171	-1.955919451	-0.96309431
H	-1.236191807	3.424936305	-1.106386332	H	-5.029833095	1.439038938	-1.058601804
H	-1.064359987	4.118615538	0.503041686	H	-5.257095517	-0.287345174	-0.654877547
H	1.04386915	4.106769726	0.597324357	H	-5.115520955	0.212167584	-2.345446553
H	1.272642924	3.46827276	-1.026111313	P	-0.02347681	-3.149210323	0.551152015
H	-3.35376301	2.891585542	-0.122492007	C	1.376873732	-4.072625258	-0.207784663
H	-2.644481786	2.724592774	1.488443063	H	2.324826707	-3.753652149	0.252891554
H	2.594039658	2.680462286	1.589037845	H	1.420291503	-3.836900046	-1.283553481
H	3.356323458	2.903413041	0.008738372	H	1.264156064	-5.162505282	-0.08450334
H	1.475260942	1.103723045	-2.336770195	C	-1.442905051	-4.076012954	-0.173836556
H	2.934105815	0.878794161	-3.351810189	H	-2.378481323	-3.774943347	0.322534781
H	2.857879031	2.233793708	-2.205088698	H	-1.312001186	-5.16522925	-0.062400153
H	-2.873809047	2.156772863	-2.284658866	H	-1.525051502	-3.834109628	-1.245813295
H	-2.960857435	0.763723237	-3.38402848	C	-0.018671202	-3.709276767	2.288083765
H	-1.495478724	1.018680867	-2.386246287	H	0.896447444	-3.341436423	2.777809212
H	-1.546511144	-0.363929838	2.939896999	H	-0.067350635	-4.807204195	2.373114661
H	-3.015867537	-0.076957857	3.937303165	H	-0.88398819	-3.261061354	2.800433652

3.4 QDPT/NEVPT2/CASSCF(14,10) on **29**

Starting from the X-ray structure (see Part II Section 3.1.1), the $S = 0$ and $S = 1$ spin states were optimized and verified according to the procedure described in Section 3.1 with the following exceptions:

- To account for relativistic effects, the ZORA approximation was employed and the corresponding recontracted ZORA-def2 basis sets were used for all elements, which included the segmented all-electron relativistically contracted (SARC) basis set for Rhenium.[264]
- The RI and RIJCOSX approximations were used in combination with the decontracted SARC/J auxiliary basis sets.

Two principal geometries (C_1 symmetry, derived from X-ray structre and C_s symmetry, obtained by rotation of one *i*Pr group and symmetrized using the ChemCraft software package) were compared for both spin states:

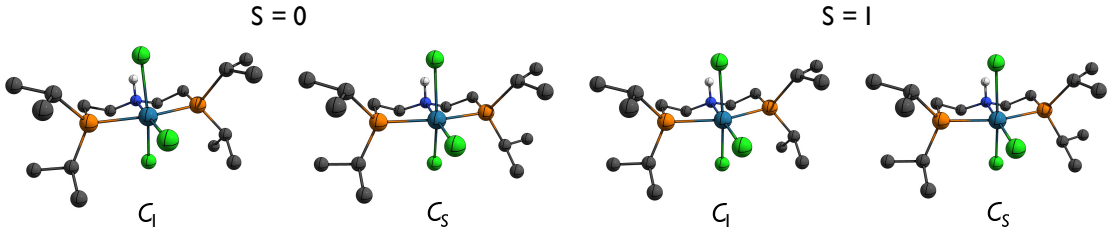

Fig. 3.3. DFT-optimized geometries of **29** for C_1 and C_S symmetric singlet and triplet states.

Tab. 3.8. Geometry parameters and relative *Gibb's* free energy of the obtained isomers of **29**.

	$S=0$		$S=1$	
	C_1	C_S	C_1	C_S
d(Re-N) / Å	2.219	2.2218	2.215	2.212
d(Re-Cl1) / Å	2.341	2.344	2.373	2.384
d(Re-Cl2) / Å	2.408	2.405	2.426	2.418
dRe-Cl3) / Å	2.381	2.379	2.390	2.38
$\measuredangle$(N1-Re-Cl1) / °	178.1	178.8	179.2	179.6
$\measuredangle$(Cl2-Re-Cl3) / °	161.4	161.6	168.3	168.4
ΔG_{rel} / kJ mol^{-1}	36.5	36.9	0.0	0.5

While the coordination geometry and energy is basically invariant between C_1 and C_S symmetry, comparison of the singlet vs. triplet states reveals the singlet to be significant higher in energy and feature a slightly different coordination environment. Hence, the $S = 1, C_1$ symmetric geometry was chosen for higher-level electron structure calculations.
For the QDPT based calculation of spin-orbit eigenstates described in Section 3.1.2, the ZORA-def2-TZVP basis sets (SARC-ZORA-TZVP for Re) and the RI-JK and RIJCOSX approximations were used along with the def2-TZVP/C auxiliary basis sets and a fine grid (GridX6 in ORCA nomenclature). The relativistic options to account for picture change effects was enabled (i.e. %ref picturechange true end). No frozen core approximation was employed and the convergence criteria were tightened by the ORCA keyword *VeryTightSCF*.

Several attempts were made to converge the calculations on the C_S symmetric triplet using symmetric constrains, however, all attempts of basis set projection from the def2-SVP to def2-TZVP failed with extreme changes in the active space.
Starting orbitals were obtained from QROs derived from the geometry optimizations at the PBE/D3BJ/RI/ZORA-def2-SVP level of theory. After an initial CASSCF(4,5) calculation including only the d-orbitals, the occupied space was inspected to identify the ligand orbitals balancing the active space and they were included in the calculation as well.
The final evaluated CASSCF(14,10) active space was corrected by strongly contracted NEVPT2 calculations[265–267] for dynamic correlation and these energies entered QDPT treatment via a mean-field operator[268] and are thus corrected also for second order effects.

3.4.1 DFT-optimized geometries

Tab. 3.9. XZY geometry data for the DFT-derived structures of **29** for the C_1 and C_S symmetry, optimized as singlet and triplet each.

	X	Y	Z		X	Y	Z
			C_1, S=0				
Re	2.527578799	8.66342235	9.317310602	H	0.342204683	4.90696198	6.813963567
Cl	0.193805405	8.741058271	9.479827063	H	0.863646734	6.61133455	7.001520683
P	2.750457286	6.309157811	9.386863735	H	0.058776385	5.783963005	8.348060642
N	4.743754073	8.593639643	9.236730327	C	5.359979292	9.812840423	8.64386167
C	5.284897002	7.308783335	8.712592381	H	5.136589075	9.793746951	7.561955178
H	6.387066205	7.291377771	8.838187423	H	6.46184916	9.769256691	8.764950667
H	5.064441496	7.283201823	7.630752879	C	4.785559628	11.06896544	9.300860602
P	2.898180697	11.00860807	9.2591073	H	5.194439597	11.97521041	8.8198394
Cl	3.030434381	8.710864202	11.67214347	H	5.07743055	11.10490825	10.36812653
C	4.631221296	6.129463521	9.433700131	C	2.481325264	11.93030541	7.668759833
H	4.909286676	6.143215808	10.50559171	H	3.058314069	11.32757355	6.937663479
H	4.989319754	5.172479249	9.016810916	C	2.932176613	13.39106897	7.578208417
C	2.250431913	5.391706578	10.95506741	H	2.304368273	14.04541322	8.208226835
H	2.649513579	6.070354815	11.73565838	H	2.835287735	13.75288611	6.536880039
Cl	2.799143833	8.630161831	6.952208244	H	3.984102877	13.53936948	7.880605953
C	2.872570441	4.001791954	11.12249991	H	4.920502447	8.616990545	10.25222412
H	2.58296644	3.572835898	12.1005337	C	0.998327714	11.75947797	7.306635132
H	3.975911245	4.020253055	11.086694	H	0.667817267	10.71508111	7.432698956
H	2.519838689	3.297347456	10.3460788	H	0.832546094	12.05060124	6.252812242
C	0.722500792	5.364021007	11.0932451	H	0.350085344	12.39584595	7.933571286
H	0.439213741	5.02628471	12.10747302	C	2.413755356	12.0384822	10.75646899
H	0.263887042	4.659760971	10.37459676	H	2.669862216	11.31930897	11.56209621
H	0.280016438	6.361731366	10.92533869	C	0.892567495	12.24455609	10.7854497
C	2.152920388	5.165451828	7.999536031	H	0.349156535	11.31021225	10.55694723
H	2.047775783	4.166659857	8.468872867	H	0.576863801	13.01299288	10.05686454
C	3.130050304	5.04703926	6.822182015	H	0.575501264	12.59065891	11.78673389
H	4.112503041	4.640950464	7.119499228	C	3.185966705	13.33989465	11.00446561
H	3.283115077	6.029270482	6.342360512	H	2.931676309	13.73604877	12.00611057

H	2.711796331	4.362619018	6.060093521	H	2.930853179	14.12233922	10.27007373
C	0.772482145	5.641707746	7.520092728	H	4.280587051	13.19813265	10.98020444

C_1, S=1

Re	-0.078958927	-0.019850918	0.065044195	H	-2.190804712	-3.859668751	-2.320467812
Cl	-2.450334257	0.052742069	0.101005993	H	-1.741781797	-2.1321891	-2.143908745
P	0.19449035	-2.396544045	0.243679378	H	-2.501537146	-2.986189898	-0.789452946
N	2.134879177	-0.086252502	0.06063405	C	2.754900167	1.121765502	-0.542317038
C	2.689036254	-1.366915827	-0.451201957	H	2.494021111	1.112916048	-1.616446803
H	3.794279053	-1.369659338	-0.346142369	H	3.860235364	1.064649038	-0.456562953
H	2.447108925	-1.413496326	-1.527827039	C	2.222378181	2.380595381	0.143624735
P	0.342717301	2.352371707	0.107095423	H	2.640973473	3.288003013	-0.326000051
Cl	0.280481593	0.033698119	2.464157723	H	2.52586605	2.392025386	1.208517806
C	2.069305892	-2.543512015	0.303776995	C	-0.091993556	3.257953232	-1.48401213
H	2.351098732	-2.498132403	1.37403047	H	0.452717946	2.628323993	-2.217263061
H	2.438813155	-3.505073483	-0.091950765	C	0.401008611	4.704517943	-1.586970048
C	-0.332489349	-3.279914097	1.816179494	H	-0.195076397	5.378860363	-0.947815457
H	0.073392151	-2.596340086	2.588697674	H	0.290390552	5.061108981	-2.628327717
Cl	0.052895505	-0.03919481	-2.321509524	H	1.463316388	4.824976652	-1.309833356
C	0.271785621	-4.675560874	1.999323555	H	2.300302911	-0.054009343	1.081884417
H	-0.022709672	-5.087160015	2.98304258	C	-1.586936243	3.133023787	-1.813930854
H	1.375464601	-4.671083878	1.962977498	H	-1.959873304	2.106470642	-1.658906678
H	-0.090866654	-5.385613976	1.232673069	H	-1.754875794	3.406613951	-2.871728016
C	-1.861129546	-3.274777598	1.94747538	H	-2.19610481	3.812616124	-1.193298308
H	-2.151953047	-3.578740683	2.969935067	C	-0.151802762	3.349674809	1.61603128
H	-2.330708052	-3.989667586	1.247035156	H	0.126391725	2.626445784	2.410665538
H	-2.281454682	-2.272188701	1.751742491	C	-1.676938924	3.517419759	1.662828243
C	-0.386474434	-3.524574797	-1.156139561	H	-2.198112155	2.572949317	1.423200736
H	-0.441550565	-4.530465732	-0.692963559	H	-2.019118515	4.291407711	0.952637198
C	0.588304141	-3.580152138	-2.338572547	H	-1.989416521	3.835765348	2.674391774
H	1.586676737	-3.957555001	-2.056964584	C	0.600499629	4.66291773	1.860669068
H	0.696957398	-2.581868485	-2.798793112	H	0.358089208	5.04501565	2.870384422
H	0.187060588	-4.261832509	-3.111551375	H	0.315230553	5.446396338	1.138259148
C	-1.788811661	-3.102776264	-1.621452368	H	1.697104437	4.542196805	1.813400174

C_S, S=0

Re	0.045039728	-0.093309332	9.69147E-05	H	0.166078445	2.585640278	5.146032363
Cl	2.360636885	-0.456916628	1.84859E-05	H	0.523604676	0.861543749	5.391788772
P	-0.249834795	-0.056037523	2.352269964	H	-1.124518613	1.376020432	4.940877405
N	-2.153216433	0.203266311	0.000140099	C	-2.673847478	0.820778111	-1.250998798
C	-2.673939444	0.820669633	1.251296798	H	-2.346941801	1.876343335	-1.24744745
H	-3.783168416	0.807858594	1.238913105	H	-3.783082557	0.807761828	-1.238962244
H	-2.346861299	1.876189754	1.247922331	C	-2.129299673	0.081693314	-2.47360951
P	-0.249680525	-0.055521255	-2.352211859	H	-2.463407179	0.577221306	-3.402305222
Cl	-0.669819488	-2.39002047	-4.23609E-05	H	-2.52152714	-0.953381775	-2.495265277
C	-2.129565245	0.081456343	2.473895242	C	0.349883284	1.463551621	-3.292752229
H	-2.522185542	-0.953463935	2.495707361	H	-0.162366944	2.262789087	-2.718439794
H	-2.463325269	0.577210096	3.40258274	C	-0.05163231	1.570108764	-4.766887048
C	0.113945104	-1.619236902	3.333329102	H	0.522134507	0.863262024	-5.391707999
H	-0.248710515	-2.375761774	2.60652123	H	0.165290205	2.587343778	-5.144816124
Cl	-0.001324297	2.28505433	0.000668425	H	-1.125520206	1.377982368	-4.939312387

C	-0.634635432	-1.819932546	4.656457808	H	-2.429219441	-0.790045257	8.1303E-05
H	-0.473902928	-2.852829492	5.020117122	C	1.858099893	1.672898281	-3.090010128
H	-1.724895875	-1.677419702	4.556655891	H	2.148758807	1.537693116	-2.034947244
H	-0.276011686	-1.137511973	5.44528451	H	2.141484183	2.696124597	-3.399045878
C	1.629942861	-1.811925492	3.482074241	H	2.451288795	0.96613227	-3.695743565
H	1.852083933	-2.85168185	3.786208385	C	0.114187119	-1.618342198	-3.333684549
H	2.046828719	-1.146323865	4.259601976	H	-0.247875542	-2.375214537	-2.606947671
H	2.161914409	-1.610029811	2.535143663	C	1.63016612	-1.810516077	-3.483233596
C	0.349729075	1.462842091	3.293299732	H	2.16246769	-1.608900135	-2.536436628
H	-0.163146331	2.262211917	2.719730975	H	2.046534019	-1.144427071	-4.260631592
C	1.857777464	1.672585769	3.089632857	H	1.852422192	-2.850065764	-3.787985479
H	2.147802395	1.537673731	2.034349933	C	-0.634977409	-1.818853062	-4.656525583
H	2.451457899	0.965761539	3.694801289	H	-0.473406629	-2.851329177	-5.021006827
H	2.141238161	2.695779481	3.398711848	H	-0.277545226	-1.135502211	-5.4450961
C	-0.050814232	1.568532111	4.767739018	H	-1.725319642	-1.677545169	-4.555897749

C_S, S=1

Re	0.071712539	-0.015441077	-2.21098E-06	H	0.120549687	2.600175732	5.131964844
Cl	2.440421232	-0.281203505	-6.26882E-05	H	0.447246785	0.874254863	5.4057981
P	-0.273726017	-0.065183363	2.380757448	H	-1.183212138	1.407950263	4.910424725
N	-2.127892727	0.216441201	0.000113528	C	-2.651405248	0.837332301	-1.244582414
C	-2.651198948	0.837101218	1.244910142	H	-2.291189639	1.882392581	-1.254404816
H	-3.760928121	0.857364042	1.222128794	H	-3.761135473	0.857559742	-1.221747524
H	-2.290918658	1.882141549	1.254820359	C	-2.148188725	0.070113873	-2.468034446
P	-0.274193196	-0.064355713	-2.380743278	H	-2.497812836	0.549038525	-3.399430832
Cl	-0.51344415	-2.361685496	-8.099E-05	H	-2.546804672	-0.963065041	-2.459884795
C	-2.147812887	0.069604734	2.468220634	C	0.334330052	1.461514364	-3.298345835
H	-2.546399152	-0.963587102	2.460045287	H	-0.15572114	2.255495747	-2.698214275
H	-2.497418398	0.548493283	3.399638317	C	-0.103856781	1.583428074	-4.761216205
C	0.10830975	-1.634313922	3.333635897	H	0.446247137	0.875693473	-5.405495739
H	-0.265817112	-2.3830658	2.604641857	H	0.119470672	2.601607922	-5.13163943
Cl	0.171918964	2.366070944	3.94839E-05	H	-1.184215145	1.409359714	-4.910036854
C	-0.622337859	-1.837769853	4.665835765	H	-2.401201273	-0.781580122	0.000101836
H	-0.459822049	-2.872473717	5.02259977	C	1.85002071	1.648847513	-3.133779378
H	-1.713452546	-1.690787725	4.580930548	H	2.177248863	1.481145543	-2.093700873
H	-0.249797827	-1.159477723	5.452012689	H	2.12809543	2.678917911	-3.423048111
C	1.627198897	-1.827201679	3.448054346	H	2.414319296	0.956898122	-3.782422585
H	1.853425088	-2.872194005	3.729191884	C	0.107588704	-1.633136403	-3.334018617
H	2.059513236	-1.174898677	4.228042862	H	-0.266554576	-2.381904762	-2.605052915
H	2.137719105	-1.60920169	2.492500616	C	1.626445485	-1.825982465	-3.448578846
C	0.335159021	1.460285228	3.298605531	H	2.136999392	-1.608044195	-2.493033577
H	-0.154891478	2.254319346	2.698524656	H	2.058771678	-1.173665783	-4.22856536
C	1.850870018	1.647512891	3.133999159	H	1.852574966	-2.870970123	-3.729782783
H	2.178047034	1.479844184	2.093890931	C	-0.623180913	-1.836399465	-4.666220773
H	2.415213038	0.955531339	3.782582706	H	-0.460725508	-2.871093056	-5.022997
H	2.128974657	2.67756524	3.423283607	H	-0.250705426	-1.158077758	-5.452415939
C	-0.10286795	1.58202774	4.761539583	H	-1.714291837	-1.689334006	-4.581296814

3.4.2 CASSCF state composition

Tab. 3.10. CASSCF state wavefunctions of the first three triplets and singlets, listing the main contributing active space occupations and their weight.

Triplets	
ROOT 0: E = -19942.24980286 Eh	
Weight	Orbital occupation
0.87176	[2222221100]
0.08309	[2222212100]
0.00603	[2212221110]
0.00472	[2212221101]
0.00333	[2122221110]
0.00322	[2122221101]
ROOT 1: E = -19941.9972794320 Eh 0.142 eV 1145.3 cm^{-1}	
0.86991	[2222212100]
0.08256	[2222221100]
0.00707	[2212212110]
0.00538	[2212212101]
0.00415	[2122212110]
0.00365	[2122212101]
ROOT 2: E = -19941.9759164604 Eh 0.723 eV 5834.0 cm^{-1}	
0.95834	[2222211200]
0.00511	[2212211201]
0.00353	[2212211210]
0.00324	[2122211201]
0.00309	[2222211002]
Singlets	
ROOT 0: E = -19941.9768947318 Eh	
0.84551	[2222222000]
0.05281	[2222220200]
0.03468	[2222202200]
0.01106	[2222211110]
0.00852	[2212222010]
0.00525	[2122222010]
0.00472	[2222122100]
0.00471	[2222221100]
0.00309	[2212122110]
0.00297	[2212222001]
ROOT 1: E = -19941.9712235491 Eh 0.154 eV 1244.7 cm^{-1}	
0.83937	[2222221100]
0.09856	[2222212100]
0.00702	[2222210210]
0.00512	[2222212010]
0.00429	[2222222000]
0.00411	[2212221110]

0.00366	[2222221001]
0.00323	[2212221101]
ROOT 2: E = -19941.9641043707 Eh 0.348 eV 2807.2 cm^{-1}	
0.84062	[2222212100]
0.09781	[2222221100]
0.0073	[2222221010]
0.00683	[2222201210]
0.00515	[2212212110]
0.00383	[2212212101]
0.00327	[2222212001]
0.0029	[2122212110]

3.4.3 QDPT state eigenvectors

Tab. 3.11. QDPT eigenvectors of the first 11 states, in the basis of the non-relativistic states.

QDPT eigenvectors					
	Energy	Weight	Spin	Root	M_S
STATE 0:	0				
		0.169538	1	0	1
		0.044763	1	1	1
		0.018389	1	2	1
		0.113456	1	0	0
		0.258238	1	1	0
		0.169538	1	0	-1
		0.044763	1	1	-1
		0.018389	1	2	-1
		0.104686	0	0	0
		0.020309	0	5	0
STATE 1:	1603.8502				
		0.074715	1	0	1
		0.136609	1	1	1
		0.453287	1	0	0
		0.096849	1	1	0
		0.074715	1	0	-1
		0.136609	1	1	-1
STATE 2:	2150.5038				
		0.463774	1	0	1
		0.463774	1	0	-1
		0.023146	0	2	0
STATE 3:	2617.1434				
		0.460602	1	1	1
		0.015706	1	2	0
		0.460602	1	1	-1
		0.032307	0	1	0
STATE 4:	3614.3358				

		0.09905	1	0	1
		0.156154	1	1	1
		0.229638	1	0	0
		0.19885	1	1	0
		0.09905	1	0	-1
		0.156154	1	1	-1
		0.027224	0	3	0
STATE 5:	3684.2718				
		0.112441	1	0	1
		0.129705	1	1	1
		0.145919	1	0	0
		0.323332	1	1	0
		0.112441	1	0	-1
		0.129705	1	1	-1
		0.017375	0	4	0
STATE 6:	5572.2206				
		0.048254	1	2	1
		0.045336	1	1	0
		0.048254	1	2	-1
		0.797872	0	0	0
STATE 7:	7557.4225				
		0.033836	1	2	1
		0.266439	1	2	0
		0.033836	1	2	-1
		0.620306	0	1	0
STATE 8:	8082.1135				
		0.170442	1	2	1
		0.090887	1	2	0
		0.170442	1	2	-1
		0.52679	0	2	0
STATE 9:	9847.189				
		0.018625	1	0	1
		0.387356	1	2	1
		0.011857	1	0	0
		0.037351	1	1	0
		0.018625	1	0	-1
		0.387356	1	2	-1
		0.061411	0	0	0
		0.01712	0	5	0
STATE 10:	10856.109				
		0.026449	1	1	1
		0.072711	1	2	1
		0.452344	1	2	0
		0.026449	1	1	-1
		0.072711	1	2	-1
		0.312257	0	1	0
STATE 11:	11101.1524				

0.024542	1	0	1
0.188459	1	2	1
0.121153	1	2	0
0.024542	1	0	-1
0.188459	1	2	-1
0.416986	0	2	0

3.4.4 CASSCF, NEVPT2 and QDPT state energies

Tab. 3.12. State energies of the first 40 states derived from CASSCF, NEVPT2 and QDPT calculations, given in cm^{-1}

	CASSCF			NEVPT2			QDPT	
STATE	ROOT	MULT	ΔE / cm^{-1}	ROOT	MULT	ΔE / cm^{-1}	ΔE / cm^{-1}	oscillator strength
0:	0	3	0	0	3	0	0	
1:	1	3	1145.3	1	3	460.6	1603.85	0.00075
2:	0	1	5619.3	0	1	2618.1	2150.5	0.00021
3:	2	3	5834	1	1	6058.8	2617.14	0.00031
4:	1	1	6864	2	1	6811.9	3614.34	0.0215
5:	2	1	8426.4	2	3	7202.3	3684.27	0.19496
6:	3	1	12058.6	3	1	12387.5	5572.22	0.00128
7:	4	1	13452.8	4	1	13840	7557.42	0.00049
8:	0	5	16770.1	5	1	18519.3	8082.11	0.00238
9:	5	1	19800.9	0	5	19890.9	9847.19	0.00004
10:	1	5	23404.6	1	5	24233	10856.11	0.00295
11:	3	3	24884.2	3	3	24775.3	11101.15	0.00465
12:	4	3	26011.5	4	3	26333.7	15018.53	0.0077
13:	5	3	28054.7	6	1	29646.1	16441.23	0.00208
14:	6	3	29488.3	5	3	29658.6	21568.53	0.02906
15:	7	3	30087.5	6	3	29895.9	22633.56	0.00023
16:	8	3	30596	7	3	31051.6	22648.37	0.00431
17:	6	1	30614.7	8	3	31383.9	22798.44	0.0002
18:	7	1	31973.5	7	1	31432.2	22877.06	0.00011
19:	9	3	32546.4	10	3	33135.4	22924.69	0.00008
20:	10	3	33649.3	9	3	33329.5	26843.64	0.02648
21:	8	1	34540.5	16	3	33365.4	26935.44	0.00001
22:	9	1	34879.8	12	1	33787.8	26953.3	0.00035
23:	11	3	36040.3	15	3	33788.3	27105.64	0.00051
24:	12	3	36201.1	8	1	34739	27159.22	0.00356
25:	10	1	37292.1	12	3	34766.2	27331.81	0.01788
26:	13	3	37479.1	11	3	34816.1	27600.38	0.00011
27:	14	3	38338.7	13	3	35405.7	27891.72	0.00099
28:	11	1	38522.8	9	1	35672	29268.85	0.0002
29:	15	3	39410.2	10	1	36484.6	30029.04	0.00295
30:	12	1	39755.5	14	3	36726.5	30117.37	0.00261
31:	16	3	39857.6	17	1	37837.8	30617.89	0.00301
32:	17	3	39919.5	22	3	37959	31769.08	0.0277
33:	13	1	40685.3	13	1	38277.1	32562.44	0.00052
34:	14	1	40868.8	11	1	38642.9	32797.66	0.04795

35:	18	3	41325.8	30	1	38787.4	33020.2	0.02169
36:	19	3	42641.6	19	3	38814.4	33154.7	0.00398
37:	15	1	42671.1	16	1	38880.6	33510.65	0.09476
38:	20	3	42947.5	17	3	38975.7	33684.73	0.07304
39:	16	1	43130.3	18	1	39160.3	34194.4	0.00426
⋮	⋮	⋮	⋮	⋮	⋮	⋮	⋮	⋮

3.4.5 Simulated influence of magnetic field on excitation between QDPT states $|0\rangle \rightarrow |4\rangle$ and $|0\rangle \rightarrow |5\rangle$

Tab. 3.13. Simulated influence of an external magnetic field on the excitation energies of the $|0\rangle \rightarrow |4\rangle$ and $|0\rangle \rightarrow |5\rangle$ excitations.

			Magnetic field along x-axis			
QDPT excitation energies	$B_x = 0$ T	$B_x = 2$ T	$B_x = 4$ T	$B_x = 6$ T	$B_x = 8$ T	$B_x = 10$ T
$\Delta E_{\|0\rangle \rightarrow \|4\rangle}$	3614.3358	3614.3369	3614.3402	3614.3457	3614.3534	3614.3633
$\Delta E_{\|0\rangle \rightarrow \|5\rangle}$	3684.2718	3684.2730	3684.2768	3684.2832	3684.2921	3684.3035
			Magnetic field along y-axis			
	$B_y = 0$ T	$B_y = 2$ T	$B_y = 4$ T	$B_y = 6$ T	$B_y = 8$ T	$B_y = 10$ T
$\Delta E_{\|0\rangle \rightarrow \|4\rangle}$	3614.3358	3614.3240	3614.2885	3614.2294	3614.1469	3614.0410
$\Delta E_{\|0\rangle \rightarrow \|5\rangle}$	3684.2718	3684.2834	3684.3184	3684.3766	3684.4580	3684.5623
			Magnetic field along z-axis			
	$B_z = 0$ T	$B_z = 2$ T	$B_z = 4$ T	$B_z = 6$ T	$B_z = 8$ T	$B_z = 10$ T
$\Delta E_{\|0\rangle \rightarrow \|4\rangle}$	3614.3358	3614.3373	3614.3419	3614.3494	3614.3599	3614.3734
$\Delta E_{\|0\rangle \rightarrow \|5\rangle}$	3684.2718	3684.2731	3684.2772	3684.2840	3684.2935	3684.3057

3.5 DFT and TDDFT calculations on the μ–N_2 bridged Re-dimer **36**

The DFT and TDDFT calculations presented in Section 3.3.1 of this thesis were performed by *Dr. Markus Finger* and *Prof. Dr. Vera Krewald*, respectively. The details of these calculations might therefore differ from the above described general procedure and are explained in detail in the corresponding publication.[269]

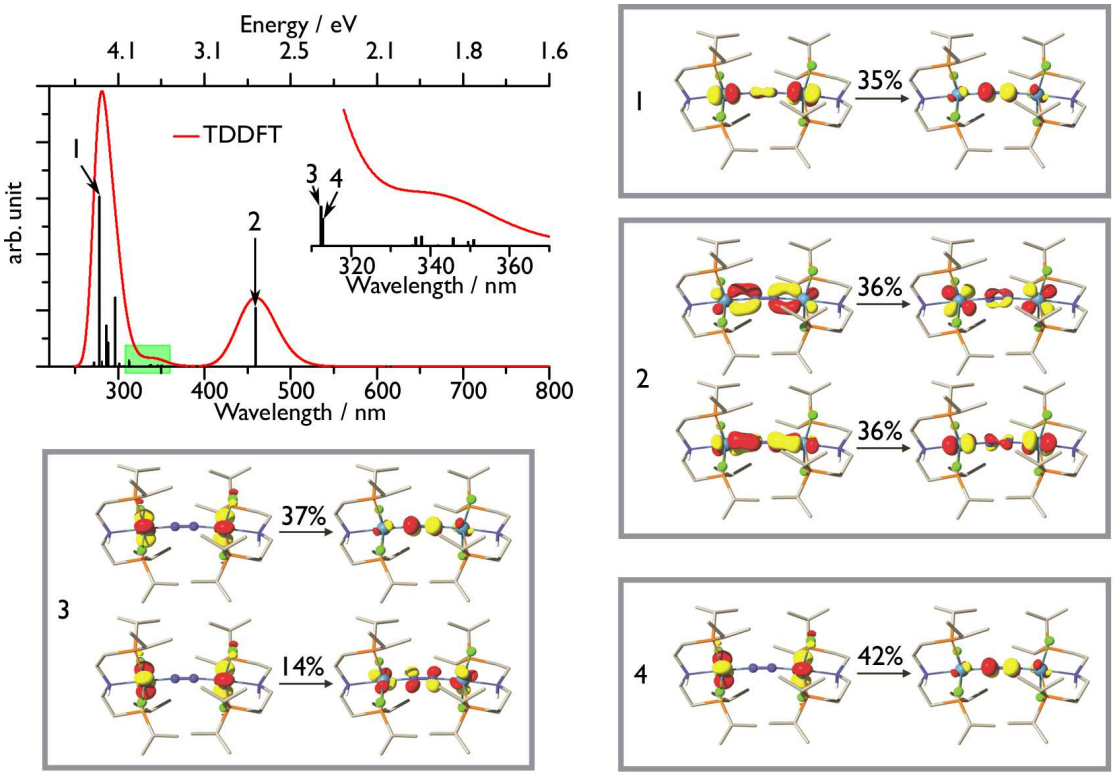

Fig. 3.4. TDDFT calculated electronic absorption spectrum of **36** with the most relevant transitions marked (1-4) and the corresponding natural transition orbitals of the most dominant contributions (weight in % given on the arrows).

3.6 Comparing the *syn* and *anti* isomers of [Re(N)Cl(HPNP^{iPr})]$^+$

DFT computations were performed with ORCA 4.0 according to the procedure described in Section 3.1. The two possible isomers which might be expected from chloride abstraction from **37**, *syn*-[Re(N)Cl(HPNP^{iPr})]$^+$ and *anti*-[Re(N)Cl(HPNP^{iPr})]$^+$, where *syn* / *anti* refers to the orientation of the N−H bond to the Re≡N bond, have been calculated and are found to be almost thermoneutral, well reflecting the appearance of two signals in the $^{31}P\{^1H\}$ NMR spectrum (see Section 3.3.2).

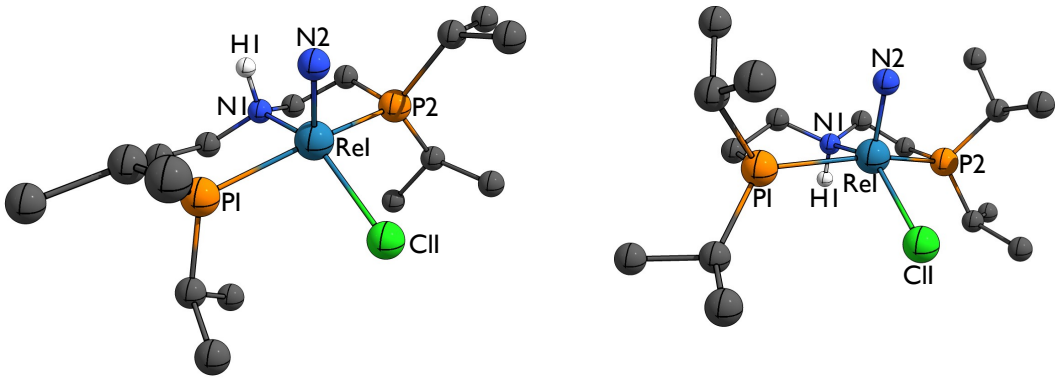

Fig. 3.5. DFT optimized structures of *syn*-[Re(N)Cl(HPNP^{iPr})]$^+$ (*left*) and *anti*-[Re(N)Cl(HPNP^{iPr})]$^+$ (*right*) (PBE/D3BJ/RI/def2-SVP). Carbon-bonded hydrogen atoms are omitted for clarity.

Tab. 3.14. Structural parameters and thermochemistry data for both isomers of [Re(N)Cl(HPNP^{iPr})]$^+$.

Distances / Å			Angles / °		
	syn	*anti*		*syn*	*anti*
Re1-N1	2.204	2.188	N1-Re1-N2	103.5	102.0
Re1-N2	1.660	1.663	N1-Re1-Cl1	144.4	144.2
Re1-Cl1	2.386	2.381	P1-Re1-P2	160.1	159.5
N1-H1	1.034	1.037	τ_5	0.26	0.26
Thermochemistry data from D3BJ-PBE0/def2-TZVPP (CPCM(CH_2Cl_2))					
$\Delta G_{anti \rightarrow syn} = 3.7\,\mathrm{kJ\,mol^{-1}}$					

3.6.1 DFT-optimized geometries

Tab. 3.15. XZY geometry data for the DFT-derived structures of *syn*-[Re(N)Cl(HPNP^{iPr})]$^+$ and *anti*-[Re(N)Cl(HPNP^{iPr})]$^+$.

	X	Y	Z		X	Y	Z
anti-[Re(N)Cl(HPNP^{iPr})]$^+$							
Re	2.485173273	6.418611957	9.825514616	H	2.010374632	4.0055001	12.14627201
Cl	0.435023642	7.208042498	10.74234263	H	1.703833952	5.053437985	13.56259999
P	3.676016195	6.5961178	11.96739671	H	2.522114743	3.475246963	13.78024342
P	1.81456204	6.92578729	7.515597672	C	4.611759493	6.701899105	7.598669245
N	4.437767162	7.034435024	9.053270228	H	4.600738084	5.596832929	7.522904712
N	2.556951759	4.764795841	9.668802168	H	5.607018561	7.059904829	7.256170607
H	4.43271385	8.069715522	9.114790416	C	3.493443911	7.328380685	6.770532352
C	5.581612567	6.568803792	9.906994869	H	3.563500637	7.001276564	5.714368183
H	6.534588218	6.955879426	9.485281868	H	3.594425968	8.435635382	6.766189139
H	5.600954261	5.463827276	9.835613562	C	0.785355021	8.426807969	7.068177144

C	5.397319269	7.029889725	11.35029718	H	1.26270949	9.224078909	7.683343053
H	5.500253468	8.135050895	11.41750194	C	0.898863772	8.800448808	5.584507991
H	6.186946742	6.60205544	11.99856471	H	1.937536942	8.989800582	5.251268545
C	3.319673525	7.949366935	13.21327828	H	0.321512977	9.728539766	5.397289113
H	3.232261856	8.848202843	12.56024843	H	0.464391056	8.015805317	4.931899007
C	4.470353344	8.157715668	14.20715968	C	-0.675308233	8.286356728	7.515337474
H	5.435457686	8.405770468	13.72475634	H	-1.184434614	9.265277316	7.406290158
H	4.622471202	7.265822229	14.84995543	H	-0.756775664	7.969655299	8.572774909
H	4.217568753	8.999347559	14.88368596	H	-1.224063361	7.563166721	6.879712079
C	1.977240746	7.741747536	13.92564922	C	1.136033494	5.450631565	6.577350456
H	1.157383716	7.532231399	13.21263277	H	0.76768608	5.891529098	5.624300201
H	1.71958119	8.660634951	14.49003482	C	2.216314249	4.409816177	6.267064297
H	2.036799226	6.914735933	14.66108531	H	1.753943561	3.55935528	5.726328872
C	3.817963669	4.974273398	12.89861329	H	2.653891371	4.000886955	7.200945161
H	4.251108836	5.272616025	13.87968281	H	3.029582189	4.798183258	5.622657307
C	4.764558385	3.98335305	12.21455455	C	-0.031969678	4.820181598	7.349227665
H	4.390848663	3.70810204	11.2073491	H	-0.799946537	5.554692585	7.650528123
H	4.801934721	3.050199406	12.81172744	H	0.336054821	4.31940447	8.266268619
H	5.803975952	4.355432958	12.128364	H	-0.520107775	4.054535637	6.712886187
C	2.430196944	4.353846534	13.11023796				

syn-[Re(N)Cl(HPNP^{iPr})]$^{+}$

Re	2.627379902	6.917532404	10.30184776	H	1.331647779	4.520651833	13.1117645
Cl	0.869136257	5.333748865	10.58719245	H	1.79237069	5.117428163	14.74616341
P	3.466818206	6.559324812	12.57973388	H	2.144118666	3.431325581	14.28346693
P	2.480381811	6.815121543	7.853504124	C	5.209995477	6.701210197	8.494666153
N	4.774356089	7.15016212	9.86349151	H	5.250785365	5.593761306	8.52675611
N	2.100843217	8.479104111	10.50311228	H	6.246496116	7.058023496	8.311760612
H	4.828757466	8.182612567	9.881480766	C	4.264294109	7.175850108	7.396343197
C	5.721277455	6.634345939	10.91375143	H	4.542961933	6.703811696	6.432641786
H	6.740081608	7.026190212	10.70487289	H	4.348686704	8.274496033	7.255924821
H	5.763869478	5.534979732	10.78218743	C	1.534777558	8.229607072	7.077544734
C	5.276230469	6.990124185	12.32895521	H	2.108631244	9.099600668	7.470693882
H	5.374262311	8.08225937	12.50625888	C	1.622466556	8.211283834	5.547686825
H	5.930725621	6.482639526	13.06596066	H	2.665106552	8.16435041	5.174962065
C	2.875410046	7.820193749	13.82748252	H	1.16988949	9.137864673	5.139447352
H	3.236428284	8.761554081	13.35475233	H	1.062430565	7.358219879	5.115718402
C	3.55306791	7.645161813	15.19089443	C	0.099809232	8.347165182	7.603602555
H	4.659284306	7.624216364	15.12114749	H	-0.337717568	9.300631596	7.244667293
H	3.220484415	6.716709487	15.69694402	H	0.065740635	8.350975023	8.710181392
H	3.278553272	8.492321316	15.85212786	H	-0.549047615	7.528491472	7.238662589
C	1.346484265	7.900603819	13.9091038	C	2.084284537	5.215609987	6.971839101
H	0.886985176	8.011468031	12.90874313	H	2.414590135	5.381760974	5.921791999
H	1.063577478	8.78564959	14.51411342	C	2.909384271	4.072163936	7.581484936
H	0.90449718	7.011515225	14.39644928	H	2.661703661	3.121923089	7.066951845
C	3.484054934	4.857667445	13.35374386	H	2.665709309	3.937111172	8.655669839
H	4.212184239	4.938219631	14.19164601	H	4.002104329	4.221305429	7.470188984
C	3.993904641	3.821432695	12.34107937	C	0.581801698	4.90905905	6.995022984
H	3.317694341	3.762815635	11.46313216	H	-0.007385197	5.64747427	6.420858752
H	4.007650589	2.817778864	12.81231225	H	0.194254037	4.874988874	8.032018141
H	5.026141455	4.024851759	11.99392841	H	0.40762243	3.916712172	6.531614933

C 2.105024884 4.472557934 13.90398425

3.7 Isomerization of $[Re(NH)Cl_2(HPNP^{iPr})]^{OTf}$

3.7.1 Method and results

All calculations were performed with ORCA 4.0 according to the procedure described in Section 3.1. Single point energies were derived with the def2-TZVPP basis sets using both the PBE and the PBE0 functional and sovlent effects were included for both THF and DCM. Four possible products for the protonation of **37** with HOTf were investigated, i.e. the *cis*- and *trans*-chloro isomers of $[Re(NH)Cl_2(HPNP^{iPr})]^+$ with either a hydrogen bonded or a non-coordinating triflate anion each (i.e. **cis-38^{OTf}**, **cis-38···OTf**, **trans-38^{OTf}** and **trans-38···OTf**). In **trans-38···OTf**, the proton was actually found to be located at the triflate anion rather than at the nitride and no additional minimum was found upon decreasing the N···H distance.

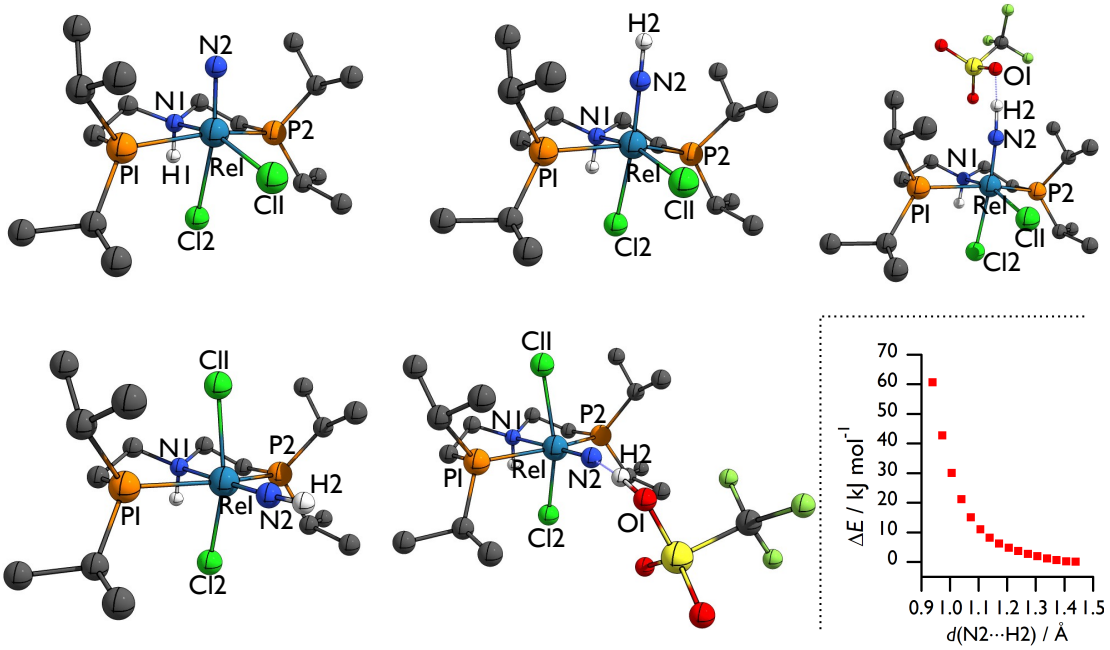

Fig. 3.6. DFT optimized structures of (*top left* to *bottom right*) **37**, **cis-38$^+$**, **cis-38···OTf**, **trans-38$^+$** and **trans-38···OTf**. Carbon-bonded hydrogen atoms are omitted for clarity. *Inset*: Relaxed surface scan (PBE/D3BJ/RI/def2-SVP) for the N2···H2 bond distance in **trans-38···OTf**.

Tab. 3.16. Structural parameters of the DFT optimized isomers. Bond lengths are given in Å, bond angles in °.

	37	exp.	**cis-38^{+}**	**cis-38···OTf**	exp.	**trans-38^{+}**	**trans-38···OTf**
Distances							
Re1-N1	2.224	2.159(2)	2.222	2.217	2.164(5)	2.408	2.482
Re1-N2	1.680	1.669(2)	1.728	1.702	1.692(5)	1.718	1.685
N2-H2			1.027	1.147	0.78(7)	1.027	1.443
H2-O1				1.378	2.166		1.092
Re1-Cl1	2.423	2.4309(7)	2.376	2.403	2.473(12)	2.414	2.452
Re1-Cl2	2.771	2.4291(7)	2.498	2.566	2.4600(14)	2.425	2.452
Angles							
N1-Re1-N2	91.9	92.65(11)	92.8	92.5	90.8(2)	179.4	177.8
Cl1-Re1-Cl2	91.7	88.23(2)	88.8	88.7	87.7(3)	157.0	155.7
P1-Re1-P2	159.6	159.92(2)	158.8	161.2	164.3(3)	154.7	156.2
Re1-N2-H2			178.0	170.7	167(5)	176.9	166.5

Tab. 3.17. Free *Gibb*'s energies for the protonation reaction of **37** with HOTf. ΔG^0 values are given in kJ mol^{-1}.

	PBE(THF)	PBE0(THF)	PBE(DCM)	PBE0(DCM)
37	0.0	0.0	0.0	0.0
cis-38^{OTf}	-13.2	-16.7	-22.8	-26.2
cis-38···OTf	-29.7	-31.6	-29.0	-31.0
trans-38^{OTf}	-22.2	-28.9	-30.9	-37.5
trans-38···OTf	-5.9	-7.7	-5.0	-6.6

3.7.2 DFT-optimized geometries

Tab. 3.18. XZY geometry data for the DFT-derived structures of **37**, **cis-38^{+}**, **cis-38···OTf**, **trans-38^{+}** and **trans-38···OTf**.

	X	Y	Z		X	Y	Z
			37				
C	0.146027254	6.25104307	8.0351485	H	-2.347494447	8.946066402	9.906482099
H	1.157973703	6.132937912	8.472246676	H	-1.065968072	9.804450602	10.81477063
H	0.231710468	6.940152297	7.163748244	C	-0.690031851	8.148267578	13.29256876
C	-0.423894967	4.901194615	7.586352154	H	-1.204719369	9.041548611	13.71287233
H	0.25853253	4.404490687	6.868401965	C	0.726028505	8.542016054	12.85889853
H	-1.394991687	5.059523324	7.071731602	H	1.235545381	7.685131716	12.37087797
C	0.663668456	2.67483371	9.292442723	H	1.322881707	8.82080674	13.75195549
H	0.555566554	1.898938799	8.50139472	H	0.741024147	9.409421363	12.16945989
C	1.994459771	3.409146317	9.096682715	H	-1.710022988	6.872201379	8.72031773
H	2.83465069	2.706081446	9.273693148	C	-0.644274721	7.028970018	14.34278283

H	2.093562441	4.237982941	9.828349196	H	-1.648581247	6.690483188	14.65657695
H	2.117067538	3.816360408	8.073371267	H	-0.09877358	7.381452502	15.24274191
C	0.604805088	2.018606396	10.67942655	H	-0.116306147	6.144179589	13.93539804
H	-0.356752198	1.50994052	10.8749693	C	-3.528834977	7.976608082	12.25944472
H	0.733410808	2.784074266	11.47001673	H	-4.015525873	7.669959359	11.30593968
H	1.420077214	1.271759839	10.77563814	C	-3.799924765	9.458232556	12.53628691
C	-2.247683199	2.782275835	8.473387969	H	-3.48330544	10.11918378	11.70483079
H	-3.010235067	3.582195929	8.335859992	H	-3.29435505	9.804136257	13.46236682
C	-1.98346715	2.072839452	7.142107792	H	-4.888551421	9.615944877	12.68503286
H	-2.908304674	1.560895462	6.803392828	C	-4.055136176	7.061169886	13.3707356
H	-1.199765188	1.292065907	7.238066615	H	-5.162354704	7.124096621	13.40614914
H	-1.678896605	2.76763225	6.334089387	H	-3.677500059	7.371197494	14.36698592
C	-2.757551599	1.829563546	9.560751742	H	-3.769757741	6.003316835	13.19893733
H	-3.75186758	1.434207907	9.267121861	Re	-1.10948082	5.504270421	10.79498931
H	-2.859764893	2.34267356	10.53864364	Cl	-2.192478623	4.057783151	12.40889909
H	-2.08323093	0.957543636	9.688121462	Cl	-3.489932378	5.911741119	9.436867735
C	-0.340013822	8.230534089	9.481209169	P	-0.810832585	3.813878579	9.071915105
H	-0.244320085	8.879969498	8.58085822	P	-1.747065014	7.606189553	11.84028278
H	0.657325976	8.171927199	9.961883089	N	-0.722701924	6.85745323	9.072608757
C	-1.383924216	8.810774692	10.44140608	N	0.501869602	5.55518395	11.2681288

cis-38^{+}

Re	4.996523348	21.20182917	5.887995897	H	4.387499586	20.41247713	1.209905018
Cl	2.516118746	21.41455044	5.684420279	H	3.880405541	21.64444464	2.420847923
P	4.62765355	19.44004325	4.210055676	H	2.675865393	20.90081793	1.316479546
N	4.236221077	19.61690197	7.247131265	H	3.217275123	19.76382599	7.111390367
N	6.647594435	20.82309289	6.231309201	H	7.617162814	20.57061739	6.45511001
C	4.534914845	19.89155541	8.680216401	P	4.597016862	22.59816691	7.873738738
H	4.065114459	19.10911199	9.315747492	C	4.010630506	21.2772982	9.070125066
H	5.63170803	19.81948586	8.819191676	H	4.289038286	21.51966937	10.11430088
C	4.553291866	18.24243627	6.769018169	H	2.901040803	21.28981544	9.021463198
H	4.081934661	17.49497597	7.444230618	C	3.252393254	23.88814588	7.908289746
H	5.650667362	18.10470099	6.834466456	H	2.397693196	23.31738556	7.483461576
C	4.048649049	18.05397025	5.334626996	C	2.909276887	24.34507824	9.330649069
H	2.938568193	18.08677967	5.316266637	H	3.746611695	24.89773029	9.804424318
H	4.346412431	17.0610939	4.944431629	H	2.619557395	23.51157594	10.00039749
C	6.186605506	18.85381347	3.345493243	H	2.048688922	25.04329028	9.288418423
H	5.798327377	18.23925777	2.502654633	C	3.565721318	25.05644	6.966407165
C	6.974098661	20.04600941	2.784871329	H	3.870771084	24.70890867	5.959938225
H	7.792221717	19.67679171	2.134194787	H	4.365804171	25.70670761	7.374440513
H	7.426732927	20.63814725	3.604614362	H	2.659930824	25.68580891	6.855610503
H	6.349859228	20.74035529	2.193702665	C	6.142378439	23.37481792	8.60229188
C	7.066011724	17.96568044	4.22877374	H	5.737785515	24.1212313	9.321911303
H	6.559715942	17.03873639	4.560644792	C	7.012287454	22.37935822	9.373598126
H	7.422840792	18.51202867	5.126506912	H	7.907658798	22.90189282	9.767110017
H	7.967849742	17.66020523	3.660527676	H	7.380885435	21.5648101	8.715729447
C	3.288247996	19.58309683	2.922684229	H	6.494530126	21.92320517	10.23942508
H	2.425059125	19.89823634	3.549049323	C	6.946800218	24.10289341	7.516392311
C	2.972446852	18.24395415	2.247090264	H	7.747377479	24.70564358	7.990500988
H	2.109864534	18.37839789	1.563177321	H	6.328915047	24.77691284	6.895658848
H	2.698248995	17.44558179	2.964607355	H	7.424994665	23.37879527	6.827443259

H	3.818322469	17.88064854	1.627795292	Cl	5.226857206	22.99428286	4.345852429
C	3.585442321	20.70251297	1.918266215				

cis-38···OTf

Re	4.853355939	21.19133672	5.94643652	H	7.415800941	20.32826177	6.816045487
Cl	2.327563323	21.46919051	5.586084296	P	4.442170404	22.58454899	7.913745166
P	4.636649078	19.40551053	4.282823489	C	3.637906264	21.32447581	9.041949879
N	3.942996454	19.64333763	7.245747838	H	3.823001663	21.55170771	10.1102278
N	6.433018979	20.75897877	6.409865606	H	2.544985599	21.42063886	8.866459131
C	4.109648217	19.90843044	8.703070445	C	3.217690054	23.99022234	7.855872589
H	3.517507563	19.16113931	9.277024119	H	2.370223324	23.50436321	7.322987336
H	5.175789354	19.73901159	8.949154697	C	2.761259261	24.45378099	9.242956636
C	4.274596712	18.25188028	6.827707266	H	3.595057807	24.90031162	9.824201639
H	3.706258005	17.53585941	7.462211113	H	2.319155593	23.6373998	9.847555713
H	5.348290331	18.08513788	7.040716001	H	1.986041968	25.24037795	9.134199235
C	3.913996568	18.04691038	5.353957232	C	3.731233134	25.14330691	6.985603714
H	2.812987749	18.11079262	5.218659057	H	4.111809172	24.78085015	6.009441056
H	4.22917132	17.04213801	5.011020383	H	4.539955462	25.70717523	7.494147343
C	6.241565394	18.75797505	3.555543948	H	2.904246861	25.85769895	6.794694402
H	5.911600313	18.17781754	2.66426624	C	5.982544354	23.20899272	8.786217902
C	7.12581866	19.92929789	3.103066415	H	5.599242377	23.99554722	9.474892253
H	7.984540699	19.54145407	2.518020825	C	6.684031185	22.12621153	9.612270615
H	7.527728927	20.47092754	3.981636451	H	7.589744137	22.557103	10.08566144
H	6.585972761	20.67040148	2.485373727	H	7.030764789	21.2790145	8.989824061
C	7.005567724	17.82359231	4.497592932	H	6.051469327	21.72036734	10.42517057
H	6.422232335	16.93716525	4.812429266	C	6.948599575	23.84364812	7.775015363
H	7.36550041	18.3428048	5.405515055	H	7.763059289	24.36565713	8.317620202
H	7.913582432	17.44809282	3.98321181	H	6.458683247	24.56767571	7.098332308
C	3.417217817	19.56614449	2.879554418	H	7.40861546	23.06260822	7.138568807
H	2.520971959	19.93783746	3.424145689	Cl	5.216383494	22.98856474	4.392525047
C	3.096124309	18.23186327	2.198748109	S	8.266182233	18.49062454	8.152946314
H	2.308059671	18.38732435	1.433033199	F	9.280539366	17.7856748	10.49858961
H	2.722157648	17.46415823	2.904780261	F	9.086210745	19.94420745	10.23681528
H	3.979541937	17.81408741	1.672242272	F	10.68315681	18.85927466	9.216014741
C	3.851873833	20.64862868	1.884793016	O	8.712604773	17.22383067	7.542942316
H	4.707549502	20.31091636	1.26471286	O	8.562990997	19.73498732	7.295655019
H	4.138658204	21.58714374	2.400358975	O	6.892777355	18.52572489	8.744466505
H	3.013820099	20.87191169	1.193064162	C	9.408672992	18.79070214	9.619774641
H	2.949051763	19.82259349	7.000856181				

trans-38^{+}

Re	4.762616794	20.91557089	6.157410902	H	4.170850427	23.02463245	10.18144989
Cl	2.356627711	21.171214	5.997657916	H	3.479375509	21.63939777	9.26077791
P	4.781100725	23.19843956	7.097851345	H	2.402863453	22.83743469	10.0357302
N	4.526900312	22.29169919	4.195730147	H	3.493918193	22.35965307	4.182042737
N	4.949756328	19.93275592	7.55434046	H	5.116050811	19.3477929	8.382157361
C	4.966865696	21.6230917	2.948798068	P	4.544405713	19.24648965	4.350140836
H	4.73558007	22.26279164	2.06857482	C	4.277138924	20.26917598	2.820374467
H	6.067647383	21.50897653	3.006108765	H	4.621282782	19.72876998	1.917574226
C	5.081969036	23.65540086	4.361260229	H	3.177969871	20.39939291	2.727069814
H	4.8474186	24.2759419	3.468283508	C	3.005714748	18.19350025	4.469893767

H	6.183821038	23.5574341	4.427170703	H	2.221907752	18.97131267	4.602027792
C	4.507911648	24.29449723	5.621215283	C	2.731984232	17.39669844	3.188976186
H	3.407560248	24.41576286	5.529864358	H	3.493973348	16.60971615	3.014148625
H	4.93599261	25.3012253	5.790703179	H	2.680074035	18.03426788	2.284668343
C	6.323866294	23.7676317	8.00219911	H	1.753927475	16.88216556	3.281581108
H	5.924889857	24.54972741	8.686399869	C	3.012395184	17.31070188	5.721743895
C	6.910669416	22.6246107	8.843566733	H	3.217419023	17.89763786	6.638610442
H	7.710024759	23.02337307	9.500015256	H	3.757135541	16.49226562	5.649727956
H	7.357407921	21.85165582	8.188177698	H	2.017563952	16.83734778	5.844083076
H	6.155711501	22.14092978	9.492501909	C	5.97974011	18.07403571	4.056285894
C	7.380960231	24.40665305	7.094486843	H	5.481470932	17.19832813	3.582971316
H	6.996334536	25.27827778	6.530133863	C	7.039097783	18.61500791	3.089313805
H	7.794004183	23.66717628	6.382094228	H	7.807916056	17.83287894	2.924562229
H	8.218061941	24.77431196	7.722279824	H	7.546845724	19.50318625	3.511300502
C	3.333916938	23.57124205	8.21957958	H	6.625034029	18.87263787	2.095152884
H	2.480882309	23.23023416	7.592853109	C	6.597559344	17.63155295	5.390902869
C	3.188204199	25.0677109	8.519981562	H	7.325407594	16.81586251	5.207096808
H	2.258976223	25.23395307	9.102040449	H	5.842138616	17.25110664	6.104856602
H	3.114845718	25.68775923	7.605070796	H	7.137789591	18.47402785	5.865317346
H	4.026462318	25.45508928	9.134631033	Cl	7.075186127	21.21195011	5.532514347
C	3.360336577	22.71654369	9.490435225				

trans-38···OTf

Re	4.727869925	21.45883878	5.724813403	H	5.635491313	23.40130434	3.47751213
Cl	2.293229432	21.62692719	5.488974662	P	4.429479989	22.71473124	7.804182493
P	4.578168832	19.53194117	4.244685439	C	3.730515421	21.44637071	8.988689744
N	3.876595173	19.70437239	7.260437966	H	3.968778044	21.70602963	10.03861628
N	5.309281104	22.6055708	4.636026253	H	2.627578501	21.51988824	8.875564654
C	4.19542193	20.02441352	8.65950415	C	3.099529018	24.02837534	7.745858193
H	3.719963604	19.29877378	9.361414828	H	2.24751077	23.44204885	7.335977003
H	5.295008658	19.93588355	8.774845883	C	2.729639096	24.58865694	9.122298917
C	4.261979402	18.36308676	6.799416754	H	3.557086186	25.18040838	9.566283629
H	3.785000325	17.56676103	7.418714992	H	2.445637774	23.79993274	9.847799984
H	5.36064687	18.27538202	6.924129807	H	1.861891677	25.27346422	9.024107579
C	3.868071471	18.18533419	5.329657307	C	3.439481984	25.12191769	6.729028247
H	2.765782775	18.2724486	5.21973886	H	3.674871271	24.70321999	5.731788747
H	4.154936824	17.18077418	4.961954096	H	4.292338518	25.74828906	7.061115153
C	6.142696741	18.8873083	3.427921709	H	2.566891941	25.79562986	6.60529423
H	5.776646473	18.38425842	2.504947679	C	5.924459022	23.52671077	8.601631894
C	7.042977371	20.06895737	3.034375907	H	5.493650731	24.36905576	9.187428865
H	7.883707033	19.7044111	2.408923826	C	6.68954518	22.60307245	9.556884904
H	7.46160083	20.54703266	3.941586625	H	7.539856076	23.16026083	10.00231851
H	6.506250888	20.84969331	2.462500386	H	7.102481467	21.73293356	9.009792836
C	6.903317065	17.86332647	4.278822246	H	6.064585687	22.23775733	10.39578631
H	6.296727456	16.96819538	4.520814917	C	6.844791276	24.0919561	7.50849899
H	7.255445923	18.32575386	5.221772178	H	7.643915381	24.7043234	7.974872052
H	7.794594541	17.51195025	3.718489248	H	6.307697688	24.72836341	6.78017936
C	3.320082009	19.70301515	2.870958614	H	7.319686711	23.26485574	6.945238107
H	2.432210591	20.05217429	3.443423631	Cl	6.830810291	20.57147165	6.619729036
C	2.998808317	18.38064003	2.167839057	S	4.650544392	24.99286291	2.318907732
H	2.177178824	18.53699992	1.438436283	F	5.671454923	26.0870736	4.530710129

H	2.669410973	17.58802571	2.869182762	F	4.445665369	27.44006273	3.330701276
H	3.867267501	17.99284467	1.595455028	F	6.461970219	26.92310795	2.674335859
C	3.708199746	20.81272869	1.887853216	O	5.818916678	23.93848906	2.544636249
H	4.584346112	20.52919448	1.269429142	O	4.623859808	25.39803595	0.910931127
H	3.933426953	21.76760868	2.399633106	O	3.426276078	24.60181364	3.043952255
H	2.864327259	21.00254427	1.193615646	C	5.359031018	26.46268327	3.271960662
H	2.869621575	19.85941166	7.085621273				

3.8 N_2 splitting and functionalization by the {Re(^{Me}NPNP^{iPr})} platform

All calculations were largely performed according to the in Section 3.1 described procedure. As the results were to be compared with those published for the splitting of **36** to **37**,[269] the procedure was modified in some points: Single point calculations were performed using the M06 functional, no additional dispersion correction was applied and the RI approximation was switched off. Furthermore, solvent effects were modeled using the SMD solvation model and the ORCA grid size was changed to 5.

The thermochemistry data for the existing *iso*-propyl substituted complexes **36**, **37** and the connecting **TS** are given here for comparision, the corresponding xyz-data can be found in the above cited publication.

Tab. 3.19. Thermochemistry data calculated for the N_2 splitting from the dimers **36** and [(μ-N_2){ReCl(^{Me}NPNP^{iPr})}$_2$] into the corresponding nitrides and subsequent methylation of the nitrides with MeOTf. All thermodynamic corrections to derive relative free energies ΔG are based on frequency calculations at the PBE/D3BJ/def2SVP level of theory. The data are given in kJ mol^{-1}.

	ΔG
36 (S = 1)	0
36 (^{BS}S = 0)	+19
TS (S=0)	175
2 × **37**	−83
2 × [Re(NMe)Cl$_2$(HPNP^{iPr})]^{OTf}	−231
[(μ-N_2){ReCl(^{Me}NPNP^{iPr})}$_2$] (S = 1)	0
[(μ-N_2){ReCl(^{Me}NPNP^{iPr})}$_2$] (^{BS}S = 0)	+3
TS (S=0)	239
2 × [Re(N)Cl(^{Me}NPNP^{iPr})]	−68
2 × [Re(NMe)Cl(^{Me}NPNP^{iPr})]^{OTf}	−266

3.8.1 DFT-optimized geometries

Tab. 3.20. XZY geometry data for the DFT-derived structures of $[Re(NMe)Cl_2(HPNP^{iPr})]^+$, $[(\mu\text{-}N_2)\{ReCl(^{Me}NPNP^{iPr})\}_2]$ (S = 1), $[(\mu\text{-}N_2)\{ReCl(^{Me}NPNP^{iPr})\}_2]$ (^{BS}S = 0), $[(\mu\text{-}N_2)\{ReCl(^{Me}NPNP^{iPr})\}_2]$ (**TS**, S = 0), $[Re(N)Cl(^{Me}NPNP^{iPr})]$ and $[Re(NMe)Cl(^{Me}NPNP^{iPr})]^+$.

	X	Y	Z		X	Y	Z
			$[Re(NMe)Cl_2(HPNP^{iPr})]^+$				
C	0.193924736	6.244767527	8.039540742	C	-0.76592672	8.203712506	13.32172106
H	1.202618041	6.098432843	8.4751646	H	-1.388718476	9.010598976	13.76743434
H	0.300941541	6.939915647	7.177833516	C	0.590950874	8.804061623	12.94027458
C	-0.415721254	4.916845876	7.579235103	H	1.224955959	8.083529088	12.3866155
H	0.247146568	4.415635997	6.847791669	H	1.143184094	9.082416583	13.86091657
H	-1.380726081	5.10483533	7.062372428	H	0.499275069	9.721689195	12.32792105
C	0.608566002	2.600497627	9.238741327	H	-1.634895109	6.906654875	8.694622172
H	0.373705305	1.789946688	8.513943566	C	-0.633331497	7.060714642	14.33763878
C	1.964830388	3.202932254	8.858876589	H	-1.60814753	6.619406689	14.61427201
H	2.763106894	2.452799036	9.032522608	H	-0.150416831	7.43652954	15.26227005
H	2.214451957	4.090122246	9.474156046	H	-0.0188534	6.231913673	13.93598648
H	2.023281902	3.496509501	7.79314469	C	-3.556724409	7.966757444	12.24017752
C	0.608776768	2.011540095	10.65612925	H	-4.050291734	7.646175914	11.29729026
H	-0.370683962	1.588162251	10.94382638	C	-3.846601691	9.450358565	12.4924895
H	0.850154788	2.781583946	11.41406384	H	-3.540647203	10.10487887	11.65256616
H	1.366946367	1.205482666	10.72523726	H	-3.358385967	9.820082507	13.41775422
C	-2.281633768	2.801373715	8.458654687	H	-4.938440798	9.586730035	12.63118715
H	-3.04998678	3.594968574	8.335227835	C	-4.054656493	7.060394639	13.37196028
C	-2.03450439	2.112437834	7.112111271	H	-5.159992254	7.1235186	13.42801752
H	-2.9690161	1.612667347	6.78515887	H	-3.660854834	7.382867515	14.35711919
H	-1.257825242	1.323013993	7.181744928	H	-3.776209175	6.000622172	13.20893181
H	-1.743321113	2.816085728	6.307425452	Re	-1.062714075	5.514301659	10.7971606
C	-2.764558271	1.833182508	9.544827396	Cl	-2.03055487	4.076431698	12.4356089
H	-3.752304186	1.423459574	9.252559389	Cl	-3.315808759	5.738721546	9.730370932
H	-2.874388401	2.332286001	10.52772649	P	-0.817691789	3.803385213	9.036589799
H	-2.076928703	0.970808186	9.659852644	P	-1.764773592	7.638248846	11.83745679
C	-0.304172366	8.246406391	9.498547055	N	-0.670944348	6.865522825	9.080177879
H	-0.187543756	8.891446061	8.599942335	N	0.579519182	5.518949593	11.34424854
H	0.681017582	8.200620632	10.0044676	C	1.910511621	5.495053037	11.82385007
C	-1.383877199	8.814983636	10.42494321	H	2.294191432	4.452321398	11.82814389
H	-2.334333533	8.938680167	9.863670817	H	1.945241517	5.873954261	12.86776745
H	-1.095190843	9.818871638	10.79177938	H	2.584098912	6.118834764	11.19691
			$[(\mu\text{-}N_2)\{ReCl(^{Me}NPNP^{iPr})\}_2]$ (S = 1)				
Re	1.95554334	8.015991958	8.700877964	N	-1.017552715	7.027617705	8.543205125
Cl	1.214019386	10.04779441	10.02806865	H	-4.103179202	8.832062666	13.62636316
P	1.984302565	9.296596241	6.646135923	H	-4.931647626	9.746818368	12.34036589
N	4.115127203	8.732299046	8.773752602	C	-4.49994813	8.754840021	12.59177804
C	4.320827881	9.953048833	7.938246646	H	-5.328126398	8.019306542	12.61267302
H	5.407962336	10.20801093	7.935336484	H	-1.771047013	9.256160529	12.81017759
H	3.781412988	10.77235965	8.451480989	H	-2.494409265	10.38153403	11.63695545

P	2.591071687	7.141446045	10.88779394	H	-4.465145552	10.52221773	10.25914224
C	3.792531009	9.793233187	6.522332689	C	-2.181622476	9.32786096	11.781454
H	4.350717486	9.011634648	5.970813886	C	-3.370114307	8.372642555	11.62819025
H	3.91870835	10.7374888	5.955764674	C	-4.180689137	10.01314009	9.309631287
C	1.681267369	8.422995713	4.993657689	H	-3.029997316	7.340388086	11.86224876
H	2.063742603	7.399733085	5.204224263	H	-5.391516402	11.29709498	8.052476762
N	0.104439012	7.357779924	8.604985693	H	-6.302532241	9.889823337	8.655156964
C	2.449469028	9.014475073	3.80663187	H	-6.373117274	8.398638019	10.17965337
H	2.201340226	8.457677927	2.878057621	H	-3.000555657	11.68684356	8.562962028
H	3.548955378	8.969779095	3.933753015	C	-5.308246001	10.21556407	8.289419479
H	2.169082191	10.07437494	3.631881925	H	-5.726711221	6.867694494	10.80865031
C	0.182222181	8.332916228	4.689670305	C	-2.87991898	10.60134677	8.76202312
H	0.010454433	7.651527072	3.830481807	H	-1.352356373	9.124047331	11.07700031
H	-0.231666697	9.319322943	4.399953187	H	-2.015043083	10.47477409	9.437588131
H	-0.416334606	7.961629755	5.54342496	C	-5.661901455	7.577060417	9.960806988
C	1.111176935	10.95792732	6.398812572	P	-3.899251793	8.210846141	9.815587994
H	1.157509358	11.13284068	5.298579624	H	-4.642375519	5.262932468	11.20143155
C	1.78733549	12.13647549	7.112230465	H	-2.085963018	5.208697528	11.86906879
H	2.824972066	12.32494172	6.773038301	H	-5.073816976	9.684654404	7.344532953
H	1.783020268	11.97691638	8.210144653	H	-2.635390601	10.0957724	7.810339692
H	1.208892494	13.06219305	6.906773249	C	-6.025008817	6.905658312	8.645663591
C	-0.341238538	10.84602378	6.858712987	H	-7.05696736	6.481699521	8.68416922
H	-0.886970062	11.78917338	6.64243076	C	-4.234817122	4.666132664	10.34195668
H	-0.355694519	10.67949511	7.951050904	H	-5.995418475	7.648887254	7.825190432
H	-0.898158047	10.01704983	6.387811878	C	-1.899426731	4.809978561	10.83801049
C	4.473489518	9.106946194	10.17905238	H	-6.266139646	4.541448651	9.510216499
H	3.808095974	9.956034682	10.43339332	H	-4.153333237	3.62253903	10.73843267
H	5.532099332	9.46001125	10.21022172	N	-2.944711073	5.163063204	9.915102119
C	4.25587929	7.982294888	11.18344233	Re	-2.905897442	6.506864541	8.385971311
H	4.301083658	8.407290267	12.20493032	H	-0.936462849	5.223731648	10.49811964
H	5.058730401	7.219105427	11.1323276	N	-5.072276135	5.823075407	8.259007617
C	1.617414086	7.626471037	12.42261843	H	-1.789225958	3.70088168	10.95116535
H	1.491252298	8.712936305	12.21070421	C	-5.211610044	4.63775334	9.16749523
C	2.28640202	7.440712676	13.78685191	Cl	-3.209838909	7.988008365	6.352259861
H	2.314231427	6.375969184	14.09187513	H	-4.985376688	3.739362935	8.565661793
H	1.707638189	7.985998596	14.56205429	C	-5.402029955	5.445656017	6.847331556
H	3.32272083	7.829772356	13.82649997	H	-5.280066695	6.378909275	6.262765118
C	4.98050932	7.606774311	8.287219422	H	-6.468243776	5.119125499	6.789598413
C	0.230850194	6.984691738	12.39038827	H	-0.62915038	3.989007153	8.627321937
H	-0.255154589	7.116681873	11.40576177	P	-2.688442072	4.72145403	6.744859548
H	-0.423450325	7.444598136	13.15876292	H	-2.900554437	2.920907326	8.232159731
H	0.280390512	5.900454483	12.61039621	C	-4.483272159	4.37645829	6.267988528
C	3.078373603	5.316250239	10.97715147	H	-0.043554438	5.686126345	6.161020499
H	3.720446357	5.263707748	10.0685065	H	-4.759316108	3.356365716	6.603929167
C	1.868214029	4.410111657	10.73190283	C	-0.774619329	3.062724576	8.042088611
H	1.219980326	4.813559275	9.931252337	C	-2.166288179	3.025606451	7.401766939
H	1.252374012	4.298509032	11.64661996	H	-0.637471555	2.198702743	8.726122894
H	2.193961643	3.393976565	10.42701015	C	-0.330428195	5.061685407	5.296038917
C	3.895671457	4.857562801	12.18769272	H	-2.183713131	6.102068347	4.931974009
H	4.307199708	3.84171724	12.00607327	H	-4.598227026	4.37444811	5.167173396
H	3.270108802	4.794901831	13.09932808	C	-1.845129273	5.052967831	5.094521118

H	4.750937867	5.524105844	12.4128699	H	0.066015444	4.04015637	5.461322542
H	5.911700406	8.013389458	7.832149991	H	0.026803979	3.008755931	7.279492974
C	4.244544973	6.66447584	7.333097405	H	0.1793434	5.466322779	4.398223556
H	5.28702792	7.017586476	9.17149088	C	-2.321959006	1.839835043	6.446091364
H	4.271175911	7.05270837	6.280010821	H	-2.201559306	0.882961832	6.998727856
N	2.891256413	6.447194405	7.798125791	H	-3.311443277	1.809733194	5.948133535
H	4.818178887	5.706204799	7.300855619	C	-2.247045999	4.209855955	3.881587536
C	2.371294083	5.161883706	7.41454193	H	-1.545287957	1.85428819	5.654815042
H	2.381451587	5.013154522	6.304050393	H	-3.338820995	4.201802289	3.695107661
H	1.326240654	5.061604303	7.75090774	H	-1.908021768	3.158517758	3.964634546
H	2.959863587	4.309506542	7.84538227	H	-1.772096745	4.632856847	2.970704813

$[(\mu\text{-}N_2)\{ReCl(^{Me}NPNP^{iPr})\}_2]$ ($^{BS}S = 0$)

Re	1.95758955	8.014366822	8.706146463	N	-1.01582931	7.024085083	8.542279218
Cl	1.211555025	10.04839491	10.026602	H	-4.09584305	8.835985801	13.62333486
P	1.984290132	9.295122773	6.648482186	H	-4.927990522	9.747688729	12.33762826
N	4.116626726	8.729872818	8.778131542	C	-4.49418585	8.756747509	12.58950767
C	4.324281375	9.947295892	7.938245922	H	-5.321051857	8.019812119	12.61274288
H	5.411996851	10.19982323	7.933325809	H	-1.765780611	9.263001603	12.80297127
H	3.787532382	10.76954988	8.449523645	H	-2.492512844	10.38564073	11.62921838
P	2.594182583	7.145758118	10.8931172	H	-4.466564989	10.52037427	10.25519965
C	3.794192345	9.784989307	6.523169578	C	-2.178084335	9.332608637	11.77481035
H	4.349202314	8.999402175	5.973950738	C	-3.365212098	8.375300806	11.62465968
H	3.923797132	10.72697792	5.953528569	C	-4.182502241	10.01141084	9.305507558
C	1.678153109	8.421069834	4.997278676	H	-3.022981725	7.343992895	11.85965394
H	2.060575493	7.397715975	5.207408232	H	-5.398578415	11.29194971	8.049889449
N	0.106041793	7.353787694	8.607519541	H	-6.305179374	9.882901422	8.655057928
C	2.445129259	9.011917306	3.809104094	H	-6.369778367	8.393921194	10.18391785
H	2.195562968	8.454732178	2.881177687	H	-3.007607034	11.68795788	8.55697582
H	3.544767106	8.96697249	3.934779965	C	-5.312356725	10.21074169	8.287249385
H	2.164718035	10.07177117	3.634182383	H	-5.718787547	6.864036669	10.81090262
C	0.178655348	8.332003045	4.695454222	C	-2.884037371	10.60266937	8.755491119
H	0.005340345	7.650266798	3.836925598	H	-1.349636527	9.128755655	11.06940068
H	-0.234660521	9.318583063	4.405570736	H	-2.017750727	10.47793113	9.429534489
H	-0.419296903	7.96182053	5.550132662	C	-5.657827647	7.573537594	9.962861088
C	1.11566712	10.95847076	6.401192721	P	-3.896450616	8.210150104	9.812914406
H	1.162617725	11.13262562	5.300893626	H	-4.64001358	5.253733076	11.20019768
C	1.79522938	12.13558563	7.113654457	H	-2.091559462	5.221626354	11.87185563
H	2.833271125	12.32094644	6.773877661	H	-5.078429514	9.679774646	7.342290038
H	1.79081919	11.97679326	8.211666147	H	-2.640099673	10.09780223	7.803245454
H	1.219264462	13.06272889	6.90771138	C	-6.024237173	6.901508534	8.648939565
C	-0.337287012	10.85048329	6.860684514	H	-7.055534168	6.47625164	8.690799486
H	-0.880541827	11.79472355	6.642924173	C	-4.231157825	4.660373601	10.33896928
H	-0.352924161	10.68500698	7.95319136	H	-5.998493227	7.644832135	7.828450279
H	-0.895731654	10.02238689	6.390081914	C	-1.899182653	4.819330788	10.84317459
C	4.474815112	9.109552442	10.18214993	H	-6.262387603	4.533942381	9.50810148
H	3.808654014	9.95888265	10.43364095	H	-4.146872647	3.615895859	10.73278909
H	5.533178029	9.463483507	10.21210193	N	-2.942462209	5.16275289	9.914345317
C	4.257815123	7.987918118	11.19015612	Re	-2.90505169	6.503831202	8.3829174
H	4.299883929	8.416533755	12.21024527	H	-0.936753563	5.235461077	10.50473598
H	5.061958391	7.225770022	11.14364573	N	-5.071468238	5.82023918	8.258690318

C	1.620578159	7.63064243	12.42797524	H	-1.784661382	3.711265179	10.9616565
H	1.497338502	8.717739014	12.21764318	C	-5.208231188	4.63300449	9.164939279
C	2.288603267	7.44105912	13.79212801	Cl	-3.21118407	7.987590489	6.35111636
H	2.313904	6.375730857	14.09529127	H	-4.980775551	3.736434412	8.56097292
H	1.710806626	7.986310364	14.5680675	C	-5.404010134	5.444695497	6.847169576
H	3.325842829	7.827596929	13.83281265	H	-5.282553162	6.378554284	6.263436499
C	4.981397623	7.601468575	8.297416875	H	-6.47048058	5.118706067	6.790943828
C	0.232536609	6.992494682	12.3934286	H	-0.636380009	3.990154377	8.629905721
H	-0.25165614	7.128051819	11.4084295	P	-2.691548962	4.720331302	6.74184038
H	-0.421395397	7.45229458	13.16215087	H	-2.903510812	2.918276631	8.227956775
H	0.279409509	5.907638571	12.61092909	C	-4.48656516	4.375766755	6.265305299
C	3.078659853	5.319950683	10.97923054	H	-0.048270396	5.6844425	6.153189872
H	3.722666685	5.268232941	10.07192496	H	-4.76294242	3.355084189	6.599260519
C	1.867084697	4.417241015	10.72794378	C	-0.777736965	3.064697797	8.042192266
H	1.224047589	4.823334663	9.924347856	C	-2.168003936	3.024900928	7.398936572
H	1.246663317	4.307004805	11.6397626	H	-0.63936326	2.199333814	8.724315643
H	2.191528411	3.400322801	10.42423475	C	-0.335671457	5.059306806	5.289045255
C	3.891856077	4.856890342	12.19073052	H	-2.189190724	6.099643467	4.927197145
H	4.302372275	3.840933423	12.00752903	H	-4.601994767	4.376093464	5.164564115
H	3.263696579	4.792703668	13.10047259	C	-1.850492536	5.050566877	5.089718823
H	4.747504117	5.521569267	12.42006034	H	0.061108195	4.037941231	5.454868626
H	5.91461708	8.00470319	7.84360414	H	0.025321971	3.015072325	7.28100133
C	4.247376556	6.657255612	7.344188198	H	0.173251719	5.463234932	4.390379001
H	5.284498413	7.01487824	9.184494394	C	-2.319851482	1.839423495	6.442387529
H	4.280548066	7.040169527	6.289247646	H	-2.198371414	0.882383331	6.99450584
N	2.88988381	6.446434948	7.800712088	H	-3.308590849	1.807859713	5.943001023
H	4.817677754	5.696695315	7.31911016	C	-2.253891851	4.206963469	3.877588285
C	2.364117367	5.16815686	7.401201775	H	-1.542077365	1.856049764	5.652229073
H	2.37804514	5.030118921	6.289258709	H	-3.345857489	4.198862652	3.692263557
H	1.317679206	5.069119133	7.733498394	H	-1.914788446	3.155669039	3.960698657
H	2.947639908	4.309524849	7.82606291	H	-1.779942395	4.629550808	2.965980094

$[(\mu\text{'}{-}\text{'}N_2)\{ReCl(^{Me}NPNP^{iPr})\}_2]$ (**TS**, S = 0)

Re	1.860305104	7.719506314	8.758951738	N	-1.328942728	7.509197349	8.314507107
Cl	2.159845367	9.52034558	10.46927057	H	-4.732526864	10.22301347	12.47143724
P	1.797529897	9.590221599	7.231327481	H	-4.868359046	11.06995777	10.90925739
N	4.346330688	8.260033909	8.510723	C	-4.937931344	10.07258651	11.39067065
C	4.460228099	9.699632973	8.18819522	H	-5.985431605	9.719685177	11.29837698
H	5.529001385	9.958932523	7.985836378	H	-2.21219135	9.656605564	12.02198229
H	4.134552758	10.25644329	9.087382493	H	-2.353515119	10.59722001	10.5131279
P	2.806243954	6.302186625	10.59579238	H	-5.271853842	10.71292409	8.86347495
C	3.594278333	10.11631603	6.998897834	C	-2.482353539	9.586398708	10.94812405
H	3.969422961	9.677347359	6.05598921	C	-3.923136912	9.089922942	10.79972004
H	3.657769061	11.2136506	6.871343235	C	-4.770320097	10.08203918	8.09574471
C	1.150524701	9.30121695	5.481859456	H	-4.003236431	8.121427478	11.34345735
H	1.530961798	8.282149491	5.254341179	H	-5.984059082	10.83925305	6.471394817
N	0.182063093	7.154092666	8.916953677	H	-6.7245698	9.433965957	7.270528625
C	1.669489061	10.28763957	4.432935568	H	-6.78149103	8.51417408	9.187801905
H	1.235025497	10.0461113	3.439625317	H	-3.790763259	11.71635932	7.04178562
H	2.772432359	10.26513198	4.322545935	C	-5.756634137	9.859176982	6.942031208
H	1.371208119	11.33102507	4.668677854	H	-6.059347069	7.282512451	10.2578342

C	-0.380116374	9.229264159	5.496903513	C	-3.516160847	10.79840361	7.602757079
H	-0.756916755	8.817442643	4.538990365	H	-1.754586852	8.911388135	10.45723219
H	-0.838320339	10.23152914	5.621013102	H	-2.859694242	11.09680888	8.437191591
H	-0.767088567	8.58137448	6.30692913	C	-5.996526092	7.732861007	9.24854063
C	0.923155573	11.20849939	7.699402784	P	-4.302846093	8.503956906	9.045582754
H	0.545531347	11.59033985	6.725259572	H	-4.674878545	6.130577135	10.97309527
C	1.801600278	12.29614799	8.326060293	H	-2.247245632	6.660777279	11.55186352
H	2.590474861	12.67334784	7.645981552	H	-5.31414437	9.200994888	6.167449648
H	2.272930465	11.92997985	9.258160055	H	-2.937634858	10.13694183	6.927312806
H	1.163865898	13.16577412	8.591919257	C	-6.217630539	6.695348236	8.154000229
C	-0.268733534	10.88628207	8.598472444	H	-7.216466259	6.206311613	8.277107636
H	-0.923209088	11.7785212	8.683857622	C	-4.240836061	5.247983011	10.41714048
H	0.082582032	10.60578672	9.60786648	H	-6.212844544	7.194912291	7.166211319
H	-0.864840618	10.03829187	8.216402507	C	-1.97893755	5.772732543	10.91263918
C	5.007431844	7.955656977	9.799405453	H	-6.238644753	4.686348283	9.684832675
H	4.67756847	8.739222402	10.51050679	H	-4.200078449	4.434384753	11.18782515
H	6.117576052	8.037516197	9.696427505	N	-2.93728605	5.489326546	9.875086919
C	4.650483182	6.576504298	10.36029011	Re	-2.894075803	6.748608129	8.133228142
H	5.191984015	6.419071405	11.31555379	H	-0.984181711	5.998023128	10.47780616
H	4.997266648	5.774631026	9.677019801	N	-5.161201256	5.662714928	8.110571822
C	2.493654681	6.986260911	12.32746161	H	-1.87522409	4.906252288	11.61515697
H	2.91184721	8.007268715	12.20229006	C	-5.192010675	4.78413151	9.314126586
C	3.218977331	6.307826669	13.49301397	Cl	-3.518369073	7.463280308	5.794505305
H	2.805449617	5.306039345	13.72494167	H	-4.865104391	3.774518238	9.002435293
H	3.095642094	6.924830185	14.40883008	C	-5.293370228	4.897125194	6.846610979
H	4.309557131	6.197032359	13.32310083	H	-5.289263764	5.648756866	6.033490903
C	4.834306695	7.420261929	7.391264375	H	-6.273061086	4.359459626	6.825792942
C	0.99397044	7.174144548	12.5991214	H	-0.07512349	4.619638395	8.571730704
H	0.47893724	7.602075732	11.71794279	P	-2.452347151	4.590771473	7.008166534
H	0.856248986	7.878287507	13.44631495	H	-2.270934969	3.510608418	9.023331528
H	0.492122447	6.224942626	12.86901557	C	-4.156099813	3.905149291	6.610036136
C	2.692043353	4.410157982	10.75950213	H	-0.419509088	6.408814307	6.045323683
H	2.603134139	4.091224094	9.704236366	H	-4.290133208	2.989236807	7.215564914
C	1.402934171	3.995908023	11.47656539	C	-0.244007566	3.549321357	8.329826821
H	0.512704865	4.508315904	11.06827091	C	-1.720530211	3.250331347	8.084955073
H	1.451046539	4.20749165	12.56220377	H	0.134517683	2.942416672	9.176823041
H	1.245457723	2.90260257	11.36214517	C	-0.301747045	5.497767667	5.431780483
C	3.920519612	3.704179018	11.34915759	H	-2.346216508	5.327749516	4.802819713
H	3.752504946	2.605574002	11.33786797	H	-4.180130493	3.576802099	5.551782649
H	4.114769321	3.994469857	12.39902265	C	-1.605380917	4.696408968	5.342675468
H	4.842657051	3.894381928	10.7663332	H	0.51915992	4.908411939	5.87884587
H	5.646407969	7.94507795	6.834028616	H	0.370886152	3.292731383	7.443263917
C	3.662740061	7.007165492	6.475681333	H	0.022257593	5.805123439	4.416076514
H	5.28506238	6.501875556	7.813232699	C	-1.949444076	1.787298391	7.702583122
H	3.330893755	7.873274319	5.872284646	H	-1.587768493	1.131802586	8.523801625
N	2.58139076	6.47055048	7.261450403	H	-3.015873548	1.534104003	7.539569673
H	4.039582002	6.256451805	5.739641981	C	-1.421241174	3.362388737	4.616296852
C	2.769705555	5.05220157	7.45247173	H	-1.393716942	1.499156854	6.787986348
H	2.823723921	4.524639023	6.468492847	H	-2.353683966	2.76417965	4.55964979
H	1.91531488	4.627888015	8.000367138	H	-0.645000213	2.740393575	5.107012947

H	3.704916221	4.757591095	8.006888398	H	-1.082666128	3.543657566	3.574272523

[Re(N)Cl(^{Me}NPNP^{iPr})]

Re	1.815958751	8.109020189	8.54029956	C	4.095846828	7.179524749	10.91552263
Cl	1.680774185	10.06803811	10.10184221	H	4.311625671	7.175201374	12.00326263
P	2.228929629	9.695142532	6.764026676	H	4.624169239	6.306506503	10.48407014
N	4.339111931	8.585891088	8.84542063	C	1.415878022	7.473602023	12.16496019
C	4.560801606	9.957741878	8.347348748	H	1.805114987	8.514972314	12.20482125
H	5.650004446	10.21191235	8.38068669	C	1.770604475	6.739594447	13.46068686
H	4.026747028	10.63937631	9.038829463	H	1.303005205	5.736419623	13.5016835
P	2.277286139	6.863698507	10.62026922	H	1.388179414	7.311413034	14.33236041
C	4.035100563	10.16640065	6.923513708	H	2.862700347	6.611641576	13.60456674
H	4.593348624	9.540198648	6.199230666	C	5.070508198	7.564215335	8.056778173
H	4.194082432	11.21995957	6.619898737	C	-0.098645821	7.573886833	11.94193724
C	2.086923922	9.11563423	4.97653931	H	-0.328490182	8.10655351	10.99886942
H	2.725873479	8.206175126	4.986864646	H	-0.562904313	8.139439638	12.77628929
N	0.244253007	7.703147222	8.119130465	H	-0.579896455	6.576052788	11.90794595
C	2.644607194	10.09290046	3.937203557	C	2.172355073	5.005820198	10.44907674
H	2.617891061	9.627556023	2.92911461	H	2.706328221	4.928939589	9.47234649
H	3.695526478	10.37994675	4.13912629	C	0.721257934	4.554979573	10.25027985
H	2.042499747	11.02236634	3.878344485	H	0.184733176	5.207464003	9.532659569
C	0.651958147	8.681870336	4.662666344	H	0.158251232	4.557546494	11.20564596
H	0.62173598	8.142437466	3.693185887	H	0.698641541	3.517742089	9.856170277
H	-0.024968113	9.556243823	4.573314106	C	2.909087119	4.165555243	11.49672628
H	0.250475548	8.011220222	5.448949224	H	2.968760442	3.111659236	11.15102231
C	1.233655196	11.30754145	6.748365496	H	2.386030032	4.159330551	12.47271413
H	1.202063423	11.59724132	5.674725537	H	3.94787025	4.509199467	11.67252851
C	1.877983697	12.45518408	7.535035542	H	5.935795571	8.030160558	7.531667953
H	2.881638434	12.72811056	7.153099518	C	4.160938354	6.820428973	7.07374477
H	1.959499966	12.19458445	8.608188245	H	5.497477856	6.823409639	8.759462098
H	1.241300735	13.36103755	7.448806221	H	4.03318269	7.427952032	6.132060297
C	-0.199482547	11.03881417	7.23174162	N	2.923096264	6.464179193	7.709605732
H	-0.823829612	11.94287462	7.070250641	H	4.703402498	5.90021678	6.740170675
H	-0.197574477	10.79758513	8.312656713	C	2.164751416	5.538969784	6.895250847
H	-0.676183619	10.18979246	6.706035262	H	1.80713052	5.974699435	5.921761572
C	4.60909436	8.485820737	10.2961182	H	1.261137594	5.191212371	7.432447214
H	4.097961649	9.345161407	10.77368337	H	2.778812832	4.641681697	6.634863684
H	5.70470478	8.58160358	10.50076901				

[Re(NMe)Cl(^{Me}NPNP^{iPr})]$^{+}$

Re	1.803363692	8.113519966	8.512002239	H	4.623278877	6.287122418	10.43932328
Cl	1.653391706	10.0030872	10.10470691	C	1.407779081	7.430952912	12.14951197
P	2.251733113	9.735207772	6.720530484	H	1.798394754	8.470828362	12.19055287
N	4.251960064	8.586486086	8.810649779	C	1.775590153	6.698232503	13.44382255
C	4.519912791	9.97380039	8.345054048	H	1.303699713	5.698642288	13.50097754
H	5.609390529	10.19187588	8.431051776	H	1.403010501	7.281773842	14.31058624
H	3.977248999	10.65331782	9.030689379	H	2.867867203	6.570880248	13.58132467
P	2.271476951	6.810357792	10.61007145	C	5.012857112	7.580701142	8.00067077
C	4.049321836	10.19868168	6.910955326	C	-0.109540365	7.528558521	11.94436904
H	4.625479624	9.585478287	6.190067071	H	-0.356732676	8.104312921	11.03175372
H	4.204613001	11.25643616	6.623895345	H	-0.563516448	8.060807909	12.80466556

C	2.119930764	9.171476945	4.930488091	H	-0.589429284	6.531890754	11.88485208
H	2.810113006	8.300421126	4.909781352	C	2.18345665	4.948041256	10.46592579
N	0.136918598	7.875077476	8.137893763	H	2.68891753	4.820556286	9.483930431
C	2.61493765	10.20711047	3.914229545	C	0.730391462	4.472419695	10.34449457
H	2.654663249	9.745683253	2.906324281	H	0.147672412	5.086430911	9.628588214
H	3.631441938	10.5831696	4.141771445	H	0.208970994	4.502601996	11.32139713
H	1.934372435	11.07899596	3.840152038	H	0.705432486	3.422186179	9.990052158
C	0.712672178	8.659480502	4.608256027	C	2.966383048	4.14875576	11.51561671
H	0.699709963	8.203028039	3.597875345	H	3.004120229	3.084181653	11.20505442
H	-0.033896908	9.479695262	4.604273971	H	2.487291272	4.182500988	12.51173398
H	0.387479023	7.886587625	5.333096466	H	4.013864023	4.489787687	11.62848231
C	1.26212634	11.3440733	6.765844498	H	5.872860109	8.074210293	7.50020348
H	1.268765833	11.66379647	5.701250806	C	4.109637001	6.851947271	7.003738616
C	1.901002982	12.45757045	7.603780565	H	5.438325045	6.832860621	8.694112347
H	2.914390466	12.73364332	7.254263634	H	3.988094142	7.452507782	6.065085136
H	1.949984509	12.17595782	8.672575022	N	2.869513256	6.532954499	7.668437893
H	1.276354156	13.37052107	7.520421687	H	4.622448294	5.915361454	6.684375967
C	-0.19137082	11.09041643	7.188445587	C	2.135650587	5.443634345	7.055295937
H	-0.77671184	12.02477422	7.070945151	H	1.697735138	5.713855222	6.058860266
H	-0.238854632	10.78820356	8.252869186	H	1.291672763	5.123900601	7.698066997
H	-0.683600864	10.31115824	6.575395493	H	2.793384416	4.559665805	6.88970945
C	4.567559294	8.467574593	10.26497705	C	-1.247383999	7.710895631	7.896925158
H	4.071893246	9.320738976	10.76675832	H	-1.480417457	7.905679066	6.828495041
H	5.666634473	8.573327608	10.41571336	H	-1.83932637	8.412131859	8.523378241
C	4.087464576	7.152119622	10.87726849	H	-1.554773725	6.667918427	8.130268033
H	4.311160154	7.145289906	11.96283647				

MeOTf

C	0.350555286	-0.047655633	-0.457374558	F	1.251373231	-0.128531451	0.521592685
S	-1.352872201	0.35798211	0.263301867	C	-2.203043266	-2.134404356	0.597781814
O	-1.175517672	1.469530085	1.192692684	O	-2.29672535	0.361755492	-0.862689695
O	-1.566083485	-0.98385609	1.193680989	H	-2.690516756	-2.673001935	1.431393932
F	0.696801426	0.913561092	-1.314750184	H	-1.447373406	-2.786926806	0.115808004
F	0.285065017	-1.222693003	-1.104349681	H	-2.961832824	-1.820479504	-0.145017857

$^{-}$OTf

C	0.262302783	-0.195782365	-0.396089987	F	0.68161702	0.823396265	-1.191394532
S	-1.502956737	0.078818457	0.244445258	F	0.366753215	-1.334389295	-1.130643898
O	-1.366532668	1.365654438	0.990143175	F	1.163606437	-0.299234775	0.616370469
O	-1.722365422	-1.138017068	1.082153459	O	-2.287134627	0.143134343	-1.025013945

Part IV

Literature

[1]B. A. Arndtsen, R. G. Bergman, T. A. Mobley, T. H. Peterson, „Selective Intermolecular Carbon-Hydrogen Bond Activation by Synthetic Metal Complexes in Homogeneous Solution“, *Acc. Chem. Res.* **1995**, *28*, 154–162, DOI 10.1021/ar00051a009.

[2]B. Thamdrup, „New Pathways and Processes in the Global Nitrogen Cycle“, *Annu. Rev. Ecol. Evol. Syst.* **2012**, *43*, 407–428, DOI 10.1146/annurev-ecolsys-102710-145048.

[3]A. E. Shilov, „Catalytic Reduction of Molecular Nitrogen in Solutions“, *Russ Chem Bull* **2003**, *52*, 2555–2562, DOI 10.1023/B:RUCB.0000019873.81002.60.

[4]H.-P. Jia, E. A. Quadrelli, „Mechanistic Aspects of Dinitrogen Cleavage and Hydrogenation to Produce Ammonia in Catalysis and Organometallic Chemistry: Relevance of Metal Hydride Bonds and Dihydrogen.“, *Chem Soc Rev* **2014**, *43*, 547–564, DOI 10.1039/c3cs60206k.

[5]Q. Cheng, „Perspectives in Biological Nitrogen Fixation Research“, *J. Integr. Plant Biol.* **2008**, *50*, 786–798, DOI 10.1111/j.1744-7909.2008.00700.x.

[6]T. Spatzal, M. Aksoyoglu, L. Zhang, S. L. A. Andrade, E. Schleicher, S. Weber, D. C. Rees, O. Einsle, „Evidence for Interstitial Carbon in Nitrogenase FeMo Cofactor“, *Science* **2011**, *334*, 940–940, DOI 10.1126/science.1214025.

[7]K. M. Lancaster, M. Roemelt, P. Ettenhuber, Y. Hu, M. W. Ribbe, F. Neese, U. Bergmann, S. DeBeer, „X-Ray Emission Spectroscopy Evidences a Central Carbon in the Nitrogenase Iron-Molybdenum Cofactor“, *Science* **2011**, *334*, 974–977, DOI 10.1126/science.1206445.

[8]R. R. Eady, „Structure-Function Relationships of Alternative Nitrogenases“, *Chem. Rev.* **1996**, *96*, 3013–3030, DOI 10.1021/cr950057h.

[9]B. M. Hoffman, D. Lukoyanov, Z.-Y. Yang, D. R. Dean, L. C. Seefeldt, „Mechanism of Nitrogen Fixation by Nitrogenase: The Next Stage“, *Chem. Rev.* **2014**, *114*, 4041–4062, DOI 10.1021/cr400641x.

[10]M. Appl in *Ullmann's Encyclopedia of Industrial Chemistry*, American Cancer Society, **2011**, DOI 10.1002/14356007.o02_o11.

[11]G. Ertl, „Surface Science and Catalysis—Studies on the Mechanism of Ammonia Synthesis: The P. H. Emmett Award Address“, *Catal. Rev.* **1980**, *21*, 201–223, DOI 10.1080/03602458008067533.

[12]Nitrogen Statistics and Information, https://www.usgs.gov/centers/nmic/nitrogen-statistics-and-information (visited on May 6, 2019).

[13]I. J. McPherson, T. Sudmeier, J. Fellowes, S. C. E. Tsang, „Materials for Electrochemical Ammonia Synthesis“, *Dalton Trans.* **2019**, *48*, 1562–1568, DOI 10.1039/C8DT04019B.

[14]A. J. Martín, T. Shinagawa, J. Pérez-Ramírez, „Electrocatalytic Reduction of Nitrogen: From *Haber-Bosch* to Ammonia Artificial Leaf“, *Chem* **2019**, *5*, 263–283, DOI 10.1016/j.chempr.2018.10.010.

[15]J. M. Smith in *Progress in Inorganic Chemistry Volume 58*, (Ed.: K. D. Karlin), John Wiley & Sons, Inc., **2014**, pp. 417–470.

[16]I. Klopsch, E. Y. Yuzik-Klimova, S. Schneider in *Nitrogen Fixation*, Topics in Organometallic Chemistry, Springer Berlin Heidelberg, **2017**, pp. 71–112, DOI 10.1007/3418_2016_12.

[17]A. D. Allen, C. V. Senoff, „Nitrogenopentammineruthenium(II) Complexes“, *Chem. Commun. (London)* **1965**, *0*, 621–622, DOI 10.1039/C19650000621.

[18]M. D. Fryzuk, S. A. Johnson, „The Continuing Story of Dinitrogen Activation“, *Coordination Chemistry Reviews* **2000**, *200-202*, 379–409, DOI 10.1016/S0010-8545(00)00264-2.

[19]B. A. MacKay, M. D. Fryzuk, „Dinitrogen Coordination Chemistry: On the Biomimetic Borderlands“, *Chem. Rev.* **2004**, *104*, 385–402, DOI 10.1021/cr020610c.

[20]R. M. Badger, „A Relation Between Internuclear Distances and Bond Force Constants“, *J. Chem. Phys.* **1934**, *2*, 128–131, DOI 10.1063/1.1749433.

[21]A. Poveda, I. C. Perilla, C. R. Pérez, „Review: Some Considerations About Coordination Compounds with End-on Dinitrogen“, *J. Coord. Chem.* **2001**, *54*, 427–440, DOI 10.1080/00958970108022654.

[22]D. F. Harrison, E. Weissberger, H. Taube, „Binuclear Ion Containing Nitrogen as a Bridging Group“, *Science* **1968**, *159*, 320–322, DOI 10.1126/science.159.3812.320.

[23]I. M. Treitel, M. T. Flood, R. E. Marsh, H. B. Gray, „Molecular and Electronic Structure of μ-Nitrogen-Decaammineruthenium(II)“, *J. Am. Chem. Soc.* **1969**, *91*, 6512–6513, DOI 10.1021/ja01051a070.

[24]J. Chatt, R. C. Fay, R. L. Richards, „Preparation and Characterisation of the Dinuclear Dinitrogen Complex, Trichloro-μ-dinitrogen-bis(tetrahydrofuran){chlorotetrakis[dimethyl-(phenyl)-phosphine]rhenium(I)}chromium(III) $[(PMe_2Ph)_4ClReN_2CrCl_3(thf)_2]$“, *J. Chem. Soc. A* **1971**, *0*, 702–704, DOI 10.1039/J19710000702.

[25]M. D. Fryzuk, T. S. Haddad, M. Mylvaganam, D. H. McConville, S. J. Rettig, „End-on versus Side-on Bonding of Dinitrogen to Dinuclear Early Transition-Metal Complexes“, *J. Am. Chem. Soc.* **1993**, *115*, 2782–2792, DOI 10.1021/ja00060a028.

[26]R. D. Sanner, J. M. Manriquez, R. E. Marsh, J. E. Bercaw, „Structure of μ-Dinitrogen-bis(bis(pentamethylcyclopentadienyl)-dinitrogenzirconium(II)), $\{(\eta^5\text{-}C_5(CH_3)_5)_2ZrN_2\}_2N_2$“, *J. Am. Chem. Soc.* **1976**, *98*, 8351–8357, DOI 10.1021/ja00442a007.

[27]C. E. Laplaza, M. J. A. Johnson, J. C. Peters, A. L. Odom, E. Kim, C. C. Cummins, G. N. George, I. J. Pickering, „Dinitrogen Cleavage by Three-Coordinate Molybdenum(III) Complexes: Mechanistic and Structural Data“, *J. Am. Chem. Soc.* **1996**, *118*, 8623–8638, DOI 10.1021/ja960574x.

[28]J. J. Curley, T. R. Cook, S. Y. Reece, P. Müller, C. C. Cummins, „Shining Light on Dinitrogen Cleavage: Structural Features, Redox Chemistry, and Photochemistry of the Key Intermediate Bridging Dinitrogen Complex“, *J. Am. Chem. Soc.* **2008**, *130*, 9394–9405, DOI 10.1021/ja8002638.

[29]C. B. Powell, M. B. Hall, „Molecular Orbital Calculations on Dinitrogen-Bridged Transition-Metal Dimers“, *Inorg. Chem.* **1984**, *23*, 4619–4627, DOI 10.1021/ic00194a042.

[30]D. E. Richardson, J. P. Sen, J. D. Buhr, H. Taube, „Preparation and Properties of Mixed-Valence (μ-Dinitrogen)Bis(Pentaammine) Complexes of Osmium and Ruthenium“, *Inorg. Chem.* **1982**, *21*, 3136–3140, DOI 10.1021/ic00138a043.

[31]M. Mercer, R. H. Crabtree, R. L. Richards, „A μ-Dinitrogen Complex with a Long N–N Bond. X-Ray Crystal Structure of $[(PMe_2Ph)_4ClReN_2MoCl_4(OMe)]$“, *J. Chem. Soc. Chem. Commun.* **1973**, *0*, 808–809, DOI 10.1039/C39730000808.

[32]M. J. Bezdek, S. Guo, P. J. Chirik, „Terpyridine Molybdenum Dinitrogen Chemistry: Synthesis of Dinitrogen Complexes That Vary by Five Oxidation States“, *Inorg. Chem.* **2016**, DOI 10.1021/acs.inorgchem.6b00053.

[33]S. Rafiq, M. J. Bezdek, M. Koch, P. J. Chirik, G. D. Scholes, „Ultrafast Photophysics of a Dinitrogen-Bridged Molybdenum Complex“, *J. Am. Chem. Soc.* **2018**, *140*, 6298–6307, DOI 10.1021/jacs.8b00890.

[34]S. Rafiq, M. J. Bezdek, P. J. Chirik, G. D. Scholes, „Dinitrogen Coupling to a Terpyridine-Molybdenum Chromophore Is Switched on by Fermi Resonance“, *Chem* **2019**, *5*, 402–416, DOI 10.1016/j.chempr.2018.11.003.

[35]P. P. Fontaine, B. L. Yonke, P. Y. Zavalij, L. R. Sita, „Dinitrogen Complexation and Extent of N≡N Activation within the Group 6 "End-On-Bridged" Dinuclear Complexes, $\{(\eta^5\text{-}C_5Me_5)M[N(i\text{-}Pr)C(Me)N(i\text{-}Pr)]\}_2(\mu\text{-}\eta^1\text{:}\eta^1\text{-}N_2)$ (M = Mo and W)“, *J. Am. Chem. Soc.* **2010**, *132*, 12273–12285, DOI 10.1021/ja100469f.

[36]M. Hirotsu, P. P. Fontaine, P. Y. Zavalij, L. R. Sita, „Extreme N≡N Bond Elongation and Facile N-Atom Functionalization Reactions within Two Structurally Versatile New Families of Group 4 Bimetallic "Side-on-Bridged" Dinitrogen Complexes for Zirconium and Hafnium“, *J. Am. Chem. Soc.* **2007**, *129*, 12690–12692, DOI 10.1021/ja0752989.

[37]A. J. Keane, B. L. Yonke, M. Hirotsu, P. Y. Zavalij, L. R. Sita, „Fine-Tuning the Energy Barrier for Metal-Mediated Dinitrogen N≡N Bond Cleavage“, *J. Am. Chem. Soc.* **2014**, *136*, 9906–9909, DOI 10.1021/ja505309j.

[38]M. Hirotsu, P. P. Fontaine, A. Epshteyn, L. R. Sita, „Dinitrogen Activation at Ambient Temperatures: New Modes of H_2 and $PhSiH_3$ Additions for an "End-On-Bridged" $[Ta(\text{IV})]_2(\mu\text{-}\eta^1\text{:}\eta^1\text{-}N_2)$ Complex and for the Bis(μ-Nitrido) $[Ta(\text{V})(\mu\text{"}-\text{"}N)]_2$ Product Derived from Facile N≡N Bond Cleavage“, *J. Am. Chem. Soc.* **2007**, *129*, 9284–9285, DOI 10.1021/ja072248v.

[39]B. L. Tran, B. Pinter, A. J. Nichols, F. T. Konopka, R. Thompson, C.-H. Chen, J. Krzystek, A. Ozarowski, J. Telser, M.-H. Baik, K. Meyer, D. J. Mindiola, „A Planar Three-Coordinate Vanadium(II) Complex and the Study of Terminal Vanadium Nitrides from N_2: A Kinetic or Thermodynamic Impediment to N–N Bond Cleavage?“, *J. Am. Chem. Soc.* **2012**, *134*, 13035–13045, DOI 10.1021/ja303360v.

[40]J. Jeffrey, M. F. Lappert, P. I. Riley, „Organozirconium Dinitrogen Complexes $[Zr(\eta\text{-}C_5H_4R')_2(\eta_2\text{-}N_2)R]$ and $[\{Zr(\eta\text{-}C_5H_5)_2R\}_2N_2]$ [R=$(Me_3Si)_2CH$, R' = H or Me]“, *Journal of Organometallic Chemistry* **1979**, *181*, 25–36, DOI 10.1016/S0022-328X(00)85734-4.

[41]G. A. Ozin, A. V. Voet, „"Sideways" Bonded Dinitrogen in Matrix Isolated Cobalt Dinitrogen, CoN_2“, *Can. J. Chem.* **1973**, *51*, 637–640, DOI 10.1139/v73-097.

[42]J. N. Armor, H. Taube, „Linkage Isomerization in Nitrogen-Labeled $[Ru(NH_3)_5N_2]Br_2$“, *J. Am. Chem. Soc.* **1970**, *92*, 2560–2562, DOI 10.1021/ja00711a066.

[43]A. Cusanelli, D. Sutton, „End-to-End Rotation of Co-Ordinated Dinitrogen in $(\eta_5\text{-}C_5Me_5)Re(CO)_2(N_2)$“, *J. Chem. Soc. Chem. Commun.* **1989**, *0*, 1719–1720, DOI 10.1039/C39890001719.

[44]A. Cusanelli, D. Sutton, „End-to-End Rotation of Rhenium-Bound Dinitrogen“, *Organometallics* **1996**, *15*, 1457–1464, DOI 10.1021/om950792j.

[45]D. V. Fomitchev, K. A. Bagley, P. Coppens, „The First Crystallographic Evidence for Side-On Coordination of N_2 to a Single Metal Center in a Photoinduced Metastable State“, *J. Am. Chem. Soc.* **2000**, *122*, 532–533, DOI 10.1021/ja993623p.

[46]K. Jonas, „π-Bonded Nitrogen in a Crystalline Nickel-Lithium Complex“, *Angew. Chem. Int. Ed. Engl.* **1973**, *12*, 997–998, DOI 10.1002/anie.197309971.

[47]C. Krüger, Y.-H. Tsay, „Molecular Structure of a π-Dinitrogen-Nickel-Lithium Complex“, *Angew. Chem. Int. Ed. Engl.* **1973**, *12*, 998–999, DOI 10.1002/anie.197309981.

[48]K. Jonas, D. J. Brauer, C. Krueger, P. J. Roberts, Y. H. Tsay, „"Side-on" Dinitrogen-Transition Metal Complexes. The Molecular Structure of $\{C_6H_5[Na \cdot O(C_2H_5)_2]_2[(C_6H_5)_2Ni]_2N_2NaLi_6(O C_2H_5)_4 \cdot O(C_2H_5)_2\}_2$“, *J. Am. Chem. Soc.* **1976**, *98*, 74–81, DOI 10.1021/ja00417a013.

[49]W. J. Evans, T. A. Ulibarri, J. W. Ziller, „Isolation and X-Ray Crystal Structure of the First Dinitrogen Complex of an f-Element Metal, $[(C_5Me_5)_2Sm]_2N_2$“, *J. Am. Chem. Soc.* **1988**, *110*, 6877–6879, DOI 10.1021/ja00228a043.

[50]M. D. Fryzuk, T. S. Haddad, S. J. Rettig, „Reduction of Dinitrogen by a Zirconium Phosphine Complex to Form a Side-on-Bridging N_2 Ligand. Crystal Structure of $\{[(Pr^i_2PCH_2SiMe_2)_2N]ZrCl\}_2(\mu\text{–}\eta^2\text{:}\eta^2\text{–}N_2)$“, *J. Am. Chem. Soc.* **1990**, *112*, 8185–8186, DOI 10.1021/ja00178a063.

[51]F. A. Cotton, D. G. Nocera, „The Whole Story of the Two-Electron Bond, with the δ Bond as a Paradigm“, *Acc. Chem. Res.* **2000**, *33*, 483–490, DOI 10.1021/ar980116o.

[52]F. Studt, L. Morello, N. Lehnert, M. D. Fryzuk, F. Tuczek, „Side-On Bridging Coordination of N_2: Spectroscopic Characterization of the Planar Zr_2N_2 Core and Theoretical Investigation of Its Butterfly Distortion“, *Chem. – Eur. J.* **2003**, *9*, 520–530, DOI 10.1002/chem.200390055.

[53]J. M. Manriquez, J. E. Bercaw, „Preparation of a Dinitrogen Complex of Bis(pentamethylcyclopentadienyl)zirconium(II). Isolation and Protonation Leading to Stoichiometric Reduction of Dinitrogen to Hydrazine“, *J. Am. Chem. Soc.* **1974**, *96*, 6229–6230, DOI 10.1021/ja00826a071.

[54]J. A. Pool, W. H. Bernskoetter, P. J. Chirik, „On the Origin of Dinitrogen Hydrogenation Promoted by $[(\eta^5\text{-}C_5Me_4H)_2Zr]_2(\mu^2,\eta^2,\eta^2\text{-}N_2)$“, *J. Am. Chem. Soc.* **2004**, *126*, 14326–14327, DOI 10.1021/ja045566s.

[55]J. A. Pool, E. Lobkovsky, P. J. Chirik, „Hydrogenation and Cleavage of Dinitrogen to Ammonia with a Zirconium Complex“, *Nature* **2004**, *427*, 527, DOI 10.1038/nature02274.

[56]R. J. Burford, M. D. Fryzuk, „Examining the Relationship between Coordination Mode and Reactivity of Dinitrogen“, *Nat. Rev. Chem.* **2017**, *1*, 0026, DOI 10.1038/s41570-017-0026.

[57]Y. Roux, C. Duboc, M. Gennari, „Molecular Catalysts for N_2 Reduction: State of the Art, Mechanism, and Challenges“, *ChemPhysChem* **2017**, *18*, 2606–2617, DOI 10.1002/cphc.201700665.

[58]*Nitrogen Fixation*, (Ed.: Y. Nishibayashi), Springer International Publishing, **2017**.

[59]*Transition Metal-Dinitrogen Complexes: Preparation and Reactivity*, (Ed.: Y. Nishibayashi), Wiley-VCH Verlag GmbH & Co. KGaA, Weinheim, Germany, **2019**, DOI 10.1002/9783527344260.

[60]J. Chatt, G. A. Heath, R. L. Richards, „The Reduction of Ligating Dinitrogen to Yield a Ligating N_2H_2 Moiety“, *J. Chem. Soc. Chem. Commun.* **1972**, 1010–1011, DOI 10.1039/C3972000101 0.

[61]J. Chatt, A. J. Pearman, R. L. Richards, „The Reduction of Mono-Coordinated Molecular Nitrogen to Ammonia in a Protic Environment“, *Nature* **1975**, *253*, 39, DOI 10.1038/253039b0.

[62]J. Chatt, R. L. Richards, „The Reactions of Dinitrogen in Its Metal Complexes“, *Journal of Organometallic Chemistry* **1982**, *239*, 65–77, DOI 10.1016/S0022-328X(00)94103-2.

[63]G. C. Stephan, C. Sivasankar, F. Studt, F. Tuczek, „Energetics and Mechanism of Ammonia Synthesis through the Chatt Cycle: Conditions for a Catalytic Mode and Comparison with the Schrock Cycle“, *Chem. Eur. J.* **2008**, *14*, 644–652, DOI 10.1002/chem.200700849.

[64]J. Chatt, G. A. Heath, G. J. Leigh, „The Formation of a Nitrogen to Carbon Bond in a Reaction of a Dinitrogen Complex“, *J. Chem. Soc. Chem. Commun.* **1972**, 444–445, DOI 10.1039/C39720000444.

[65]J. Chatt, G. A. Heath, N. E. Hooper, G. J. Leigh, „Direct Formation of Acylazo- and Aroylazo-Rhenium(III) Complexes from Rhenium(I) Dinitrogen Complexes“, *Journal of Organometallic Chemistry* **1973**, *57*, C67–C68, DOI 10.1016/S0022-328X(00)86587-0.

[66]D. V. Yandulov, R. R. Schrock, „Catalytic Reduction of Dinitrogen to Ammonia at a Single Molybdenum Center“, *Science* **2003**, *301*, 76–78, DOI 10.1126/science.1085326.

[67]D. V. Yandulov, R. R. Schrock, „Studies Relevant to Catalytic Reduction of Dinitrogen to Ammonia by Molybdenum Triamidoamine Complexes“, *Inorg. Chem.* **2005**, *44*, 1103–1117, DOI 10.1021/ic040095w.

[68]R. R. Schrock, „Catalytic Reduction of Dinitrogen to Ammonia by Molybdenum: Theory versus Experiment“, *Angew. Chem. Int. Ed.* **2008**, *47*, 5512–5522, DOI 10.1002/anie.200705246.

[69]F. Neese, „The Yandulov/Schrock Cycle and the Nitrogenase Reaction: Pathways of Nitrogen Fixation Studied by Density Functional Theory“, *Angew. Chem. Int. Ed.* **2006**, *45*, 196–199, DOI 10.1002/anie.200502667.

[70]W. Thimm, C. Gradert, H. Broda, F. Wennmohs, F. Neese, F. Tuczek, „Free Reaction Enthalpy Profile of the Schrock Cycle Derived from Density Functional Theory Calculations on the Full [MoHIPTN_3N] Catalyst“, *Inorg. Chem.* **2015**, *54*, 9248–9255, DOI 10.1021/acs.inorgchem.5b00787.

[71]A. Sharma, M. Roemelt, M. Reithofer, R. R. Schrock, B. M. Hoffman, F. Neese, „EPR/ENDOR and Theoretical Study of the Jahn–Teller-Active [HIPTN_3N]Mo(V)L Complexes (L = N^-, NH)“, *Inorg. Chem.* **2017**, *56*, 6906–6919, DOI 10.1021/acs.inorgchem.7b00364.

[72]J. S. Anderson, J. Rittle, J. C. Peters, „Catalytic Conversion of Nitrogen to Ammonia by an Iron Model Complex“, *Nature* **2013**, *501*, 84–87, DOI 10.1038/nature12435.

[73]S. E. Creutz, J. C. Peters, „Catalytic Reduction of N_2 to NH_3 by an Fe–N_2 Complex Featuring a C-Atom Anchor“, *J. Am. Chem. Soc.* **2014**, *136*, 1105–1115, DOI 10.1021/ja4114962.

[74]J. Rittle, J. C. Peters, „An Fe-N_2 Complex That Generates Hydrazine and Ammonia via Fe=NNH_2: Demonstrating a Hybrid Distal-to-Alternating Pathway for N_2 Reduction“, *J. Am. Chem. Soc.* **2016**, *138*, 4243–4248, DOI 10.1021/jacs.6b01230.

[75]N. B. Thompson, M. T. Green, J. C. Peters, „Nitrogen Fixation via a Terminal Fe(IV) Nitride“, *J. Am. Chem. Soc.* **2017**, *139*, 15312–15315, DOI 10.1021/jacs.7b09364.

[76]M. J. Chalkley, T. J. Del Castillo, B. D. Matson, J. P. Roddy, J. C. Peters, „Catalytic N_2-to-NH_3 Conversion by Fe at Lower Driving Force: A Proposed Role for Metallocene-Mediated PCET“, *ACS Cent. Sci.* **2017**, DOI 10.1021/acscentsci.7b00014.

[77]K. Arashiba, Y. Miyake, Y. Nishibayashi, „A Molybdenum Complex Bearing PNP-Type Pincer Ligands Leads to the Catalytic Reduction of Dinitrogen into Ammonia“, *Nat. Chem.* **2011**, *3*, 120–125, DOI 10.1038/nchem.906.

[78]H. Tanaka, Y. Nishibayashi, K. Yoshizawa, „Interplay between Theory and Experiment for Ammonia Synthesis Catalyzed by Transition Metal Complexes“, *Acc. Chem. Res.* **2016**, *49*, 987–995, DOI 10.1021/acs.accounts.6b00033.

[79]A. Eizawa, K. Arashiba, H. Tanaka, S. Kuriyama, Y. Matsuo, K. Nakajima, K. Yoshizawa, Y. Nishibayashi, „Remarkable Catalytic Activity of Dinitrogen-Bridged Dimolybdenum Complexes Bearing NHC-Based PCP-Pincer Ligands toward Nitrogen Fixation“, *Nat. Commun.* **2017**, *8*, 14874, DOI 10.1038/ncomms14874.

[80]K. Arashiba, A. Eizawa, H. Tanaka, K. Nakajima, K. Yoshizawa, Y. Nishibayashi, „Catalytic Nitrogen Fixation via Direct Cleavage of Nitrogen–Nitrogen Triple Bond of Molecular Dinitrogen under Ambient Reaction Conditions“, *BCSJ* **2017**, *90*, 1111–1118, DOI 10.1246/bcsj.20170197.

[81]Y. Ashida, K. Arashiba, K. Nakajima, Y. Nishibayashi, „Molybdenum-Catalysed Ammonia Production with Samarium Diiodide and Alcohols or Water“, *Nature* **2019**, *568*, 536, DOI 10.1038/s41586-019-1134-2.

[82]C. E. Laplaza, C. C. Cummins, „Dinitrogen Cleavage by a Three-Coordinate Molybdenum(III) Complex“, *Science* **1995**, *268*, 861–863, DOI 10.1126/science.268.5212.861.

[83]Q. Cui, D. G. Musaev, M. Svensson, S. Sieber, K. Morokuma, „N_2 Cleavage by Three-Coordinate Group 6 Complexes. W(III) Complexes Would Be Better Than Mo(III) Complexes“, *J. Am. Chem. Soc.* **1995**, *117*, 12366–12367, DOI 10.1021/ja00154a052.

[84]M. Kol, R. R. Schrock, R. Kempe, W. M. Davis, „Synthesis of Molybdenum and Tungsten Complexes That Contain Triamidoamine Ligands of the Type $(C_6F_5NCH_2CH_2)_3N$ and Activation of Dinitrogen by Molybdenum“, *J. Am. Chem. Soc.* **1994**, *116*, 4382–4390, DOI 10.1021/ja00089a028.

[85]K.-Y. Shih, R. R. Schrock, R. Kempe, „Synthesis of Molybdenum Complexes That Contain Silylated Triamidoamine Ligands. A μ-Dinitrogen Complex, Methyl and Acetylide Complexes, and Coupling of Acetylides“, *J. Am. Chem. Soc.* **1994**, *116*, 8804–8805, DOI 10.1021/ja00098a048.

[86]E. Solari, C. D. Silva, B. Iacono, J. Hesschenbrouck, C. Rizzoli, R. Scopelliti, C. Floriani, „Photochemical Activation of the N≡N Bond in a Dimolybdenum–Dinitrogen Complex: Formation of a Molybdenum Nitride“, *Angew. Chem. Int. Ed.* **2001**, *40*, 3907–3909, DOI 10.1002/1521-3773(20011015)40:20<3907::AID-ANIE3907>3.0.CO;2-#.

[87]G. Christian, R. Stranger, B. F. Yates, D. C. Graham, „Ligand Rotation in $[Ar(R)N]_3M\text{-}N_2\text{-}M'[N(R)Ar]_3$ (M, M' = Mo(iii), Nb(III; R = ^{i}Pr and ^{t}Bu) Dimers“, *Dalton Trans.* **2005**, 962–968, DOI 10.1039/B413766C.

[88]N. J. Brookes, D. C. Graham, G. Christian, R. Stranger, B. F. Yates, „The Influence of Peripheral Ligand Bulk on Nitrogen Activation by Three-Coordinate Molybdenum Complexes—A Theoretical Study Using the ONIOM Method“, *J. Comput. Chem.* **2009**, *30*, 2146–2156, DOI 10.1002/jcc.21199.

[89]M. H. Chisholm, F. A. Cotton, B. A. Frenz, W. W. Reichert, L. W. Shive, B. R. Stults, „The Molybdenum-Molybdenum Triple Bond. 1. Hexakis(Dimethylamido)Dimolybdenum and Some Homologs: Preparation, Structure, and Properties“, *J. Am. Chem. Soc.* **1976**, *98*, 4469–4476, DOI 10.1021/ja00431a024.

[90]Y.-C. Tsai, M. J. A. Johnson, D. J. Mindiola, C. C. Cummins, W. T. Klooster, T. F. Koetzle, „A Cyclometalated Resting State for a Reactive Molybdenum Amide: Favorable Consequences of β-Hydrogen Elimination Including Reductive Cleavage, Coupling, and Complexation“, *J. Am. Chem. Soc.* **1999**, *121*, 10426–10427, DOI 10.1021/ja9917464.

[91]J. C. Peters, J.-P. F. Cherry, J. C. Thomas, L. Baraldo, D. J. Mindiola, W. M. Davis, C. C. Cummins, „Redox-Catalyzed Binding of Dinitrogen by Molybdenum N-Tert-Hydrocarbylanilide Complexes: Implications for Dinitrogen Functionalization and Reductive Cleavage“, *J. Am. Chem. Soc.* **1999**, *121*, 10053–10067, DOI 10.1021/ja991435t.

[92]Y.-C. Tsai, C. C. Cummins, „Base-Catalyzed Dinitrogen Cleavage by Molybdenum Amides“, *Inorganica Chimica Acta*, Protagonists in Chemistry: Richard R. Schrock **2003**, *345*, 63–69, DOI 10.1016/S0020-1693(02)01344-0.

[93]M. Pucino, F. Allouche, C. P. Gordon, M. Wörle, V. Mougel, C. Coperet, „Reactive Coordinatively Saturated Mo(III) Complex: Exploiting the Adaptive Hapticity of Tris(Tert-Butoxy)Silanolate Ligands“, *Chem. Sci.* **2019**, 10.1039.C9SC01955C, DOI 10.1039/C9SC01955C.

[94]I. Klopsch, M. Finger, C. Würtele, B. Milde, D. B. Werz, S. Schneider, „Dinitrogen Splitting and Functionalization in the Coordination Sphere of Rhenium“, *J. Am. Chem. Soc.* **2014**, *136*, 6881–6883, DOI 10.1021/ja502759d.

[95]B. M. Lindley, R. S. van Alten, M. Finger, F. Schendzielorz, C. Würtele, A. J. M. Miller, I. Siewert, S. Schneider, „Mechanism of Chemical and Electrochemical N_2 Splitting by a Rhenium Pincer Complex“, *J. Am. Chem. Soc.* **2018**, *140*, 7922–7935, DOI 10.1021/jacs.8b03755.

[96]G. A. Silantyev, M. Förster, B. Schluschaß, J. Abbenseth, C. Würtele, C. Volkmann, M. C. Holthausen, S. Schneider, „Dinitrogen Splitting Coupled to Protonation“, *Angew. Chem. Int. Ed.* **2017**, *56*, 5872–5876, DOI 10.1002/anie.201701504.

[97]J. M. Smith, R. J. Lachicotte, K. A. Pittard, T. R. Cundari, G. Lukat-Rodgers, K. R. Rodgers, P. L. Holland, „Stepwise Reduction of Dinitrogen Bond Order by a Low-Coordinate Iron Complex“, *J. Am. Chem. Soc.* **2001**, *123*, 9222–9223, DOI 10.1021/ja016094+.

[98]J. M. Smith, A. R. Sadique, T. R. Cundari, K. R. Rodgers, G. Lukat-Rodgers, R. J. Lachicotte, C. J. Flaschenriem, J. Vela, P. L. Holland, „Studies of Low-Coordinate Iron Dinitrogen Complexes“, *J. Am. Chem. Soc.* **2006**, *128*, 756–769, DOI 10.1021/ja052707x.

[99]M. M. Rodriguez, E. Bill, W. W. Brennessel, P. L. Holland, „N_2 Reduction and Hydrogenation to Ammonia by a Molecular Iron-Potassium Complex“, *Science* **2011**, *334*, 780–783, DOI 10.1126/science.1211906.

[100]T. M. Figg, P. L. Holland, T. R. Cundari, „Cooperativity Between Low-Valent Iron and Potassium Promoters in Dinitrogen Fixation“, *Inorg. Chem.* **2012**, *51*, 7546–7550, DOI 10.1021/ic300150u.

[101]K. C. MacLeod, D. J. Vinyard, P. L. Holland, „A Multi-Iron System Capable of Rapid N_2 Formation and N_2 Cleavage“, *J. Am. Chem. Soc.* **2014**, *136*, 10226–10229, DOI 10.1021/ja505193z.

[102]G. K. B. Clentsmith, V. M. E. Bates, P. B. Hitchcock, F. G. N. Cloke, „Reductive Cleavage of Dinitrogen by a Vanadium Diamidoamine Complex: The Molecular Structures of $[V(Me_3SiN\{CH_2CH_2NSiMe_3\}_2)(\mu\text{-}N)]_2$ and $K[V(Me_3SiN\{CH_2CH_2NSiMe_3\}_2)(\mu\text{-}N)]_2$“, *J. Am. Chem. Soc.* **1999**, *121*, 10444–10445, DOI 10.1021/ja9921219.

[103]F. Studt, V. M. E. Lamarche, G. K. B. Clentsmith, F. G. N. Cloke, F. Tuczek, „Vibrational and Electronic Structure of the Dinuclear Bis(μ-Nitrido) Vanadium(V) Complex [V(N{N"}$_2$)(μ-N)]$_2$: Spectroscopic Properties of the M$_2$(μ-N)$_2$ Diamond Core“, *Dalton Trans.* **2005**, *0*, 1052–1057, DOI 10.1039/B418856J.

[104]V. M. E. Bates, G. K. B. Clentsmith, F. G. N. Cloke, J. C. Green, H. D. Ll. Jenkin, „Theoretical Investigation of the Pathway for Reductive Cleavage of Dinitrogen by a Vanadium Diamidoamine Complex“, *Chem. Commun.* **2000**, *0*, 927–928, DOI 10.1039/B002534H.

[105]I. Fischler, E. K. von Gustorf, „Chemische und biologische Aspekte der Fixierung und Reduktion molekularen Stickstoffs“, *Naturwissenschaften* **1975**, *62*, 63–70, DOI 10.1007/BF00592178.

[106]T. M. Buscagan, P. H. Oyala, J. C. Peters, „N$_2$-to-NH$_3$ Conversion by a Triphos–Iron Catalyst and Enhanced Turnover under Photolysis“, *Angew. Chem. Int. Ed.* **2017**, *56*, 6921–6926, DOI 10.1002/anie.201703244.

[107]M. J. A. Johnson, P. M. Lee, A. L. Odom, W. M. Davis, C. C. Cummins, „Atom-Bridged Intermediates in N- and P-Atom Transfer Reactions“, *Angew. Chem. Int. Ed. Engl.* **1997**, *36*, 87–91, DOI 10.1002/anie.199700871.

[108]A. S. Huss, J. J. Curley, C. C. Cummins, D. A. Blank, „Relaxation and Dissociation Following Photoexcitation of the (μ-N$_2$)[Mo(N[^{t}Bu]Ar)$_3$]$_2$ Dinitrogen Cleavage Intermediate“, *J. Phys. Chem. B* **2013**, *117*, 1429–1436, DOI 10.1021/jp310122x.

[109]H. Kunkely, A. Vogler, „Photolysis of Aqueous [(NH$_3$)$_5$Os(μ-N$_2$)Os(NH$_3$)$_5$]$^{5+}$: Cleavage of Dinitrogen by an Intramolecular Photoredox Reaction“, *Angewandte Chemie International Edition* **2010**, *49*, 1591–1593, DOI 10.1002/anie.200905026.

[110]H. Kunkely, A. Vogler, „Photolysis of Aqueous [Os(NH$_3$)$_5$(N$_2$)]$^{2+}$: Dismutation of Coordinated Dinitrogen“, *Inorganica Chimica Acta* **2012**, *391*, 229–231, DOI 10.1016/j.ica.2012.04.021.

[111]A. Vogler, H. Kunkely, „Photooxidation of Coordinated Dinitrogen. Photolysis of the ClO$_2$ Adduct of [(NH$_3$)$_5$Os(μ-N$_2$)Os(NH$_3$)$_5$]$^{5+}$“, *Inorganic Chemistry Communications* **2012**, *18*, 73–74, DOI 10.1016/j.inoche.2012.01.013.

[112]H. Kunkely, A. Vogler, „Photolysis of Aqueous [Os(NH$_3$)$_5$(N$_2$)]$^{2+}$. Photoreduction of Coordinated Dinitrogen to Hydrazine as a Model for a New Type of Artificial Photosynthesis?“, *Z. Für Naturforschung B* **2014**, *67*, 488–490, DOI 10.5560/znb.2012-0080.

[113]V. Krewald, L. González, „A Valence-Delocalised Osmium Dimer Capable of Dinitrogen Photocleavage: Ab Initio Insights into Its Electronic Structure“, *Chem. – Eur. J.* **2018**, *24*, 5112–5123, DOI 10.1002/chem.201704651.

[114]T. Miyazaki, H. Tanaka, Y. Tanabe, M. Yuki, K. Nakajima, K. Yoshizawa, Y. Nishibayashi, „Cleavage and Formation of Molecular Dinitrogen in a Single System Assisted by Molybdenum Complexes Bearing Ferrocenyldiphosphine“, *Angew. Chem. Int. Ed.* **2014**, *53*, 11488–11492, DOI 10.1002/anie.201405673.

[115]C. Rebreyend, B. de Bruin, „Photolytic N$_2$ Splitting: A Road to Sustainable NH$_3$ Production?“, *Angew. Chem. Int. Ed.* **2015**, *54*, 42–44, DOI 10.1002/anie.201409727.

[116]A. J. Keane, W. S. Farrell, B. L. Yonke, P. Y. Zavalij, L. R. Sita, „Metal-Mediated Production of Isocyanates, R$_3$EN=C=O from Dinitrogen, Carbon Dioxide, and R$_3$ECl“, *Angew. Chem. Int. Ed.* **2015**, *54*, 10220–10224, DOI 10.1002/anie.201502293.

[117]M. D. Fryzuk, J. B. Love, S. J. Rettig, V. G. Young, „Transformation of Coordinated Dinitrogen by Reaction with Dihydrogen and Primary Silanes“, *Science* **1997**, *275*, 1445–1447, DOI 10.1126/science.275.5305.1445.

[118]L. Morello, J. B. Love, B. O. Patrick, M. D. Fryzuk, „Carbon-Nitrogen Bond Formation via the Reaction of Terminal Alkynes with a Dinuclear Side-on Dinitrogen Complex“, *J. Am. Chem. Soc.* **2004**, *126*, 9480–9481, DOI 10.1021/ja049490b.

[119]W. H. Bernskoetter, E. Lobkovsky, P. J. Chirik, „Nitrogen–Carbon Bond Formation from N_2 and CO_2 Promoted by a Hafnocene Dinitrogen Complex Yields a Substituted Hydrazine“, *Angew. Chem. Int. Ed.* **2007**, *46*, 2858–2861, DOI 10.1002/anie.200604099.

[120]J. Fritzsche, H. Struve, „Ueber Die Osman-Osmiumsäure“, *J. Für Prakt. Chem.* **1847**, *41*, 97–113, DOI 10.1002/prac.18470410113.

[121]R. A. Eikey, M. M. Abu-Omar, „Nitrido and Imido Transition Metal Complexes of Groups 6–8“, *Coordination Chemistry Reviews* **2003**, *243*, 83–124, DOI 10.1016/S0010-8545(03)00048-1.

[122]C. J. Ballhausen, H. B. Gray, „The Electronic Structure of the Vanadyl Ion“, *Inorg. Chem.* **1962**, *1*, 111–122, DOI 10.1021/ic50001a022.

[123]J. M. Mayer, „Why Are There No Terminal Oxo Complexes of the Late Transition Metals? Or The Importance of Metal–Ligand π Antibonding Interactions“, *Comments Inorg. Chem.* **1988**, *8*, 125–135, DOI 10.1080/02603598808035790.

[124]K. G. Caulton, „The Influence of π-Stabilized Unsaturation an Filled/Filled Repulsions in Transition Metal Chemistry“, *New J. Chem.* **1994**, *18*, 25–41.

[125]J. F. Berry, „Terminal Nitrido and Imido Complexes of the Late Transition Metals“, *Comments Inorg. Chem.* **2009**, *30*, 28–66, DOI 10.1080/02603590902768875.

[126]W. D. Wagner, K. Nakamoto, „Formation of Nitridoiron(V) Porphyrins Detected by Resonance Raman Spectroscopy“, *J. Am. Chem. Soc.* **1988**, *110*, 4044–4045, DOI 10.1021/ja00220a057.

[127]W. D. Wagner, K. Nakamoto, „Resonance Raman Spectra of Nitridoiron(V) Porphyrin Intermediates Produced by Laser Photolysis“, *J. Am. Chem. Soc.* **1989**, *111*, 1590–1598, DOI 10.1021/ja00187a010.

[128]K. Meyer, E. Bill, B. Mienert, T. Weyhermüller, K. Wieghardt, „Photolysis of *cis*- and *trans*-$[Fe(III)(Cyclam)(N_3)_2]^+$ Complexes: Spectroscopic Characterization of a Nitridoiron(V) Species“, *J. Am. Chem. Soc.* **1999**, *121*, 4859–4876, DOI 10.1021/ja983454t.

[129]N. Aliaga-Alcalde, S. D. George, B. Mienert, E. Bill, K. Wieghardt, F. Neese, „The Geometric and Electronic Structure of [(Cyclam-Acetato)Fe(N)]+: A Genuine Iron(V) Species with a Ground-State Spin S=1/2“, *Angew. Chem. Int. Ed.* **2005**, *44*, 2908–2912, DOI 10.1002/anie.200462368.

[130]J. F. Berry, E. Bill, E. Bothe, S. D. George, B. Mienert, F. Neese, K. Wieghardt, „An Octahedral Coordination Complex of Iron(VI)“, *Science* **2006**, *312*, 1937–1941, DOI 10.1126/science.1128506.

[131]„A Tetrahedrally Coordinated $L_3Fe{-}N_x$ Platform“.

[132]C. Vogel, F. W. Heinemann, J. Sutter, C. Anthon, K. Meyer, „An Iron Nitride Complex“, *Angew. Chem. Int. Ed.* **2008**, *47*, 2681–2684, DOI 10.1002/anie.200800600.

[133]J. J. Scepaniak, M. D. Fulton, R. P. Bontchev, E. N. Duesler, M. L. Kirk, J. M. Smith, „Structural and Spectroscopic Characterization of an Electrophilic Iron Nitrido Complex“, *J. Am. Chem. Soc.* **2008**, *130*, 10515–10517, DOI 10.1021/ja8027372.

[134]A. K. Maity, J. Murillo, A. J. Metta-Magaña, B. Pinter, S. Fortier, „A Terminal Iron(IV) Nitride Supported by a Super Bulky Guanidinate Ligand and Examination of Its Electronic Structure and Reactivity“, *J. Am. Chem. Soc.* **2017**, *139*, 15691–15700, DOI 10.1021/jacs.7b06919.

[135]J.-U. Rohde, T. A. Betley, T. A. Jackson, C. T. Saouma, J. C. Peters, L. Que, „XAS Characterization of a Nitridoiron(IV) Complex with a Very Short Fe-N Bond“, *Inorg. Chem.* **2007**, *46*, 5720–5726, DOI 10.1021/ic700818q.

[136]R. Hoffmann, „Building Bridges Between Inorganic and Organic Chemistry (Nobel Lecture)“, *Angew. Chem. Int. Ed. Engl.* **1982**, *21*, 711–724, DOI 10.1002/anie.198207113.

[137]A. Walstrom, M. Pink, X. Yang, J. Tomaszewski, M.-H. Baik, K. G. Caulton, „A Facile Approach to a d^4 Ru≡N: Moiety“, *J. Am. Chem. Soc.* **2005**, *127*, 5330–5331, DOI 10.1021/ja050361k.

[138]B. Askevold, J. T. Nieto, S. Tussupbayev, M. Diefenbach, E. Herdtweck, M. C. Holthausen, S. Schneider, „Ammonia Formation by Metal–Ligand Cooperative Hydrogenolysis of a Nitrido Ligand“, *Nat Chem* **2011**, *3*, 532–537, DOI 10.1038/nchem.1051.

[139]J. Schöffel, A. Y. Rogachev, S. DeBeer George, P. Burger, „Isolation and Hydrogenation of a Complex with a Terminal Iridium–Nitrido Bond“, *Angew. Chem. Int. Ed.* **2009**, *48*, 4734–4738, DOI 10.1002/anie.200901494.

[140]M. G. Scheibel, B. Askevold, F. W. Heinemann, E. J. Reijerse, B. de Bruin, S. Schneider, „Closed-Shell and Open-Shell Square-Planar Iridium Nitrido Complexes“, *Nat Chem* **2012**, *4*, 552–558, DOI 10.1038/nchem.1368.

[141]M. G. Scheibel, Y. Wu, A. C. Stückl, L. Krause, E. Carl, D. Stalke, B. de Bruin, S. Schneider, „Synthesis and Reactivity of a Transient, Terminal Nitrido Complex of Rhodium.“, *J Am Chem Soc* **2013**, *135*, 17719–17722, DOI 10.1021/ja409764j.

[142]W. A. Nugent, J. M. Mayer, *Metal-Ligand Multiple Bonds: The Chemistry of Transition Metal Complexes Containing Oxo, Nitrido, Imido, Alkylidene, or Alkylidyne Ligands*, Wiley-Interscience, **1988**.

[143]E. D. Hedegård, J. Bendix, S. P. A. Sauer, „Partial Charges as Reactivity Descriptors for Nitrido Complexes“, *Journal of Molecular Structure: THEOCHEM* **2009**, *913*, 1–7, DOI 10.1016/j.theochem.2009.06.042.

[144]T. J. Crevier, J. M. Mayer, „Direct Attack of Phenyl Anion at an Electrophilic Osmium-Nitrido Ligand“, *J. Am. Chem. Soc.* **1998**, *120*, 5595–5596, DOI 10.1021/ja980548u.

[145]T. J. Crevier, J. M. Mayer, „Insertion of an Osmium Nitride into Boron-Carbon Bonds“, *Angewandte Chemie International Edition* **1998**, *37*, 1891–1893, DOI 10.1002/(SICI)1521-3773(19980803)37:13/14<1891::AID-ANIE1891>3.0.CO;2-Y.

[146]T. J. Crevier, B. K. Bennett, J. D. Soper, J. A. Bowman, A. Dehestani, D. A. Hrovat, S. Lovell, W. Kaminsky, J. M. Mayer, „C—N Bond Formation on Addition of Aryl Carbanions to the Electrophilic Nitrido Ligand in TpOs(N)Cl_2“, *J. Am. Chem. Soc.* **2001**, *123*, 1059–1071, DOI 10.1021/ja0028424.

[147]E. L. Sceats, J. S. Figueroa, C. C. Cummins, N. M. Loening, P. Van der Wel, R. G. Griffin, „Complexes Obtained by Electrophilic Attack on a Dinitrogen-Derived Terminal Molybdenum Nitride: Electronic Structure Analysis by Solid State CP/MAS ^{15}N NMR in Combination with DFT Calculations“, *Polyhedron*, Special Issue in Honour of M.L.H. Green **2004**, *23*, 2751–2768, DOI 10.1016/j.poly.2004.08.010.

[148]J. J. Curley, A. F. Cozzolino, C. C. Cummins, „Nitrogen Fixation to Cyanide at a Molybdenum Center“, *Dalton Trans.* **2011**, *40*, 2429–2432, DOI 10.1039/C0DT01326A.

[149]H. Henderickx, G. Kwakkenbos, A. Peters, J. van der Spoel, K. de Vries, „Direct Formation of an Organonitrogen Compound from a Molybdenum Nitrido Species“, *Chem. Commun.* **2003**, 2050–2051, DOI 10.1039/B305774G.

[150]Q. Liao, A. Cavaillé, N. Saffon-Merceron, N. Mézailles, „Direct Synthesis of Silylamine from N_2 and a Silane: Mediated by a Tridentate Phosphine Molybdenum Fragment“, *Angew. Chem. Int. Ed.* **2016**, *55*, 11212–11216, DOI 10.1002/anie.201604812.

[151]Q. Liao, N. Saffon-Merceron, N. Mézailles, „N_2 Reduction into Silylamine at Tridentate Phosphine/Mo Center: Catalysis and Mechanistic Study“, *ACS Catal.* **2015**, *5*, 6902–6906, DOI 10.1021/acscatal.5b01626.

[152]M. F. Espada, S. Bennaamane, Q. Liao, N. Saffon-Merceron, S. Massou, E. Clot, N. Nebra, M. Fustier-Boutignon, N. Mézailles, „Room-Temperature Functionalization of N_2 to Borylamine at a Molybdenum Complex“, *Angew. Chem.* **2018**, *130*, 13047–13050, DOI 10.1002/ange.201805915.

[153]I. Klopsch, M. Kinauer, M. Finger, C. Würtele, S. Schneider, „Conversion of Dinitrogen into Acetonitrile under Ambient Conditions“, *Angew. Chem. Int. Ed.* **2016**, *55*, 4786–4789, DOI 10.1002/anie.201600790.

[154]I. Klopsch, F. Schendzielorz, C. Volkmann, C. Würtele, S. Schneider, „Synthesis of Benzonitrile from Dinitrogen“, *Z. Für Anorg. Allg. Chem.* **2018**, *644*, 916–919, DOI 10.1002/zaac.201800181.

[155]G. P. Connor, B. Q. Mercado, H. M. C. Lant, J. M. Mayer, P. L. Holland, „Chemical Oxidation of a Coordinated PNP-Pincer Ligand Forms Unexpected Re–Nitroxide Complexes with Reversal of Nitride Reactivity“, *Inorg. Chem.* **2019**, DOI 10.1021/acs.inorgchem.9b01075.

[156]L. M. Duman, W. S. Farrell, P. Y. Zavalij, L. R. Sita, „Steric Switching from Photochemical to Thermal Reaction Pathways for Enhanced Efficiency in Metal-Mediated Nitrogen Fixation“, *J. Am. Chem. Soc.* **2016**, *138*, 14856–14859, DOI 10.1021/jacs.6b09789.

[157]L. M. Duman, L. R. Sita, „Closing the Loop on Transition-Metal-Mediated Nitrogen Fixation: Chemoselective Production of $HN(SiMe_3)_2$ from N_2, Me_3SiCl, and X—OH (X = R, R_3Si, or Silica Gel)“, *J. Am. Chem. Soc.* **2017**, *139*, 17241–17244, DOI 10.1021/jacs.7b08859.

[158]M. P. Shaver, M. D. Fryzuk, „Activation of Molecular Nitrogen: Coordination, Cleavage and Functionalization of N_2 Mediated By Metal Complexes“, *Adv. Synth. Catal.* **2003**, *345*, 1061–1076, DOI 10.1002/adsc.200303081.

[159]J. J. Scepaniak, C. G. Margarit, J. N. Harvey, J. M. Smith, „Nitrogen Atom Transfer from Iron(IV) Nitrido Complexes: A Dual-Nature Transition State for Atom Transfer“, *Inorg. Chem.* **2011**, *50*, 9508–9517, DOI 10.1021/ic201190c.

[160]J. J. Scepaniak, R. P. Bontchev, D. L. Johnson, J. M. Smith, „Snapshots of Complete Nitrogen Atom Transfer from an Iron(IV) Nitrido Complex“, *Angew. Chem. Int. Ed.* **2011**, *50*, 6630–6633, DOI 10.1002/anie.201102028.

[161]S. B. Muñoz, W.-T. Lee, D. A. Dickie, J. J. Scepaniak, D. Subedi, M. Pink, M. D. Johnson, J. M. Smith, „Styrene Aziridination by Iron(IV) Nitrides“, *Angew. Chem. Int. Ed.* **2015**, *54*, 10600–10603, DOI 10.1002/anie.201503773.

[162]D. W. Crandell, S. B. Muñoz, J. M. Smith, M.-H. Baik, „Mechanistic Study of Styrene Aziridination by Iron(IV) Nitrides“, *Chem. Sci.* **2018**, *9*, 8542–8552, DOI 10.1039/C8SC03677B.

[163]W.-L. Man, W. W. Y. Lam, S.-M. Yiu, T.-C. Lau, S.-M. Peng, „Direct Aziridination of Alkenes by a Cationic (Salen)Ruthenium(VI) Nitrido Complex“, *J. Am. Chem. Soc.* **2004**, *126*, 15336–15337, DOI 10.1021/ja045845f.

[164]S. N. Brown, „Insertion of a Metal Nitride into Carbon-Carbon Double Bonds“, *J. Am. Chem. Soc.* **1999**, *121*, 9752–9753, DOI 10.1021/ja992385v.

[165]A. G. Maestri, S. D. Taylor, S. M. Schuck, S. N. Brown, „Cleavage of Conjugated Alkenes by Cationic Osmium Nitrides: Scope of the Reaction and Dynamics of the Azaallenium Products“, *Organometallics* **2004**, *23*, 1932–1946, DOI 10.1021/om034404m.

[166]A. Walstrom, H. Fan, M. Pink, K. G. Caulton, „Unexpected Selectivity in Electrophilic Attack on (PNP)RuN“, *Inorganica Chimica Acta*, Protagonist in Chemistry: Paul S. Pregosin **2010**, *363*, 633–636, DOI 10.1016/j.ica.2008.11.010.

[167]A. Walstrom, M. Pink, H. Fan, J. Tomaszewski, K. G. Caulton, „Radical (NO) and Nonradical (N_2O) Reagents Convert a Ruthenium(IV) Nitride to the Same Nitrosyl Complex“, *Inorg. Chem.* **2007**, *46*, 7704–7706, DOI 10.1021/ic700789y.

[168]N. Tsvetkov, M. Pink, H. Fan, J.-H. Lee, K. G. Caulton, „Redox and Lewis Acid Reactivity of Unsaturated OsII“, *Eur. J. Inorg. Chem.* **2010**, *2010*, 4790–4800, DOI 10.1002/ejic.201000503.

[169]A. Okuniewski, D. Rosiak, J. Chojnacki, B. Becker, „Coordination Polymers and Molecular Structures among Complexes of Mercury(II) Halides with Selected 1-Benzoylthioureas“, *Polyhedron* **2015**, *90*, 47–57, DOI 10.1016/j.poly.2015.01.035.

[170]D. Sieh, J. Schöffel, P. Burger, „Synthesis of a Chloro Protected Iridium Nitrido Complex“, *Dalton Trans.* **2011**, *40*, 9512–9524, DOI 10.1039/C1DT10886G.

[171]D. Sieh, P. Burger, „Si–H Activation in an Iridium Nitrido Complex—A Mechanistic and Theoretical Study“, *J. Am. Chem. Soc.* **2013**, *135*, 3971–3982, DOI 10.1021/ja311905h.

[172]J. Schöffel, N. Šušnjar, S. Nückel, D. Sieh, P. Burger, „4d vs. 5d – Reactivity and Fate of Terminal Nitrido Complexes of Rhodium and Iridium“, *Eur. J. Inorg. Chem.* **2010**, *2010*, 4911–4915, DOI 10.1002/ejic.201000899.

[173]J. Abbenseth, M. Finger, C. Würtele, M. Kasanmascheff, S. Schneider, „Coupling of Terminal Iridium Nitrido Complexes“, *Inorg. Chem. Front.* **2016**, *3*, 469–477, DOI 10.1039/C5QI00267B.

[174]F. Schendzielorz, master's thesis, Georg-August-Universität, Göttingen, **2014**.

[175]M. M. Konnick, S. M. Bischof, D. H. Ess, R. A. Periana, B. G. Hashiguchi, „Base Accelerated Generation of N_2 and NH_3 from an Osmium Nitride“, *Journal of Molecular Catalysis A: Chemical* **2014**, *382*, 1–7, DOI 10.1016/j.molcata.2013.10.019.

[176]J. T. Anhaus, T. P. Kee, M. H. Schofield, R. R. Schrock, „Planar "20-Electron" Osmium Imido Complexes. A Linear Imido Ligand Does Not Necessarily Donate Its Lone Pair of Electrons to the Metal“, *J. Am. Chem. Soc.* **1990**, *112*, 1642–1643, DOI 10.1021/ja00160a061.

[177]J. R. Wolf, G. C. Bazan, R. R. Schrock, „Exchange of Oxo Ligands in OsO_4 with Imido Ligands in $Mo(NAr)_2(O\text{-}t\text{Bu})_2$. A Facile Route to $Os(NAr)_2O_2$ and $Os(NAr)_3O$ and Osmium(IV) Complexes of the Type $Os(NAr)_2L_2$ (NAr = N-2,6-C_6H_3-Iso-Pr_2; L = a Phosphine)“, *Inorg. Chem.* **1993**, *32*, 4155–4156, DOI 10.1021/ic00071a032.

[178]M. H. V. Huynh, P. S. White, C. A. Carter, T. J. Meyer, „Formation and Reactivity of the Osmium(IV)–Cyanoimido Complex $[Os(IV(bpy)(Cl)_3(NCN)]^-$“, *Angew. Chem. Int. Ed.* **2001**, *40*, 3037–3039, DOI 10.1002/1521-3773(20010817)40:16<3037::AID-ANIE3037>3.0.CO;2-0.

[179]M. H. V. Huynh, R. T. Baker, D. L. Jameson, A. Labouriau, T. J. Meyer, „Formation and Reactivity of the Os(IV)-Azidoimido Complex, PPN|[Os(IV)|(bpy)(Cl)3|(N4)]“, *J. Am. Chem. Soc.* **2002**, *124*, 4580–4582, DOI 10.1021/ja0122086.

[180]I. Klopsch, PhD thesis, Georg-August-Universität, Göttingen, **2016**.

[181]U. Abram, A. Hagenbach, „*Trans*-$[TcNCl_2(Ph_3PNH)_2]$ — Synthesis and Structure“, *Z. Für Anorg. Allg. Chem.* **2002**, *628*, 1719–1720, DOI 10.1002/1521-3749(200208)628:8<1719::AID-ZAAC1719>3.0.CO;2-0.

[182]M. Bertoli, A. Choualeb, D. G. Gusev, A. J. Lough, Q. Major, B. Moore, „PNP Pincer Osmium Polyhydrides for Catalytic Dehydrogenation of Primary Alcohols“, *Dalton Trans.* **2011**, *40*, 8941–8949, DOI 10.1039/C1DT10342C.

[183]N. Lease, E. M. Pelczar, T. Zhou, S. Malakar, T. J. Emge, F. Hasanayn, K. Krogh-Jespersen, A. S. Goldman, „PNP-Pincer Complexes of Osmium: Comparison with Isoelectronic (PCP)Ir and $(PNP)Ir^+$ Units“, *Organometallics* **2018**, *37*, 314–326, DOI 10.1021/acs.organomet.7b00738.

[184]I. Ivančič, D. Degobbis, „An Optimal Manual Procedure for Ammonia Analysis in Natural Waters by the Indophenol Blue Method“, *Water Research* **1984**, *18*, 1143–1147, DOI 10.1016/0043-1354(84)90230-6.

[185]J. Abbenseth, S. C. Bete, M. Finger, C. Volkmann, C. Würtele, S. Schneider, „Four- and Five-Coordinate Osmium(IV) Nitrides and Imides: Circumventing the “Nitrido Wall”“, *Organometallics* **2018**, *37*, 802–811, DOI 10.1021/acs.organomet.7b00707.

[186]J. D. Buhr, H. Taube, „Oxidation of $[Os(NH_3)_5CO]^{2+}$ to $[Os(NH_3)_4CO)_2(N_2)]^{4+}$“, *Inorg. Chem.* **1979**, *18*, 2208–2212, DOI 10.1021/ic50198a032.

[187]D. C. Ware, H. Taube, „Substitution-Induced Nitrogen-Nitrogen Coupling for Nitride Coordinated to Osmium(VI)“, *Inorg. Chem.* **1991**, *30*, 4605–4610, DOI 10.1021/ic00024a029.

[188]T. J. Meyer, M. H. V. Huynh, „The Remarkable Reactivity of High Oxidation State Ruthenium and Osmium Polypyridyl Complexes“, *Inorg. Chem.* **2003**, *42*, 8140–8160, DOI 10.1021/ic020731v.

[189]H.-W. Lam, C.-M. Che, K.-Y. Wong, „Photoredox Properties of $[OsN(NH_3)_4]^{3+}$ and Mechanism of Formation of $[\{Os(NH_3)_4(CH_3CN)\}_2N_2]^{5+}$ through a Nitrido-Coupling Reaction“, *J. Chem. Soc. Dalton Trans.* **1992**, *0*, 1411–1416, DOI 10.1039/DT9920001411.

[190]K. D. Demadis, T. J. Meyer, P. S. White, „Localization in *trans,trans*-$[(Tpy)(Cl)_2Os(III)(N_2)Os(II)(Cl)_2(Tpy)]^+$ (Tpy = 2,2‘:6‘,2“-Terpyridine)“, *Inorg. Chem.* **1997**, *36*, 5678–5679, DOI 10.1021/ic970885o.

[191]D. Adhikari, F. Basuli, H. Fan, J. C. Huffman, M. Pink, D. J. Mindiola, „P=N Bond Formation via Incomplete N-Atom Transfer from a Ferrous Amide Precursor“, *Inorg. Chem.* **2008**, *47*, 4439–4441, DOI 10.1021/ic800182m.

[192]V. Vreeken, L. Baij, B. de Bruin, M. A. Siegler, J. I. van der Vlugt, „N-Atom Transfer via Thermal or Photolytic Activation of a Co-Azido Complex with a PNP Pincer Ligand“, *Dalton Trans.* **2017**, *46*, 7145–7149, DOI 10.1039/C7DT01712J.

[193]Y. Zhang, P. Tong, D. Yang, J. Li, B. Wang, J. Qu, „Migratory Insertion and Hydrogenation of a Bridging Azide in a Thiolate-Bridged Dicobalt Reaction Platform“, *Chem. Commun.* **2017**, *53*, 9854–9857, DOI 10.1039/C7CC05092E.

[194]V. Vreeken, M. A. Siegler, B. de Bruin, J. N. H. Reek, M. Lutz, J. I. van der Vlugt, „C–H Activation of Benzene by a Photoactivated Ni(II)(Azide): Formation of a Transient Nickel Nitrido Complex“, *Angew. Chem. Int. Ed.* **2015**, *54*, 7055–7059, DOI 10.1002/anie.201501437.

[195]J. Abbenseth, M. Diefenbach, S. C. Bete, C. Würtele, C. Volkmann, S. Demeshko, M. C. Holthausen, S. Schneider, „A Square-Planar Osmium(II) Complex“, *Chem. Commun.* **2017**, DOI 10.1039/C7CC01569K.

[196]A. W. Addison, T. N. Rao, J. Reedijk, J. van Rijn, G. C. Verschoor, „Synthesis, Structure, and Spectroscopic Properties of Copper(II) Compounds Containing Nitrogen–Sulphur Donor Ligands; the Crystal and Molecular Structure of Aqua[1,7-Bis(N-Methylbenzimidazol-2-Yl)-2,6-Dithiaheptane]Copper(II) Perchlorate“, *J. Chem. Soc. Dalton Trans.* **1984**, *0*, 1349–1356, DOI 10.1039/DT9840001349.

[197]S. P. Semproni, W. S. McNeil, R. A. Baillie, B. O. Patrick, C. F. Campana, P. Legzdins, „Ground-State Electronic Asymmetry in $Cp^*W(NO)(\eta_1\text{–Isonitrile})_2$ Complexes“, *Organometallics* **2010**, *29*, 867–875, DOI 10.1021/om901018n.

[198]J. Bauer, H. Braunschweig, C. Hörl, K. Radacki, J. Wahler, „Synthesis of Zwitterionic Cobaltocenium Borate and Borata-Alkene Derivatives from a Borole-Radical Anion“, *Chem. – Eur. J.* **2013**, *19*, 13396–13401, DOI 10.1002/chem.201302201.

[199]P. O. Lagaditis, B. Schluschaß, S. Demeshko, C. Würtele, S. Schneider, „Square-Planar Cobalt(iii) Pincer Complex“, *Inorg. Chem.* **2016**, *55*, 4529–4536, DOI 10.1021/acs.inorgchem.6b00369.

[200]F. Schneck, M. Finger, M. Tromp, S. Schneider, „Chemical Non-Innocence of an Aliphatic PNP Pincer Ligand“, *Chem. Eur. J.* **2017**, *23*, 33–37, DOI 10.1002/chem.201604407.

[201]W. E. Truce, D. G. Brady, „Stereochemistry of Amine Additions to Acetylenic Sulfones and Carboxylic Esters“, *J. Org. Chem.* **1966**, *31*, 3543–3550, DOI 10.1021/jo01349a018.

[202]T. L. Brown, K. J. Lee, „Ligand Steric Properties“, *Coordination Chemistry Reviews* **1993**, *128*, 89–116, DOI 10.1016/0010-8545(93)80025-Z.

[203]B. N. Figgis, J. Lewis, „The Magnetic Properties of Transition Metal Complexes“, *Prog. Inorg. Chem.*, Progress in Inorganic Chemistry **1964**, DOI 10.1002/9780470166079.ch2.

[204]J. Chatt, G. J. Leigh, D. M. P. Mingos, „Configurations of Some Complexes of Rhenium, Ruthenium, Osmium, Rhodium, Iridium, and Platinum Halides with Mono(Tertiary Phosphines) and Mono(Tertiary Arsines)“, *J. Chem. Soc. A* **1969**, *0*, 1674–1680, DOI 10.1039/J19690001674.

[205]D. F. Evans, „400. The Determination of the Paramagnetic Susceptibility of Substances in Solution by Nuclear Magnetic Resonance“, *J. Chem. Soc.* **1959**, *0*, 2003–2005, DOI 10.1039/JR9590002003.

[206]P. Zanello, *Inorganic Electrochemistry: Theory, Practice and Application*, The Royal Society of Chemistry, **2003**, DOI 10.1039/9781847551146.

[207]C. Kiene, Bachelor's thesis, Georg-August-Universität, Göttingen, **2019**.

[208]C. A. Tolman, „Steric Effects of Phosphorus Ligands in Organometallic Chemistry and Homogeneous Catalysis“, *Chem. Rev.* **1977**, *77*, 313–348, DOI 10.1021/cr60307a002.

[209]M. Käß, A. Friedrich, M. Drees, S. Schneider, „Ruthenium Complexes with Cooperative PNP Ligands: Bifunctional Catalysts for the Dehydrogenation of Ammonia–Borane“, *Angew. Chem. Int. Ed.* **2009**, *48*, 905–907, DOI 10.1002/anie.200805108.

[210]B. Askevold, M. M. Khusniyarov, E. Herdtweck, K. Meyer, S. Schneider, „A Square-Planar Ruthenium(II) Complex with a Low-Spin Configuration“, *Angew. Chem. Int. Ed.* **2010**, *49*, 7566–7569, DOI 10.1002/anie.201002296.

[211]F. J. V. Santos, C. A. Nieto de Castro, J. H. Dymond, N. K. Dalaouti, M. J. Assael, A. Nagashima, „Standard Reference Data for the Viscosity of Toluene“, *J. Phys. Chem. Ref. Data* **2006**, *35*, 1–8, DOI 10.1063/1.1928233.

[212]Tetrahydrofuran - High Purity Solvents, https://www.sigmaaldrich.com/chemistry/solvents/tetrahydrofuran-center.html (visited on Feb. 15, 2019).

[213]Nitrogen, https://webbook.nist.gov/cgi/cbook.cgi?ID=C7727379&Units=SI&Mask=1000#Diatomic (visited on Feb. 19, 2019).

[214]J. Chatt, J. R. Dilworth, R. L. Richards, „Recent Advances in the Chemistry of Nitrogen Fixation“, *Chem. Rev.* **1978**, *78*, 589–625, DOI 10.1021/cr60316a001.

[215]F. Neese, „Prediction of Molecular Properties and Molecular Spectroscopy with Density Functional Theory: From Fundamental Theory to Exchange-Coupling“, *Coordination Chemistry Reviews*, Theory and Computing in Contemporary Coordination Chemistry **2009**, *253*, 526–563, DOI 10.1016/j.ccr.2008.05.014.

[216]G. Christian, R. Stranger, B. F. Yates, C. C. Cummins, „Rationalizing the Different Products in the Reaction of N_2 with Three-Coordinate MoL_3 Complexes“, *Dalton Trans.* **2007**, *0*, 1939–1947, DOI 10.1039/B701050H.

[217]T. Rodima, I. Kaljurand, A. Pihl, V. Mäemets, I. Leito, I. A. Koppel, „Acid-Base Equilibria in Nonpolar Media. 2. Self-Consistent Basicity Scale in THF Solution Ranging from 2-Methoxypyridine to EtP_1(Pyrr) Phosphazene“, *J. Org. Chem.* **2002**, *67*, 1873–1881, DOI 10.1021/jo016185p.

[218]K. C. Mullane, H. Ryu, T. Cheisson, L. N. Grant, J. Y. Park, B. C. Manor, P. J. Carroll, M.-H. Baik, D. J. Mindiola, E. J. Schelter, „C–H Bond Addition across a Transient Uranium–Nitrido Moiety and Formation of a Parent Uranium Imido Complex“, *J. Am. Chem. Soc.* **2018**, *140*, 11335–11340, DOI 10.1021/jacs.8b06090.

[219]J. R. Dilworth, J. S. Lewis, J. R. Miller, Y. Zheng, „Rhenium Complex of a Triply Deprotonated Chelated Thiosemicarbazide and Its Conversion to a Nitride Complex via a Hydrazide Intermediate. Crystal Structure of $[ReCl_2(NH)(NHNH_2)(PPh_3)_2]$“, *J. Chem. Soc. Dalton Trans.* **1995**, *0*, 1357–1361, DOI 10.1039/DT9950001357.

[220]A. Haug, J. Strähle, „Synthese und Struktur von $[Re(NH)Cl_2(PMe_2Ph)_3][TaCl_6]$ und $[(Me_2PhP)_3Cl_2Re{\equiv}N]_2VOCl_2$“, *Z. Für Anorg. Allg. Chem.* **1998**, *624*, 1746–1750, DOI 10.1002/(SICI)1521-3749(1998110)624:11<1746::AID-ZAAC1746>3.0.CO;2-2.

[221]W.-H. Leung, J. L. C. Chim, I. D. Williams, W.-T. Wong, „Reactions of Nitridorhenium(V) and -Osmium(VI) Complexes with Acylating Agents“, *Inorg. Chem.* **1999**, *38*, 3000–3005, DOI 10.1021/ic981244b.

[222]D. Davidson, H. Skovronek, „The Acylation of Amides“, *J. Am. Chem. Soc.* **1958**, *80*, 376–379, DOI 10.1021/ja01535a032.

[223]B. M. Lindley, Q. J. Bruch, P. S. White, F. Hasanayn, A. J. M. Miller, „Ammonia Synthesis from a Pincer Ruthenium Nitride via Metal–Ligand Cooperative Proton-Coupled Electron Transfer“, *J. Am. Chem. Soc.* **2017**, *139*, 5305–5308, DOI 10.1021/jacs.7b01323.

[224]D. Barrón, J. Barbosa, „Acid–Base Behaviour of Substituted Phenolic Substances and Resolution of Acid Strength in Tetrahydrofuran“, *Analytica Chimica Acta* **2000**, *403*, 339–347, DOI 10.1016/S0003-2670(99)00635-2.

[225]J. Barbosa, D. Barrón, E. Bosch, M. Rosés, „Resolution of Acid Strength in Tetrahydrofuran of Substituted Benzoic Acids“, *Analytica Chimica Acta* **1992**, *265*, 157–165, DOI 10.1016/0003-2670(92)85165-3.

[226]J. Abbenseth, PhD thesis, Georg-August-Universität, Göttingen, **2019**.

[227]C. He, M. J. Gaunt, „Ligand-Enabled Catalytic C-H Arylation of Aliphatic Amines by a Four-Membered-Ring Cyclopalladation Pathway“, *Angew. Chem. Int. Ed.* **2015**, *54*, 15840–15844, DOI 10.1002/anie.201508912.

[228]J. Meiners, A. Friedrich, E. Herdtweck, S. Schneider, „Facile Double C-H Activation of Tetrahydrofuran by an Iridium PNP Pincer Complex“, *Organometallics* **2009**, *28*, 6331–6338, DOI 10.1021/om9006906.

[229]G. W. Parshall, L. W. Shive, F. A. Cotton in *Inorganic Syntheses*, *Vol. XVII*, John Wiley & Sons, Ltd, **1977**, pp. 110–112, DOI 10.1002/9780470132487.ch31.

[230]G. Rouschias, G. Wilkinson, „The Preparation and Reactions of Trihaolgeno(Alkanonitrile)Bis-(Triphenylphosphine)Rhenium(III) Complexes“, *J. Chem. Soc. Inorg. Phys. Theor.* **1967**, 993, DOI 10.1039/j19670000993.

[231]S. H. Babcock, H. P. Lankelma, E. Vopicka in *Inorganic Syntheses*, *Vol. I*, John Wiley & Sons, Ltd, **1939**, pp. 10–11, DOI 10.1002/9780470132326.ch4.

[232]J.-M. Lalancette, G. Rollin, P. Dumas, „Metals Intercalated in Graphite. I. Reduction and Oxidation“, *Can. J. Chem.* **1972**, *50*, 3058–3062, DOI 10.1139/v72-485.

[233]V. W. Manner, T. F. Markle, J. H. Freudenthal, J. P. Roth, J. M. Mayer, „The First Crystal Structure of a Monomeric Phenoxyl Radical: 2,4,6-Tri-Tert-Butylphenoxyl Radical“, *Chem. Commun.* **2007**, 256–258, DOI 10.1039/B712872J.

[234]M. Brookhart, B. Grant, A. F. Volpe, „$[(3,5\text{-}(CF_3)_2C_6H_3)_4B]^-[H(OEt_2)_2]^+$: A Convenient Reagent for Generation and Stabilization of Cationic, Highly Electrophilic Organometallic Complexes“, *Organometallics* **1992**, *11*, 3920–3922, DOI 10.1021/om00059a071.

[235]A. Martinsen, J. Songstad, R. Larsson, M. Pouchard, P. Hagenmuller, A. F. Andresen, „Preparation and Properties of Some Bis(Triphenylphosphine)Iminium Salts, $[(Ph_3P)_2N]X$.“, *Acta Chem. Scand.* **1977**, *31a*, 645–650, DOI 10.3891/acta.chem.scand.31a-0645.

[236]D. Adhikari, S. Mossin, F. Basuli, J. C. Huffman, R. K. Szilagyi, K. Meyer, D. J. Mindiola, „Structural, Spectroscopic, and Theoretical Elucidation of a Redox-Active Pincer-Type Ancillary Applied in Catalysis“, *J. Am. Chem. Soc.* **2008**, *130*, 3676–3682, DOI 10.1021/ja7108486.

[237]T. J. Herrington, A. J. W. Thom, A. J. P. White, A. E. Ashley, „Novel H_2 Activation by a Tris[3,5-Bis(Trifluoromethyl)Phenyl]Borane Frustrated Lewis Pair“, *Dalton Trans.* **2012**, *41*, 9019–9022, DOI 10.1039/C2DT30384A.

[238]*APEX3 V2016.9-0 (SAINT/SADABS/SHELXT/SHELXL)*, Bruker AXS Inc., **2016**.

[239]G. M. Sheldrick, „SHELXT – Integrated Space-Group and Crystal-Structure Determination“, *Acta Cryst A* **2015**, *71*, 3–8, DOI 10.1107/S2053273314026370.

[240]G. M. Sheldrick, „Crystal Structure Refinement with SHELXL“, *Acta Cryst C* **2015**, *71*, 3–8, DOI 10.1107/S2053229614024218.

[241]G. M. Sheldrick, „A Short History of SHELX“, *Acta Cryst A* **2008**, *64*, 112–122, DOI 10.1107/S0108767307043930.

[242]N. Elgrishi, K. J. Rountree, B. D. McCarthy, E. S. Rountree, T. T. Eisenhart, J. L. Dempsey, „A Practical Beginner's Guide to Cyclic Voltammetry“, *J. Chem. Educ.* **2018**, *95*, 197–206, DOI 10.1021/acs.jchemed.7b00361.

[243]G. A. Bain, J. F. Berry, „Diamagnetic Corrections and Pascal's Constants“, *J. Chem. Educ.* **2008**, *85*, 532, DOI 10.1021/ed085p532.

[244]W. Haberditzl, „Advances in Molecular Diamagnetism“, *Angew. Chem. Int. Ed. Engl.* **1966**, *5*, 288–298, DOI 10.1002/anie.196602881.

[245]E. Bill, JULX, *Program for Simulation of Molecular Magnetic Data*, Max-Planck Institute for Chemical Energy Conversion, Mülheim/Ruhr, **2008**.

[246]F. Neese, „The ORCA Program System“, *Wiley Interdiscip. Rev. Comput. Mol. Sci.* **2012**, *2*, 73–78, DOI 10.1002/wcms.81.

[247]F. Neese, „Software Update: The ORCA Program System, Version 4.0“, *Wiley Interdiscip. Rev. Comput. Mol. Sci.* **2018**, *8*, e1327, DOI 10.1002/wcms.1327.

[248]J. P. Perdew, K. Burke, M. Ernzerhof, „Generalized Gradient Approximation Made Simple“, *Phys. Rev. Lett.* **1996**, *77*, 3865–3868, DOI 10.1103/PhysRevLett.77.3865.

[249]J. P. Perdew, M. Ernzerhof, K. Burke, „Rationale for Mixing Exact Exchange with Density Functional Approximations“, *J. Chem. Phys.* **1996**, *105*, 9982–9985, DOI 10.1063/1.472933.

[250]F. Weigend, R. Ahlrichs, „Balanced Basis Sets of Split Valence, Triple Zeta Valence and Quadruple Zeta Valence Quality for H to Rn: Design and Assessment of Accuracy“, *Phys. Chem. Chem. Phys.* **2005**, *7*, 3297–3305, DOI 10.1039/B508541A.

[251]D. Andrae, U. Häußermann, M. Dolg, H. Stoll, H. Preuß, „Energy-Adjusted Ab Initio Pseudopotentials for the Second and Third Row Transition Elements“, *Theoret. Chim. Acta* **1990**, *77*, 123–141, DOI 10.1007/BF01114537.

[252]O. Treutler, R. Ahlrichs, „Efficient Molecular Numerical Integration Schemes“, *J. Chem. Phys.* **1995**, *102*, 346–354, DOI 10.1063/1.469408.

[253]K. Eichkorn, O. Treutler, H. Öhm, M. Häser, R. Ahlrichs, „Auxiliary Basis Sets to Approximate Coulomb Potentials“, *Chem. Phys. Letters* **1995**, *240*, 283–290, DOI 10.1016/0009-2614(95)00621-A.

[254]K. Eichkorn, O. Treutler, H. Öhm, M. Häser, R. Ahlrichs, „Auxiliary Basis Sets to Approximate Coulomb Potentials (Chem. Phys. Letters 240 (1995) 283-290)“, *Chem. Phys. Letters* **1995**, *242*, 652–660, DOI 10.1016/0009-2614(95)00838-U.

[255]K. Eichkorn, F. Weigend, O. Treutler, R. Ahlrichs, „Auxiliary Basis Sets for Main Row Atoms and Transition Metals and Their Use to Approximate Coulomb Potentials“, *Theor Chem Acta* **1997**, *97*, 119–124, DOI 10.1007/s002140050244.

[256]F. Neese, F. Wennmohs, A. Hansen, U. Becker, „Efficient, Approximate and Parallel Hartree–Fock and Hybrid DFT Calculations. A 'Chain-of-Spheres' Algorithm for the Hartree–Fock Exchange“, *Chemical Physics*, Moving Frontiers in Quantum Chemistry: **2009**, *356*, 98–109, DOI 10.1016/j.chemphys.2008.10.036.

[257]F. Weigend, „Accurate Coulomb-Fitting Basis Sets for H to Rn“, *Phys. Chem. Chem. Phys.* **2006**, *8*, 1057–1065, DOI 10.1039/B515623H.

[258]S. Grimme, J. Antony, S. Ehrlich, H. Krieg, „A Consistent and Accurate Ab Initio Parametrization of Density Functional Dispersion Correction (DFT-D) for the 94 Elements H-Pu“, *J. Chem. Phys.* **2010**, *132*, 154104, DOI 10.1063/1.3382344.

[259]S. Grimme, S. Ehrlich, L. Goerigk, „Effect of the Damping Function in Dispersion Corrected Density Functional Theory“, *J. Comput. Chem.* **2011**, *32*, 1456–1465, DOI 10.1002/jcc.21759.

[260]S. Grimme, „Supramolecular Binding Thermodynamics by Dispersion-Corrected Density Functional Theory“, *Chem. – Eur. J.* **2012**, *18*, 9955–9964, DOI 10.1002/chem.201200497.

[261]A. Klamt, G. Schüürmann, „COSMO: A New Approach to Dielectric Screening in Solvents with Explicit Expressions for the Screening Energy and Its Gradient“, *J. Chem. Soc. Perkin Trans. 2* **1993**, *0*, 799–805, DOI 10.1039/P29930000799.

[262]V. Barone, M. Cossi, „Quantum Calculation of Molecular Energies and Energy Gradients in Solution by a Conductor Solvent Model“, *J. Phys. Chem. A* **1998**, *102*, 1995–2001, DOI 10.1021/jp9716997.

[263]Chemcraft - graphical software for visualization of quantum chemistry computations. https://www.chemcraftprog.com.

[264]D. A. Pantazis, X.-Y. Chen, C. R. Landis, F. Neese, „All-Electron Scalar Relativistic Basis Sets for Third-Row Transition Metal Atoms“, *J. Chem. Theory Comput.* **2008**, *4*, 908–919, DOI 10.1021/ct800047t.

[265]C. Angeli, R. Cimiraglia, S. Evangelisti, T. Leininger, J.-P. Malrieu, „Introduction of N-Electron Valence States for Multireference Perturbation Theory“, *J. Chem. Phys.* **2001**, *114*, 10252–10264, DOI 10.1063/1.1361246.

[266]C. Angeli, R. Cimiraglia, J.-P. Malrieu, „N-Electron Valence State Perturbation Theory: A Fast Implementation of the Strongly Contracted Variant“, *Chemical Physics Letters* **2001**, *350*, 297–305, DOI 10.1016/S0009-2614(01)01303-3.

[267]C. Angeli, R. Cimiraglia, J.-P. Malrieu, „N-Electron Valence State Perturbation Theory: A Spinless Formulation and an Efficient Implementation of the Strongly Contracted and of the Partially Contracted Variants“, *J. Chem. Phys.* **2002**, *117*, 9138–9153, DOI 10.1063/1.1515317.

[268]B. A. Heß, C. M. Marian, U. Wahlgren, O. Gropen, „A Mean-Field Spin-Orbit Method Applicable to Correlated Wavefunctions“, *Chemical Physics Letters* **1996**, *251*, 365–371, DOI 10.1016/0009-2614(96)00119-4.

[269]F. Schendzielorz, M. Finger, J. Abbenseth, C. Würtele, V. Krewald, S. Schneider, „Metal-Ligand Cooperative Synthesis of Benzonitrile by Electrochemical Reduction and Photolytic Splitting of Dinitrogen“, *Angew. Chem.* **2019**, *131*, 840–844, DOI 10.1002/ange.201812125.

Part V

Appendix

Crystal structures

A

A.1 [Os(NBAr$^{F}_{18}$)(PNP^{tBu})] (**5**)

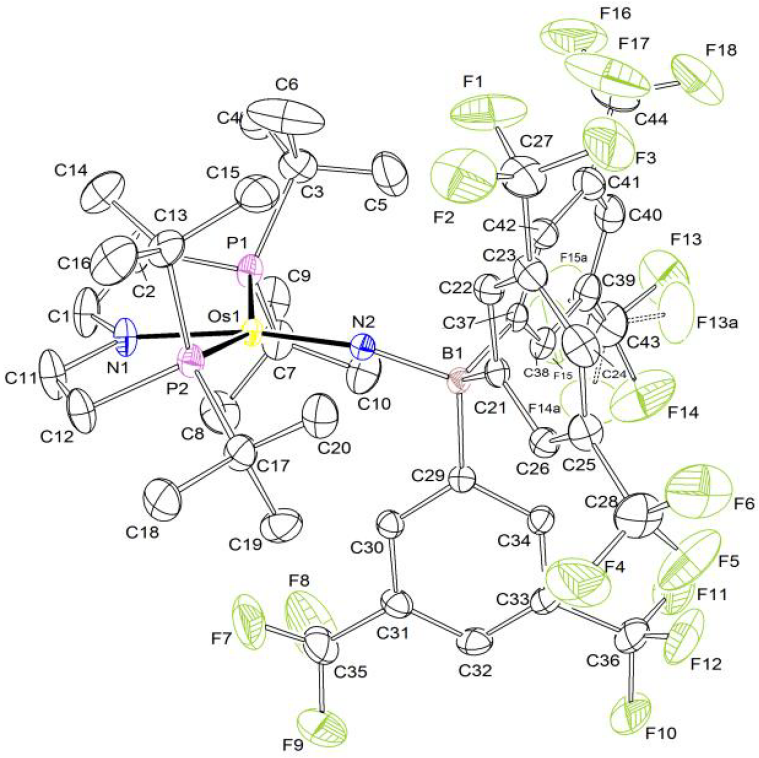

Fig. A.1. Thermal ellipsoid plot of **5** with the anisotropic displacement parameters drawn at the 50 % probability level. The asymmetric unit contains one disordered complex molecule. The disordered complex molecule was refined with population of 0.67(2) on the main domain using some restraints (SADI, RIGU).

Tab. A.1. Crystal data and structure refinement of **5**.

Identification code	**5**
Empirical formula	$C_{44}H_{53}BF_{18}N_2OsP_2$
Formula weight	1214.83
Temperature	173(2) K
Wavelength	0.71073 Å
Crystal system	Monoclinic

Space group	$P2_1/n$	
Unit cell dimensions	a = 14.2710(5) Å b = 22.0590(7) Å c = 15.7378(5) Å	$alpha = 90°$ $beta = 90.4440(10)°$ $gamma = 90°$
Volume	4954.2(3) $Å^3$	
Z	4	
Density (calculated)	1.629 Mg/m^3	
Absorption coefficient	2.740 mm^{-1}	
F(000)	2416	
Crystal size	0.241 x 0.162 x 0.153 mm^3	
Crystal shape and color	Block, dark red	
Theta range for data collection	2.255 to 30.605°	
Index ranges	-20≤h≤20, -31≤k≤31, -22≤l≤22	
Reflections collected	216917	
Independent reflections	15244 [R(int) = 0.0544]	
Completeness to theta = 25.242°	99.90 %	
Refinement method	Full-matrix least-squares on F^2	
Data / restraints / parameters	15244 / 366 / 653	
Goodness-of-fit on F^2	1.066	
Final R indices [I>2sigma(I)]	R1 = 0.0265	wR2 = 0.0482
R indices (all data)	R1 = 0.0499	wR2 = 0.0551
Largest diff. peak and hole	0.795 and -0.746 $eÅ^{-3}$	

A.2 $[Os(NSiMe_3)(PNP^{tBu})]^{BPh_4}$ ($\mathbf{6}^{\mathbf{BPh_4}}$)

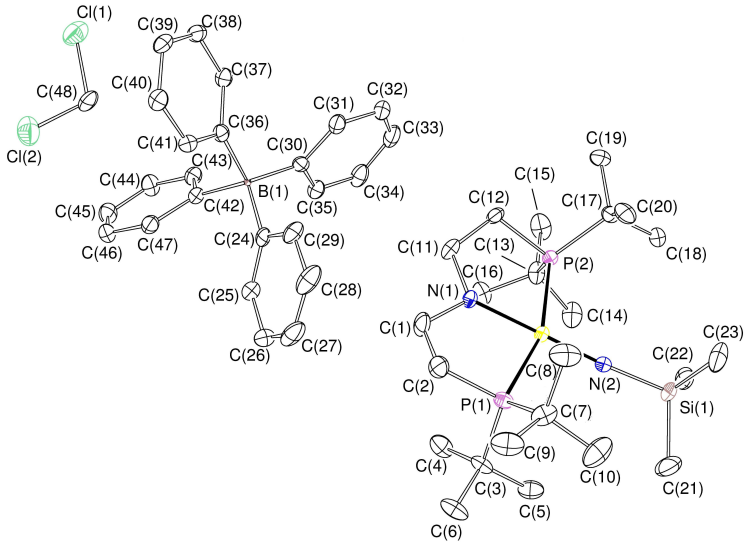

Fig. A.2. Thermal ellipsoid plot of $\mathbf{6}^{BPh_4}$ with the anisotropic displacement parameters drawn at the 50 % probability level. All hydrogen atoms are omitted for clarity. The asymmetric unit contains one complex molecule, one CH_2Cl_2 solvent molecule and two different anions at the same position (BPh_4^- and Br^-). The two alternative anions were refined with occupation factors of 0.95 for BPh_4^- and 0.05 for Br^- using EXYZ and EADP commands. Possible room filling solvent molecules next to Br^- were not found due to overlay with phenyl groups of BPh_4^- and low occupancy.

Tab. A.2. Crystal data and structure refinement of $\mathbf{6}^{\mathbf{BPh_4}}$.

Identification code	$\mathbf{6}^{BPh_4}$
Empirical formula	$C_{24}H_{55}Cl_2N_2OsP_2Si(BC_{24}H_{20})_{0.95}(Br)_{0.05}$
Formula weight	1030.07
Temperature	100(2) K
Wavelength	0.71073 Å
Crystal system	Monoclinic
Space group	$P2_1/c$
Unit cell dimensions	a = 17.7529(7) Å $\quad \alpha = 90°$ b = 21.2994(7) Å $\quad \beta = 109.088(2)°$ c = 13.7921(5) Å $\quad \gamma = 90°$
Volume	4928.4(3) Å^3
Z	4
Density (calculated)	1.388 Mg/m^3

Absorption coefficient	2.858 mm^{-1}	
F(000)	2117	
Crystal size	0.162 x 0.103 x 0.065 mm^3	
Crystal shape and color:	Block, green-brown	
Theta range for data collection	2.265 to 30.508°	
Index ranges	-24≤h≤25, -30≤k≤30, -19≤l≤19	
Reflections collected	100115	
Independent reflections	14845 [R(int) = 0.1174]	
Completeness to theta = 25.242°	99.90 %	
Absorption correction	Numerical	
Max. and min. transmission	0.9393 and 0.7241	
Refinement method	Full-matrix least-squares on F^2	
Data / restraints / parameters	14845 / 0 / 529	
Goodness-of-fit on F^2	1.16	
Final R indices [I>2sigma(I)]	R1 = 0.0493	wR2 = 0.0802
R indices (all data)	R1 = 0.1099	wR2 = 0.0994
Largest diff. peak and hole	2.098 and -1.723 $eÅ^{-3}$	

A.3 [Os(NPMe$_3$)(PNP^{tBu})] (**7**)

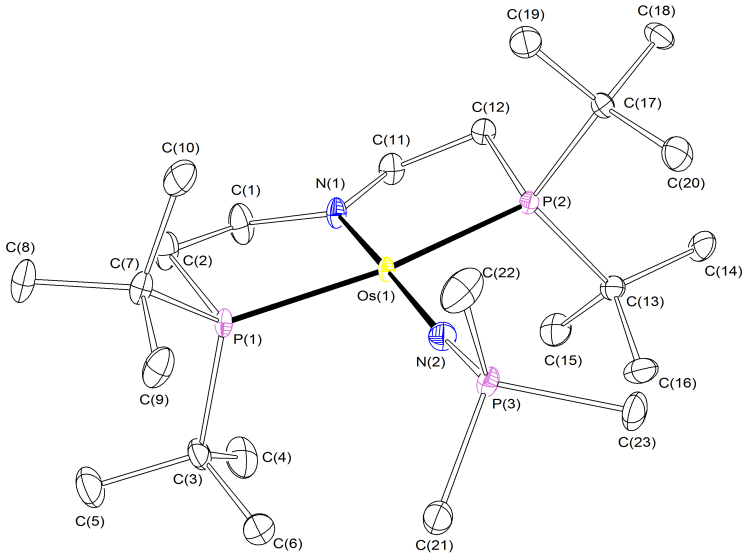

Fig. A.3. Thermal ellipsoid plot of **7** with the anisotropic displacement parameters drawn at the 50 % probability level All hydrogen atoms are omitted for clarity.

Tab. A.3. Crystal data and structure refinement of **7**.

Identification code	**7**	
Empirical formula	$C_{23}H_{53}N_2OsP_3$	
Formula weight	640.78	
Temperature	100(2) K	
Wavelength	0.71073 Å	
Crystal system	Monoclinic	
Space group	$P2_1/c$	
Unit cell dimensions	a = 11.2796(7) Å b = 16.1565(10) Å c = 15.9319(11) Å	$\alpha = 90°$ $\beta = 100.141(3)°$ $\gamma = 90°$
Volume	2858.1(3) Å^3	
Z	4	
Density (calculated)	1.489 Mg/m^3	
Absorption coefficient	4.642 mm^{-1}	
F(000)	1304	
Crystal size	0.228 x 0.216 x 0.138 mm^3	

Crystal shape and color	Block, clear light brown	
Theta range for data collection	2.226 to 28.372°	
Index ranges	-15≤h≤15, -21≤k≤21, -21≤l≤20	
Reflections collected	41683	
Independent reflections	7138 [R(int) = 0.0536]	
Completeness to theta = 25.242°	100.00 %	
Absorption correction	Semi-empirical from equivalents	
Max. and min. transmission	0.7457 and 0.5893	
Refinement method	Full-matrix least-squares on F^2	
Data / restraints / parameters	7138 / 0 / 277	
Goodness-of-fit on F^2	1.027	
Final R indices [I>2sigma(I)]	R1 = 0.0265	wR2 = 0.0458
R indices (all data)	R1 = 0.0404	wR2 = 0.0491
Largest diff. peak and hole	1.080 and -0.937 $eÅ^{-3}$	

A.4 $[OsH_4(HPNP^{tBu})]$ (**8**)

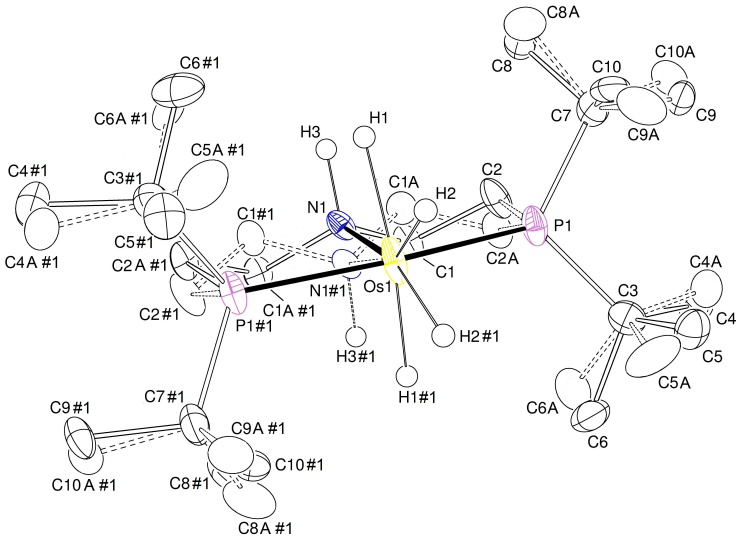

Fig. A.4. Thermal ellipsoid plot of 4 with the anisotropic displacement parameters drawn at the 50i % probability level. All C-H hydrogen atoms are omitted for clarity. The asymmetric unit contains a half complex molecule which is disordered in two positions. The disorder was refined with site occupation factors of 0.5 for both sites using PART commands and some restraints on the anisotropic displacement parameters (RIGU). All Os-H hydrogen atoms were found from the residual density map and isotropically refined. The isotropically refined N-H hydrogen atom was found from the residual density map and constrained to 1.2 U_{eq} of the connected atom.

Tab. A.4. Crystal data and structure refinement of **8**.

Identification code	**8**	
Empirical formula	$C_{20}H_{49}NOsP_2$	
Formula weight	555.74	
Temperature	100(2) K	
Wavelength	0.71073 Å	
Crystal system	Monoclinic	
Space group	$C2/c$	
Unit cell dimensions	a = 22.7190(17) Å b = 7.3382(6) Å c = 14.6831(13) Å	$\alpha = 90°$ $\beta = 104.993(4)°$ $\gamma = 90°$
Volume	2364.6(3) $Å^3$	
Z	4	
Density (calculated)	1.561 Mg/m^3	

Absorption coefficient	5.532 mm^{-1}	
F(000)	1128	
Crystal size	0.279 x 0.094 x 0.071 mm^3	
Crystal shape and color:	Block, yellow-orange	
Theta range for data collection	2.872 to 27.875°	
Index ranges	-29≤h≤29, -9≤k≤9, -19≤l≤19	
Reflections collected	64019	
Independent reflections	2827 [R(int) = 0.0423]	
Completeness to theta = 25.242°	100.00 %	
Absorption correction	Semi-empirical from equivalents	
Max. and min. transmission	0.7458 and 0.6663	
Refinement method	Full-matrix least-squares on F^2	
Data / restraints / parameters	2827 / 36 / 210	
Goodness-of-fit on F^2	1.213	
Final R indices [I>2sigma(I)]	R1 = 0.0255	wR2 = 0.0461
R indices (all data)	R1 = 0.0334	wR2 = 0.0488
Largest diff. peak and hole	1.157 and -2.106 $eÅ^{-3}$	

A.5 $[Os(CN^tBu)_2Cl\{N(CH_2CH_2P^tBu_2)(=CHCH_2P(^tBu)_2=NH)\}]^{BAr^F_{24}}$ ($\mathbf{11}^{BAr^F_{24}}$)

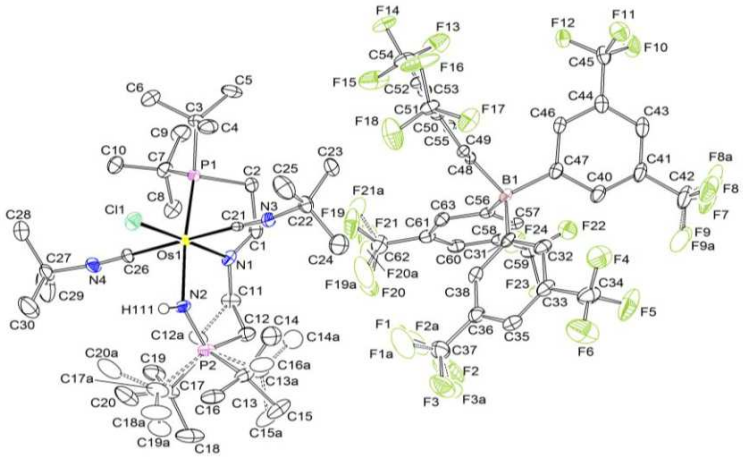

Fig. A.5. Thermal ellipsoid plot of $\mathbf{11}^{BAr^F_{24}}$ with the anisotropic displacement parameters drawn at the 50 % probability level. The asymmetric unit contains one disordered complex molecule and one BAr^F_{24} anion with three disordered CF_3 groups. The disordered complex molecule was refined with population of 0.869(2) on the main domain using some restraints and constrains (SADI, EADP). The disordered CF_3 groups were refined with populations of 0.776(7), 0.53(2) and 0.60(4) on their main domains using some restraints (SADI, RIGU). The N-H hydrogen atom was found from the residual density map and isotropically refined.

Tab. A.5. Crystal data and structure refinement of $\mathbf{11}^{BAr^F_{24}}$.

Identification code	$\mathbf{11}^{BAr^F_{24}}$	
Empirical formula	$C_{62}H_{74}BClF_{24}N_4OsP_2$	
Formula weight	1629.65	
Temperature	100(2) K	
Wavelength	0.71073 Å	
Crystal system	Monoclinic	
Space group	$P2_1/c$	
Unit cell dimensions	a = 19.189(2) Å b = 18.6585(19) Å c = 19.091(2) Å	$\alpha = 90°$ $\beta = 90.631(5)°$ $\gamma = 90°$
Volume	6835.0(12) $Å^3$	
Z	4	
Density (calculated)	1.584 Mg/m^3	

Absorption coefficient	2.059 mm^{-1}	
F(000)	3272	
Crystal size	0.292 x 0.158 x 0.124 mm^3	
Crystal shape and color	Block, clear intense yellow	
Theta range for data collection	1.852 to 30.630°	
Index ranges	-27≤h≤26, -26≤k≤26, -27≤l≤27	
Reflections collected	291617	
Independent reflections	20995 [R(int) = 0.1089]	
Completeness to theta = 25.242°	100.00 %	
Max. and min. transmission	0.7461 and 0.6423	
Refinement method	Full-matrix least-squares on F^2	
Data / restraints / parameters	20995 / 609 / 1002	
Goodness-of-fit on F^2	1.037	
Final R indices [I>2sigma(I)]	R1 = 0.0351	wR2 = 0.0659
R indices (all data)	R1 = 0.0639	wR2 = 0.0759
Largest diff. peak and hole	2.766 and -1.532 eÅ^{-3}	

A.6 [OsCl(CN^{t}Bu)(PNP^{tBu})] (**15**)

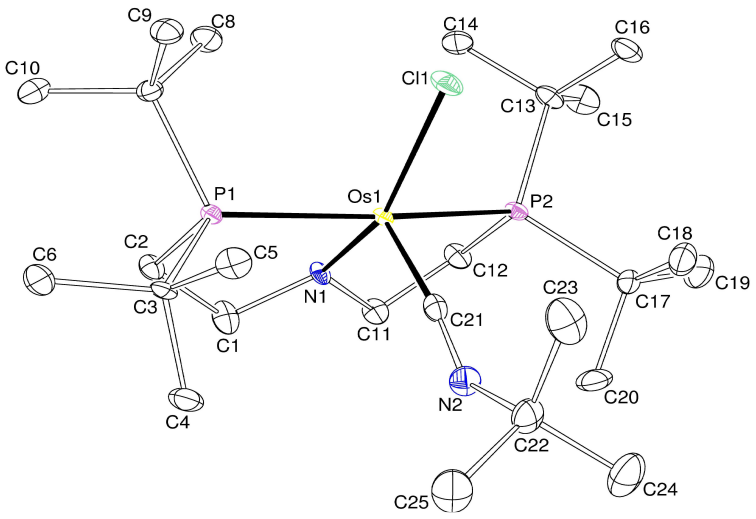

Fig. A.6. Thermal ellipsoid plot of **15** with the anisotropic displacement parameters drawn at the 50 % probability level. The asymmetric unit contains one complex molecule.

Tab. A.6. Crystal data and structure refinement of **15**.

Identification code	**15**	
Empirical formula	$C_{25}H_{53}ClN_2OsP_2$	
Formula weight	669.28	
Temperature	100(2) K	
Wavelength	0.71073 Å	
Crystal system	Monoclinic	
Space group	$P2_1/c$	
Unit cell dimensions	a = 19.7104(12) Å b = 9.7951(6) Å c = 16.4534(10) Å	$\alpha = 90°$ $\beta = 114.422(2)°$ $\gamma = 90°$
Volume	2892.4(3) $Å^3$	
Z	4	
Density (calculated)	1.537 Mg/m^3	
Absorption coefficient	4.627 mm^{-1}	
F(000)	1360	
Crystal size	0.214 x 0.188 x 0.036 mm^3	
Crystal shape and color	Plate, clear intense brown	
Theta range for data collection	2.270 to 28.402°	
Index ranges	$-26 \leq h \leq 26$, $-13 \leq k \leq 13$, $-22 \leq l \leq 21$	
Reflections collected	129552	
Independent reflections	7246 [R(int) = 0.0843]	
Completeness to theta = 25.242°	100.00 %	
Max. and min. transmission	0.7457 and 0.6125	
Refinement method	Full-matrix least-squares on F^2	
Data / restraints / parameters	7246 / 0 / 295	
Goodness-of-fit on F^2	1.048	
Final R indices [I>2sigma(I)]	R1 = 0.0240,	wR2 = 0.0348
R indices (all data)	R1 = 0.0476	wR2 = 0.0387
Largest diff. peak and hole	0.623 and -0.993 $eÅ^{-3}$	

A.7 [(μ–N_2){ReCl(PNP^{tBu})}$_2$] (**XX**)

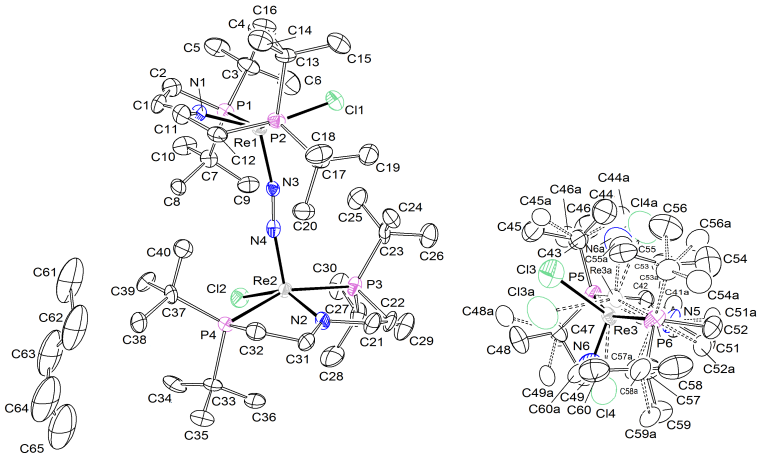

Fig. A.7. Thermal ellipsoid plot of **XX** with the anisotropic displacement parameters drawn at the 50 % probability level. The asymmetric unit contains one dimeric species, a monomeric species and a half pentane solvent molecule. The monomeric species was refined as two different disordered complex molecules ([$ReCl_2$(PNP^{tBu})] (**XIX**) and [ReNCl(PNP^{tBu})] (**XXI**) with occupation factors of 0.5 for both complexes) using some restraints and constraints (SADI, RIGU, EADP). The pentane solvent molecule was refined using some restraints and constraints (SADI, RIGU, DFIX).

Tab. A.7. Crystal data and structure refinement of **XX**.

Identification code	**XX**	
Empirical formula	$C_{40}H_{88}Cl_2N_4P_4Re$ (100 %) $C_{20}H_{44}Cl_2NP_2Re$ (50 %) $C_{20}H_{44}ClN_2P_2Re$ (50 %) C_5H_{12} (50 %)	
Formula weight	1835.27	
Temperature	100(2) K	
Wavelength	0.71073 Å	
Crystal system	Monoclinic	
Space group	$P2_1/c$	
Unit cell dimensions	a = 12.4165(8) Å b = 33.602(2) Å c = 19.7243(14) Å	$\alpha = 90°$ $\beta = 101.313(2)°$ $\gamma = 90°$
Volume	8069.5(9) Å^3	
Z	4	
Density (calculated)	1.511 Mg/m^3	

Absorption coefficient	4.761 mm^{-1}	
F(000)	3704	
Crystal size	0.217 x 0.085 x 0.064 mm^3	
Crystal shape and color	Plate, clear dark brown	
Theta range for data collection	2.228 to 26.451°	
Index ranges	-15≤h≤15, -39≤k≤42, -24≤l≤24	
Reflections collected	143213	
Independent reflections	16610 [R(int) = 0.1745]	
Completeness to theta = 25.242°	99.90 %	
Refinement method	Full-matrix least-squares on F^2	
Data / restraints / parameters	16610 / 469 / 963	
Goodness-of-fit on F^2	1.077	
Final R indices [I>2sigma(I)]	R1 = 0.0639	wR2 = 0.1178
R indices (all data)	R1 = 0.1113	wR2 = 0.1328
Largest diff. peak and hole	2.340 and -1.787 $eÅ^{-3}$	

A.8 [ReHCl(PNP^{tBu})] (**17**)

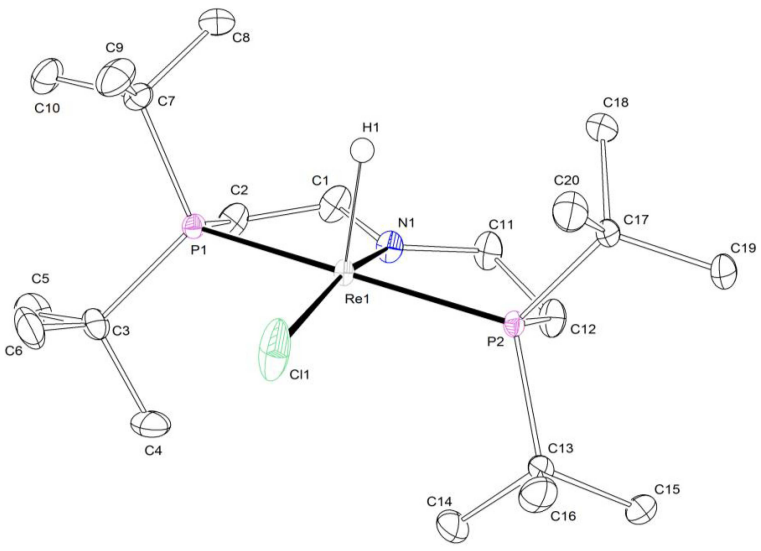

Fig. A.8. Thermal ellipsoid plot of **17** with the anisotropic displacement parameters drawn at the 50 % probability level. The asymmetric unit contains one complex molecule. The isotropically refined Re-H hydrogen atom was found from the residual density map and constrained to 1.2 U_{eq} of the connected rhenium atom.

Tab. A.8. Crystal data and structure refinement of **17**.

Identification code	**17**	
Empirical formula	$C_{20}H_{45}ClNP_2Re$	
Formula weight	583.16	
Temperature	103(2) K	
Wavelength	0.71073 Å	
Crystal system	Monoclinic	
Space group	$P2_1/c$	
Unit cell dimensions	a = 12.1666(5) Å b = 16.1172(7) Å c =12.8698(6) Å	$\alpha = 90°$ $\beta = 104.311(2)°$ ° $\gamma = 90°$
Volume	2445.35(19) $Å^3$	
Z	4	
Density (calculated)	1.584 Mg/m^3	
Absorption coefficient	5.214 mm^{-1}	
F(000)	1176	
Crystal size	0.204 x 0.156 x 0.078 mm^3	
Crystal shape and color	Block, clear dark brown	
Theta range for data collection	2.420 to 30.602°	
Index ranges	-17≤h≤17, -23≤k≤23, -18≤l≤18	
Reflections collected	94866	
Independent reflections	7511 [R(int) = 0.0618]	
Completeness to theta = 25.242°	99.9 %	
Max. and min. transmission	0.7461 and 0.5615	
Refinement method	Full-matrix least-squares on F^2	
Data / restraints / parameters	7511 / 0 / 241	
Goodness-of-fit on F^2	1.028	
Final R indices [I>2sigma(I)]	R1 = 0.0227	wR2 = 0.0371
R indices (all data)	R1 = 0.0358	wR2 = 0.0399
Largest diff. peak and hole	1.819 and -1.218 $eÅ^{-3}$	

A.9 $[(N,N\text{–}C_2H_4N_2)\{ReCl(PNP^{tBu})\}_2]^{(OTf)_2}$ ($\mathbf{19^{(OTf)_2}}$)

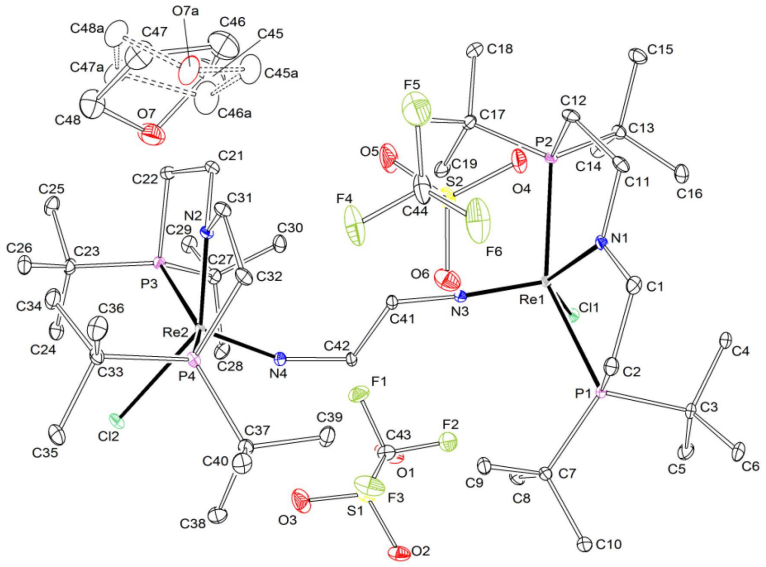

Fig. A.9. Thermal ellipsoid plot of $\mathbf{19^{(OTf)_2}}$ with the anisotropic displacement parameters drawn at the 50 % probability level. The asymmetric unit contains one complex molecule, two $CF_3SO_3^-$ anions and one disordered THF solvent molecule. The disordered solvent molecule was refined with population of 0.620(5) on the main domain.

Tab. A.9. Crystal data and structure refinement of $\mathbf{19^{(OTf)_2}}$.

Identification code	$\mathbf{19^{(OTf)_2}}$	
Empirical formula	$C_{48}H_{100}Cl_2F_6N_4O_7P_4Re_2S_2$	
Formula weight	1590.61	
Temperature	101(2) K	
Wavelength	0.71073 Å	
Crystal system	Monoclinic	
Space group	$P2_1/c$	
Unit cell dimensions	a = 15.8769(5) Å	$\alpha = 90°$
	b = 27.6973(9) Å	$\beta = 117.5340(10)°$
	c = 16.3093(5) Å	$\gamma = 90°$
Volume	6359.6(4) $Å^3$	
Z	4	
Density (calculated)	1.661 Mg/m^3	
Absorption coefficient	4.119 mm^{-1}	
F(000)	3208	

Crystal size	0.266 x 0.237 x 0.153 mm^3	
Crystal shape and color	Block, clear intense brown	
Theta range for data collection	2.502 to 30.589°	
Index ranges	-22≤h≤22, -39≤k≤39, -23≤l≤23	
Reflections collected	263962	
Independent reflections	19533 [R(int) = 0.0628]	
Completeness to theta = 25.242°	99.9 %	
Refinement method	Full-matrix least-squares on F^2	
Data / restraints / parameters	19533 / 0 / 746	
Goodness-of-fit on F^2	1.07	
Final R indices [I>2sigma(I)]	R1 = 0.0274	wR2 = 0.0470
R indices (all data)	R1 = 0.0390	wR2 = 0.0494
Largest diff. peak and hole	1.955 and -1.466 $eÅ^{-3}$	

A.10 $[Re(O)Cl(PNP^{tBu})]BPh_4$ (**20^{BPh_4}**)

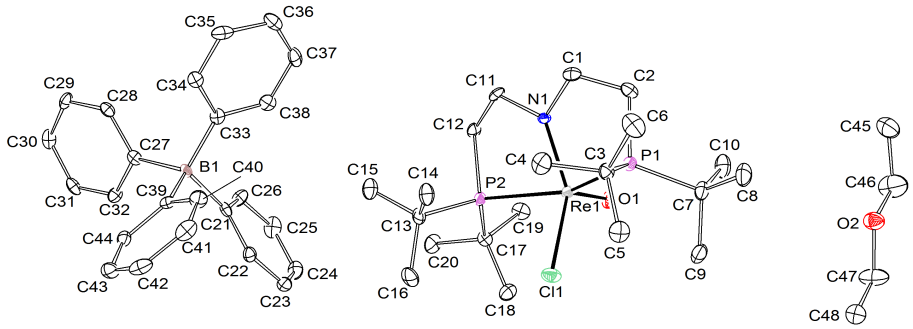

Fig. A.10. Thermal ellipsoid plot of **20^{BPh_4}** with the anisotropic displacement parameters drawn at the 50 % probability level. The asymmetric unit contains one complex molecule, one BPh_4^- anion and one diethyl ether solvent molecule.

Tab. A.10. Crystal data and structure refinement of **20^{BPh_4}**.

Identification code	**20^{BPh_4}**
Empirical formula	$C_{48}H_{74}BClNO_2P_2Re$
Formula weight	991.48
Temperature	100(2) K

Wavelength	0.71073 Å	
Crystal system	Triclinic	
Space group	$P\bar{1}$	
Unit cell dimensions	a = 11.124(3) Å b = 14.432(4) Å c = 16.248(4) Å	α = 113.774(13)° β = 92.511(8)° γ = 90.987(9)°
Volume	2383.3(11) $Å^3$	
Z	2	
Density (calculated)	1.382 Mg/m^3	
Absorption coefficient	2.709 mm^{-1}	
F(000)	1024	
Crystal size	0.084 x 0.040 x 0.035 mm^3	
Crystal shape and color	Block, clear pale yellow	
Theta range for data collection	2.228 to 26.628°	
Index ranges	-13≤h≤13, -18≤k≤18, -20≤l≤20	
Reflections collected	93699	
Independent reflections	9615 [R(int) = 0.1652]	
Completeness to theta = 25.242°	97.6 %	
Refinement method	Full-matrix least-squares on F^2	
Data / restraints / parameters	9615 / 0 / 519	
Goodness-of-fit on F^2	1.021	
Final R indices [I>2sigma(I)]	R1 = 0.0403	wR2 = 0.0615
R indices (all data)	R1 = 0.0646	wR2 = 0.0670
Largest diff. peak and hole	1.159 and -1.339 $eÅ^{-3}$	

A.11 [Re(N)Cl(P=N=P$^{t\mathrm{Bu}}$)] (**22**)

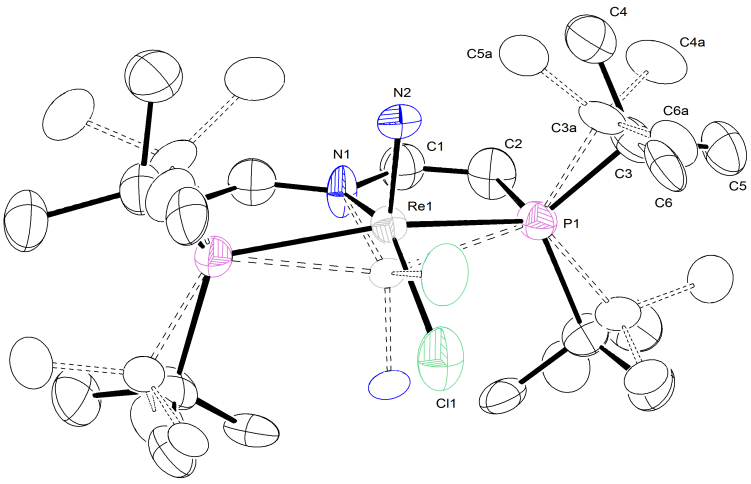

Fig. A.11. Thermal ellipsoid plot of **22** with the anisotropic displacement parameters drawn at the 50 % probability level. The asymmetric unit contains a half disordered complex molecule. The disorder was refined with site occupation factors of 0.5 for both sites using PART commands and some restraints (RIGU). The structure was refined as an inversion twin using the twin law -100 0-10 00-1 (BASF: 0.50(3)).

Tab. A.11. Crystal data and structure refinement of **22**.

Identification code	**22**	
Empirical formula	$C_{20}H_{40}ClN_2P_2Re$	
Formula weight	592.13	
Temperature	100(2) K	
Wavelength	0.71073 Å	
Crystal system	Tetragonal	
Space group	$P\bar{4}2_1m$	
Unit cell dimensions	a = 12.0771(7) Å b = 12.0771(7) Å c = 8.3696(6) Å	$\alpha = 90°$ $\beta = 90°$ $\gamma = 90°$
Volume	2383.3(11) Å^3	
Z	2	
Density (calculated)	1.611 Mg/m^3	
Absorption coefficient	5.225 mm^{-1}	
F(000)	592	
Crystal size	0.234 x 0.229 x 0.130 mm^3	

Crystal shape and color	Block, light brown	
Theta range for data collection	2.385 to 27.443°	
Index ranges	-15≤h≤15, -15≤k≤15, -10≤l≤10	
Reflections collected	20488	
Independent reflections	1492 [R(int) = 0.0883]	
Completeness to theta = 25.242°	100 %	
Max. and min. transmission	0.7457 and 0.5234	
Refinement method	Full-matrix least-squares on F^2	
Data / restraints / parameters	1492 / 36 / 121	
Goodness-of-fit on F^2	1.151	
Final R indices [I>2sigma(I)]	R1 = 0.0444	wR2 = 0.0841
R indices (all data)	R1 = 0.0611	wR2 = 0.0925
Largest diff. peak and hole	1.888 and -1.191 eÅ^{-3}	

A.12 [Re(bipy)Cl(PNP^{tBu})]^{BPh_4} (**27^{BPh_4}**)

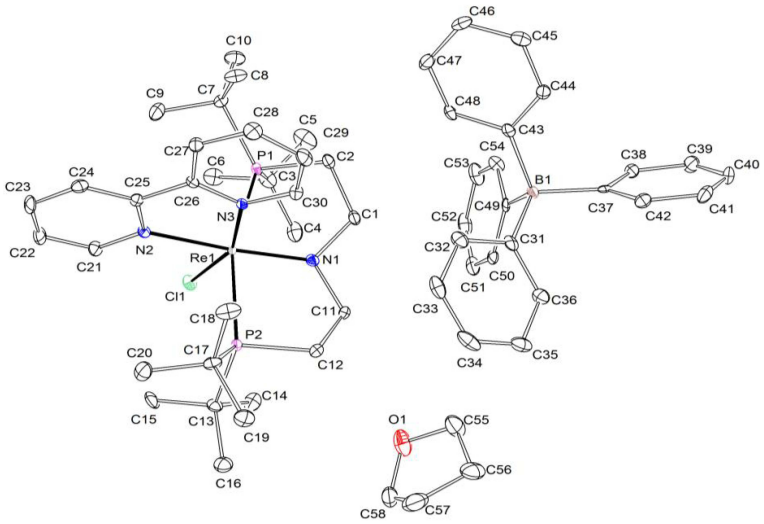

Fig. A.12. Thermal ellipsoid plot of **27^{BPh_4}** with the anisotropic displacement parameters drawn at the 50 % probability level. The asymmetric unit contains one complex molecule, one THF molecule and one BPh_4^- anion.

Tab. A.12. Crystal data and structure refinement of **27^{BPh_4}**.

Identification code	**27^{BPh_4}**

Empirical formula	$C_{58}H_{80}BClN_3OP_2Re$	
Formula weight	1129.65	
Temperature	100(2) K	
Wavelength	0.71073 Å	
Crystal system	Monoclinic	
Space group	$P2_1/n$	
Unit cell dimensions	a = 21.0255(10) Å b = 13.6445(7) Å c = 21.1205(11) Å	$\alpha = 90°$ $\beta = 117.775(2)°$ $\gamma = 90°$
Volume	5361.0(5) $Å^3$	
Z	4	
Density (calculated)	1.611 Mg/m^3	
Absorption coefficient	1.400 mm^{-1}	
F(000)	2336	
Crystal size	0.271 x 0.122 x 0.106 mm^3	
Crystal shape and color	Plate, dark red	
Theta range for data collection	2.190 to 29.218°	
Index ranges	-28≤h≤27, -18≤k≤18, -29≤l≤29	
Reflections collected	240096	
Independent reflections	14515 [R(int) = 0.1752]	
Completeness to theta = 25.242°	99.9 %	
Max. and min. transmission	0.7458 and 0.6637	
Refinement method	Full-matrix least-squares on F^2	
Data / restraints / parameters	14515 / 0 / 616	
Goodness-of-fit on F^2	1.054	
Final R indices [I>2sigma(I)]	R1 = 0.0454	wR2 = 0.0571
R indices (all data)	R1 = 0.0777	wR2 = 0.0636
Largest diff. peak and hole	1.622 and -1.415 $eÅ^{-3}$	

A.13 [$ReCl_3(HPNP^{iPr})$] (**29**)

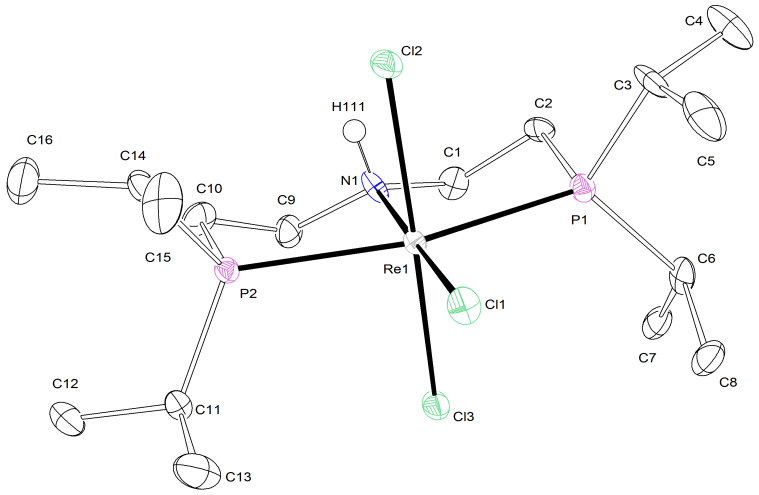

Fig. A.13. Thermal ellipsoid plot of **29** with the anisotropic displacement parameters drawn at the 50 % probability level. The asymmetric unit contains one complex molecule. The N-H hydrogen atom was found from the residual density map and isotropically refined. The structure was refined as an inversion twin using the twin law -100 0-10 00-1 (BASF: 0.015(9)).

Tab. A.13. Crystal data and structure refinement of **29**.

Identification code	**29**	
Empirical formula	$C_{16}H_{37}Cl_3NP_2Re$	
Formula weight	597.95	
Temperature	100(2) K	
Wavelength	0.71073 Å	
Crystal system	Orthorhombic	
Space group	$P2_12_12_1$	
Unit cell dimensions	a = 7.3805(3) Å b = 13.0720(6) Å c = 23.6017(11) Å	$\alpha = 90°$ $\beta = 90°$ $\gamma = 90°$
Volume	2277.04(18) $Å^3$	
Z	4	
Density (calculated)	1.744 Mg/m^3	
Absorption coefficient	5.829 mm^{-1}	
F(000)	1184	

Crystal size	0.223 x 0.105 x 0.074 mm^3	
Crystal shape and color	Block, clear light brown	
Theta range for data collection	2.325 to 30.543°	
Index ranges	-10≤h≤10, -18≤k≤17, -33≤l≤33	
Reflections collected	55467	
Independent reflections	6973 [R(int) = 0.1341]	
Completeness to theta = 25.242°	99.9 %	
Max. and min. transmission	0.7461 and 0.5961	
Refinement method	Full-matrix least-squares on F^2	
Data / restraints / parameters	6973 / 0 / 221	
Goodness-of-fit on F^2	1.034	
Final R indices [I>2sigma(I)]	R1 = 0.0434	wR2 = 0.0497
R indices (all data)	R1 = 0.0775	wR2 = 0.0549
Absolute structure parameter	0.015(9)	
Largest diff. peak and hole	1.078 and -1.629 eÅ^{-3}	

A.14 $[ReCl_3(PNP^{iPr})]$ (**31**)

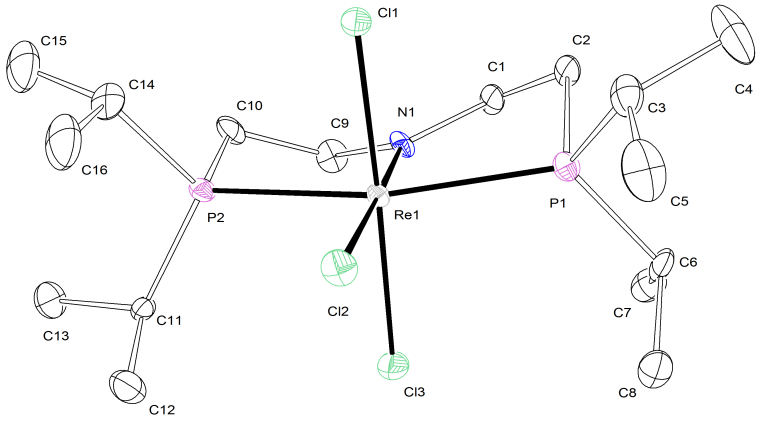

Fig. A.14. Thermal ellipsoid plot of **31** with the anisotropic displacement parameters drawn at the 50 % probability level. The asymmetric unit contains one complex molecule. The structure was refined using some restraints and constraints (RIGU, EADP).

Tab. A.14. Crystal data and structure refinement of **31**.

Identification code	**31**

Empirical formula	$C_{16}H_{36}Cl_3NP_2Re$	
Formula weight	596.95	
Temperature	113(2) K	
Wavelength	0.71073 Å	
Crystal system	Orthorhombic	
Space group	$P2_12_12_1$	
Unit cell dimensions	a = 7.3389(5) Å b = 12.6285(7) Å c = 24.1756(14) Å	$\alpha = 90°$ $\beta = 90°$ $\gamma = 90°$
Volume	2240.6(2) $Å^3$	
Z	4	
Density (calculated)	1.770 Mg/m^3	
Absorption coefficient	5.923 mm^{-1}	
F(000)	1180	
Crystal size	0.099 x 0.050 x 0.038 mm^3	
Crystal shape and color	Block, clear dark red-orange	
Theta range for data collection	2.332 to 28.342°	
Index ranges	$-9 \leq h \leq 9$, $-16 \leq k \leq 16$, $-32 \leq l \leq 32$	
Reflections collected	67072	
Independent reflections	5593 [R(int) = 0.1661]	
Completeness to theta = 25.242°	99.9 %	
Max. and min. transmission	0.7410 and 0.6416	
Refinement method	Full-matrix least-squares on F^2	
Data / restraints / parameters	5593 / 24 / 204	
Goodness-of-fit on F^2	1.041	
Final R indices [I>2sigma(I)]	R1 = 0.0428	wR2 = 0.0594
R indices (all data)	R1 = 0.0601,	wR2 = 0.0631
Absolute structure parameter	0.013(6)	
Largest diff. peak and hole	1.024 and -2.523 $eÅ^{-3}$	

A.15 $[ReCl_2(thf)(PNP^{iPr})]$ (**32**)

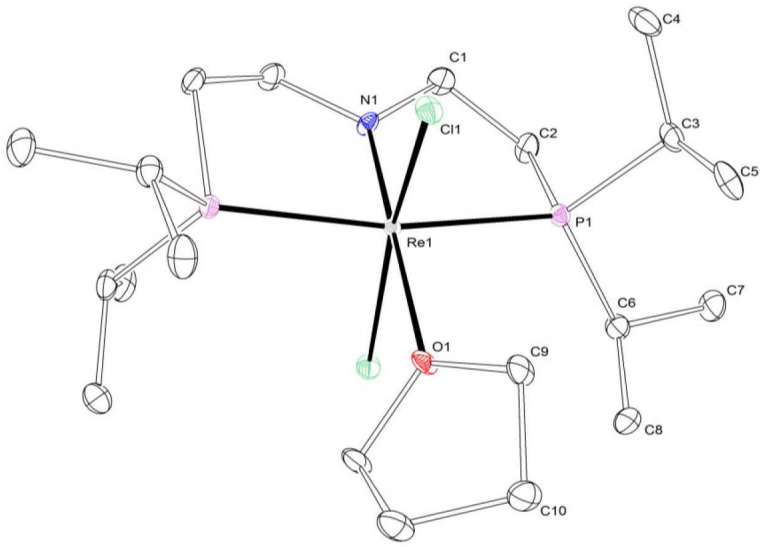

Fig. A.15. Thermal ellipsoid plot of **32** with the anisotropic displacement parameters drawn at the 50 % probability level. The asymmetric unit contains a half complex molecule.

Tab. A.15. Crystal data and structure refinement of **32**.

Identification code	**32**	
Empirical formula	$C_{20}H_{44}Cl_2NOP_2Re$	
Formula weight	633.6	
Temperature	113(2) K	
Wavelength	0.71073 Å	
Crystal system	Monoclinic	
Space group	$C2/c$	
Unit cell dimensions	a = 18.2122(7) Å b = 11.0408(4) Å c = 12.5053(6) Å	$\alpha = 90°$ $\beta = 101.887(2)°$ $\gamma = 90°$
Volume	2460.61(18) $Å^3$	
Z	4	
Density (calculated)	1.710 Mg/m^3	
Absorption coefficient	5.297 mm^{-1}	
F(000)	1272	
Crystal size	0.171 x 0.128 x 0.035 mm^3	

Crystal shape and color	Plate, clear light green-brown	
Theta range for data collection	2.286 to 30.609°	
Index ranges	-26≤h≤26, -15≤k≤15, -17≤l≤17	
Reflections collected	46525	
Independent reflections	3777 [R(int) = 0.0759]	
Completeness to theta = 25.242°	100 %	
Max. and min. transmission	0.7461 and 0.6072	
Refinement method	Full-matrix least-squares on F^2	
Data / restraints / parameters	3777 / 0 / 128	
Goodness-of-fit on F^2	1.07	
Final R indices [I>2sigma(I)]	R1 = 0.0243	wR2 = 0.0365
R indices (all data)	R1 = 0.0377	wR2 = 0.0389
Largest diff. peak and hole	1.521 and -1.126 eÅ^{-3}	

A.16 [$ReCl_2(PNP^{iPr})$] (**30**)

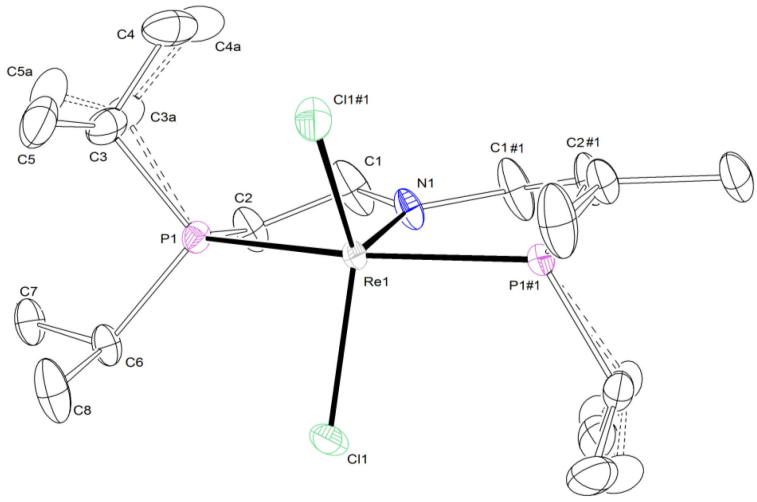

Fig. A.16. Thermal ellipsoid plot of **30** with the anisotropic displacement parameters drawn at the 50 % probability level. The asymmetric unit contains a half disordered complex molecule. The disordered complex molecule was refined with population of 0.52(2) on the main domain using some constraints (EADP).

Tab. A.16. Crystal data and structure refinement of **30**.

Identification code	**30**

Empirical formula	$C_{16}H_{36}Cl_2NP_2Re$	
Formula weight	561.5	
Temperature	113(2) K	
Wavelength	0.71073 Å	
Crystal system	Monoclinic	
Space group	$C2/c$	
Unit cell dimensions	a = 14.7630(7) Å b = 7.4571(4) Å c = 20.3176(10) Å	$\alpha = 90°$ $\beta = 106.718(2)°$ $\gamma = 90°$
Volume	2142.20(19) $Å^3$	
Z	4	
Density (calculated)	1.741 Mg/m^3	
Absorption coefficient	6.069 mm^{-1}	
F(000)	1112	
Crystal size	0.604 x 0.171 x 0.160 mm^3	
Crystal shape and color	Plate, clear pale yellow-violet	
Theta range for data collection	2.881 to 28.348°	
Index ranges	-19≤h≤19, -9≤k≤9, -27≤l≤27	
Reflections collected	36014	
Independent reflections	2658 [R(int) = 0.0627]	
Completeness to theta = 25.242°	99.9 %	
Max. and min. transmission	0.7457 and 0.4736	
Refinement method	Full-matrix least-squares on F^2	
Data / restraints / parameters	2658 / 0 / 117	
Goodness-of-fit on F^2	1.102	
Final R indices [I>2sigma(I)]	R1 = 0.0216	wR2 = 0.0460
R indices (all data)	R1 = 0.0248	wR2 = 0.0631
Largest diff. peak and hole	1.703 and -1.240 $eÅ^{-3}$	

A.17 [Re(N)Cl(PNP^{iPr})] (**34**)

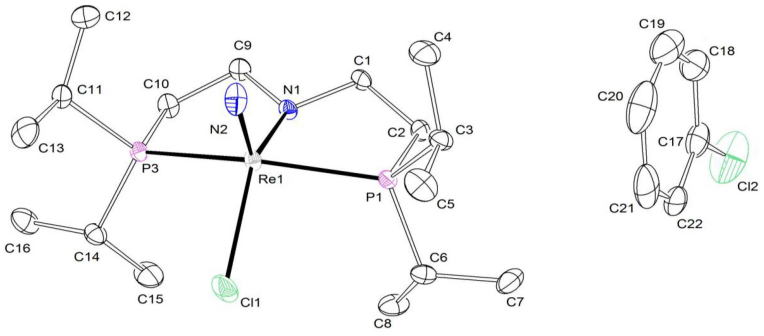

Fig. A.17. Thermal ellipsoid plot of **34** with the anisotropic displacement parameters drawn at the 50 % probability level. The asymmetric unit contains one complex molecule and one chlorobenzene solvent molecule.

Tab. A.17. Crystal data and structure refinement of **34**.

Identification code	**34**
Empirical formula	$C_{22}H_{41}Cl_2N_2P_2Re$
Formula weight	652.61
Temperature	120(2) K
Wavelength	0.71073 Å
Crystal system	Monoclinic
Space group	$P2_1/c$
Unit cell dimensions	a = 13.5319(7) Å, $\alpha = 90°$ b = 14.5498(7) Å, $\beta = 102.555(2)°$ c = 14.0355(7) Å, $\gamma = 90°$
Volume	2697.3(2) Å^3
Z	4
Density (calculated)	1.607 Mg/m^3
Absorption coefficient	4.834 mm^{-1}
F(000)	1304
Crystal size	0.220 x 0.114 x 0.058 mm^3
Crystal shape and color	Block, clear intense yellow
Theta range for data collection	2.356 to 30.610°
Index ranges	-19≤h≤19, -20≤k≤20, -20≤l≤20

Reflections collected	94562	
Independent reflections	8294 [R(int) = 0.0768]	
Completeness to theta = 25.242°	99.9 %	
Max. and min. transmission	0.7461 and 0.5667	
Refinement method	Full-matrix least-squares on F^2	
Data / restraints / parameters	8294 / 0 / 270	
Goodness-of-fit on F^2	1.028	
Final R indices [I>2sigma(I)]	R1 = 0.0269	wR2 = 0.0385
R indices (all data)	R1 = 0.0502	wR2 = 0.0430
Largest diff. peak and hole	0.930 and -1.091 eÅ^{-3}	

A.18 [ReCl(N_2)$_2$(HPNP^{iPr})] (**35**)

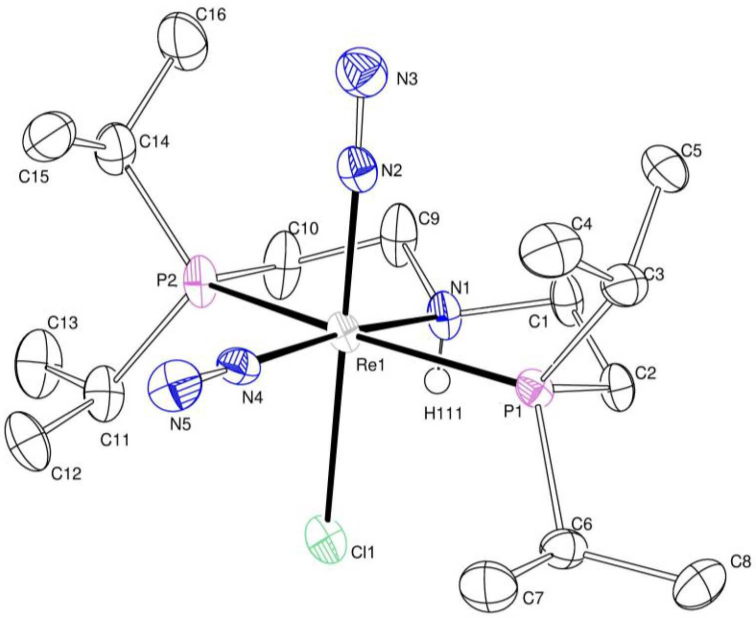

Fig. A.18. Thermal ellipsoid plot of**35** with the anisotropic displacement parameters drawn at the 50 % probability level. The asymmetric unit contains one complex molecule. The N-H hydrogen atom was found from the residual density map and isotropically refined.

Tab. A.18. Crystal data and structure refinement of **35**.

Identification code	**35**
Empirical formula	$C_{16}H_{37}ClN_5P_2Re$

Formula weight	583.09	
Temperature	100(2) K	
Wavelength	0.71073 Å	
Crystal system	Monoclinic	
Space group	$P2_1/n$	
Unit cell dimensions	a = 8.4054(4) Å b = 12.8887(6) Å c = 21.2215(9) Å	$\alpha = 90°$ $\beta = 96.241(2)°$ $\gamma = 90°$
Volume	2285.40(18) $Å^3$	
Z	4	
Density (calculated)	1.695 Mg/m^3	
Absorption coefficient	5.584 mm^{-1}	
F(000)	1160	
Crystal size	0.255 x 0.140 x 0.133 mm^3	
Crystal shape and color	Block, clear pale yellow-green	
Theta range for data collection	2.495 to 30.597°	
Index ranges	-12≤h≤12, -18≤k≤18, -29≤l≤30	
Reflections collected	89022	
Independent reflections	7010 [R(int) = 0.0572]	
Completeness to theta = 25.242°	100 %	
Max. and min. transmission	0.7461 and 0.6204	
Refinement method	Full-matrix least-squares on F^2	
Data / restraints / parameters	7010 / 0 / 238	
Goodness-of-fit on F^2	1.05	
Final R indices [I>2sigma(I)]	R1 = 0.0264	wR2 = 0.0502
R indices (all data)	R1 = 0.0423	wR2 = 0.0557
Largest diff. peak and hole	1.740 and -0.868 $eÅ^{-3}$	

A.19 $[(\mu\text{-}N_2)\{ReCl_2(HPNP^{iPr})\}_2]$ (**36**)

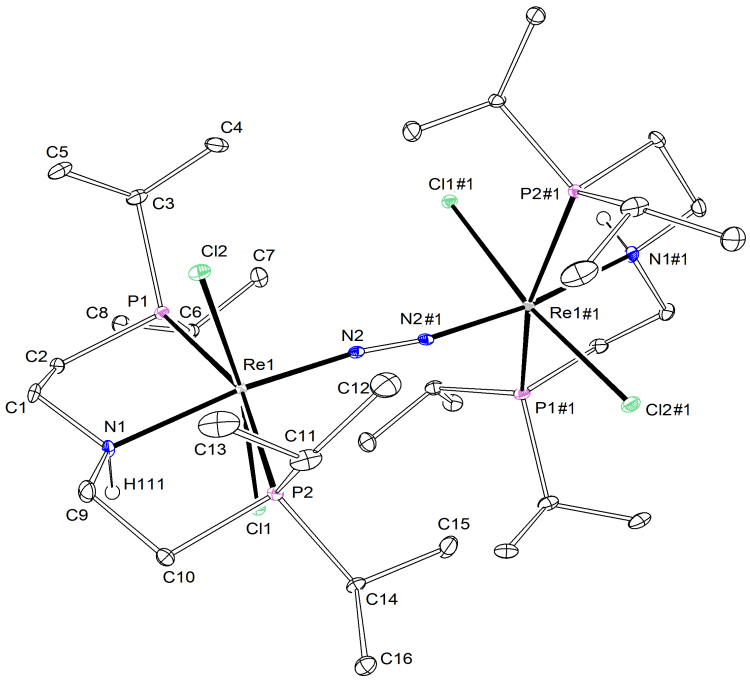

Fig. A.19. Thermal ellipsoid plot of **36** with the anisotropic displacement parameters drawn at the 50 % probability level. The asymmetric unit contains one complex molecule. The N-H hydrogen atom was found from the residual density map and isotropically refined.

Tab. A.19. Crystal data and structure refinement of **36**.

Identification code	**36**	
Empirical formula	$C_{32}H_{74}Cl_4N_4P_4Re_2$	
Formula weight	1153.03	
Temperature	101(2) K	
Wavelength	0.71073 Å	
Crystal system	Monoclinic	
Space group	$C2/c$	
Unit cell dimensions	a = 16.7163(11) Å b = 14.5042(10) Å c = 18.2802(12) Å	$\alpha = 90\,°$ $\beta = 96.445(2)\,°$ $\gamma = 90\,°$
Volume	4404.1(5) $Å^3$	
Z	4	
Density (calculated)	1.739 Mg/m^3	

Absorption coefficient	5.908 mm^{-1}	
F(000)	2288	
Crystal size	0.085 x 0.043 x 0.036 mm^3	
Crystal shape and color	Block, clear intense blue-green	
Theta range for data collection	2.242 to 28.367 °	
Index ranges	-22≤h≤22, -19≤k≤19, -24≤l≤24	
Reflections collected	73468	
Independent reflections	5510 [R(int) = 0.0773]	
Completeness to theta = 25.242 °	99.90 %	
Refinement method	Full-matrix least-squares on F^2	
Data / restraints / parameters	5510 / 0 / 220	
Goodness-of-fit on F^2	1.062	
Final R indices [I>2sigma(I)]	R1 = 0.0262	wR2 = 0.0410
R indices (all data)	R1 = 0.0376	wR2 = 0.0432
Largest diff. peak and hole	1.422 and -1.299 eÅ^{-3}	

A.20 [Re(N)Cl$_2$(HPNP^{iPr})] (**37**)

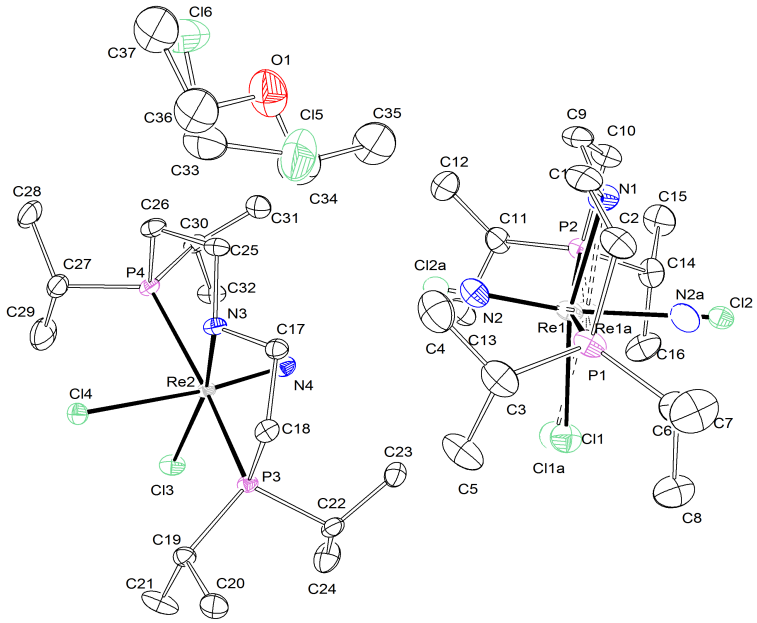

Fig. A.20. Thermal ellipsoid plot of **37** with the anisotropic displacement parameters drawn at the 50% probability level. The asymmetric unit contains one disordered complex molecule, one complex molecule without disorder and a dichloromethane and molecule which is one the same position as a diethylether molecule. The disordered complex molecule was refined with population of 0.962(2) on the main domain using some restraints and constraints (SADI, EADP). The solvent molecules were set to a population of 0.7 for the dichloromethane molecule and 0.3 for the diethylether molecule using some restraints and constrains (DFIX, EADP, RIGU, SADI).

Tab. A.20. Crystal data and structure refinement of **37**.

Identification code	**37**	
Empirical formula	$C_{33.90}H_{77.40}Cl_{5.40}N_4O_{0.30}P_4Re_2$	
Formula weight	1233.7	
Temperature	100(2) K	
Wavelength	0.71073 Å	
Crystal system	Monoclinic	
Space group	$P2_1/n$	
Unit cell dimensions	a = 14.1911(7) Å b = 18.7893(10) Å c = 19.6013(10) Å	$\alpha = 90°$ $\beta = 106.477(2)°$ $\gamma = 90°$
Volume	5011.9(4) Å^3	
Z	4	

Density (calculated)	1.635 Mg/m^3	
Absorption coefficient	5.270 mm^{-1}	
F(000)	2452	
Crystal size	0.314 x 0.266 x 0.103 mm^3	
Crystal shape and color	Block, clear intense brown	
Theta range for data collection	2.168 to 28.381°	
Index ranges	$-18 \leq h \leq 18$, $-25 \leq k \leq 25$, $-26 \leq l \leq 26$	
Reflections collected	230643	
Independent reflections	12540 [R(int) = 0.0407]	
Completeness to theta = 25.242°	99.9 %	
Max. and min. transmission	0.7461 and 0.6204	
Refinement method	Full-matrix least-squares on F^2	
Data / restraints / parameters	12540 / 83 / 507	
Goodness-of-fit on F^2	1.178	
Final R indices [I>2sigma(I)]	R1 = 0.0228	wR2 = 0.0467
R indices (all data)	R1 = 0.0289	wR2 = 0.0504
Largest diff. peak and hole	1.177 and -0.974 $eÅ^{-3}$	

A.21 *cis*-[Re(NH)Cl$_2$(HPNP^{iPr})]^{OTf} (**cis-38^{OTf}**)

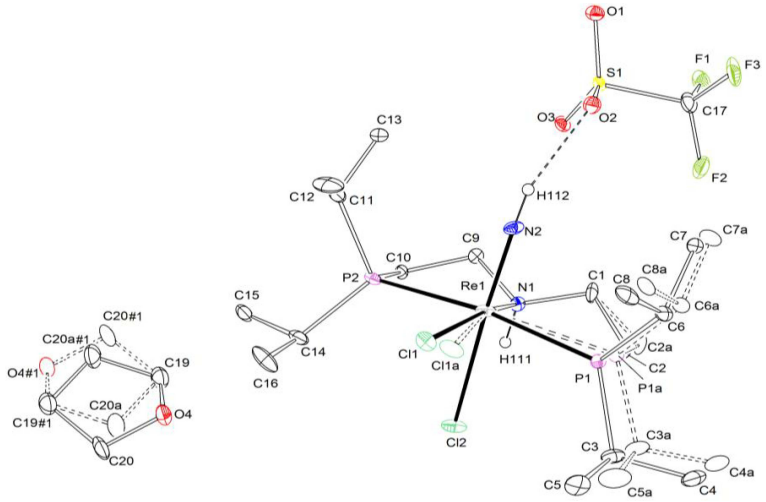

Fig. A.21. Thermal ellipsoid plot of **cis-38^{OTf}** with the anisotropic displacement parameters drawn at the 50% probability level. The asymmetric unit contains one disordered complex molecule, one $CF_3SO_3^-$ anion and a half disordered THF solvent molecule. The disordered complex molecule and the disordered THF solvent molecule were refined with site occupation factors of 0.5 for both sites using PART commands and some restraints and constraints (SADI, RIGU, EADP). All N-H hydrogen atoms were found from the residual density map and isotropically refined.

Tab. A.21. Crystal data and structure refinement of **cis-38^{OTf}**.

Identification code	**cis-38^{OTf}**	
Empirical formula	$C_{16}H_{38}Cl_2N_2P_2Re \cdot CF_3SO_3 \cdot \frac{1}{2} C_4H_8O$	
Formula weight	762.64	
Temperature	101(2) K	
Wavelength	0.71073 Å	
Crystal system	Monoclinic	
Space group	$P2_1/n$	
Unit cell dimensions	a = 7.4700(4) Å	$\alpha = 90°$
	b = 32.5017(18) Å	$\beta = 102.681(2)°$
	c = 12.4358(8) Å	$\gamma = 90°$
Volume	2945.6(3) Å^3	
Z	4	
Density (calculated)	1.720 Mg/m^3	
Absorption coefficient	4.530 mm^{-1}	

F(000)	1520	
Crystal size	0.162 x 0.060 x 0.054 mm^3	
Crystal shape and color	Plate, clear light blue	
Theta range for data collection	2.507 to 28.384°	
Index ranges	$-9 \leq h \leq 9$, $-43 \leq k \leq 43$, $-16 \leq l \leq 16$	
Reflections collected	98467	
Independent reflections	7353 [R(int) = 0.1698]	
Completeness to theta = 25.242°	99.9 %	
Refinement method	Full-matrix least-squares on F^2	
Data / restraints / parameters	7353 / 136 / 393	
Goodness-of-fit on F^2	1.079	
Final R indices [I>2sigma(I)]	R1 = 0.0514	wR2 = 0.0724
R indices (all data)	R1 = 0.0908	wR2 = 0.0805
Largest diff. peak and hole	1.498 and -1.862 $eÅ^{-3}$	

A.22 *trans*-[Re(NH)Cl$_2$(HPNP$^{i\mathrm{Pr}}$)]$^{\mathrm{BAr}^{\mathrm{F}}_{24}}$ (**trans-38$^{\mathrm{BAr}^{\mathrm{F}}_{24}}$**)

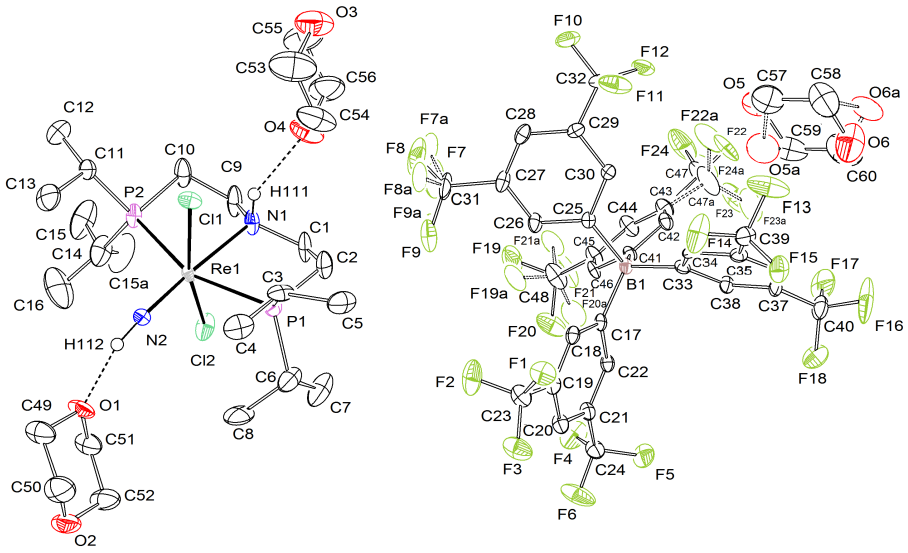

Fig. A.22. Thermal ellipsoid plot of **trans-38$^{\mathrm{BAr}^{\mathrm{F}}_{24}}$** with the anisotropic displacement parameters drawn at the 50 % probability level. The asymmetric unit contains one complex molecule, three dioxane solvent molecules and one $\mathrm{BAr}^{\mathrm{F}-}_{24}$ anion. The disordered complex molecule was refined with population of 0.876(9) on the main domain using some restraints (RIGU, SADI). One disordered dioxane solvent molecule was refined with population of 0.67(1) on the main domain using some restraints (RIGU, SADI). The disordered $\mathrm{BAr}^{\mathrm{F}-}_{24}$ anion was refined with population of 0.70(1), 0.73(2) and 0.876(9) on their main domains using some restraints (RIGU, SADI). Both N-H hydrogen atoms were found from the residual density map and isotropically refined.

Tab. A.22. Crystal data and structure refinement of **trans-38$^{\mathrm{BAr}^{\mathrm{F}}_{24}}$**.

Identification code	**trans-38$^{\mathrm{BAr}^{\mathrm{F}}_{24}}$**	
Empirical formula	$C_{60}H_{74}BCl_2F_{24}N_2O_6P_2Re$	
Formula weight	1705.06	
Temperature	100(2) K	
Wavelength	0.71073 Å	
Crystal system	Monoclinic	
Space group	$P2_1/c$	
Unit cell dimensions	a = 14.6803(12) Å b = 30.215(2) Å c = 17.4634(15) Å	$\alpha = 90°$ $\beta = 114.467(3)°$ $\gamma = 90°$
Volume	7050.5(10) Å^3	
Z	4	

Density (calculated)	1.606 Mg/m^3	
Absorption coefficient	1.957 mm^{-1}	
F(000)	3424	
Crystal size	0.100 x 0.086 x 0.038 mm^3	
Crystal shape and color	Plate, clear light blue	
Theta range for data collection	2.378 to 25.360°	
Index ranges	$-17 \leq h \leq 17$, $-36 \leq k \leq 36$, $-20 \leq l \leq 21$	
Reflections collected	143381	
Independent reflections	12865 [R(int) = 0.1675]	
Completeness to theta = 25.242°	99.9 %	
Refinement method	Full-matrix least-squares on F^2	
Data / restraints / parameters	12865 / 947 / 1021	
Goodness-of-fit on F^2	1.139	
Final R indices [I>2sigma(I)]	R1 = 0.0572	wR2 = 0.0914
R indices (all data)	R1 = 0.0849	wR2 = 0.0984
Largest diff. peak and hole	0.771 and -2.023 $eÅ^{-3}$	

A.23 $[Re(NBAr^{F}_{18})Cl_2(HPNP^{iPr})]$ (**39**)

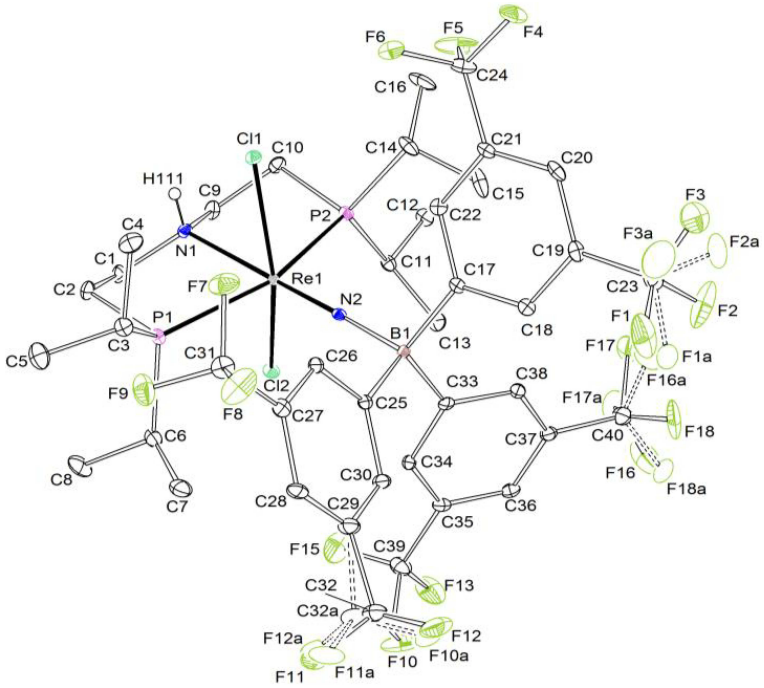

Fig. A.23. Thermal ellipsoid plot of **39** with the anisotropic displacement parameters drawn at the 50% probability level. The asymmetric unit contains one disordered complex molecule. The three disordered CF_3 groups were refined in two different positions with population of 0.640(4), 0.793(8) and 0.731(7) on their main domains using PART commands and some restraints and constrains (RIGU, EADP). The N-H hydrogen atom was found from the residual density map and isotropically refined.

Tab. A.23. Crystal data and structure refinement of **39**.

Identification code	**39**	
Empirical formula	$C_{40}H_{46}BCl_2F_{18}N_2P_2Re$	
Formula weight	1226.64	
Temperature	103(2) K	
Wavelength	0.71073 Å	
Crystal system	Monoclinic	
Space group	$C2/c$	
Unit cell dimensions	a = 25.0171(15) Å b = 12.5947(7) Å c = 32.3189(19) Å	$\alpha = 90°$ $\beta = 108.879(2)°$ $\gamma = 90°$
Volume	9635.3(10) Å^3	
Z	8	

Density (calculated)	1.691 Mg/m^3	
Absorption coefficient	2.801 mm^{-1}	
F(000)	4848	
Crystal size	0.339 x 0.240 x 0.151 mm^3	
Crystal shape and color	Block, clear intense blue-green	
Theta range for data collection	2.423 to 28.370°	
Index ranges	$-33 \leq h \leq 33$, $-16 \leq k \leq 16$, $-43 \leq l \leq 43$	
Reflections collected	133858	
Independent reflections	12043 [R(int) = 0.1225]	
Completeness to theta = 25.242°	99.9 %	
Refinement method	Full-matrix least-squares on F^2	
Data / restraints / parameters	12043 / 450 / 694	
Goodness-of-fit on F^2	1.059	
Final R indices [I>2sigma(I)]	R1 = 0.0445	wR2 = 0.0676
R indices (all data)	R1 = 0.0758	wR2 = 0.0741
Largest diff. peak and hole	1.038 and -1.278 $eÅ^{-3}$	

A.24 $[ReCl_3(P{=}NP^{iPr})]$ (**40**)

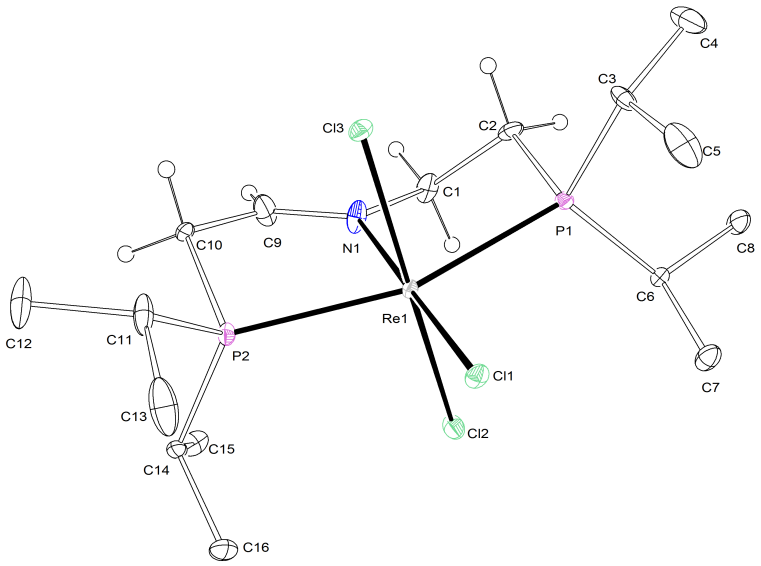

Fig. A.24. Thermal ellipsoid plot of **40** with the anisotropic displacement parameters drawn at the 50 % probability level. The asymmetric unit contains one complex molecule. The structure was refined as an inversion twin using the twin law -100 0-10 00-1 (BASF: 0.016(7)).

Tab. A.24. Crystal data and structure refinement of **40**.

Identification code	**40**	
Empirical formula	$C_{16}H_{35}Cl_3NP_2Re$	
Formula weight	595.94	
Temperature	102(2) K	
Wavelength	0.71073 Å	
Crystal system	Orthorhombic	
Space group	$P2_12_12_1$	
Unit cell dimensions	a = 7.2793(2) Å	$\alpha = 90°$
	b = 12.8079(4) Å	$\beta = 90°$
	c = 23.9040(7) Å	$\gamma = 90°$
Volume	2228.63(11) $Å^3$	
Z	4	
Density (calculated)	1.776 Mg/m^3	
Absorption coefficient	5.955 mm^{-1}	
F(000)	1176	

Crystal size	0.217 x 0.122 x 0.089 mm^3	
Crystal shape and color	Block, clear intense orange	
Theta range for data collection	2.331 to 28.353°	
Index ranges	-9≤h≤9, -17≤k≤16, -31≤l≤31	
Reflections collected	42851	
Independent reflections	5555 [R(int) = 0.0666]	
Completeness to theta = 25.242°	99.9 %	
Refinement method	Full-matrix least-squares on F^2	
Data / restraints / parameters	5555 / 0 / 217	
Goodness-of-fit on F^2	1.033	
Final R indices [I>2sigma(I)]	R1 = 0.0245	wR2 = 0.0423
R indices (all data)	R1 = 0.0301	wR2 = 0.0435
Absolute structure parameter	0.016(7)	
Largest diff. peak and hole	0.791 and -1.120 $eÅ^{-3}$	

List of chemical compounds

B

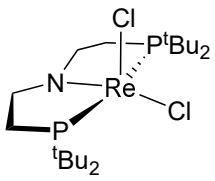

XIX

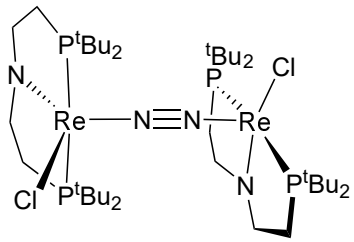

XX

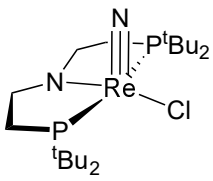

XXI

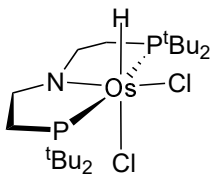

1

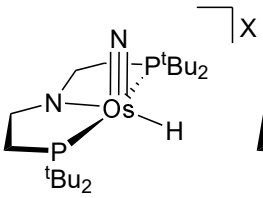

2^{X}

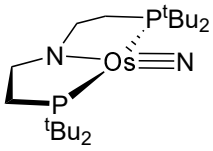

3

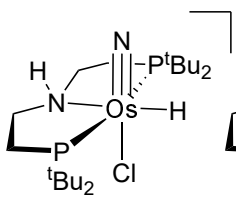

4^{Cl}

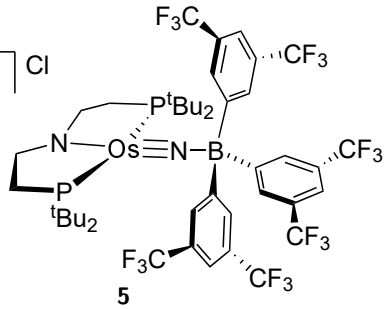

5

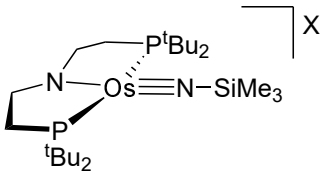

6^{X}

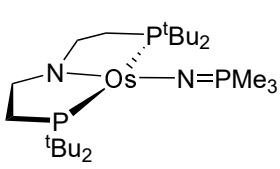

7

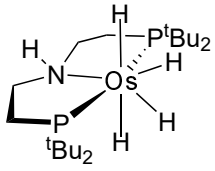

8

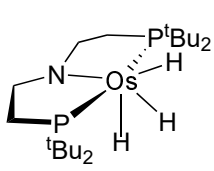

9

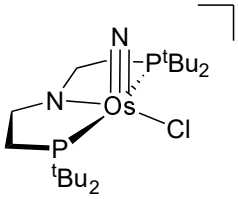

$10^{BAr^{F}_{24}}$

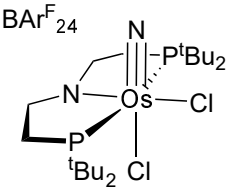

10-Cl

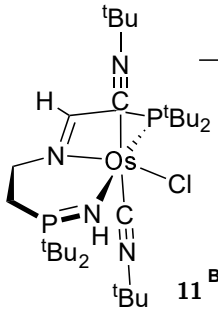

$11^{BAr^{F}_{24}}$

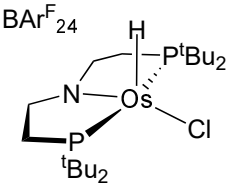

12^{BPh_4}

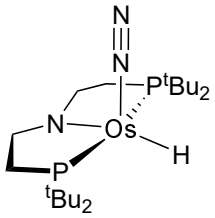

13

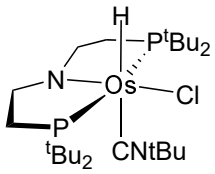

14^{BPh_4}

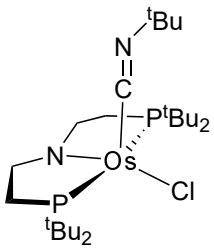

15

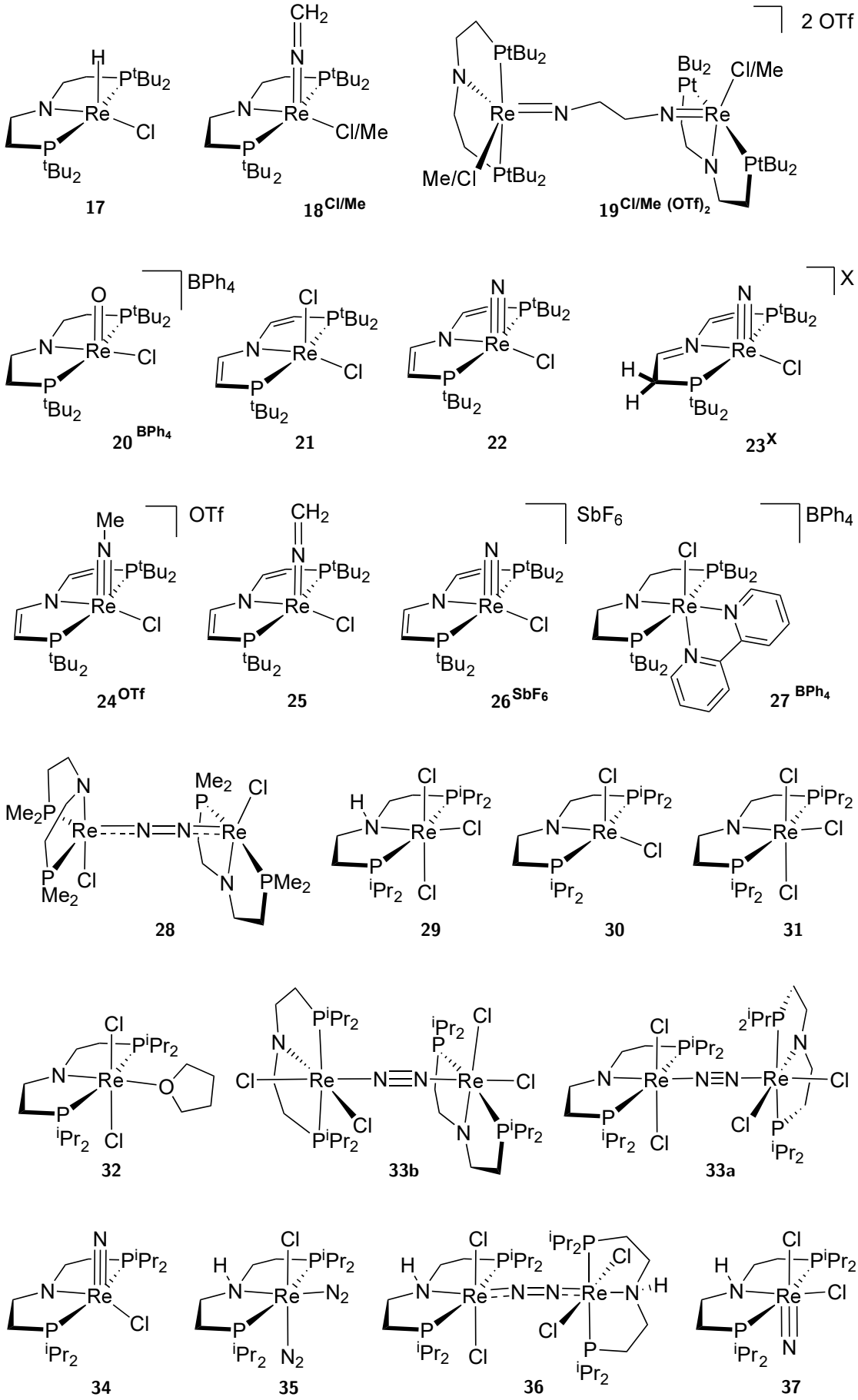
17
18Cl/Me
19Cl/Me (OTf)2
2 OTf
20BPh4
BPh4
21
22
23X
X
24OTf
OTf
25
26SbF6
SbF6
27BPh4
BPh4
28
29
30
31
32
33b
33a
34
35
36
37

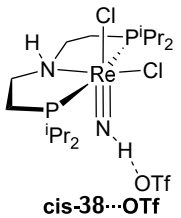

cis-38···OTf

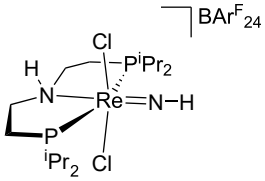

trans-38$^{BArF_{24}}$

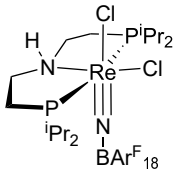

cis-39

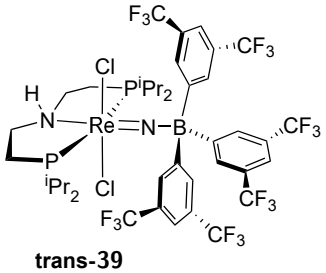

trans-39

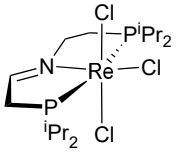

40

C

List of abbreviations

ATR-IR	attenuated total reflection infrared
BDE	bond dissociation enthalpy
bipy	2,2'-bipyridine
CASSCF	complete active space self consistent field
CC	coupled cluster
CE	counter electrode
COSY	correlation spectroscopy
CPE	controlled potential electrolysis
CV	cyclic voltammetry
d	doublet
DBU	1,8-diazabicyclo[5.4.0]undec-7-ene
dd	doublet of doublets
DCM	dichloromethane
DCP	2,6-dichlorophenol
DFT	density functional theory
DOSY	diffusion ordered spectroscopy
EPR	electron paramagnetic resonance
ESI	electron spray ionization
eq	equivalent
eq.	equation
FMO	frontier molecular orbital
FWHM	full width at half maximum
GC	glassy carbon
hept	heptet
HMBC	heteronuclear multiple bond correlation
HMDSO	hexamethyldisiloxane
HOMO	highest occupied molecular orbital
HSQC	heteronuclear single quantum coherence
IC	internal conversion
iR	internal resistance
IR	infrared
ISC	inter system crossing
KHMDS	potassium bis(trimethylsilyl)amide
KO^{t}Bu	potassium *tert*-butoxide

LED	light-emitting diode	141
LIFDI	liquid injection field desorption ionization	62
LUMO	lowest unoccupied molecular orbital	3
m	multiplet	142
MIR	mid infrared	91
MLCT	metal-ligand charge transfer	11
MO	molecular orbital	8
NBO	natural bonding orbital	53
NCS	*N*-chlorosuccinimide	36
NHC	N-heterocyclic carbene	17
NIR	near infrared	90
NMR	nuclear magnetic resonance	40
NEVPT2	N-electron valence state perturbation theory	88
NOESY	nuclear *Overhauser* effect spectroscopy	50
NPA	natural population analysis	54
PCET	proton coupled electron transfer	17
QDPT	quasi-degenerate perturbation theory	88
QRO	quasi-restricted orbital	134
RE	reference electrode	73
RMSD	root-mean-square deviation (of atomic positions)	77
RT	room temperature	33
s	singlet	147
SOC	spin-orbit coupling	67
SOMO	singly occupied molecular orbital	41
spin-sys	spin system	142
SQUID	superconducting quantum interference device	10
t	triplet	150
TDDFT	time-dependent density functional theory	27
TEMPOH	1-hydroxyl-2,2,6,6-tetramethylpiperidine	39
TIP	temperature independent paramagnetism	67
TTBP	2,4,6-tris-*tert*-butylphenoxy radical	36
THF	tetrahydrofurane	49
UV	ultraviolet	24
UV/vis	ultraviolet/visible	26
VER	vibrational energy relaxation	26
vs.	*versus*	49
vt	virtual triplet	145
VT-NMR	variable temperature nuclear magnetic resonance	68
WE	working electrode	73